中国科学院紫金山天文台

Research Annual Report

2017

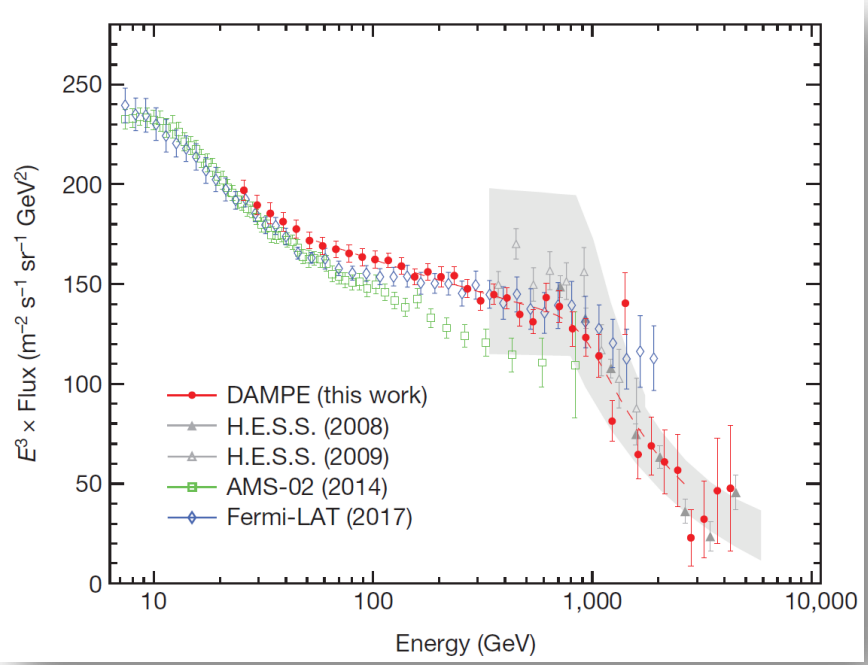

Purple Mountain Observatory CAS

中国科学院紫金山天文台

2017 科研工作年度报告

中国科学院紫金山天文台科技处

2018 年 7 月

Cover: Dark Matter Particle Explorer published its measurement of electrons and positrons in a very wide energy range

封面：暗物质粒子探测卫星发布首批科学成果

中国科学院紫金山天文台
科技处

地 址：南京市北京西路 2 号
邮 编：210008
电 话：+86-25-8333-2288, 2158
传 真：+86-25-8333-2288
电 邮：pmokjc@pmo.ac.cn
http://www.pmo.cas.cn

目 录

目 录 I

2017 年度科研工作总结 1

一、科研工作总体情况 1

ABSTRACT LIST OF PUBLICATIONS IN 2017 ..... **28**

I. DARK MATTER & SPACE ASTRONOMY **29**

1-01 Cosmic Gamma Ray Bursts, Neutron Stars, and Relevant Physics **29**

（1）A parameterized energy correction method for electromagnetic showers in BGO-ECAL of DAMPE 29

（2）Revealing Physical Activity of GRB Central Engine with Macronova/Kilonova Data 29

（3）GRB 111005A at z=0.0133 and the Prospect of Establishing Long-Short GRB/GW Association 29

（4）Multi-messenger Observations of a Binary Neutron Star Merger 29

（5）The GW170817/GRB 170817A/AT 2017gfo Association: Some Implications for Physics and Astrophysics 41

1-02 High-energy Solar physics 41

（6）Shapes of Ne-20 de-excitation line in solar flare 41

（7）The Confined X-class Flares of Solar Active Region 2192 (vol 801, L23, 2015) 41

（8）On the time evolution of brightness, volume and height of a coronal source in an M-class flare 42

（9）Generation Mechanisms of Quasi-parallel and Quasi-circular Flare Ribbons in a Confined Flare 42

（10）Formation and Initiation of Erupting Flux Rope and Embedded Filament Driven by Photospheric Converging Motion 42

（11）Search for the gamma-ray emission from M33 with the Fermi Large Area Telescope 42

（12）Molecular Gas toward the Gemini OB1 Molecular Cloud Complex. I. Observation Data 42

（13）The Molecular Structures of the Local Arm and Perseus Arm in the Galactic Region of l = [139 degrees.75, 149 degrees.75], b = [-5 degrees.25, 5 degrees.25]..43

（14）Characteristics of events with metric-to-decahectometric type II radio bursts associated with CMEs and flares in relation to SEP events 43

（15）Observational Evidence of Magnetic Reconnection for Brightenings and Transition Region Arcades in IRIS Observations 43

（16）Spectroscopic Observations of Magnetic Reconnection and Chromospheric Evaporation in an X-shaped Solar Flare 43

（17）Spectroscopic Observations of Magnetic Reconnection and Chromospheric Evaporation in an X-shaped Solar Flare 44

（18）A Study of Fermi-LAT GeV gamma-Ray Emission toward the Magnetar-harboring Supernova Remnant Kesteven 73 and Its Molecular

Environment 44
（19）Generation Mechanisms of Quasi-parallel and Quasi-circular Flare Ribbon in a Confined Flare 44
（20）Statistical study of co-rotating interaction region properties with STEREO and ACE observations 44
1-03 Multi-Band Observation Solar Activity 45
（21）Simultaneous Transverse and Longitudinal Oscillations in a Quiescent Prominence Triggered by a Coronal Jet 45
（22）INITIATION PROCESSES FOR THE 2013 MAY 13 X1.7 LIMB FLARE 45
（23）THE INTERPRETATION OF THE MULTI-WAVELENGTH AFTERGLOW EMISSION OF SHORT GRB 140903A 45
（24）NIHAO - VIII. Circum-galactic medium and outflows - The puzzles of H I and O VI gas distributions Gutcke, ...45
（25）Quasi-periodic pulsations with periods that change depending on whether the pulsations have thermal or nonthermal components.....46
（26）One-Minute Quasi-Periodic Pulsations Seen in a Solar Flare 46
（27）The Eruption of a Small-scale Emerging Flux Rope as the Driver of an M-class Flare and of a Coronal Mass Ejection 46
（28）High-resolution Observations of Sympathetic Filament Eruptions by NVST .46
（29）Large-amplitude Longitudinal Oscillations in a Solar Filament.....47
（30）Solar Tornadoes Triggered by Interaction between Filaments and EUV Jets.47
（31）Explosive Chromospheric Evaporation Driven by Nonthermal Electrons around One Footpoint of a Solar Flare Loop 47
（32）Blob Formation and Ejection in Coronal Jets due to the Plasmoid and Kelvin-Helmholtz Instabilities 47
（33）Steep Decay Phase Shaped by the Curvature Effect. II. Spectral Evolution ...48
（34）Steep Decay Phase Shaped by the Curvature Effect. I. Flux Evolution.....48
（35）Statistical properties of bipolar magnetic regions.....48
（36）Terrestrial planet formation under migration: systems near the 4:2:1 mean motion resonance.....48
（37）Interaction of Two Filaments in a Long Filament Channel Associated with Twin Coronal Mass Ejections.....49
（38）Location of energy source for coronal heating on the photosphere 49
（39）Pre-flare coronal dimmings 49
（40）LITTLE THINGS (vol 144, 134, 2012).....49
（41）Design Study on the Digital Correlator Using for Radio Holography 50
（42）Metal enrichment signatures of the first stars on high-z DLAs.....50
（43）Doppler Shift Oscillations from a Hot Line Observed by IRIS 50
（44）Quasi-periodic pulsations with multiple periods in hard X-ray emission 50
（45）Large-amplitude Longitudinal Oscillations Triggered by the Merging of Two
（46）Solar Filaments: Observations and Magnetic Field Analysis.....51
（47）Acceleration and Radiation of High-Energy Cosmic Particles 51
（46）EVOLUTION OF HIGH-ENERGY PARTICLE DISTRIBUTION IN MATURE SHELL-TYPE SUPERNOVA REMNANTS.....51
（47）Anomalous Distributions of Primary Cosmic Rays as Evidence for Time-dependent Particle Acceleration in Supernova Remnants 51
（48）Evaluation of dimension of fractal time series with the least square method51
（49）Measure the Propagation of a Halo CME and Its Driven Shock with the Observations from a Single Perspective at Earth.....52
（50）Calibration of the Mengcheng Solar Radio Spectrometer 52
1-04 Physics of Dark Matter Indirect Detection 52
（51）A gamma-ray Quasi-periodic Modulation in the Blazar PKS 0301-243?.....52

Purple Mountain Observatory
Chinese Academy of Sciences

ADD :2 West Beijing Road,
Nanjing 210008, China
TEL : +86-25-83332288
FAX : +86-25-83332288
Email :pmokjc@pmo.ac.cn
http://www.pmo.cas.cn

Editor Commettee

Darun XIONG,
Ji YANG, Jin CHAN, Zhangyin ZHAO,
Sheng-Cai SHI, Yuehua MA,
Weiqun GAN, Daming WEI,
Haisheng JI, Lifan WANG,
Xi KANG, Yu GAO, Hongchi WANG,
Ye XU, Jin Xu, Dazhi YAO,
Yanning FU, Weibiao XU,
Jianghui JI, Haibin ZHAO ,
YiZhong FAN, Siming LIU,
Xuefeng WU, Xianzhong ZHENG,
Xuepeng CHEN, Yingxi ZUO

Sub-Editor

Jianxin HUI huijx@pmo.ac.cn
Lilin lilin@pmo.ac.cn
xuemeiChen xmchen@pmo.ac.cn

Excutive Editor

Ningzongjun
ningzongjun@pmo.ac.cn

Division of

（52）Neutron Star-Black Hole Coalescence Rate Inferred from Macronova Observations.....52
（53）Possible Correlations between the Emission Properties of SGRBs and Their Offsets from the Host Galaxies.....52
（54）Revisiting SNR Puppis A with Seven Years of Fermi Large Area Telescope Observations.....53
（55）Millimeter observations of the disk around GW Orionis.....53
（56）Possible Quasi-periodic Modulation in the z=1.1 Gamma-Ray Blazar PKS 0426-380.....53
（57）Possible Dark Matter Annihilation Signal in the AMS-02 Antiproton Data.....53
（58）Light bending in infinite derivative theories of gravity.....53
（59）Constraining the PopIII IMF with high-z GRBs.....54
（60）Limits on dark matter annihilation cross sections to gamma-ray lines with subhalo distributions in N-body simulations and Fermi LAT data.....54
（61）gamma-Ray emission signals in the massive graviton mediated dark matter model.....54
（62）Evaluating the Bulk Lorentz Factors of Outflow Material: Lessons Learned from the Extremely Energetic Outburst GRB 160625B.....54
（63）Revisiting Quasi-periodic Modulation in gamma- Ray Blazar PKS 2155-304 with Fermi Pass 8 Data.....54
（64）Spectroscopic identification of r-process nucleosynthesis in a double neutron-star merger.....55
（65）An X-Ray Periodicity of similar to 1.8 hr in Narrow-line Seyfert 1 Galaxy Mrk 766.....55
（66）Direct detection of a break in the teraelectronvolt cosmic-ray spectrum of electrons and positrons.....55
（67）The unpolarized macronova associated with the gravitational wave event GW 170817.....56
（68）GRB 111005A at z = 0.0133 and the Prospect of Establishing Long-Short GRB/GW Association.....56
1-05 Laboratory for Dark Matter and Space Astronomy..... 57
（69）LIKEDM: Likelihood calculator of dark matter detection.....57
（70）HESS J1427-608: AN UNUSUAL HARD, UNBROKEN gamma-RAY SPECTRUM IN A VERY WIDE ENERGY RANGE.....57
（71）On-orbit Status and Light Attenuation Behavior of the DAMPE-PSD.....57
（72）A radiation transfer model for the Milky Way: I. Radiation fields and application to high-energy astrophysics.....57
（73）Compact Resolved Ejecta in the Nearest Tidal Disruption Event.....58
（74）3FGL J1924.8-1034: A spatially extended stable unidentified GeV source?.....58
（75）Quality control of mass production of PMT modules for DAMPE.....58
（76）Propagation of cosmic rays in the AMS-02 era.....58
（77）Calibrating a physical model based on Geant4 to calculate cosmogenic nuclide production rates on lunar surface.....58
（78）AMS-02 positron excess and indirect detection of three-body decaying dark matter.....59
（79）Thermal Design and Validation of DAMPE BGO Calorimeter.....59
（80）Synthesis of ZnO nanoporous structure materials by two-step thermal oxidation of Zn film.....59
（81）CALIFA reveals prolate rotation in massive early-type galaxies: A polar galaxy merger origin?.....59
（82）The DArk Matter Particle Explorer mission.....59
（83）Offline software for the DAMPE experiment.....60

（84）Temperature effects on MIPs in the BGO calorimeters of DAMPE 60
（85）Validation of the Ability of Full Configuration Interaction Quantum Monte Carlo for Studying the 2D Hubbard Model 60
（86）Statistical study of co-rotating interaction region properties with STEREO and ACE observations 61
1-06 UV/X-ray Astronomy Research Group 61
（87）A timing view of the heartbeat state of GRS 1915+105 61
（88）Joint fit of Warm Absorbers in COS and HETG spectra of NGC 3783 61
（89）Current Investigations on Young Star Cluster NGC 3603 in X-ray 61
II. ANTARCTIC ASTRONOMY RADIO ASTRONOMY **63**
2-01 Stellar Structure, Evolution and Pulsation **63**
（91）On the effect of turbulent anisotropy on pulsation stability of stars 63
（92）Turbulent Convection and Pulsation Stability of Stars 63
2-02 Center for Antarctic Astronomy 63
（93）INTERSTELLAR-MEDIUM MAPPING IN M82 THROUGH LIGHT ECHOES AROUND SUPERNOVA 2014 63
（94）Optical Sky Brightness and Transparency during the Winter Season at Dome A Antarctica from the Gattini-All-Sky Camera 63
（95）IC 630: Piercing the Veil of the Nuclear Gas 64
（96）Evolution of Mass and Velocity Field in the Cosmic Web: Comparison Between Baryonic and Dark Matter 64
（97）Variable Stars Observed in the Galactic Disk by AST3-1 from Dome A, Antarctica 64
（98）Cosmological Inference from Host-Selected Type Ia Supernova Samples 65
（99）Detection of a possible superluminous supernova in the Epoch of Reionization 65
（100）OzDES multifibre spectroscopy for the Dark Energy Survey: 3-yr results and first data release 65
（101）The Influence of Host Galaxies in Type Ia Supernova Cosmology 66
（102）A hybrid type Ia supernova with an early flash triggered by helium-shell detonation 66
（103）Preheating of the Intergalactic Medium by Gravitational Collapse and Ultraviolet Background 66
（104）Follow Up of GW170817 and Its Electromagnetic Counterpart by Australian-Led Observing Programmes 67
（105）Optical observations of LIGO source GW 170817 by the Antarctic Survey Telescopes at Dome A, Antarctica 67
（106）Average Spectral Properties of Type Ia Supernova Host Galaxies 68
（107）Average Spectral Properties of Type Ia Supernova Host Galaxies 68
2-03 Galaxy Cosmology and Dark Energy 68
（108）Backflows by active galactic nuclei jets: global properties and influence on supermassive black hole accretion 68
（109）NIHAO XII: galactic uniformity in a Lambda CDM universe 69
（110）NIHAO VII: predictions for the galactic baryon budget in dwarf to Milky Way mass haloes 69
（111）Constraints on the Evolution of the Galaxy Stellar Mass Function. I. Role of Star Formation, Mergers, and Stellar Stripping 69
（112）What is the right way to quench star formation in semi-analytic models of galaxy formation? 69
（113）The spatial alignment of galaxies on different scales:A review on the theoretical and observational progress 70
（114）The Frontier Fields lens modelling comparison project 70
（115）Halo Intrinsic Alignment: Dependence on Mass, Formation Time, and

Environment 70
（116）A general explanation on the correlation of dark matter halo spin with the large-scale environment 71
（117）How to co-add images? I. A new iterative method for image reconstruction of dithered observations 71
（118）Constraints on the Evolution of the Galaxy Stellar Mass Function. II. The Quenching Timescale of Galaxies and Its Implication for Their Star Formation Rates71
（119）The Sloan Lens ACS Survey. XIII. Discovery of 40 New Galaxy-scale Strong Lenses 71
（120）The Sloan Lens ACS Survey. XIII. Discovery of 40 New Galaxy-scale Strong Lenses 72
（121）Testing PSF Interpolation in Weak Lensing with Real Data 72
2-04 Star Formation in Galaxies 72
（122）Dense gas in low-metallicity galaxies....72
（123）HIFI Spectroscopy of H2O Submillimeter Lines in Nuclei of Actively Star-forming Galaxies 72
（124）ALMA Maps of Dust and Warm Dense Gas Emission in the Starburst Galaxy IC 5179....73
（125）Testing the universality of the star-formation efficiency in dense molecular gas....73
（126）ALMA [N II] 205 mu m Imaging Spectroscopy of the Interacting Galaxy System BRI 1202-0725 at Redshift 4.7....74
（127）Neutral Carbon Emission in Luminous Infrared Galaxies: The [CI] Lines as Total Molecular Gas Tracers....74
（128）A Herschel Space Observatory Spectral Line Survey of Local Luminous Infrared Galaxies from 194 to 671 Microns 74
（129）HC3N observations of nearby galaxies 74
（130）Dense Gas in the Outer Spiral Arm of M51 75
（131）Extinction Correction Significantly Influences the Estimate of the Ly alpha Escape Fraction....75
（132）High Dense Gas Fraction in Intensely Star-forming Dusty Galaxies....75
（133）VALES: IV. Exploring the transition of star formation efficiencies between normal and starburst galaxies using APEX/SEPIA Band-5 and ALMA at low redshift 76
（134）Molecular gas in the Herschel-selected strongly lensed submillimeter galaxies at z 2-4 as probed by multi-J CO lines 76
（135）Molecular gas in the Herschel-selected strongly lensed submillimeter galaxies at z similar to 2-4 as probed by multi-J CO lines 76
（136）Molecular gas in the Herschel-selected strongly lensed submillimeter galaxies at z similar to 2-4 as probed by multi-J CO lines 76
（137）Homologous Circular-ribbon Flares Driven by Twisted Flux Emergence 77
2-05 Molecular Clouds and Star Formation 77
（138）A simple criterion for selecting disks with evidence for dust growth and settling....77
（139）Kinetic temperature of massive star-forming molecular clumps measured with formaldehyde III. The Orion molecular cloud 1....77
（140）L1188: A Promising Candidate for Cloud-Cloud Collisions Triggering the Formation of Low-and Intermediate-mass Stars 78
（141）On the local stellar populations....78
（142）The barium-to-iron enrichment versus age relation of ancient disc stars ...78
（143）SiS in the Circumstellar Envelope of IRC+10216: Maser and Quasi-thermal Emission....79
（144）First Results from BISTRO: A SCUBA-2 Polarimeter Survey of the Gould Belt79
（145）First Millimeter Detection of the Disk around a Young, Isolated,

Planetary-mass Object.....79
（146）NGC 1980 Is Not a Foreground Population of Orion: Spectroscopic Survey of Young Stars with Low Extinction in Orion.....80
（147）A Curved Magnetic Field in the Ring-like Shell of Bubble N4 80
（148）Multiplicity among Solar-type Stars 80
（149）How Do Stars Gain Their Mass? A JCMT/SCUBA-2 Transient Survey of Protostars in Nearby Star-forming Regions 80
（150）A simple criterion for selecting disks with evidence for dust growth and settling.....81
（151）The properties of the inner disk around HL Tau: Multi-wavelength modeling of the dust emission 81
（152）Stellar variability from Dome A, Antarctica 81
2-06 Galaxy formation and wide Field Sky Survey..... 82
（153）THE QUENCHED MASS PORTION OF STAR-FORMING GALAXIES AND THE ORIGIN OF THE STAR FORMATION SEQUENCE SLOPE 82
（154）First Spectroscopic Confirmations of z similar to 7.0 Ly alpha Emitting Galaxies in the LAGER Survey 82
（155）The Origins of UV-optical Color Gradients in Star-forming Galaxies at z similar to 2: Predominant Dust Gradients but Negligible sSFR Gradients 82
（156）An Imperfectly Passive Nature: Bright Submillimeter Emission from Dust-obscured Star Formation in the z=3.717 "Passive" System, ZF 20115 83
（157）First Results from the Lyman Alpha Galaxies in the Epoch of Reionization (LAGER) Survey: Cosmological Reionization at z similar to 7.....83
（158）AGN-host connection at 0.5 < z < 2.5: A rapid evolution of AGN fraction in red galaxies during the last 10 Gyr 84
（159）DEEP CFHT Y-BAND IMAGING OF VVDS-F22 FIELD. I. DATA PRODUCTS AND PHOTOMETRIC REDSHIFTS 84
2-07 High – energy time-domain astronomy 84
（160）A Further Test of Lorentz Violation from the Rest-frame Spectral Lags of Gamma-Ray Bursts 84
（161）A New Measurement of the Spectral Lag of Gamma-Ray Bursts and its Implications for Spectral Evolution Behaviors 85
（162）Constraining Anisotropic Lorentz Violation via the Spectral-lag Transition of GRB 160625B.....85
（163）New test of weak equivalence principle using polarized light from astrophysical events 85
（164）An Improved Method to Measure the Cosmic Curvature 85
（165）Impact of a Locally Measured H-0 on the Interpretation of Cosmic-chronometer Data.....86
（166）New limits on the photon mass with radio pulsars in the Magellanic clouds86
（167）Gamma-ray burst cosmology: Hubble diagram and star formation history 86
（168）A New Test of Lorentz Invariance Violation: The Spectral Lag Transition of GRB 160625B.....86
（169）The Observer's Guide to the Gamma-Ray Burst Supernova Connection 86
（170）Strongly lensed gravitational waves and electromagnetic signals as powerful cosmic rulers.....87
（171）Hyperaccreting Black Hole as Gamma-Ray Burst Central Engine. II. Temporal Evolution of the Central Engine Parameters during the Prompt and Afterglow Phases.....87
（172）Model-independent Constraints on Cosmic Curvature and Opacity 87
（173）Lorentz factor - Beaming corrected energy/luminosity correlations and GRB central engine models 87
（174）Afterglows and Kilonovae Associated with Nearby Low-luminosity

Short-duration Gamma-Ray Bursts: Application to GW170817/GRB 170817A.....88
（175）Multimessenger tests of the weak equivalence principle from GW170817 and its electromagnetic counterparts 88
（176）A Further Test of Lorentz Violation from the Rest-frame Spectral Lags of Gamma-Ray Bursts 88
2-08 Gas distribution and Properties of the Milky Way 89
（177）Is HESS J1912+101 Associated with an Old Supernova Remnant? 89
（178）Multifrequency VLBA polarimetry of the high-redshift GPS quasar OQ17289
（179）Molecular Clouds in the Extreme Outer Galaxy between l.=34 degrees.75 to 45 degrees.25 89
（180）Kinematics of a Young Low-mass Star-forming Core: Understanding the Evolutionary State of the First-core Candidate L1451-mm.....89
（181）Molecular Environments of Three. Large Supernova Remnants in the Third Galactic Quadrant: G205.5+0.5, G206.9+2.3, and G213.0-0.6 90
（182）A Turbulent Origin for the Complex Envelope Kinematics in the Young Low-mass Core Per-bolo 58 Maureira, ...90
（183）A Turbulent Origin for the Complex Envelope Kinematics in the Young Low-mass Core Per-bolo 58.....90
2-09 Millimeter & Sub-Millimeter Wave Laboratory 91
（184）Characterization of a Free-Standing Membrane Supported Superconducting Ti Transition Edge Sensor.....91
（185）Optoelectronic Control of an External Cavity Quantum Cascade Laser Using a Graphene Loaded Metamaterial Array.....91
（186）Observations of the Hydroxyl Radical in C/2013 US10 (Catalina) at 18cm Wavelength.....91
（187）Guest Editorial Mini-Special Issue on the 27th International Symposium on Space Terahertz Technology 91
（188）THz Vector Field Measurement Comparison Between On-the-Fly and Step Scan Method 91
（189）External amplitude and frequency modulation of a terahertz quantum cascade laser using metamaterial/graphene devices.....92
（190）Analysis of 220-GHz Low-Loss Quasi-Elliptic Waveguide Bandpass Filter ...92
（191）WR-3 Band Quasi-Elliptical Waveguide Filters Using Higher Order Mode Resonances.....92
（192）A 240-GHz Wideband Ridged Waveguide Filter Based on MEMS Process ..92
（193）Development of ultra high sensitivity superconducting THz detectors.....93
（194）Terahertz and far-infrared windows opened at Dome A in Antarctica 93
（195）High Efficiency and Wideband 300 GHz Frequency Doubler Based on Six Schottky Diodes.....93
（196）超高灵敏度太赫兹超导探测技术发展 93
2-10 Telescope Technology Laboratory 93
（197）Failure analysis of a frangible composite cover: A transient-dynamics study93
（198）Two Methods to Broaden the Bandwidth of a Nonlinear Piezoelectric Bimorph Power Harvester 94
（199）Research on a bimorph piezoelectric deformable mirror for adaptive optics in optical telescope.....94
（200）Linear and nonlinear analysis of the thermal effects of beam piezoelectric bending actuator on adaptive optics.....94
（201）A combined analysis of PandaX, LUX, and XENON1T experiments within the framework of dark matter effective theory.....94
2-11 Delingha millimeter wave Observation Station 94
（202）Two-dimensional Molecular Gas and Ongoing Star Formation around H II Region Sh2-104.....95

（203）Towards a three-dimensional distribution of the molecular clouds in the Galactic Centre 95
（204）Large-field CO(1-0) observations toward the Galactic historical supernova remnants: a large cavity around Tycho's supernova remnant 95
（205）A 95 GHz methanol emission survey toward eight small supernova remnants 95
（206）A New 95GHz Methanol Maser Catalog. I. Data 96
（207）Techniques for Accurate Parallax Measurements for 6.7 GHz Methanol Masers 96
（208）CO(J=1-0) Observations of a Filamentary Molecular Cloud in the Galactic Region Centered at l=150 degrees, b=3 degrees.5 96
（209）Molecular Lines of CO Isotopes of the High Galactic Latitude Cloud HSVMT 27 96
III. ..... APPLIED CELESTIAL MECHANICS AND SPACE OBJECT & DEBRIS RESEARCH 98
3-01 Center for Space Object and Debris Research 98
（210）The secular analytical solution of the orbital plane using Lindstedt-Poincare method 98
（211）Approximate expressions of mean eddy current torque acted on space debris 98
（212）Long-term dynamical evolution of Tundra-type orbits 98
（213）The fast co-adding algorithm of QCT 98
（214）Blind deconvolution with principal components analysis for wide-field and small-aperture telescopes 99
（215）Satellite-based entanglement distribution over 1200 kilometers 99
（216）Investigations of associated multi-band observations for GEO space debris99
（217）Analytic model for the long-term evolution of circular Earth satellite orbits including lunar node regression 99
（218）Image Restoration Based on Statistic PSF Modeling for Improving the Astrometry of Space Debris 100
（219）The Representation of OTA Images' Astrometric Results with WCS-SIP Coefficients 100
（220）Probabilistic Data Association Method for Space Object Tracking 100
（221）Analysis of Nighttime Infrared Cloud Cover at Yaoan Astronomical Station100
（222）Research Progress on Ground-based Infrared Observations of Space Objects 100
（223）Deep Learning for Mid-Term Forecast of Daily Index of Solar 10.7 cm Radio Flux 101
（224）姚安天文观测站的夜间红外云量特征分析 101
（225）空间目标的地基红外观测研究进展 101
（226）The secular analytical solution of the orbital plane using Lindstedt-Poincaré method 101
3-02 Satellite Precise Orbit Determination and Application 102
（227）农村资本流动涡旋模型及应用——以山东商河大蒜产业为例.....102
IV. .....PLANETARY SCIENCES AND DEEP SPACE EXPLORATION 102
4-01 Near Earth O bject Survey and Solar System Bodies 102
（228）Obliquity evolution of the minor satellites of Pluto and Charon 102
（229）Transiting Exoplanet Monitoring Project (TEMP). II. Refined System Parameters and Transit Timing Analysis of HAT-P-33b 102
（230）Feature-rich transmission spectrum for WASP-127b Cloud-free skies for the puffiest known super-Neptune?.....103
（231）The GTC exoplanet transit spectroscopy survey VI. Detection of sodium in WASP-52b's cloudy 103
（232）The GTC exoplanet transit spectroscopy survey V. A spectrally-resolved

Rayleigh scattering slope in GJ 3470b 103
（233）The GTC exoplanet transit spectroscopy survey VII. An optical transmission spectrum of WASP-48b.....104
（234）Obliquity evolution of the minor satellites of Pluto and Charon.....104
4-02 Ephemerial Astronomy and Astronomical Reference System 104
（235）Solar System and stellar tests of noncommutative spectral geometry 104
（236）Deep Imaging of the HCG 95 Field. I. Ultra-diffuse Galaxies 105
（237）The orbital configuration of the two interacting Jupiters in HD 155358 system.....105
（238）Classical tests of photons coupled to Weyl tensor in the Solar System.....105
（239）A prediction method for ground-based stellar occultations by ellipsoidal solar system bodies and its application 105
（240）Improved Solar System bounds on the cosmologically viable f (G) gravity106
（241）Gravitational time advancement under gravity's rainbow 106
（242）Application of Close Encounters in Determining the Masses of Asteroids 106
（243）Solar system and binary pulsars tests of the minimal momentum uncertainty principle.....106
（244）Stability Analysis of the Two Possible 2:1 MMR Systems 106
4-03 The Sun and Solar System Plasmas 107
（245）Low-frequency electromagnetic cyclotron waves in and around magnetic clouds: STEREO observations during 2007-2013 107
（246）Effects of ion thermal pressure on wave properties of electromagnetic ion cyclotron waves in a H+-He+-O+ plasma 107
（247）Magnetospheric Multiscale Observations of Electron Vortex Magnetic Hole in the Turbulent Magnetosheath Plasma 107
（248）Radial Variations of Outward and Inward Alfvenic Fluctuations Based on Ulysses Observations.....107
（249）Research Progress of Electron Cyclotron Maser Emission on Solar Physics108
（250）A self-consistent mechanism for electron cyclotron maser emission and its application to type III solar radio bursts 108
（251）Chaos-induced resistivity of collisionless magnetic reconnection in the presence of a guide field Shang,.....108
（252）Time-dependent Occurrence Rate of Electromagnetic Cyclotron Waves in the Solar Wind: Evidence for the Effect of Alpha Particles? 109
（253）A statistical study of kinetic-size magnetic holes in turbulent magnetosheath: MMS observations.....109
（254）电子回旋脉泽辐射机制在太阳物理中的进展 109
（255）Radial Variations of Outward and Inward Alfvénic Fluctuations Based on Ulysses Observations,.....109
（256）Properties of Whistler Waves in Warm Electron Plasmas 110
（257）Applying the cold plasma dispersion relation to whistler mode chorus waves: EMFISIS wave measurements from the Van Allen Probes.....110
4-04 Near Earth Object Telescope 110
（258）Detection of Faint Asteroids Based on Image Shifting and Stacking Method110
（259）Analysis for Cellinoid shape model in inverse process from lightcurves ...110
（260）Scattering Law Analysis Based on Hapke and Lommel-Seeliger Models for Asteroidal Taxonomy 111
4-05 Laboratory for Planetary Science and Deep Space Exploration 111
（261）Drilling, sampling, and sample-handling system for China's asteroid exploration mission 111
（262）Surface thermophysical properties on the potentially hazardous asteroid (99942) Apophis 111
（263）Long-lived Dust Asymmetries at Dead Zone Edges in Protoplanetary Disks111

（264）Thermophysical characteristics of the large main-belt asteroid (349) Dembowska 112
（265）The Scattering Outcomes of Kepler Circumbinary Planets: Planet Mass Ratio 112
（266）Tidal Evolution of the Kepler Planets with Radii Less than 4 R_ 112
（267）基于图像位移叠加方法探测暗弱小行星 112
（268）晚期月海玄武岩的矿物变化 113
（269）Using Chebyshev polynomial interpolation to improve the computational efficiency of gravity models near an irregularly-shaped asteroid 113
（270）Near Mean-motion Resonances in the System Observed by Kepler: Affected by Mass Accretion and Type I Migration 113
（271）Near Mean-motion Resonances in the System Affected by Mass Accretion and Type I MigrationObserved by Kepler: 113
4-06 Laboratory for Astrochemistry and Planetary Sciences 113
（272）Optical spectroscopic characterizations of laser irradiated olivine grains.113
Late Oligocene crustal anatexis and melt/fluid migration in the Ailao Shan tectonic
（273）belt: Evidences from zircon U-Pb ages and trace element compositions..114
（274）New understanding on Ximeng Group in Three River area, western Yunnan: Evidence from structural characterization and zircon U-Pb dating 114
（275）The petrology and chronology of NWA 8009 impact melt breccia: Implication for early thermal and impact histories of Vesta 114
（276）Petrogenesis of late Eocene high Ba-Sr potassic rocks from western Yangtze Block, SE Tibet: A magmatic response to the Indo-Asian collision 115
（277）Chronology,Petrogenesis and Links with Extrusion Tectonics of Cangyuan Cenozoic Intermediate to Acid Intrusive Rocks in Baoshan Block,Eastern Tibetan Plateau.....115
（278）PETROLOGY, MINERALOGY AND IN SITU U-PB DATING OF NORTHWEST AFRICA 11042. 115
（279）滇西三江地区西盟群的再认识——来自构造变形特征及锆石 U-Pb 年代学的证据.....115
（280）哀牢山构造带晚渐新世地壳深熔与熔/流体迁移:锆石 U-Pb 年龄与微量元素证据.....116
（281）青藏高原东缘保山地块沧源新生代中酸性侵入岩年代学、岩石成因与地块挤出.....116
（282）NWA 4898 月球高铝玄武岩岩石成因研究.....116
（283）月海玄武岩 NWA 10597 的岩相特征及成因探讨 116
（284）Optical spectroscopic characterizations of laser irradiated olivine grains.117
4-07 Planetary Spectroscopy Group.....117
（285）Submicroscopic metallic iron in lunar soils estimated from the in situ spectra of the Chang'E-3 mission.....117
（286）Effect of Topography Degradation on Crater Size-Frequency Distributions: Implications for Populations of Small Craters and Age Dating 117
紫台历年发表论文情况 118
学术报告..... 118
专利 119
2017 年度发表科研论文、专著、专利一览表 121
紫台历年主要科研项目统计 123
2017 年度在研科研项目..... 123
学术报告 124

国际合作与台内学术报告统计 127
中国 2017 年度“十大天文科技进展” 128

2017 年度科研工作总结

一、科研工作总体情况

1、概述

2017 年，紫台在研项目 344 项，其中新增 131 项；应结题项目 119 项，将于 2018 年 8 月底前完成结题。全年收到财务到账经费通知 169 笔，共计 1.77 亿元，比 2016 年增加 8%，其中项目合同经费 1.51 亿元（基础类：88%，应用类：12%）。2017 年度在研项目实际入账 1.3471 亿元。2016 年度应结题课题 164 项，延期课题 24 项，实际结题率 85%。2017 年度共清理课题账号 80 个，其中财政类 39 个，非财政类 41 个。

2017 年，紫台共发表论文 286 篇，其中第一单位 162 篇，SCI 论文 233 篇，第一单位 SCI 论文 121 篇；著作 1 篇；申请专利 14 项，授权专利 10 项，软件登记 12 项。（附件 2）专利资助及奖励：专利资助 2.4 万、专利奖励 1 万+0.5 万，合计：39000 元，荣获鼓楼区知识产权工作"先进个人"称号。

2、 重要进展和重大成果

牵头组织国家重大科研仪器研制项目"太赫兹超导阵列成像系统"；国牵头组织家重点研发计划"恒星形成和星际介质的研究"申报工作，并获得资助（承担课题任务 4 项），总经费 4667 万元；牵头组织 973 项目"利用南极巡天望远镜在超新星宇宙学及太阳系外行星方面的前沿研究"和"暗物质粒子探测卫星的相关科学研究"的自验收；牵头组织九宫山天文台米级望远镜设计方案评审及选址工作。

二、研究活动进展

Ⅰ. 暗物质与空间天文研究部

1-01 宇宙伽马暴、中子星及相关物理研究团组

2017 年 8 月 17 日，人类首次观测到双中子星并合产生的引力波事件，并在首次观测到了引力波事件的电磁对应体。本团组成员参加了两项基于欧洲南方天文台甚大望远镜的观测项目，这两个项目在对首个引力波光学对应体的观测中，获得了国际上最完整的光谱观测资料（Pian et al. 2017, Nature）和首次巨新星的偏振观测资料（Covino et al. 2017, Nature Astronomy），并加入了 LIGO 合作组主导的多信使观测引力波源的文章（LIGO scientific collaboration et al., 2017, ApJ Letter）。

针对这次双中子星并合事件，我们进行了深入的研究。伽玛暴与引力波之间有 1.7 秒的时间差，这可以用来限制引力波速度与光速之间的偏差（达到 10-16 量级），还可以检验弱等效原理。巨新星与镧系元素的发现基本排除了该事件起源于双夸克星并合的模型。基于很高的双中子星并合率以及较大的抛射物质量，可以断言双中子星并合是超重元素的主要产地。我们还把 GRB170817A 与其他短暴进行了比较，看它的性质是不是很独特。结果发现如果把一些很亮的短暴如 GRB130603B 偏轴观测，则它的性质跟 GRB170817A 比较类似。另外我们还发现在现有的短暴中也有一些短暴的能量较小，跟 GRB170817A 类似，因此我们得出结论这次引力波事件对应的短伽玛暴可能并不是独特的。同时我们发现对一些距离很近的短暴没有观测到对应的光学辐射，这表明双中子星并合产生的巨新星的光度可能互不相同。

这次事件也基本确认了短暴是起源于双致密星并合，而这类系统在诞生时往往有较大的 kick 速度，因此产生短暴时与星系中心有一个偏离度。我们研究了这个偏离度与伽玛暴余辉辐射的关系，发现它们之间存在较好的相关性，并且这个相关性可以用标准的余辉模型较好的解释。

通过分析此前发生的短伽玛暴的观测资料，我们在 GRB150424A 和 GRB160821B 中新发现这两个短暴的喷流存在拐折的证据。通过系统分析近距离短暴，我们发现近邻宇宙中子星并合率很高，并且更多的短暴喷流不指向地球（偏轴），这类偏轴的事件能进一步提高伽玛暴 / 引力波成协事件的探测率。

2017 年，中国科学卫星系列首发星暗物质粒子探测卫星发布了首批科学成果。本团组的成员也参与了相关的数据分析等工作。

1-02 太阳高能物理研究团组

1、先进天基太阳天文台（ASO-S）获先期工程启动

作为 ASO-S 首席科学家单位、ASO-S 科学应用系统总师单位、ASO-S 卫星系统载荷 HXI 主任设计师单位、ASO-S 卫星系统载荷 LST 科学家单位，2017 年我们在卫星立项中发挥了重要作用。经过前期各系统需求论证、卫星平台与载荷协调、卫星与各载荷方案阶段策划、经费预算讨论、各系统方案论证、先期启动任务论证等一系列工作，2017 年 6 月 16 日，ASO-S 项目通过了由先导专项卫星工程总体组织的工程立项综合论证评审，标志着 ASO-S 完成了工程立项审批的依据。由于立项批复尚需中咨公司的评估，以及和其他卫星项目的协调，为了避免时间上的损失，早在今年 3 月

我们就打报告要求提前拨付经费先期启动载荷研制。2017 年 8 月 22 日 ,项目收到重任局批复同意 ASO-S 先期启动，并下拨先期启动经费。2017 年 9 月 7 日 , ASO-S 卫星项目先期启动会在上海召开 ,会议明确将 2017 年 9 月 1 日定为 ASO-S 方案设计阶段的起点。

之后，配合中咨公司，开展 ASO-S 卫星系统和科学应用系统的可行性和经费概算评估 ;开展各载荷科学指标和定标需求论证、关键技术攻关方案论证、以及初步方案设计论证。期间，就 ASO-S 载荷 LST 和 HXI 专门召开了两次国际会议，听取国际同行对载荷设计的咨询意见。同时，针对 ASO-S 未来科学产出的准备工作也在加紧展开，申请的基金委天文联合基金重点项目获得批准 ,首席科学家卫星科学准备项目也已经完成任务书上报 ,已经启动了 HXI 算法调研、LST 谱线诊断、数据分析中心框架规划等工作。目前 ,ASO-S 项目方案设计阶段正在紧张实施之中 ,预计今年年底可以获得中科院的正式立项批复。

2、耀斑及相关研究

退激发伽马射线通常具有明显的多普勒效应 ,谱线轮廓的加宽和红移变化与耀斑加速离子的物理特性有关。Chen& Gan (2017)详细计算 20Ne 1.634MeV 线的谱线轮廓变化 ,深入探讨了该谱线轮廓与耀斑加速离子能谱、成分，以及耀斑发生位置的变化关系 ,发展了一套以谱线轮廓分析来推求耀斑加速离子特性的方法。相比过去的全能谱拟合方法，谱线轮廓方法受拟合模型的影响较小，并且具有拟合自由度低、响应快速的优点，是一套更为直接和直观的伽马射线能谱分析方法。Firoz et al.(2017)详细研究了一个 M 级耀斑的 RHESSI 观测结果 ,集中考察 6-12keV 和 12-18keV 发射源在耀斑后相的演化 ,发现无论在空间位置还是在上升速度上均有差异，平均强度与发射体积之间存在幂律关系，虽然幂律指数有所不同，但与理论模型预测的接近，说明日冕源基本处于绝热膨胀状态。Li et al. (2017)对一个非典型 X 形状耀斑的磁重联和色球蒸发过程进行了光谱诊断。发现 Si IV 谱线（形成于过渡区）在分界线附近出现两翼增宽，速度达 200 km/s,可用磁重联（发生在过渡区）产生的双向流来解释。耀斑通常是在日冕发生磁重联释放能量，重联的光谱证据也多来自高温谱线，且多是探测到向下的出流，即红移。而在此奇异的 X 形耀斑中 ,磁重联可发生在较低的位置 : 从日冕沿分界线向下到过渡区甚至高色球层。我们则探测到了发生在过渡区的磁重联产生的双向流。此外还发现在耀斑足点处 Si IV 谱线呈现整体红移 ,同时高温 Fe XXI 谱线出现蓝移 ,符合色球蒸发/压缩模型。实际上 ,以往发现 Si IV 谱线在足点处多呈现红不对称 ,主要表现为一个静止分量叠加一个红移分量，而我们则发现了 Si IV 的整体红移，这可能与耀斑加热过程，如热还是非热成分有关，这也值得进一步通过数值模拟来研究。Su et al. (2017，待发表)完成了 DEM（等离子体的微分发射度）计算的改进工作，结果的准确度比现有方法提高了两个数量级 ,由此估计出的 X 射线热辐射同观测吻合很好。因投稿到 Nature Astronomy 被耽搁，现正转投 ApJ。该工作是由 EUV 图像的表观研究向等离子体性质的量化研究转变的一个基础性工作 ,将对基于 EUV 图像和 X 射线数据的等离子体研究 ,磁重联能量释放，等离子体加热过程，粒子加速过程等，尤其是耀斑触发过程的系统性研究，产生极其重要的影响。

苏杨的另两项工作也取得了阶段性进展 :（1）电流片研究方面，已选取多个典型的太阳爆发事件，正在指导学生分析一组独特的数据，并利用已经改进的 DEM 计算方法，从多个角度多个波段对电流片和尖角状结构的性质进行详细分析，预计将产生一篇较为重要的文章 ;（2）粒子加速联系着磁场重联的能量释放，耀斑中的等离子体加热等，是太阳物理研究的一个热点。通过系统性的搜寻，找到了一类较为奇特的高能硬 X 射线爆发 ,这些爆发往往发生在另一个耀斑的衰减相 ,却能产生很强的硬 X 射线辐射 ,甚至可以超过主耀斑相的流量，然而其产生的热辐射却不明显。结合多波段观测资料，我们将对该爆发的高能非热电子进行详细分析，并理解其与耀斑主相的关系，揭示其背后的物理过程。

3、CME 及相关研究

Zhao et al. (2017)采用了 2.5 维 MHD 数值方法，研究了初始拱状线性无力场在底部受沿磁中性线缓慢汇聚运动情况下，导致产生 CME 的磁绳形成和演化过程。汇聚运动使磁场极性反转，在磁绳中形成磁重联，当发展到一定地步，出现 CME 爆发。该研究阐明，汇聚运动是磁绳产生并触发 CME 的一个可能的机制。此外，还研究了磁绳与日珥在热动力学、磁场和力学平衡等方面的性质，特别是该研究展示了磁绳从初始相到加速相的详细演化过程 ,从中突显出磁重联的作用。Lu et al. (2017)首次利用单视角卫星 SOHO/LASCO C2 观测进行对地晕状 CME 三维结构的重构。该重构方法结合了白光日冕 Thomson 散射的偏振特性，去除了所研究晕状 CME 中的非相关结构，基于偏振度测量给出了每一像素的视向距离。考虑到对地晕状 CME 中心通常由于遮光板的原因无法进行偏振法重构 ,为了弥补这一部分信息损失，我们对遮光板外的 CME 三维偏振重构结果进行了 GCS 三维磁通量绳形状的模拟，从而获得三维 CME 的完整结构。该方法可为分析 ASO-S 上的 LST 白光日冕仪数据提供借鉴，下一步工作是通过与 LST 视场接近的 STEREO/COR1 大量 CME 偏振测量数据的应用测试，来进行自动化的完善。

缓变性太阳能量粒子事件（SEP）通常是 CME 驱动激波加速的，而激波通常与二型射电暴密切相关。Prakash et al. (2017)研究了 m-to-DH（米波到百米波段）二型暴相关的 1997 至 2012 年间的太阳爆发事件，寻找了能否产生缓变 SEP 的观测特征。发现有缓变 SEP 的事件 CME 具有更高速度、更大减速度 ;有缓变 SEP 的事件耀斑峰值能量更高、但是耀斑持续时间接近；有缓变 SEP 的事件的射电二型暴形成高度更低。这些统计特性为 SEP 预报提供了线索。

小尺度短时标爆发事件是研究较少的一类爆发事件。Ying et al. (2017, 已投稿）所研究的这个 CME 和激波事件伴随有一个 M 级耀斑，源区位于活动区边缘仅 25*50arcsec^2 大小。虽然尺度很小，但是利用 SDO/AIA 的数据，我们发现 CME 的速度和加速度等运动学特征均超出了之前统计结果的最大值，利用 II 型暴的动态频谱图发现该 CME 驱动的激波形成高度异常的低，激波马赫数很高。该小尺度爆发与 James Chen 预测到的磁通量绳足点分离距离越小，CME 加速越快相一致。小尺度短时标爆发事件除了上述的特殊之处，和大尺度事件也有相似之处，其耀斑和 CME 间的能量分配大小尺度事件都基本相等。这是首次对小尺度短时标爆发事件的耀斑、CME 和激波进行的系统研究。

4、太阳磁场相关研究

Zhao et al. (2017)重点研究了浮现区中小尺度的磁场结构与浮现区域内部的增亮之间的关系，具体包括对 11850 活动区和 12585 活动区的研究,我们重点关注浮现区低层大气的增亮，而该区域的磁场特性无法用无力场来描述，我们因此选择有力场外推的方法来进行研究，这也是首次将有力场外推方法应用于局部增亮的研究。我们的研究发现不同的磁场位型下等离子体具有不同的加热效应；外推的结果很好地显示在活动区浮现的过程中，磁场秃斑位置以及秃斑分界层处的重联可以在低层大气产生亮点以及亮的拱状结构。我们的工作为磁场重联在磁流管浮现过程中的重要作用提供了有力的证据。此外，我们还使用空间 IRIS 卫星以及 HINODE 卫星与地面 BBSO 的联合观测数据开展研究，该联合观测涵盖了光球高分辨率的磁场以及从太阳低层到高层大气的多个辐射波段，对于研究小尺度的能量释放位置和释放范围具有重要意义。通过 STEREO 卫星和 ACE 卫星对共转作用区的同时观测，Huang et al.（2017））统计分析了从 2007 年到 2010 年的 28 个 CIR 事例。根据卫星的位置和观测时间的差异计算了 CIR 的性质，速度，磁场强度以及等离子体温度的变化，与预期模型符合较好，但是粒子密度下降过快，超过了正常的预期变化，通过具体分析，给出了几种可能性。

5、其它

今年团组国际合作比较活跃，主办了两次国际会议，邀请了十多位外宾来访交流。团组成员也参加了近 20 人次的国际会议，包括：首届中欧太阳物理研讨会、第 4 届亚太太阳物理研讨会、第 16 届 RHESSI 年会等。此外，还主办了全国太阳物理战略研讨会，一系列的 ASO-S 项目会议，全国太阳高能物理数据处理和分析讲习班，以及天宫 2 号载荷 POLAR 数据分析会等。

团组成员承担的修购专项“太阳多通道近红外光谱仪升级”项目年内顺利验收。基于 POLAR 分析联合基金重点项目的太阳高能数据库的前期硬件设施已到位运行。

1-03 太阳活动的多波段观测研究团组

本年度我们通过发表科学论文，除了前面所述的亮点成果，我们还在以下几个方面取得了进展： 1）首次报道日冕喷流触发的同时存在的横向和纵向日珥振荡。2）暗条纵向振荡期间有物质泄漏，而且泄漏前后不同地方振荡周期和幅度都有明显的变化，即暗条南部振荡幅度先增加后衰减，而暗条北部振荡幅度先减小后增加。通过引入暗条纤维-纤维相互作用，我们提出了一个模型来解释复杂的暗条振荡行为。3）在耀斑脉冲相前 90 多分钟，磁绳两个足点附近就出现了窄的日冕暗化现象，面积随时间缓慢增加，亮度随时间逐渐减弱，在 171，193，211 埃等极紫外波段最明显。这种耀斑前日冕暗化被解释为在磁绳缓慢上升阶段，磁绳外层冕环系统逐渐膨胀引起的密度降低引起的亮度减弱。 4）详细研究了耀斑环中的多普勒速度振荡现象，首次在高温（ log T ≈ 7.05）谱线（Fe XXI 1354.09 Å）上发现了周期大约为 3.1 分钟的 kink 振荡。根据 kink 振荡的模型，我们估算出耀斑环中的磁场强度大约为 68 高斯。5) 使用 Fermi/GBM 的观测数据，我们首次发现短周期的 QPPs 主要出现在能量低的 X 射线能段，而且出现在耀斑脉冲相的开始阶段，长周期的 QPPs 则出现在能量高的 X 射线能段，主要存在在于耀斑脉冲相的后期阶段。6) 使用 RHESSI 的观测数据，我们发现耀斑的振荡周期在其热辐射成分上（SXR 波段）大约是 50 秒，而在非热辐射（ HXR 和微波辐射 ）中则约为 100 秒。并且两种振荡都发生在耀斑的脉冲相期间，而且几乎是同时的。这个结果是首次被观测到，对于耀斑的 QPPs 模型提出了新的挑战。7) 使用 IRIS 和 SDO 的联合观测，我们第一次从成像和光谱两个方面发现了爆发式色球蒸发的观测证据。同时微波和硬 X 射线的脉冲辐射都与谱线的多普勒速度有着很好的对应关系，说明爆发式的色球蒸发是由非热电子驱动的。8) 使用 SOHO/MDI 的观测数据，我们发展了一套自动识别太阳活动区中偶极磁场的程序，并研究了它们的统计性质。我们发现偶极磁场的面积和磁通量强度都服从幂律分布。我们还发现偶极磁场的方向角分布服从'黑尔极性定律'，同时向太阳赤道方向有稍微的倾斜。最后我们发现偶极磁场同样存在南北不对称性。9）宿英娜等用位于云南抚仙湖的一米新真空太阳望远镜（NVST）观测到 2015 年 10 月 15 日的两个暗条爆发。这两个暗条起始于活动区 NOAA 12434，并向南延伸到宁静区。结合 SDO/AIA 的大视场观测，我们还发现了更高处的大尺度宁静暗条通道的存在。爆发前，左边暗条比较窄而暗，右边暗条则并不明显。在 03:01 UT 时，左边暗条附近开始增亮，并伴随着其南半部分的缓慢上升和膨胀，同时开始表现出扭转结构。随着增亮的不断增强，暗条的扭转结构也越来越清晰。左边暗条在上升过程中还表现出顺时针的旋转运动。左边暗条在 03:36 UT 开始爆发，并在 03:45 UT 达到峰值。此时我们在 94 Å 波段观察到清晰的亮弧结构。在左边暗条爆发时，右边暗条开始快速上升，并在部分波段有增亮现象。右边暗条上升过程中也表现出扭转结构和顺时针的旋转运动。两次爆发一前一后、一强一弱，但暗条物质并没有被抛射出去，而是沿着大尺度暗条通道向南运动。我们应用“磁通量绳插入法” 模

拟日冕中暗条的磁场结构。对左边暗条，我们首先保持其角向磁场不变，而增加轴向磁场。我们发现磁通量绳的剪切增加，但并不会爆发，这与观测不符。然后我们保持其轴向磁场不变，而不断增加角向磁场。经过一系列模拟，我们得出了与观测最接近的模型，其磁通量绳的扭转角为 4.2 ，大于扭折不稳定性的阈值。因此，左边暗条爆发很可能是由扭折不稳定性引发的。经过进一步模拟，我们发现左边暗条的上升会引发 X-point 处的磁重联，重联形成的磁力线和观测到的亮弧形结构比较吻合。结合两个爆发的时间关系，我们认为右边暗条爆发是由磁重联引起的束缚磁场的减弱引发的。 10）宿英娜等对相继发生在 2015 年 8 月 7 日～8 日的 5 个耀斑的来自美国大熊湖天文台 1.6 米太阳望远镜(BBSO/GST)的高分辨率观测资料进行深入分析研究。主要耀斑区域是由多束暗条结构组成的拱形暗条系，该暗条系被准圆形的亮耀斑带包围。我们利用两种方法研究该活动区的磁场结构和演化：非线性无力场外推和磁通量绳插入法。通过外推出的非线性无力场中的磁场缠绕的分布我们可以识别出多个磁绳结构，这与观测中的多束暗条结构一致。模型显示该区域的暗条结构拥有混合极性的磁螺度，即在北部（南部）极性为正（负）。非线性无力场中的准分阶层的足点和观测的耀斑带一致。沿着环绕耀斑区的 Dome 形准分阶层的准圆形足点所画出的磁力线与有强磁螺度和 Poynting flux 注射的区域相连。位于拱形暗条系东边的双带的精细结构与准分阶层的足点的精细结构一致。我们发现磁缠绕随时间逐渐增强，这与耀斑前 26 小时内有正螺度的注射的观测相符。因此，我们的结论是这些准圆形的耀斑是由与含有混合极性的磁螺度的拱形暗条系相关的准分阶层处的磁重联所致。

1-04 暗物质与空间天文台实验室

1、暗物质粒子探测卫星“悟空”号获得世界上最精确的 TeV 电子宇宙射线能谱

暗物质粒子探测卫星 2015 年 12 月 17 日发射升空，2016 年 3 月 18 日正式交付紫金山天文台。卫星在轨运行的前 530 天共采集了约 28 亿颗高能宇宙射线，其中包含约 150 万例 25GeV 以上的电子宇宙射线。基于这些数据科研人员成功获取了目前国际上精度最高的 TeV 电子宇宙射线探测结果，如下图所示。该成果于北京时间 2017 年 11 月 30 日在 Nature 杂志在线发表。

与之前结果相比：

(1)悟空号的电子宇宙射线的能量测量范围比起国外的空间探测设备（AMS-02, Fermi-LAT）有显著提高，拓展了我们观察宇宙的窗口。

(2) 悟空号测量到的 TeV 电子的能量最准、“纯净”程度最高（也就是其中混入的质子数量最少）。

(3) 悟空号首次直接测量到了电子宇宙射线能谱在~1 TeV 处的拐折，该拐折反映了宇宙中高能电子辐射源的典型加速能力，其精确的下降行为对于判定部分（能量低于 1 TeV）电子宇宙射线是否来自于暗物质起着关键性作用。

此外，悟空号的数据初步显示在~1.4 TeV 处存在能谱精细结构。目前悟空号运行状态极佳，正持续收集数据，一旦该精细结构得以确证，将是粒子物理或天体物理领域的重大发现。

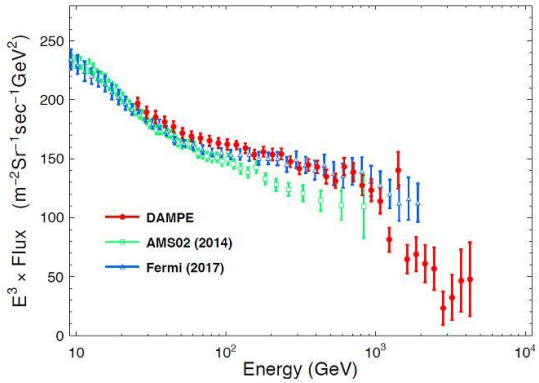

图 1 :悟空号工作 530 天得到的高精度宇宙射线电子能谱（红色数据点），以及和美国费米卫星测量结果（蓝点）、丁肇中先生领导的阿尔法磁谱仪的测量结果（绿点）的比较。

2、暗物质粒子探测卫星“悟空”号成功发射两周年

2017 年 12 月 17 日，暗物质粒子探测卫星发射升空两周年。目前卫星状态表现优异，其中 4 个有效载荷中，塑料阵列探测器（328 通道）、BGO量能器（1848 通道）、中子探测器（4 通道）都 100%正常工作，硅微条阵列探测器（73728 通道)99.9%正常工作 ,也大幅度优于原定的 98%的指标。整个探测器在粒子的电荷测量、能量测量、方向测量、粒子鉴别等性能均全面实现或超过了设计指标。迄今已完成全天区覆盖四次，共探测有效事例 38 亿多个。

3、ASO-S 卫星启动先期立项，我室承担 HXI 载荷研制任务

2017 年 8 月 22 日，中国科学院重大任务局批复同意 ASO-S 先期启动 ,并下拨先期启动经费。2017 年 9 月 7 日，ASO-S 卫星项目先期启动会在上海召开，会议明确将 2017 年 9 月 1 日定为 ASO-S 方案设计阶段的起点。目前，以我室承担的 HXI 载荷（三大主载荷之一）已正式进入方案研制阶段。

1-05 宇宙高能粒子的加速和辐射研究团组

本年度在国家重大科技项目方面围绕宇宙线的起源问题，我们正在参与由高能所牵头的国家重点研发计划（LHAASO 项目）的申请，组织参加和 LHAASO 相关的会议三次；同时结合暗物质粒子卫星“悟空”的科学目标申请的国家自然科学基金联合基金培育项目已获批；在国际合作方面，申请的中国科学院与美国能源部下属洛斯阿拉莫斯国家实验室的国际合作重点项目获得资助、和德国马克思-普

朗克太阳系研究所一起申请的国家自然科学基金委国际合作研究项目也获得资助；团组科研助理曾厚敦获得国家自然科学基金青年基金，周晓伟获得中科院公派出国留学项目的资助正在德国交流访问。

曾厚敦和周晓伟是本团组新进的两名助理研究员，作为核心骨干，他们分别在超新星遗迹多波段观测研究和等离子体物理等领域开展科研工作；博士研究生卢磊完成在德国马普所的访问，回国完成博士毕业论文并顺利通过答辩，已申请 ASO-S 项目的冠名博士后；博士生乔冰强作为和高能所联合培养的研究生已经在宇宙射线观测的月影分析方面取得了阶段性成果；博士生张平继续在瑞士 PSI 研究所执行基金委留学计划，完成了对 2015 年 8 月 27 日用中国科学技术大学蒙城太阳射电频谱仪观测到的一个 M 级耀斑的多波段观测数据分析，发现耀斑环塌缩导致的高能粒子加速可以解释其中的高能辐射，这一工作已经投稿，预期近期会被 A&A 接受并发表；博士生张轶然、王璐、屈艳坤分别在超新星遗迹激波粒子加速、太阳耀斑的射电光变特征、类星体光变分析方面取得了一些成果；博士研究生石召东正在学习磁流体数值模拟等高能天体物理研究工具。首席还参与第四届全球华人空间天气会议（北京）、第 7 届东亚等离子体暑期学校和研讨会（威海）、第 8 届 LHAASO 国际会议的组织（上海），王璐组织了一期青促会太阳射电研究会议。

结合最近观测到的宇宙射线能谱的反常精细结构和超新星遗迹的多波段观测，张轶然利用随时间演化的扩散激波粒子加速理论成功地解释了有关观测现象。该工作对于超新星遗迹中粒子加速过程的研究有重要意义，有望解决超新星遗迹射电能谱随遗迹演化而变硬，伽玛射线辐射的双幂律谱特征等长期困扰这一研究方向的关键科学问题，为进一步发展宇宙射线的超新星遗迹起源学说奠定了基础。

在太阳耀斑的多波段观测分析研究方面，通过对一个 M 级耀斑的详细分析，进一步说明太阳耀斑中粒子加速过程的多样性。一个耀斑中占主导地位的粒子加速过程和参与耀斑过程的磁场结构的演化密切相关，我们因此有可能把太阳磁场的多波段观测和耀斑的粒子加速过程研究结合起来进一步深化有关理论，加深对相关现象的认识。

1-06 暗物质间接探测的相关科学研究团组

本团队 2017 年的工作重心是参加暗物质粒子探测卫星的物理事例数据处理，并负责科学结果的成文以及物理解读。在该方面发表“DAMPE”项目论文 1 篇（Astroparticle Physics）以及 Nature 论文一篇（报道了 25GeV-4.6TeV 的电子宇宙射线能谱）；本团队负责人受卫星首席科学家常进研究员的委托完成了论文的投稿及发表。在我们的 nature 论文中直接探测到了电子宇宙射线在 0.9TeV 处的能谱拐折，并且得到了 1.4TeV 处电子能谱超出的初步迹象，引发了研究热潮。

本团队还在暗物质间接探测的相关理论研究方面在 PRL，PRD 等杂志发表论文 4 篇. 特别是我们分析了 AMS-02 反质子的数据，发现在 GeV 能区存在着超出，可以解读为~50GeV 的暗物质粒子的湮灭。更为有意思的是该信号和银河系中心的 GeV 超出可以自洽的予以解释。该文在 PRL 发表并引发广泛的关注，被丁肇中先生等人在会议报告中引用。

我们还投入部分人力，在引力波天文方面做了一系列的工作，尤其是实际性参与了 GW170817 的电磁辐射对应体的观测，作为合作者发表 Nature（报道了世界上最好的 macronova 的光谱数据，直接得到了比铁更重元素产生的证据）及 Nature Astronomy（对 macronova 进行了首次偏振测量）论文各一篇；另在 ApJL 发表理论论文 4 篇（含 2 篇对 GW170817 的电磁观测数据进行深入解读并讨论其物理意义）；尚有多篇论文在审稿当中。

1）紫台科学家在反质子数据中发现疑似暗物质信号

现代天文学观测表明宇宙由 5%的普通物质，25%的暗物质和 70%的暗能量构成。暗物质的粒子本质是当前物理学面临的重大问题，相关研究可望带来物理学新的革命。通过宇宙线反物质粒子和伽马射线间接探测暗物质粒子湮灭或衰变的产物是暗物质粒子探测的三种主要手段之一（图1），世界各国目前运行有数个空间探测仪器试图进行暗物质粒子间接探测，其中最广为人知的是丁肇中先生领导的阿尔法磁谱仪实验（AMS-02），我国也于 2015 年 12 月 17 日发射了“悟空号”卫星。

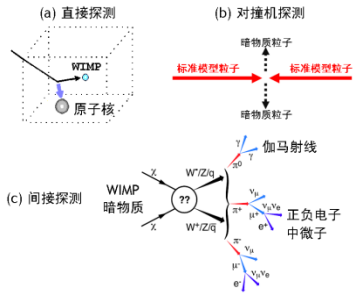

图 1. 三种探测暗物质粒子的原理示意图 。

位于国际空间站上的 AMS-02 实验与悟空号等实验相比，它可以精确分辨正、反粒子。我们所生存的宇宙主要由正物质构成，但仍然存在少量的反物质粒子，产生于高能宇宙射线粒子与星际介质的相互碰撞。而暗物质湮灭或衰变产生的是等量的正、反粒子。因此在反物质粒子中寻找暗物质信号相对比较容易，因为背景（即宇宙线起源的反粒子）更低。然而受限于宇宙射线的起源、传播、星际介质分布等的不确定性，长期以来背景模型的误差很大，人们未能在反质子数据中找到明确的暗物质信号。最近，紫金山天文台的研究人员对 AMS-02 最新测量的 B/C 比例及质子能谱数据进行了整体拟合，显著地改善了对宇宙线传播过程的理解和对传播参数的限制，有效地缩小了背景模型的不确定度。他们的进一步研究发现 AMS-02 的反质子宇宙线能谱和天体

物理背景的预期并不完全一致，而是在 1-10 GeV 的能区存在 “超出”。他们发现加入暗物质湮灭的贡献可以很好地拟合观测数据（见图 2），所需的暗物质粒子的质量约为 50 GeV，与银河系中心、矮星系、星系团方向的伽马射线数据中呈现的一些疑似暗物质信号对应的参数（质量和/或湮灭截面、能道）一致。悟空号等独立实验的数据将有望对这一疑似信号进行深入检验。无独有偶，德国的一个研究小组也独立地得到了相同的结论。这两篇论文于 2017 年 5 月 9 日在 Physics Review Letters（《物理评论快报》)同时发表，且均入选 “Editor’s suggestions” 以及 “Featured in Physics” 在美国物理学会（APS）网站予以重点报道（https://journals.aps.org/prl/abstract/10.1103/PhysRevLett.118.191101; https://journals.aps.org/prl/abstract/10.1103/PhysRevLett.118.191102）。中方论文的第一作者为南大物理系在紫金山天文台范一中团组进行联合培养的博士研究生崔明阳，通讯作者为袁强和范一中，合作者还包括台湾 “国家理论科学研究中心” 的学者蔡岳霖。

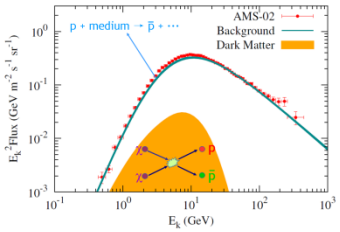

图 2. 反质子背景模型和 AMS-02 数据的比较：1-10 GeV 能段数据存在 “超出”，可以用质量约为 50 GeV 的暗物质粒子的湮灭予以解释。

1-07 紫外及 X 射线天文研究团组

1、首次对 NGC3783 这个 AGN 同时观测的高分辨率 X 射线与紫外光谱进行了联合拟合；

2、探索了利用时变信息研究盘冕相互作用这样一条新途径，并首次使用能量-频率-相位延迟图研究盘冕相互作用的细节。

（1）科学研究上，我们分别在 X 射线双星时变、巨 H II 区内多态气体的运动学，以及星系吸积和反馈的观测和模拟等几个方面继续深入研究。

首先，星系吸积和反馈的观测和模拟以及星系团温热气体的研究工作是本团组的重要方向。我们分别在 AGN 反馈的出现频次问题、星暴星系电离外流风的速度、AGN 外流风的多波段研究，以及 X 射线二维光谱的研究等方面深入展开，进展良好。1）活动星系核（AGN）状态在一个星系中出现的频次，即其反馈模式，对星系演化过程非常重要，但却是一个未知的量。在离我们最近的仙女座大星云 M31 中观测到较强的 OVII 禁线，但电荷交换过程不足以解释。我们构建了热气体共振散射的光谱模型，用于解释谱线比值与谱线轮廓的变化，并首次给出其核球热气体的湍动速度。此外，我们基于构建了 AGN 熄灭后周围热气体的动力学非平衡态光致电离光谱演化模型，自然的解释 M31 核球部分的 X 射线光谱的复杂谱线性质，表明这个星系在四五十万年前曾是个明亮的 AGN。这个事例示范了从宁静星系来研究 AGN 反馈频次的可行性，相关工作正在撰写论文。2）我们基于 M83 的多次 XMM-Newton 高分辨率光谱的数据，首次直接测量了其电离外流气体速度。其核心区域光谱谱线特征显示外流速度约为 1200 公里每秒。我们正在从两种独立方法去对比速度值，确认物理过程的自洽性。3）AGN 外流风的研究中，我们采用此前改进的 XSTAR 软件，首次对 NGC3783 这个 AGN 同时观测的高分辨率 X 射线与紫外光谱进行了联合拟合，对两个波动的温吸收外流气体的特性进行了统一的限制。发现前人提出的连续外流风并不适用，而更倾向于波动性的外流夹杂着球形小团块的方式。此工作已经发表在 RAA 上。4）XMM-Newton 高分辨率光谱的数据其实兼具高能谱分辨率（R=150-800）与一定的空间分辨率（0.5 角分）。但是此前只有一维光谱的应用。我们开始发展对多次观测数据叠加，并使用 MCMC 方法进行而二维光谱拟合的工具。这对弥散热气体的研究有极大的用途，并为将发射的 Hitomi 二代及 ARCUS 等 X 射线卫星做出预先研究准备。5）我们选取了一个星系团/类星体对样本，目的是为了研究星系团中气体的物理和动力学状态，及其对星系团中星系星周介质的影响．结合 X 射线空间望远镜 Chandra 和 XMM-newton，地面光学 SDSS 巡天数据，以及射电 NVSS 和 FIRST 的巡天数据．我们估算星系团中热气体和星系相对于星系团总质量的重子物质比例，并且通过多种方法判定了星系团的动力学状态．结合将来的哈勃空间望远镜紫外光谱仪 COS 对背景类星体的观察，能使我们研究星系团中温气体和温热气体的性质，进而通过联系星系团中多种不同状态的气体能使我们研究星系团气体复杂的加热/冷却机制和动力学过程．其研究结果对于我们理解宇宙中大尺度结构的形成和重子的演化十分重要．也能使我们更好的利用星系团作为研究宇宙学的探针．文章即将完成并投稿．

其次，在 X 射线双星时变研究中，我们探索了利用时变信息研究盘冕相互作用这样一条新途径，并首次使用能量-频率-相位延迟图研究盘冕相互作用的细节。我们利用之前提出了两种研究 X 射线变化起源的方法，即幅度比值谱方法（Yan et al. 2013 ApJ, 767, 44）和能量-频率-功率图方法（Yan et al. 2017 MNRAS, 465, 1926），应用到黑洞双星 GRS 1915+105 处于 “心跳态” 的 RXTE 数据，研究了 X 射线变化起源以及吸积流盘和冕之间的相互作用。相关结果已发表（Yan et al. 2018 MNRAS, 474, 1214）。

最后我们完成了旋涡星系 M101 的巨 H II 区内多态气体运动学的研究工作。该工作的目标为通过研究巨 H II 区内多态气体的运动学和热力学性质，研究恒星活动的反馈。我们完善了利用拟合光谱能量分布分析年轻星族性质的方法，

撰写相关论文并投稿。

（2）技术发展上，我们已经完成天文联合重点项目紫外巡天卫星有效载荷 HI Lyalpha 光谱仪的光学设计方案，准备交付加工光学器件。我们完成了科工局民用航天项目的任务书，开展了科学和技术启动咨询会，并积极为项目的实施以及后续发展争取各种国际国内合作资源。

（3）教学上，本年度秋季在南京大学本科开设《高能宇宙探索课》，紫台开设《文献阅读和学术公众报告研讨课》课程。

II．南极天文及射电天文研究部

2-01 恒星结构、演化和脉动的研究团组

1）完成了以引力透镜计划（OGLE）高光度脉动红变星的线性非绝热脉动计算，并证认了 Wood 和 OGLE 发现的脉动红巨星的五个周光关系 C,C′，B, A 和 A′ 为高光度红巨星径向脉动的基模¯4 阶泛音。

2）研究了红巨星αUMa 的脉动并对其脉动模式进行了模式证认。

3 对食双星 V551Aur 中脉动子星的脉动进行了星震学了理论诊断。得到双星系统二子星的质量、年龄、光度、有效温度和脉动模式。

我长期追求的科学目标是探求恒星对流理论以及与之相关的恒星结构、演化和脉动稳定性问题。近十余年来，由于引力透镜计划 OGLE, MACHO,近红外巡天 2MASS,以及空间 CoRoT 和 Kepler 卫星相继投入，红变星及小振幅的δ Scuti 和γDoradus 变星的观测研究取得了重大的进展，所以近年我将研究的重点重新转回到变星脉动理论方面。这就是我国家自然科学基金项目《脉动变星的理论研究》的研究背景和近五年来的主要研究内容。这是一个长期的科学目标，彻底搞定这个问题尚需时日，我个人认为到目前取得二项重要进展。

（1）高光度红巨星的脉动模式证认和激发机制

长期以来，造父变星是脉动区外低温红变星脉动的激发机制仍是一个尚未完全搞清和存在争议的问题。人们一直认为对流单纯只是一种脉动的阻尼机制。在发现太阳五分钟振荡之后，湍流随机激发机制由于其物理意义的简单直观，并得到太阳 P 模有限带宽观测的强有力的支持，以及自然而然消除了脉动限幅机制的困扰等众多优点而广被天文界接受，成为一种主导天文界的主流观点，并且进而推广到解释几乎所有低温红巨星的脉动激发机制，甚至于到 OGLE 高光度小变幅红变星(OSARGs)的脉动。对这个问题我们一直持有不同的观点，认为将对流视为单纯仅为脉动的阻尼机制本身就是片面的，并不合乎事实。实际上，对流引起恒星内部能量、动量的非局部传输与交换以及物质的混合。后者(物质的混合)即恒星演化所谓 overshooting; 而前二者即影响恒星脉动的所谓对流与脉动的热力学(通过对流热流)和动力学耦合（湍流压与湍流粘滞性）。为了正确处理对流与脉动的耦合，我们发展了一种 anisotrpic and non-local time-depent theory of convection。我们的研究表明，在远离对流区边界的对流区内部，对流与脉动的热力学耦合，确实是脉动的一种阻尼机制，是产生造父变星脉动不稳定区红端边界的主要原因。这是因为在恒星脉动过程中，对流（热）流总是稍稍滞后恒星密度的变化，即在恒星脉动的高温高密度相位，转移出更多的热量，而在脉动的低温和低密度相位，转移出较少的热量。这就犹如一匹致冷机的工作原理，将脉动动能转化为热能，是脉动的阻尼机制。而湍流压通常总是一种脉动的激发机制。这是因为由于湍流运动的惯性，湍流压总是稍稍滞后密度的变化，这样在 Pt¯V 功图上形成一个正向的卡诺循环，即将湍动动能转化为恒星的脉动动能。定量的分析表明，热对流的阻尼作用反比于脉动的频率，湍流压的激发作用在ωτc ∝τc /P~1 达到极大。其中τc 是对流运动的惯性时标，而 ω和 P 是脉动的圆频率和周期。湍流压对红变星脉动的激发起了至关重要的作用。湍流粘滞性是将脉动动能转化为湍动动能，最终在湍流谱的高波数区，通过分子粘滞性转化为热能。所以它是脉动的阻尼机制。对流热对流，湍流压和湍流粘滞性三种因素的相对大小随着恒星的质量、光度和有效温度变化，所以其总合效应，时而表现为阻尼，时而表现为脉动的激发作用。我们的研究表明，对低光度的红巨星，其脉动的性质表现得像类太阳振动，其低阶的 P 模是脉动稳定的，而中高阶 P 模却是脉动不稳定的。随着恒星的光度增大，脉动最不稳定模向低频推移。到高光度红巨星，中高阶 P 模变得脉动稳定，而低阶 P 模却变得脉动不稳定。

（2）高光度红巨星表现像 Mira-like 的脉动性质

利用我们 anisotropic and non-local time dependent theory of convection,我们计算了高光度红巨星的线性非绝热脉动，得到①观测到的高光度红巨星周光关系的 5 个分立 C, C′，B, A and A′，分别是红巨星径向基模¯4 阶泛音。②这些低阶径向模是可以自激的。辐射压对红巨星脉动的激发起了至关重要的作用。

2-02 南极天文中心

南极巡天望远镜观测到引力波事件（GW 170817A）的光学对应体。南极巡天望远镜 AST3 是唯一在南极观测到发生于 2017 年 8 月 17 日（GW 170817A）引力波事件光学对应体的望远镜(Science Bulletin， Volume 62, Issue 21,（2017）, & 2017 PASP,34,69)。

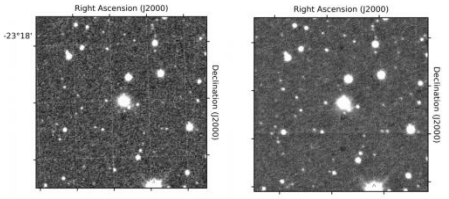

图 1.2017 年 8 月 23 日（左）和 18 日（右）对 GW 180817A 天区的观测图像

由于事件的宿主星系为赤纬-23 度，靠近 AST3 地平的位置， AST3 取消了原有的软件限位, 在目标地平高度极低的情况下(15 30 度)采集了 8 天的有效数据（18 号、20 号、21 日、23 号、24 号、25 号、27 号、28 号），共 218 张图像数据。其中 18 号、23 号和 24 号的观测数据质量最优，5 分钟的曝光在消光接近 3 星等时，极限星等仍达到了 18.5 等， 这也提供了足够的深度使 AST3 有机会对该引力波较早期的光学信号进行跟踪探测。

对不同类型的 Ia 超新星的宿主星系的光谱特征和金属丰度进行了统计分析。

利用 1338 颗光谱和光度证认了 Ia 超新星，进行统计分析：发现大质量和低恒星形成的宿主星系的 Ia 超新星更亮和光度下降更快。

2-03 星系宇宙学和暗能量研究团组

完成了目前国际上最大规模的弱引力透镜模拟

1 ,完成了目前国际上领先的弱引力透镜模拟(Wei et al. 2018, ApJ in Press)。该模拟具有大天区（全天）、高精度、物质场和星系同时解析等特点，在国际上属于首次完成的弱引力透镜全天的成图模拟。利用该模拟数据，可以系统研究引力场对星系形状的效应，可以研究不同类型、亮度星系的内秉形状相关等。在本项研究中，我们发现不同类型的星系能够贡献不同的 GI 效应。目前传统的理论很难解释透镜巡天测量到的正 GI 信号，我们发现这主要是由旋涡星系引起的。这意味着将来的弱引力透镜模型还需要进一步改进。文章已经被 ApJ 接受，即将发表。利用该模拟数据，可以定量确定目前弱引力透镜巡天的系统误差等，还可以为将来的透镜巡天确定观测样本的选择等科学目标服务，具有重要的理论和应用价值。

2，暗晕的空间指向研究。利用目前国际领先的 ELUCID 数值模拟，研究了暗物质晕的空间指向相关及其对暗晕质量，形成时间和环境的依赖。我们首次发现，除了以往研究发现的暗晕空间指向相关对暗晕质量存在相关以外，其空间指向还依赖于暗晕的形成时间和大尺度环境：在给定质量出，年老暗晕的空间指向性比年轻暗晕要高，在密集环境下暗晕的指向性比稀疏环境下暗晕的指向性要高。为了解释这个模拟结果，我们在经典的暗晕指向模型基础上进行了修改，发现暗晕的空间偏袒因子可以很好的解释模拟结果。这个结果对发展精确的星系内秉指向相关理论非常有用。我们的文章发表后，大尺度结构领域的理论开拓者之一，美国科学院院士 Marc Kamionkowski 教授专门写信对我们表示祝贺。该研究成果发表在 ApJ 杂志。(Xia et al. 2017, ApJ, 848, 22).

3, 星系的空间指向。星系在空间分布并非随机的，而是在不同尺度上存在不同的空间指向排列现象，比如在小尺度上，卫星星系倾向于分布在中央星系的主轴附近，而且其信号强弱与中央星系的颜色和质量有关；在大尺度上，中央星系的主轴之间也存在相关性，中央星系跟大尺度环境之间也存在指向相关。如何理解这些不同尺度的星系指向相关是数值模拟和理论研究的主要方向。过去的 5-10 年康熙研究员在星系的空间排列方面开展了大量工作，其研究成果引起了同行的高度关注，相关文章引用 200 次以上。中国科学杂志邀请康熙研究员就星系的空间排列写了一篇综述文章，就星系空间排列的研究现状，物理起源进行了详细阐述。文章发表在中国科学物理天文学专刊(2017SSPMA, 47d9803)。

4 ,利用最新的强引力透镜系统研究椭圆星系的内部物质轮廓。舒轶平等利用哈勃通过一个高效的强引力透镜挑选方法，我和合作者们从斯隆数字巡天近一百万条光谱中筛选出了 135 个强引力透镜候选者。随后利用哈勃太空望远镜的图像数据，从中证认出 40 个全新的强引力透镜系统。这一发现将已知的强引力透镜数目提高了 10%。此外，通过拟合观测数据，我们得到了 40 个透镜星系的质量分布。结合其它已知的强引力透镜样本，我们发现椭圆星系中心的密度分布和星系的质量存在较强的相关性，这表明星系演化过程中冷却和反馈机制的效率会随星系质量而变化 。文章发表在 ApJ 杂志(Shu et al., 2017, ApJ, 851,48)。

5，星系质量函数的演化。目前星系形成模型需要解释在不同宇宙时刻的星系质量函数的演化，了解那些是主导星系质量函数演化的物理过程。团组的博士后 Contini Emanuele 和合作导师康熙研究员一起发展了一个经验的解析模型来研究星系质量的演化，考察星系并合、恒星形成与终止过程对质量函数的影响。与以外模型不一样，我们的模型最大限度利用了观测的数据，我们强迫所有的星系在高红移具有‘正确’的恒星质量，利用观测给出的恒星形成率 - 恒星质量关系，结合数值模拟给出的星系并合树，考虑合理的星系质量剥离模型，这样可以预言星系质量函数的演化。我们发现，星系的并合和潮汐质量剥离对星系质量演化非常重要，我们发现模型预言的大质量星系的演化比早期测量的质量要大，而更最近的观测数据更加接近。2017 年在这个研究方面我们共发表了 2 篇文章(Contini Emanuele et al., 2017, ApJ, 837, 27; Contini Emanuele et al. 2017，849, 156).

6，暗晕角动量与大尺度结构的相关性。利用 SDSS 巡天数据研究者发现星系的角动量方向与大尺度结构，特别是纤维状结构(Filament)指向之间存在相关性，且这种相关性依赖于星系的质量或形态，如旋涡星系的角动量与 Filament 的方向倾向于平行，而椭圆星系的角动量与 Filament 的方向倾向于垂直。如何理解这种相关性及其对星系质量的依赖是目前理论研究面临的主要问题。王鹏和康熙等人利用宇宙学数值模拟研究了这种相关性，他们发现这种相关性主要由暗晕的形成时间和进入 Filament 时间的先后顺序决定：对于大质量暗晕，其先进入 Filament,并且在其中吸积了大量

物质 ,由于处在 Filament 的物质主要沿着 Filament 进入暗晕，因此其吸积物质的轨道角动量转化为暗晕角动量，其方向与 Filament 垂直。而对于低质量暗晕，由于其形成时间早于进入 Filament,因此其角动量主要形成于 wall 中，导致其角动量于 Filament 平行。该研究结果很好的解释了星系角动量 - 大尺度结构的相关性。研究成果发表在 MNRAS Letter (Wang et al. 2017, MNRAS Letter, 468, 123)。

2-04 星系中的恒星形成研究团组

1）第一次对近邻星系的水的观测研究

2）含 H2O 的强引力透镜星系中分子气体的研究。

团组成员负责 JCMT 的大项目（MALATANG） 今年是数据全部观测结束的一年，项目利用 JCMT 望远镜的多波束接收机 HARP 对一批近邻星系的 HCN 和 HCO+ 发射线进行成图观测。本项目已经积累了 390 小时的观测时间，大量的数据有待细致处理。本项目的观测结果，对连接河内分子云团与河外星系的整体探测，有重要意义。现有的观测结果，缺失了红外光度 L ~ 104 至 107 （单位：太阳光度）之间的恒星形成单元的空白，本项目的数据分辨率可以填补上这个空白。

Perseus 分子云中年轻星体（YSO）的吸积活动研究。在 Spitzer 的观测中人们证认出了大量的 YSO，但是很多 YSO 缺少光谱数据的进一步确认。LAMOST 的巡天数据提供了海量的光谱 ,我们利用 LAMOST 的光谱数据对 Perseus 分子云中的 YSO 进行了研究，我们主要研究了这些 YSO 的恒星性质以及它们的吸积活动。通过光谱分析，这些 YSO 都是低质量的年轻星体，并且具有较强的吸积活动。进一步分析其他波段的数据，我们发现这些 YSO 的吸积活动和它们的 X 射线光度之间也存在着正相关的关系。这项工作已经完成，正在准备投稿中。

大质量恒星和星团的形成的触发机制。我们利用 PMO-13.7m 望远镜对 S235 区域进行观测研究，发现其中的恒星形成很可能由两片分子云通过云云碰撞过程所触发。S235 中两片分子云相对速度约为 5km/s，并且它们之间有桥状结构连接说明它们在物理上有相互作用，另外在空间分布上也是互补的，表明它们很可能在相互碰撞。利用 13CO 的数据，我们找到了 10 个分子云团块并计算其核形成效率 (CFE，2.6~30.6%)和恒星形成效率(SFE，8~25%)，并发现其空间分布上有明显区别。面向碰撞矢量方向上的区域的 CFE 和 SFE 在数值上更大(>10%)，而另一区域则有较小的 CFE 和 SFE(<10%)，表明云云碰撞可以提高核的形成效率和恒星形成效率，从而触发更多的恒星形成。这篇文章将于近期发表。

HII 区周围团块性质与恒星形成研究。大质量恒星形成的机制和环境一直没有得到清楚的认识，分子云核是恒星形成的地点，因此对分子云核的性质、所处环境等进行统计研究有助于对此问题的探索。The Milky Way Project (WMP) 巡天项目(|l|≤65°, |b|≤1°)得到 5106 个红外尘泡的列表，其中包括了一部分已知 HII 区及 HII 区候选体。本工作在此范围内选择了一批已知 HII 区样本并对部分 HII 区候选体进行证认，共得到 49 个样本。然后利用 Herschel70 – 500 μm 尘埃连续谱数据通过灰体谱 SED 拟合得到氢分子柱密度图，证认位于尘泡边缘及尘泡附近的分子云团块及云核样本，并对这些样本的物理性质做了讨论。统计表明 HII 区周围存在具备大质量恒星形条件的云核，团块或云核的分布数目从其半径开始向外呈递减趋势，因此 HII 区的扩张可能触发了恒星形成，而是否有一定比例的大质量恒星形成可能由 HII 区扩张触发仍在统计中。下一步本工作即将对相同范围内的年轻星进行证认，从年轻星的角度对 HII 区周围的恒星形成尤其是大质量恒星形成进行统计研究。此工作仍在进行中。

近邻矮星系群中恒星形成历史（SFH）对恒星质量估计的影响。基于 40 个本地近邻矮星系的金属丰度的演化和恒星形成历史，我们研究了 SFH，金属丰度和尘埃消光对 UV-到-NIR 颜色-质光比（color-logYstar(λ)）分布和近邻宇宙星系的质量估计的影响。发现 1）前人修正过的近邻星系的 color-logYstar (λ)关系；2）光学 color-logYstar(λ)关系在金属丰度更高的地方更宽、更深；3）SFH 形状参数 "集中" 对 color-logYstar(λ)关系没有很大影响；4）对于给定波长决定的年龄和金属丰度来说，金属丰度演化对光学而不是 NIR 的质光比有很大不确定性等结果。这一工作发表在 APJ 上。

近邻星系中水的观测研究。与传统的用来示踪致密的星系介质区域的分子探针（例如 CO 和 HCN)不同，水分子通常示踪的是恒星形成区或者被 AGN 加热的极端物理环境。我们利用 Hershcel 远红外空间望远镜的 HIFI(Heterodyne Instrument for the Far Infrared)频谱仪第一次对近邻星系（星系核中心）水分子（o-H2O 和 p-H2O）转动能级谱线的系统观测和研究。在 9 个近邻的恒星形成活跃的星系中，除了 Antennae 星系，都观测到了很强的水分子发射和 / 或者吸收线。这说明水分子谱线并不来自于仅小范围的非常致密区域， 而是像 CO 一样源自于星系（核）中的延展的大范围物理区域。 另外，低阶水线的发射线特征要比中阶水发射线的速度更加延展，表明低阶水线来自于一个更加延展的物理区域。 由于吸收和发射特征的相互混合，各个星系的水分子基态和低阶谱线呈现出形状各异的谱线轮廓。通过最新的 3D, non-LTE 辐射转移代码- 'β3D' 来进行辐射转移模拟 ,结合文献的 SPIRE/PACS 观测到的星系其它各阶水线。

含 H2O 的强引力透镜星系中分子气体的研究。我们从 Herschel-ATLAS 巡天获得的源表中仔细地挑选出了一组受强引力透镜作用的具有 H2O 谱线探测的 16 个亚毫米星系，使用 IRAM 三十米单天线毫米波射电望远镜对样本中

亚毫米星系中的多能级 CO 谱线进行了观测。通过分析 CO 发射线的谱线轮廓，我们发现引力透镜的非均匀放大效应会引起对观测到的谱线宽度的低估，这个低估最大可以到 2 倍左右。通过基于大速度梯度 (LVG) 的 CO 谱线辐射转移模型，并利用结合了贝叶斯思想的马尔可夫链蒙特卡洛方法，此工作求出了多能级 CO 谱线所示踪的分子气体的物理性质，包括:分子气体的体密度、温度以及 CO 分子的柱密度。通过对样本整体的统计分析，我们发现星系整体的气体热压力与其恒星形成效率呈紧密的线性相关。此工作同时还研究了星系整体的分子气体性质与星系整体恒星形成性质之间的关系:我们计算出了这些被强引力作用的星系的气尘比以及气体耗散时标，发现样本星系具有的这些性质与其他亚毫米星系并无差异。最后，我们对比了样本星系的 CO 谱线和 H2O 谱线的线宽，发现这两者符合的比较好。这意味着这两种分子气体辐射分部的空间区域较为类似，此结果已经发表。

M51 中高空间分辨率的恒星形成效率。我们利用 NOEMA 干涉阵望远镜对星系 M51 外围旋臂上分子云集合的 HCN J=1-0 和 HCO+ J=1-0 谱线进行了的 100 pc 空间分辨率的观测，得到了 6 个分子云集合的致密分子气体谱线光度。通过比较不同尺度天体(十几 kpc 的星系、1 kpc 左右的星系盘上局部区域、100 pc 左右的分子云集合和 1 pc 左右的银河系内分子云核)的致密分子气体质量(L_HCN 1−0)和恒星形成率(L_IR)的关系，我们发现 L_HCN 1−0 和 L_IR 的线性相关性在空间尺度小至 100 pc 的分子云集合中依然成立。同时,我们发现有大质量恒星正在形成的分子云集 B 合的致密分子气体的恒星形成效率(L_IR/L_HCN 1−0 和 L_IR/L_HCO+ 1−0)相对较高，此工作已经发表。

(超) 亮红外星系样本中的 [CI](1-0) 和 [CI](2-1) 线的分析研究。通过研究 CO(1-0) 和 [CI] 线光度之间的关系，发现 L’ _{CO(1-0)} 与 L'_{[CI](1-0)} 和 L'_{[CI](2-1)} 之间都存在较好的线性关系，表明在 (超) 亮红外星系中 [CI] 可以作为总分子气体质量探针。同时发现 L'_{[CI](1-0)}/L'_{CO(1-0)} 和 f_{60}/f_{100}之间不存在关系，L'_{[CI](2-1)}/L'_{CO(1-0)} 和 L'_{[CI](2-1)}/L'_{[CI](1-0)} 与 f_{60}/f_{100}, 分别存在较弱和较温和的关系。假设 [CI] 为光学薄的，进一步计算了[CI] 的激发温度，碳的质量以及平均的 [CI] 线光度到 H_2 质量的转换因子。使用 [CI] 的转换因子获得的 H_2 的质量大体上和利用 L'_{CO(1-0)} 以及 CO 的转换因子获得的 H_2 质量相等，此工作已经发表。

对致密分子气体探针 HC3N 的观测研究。由于多数常用的致密分子气体探针，如 HCN，HCO+ 等多为光厚谱线，使得计算致密分子气体质量时会有一定的偏差。而像 HC3N 一样的光薄谱线，可以提供更准确的致密分子气体质量测算。我们使用 Effelsberg 100 米和 SMT 10 米望远镜分布对 HC3N 2-1 和 24-23 的发射线进行了观测。受天气设备影响，探测率较低。我们对 HC3N 和 HCN 在不同星系中的比值进行了讨论。

2-05 分子云与恒星形成研究团组

1）发现云云碰撞触发中低质量恒星形成的理想候选体

2）通过近红外偏振测量获得了环形分子壳层上的磁场方向和强度

1. “银河画卷”计划取得重要科学成果。云云碰撞是恒星触发形成的一种重要机制，然而迄今为止在观测方面可以用来深入研究该机制的候选对象并不是很多，而且已知的云云碰撞案例中绝大多数是伴随着大质量恒星形成的，却鲜有只触发中低质量恒星形成的例子。利用“银河画卷”谱线巡天数据发现：位于仙王座气泡（Cepheus bubble）边缘的分子云复合体 L1188 由两个几乎相互垂直的长条形分子云 L1188a 和 L1188b 组成，而且在两个分子云交叉的区域内的分子气体具备云云碰撞所可能表现的各种典型运动学特征。结合在交叉区域增强的年轻星分布特征，推断出其中的恒星形成很可能是通过发生在大约一百万年前的一场云云碰撞所触发的。进一步的研究还发现，该分子复合体中的云核都不足以形成大质量恒星，从而使 L1188 成为不可多得的研究云云碰撞触发中低质量恒星形成的理想候选体，有待进一步高分辨率的研究。研究团队已经分别获得 IRAM-30 米和 JCMT-15 米毫米波望远镜的观测数据，将对其中的分子云核特性和恒星形成触发过程开展深入研究。论文发表在 Astrophysical Journal Letters 上。2017 年度分子云与恒星形成团组负责完成了“银河画卷”计划约 60 平方度天区的观测、数据检查和数据入库，为“银河画卷”计划的最终完成以及 2018 年度的科学研究奠定了良好基础。

2．大质量恒星形成研究取得重要进展。通过近红外偏振测量获得了环形分子壳层上的磁场方向和强度，发现磁场方向受到膨胀气体的挤压，形成与环形分子壳层平行的结构，磁场强度得到明显增强。研究结果显示，环形分子壳层上得到增强的磁场强度能够显著减弱由大质量恒星引起的触发恒星形成活动。论文发表在 ApJ。对位于 M17 中的一个热分子核的红外对应体进行了细致的研究。该热核的红外对应体与数个水脉泽斑相关，在其周围没有发现 I 型和 II 型甲醇脉泽。结合已经发表的 VERA 的三角视差观测发现这些水脉泽斑的自行运动相对于这个红外对应体呈现向外膨胀的运动，说明该区域可能存在分子外流以及盘吸积过程。这些观测证据说明热核的红外对应体很有可能是一个正在吸积物质的大质量原恒星。

3．原行星盘结构和演化研究取得系列重要成果。通过国际合作，对 HL Tau 原行星盘的 ALMA 和 VLA 观测资料做了细致的辐射转移模拟，限制了盘中尘埃亮环的性质并找到了早期行星形成过程的证据。论文发表在 A&A 杂志。通过细致的参量空间研究，分析了盘的张开程度和标高等关键结

构参量如何改变能谱分布的整体形态，并以此提出了一个挑选发生尘埃生长和沉降原行星盘的实用判据。研究结果发表在 Ap&SS 杂志。成功申请到国际 IRAM 30 米望远镜对 Taurus 恒星形成区中 2 个原行星盘的毫米波观测，用于更好地限制盘的结构以及研究盘中早期行星形成过程。发展了用于分析即将到来的 JWST 原行星盘光谱数据资料的工具，研究盘的化学结构。

2-06 毫米波和亚毫米波技术实验室

1、成功研制我国首台太赫兹超导阵列成像系统；

2、南极 5 米太赫兹望远镜关键技术预先研究取得实质进展。

1）国家重大科研仪器研制项目（部门推荐）"太赫兹超导阵列成像系统" 顺利通过国家基金委组织的项目验收。该项目攻克了两种国际前沿的超导探测器芯片技术--超导动态电感探测器（MKIDs）和超导相变边缘探测器（TES），实现了我国大规模二维阵列超导探测器芯片技术"零"的突破，其中 MKIDs 探测器芯片在像素规模、灵敏度及工作频段等指标方面均处于国际同类探测器的前沿水平。此外，还攻克了大规模 MKIDs 探测器阵列频分复用读出、太赫兹波段大视场成像光学设计仿真、以及低漏热亚 K 低温制冷平台设计三项主要关键技术。在上述技术突破基础上，成功研制了一台 850 微米波段 8 8 像元和一台 350 微米波段 32x32 像元超导阵列成像系统，灵敏度均优于地面观测设备背景极限。该仪器的成功研制使我国跻身大规模阵列超导探测器技术领域国际前沿，为我国天文观测研究提供了一种全新的成像探测手段。

2）南极 5 米太赫兹望远镜关键技术预先研究方面，完成了基于 Nb/NbN 混合超导隧道结（与俄罗斯科学院 IREE 研究所合作）的 350 微米波段超导 SIS 混频器芯片的初步性能表征，启动了 450 微米波段超导 SIS 混频器芯片的设计、350/450 微米波段多波束接收机的相关研制工作；开展了 200 微米波段超导 HEB 混频器原理芯片的中频带宽、稳定性及噪声温度的偏压及温度相关性等研究，启动了该波段多波束接收机的相关研制工作；与上海讯析电子科技有限公司联合研制了 4GHz 带宽实时数字 FFT 频谱仪系统，性能达到南极 5 米太赫兹望远镜的需求。此外，还完成运控系统详细架构设计、以及基于低功耗存储服务器的大容量冷存储原型验证系统。

3）载人航天工程 2 米多功能光学设施高灵敏度太赫兹探测模块研制方面，通过了设施总体对太赫兹模块基于 CZ-5B 运载火箭的初步设计方案评审，完成了模块关键技术攻关方案评审；完成了 8-10K 空间制冷机方案设计与风险评估的招标与合同签订；完成了太赫兹模块增加肖特基探测器的可行性研究；通过与主光机集同设计，签订了太赫兹模块的电接口和热接口 IDS，启动了相关研制工作；完成了综合电控组件原理样机的电装和初步软件编程，完成了频谱处理板卡原理样机的研制与初步性能测试；完成了基建技改项目申请建议书评审，启动了超导混频器芯片制备超净室及模块装调洁净间的改造工程。

4）国家重大科研仪器研制项目（部门推荐）"多波段多大气成分主被动综合探测系统" 的 "太赫兹辐射波谱仪" 课题进展顺利，完成了系统的集成、测试及性能优化，并实现了在德令哈和羊八井外场对太赫兹大气臭氧发射谱线等的双波段同时观测，通过了项目对课题的现场技术测试。

5）中科院先导专项项目 "阿里台址 CMB 观测条件评估与阿里 1 号辅助标定研究" 课题进展顺利，阿里原初引力波台址大气透过率测试仪器性能得到进一步提升，继续开展了阿里台址太赫兹远红外波段大气透过率特性测量。中科院先导专项项目 "面向天文应用的高灵敏度太赫兹超导探测器关键技术研究" 通过结题验收，针对南极 5 米太赫兹望远镜研制的高灵敏度超导相干和非相干探测器被遴选为项目研究亮点。

6）在超导探测器技术研究及应用方面，太赫兹超导探测器研制平台（一期）运行正常；重点研发计划项目课题 "光子数可分辨超导相变边缘单光子探测器及其读出电路" 启动实施，超导 TES 光子探测器芯片制备和光学反射腔研制取得初步进展；继续开展了量子级联激光器和超导热电子混频器集成接收技术研究，构建的中红外波段（10 微米）高灵敏度外差式接收机系统灵敏度突破 7 倍量子噪声极限，反射式成像系统空间分辨率达到 400 微米。

2-07 德令哈毫米波观测基地

1）2017 年度，"银河画卷计划" 共计完成 1000 个巡天单元（每个单元 30'×30'大小）；

2）积极开展国际合作研究，在国际重大天文研究计划贝塞尔 BeSSeL Survey (Bar and Spiral Structure Legacy Survey)项目中扮演重要角色。进一步证实了银河系本地臂，发现了连接本地臂和人马臂的一个子结构，这是至今发现的银河系内最长的子结构，解决了关于天鹅座 X 恒星形成复合体内天体距离的长期争论。

基地运行的 13.7 米毫米波射电望远镜在 2004 年进行了一次机械系统大修，再此之后每年都做定期的检修，截止现在已经运行了 13 年，为了保证望远镜机械系统正常的工作，在今年夏季通过合同对外承包的方式，由长期对 13.7 米毫米波射电望远镜承担机械系统维护的毕振荣同志总负责本次的机械系统大修。今年对天线机械系统做了全面检修，更换了高速箱、传动箱内所有的轴承，更换了高速箱与传动箱间的连轴器，俯仰传动箱和高速箱的罩壳上新切割了传动箱安装孔，加装了盖板，防止电磁辐射。为了能及时发现机械系统异常，开发了电机电流实时监测系统。更换制冷机，更换真空计（新款 E-9torr），更换损伤的氦气管，压缩机前增加空调等；更换 BEAM6 混频器[采用新的 BiasT]，更换

Beam4、Beam8、Beam7 混频器的磁铁，抑制台阶分裂；更换 Beam9（USB）、Beam9（LSB)、Beam2（LSB)链路 HEMT 放大器，更换杜瓦内部分老化的偏置电缆。按照插座产品的第三版国家标准更换平台上的电源插座，优化平台布局。截止到 2017 年年底，“银河画卷计划”巡天工作完成 6380 个巡天单元（总共 10941 个单元，每个单元 30′×30′大小,完成 58.3%），包括 M17, Aqualia Rift, Cygnus X, W3/W4/W5, GEM OB1, Monoceros Nebula, Maddalena Cloud, 和 Califirnia Cloud 等比较有名的天体目标，对其中的分子云演化和恒星形成过程进行了研究，数据质量完全符合科学家的要求，彰显了“超导成像频谱仪系统+OTF 观测模式”的强大威力。运行在 13.7 米望远镜的超导成像频谱仪系统，数据存储空间由原来的 40TB 升级到 300TB 容量，满足银河画卷数据存储需求。为了确保来之不易的天文观测数据的安全存储，建立了 30TB 的毫米波主题数据库离线备份系统。

中国科学院紫金山天文台“银河画卷”巡天团队利用德令哈 13.7 米望远镜一氧化碳及其同位素北天银道面巡天观测数据，在银经范围 34.75 到 45.25 度，银纬范围 - 5.25 度到 5.25 度范围，速度空间位于外旋臂之外区域，共找到 168 个分子云，这些分子云中只有极个别是已知的。研究发现这些分子云的尺度和线宽也显示了一定的关系，但是与内盘分子云的尺度线宽关系略有差异。这些分子云很好的示踪了近年 Dame & Thaddeus 2011 年新发现的外盾牌 - 半人马臂，从而为这条旋臂的真实性提供了强有力的观测证据。研究还发现这些分子云示踪了银河系分子气体遥远外盘的翘曲幅度非常大，同时分子气体所示踪的翘曲幅度与原子气体，尘埃，和恒星示踪的盘的翘曲幅度相当。这些研究结果已经在美国的《天体物理学杂志增刊》（The Astrophysical Journal Supplement Series）上发表。文章见 2017ApJS..230...17S。

紫金山天文台和上海天文台研究团队利用 13.7 米毫米波射电望远镜共观测了 1020 个 BGPS 源，探测到了 213 个发射，并通过和 HCO+热线宽比较判断认为 205 个极可能是脉泽，其中有 144 个（占 70%）是首次探测到的。本次观测是一次搜寻目标最多，探测到最多 I 型甲醇脉泽的观测。结合以前 95 GHz 甲醇脉泽的系统观测进行整理编表，得到含有 481 个 95 GHz 甲醇脉泽的编表和 37 脉泽候选体，这是目前最大的 95 GHz I 型甲醇脉泽样本。这项工作为研究 95 GHz I 型甲醇脉泽的环境，脉泽抽运机制，以及未来的高分辨率观测奠定了基础，是位于北半球发现最多 I 型甲醇脉泽的望远镜。文章见 2017ApJS..231...20Y

紫金山天文台研究人员利用 MWISP 的 CO 巡天数据对 TeV 源 HESS J1912+101 进行了研究。结合 JCMT CO(3--2)数据和 VGPS HI 21cm 原子气体数据，分析揭示了 60km/s 的气体与这个高能源有物理联系。受到扰动的气体速度达到 20--40km/s，不但在形态上展现出二者具有空间相似性，运动学分析也表明这些被激波聚集、加速、加热的气体可能来自于一个年老的超新星遗迹爆炸。相对应地，距离估算为 4.1kpc ,SNR 年龄约为 0.7--2.0x10^5 years。我们的结论是，具有环形壳层分布的 TEV 源 HESS J1912+101 是一个年老超新星遗迹爆炸后，激波与其周围的致密分子气体相互作用的结果。更有趣的是，我们的距离和年龄估算，与这个高能源几何中心的一个脉冲星的物理性质一致。这表明二者可能有直接的物理联系。文章见 2017ApJ...845...48S。

南京大学研究团队利用 13.7 米毫米波射电望远镜在 Fermi-LAT 7.6 年的观测数据中，发现一个位于超新星遗迹 Kes73 的西边的延展的伽马射线源。分析表明该伽马射线的能谱不能仅靠纯的轻子辐射或是纯的来自磁星的辐射产生，因此必定存在一个强子发射的成分。研究人员利用该区域的毫米波 CO 分子谱线观测研究了星际分子环境。CO 谱线观测表明了分子云与超新星遗迹边界西部多波段观测得到的形态一致。沿西北边界的蓝翼，速度范围在 85–88 km/s 之间的 12CO(J=2-1)/12CO(J=1-0)谱线强度比显著提升到 1.1，这为超新星遗迹和分子云之间的存在相互作用提供了运动学证据，也表明由超新星遗迹和周围分子云相互作用而产生的强子可为伽马射线做出贡献。因此，该伽马射线谱可以解释为一个纯的强子发射或是磁星和强子发射的混合。如果是纯的强子发射，质子的谱指数为 2.4，与弥散激波加速理论的本质一致。如果是磁星和强子混合辐射，磁场的耗散率要大于 1036 erg s−1 才能驱动磁星的曲率辐射。文章见 2017ApJ...851..37

国家天文台徐金龙副研究员及其研究小组与紫金山天文台研究人员利用紫金山天文台青海观测站的 13.7 米毫米波望远镜以及 Herschel、WISE 等多波段数据，详细研究了电离氢区 SH2-104，首次揭示了该电离氢区周围的分子气体是二维片状的。通过对电离氢区 SH2-104 周围介质的结构和动力学分析，发现该电离氢区周围的介质是环状的二维结构，并不是球壳状的三维结构。有趣的是为何包裹三维电离氢区周围的分子气体是二维环状结构，以及环状结构的中心是空的而没有相应的分子气体辐射？通过该小组系列文章的研究揭示银河系内部分星际介质就是二维片状的，只是这类片状介质存在一定厚度。当位于此类介质中膨胀电离氢区的尺度大于周围片状介质的厚度时，展现了我们所看到的 SH2-104 周围二维环状结构。该研究成果近日发表在国际天文学期刊《天体物理学报》上（https://doi.org/10.3847/1538-4357/aa8ee0）。

北京师范大学研究团队利用 13.7 米毫米波射电望远镜在 5 个源中成功探测到了 SiO (v=1, J=2−1)的脉泽发射，通过研究演化星中的硅酸盐尘埃和 SiO 脉泽辐射的关系，来探究硅酸盐的形成机制，结合 SiO (v=1, J=1–0) 的档案数据，对一个含有 21 个 SiO (v=1, J=2–1)源和 28 个 SiO (v=1, J=1–0)源的样本，分析研究 SiO 脉泽的积分强度和硅酸盐

尘埃发射。研究结果表明它们两者之间存在明显的相关关系，而这并不与 SiO 分子是形成硅酸盐尘埃的种子的假设相矛盾。另一方面，研究人员还发现氧化硅脉泽和硅酸盐结晶之间无相关关系，这可能预示着硅酸盐结晶与质量损失率不相关。文章见 2017AJ....153..176L

围绕 13.7 米毫米波射电望远镜的建设、技术创新，成就出一批活跃在国际学科前沿的有影响的科研骨干。他们在使用基地望远镜的同时，积极申请其他国际一流望远镜，如德国 Effelsberg100m ,日本 Nobeyama45m ,美国的 VLA、VLBA 以及欧洲的 EVN 等的观测，做出了许多国际一流工作。

随着我国深空航天、现代国防等方面对 UT1 的精度和及时性需求的增长，自主测量和提供 UT1 的问题表现得更加迫切和重要，由国家授时中心主导，在我国建立了 UT1 测量网，其中一台设备天顶筒望远镜就落户在我基地。基地工作人员主要完成了选址、基础建设、协助安装调试等工作，目前设备运行良好。随着恢复我国的自主 UT1 测量与服务能力，彻底解决当前过度依赖 IERS 的不利局面,弥补国家安全漏洞，为我国航天、卫星导航、深空探测等战略领域提供可靠的 UT1 数据，满足国家急需。该项目通过网络实现远程观测，遇到设备故障，基地工作人员给予现场技术支持。

为了充分利用 1.2 米量子科学实验专用望远镜，中国科学技术大学团队在该望远镜上成功安装了二通道天文成像仪系统，通过宽窄波段结合的方法进行反响映射测量。计划获得 100 个活动星系核的反响映射测量，大幅改善反响映射测量活动星系核样本的参数空间覆盖，为其他波段研究提供黑洞质量测量的独特样本，已成功实现了远程观测（基地观测人员给予相关协助）；协助量子可研团队，完成了量子隐形传态实验平台基础建设工作，并协助完成设备安装调试工作。在基地工作人员的协助下，顺利保障了 1.2 米量子卫星专用望远镜的量子测试测试工作。

在中国 SONG 项目团队的精诚合作下，项目已经取得巨大进展：50BiN 双筒望远镜观测了包括疏散星团、食双星、超新星等十个目标，发表论文 2 篇； SONG 1 米望远镜与丹麦 SOONG 1 米望远镜成功实现了联合观测，对 Gamma Cephei，Gamma Per 等 10 余颗恒星进行联合时域观测，已完成数据处理，获得前期科学结果，发表论文 1 篇。得益于西华师范大学成立了天文台、天文系和西华师范大学 - 国家天文台 - 紫金山天文台联合实测天体物理中心，西华师范大学在基地挂牌建立了“实习基地”，完成西华师范大学天文系大学本科生 3 批次实习工作。

为了给 AIMS 找到一个适合红外太阳观测台址，协助怀柔基地研究人员在站上安装“用于太阳磁场精确测量的中红外观测系统”，包含一台带有太阳直接辐射、温度、湿度、风速和风向五要素的气象站和一台工作波长为 750-1000nm 近红外水汽仪，用于测量红外天空背景亮度、水汽含量和太阳可观测时间的考察测量，基地安排专门的工作人员负责设备的运维。

作为青海省爱国主义教育基地和科普教育基地，依靠 13.7 米射电望远镜、天文展板长廊、SONG 项目、1.2 米量子望远镜等设备宣传科普知识增强我站的综合实力和知名度，为提高全州地区及全省的科学文化素质、辐射带动旅游建设做出新的贡献。根据国家、台本部、青海省、海西州政府的要求积极参加各种科普活动。完成了澳门科学技术发展基金会组织的“2017 青海-天文-地质科普夏令营”活动；青海观测站科普部组织相关人员首次以网络直播的形式参加了由腾讯公司组织的 2017 年英仙座流星雨直播工作，本次流星雨播报以现场手机实时摄录和图片拍摄的方式进行。2017 累计接待科研院所、科技团组、夏令营、旅游团等 600 人次。

在台基建处领导的指导下，完成 2017 年度《青海观测站科研辅助用房修缮项目》，本项目通过对科研辅助用房上下水系统修缮、食堂改造、车间维修等内容，通过该项目的实施，极大地提高了青海观测站的竞争实力，使得青海观测站科研平台基础能力有了大的提升，为观测站承担高水平的科学研究提供基础支撑保障。

2-08 星系形成与大视场巡天团组

1. 恒星形成星系中的年老星族质量比例和恒星形成主序斜率的起源研究 （Pan Z.Z. et al.,2017, ApJ, 834, 39）：恒星形成星系在恒星形成率（log SFR）_质量（log M）图上排列成一个紧密序列（通常称为恒星形成主序）。这个序列在小质量端的斜率为 1.0 左右，但是在大质量端斜率明显小于 1.0。通常认为大质量端的斜率变平与星系中的年老星族成分含量有关，因为年老星族成分对星系质量有贡献，却与 SFR 没有任何关系，因此拉平了 log SFR-log M 关系。我们在本工作中构建了一个简单模型，通过恒星形成主序的拉平效应，定量计算恒星形成星系中的年老星族质量比例。我们还解释了为何恒星形成主序的斜率在小质量端为何是 1.0。我们认为小质量星系受到 quenching 效应的影响很小，因而它们一直能够长期保持一个稳定的 SFR。这样一来 M 和 SFR 就形成了一个简单的线性关系 M~SFR*t，其中 t 表征的是宇宙年龄。在对数空间，log SFR-log M 关系自然有一个 1.0 的斜率。通过检验小质量端恒星形成主序随红移的演化，我们发现这种解释能够被观测所支持。

2. 测定给出 100 亿年前宇宙中恒星形成星系 Lya 光子逃逸比例（F.X. An, X. Z. Zheng, et al. 2017, ApJ, 835, 116）：来自恒星形成星系的 Lya 光子逃逸比例是估测星系际介质中性度的关键测量参数，对理解宇宙如何再电离过程至关重要。红移 z=2.24 对应 100 亿年前的宇宙时期，Lya 发射线红移至光学窗口，是可以大样本详尽研究星系 Lya 光子逃逸的最低红移窗口。利用我们获得 CDFS 天区的光学和近红外窄波段深度成像数据，我们测定 z=2.24 处星系的 Lya 和

Ha 发射线 ,估计单个星系和星系平均的 Lya 光子逃逸比例，给出估计值为（3.7+-1.4）% 。我们发现 Lya 光子逃逸比例与星系消光量反相关 ,消光强的星系 Lya 光子逃逸比例低。同时 ,我们指出采用不同的消光改正方法对估计 Lya 光子逃逸比例影响很大，偏差值可达 1%。

3. 近邻宇宙极疏散星系探测研究(Shi D.D., Zheng X.Z. et al. 2017, ApJ,846， 26)： 极深光学图像观测探测到一类特殊极疏散星系（ultra-diffuse galaxies），因其尺度大（半光半径>1.5kpc),中心面亮度极低(>24mag arcsec-2 ）而与正常星系在参数空间的分布区域显著不同。其成因和演化机制是否与正常星系的截然不同 ,而预示新的星系形成机制？ 我们利用中国科学院紫金山天文台盱眙观测站 1 米施密特大视场巡天望远镜的 g 和 r 波段在 Hickson Compact Group 95（HCG 95）3 度×3 度区域内探测到了 105 个极疏散星系候选体，其中包括 68 个极有可能的极疏散星系和 37 个可能的极疏散星系候选体，与两个贫星系团成协。有意思的是，在这些极疏散星系候选体当中有一个 UDG（H95F）被甚大阵（VLA）观测，它的红移与 HCG 95 的红移一致，被认为是 HCG 95 星系群中的一个成员星系 H95F，并发现其中性氢的质量为 1.1×109M⊙，恒星质量为 1.8×108M⊙。在我们场中探测到极疏散星系候选体样本的颜色分布比较广泛 ,虽然多数极疏散星系样本处于红序阶段，但仍有三分之一极疏散星系的颜色偏蓝，与恒星形成星系颜色类似。颜色偏蓝的极疏散星系表明它们仍在进行恒星形成。我们的研究结果首次表明，光学极深测光探测到的极疏散星系与 HI 巡天探测到的富 HI 气体暗星系（almost dark galaxies）有重叠。其颜色分布广泛，表明它们的形成历史和演化阶段显著不同。在 HCG95 天区富气的极疏散星系的形成与此天区内富含 H I 的大尺度结构中，两个晚期形成贫星系团的成员星系缓慢形成过程中吸积气体角动量大、形成的星系盘面亮度极低有关。

4. 低红移星系中性氢和光学盘尺寸对比研究（Pan, Wang, Zheng & Kong, 2018, submitted to ApJ)：盘星系的恒星盘嵌在一个尺寸更大的中性氢气体（HI）盘中。气体盘的性质对星系的后续的演化有重要影响，但是对 HI 气体盘性质的研究却不多，这是因为目前空间可分辨的 HI 观测数据还比较少。王菁等人研究了 500 星系的 HI 气体盘后发现，星系的 HI 盘尺寸（DHI）和 HI 气体的质量（MHI）有一个非常紧密的关系。我们利用王菁等人的 DHI—MHI 关系，对大约 10000 个仅有 MHI 观测的星系估计了它们的 HI 气体盘尺寸，然后跟星系的恒星盘尺寸（Dopt）做了对比研究。我们发现，当星系的 HI 气体/恒星质量比大于 20%时，星系的 DHI/Dopt 比值约为 2.0，且该比值与气体/恒星质量比几乎没有相关性。但是当气体/恒星质量比进一步减小时，DHI/Dopt 比值就会随气体/恒星质量比的减小而降低。我们因此认为，当星系的气体含量足够丰富时，星系恒星盘的增长会受到气体含量的调控 ,因此这两个成分的尺寸比例能够维持在 2.0 附近。但是当 HI 气体的供给被切断之后，星系的恒星盘尺寸的增长就会受到限制。这为我们理解为何贫气体星系总是核球主导而非盘主导提供一个合理解释。

5. 大质量恒星形成星系恒星+气体成分的演化研究（Pan, Zheng & Kong, 2018, to be submitted)：大质量星系的演化历史是天体物理研究中的一个重要问题。要研究这个课题，一个关键点如何确定在宇宙不同时期前身星系的物理特性。在这个工作中，我们研究了近邻宇宙中银河系质量(10^10.7 太阳质量)大小的恒星形成星系从红移 1.5 以来的恒星+气体成分的演化。假设前身星系在不同红移时都是一个典型的恒星形成星系，我们就可以回推银河系在不同红移时应该有多大的质量。根据星系的质量—恒星形成率关系，我们可以推断前身星系的分子氢气体质量。我们发现银河系的恒星质量增长要显著慢于恒星+气体总质量的增长。有了恒星+气体总质量随时间的增长曲线，我们可以得到星系的净吸积率随时间的演化。我们发现在最近的 30 亿年里，星系的净吸积率要比恒星形成率低 5-12 倍，这说明星系吸积率的显著降低是恒星形成熄灭的主要原因。我们还发现恒星死亡带来的气体回馈对维持星系的恒星形成率起到显著作用。

6. 发展了一套利用机器学习的方法用来证认单天线探测到的亚毫米源的多波段对应体 （An F.X. et al. 2018, submitted)：亚毫米星系是大质量，被尘埃遮蔽的星暴星系。在当今宇宙中这类星系非常少，但它的数目随着红移的增加而增加，并且在红移 2-3 的时候数密度达到了顶峰。这类星系的恒星形成率高达 100-1000Msun/yr，使得它在不到一亿年的时间内增长成大质量星系(M>10^{11}Msun). 所以 ,亚毫米星系被认为是低红移处的大质量年老星系以及我们当今宇宙中的大质量椭圆星系的祖先。自从 1990 年在亚毫米波段发现了这类亚毫米亮的星系以来 ,数以万计的亚毫米星系已经被探测到。然而，单天线亚毫米望远镜的分辨率非常低，一般为 10-30 角秒。这是对亚毫米源进行后续分析，以及研究其与其它星系演化关系的最大阻碍。我们利用目前最大的亚毫米、毫米干涉阵（ALMA）探测到的高分辨率的亚毫米星系以及 UDS 场的多波段数据发展了一套机器学习的方法用来证认单天线探测到的亚毫米源的多波段对应体。我们首先利用 ALMA 探测到的亚毫米星系以及其多波段的特性建立了一个训练样本 ,我们结合机器学习的方法来分辨训练样本中亚毫米星系和非亚毫米星系的区别。我们首先利用训练样本对我们的方法做了一个自我测试 ,发现我们的方法可以证认出 87%的 ALMA 探测到的亚毫米星系。接着我们将方法应用到另外一个完全独立的 ,同时具备单天线亚毫米观测以及 ALMA 观测的场（ECDFS），证认出了 80%的 ALMA 探测到的亚毫米星系。这说明我们的方法可以成功证认单天线亚毫米源的多波段对应体。我们计划将我们的方法应用于那些还没有被亚毫米干涉阵观测或者不在亚毫米干涉阵观测范围内的单天线亚毫米观测样本，从而得到一个统计上足够大的亚毫米星系对应体的样本用来研究

亚毫米星系的形成与演化以及它和其它天体的演化关系。

2-09 高能时域天文团组

1、参与发现首例引力波电磁对应体及其理论研究进展

2017 年 8 月 17 日，LIGO 和 Virgo 共同探测到首例来自双中子星并合的引力波事件 GW 170817，这次联合探测更具体地给出了引力波发生的方向和距离。从 8 月 18 日至 28 日，中国南极天文合作团队利用正在南极昆仑站运行的第二台南极巡天望远镜 AST3-2，克服了望远镜限位等技术难点，对该引力波源所在的宿主星系开展了密集观测，在 8 月 18 日即引力波信号探测到的 25 小时后，成功探测到该引力波对应的光学辐射。这是我国天文观测设备与国际其他观测设备一起，见证了天文学史上里程碑式的重大事件，共同证实了双中子星并合事件是宇宙中大部分超重元素（包括金、银以及镧系元素、锕系元素等）的起源，回答了 21 世纪宇宙物理学领域 11 个重大科学问题之一。AST3-2 的观测结果于 2017 年 11 月在中国期刊《科学通报》英文版 Science Bulletin 上作为封面文章发表（Hu, Wu et al., 2017, Science Bulletin，亮点工作之一），吴雪峰是此工作的第二作者、理论负责人。该探测结果在 2017 年 10 月 17 日中央电视台以及国内多家极具影响力的媒体广泛宣传报道，特别是十九大召开期间作为十九大代表的中科院院长在接受央视采访时提到南极巡天望远镜的这一观测成果。

基于 LIGO/VIRGO 引力波与电磁对应体联合探测科学合作以及中澳天文合作，吴雪峰还参与了此次事件的 2 项国际合作工作（Abbott, 2017, ApJL；Andreoni, 2017, PASA）；基于 GW170817 的观测数据，参加了 1 项国内合作的理论工作（Xiao, Liu, Dai & Wu, 2017, ApJL）。

长时标伽玛射线暴和超新星起源于大质量恒星坍缩，而短时标伽玛暴被认为产生于中子星双星并合。在过去的近 20 年里，已经发现一些长时标伽玛暴和 Ic 型超新星成协，最近几年也发现与短暴成协的几例巨新星（macronovae / kilonovae）。这两类现象都预期伴随着宇宙高频引力波事件。吴雪峰等对伽玛暴-超新星关联性（包括短暴-巨新星）从观测和理论模型上作了最新的详细综述（Can, Wang, Dai & Wu, 2017, Advances in Astronomy），将作为这一领域的"Observer's Guide"，为未来引力波电磁对应体的研究提供参考。

2、物理学基本假设的天文学检验

（1）检验弱等效原理：爱因斯坦等效原理预言，光子在引力场中传播，穿越的时间和没有引力场情况是不同的。这种效应也被称之为 Shapiro 延迟。弱等效原理可以通过对比宇宙学暂现源同时释放的不同能量光子在通过同一个引力场所用的时间差来检验，即比较不同能量光子在银河系引力场（甚至更大尺度的引力场）中传播对应的后牛顿参数γ值的差别是否为零。魏俊杰、吴雪峰及合作者利用引力波事件 GW 170817 和成协短伽玛暴 GRB 170817A 到达地球的时间差 1.7 秒，以及 GW 170817 和千新星首次探测到的时间差 10.9 小时，对弱等效原理进行了引力波/电磁波的多信使检验（Wei, Zhang, Wu, Gao, Meszaros, Zhang, Dai, Zhang & Zhu, 2017, JCAP）。吴雪峰、魏俊杰及其合作者还提出，利用来自同一宇宙学暂现源的不同偏振光子到达地球的时间差，可以对弱等效原理进行高精度检验，并利用伽玛暴（GRB 120308 和 GRB 100826A）、快速射电暴（150807）不同偏振辐射经过本超星系团 Laniakea 引力场后到达地球的时间差，将弱等效原理破缺的上限严格限制到了 10^(-16)量级（Wu, Wei, Lan, Gao, Dai & Meszaros, 2017, PRD）。

（2）限制洛伦兹不变性破缺：伽玛暴的能谱时延已被广泛地用来限制洛伦兹不变性破缺。然而，目前所有这类相关研究都是利用观测坐标系下两个固定能段的光变曲线之间的到达时间差来限制洛伦兹不变性破缺。由于不同的伽玛暴具有不同的红移，观测坐标系下的能谱时延并不能真实反映静止坐标系下的能谱时延，因此观测坐标系下得到的能谱时延对能量有一定的依赖性，从而可能造成限制洛伦兹不变性破缺的不确定性。正确的处理方法应该是先在静止坐标系下选定两个能段，每个伽玛暴通过各自的红移修正得到观测坐标系下的两个能段，然后再对每个伽玛暴分析各自两个观测坐标系能段所对应光变曲线之间的到达时间差，最后再利用所得的到达时间差限制洛伦兹不变性破缺。魏俊杰和吴雪峰首次利用 56 个已知红移的伽玛暴的静止坐标系能谱时延分析了洛伦兹不变性破缺效应及其对红移的依赖性，发现现有数据并没有证据表明洛伦兹不变性存在破缺，也没有证据表明洛伦兹不变性破缺效应会随红移发生演化（Wei & Wu, 2017, ApJ, 851, 127）。此外，魏俊杰、吴雪峰等利用迄今为止唯一一个能谱时延数据丰富、存在从正延迟转变到负延迟特征的伽玛暴 GRB 160625B，基于该暴不同能段光变曲线得到的其它高能段和最低能段光变之间的达到时间差，假设观测时间延迟既来自内禀时间延迟的贡献，又来自洛伦兹不变性破缺效应所造成的时间延迟的贡献，对一阶、二阶洛伦兹不变性破缺作出了强有力的保守限制（Wei, Zhang, Shao, Wu, & Meszaros, 2017, ApJL）。审稿人认为此工作提出了一种新颖的分析方法，对目前的量子引力研究领域的发展具有潜在价值（亮点工作之二）。魏俊杰、吴雪峰等还利用该暴的数据，对洛伦兹不变性破缺的各向同性和非各向同性的系数进行了限制（Wei, Wu, Zhang, Shao, Meszaros, & Kostelecký, 2017, ApJ）。

（3）限制光子静止质量上限：根据爱因斯坦狭义相对论，如果光子静止质量不为零，那么会引起光子速度的色散，即光子在真空中的传播速度不再是光速，而是跟光子的频率有关。频率越高的光子其速度也越快。假设某一天体同时发出两个不同频率的光子（通常采用短时标爆发天体），则通过测量不同光子到达探测器的飞行时间差，来限制光子静止质量。近期，魏俊杰、吴雪峰等利用大、小麦哲伦星云的 2 颗

射电脉冲星不同射电频率脉冲到达地球的时间差，把光子静止质量的上限提高到 10^(-45)克（Wei, Zhang, Zhang, & Wu, 2017, RAA）。

3、伽玛暴及余辉的研究进展

（1）伽玛暴中心引擎的研究：超吸积恒星级黑洞被认为是伽玛暴中心引擎的候选体。近几年来 Fermi 和 Swift 卫星观测到的伽玛暴丰富数据可以限制中心引擎模型。吴雪峰参与的合作工作考虑正反中微子湮灭过程和 Blandford-Znajek（BZ）过程这 2 种中心引擎机制，详细研究了伽玛暴瞬时辐射阶段和余辉阶段这 2 种中心引擎的物理参数如何随时间演化，得到在通常情况下 BZ 过程产生的伽玛暴喷流光度更高，并可能在余辉后期继续活动。此外，初始自转很小的黑洞其中心引擎可能首先通过中微子湮灭形成一个热的“火球”，然后通过 BZ 过程产生波印廷流主导的磁化喷流。该研究表明黑洞的晚期吸积，可以解释伽玛暴余辉阶段的奇异行为，如耀发、增亮和平台辐射（Lei, Zhang, Wu & Liang, 2017, ApJ）。吴雪峰及其合作者基于伽玛暴样本，包括这些伽玛暴的伽玛射线能量、平均光度，以及根据模型得到的初始洛伦兹因子和喷流半张角等，基于这些物理量之间的统计相关性，发现观测数据与 BZ 机制更为一致（Yi, Lei, Zhang, Dai, Wu & Liang, 2017, JHEAp）。

（2）从重子火球到磁化火球演化的特殊伽玛暴 GRB 160625B 研究：伽玛暴喷流的物质组成一直是伽玛暴研究领域中的一个前沿热点课题。吴雪峰参与的特殊伽玛暴 GRB 160625B 研究工作（Zhang, B. B., Zhang, B., Castro-Tirado, A. J., Dai, Z. G., Tam, P.-H. T., Wang, X. Y., Hu, Y. D., Karpov, S., Pozanenko, A., Zhang, F. W., Mazaeva, E., Minaev, P., Volnova, A., Oates, S., Gao, H., Wu, X. F., Shao, L., et al., 2017, Nature Astronomy），从伽玛射线和光学观测数据分析中，发现这个伽玛暴的瞬时辐射包括三次孤立的爆发期，3 次爆发期的持续时间分别约为 0.8 秒、35 秒和 212 秒。该暴光度极高，因此能够对最初的前兆辐射到主暴再到后期的延展辐射这 3 次爆发进行详细的时间分辨光谱分析，发现前 2 次爆发的能谱特性明显和第 3 次不同，清楚地展示了该暴从一开始的热辐射，最后向非热辐射转变，第一次在观测上表明了在单个伽玛暴中物质组成从重子物质主导的火球过渡到波印廷流主导的磁化喷流。

（3）伽玛暴能谱时延的大样本研究：吴雪峰及其合作者对由 Fermi/GBM 监测到的 50 个单脉冲伽玛暴的能谱时延特性进行了系统的研究（Shao, Zhang, Wang, Wu, et al., 2017, ApJ, 844, 126）。通过将光变曲线细分到多个连续不同的能段，从而得到了与能量通道选择无关的能谱时延，并进行了详细的统计研究，发现脉冲的能谱时延和脉冲宽度随光子能量都成类似的幂律依赖关系，这种关系极有可能是伽玛暴喷流辐射的相对论几何效应导致的。这一工作还研究了伽玛暴脉冲的能谱演化行为，发现能谱时延可忽略的伽玛暴脉冲通常具有较短的持续时间，并且能谱硬度似乎随流量强度具有“跟踪”行为。另外，具有显著能谱时延的伽玛暴脉冲通常具有较长的持续时间，并伴随从硬到软的能谱演化行为。

4、宇宙学模型的多途径限制

（1）利用引力波及其电磁对应体的强引力透镜事件开展宇宙学暗能量状态方程的研究：自 2015 年 9 月，引力波的直接探测已经变成现实。目前已经探测到 5 例双黑洞并合产生的引力波事件，以及 1 例双中子星并合产生的引力波事件，人类探索宇宙已经进入引力波时代。未来，随着 LIGO 的升级，以及国际上其它引力波天文台的投入观测，将会有越来越多的引力波事件被探测到。这其中，一些引力波事件的引力波信号和电磁对应体信号，在到达地球之前的传播路径上，有可能被某个星系（如类星体）作为“透镜”，产生强引力透镜过程，从而兵分多路，最终地球观测者探测到该引力波事件的多重像。之前的工作已经表明，多重像彼此之间到达时间差τ，以及“透镜”星系的速度弥散σ，可以单独用来作为“标准烛光”，限制宇宙学模型参数的大小。我们最近发现，时间差τ和“透镜”星系速度弥散σ的组合，即τ/σ^ 2，可以更好地限制宇宙学模型。魏俊杰和吴雪峰的模拟计算显示，未来探测到 50 个左右的强引力透镜化的引力波及其电磁对应体事件，在限制宇宙学方面（暗能量状态方程 w 参数），其效果可以和目前 Union 2.1 样本中 580 个 Ia 型超新星的限制结果相当。这个结果对未来利用引力波事件作为宇宙学探针具有较为重要的参考价值（Wei & Wu, 2017, MNRAS）。

（2）基于 H(z)的“宇宙时钟”方法研究宇宙膨胀历史：通过测量古老星系的微分年龄(Differential Age)，天文学家可以测出宇宙膨胀率 H(z)。利用这种宇宙学模型无关的方法所测得的哈勃参数 H(z)习惯被称为“宇宙时钟”（“Cosmic Chronometer”）。前人分析发现最新的 30 个 H(z)数据支持宇宙加速膨胀。魏俊杰、吴雪峰及其合作者指出宇宙加速膨胀的结果实际上是由于这 30 个 H(z)数据被额外引入了一个比较高的哈勃常数 H_0 导致的。如果不引入 H_0，而是仅仅分析这 30 个 H(z)数据，他们发现这些数据倾向于支持匀速膨胀的宇宙学模型（Wei, Wu, & Melia, 2017, ApJ, 835, 270）。

（3）利用模型无关方法限制宇宙曲率参数：魏俊杰和吴雪峰率先提出一种宇宙学模型无关的新方法，通过结合最新的哈勃参数 H(z)和 Ia 型超新星数据来限制宇宙曲率。基于 H(z)数据，他们利用模型无关的高斯重构方法来构造距离模数 μ_H (z)，其中 μ_H (z)依赖于宇宙曲率参数Ω_k。通过比较 Ia 型超新星的距离模数 μ_SN (z)和 μ_H (z)，他们对Ω_k 作出限制。他们发现所测得的Ω_k 值与零非常吻合，表明在现有的观测数据水平上平坦宇宙仍然被支持（Wei & Wu, 2017, ApJ, 838, 160）。紧接着，魏俊杰及其合作者利用相同的高斯重构方法同时限制宇宙曲率和宇宙不透明度，他们

发现平坦且透明的宇宙仍然被现有的观测数据所支持（Wang, Wei, Li, Xia, & Zhu, 2017, ApJ, 847, 45）。

（4）伽玛暴宇宙学研究：Ia 型超新星作为宇宙“标准烛光”的不足之处就是不能探测到高红移的这类天体。伽玛暴的可探测红移远远超过 Ia 型超新星，因此可以作为一个探索高红移宇宙的强大工具，包括探索宇宙早期的恒星形成。魏俊杰和吴雪峰利用伽玛暴建立高红移处的哈勃图，并提出高红移伽玛暴可以限制高红移宿主星系中暗物质晕的最小质量，以及在暗物质晕中的恒星形成过程（Wei & Wu, 2017, IJMPD）。

5、时域巡天观测数据处理方法的研究

（1）研究了如何判断给定离散数据点是否为一光滑曲线抽样的方法，并结合变星候选体的周期假警率来判断该候选体是否为变星。变星的判断有很多方法，其中一种是 Js 指数，Js 值越大是变星的可能性越大，但用这个量在 TNTS 数据变星搜寻中存在一些问题。考虑到对每颗星的星等都可以得到其最可能的周期图像，如果该星的确存在周期变化，那么上述周期图像中的数据点应该像一条光滑曲线，反之就会比较弥散。比较数据点和平滑以后的数据点的相关性可以比较好地判断这些数据点看起来是比较像光滑曲线还是比较弥散。利用这一方法结合周期假警率等参数就可以用来搜寻变星。实际分析 TNTS 巡天数据，这个方法的确可以按照可能性大小来对变星候选体排序。

（2）研究了暂现源观测中普遍使用的图像相加和相减方法，特别是研究了最新的根据统计学原理提出的图像相加和相减方法以及相应的代码。研究了在巡天项目中用传统图像相减方法处理后如何筛选暂现源的方法，准备研究用新的图像相减方法处理后如何筛选暂现源。暂现源观测中目前较广泛使用的图像相减软件是 hotpants。类似的图像相减方法一般会经过很多条件筛选后得到真实的暂现源。而 2015、2016 年基于统计学原理发展的新的图像相加和相减方法，原则上要比传统方法好。目前正在开展的这方面工作包括：参考已有的代码，写出基于新方法的暂现源观测 pipeline，并在实际观测中测试、改进，并同传统方法加以比较。

2-10 银河系气体分布与性质研究团组

（1）基于“银河画卷”巡天，团组成员对银道面的超新星遗迹开展了系统的观测研究。针对核坍缩型超新星遗迹，团组苏扬博士等人对一组样本进行了大视场观测，研究了遗迹的星周气体环境，发现了高能宇宙线和超新星遗迹星周气体之间的潜在联系（Su et al. 2017a,b）。针对热核型超新星遗迹，团组陈学鹏等人对第谷超新星遗迹进行了大视场高灵敏度的观测，发现了围绕该遗迹的巨大气体空腔（测量到的空腔半径值介于 13-27pc 之间）。这个巨型空腔的发现支持了热核型超新星的吸积理论模型（Chen et al. 2017）。

（2）基于“银河画卷”巡天，团组孙燕博士等人观测了银道面第一象限 34.75-45.25 度、遥远外旋臂上的分子气体，证认了约 169 个分子云，建立了迄今为止国际上最大的遥远外臂 Extreme Outer Galaxy (EOG)分子云样本，并详细分析了这些分子云的基本性质。该项工作极大地促进了外旋臂上分子云与恒星形成的研究，有助于我们理解在不同旋臂、不同环境（气体密度和金属丰度）下恒星形成的异同。该项工作发表在国际核心期刊 The Astrophysical Journal Supplement Series（Sun et al. 2017）。

（3）基于“银河画卷”巡天，并结合空间红外望远镜，团组研究生熊放（导师陈学鹏研究员）对 G150 区域的巨纤维状分子云进行多波段观测研究。我们发现该巨分子云由“主纤维状分子云”和近十个“子纤维状分子云”组成；大部分搜寻得到的分子云核坐落在纤维状分子云中，而且“主纤维状分子云”和若干个“子纤维状分子云”上的云核已经有恒星形成的表象。该项工作有助于更好地理解恒星形成早期的初始状态（Xiong & Chen et al. 2017）。

2-11 天文望远镜技术实验室

1）自适应光学研究方面取得重要成果。

自适应光学研究方面取得重要成果。基于力学领域的主/偏场理论，提出了一类新型连续镜面分立压电变形镜，创新了变形镜结构与工作机制，发展了新的力学控制方法与理论，有望极大拓展变形镜带宽和增大其量程。首先，建构了该类变形镜两种新型促动器的主/偏场理论模型，研究了结构因素与环境因素对促动器性能影响规律。其次，建构了以两种新型促动器为驱动的连续镜面分立压电变形镜力学控制模型，发展了自适应光学分立式压电变形镜力学控制新理论。以上一系列的研究成果得到了国际同行科学家高度评价，相关的成果分别发表在国际顶级的光学期刊 Optics Express 和国际知名的学术权威期刊 Journal of Intelligent Material Systems and Structures 等 SCI 期刊上，并获得多项国家授权专利和软件著作权，其中一项名为“一种以梁型压电促动器为驱动的变形镜”实用新型授权专利获 2017 年度南京市优秀专利奖。

南极 5 米太赫兹望远镜（DATE5）温控系统设计。分别与重庆大学工程热物理研究所以及南京航空航天大学微小卫星中心合作，开展南极 5 米太赫兹望远镜总体热控深化设计方案研究，其中南京航空航天大学设计方案已经完成台内评审。同时，我们自己也独立建立 DATE5 温控系统流体动力学模型，进行仿真计算，与合作方设计结果对比验证。

完成 DATE5 缩比天线（1.2 米口径）的研制、集成与测试。分别与上海复合材料有限公司和中国电科 54 所合作，研制完成了碳纤维结构 1.2 米口径太赫兹天线反射面系统（包括面板和背架等）和高精度斜轴式天线转台，反射面综合调整精度优于 20 微米。依托该天线开展斜轴式望远镜运动特性的实验研究（包括指向特性、跟踪特性以及伺服控制特性）以及反射面电调实验等。为开展天线热控实验，完成

斜轴式转台保温罩的设计，包含玻璃纤维蒙皮、气凝胶夹芯结构保温罩主体以及转轴间迷宫封沿等。

太赫兹碳纤维原型面板的试制工作取得阶段性成果。与上海复合材料科技有限公司合作，将碳纤维原型面板的表面加工精度进一步提高为 3.4μm rms（常温下三坐标仪测试结果）。同时为了提升面板的热稳定性，采用了全碳（格栅，碳管夹芯结构）结构设计方案，新型结构面板的低温性能仍在测试当中。

围绕 DATE5 继续开展天线测量研究。（1）继续开展近场全息测量研究，针对 1.2 米 THz 天线，完成了主焦和卡焦接收方式下全息测量系统软硬件研制，完成了用于 DATE5 天线全息测量的 W 波段宽波束主焦馈源的设计、仿真、加工和初步测试，完成了基于 FPGA 的数字相关器研制（与上海讯析公司合作）和测试，目前正在开展近场全息测量实验。（2）开展射电望远镜波前测量中的非相干方法研究，已初步完成了非相干波前检测方法的建模仿真研究。（3）开展南极 5 米太赫兹望远镜指向与调焦校准精度分析研究，针对 660GHz 工作频段，挑选在南极台址可用来验证望远镜指向与调焦模型的候选射电校准源，对指向校准与副面调焦所能达到的精度进行估算，初步确定了满足校准精度要求的若干射电源，此项工作投稿天文学报并已经过一轮审稿和修改。参加中、美、智三方合作项目——中智宇宙学亚毫米波望远镜(CST)升级设计方案研究。本团组王海仁博士参加该项目，建立了 CST 三维参数化有限元模型和伺服控制模型，为 CST 后续升级设计工作打下了基础。该工作得到了著名科学家、CSO 天文台台长、加州理工学院教授 Sunil Golwala 博士等人的高度评价。

围绕基金重大项目继续开展极端台址环境下的太赫兹望远镜关键组件特性研究，与燕山大学极端条件下机械结构和材料科学国防重点学科实验室签订合作备忘录，共同开展面向南极天文需求的望远镜低温运动机械合作研究，2017 年度已完成 DATE5 副镜并联调整机构的方案设计以及主反射面面板电调促动器的样机研制；

其它工作。（1）参与中日合作西藏阿里 HinOTORI 50cm 望远镜的建设安装，2017 年 9 月-10 月在阿里台址现场完成了 4 米圆顶的现场安装和望远镜的初期调试观测工作。（2）完成了基于 Linux 操作平台的滨松可见光探测器的读出电路设计。（3）完成了步入式低温环境实验舱在仙林新园区的安装、调试以及验收工作。（4）完成了望远镜测试外场工程开工前所有准备工作，包含设计方案，地质勘探以及招标等。

2-12 基于 SKA 的宇宙学研究团组

主要从事宇宙学和射电天文的数据分析，参加会议报告 6 次，其中邀请报告 3 次、口头报告 5 次、墙报 1 次

III．应用天体力学和空间目标与碎片研究部

3-01 空间目标与碎片观测研究中心

1）中心代表中科院参加了“天宫二号/天舟一号”空间碎片预警监测任务，在危险空间碎片（特别是大椭圆空间碎片）的监测上发挥了重要作用，保障了“天宫二号/天舟一号”的飞行安全，为我院争得了荣誉。

2）“地球同步轨道区域空间碎片运动特征研究与观测编目”、“大相对口径中高轨空间碎片探测望远镜研制”两个项目均通过省部级科技进步二等奖（单位排名第一）的答辩。

2017 年中心参加了多项国家任务，并得到了各方好评。主要有：

① “天宫二号/天舟一号”空间碎片预警监测；

② 日本卫星应急搜索监测；

③ “天宫一号”应急观测；

④ 我国卫星和火箭减缓辅助评估观测；

⑤ 中国长征 3 号乙火箭体陨落期国际联测；

⑥ 小行星 2012TC4 监测试验；

⑦ 姚安 1017 中高轨监测试验；

课题进展情况：继续深入开展人造天体的一些特殊轨道的长期演化规律、空间碎片的观测方法、空间碎片非质点旋转运动特征提取及分析、大气模型修正等方面的工作。

基于 QCT（多通道望远镜）与 UKIRT，开展了中美针对 GEO 区域空间碎片的首次多波段联测，发现了同类型火箭体在红外波段的色指数聚类特性，并得到了该批目标的多波段光变曲线。结合后随的观测数据，分析了目标光变周期受不同观测时间、不同观测站址的影响，发现存在光变周期多站、多次观测始终一致的目标。

基于 2013-2015 年 EnviSat 光学观测数据中镜面反射时刻，考虑其角动量绕轨道面法向的进动规律，拟合获取了其旋转周期变化，该拟合结果是目前所有关于 EnviSat 旋转状态拟合文献中最优的。

在轨道演化研究方面，首次给出近圆中高轨道目标在考虑月球轨道面进动影响下非共振状态下的长期演化轨道分析模型，分析了共振状态下的相空间结构。在此基础上，分析了近圆轨道人造天体的不稳定区域。

采用双平均化方法，建立了中高轨空间目标轨道的长期模型，给出了一套高效率的轨道演化软件；采用 Lindstedt-Poincaré方法，给出了周期系数微分方程组的级数解，建立了中高轨轨道平面的长期分析解。

在望远镜主控软件中嵌入云量监测模块，利用实时云图信息对空间碎片观测调度进行优化。实际测试表明：在多云天气条件下，提高预报密度，可明显提升观测效率。这一工作模式对未来实现望远镜的高效率、智能化观测具有重要意

义。

3-02 卫星精密定轨及应用研究团组

1）国家重点型号项目 B 分系统在试验场完成测试

2）国家重大型号项目 A 子项软件得到后续的采购合同

国家重点型号项目 B 分系统在试验场多次参加和配合总体单位进行了全系统对接联调，软件通过了实测数据检验，各项功能经对接测试完全符合合同规定的要求，定轨和预报精度经总体单位和用户确认达到了规定的技术要求，其中预报精度能够满足大时间跨度对雷达窄波束的引导跟踪要求，优于美国双行根数采用的 SGP4 模型，得到总体单位的充分认可，软件对试验期间所获取的大量实测数据进行了处理和精度分析，为总体单位进行设备的精度标校和全系统通过出所验收提供了可靠支持。

国家重大型号项目 A 子项软件在小面阵实测环境下展现了优越的编目性能，自动化程度较以往的同类软件大幅提升，得到相关部门的充分肯定，2017 年度总体单位又与团组签订了该软件的采购合同，采购经费 340 万元，该软件将在后续型号设备中得到采用。此外，团组 2017 度还配合总体单位进行了系统鉴定定型的部分工作，协助总体单位完成了系统鉴定定型试验总案评审。

Ⅳ．行星科学和深空探测研究部

4-01 近地天体探测和太阳系天体研究团组

1）在一颗系外天王星的大气中发现了瑞利散射的光谱证据

2）发现系外热木星 WASP-52b 可能存在大气热成层

对多颗热木星和热天王星进行巡天观测，利用凌星现象获取它们的大气透射谱，进而根据光谱特征分析得到大气组成成分。

对多颗热木星和热天王星进行巡天观测，利用凌星现象获取它们的大气透射谱，进而根据光谱特征分析得到大气组成成分。

（1）在系外天王星 GJ 3470b 的大气中发现了瑞利散射的光谱证据，GJ 3470b 是一颗绕 M 型矮星公转、质量比天王星略小的系外行星。利用 10.4 米 GTC 望远镜的 OSIRIS 光学光谱仪观测了该行星的 3 次凌星现象，获取了高质量的大气透射谱。该谱与氢氦占主导的大气中产生的瑞利散射特征一致，该瑞利散射可能来自于氢分子，也可能来自于小颗粒物云霾，但大气包层中的氢氦比例一定较高，才能维持与观测相符的大气平均分子质量。这个结果说明将木星级的比较学研究延拓至更小质量、更小尺寸的行星是可行的，M 型矮星的行星系统将会是此类研究的主要目标。这是目前利用地基望远镜观测到大气信号（非无特征水平光谱）的最小尺寸系外行星。

（2）根据探测到的钠钾原子的吸收轮廓，发现太阳系外热木星 WASP-52b 可能存在大气热成层；极其膨大的超级海王星 WASP-127b 的大气展现了令人疑惑的包括瑞利散射、钠原子、TiO/VO 在内的丰富光谱特征；在极热热木星 WASP-48b 的大气中发现了 TiO/VO 的可能证据。利用 10.4 米 GTC 望远镜的 OSIRIS 光学光谱仪，获取了热木星 WASP-52b 的光谱分辨率约为 30 的大气透射谱，该谱呈现的连续谱显示其大气中存在光学厚的云层，屏蔽了该极其膨大的热木星大气中可能出现的丰富光谱特征。从观测的高质量数据中分析得到了信噪比可观的光谱分辨率约为 370 的大气透射谱，该谱展现了来自钠原子的、显著的窄吸收线心，钾原子的共振双线也可能被分辨出来了。这些窄线心的探测发现，说明即便存在光学厚的云层，只要光谱分辨率足够高，云层上空的微弱原子吸收还是能够被探测到的。钠钾原子的吸收轮廓显示该行星的大气在所探测到的压强范围内，高度每增加 1km，温度平均升高 0.88K，暗示可能存在热成层。这对于研究高层大气的加热机制、行星外部环境的影响有重要意义。

4-02 历算和天文参考系团组

完成了国家标准《农历的编算和颁行》的制订工作

国家标准《农历的编算和颁行》的制订工作是我们的一个亮点工作。农历是我国目前仍在颁行的中国传统历法，是我国传统节假日安排的法定依据，其在传承华夏文化、维系华人世界等方面具有无可替代的重要意义。农历的日期编排依赖于太阳和月球的精确预报位置，其编算具有很强的专业性。为了有效维护农历作为国家历法的科学性、统一性和严肃性，由中国科学院提出并归口管理，中国科学院紫金山天文台于 2014 年牵头承担了中国国家标准化委员会下达的《农历的编算和颁行》标准制订项目。经过全国天文、历法、历史、民俗等各有关方面专家两年多的共同参与，该标准于今年 5 月正式颁布，其核心内容有：太阳和月球视位置预报的精度要求和符合国际天文联合会决议的规范模型，以及农历日期的编排规则和表示方法。

此外，结合研究生培养，我们在包括相对论基本天文学、河外射电参考架局部扭曲的成因，以及恒星、双恒星和多恒星系统，系外双行星系统，太阳系行星、天然卫星和小行星等运动学和动力学研究方面也做了大量研究工作，有些研究已经取得了一些很有价值的新结果，共发表了 8 篇学术论文。

4-03 太阳和太阳系等离子体研究团组

1）利用卫星数据揭示了阿尔文扰动的新观测特征；

2）建立太阳耀斑环中快电子束流-回流系统激发动力学阿尔文波的物理机制；

3）提出热电子效应可以导致哨声波的频率延展至电子回旋频率。

本年度科研工作承接本团组的研究特色和优势，系统研究了阿尔文波及动力学阿尔文波线性不稳定性激发机制的理论和应用，以及湍流相关理论和观测，取得多方面的科研成果：

太阳风阿尔文波研究

在之前工作的基础上，利用 Ulysses 卫星进一步研究外传和内传阿尔文扰动的径向演化问题。基于该卫星的磁场和等离子体数据，可以选择阿尔文扰动事件，再利用 CHYL 方法对这些事件进行处理，根据推导得到的公式，可以得到基于 Walen 斜率的内传与外传阿尔文波振幅比或能量比。同以前研究类似，得到的径向演化显示，该能量比随日心距离单调增长，这意味着内传阿尔文波的贡献或其产生率也随之增大；同时内传主导的阿尔文扰动相较外传的相对扰动强度也逐渐增加。进一步的统计研究表明，太阳风高速流中外传主导的阿尔文扰动发生率比以往的研究结果更高（平均每天约 83%的时间）。该工作中计算的能量比采用的方法，相比以前用平均的方法所得结果更为准确，更加接近太阳风等离子体的实际情况。内传主导的阿尔文扰动的持续时间占所有阿尔文扰动事件的比例也随日心距离单调增加，在大于 4AU 之后是 Voyager 2 观测结果的两倍以上。这些结果从定性和定量两方面揭示了阿尔文扰动的新观测特征，对建立太阳风扰动演化的模型提供了新的限制条件。

太阳大气动力学阿尔文波研究

研究了直接激发动力学阿尔文波不稳定性的物理机制之一，提出快电子束流-回流系统中，通过共振和非共振的波-粒相互作用，动力学阿尔文波的线性不稳定产生机制。 研究结果表明，在如太阳耀斑环等低 beta（热压-磁压比）等离子体环境中，当快电子速度略微超过当地阿尔文速度时，动力学阿尔文波可以有效生长。动力学阿尔文波的生长率随着快电子束速度的增大而增大，随垂直波数的增大而减小。电子束流提供其不稳定性生长的自由能。这些结果对理解空间和天体等离子体中束流耗散和等离子体活动现象有着重要的潜在应用价值。

地球磁层哨声波研究，结合了等离子体流体和动力论模型，揭示了地球磁层中重离子成分比和温度各向异性对有效激发氧带电磁离子回旋波的影响、以及对电磁离子回旋波禁带宽带的影响；揭示了太阳和行星低密度强磁场等离子体中哨声波新特征，首先提出热电子效应可以导致哨声波的频率延展至电子回旋频率。

4-04 行星科学与深空探测实验室

(1) 图塔蒂斯小行星的研究成果入选“十八大”以来中科院创新成果展

(2) 小行星深空探测创新交叉团队入选中国科学院创新交叉团队

（1）小行星表面热物理性质

Dembowska（349）小行星是一颗主带小行星，它很亮，自转很快，自转轴与轨道面的夹角很小；它的近红外反射光谱与灶神星的光谱十分相似，所以可能发生过熔融分异历史。它的轨道半长径为 2.92379 AU，靠近太阳系“雪线”，所以可能有水冰的存在。但是，至今为止，我们对于这颗小行星的基本物理信息仍不完全确定。利用 ATPM 分析 Dembowska 的三组热红外观测数据，获得了其表面热惯量，粗糙度，反照率等基本热物理信息（表 1）。基于以上得到的基本热物理信息模拟其任意轨道时刻的表面及次表面温度环境（图 1-3）。研究结果发现 Dembowska 表面南北两极温度变化较大（40～200K），赤道温度变化较小（150～180K），但都有很长时间温度高于 150 K，所以表面不太可能保存水冰。研究发现：Dembowska 南北次表层一定深度以下，温度达到 150 K 以下，水冰可以稳定存在(Yu, Yang & Ji et al. MNRAS,2017)。

表 1. Dembowska 的基本热物理参数

Properties	1σ value	3σ value
Thermal inertia Γ($Jm^{-2}s^{-0.5}K^{-1}$)	20^{+6}_{-8}	20^{+18}_{-20}
Roughness fraction f_r	$0.4^{+0.4}_{-0.3}$	$0.4^{+0.6}_{-0.4}$
Geometric albedo p_v	$0.317^{+0.013}_{-0.011}$	$0.317^{+0.045}_{-0.04}$
Effective diameter D_{eff} (km)	154^{+4}_{-2}	154 ± 10

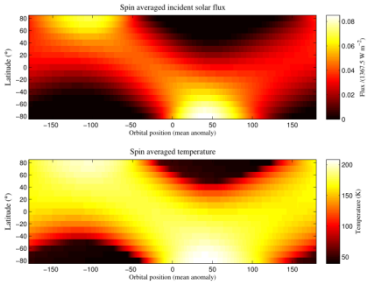

图 1.Dembowska 轨道不同时刻的表面光照和温度分布。

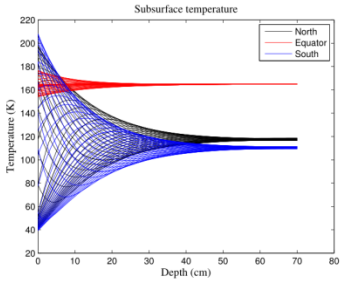

图 2. Dembowska 次表层温度分布。

Apophis 小行星是一颗对地球具有潜在撞击威胁的阿登型近地小行星，对其轨道运动的预测具有十分重要的意义。然而 Apophis 体积较小，形状不规则，使得其具有显著的 Yarkovsky 轨道漂移效应。所以估算 Apophis 的轨道漂移速率是准确预测其轨道运动的前提。为了估算 Apophis 的轨道漂移速率，需要知道其表面热惯量，粗糙度，反照率等

基本热物理参数（图 11）。我们用 Advanced thermophysical model 分析了 Herschel/PACS 和 CanariCam/GTC 获取的 Apophis 的热红外观测数据，获得 Apophis 的基本热物理参数（表 2） (Yu, Ji & Ip, RAA, 2017)。

表 2. Apophis 的基本热物理参数

Properties	Value
Thermal inertia Γ($Jm^{-2}s^{-0.5}K^{-1}$)	100^{+240}_{-80}
Roughness fraction f_r	0.48~1.0
Geometric albedo p_v	$0.28^{+0.024}_{-0.019}$
Effective diameter D_{eff} (m)	382^{+14}_{-16}
Mass (kg)	$(5.541^{+0.98}_{-1.04}) \times 10^{10}$

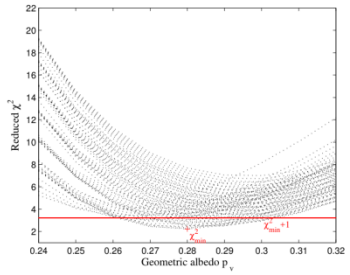

图 3. pv～χ2 曲线给出几何反照率的 1σ值域。

2.Bennu 小行星形状形成

利用 N-body 数值模型 Mass-spring 程序包研究了小体积碎石撞击对 Bennu 表面本征震动频率的激发及其与 Bennu 形状演化的关系，在 Scheeres 等人工作的基础上，进一步解释了赤道形状可能的起源（Zhao et al., in prep. 2017a）。

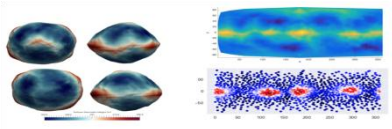

图 4. 左图：Bennu 的形状模型。右上图：Bennu 表面海拔分布，右下图：赤道撞击产生的 Bennu 表面震动能量分布。

3. 建立三维辐射转移模型研究 67P 彗发中水分子分布特性

利用三维辐射转移程序 LIME，基于 Haser 公式建立的彗发模型，对 Rosetta 观测初期阶段彗核活动中水分子的运动和分布进行了分析，验证了 Hapi 地区活动较为剧烈的结论（Zhao et al., in prep. 2017b）。

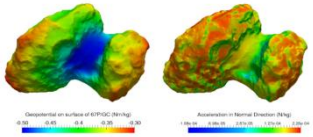

图 5. 2014-07-11T22:02:33 67p 彗星表面温度和水分子产生率分布。

4. 揭示 4179 Toutatis 小行星可能的形成机制

4179 Toutatis 具有奇特的形状和非常缓慢的自转，地面雷达和嫦娥二号光学图像均显示该小行星具有延展型的密接双小行星结构（由两个瓣组成），并且连结处位于身体的长轴上。据推测该小行星的形成机制源于一次两部分结构的低速撞击。如果 Toutatis 的母体是一颗近地双小行星，在近距离飞越地球的过程中，由于地球的引力改变了该双小行星的相互轨道，并有可能影响该系统主星和卫星的自转和形状。假设该系统为双同步自旋双小行星，卫星相对主星的距离为 4 倍主星半径，并且两部分均考虑为由无粘附力作用下的自引力球形粒子聚合体所构成。利用 pkdgrav 程序，考虑了软球离散元模型。结果表明，在合适的参数下，这种机制很容易形成密接双小行星，但发现两者之间的相互碰撞很难用来解释主星延展型结构。然而，在飞越距离约为 1.4-1.5 倍地球半径情况下，获得一组与目前 Toutatis 形状相似的密接双小行星，表明该机制可以解释 Toutatis 目前的形状（Hu et al., in prep. 2017）。

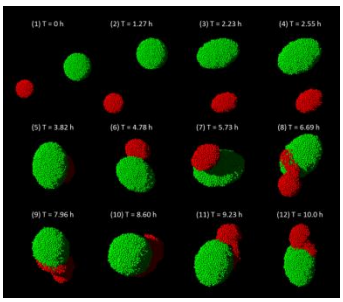

图 6. Toutatis 的密接双小行星形成。

5. 行星生长过程对共振构型的影响

通过考虑行星的生长过程研究对行星之间进入共振构型的影响，可能存在的向外的第一类轨道迁移也是影响行星能否进入共振的一个重要因素。通过考虑这两个因素的影响，可得到行星质量的增长以及向外的轨道迁移会增大进入 3:2 共振的概率，内部两行星更容易处于近共振位置，且更平坦的盘易于行星形成共振构型，如果行星存在向外的轨道迁移则大大提高进入 3:2 共振的概率，最终得到的行星之间的质量关系与目前的观测结果相符(Wang & Ji, AJ, 2017)。

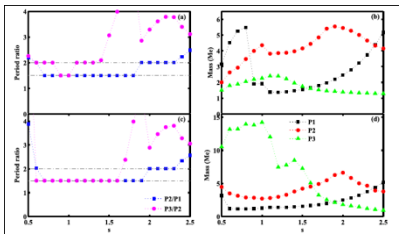

图 7. 行星质量增长过程对进入 2：1 和 3：2 共振的影响。

6. 行星之间进入近共振构型的形成机制研究

针对目前 Kepler 计划观测到的多行星系统中轨道周期的分布情况发现，大部分的行星在演化过程中进入共振后会脱离共振到达近共振构型。提出了一种可能的形成机制解释这一过程。行星在进入共振后将嵌在一起迁移，而此时若气体盘仍存在时，行星由于进入共振而被激发的偏心率则会被抑制，与此同时行星将会有小幅度的轨道迁移过程，从而脱离共振到达目前的近共振构型。在此形成机制基础上我们进行了大量的数值计算，从统计上发现该机制可以解释目前的近共振构型的形成（Wang et al., in prep. 2017a）。

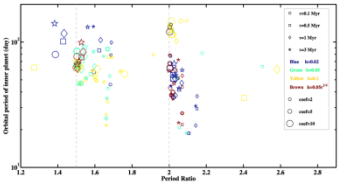

图 8. 行星周期比的数值模拟结果与内行星轨道周期的关系。

7. 多行星系统稳定性研究

目前发现的多行星系统中有很多是处于共振或者近共振构型，尤其是随着 Trappist-1 系统的发现，在该系统中七颗行星两两之间轨道周期处于简单的整数比，因此共振构型可能是多行星系统长期稳定存在的一个构型。若考虑了气体盘的存在下行星的轨道迁移过程，检验了多行星系统的稳定需要的条件。研究发现气体盘的消散时标较长的情况下系统更容易稳定，但是共振构型行系统的稳定区域较小。当系统中存在行星较快或者较高的质量损失时系统可能由稳定状态变为不稳定（Wang et al., in prep. 2017b）。

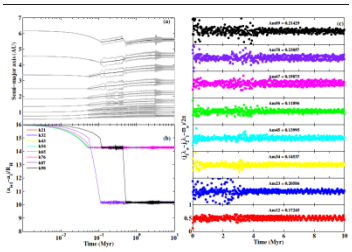

图 9. Trappist-1 系统的轨道演化与共振构型形成。

8. Proxima Centauri 系统动力学及稳定性

在 Proxima b 准确的部分轨道参数的基础上，Proxima b 和 Proxima c 的升交点经度分别取 0、90、180 和 270 度，应用 MEGNO 混沌性指标，对非共面情形进行模拟计算，得到 16 张$(\cos i_c, \cos i_b)$的混沌稳定性图像。通过对比相互倾角的图像（左）和 MEGNO 稳定性图像（右），可以看出两颗行星相互倾角大的图像区域对应着 MEGNO 值大的混沌图像区域，说明相互倾角较大的情形更容易发生系统混沌现象，很有可能导致系统的不稳定性。经过对各种情况进行仔细对比，可以看出相互倾角约小于50^0的时候，利于保持系统的稳定，这对 Proxima Centauri 行星系统及其行星参数范围的研究方法具有重要的意义（Meng et al., in prep. 2017）。

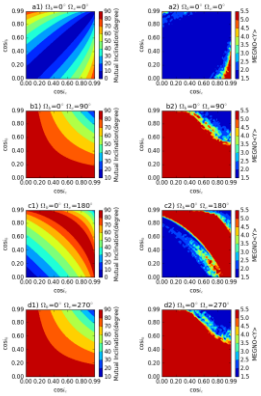

图 10. 非共面情形的图像，相互倾角图像和 MEGNO 的混沌稳定性图像的比较。

9.揭示 Kepler 环双星系统中行星的轨道形成机制

Kepler 空间望远镜的一个重大发现是在主序双星周围发现了环双星的行星（CBP）。行星在盘中的迁移模型不能很好解释 Kepler-34b 和 Kepler-413b 的轨道构型。我们提出了一种新的机制-即目前观测到的 CBP 轨道构型由双星系统中行星与行星间的散射机制所致。对多颗 CBP 在盘中迁移的模拟工作显示，这些天体首先会进入轨道共振构型，而随着盘中气体的消散，它们之间会发生散射。研究发现，行星的质量比和初始的相对位置是决定行星轨道空间分布的两个重要因素，行星与行星间的散射机制很好地解释了目前 Kepler 所观测到的 CBP 轨道构型,例如 Kepler-34b 的形成过程 (Gong & Ji, AJ, 2017)。

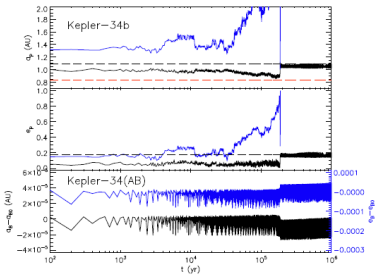

图 11. Kepler-34b 的形成过程。红虚线为 Keple-34（AB）周围的不稳定边界，黑虚线为目前的观测位置。

10. 旋涡在原行星盘中气体的探测能力与特征

以 IRS 48 disk 为例，使用 LA-COMPASS 和 RADMC-3D 进行 2D 的流体模拟和 3D 的辐射转移计算，并使用 CASA 模拟 ALMA 特定构型下的观测，给出旋涡在不同情况下的在原行星盘中的图像特征，同时考虑了影响旋涡在原行星盘中的探测能力的不同因素。图 12 给出不同情

况下的模型的尘埃连续谱，CO 气体 J=3-2 转动发射线的谱线强度，速度分速，速度弥散。从中可看到不同情况下旋涡特征，从而为在原行星盘中观测旋涡提供了相应依据(Huang P., et al.，in prep.，2017)。

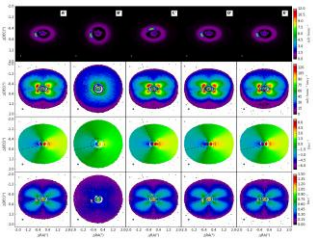

图 12.从上至下，为盘的尘埃连续谱，CO 气体 J=3-2 转动发射线的谱线强度，速度分速，速度弥散。而从左至右为不同盘模型：标准模型，改变倾角，改变旋涡位置，改变噪声水平，改变速度分辨率的模型。虚线与虚线椭圆交点为旋涡的中心位置。

11. 对玻璃陨石开展了高精度钾同位素分析

利用 Wang 和 Jacobsen（2016a）最近发展的高精度钾同位素测试方法，分析了来自三个不同散落区的七个玻璃陨石的钾同位素成分。所有玻璃陨石的钾同位素成分分布范围窄（δ41KBSE: −0.10 ± 0.03‰ 至 0.16 ± 0.04‰），与不同构造背景的地球玄武岩代表的均一的全岩硅酸盐地球（BSE）无异（图 13）。根据多个挥发性元素同位素体系在玻璃陨石和月球样品之间的对比，我们认为挥发性元素在玻璃陨石中丢失的机制和条件完全不同于月球。月岩中的重钾同位素反映了月球形成大撞击事件的主要特征（Wang and Jacobsen，2016b），而月球的 Cu 和 Zn 同位素分异更有可能是岩浆洋蒸发或晚期撞击蚀变的结果。钾同位素因此成为研究月球起源和行星分异的更可靠的工具(Jiang et al., in prep. 2017)。

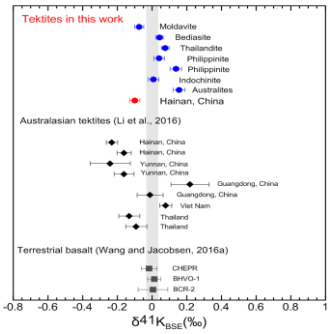

图 13. 玻璃陨石的钾同位素成分。灰色阴影区代表不同构造背景（大陆、地幔羽和洋中脊）的三种地球玄武岩的钾同位素成分（Wang and Jacobsen, 2016a）。在误差范围内，不同类型玻璃陨石的钾同位素成分无明显差异。

12. 利用切比雪夫多项式提出了一种新的小天体引力场计算方法

在小行星深空探测任务中，小行星的临近动力学环境对探测器轨道的影响至关重要。但由于小天体形状复杂，利用传统的球谐系数展开法和新的多面体方法都存在一些问题。在这个工作中，提出了一种三维空间（沿着三个球坐标）自适应分割方法，在每一块空间单元里用三维切比雪夫多项式方法做拟合。通过对 Toutatis 附近探测器轨道外推做了对比之后，发现该方法确实可能有效地提高计算效率（可提升成百上千倍），并且误差在一定情况下可以接受(Hu et al., RAA, 2017)。

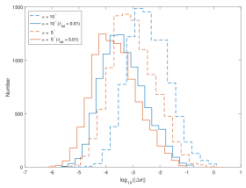

图 14. 在不同的参数下，利用该方法计算的 Toutatis 附近的轨道与真实轨道的差别（误差）。

13 使用 MWA 探测空间碎片

在对流星的观测过程中，发现了其他的射电暂现现象，主要是低轨道卫星对调频广播信号的反射。通过将反射信号与卫星轨道进行对比确认，探测到的最小卫星为立方卫星（cubesat），轨道高度为 600 km，大小为数十厘米。这证明了利用 FM 广播信号来探测空间碎片是可行的。图 15 为默奇森宽场阵列探测到的立方卫星，Duchifat-1。图像按时间先后顺序从左向右排列，每张图像的积分时间为 2 秒。黄色圆圈代表根据卫星轨道根数推算出的卫星在 2 秒积分时间开始时的位置。为了减小背景辐射产生的噪声，这里给出的是相邻图像相减之后的结果 (Zhang et al., submitted to MNRAS, 2017) 。

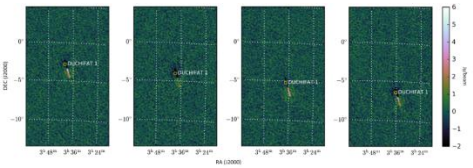

图 15. 默奇森宽场阵列探测到的立方卫星 Duchifat-1。

4-05 天体化学和行星科学实验室

在普通球粒陨石中确定了太阳系早期冲击事件的时间表；发现了月球大碰撞事件在太阳系内普遍存在，影响到小行星带。

1. 揭示灶神星壳体中锆石应为变质，而非岩浆成因，主要来自填隙物部分熔融熔体的再结晶，与早期全球热变质过程中的再加热事件有关。结合同位素年代学，限定灶神星壳广泛存在的热变质应发生于 4.55 Ga。发现灶神星存在一个 ~4.1–4.2 Ga 的冲击变质峰期，与月球冲击年龄谱图中的峰值年代一致，表明内太阳系在~4.1–4.3 Ga 之间很可能存在一期广泛的强烈冲击过程。相关成果发表于 Geochimica et

Cosmochimica Acta 204, 159–178.

2. L 群球粒陨石 NWA 7251 的磷酸盐记录了两期冲击变质年龄，一期为 4.40 Ga，另一期为 0.47 Ga；0.47 Ga 发生的冲击变质事件使 NWA 7251 发生了熔融。L 群球粒陨石 NWA 7251 冲击熔融体中的磷灰石 Cl/F 比值分布范围比较大，可能与脱气作用有关。相关成果在 Meteoritics & Planetary Science 审稿中。

3. 通常认为冲击之后的持续高温是造成同位素重置的决定性因素。然而，我们的工作显示寺巷口陨石磷灰石 U-Pb 同位素体系受重置程度与高压相变程度具有显著的正相关，表明受到冲击过程中极端 P-T-t 条件的影响。相关成果在 Meteoritics & Planetary Science 审稿中。

4. 小型天体之间的撞击事件可能无法产生充足的热量使全岩同位素时钟重置，因而难以获得其准确撞击年龄。通过原位微区手段测定陨石中局部冲击熔融脉中磷酸盐高压相 U-Pb 同位素组成，为解决这一难题提供途径。相关成果即将投稿。

5. 发现 HED 中存在 4.530 Ga 左右的一期重要热变质冷却事件，很可能与岩浆活动快速衰减有关。灶神星的热变质冷却很可能较早便发生。首次在非角砾化 HED 族陨石中识别到确凿的早期多阶段热事件，与前人在非角砾化 HED 族陨石中观察到的存在再加热岩相学证据一致。这表明前人通过 HED 全岩 Ar-Ar 定年获得的 4.48 Ga 峰值年龄很可能为多期热事件的混合年龄，没有明确的地质学意义。相关成果在 Geochimica et Cosmochimica Acta 审稿中。

6. 揭示 NWA 11042 为一块不含球粒、具岩浆结构的陨石，其结构及矿物组成特征与火星陨石相似，但同位素组成与 L 群球粒陨石一致。经过详细岩矿学及同位素年代学分析，确定该样品为来自 L 群球粒陨石母体的熔融产物，并记录了母体上的两期强烈的冲击事件。相关成果即将投稿。

在上述科研工作的基础上，课题组还积极参与到公众科普活动中，组织和参与了形式多样的系列大众科普活动，其中包括：1）与南京图书馆和现代快报共同组织为期十七天的“天外客大型星空陨石展”，累计约有 10 万人到馆参观。公众通过近距离地接触陨石，加深了对人类大家园太阳系的感触和认识。活动经过现代快报、南京电视台等媒体报道，将天文知识传播给更广的人群，取得了良好的科学宣传效果。2）参与南京分院举办的“紫金”科学探究计划，指导南师附中学生进行行星科学有关科研工作，为培养中学生的科研兴趣和科学素养，配合中国科学院科学科普传播工作贡献了力量。

4-06 近地天体望远镜 团组室

1）近地天体望远镜新发现 10 个近地小行星，其中一个是对地球构成潜在威胁的近地小行星。

2）近地天体望远镜新发现 1 个彗星。

本年度近地天体望远镜发现了 10 个新的近地小行星，包括 1 个 Aten 型、4 个 Apollo 型，5 个 Amor 型。其中 2017 BL3 是一个 Apollo 型潜在威胁小行星（轨道根数：a=1.61AU,e=0.69,i=12.28,q=0.50AU）。截止目前近地天体望远镜已经发现了 15 个新的近地小行星。2017 年 1 月近地天体望远镜发现近地天体的工作上报中国科学院《要情》——《紫金山天文台新发现三个不同类型的近地小行星》，上报领导参阅材料《近地天体监测预警研究的进展、意义和建议》，引起党和国家领导人高度重视和批复。

表 1. 2017 年度新发现近地小行星概况

编号	轨道类型	发现日期
2017 BK3	Amor	2017/1/21
2017 BL3	Apollo (PHA)	2017/1/21
2017 BM3	Aten	2017/1/22
2017 DC120	Amor	2017/2/28
2017 GS4	Apollo	2017/4/1
2017 KR27	Apollo	2017/5/26
2017 OD1	Amor	2017/7/19
2017 QS17	Apollo	2017/8/23
2017 QQ32	Amor	2017/8/27
2017 RU17	Amor	2017/9/12

2017 年 3 月 1 日近地天体望远镜发现彗星 C/2017 E2 (Tsuchinshan)，左图显示了该彗星的轨道，轨道倾角 i=79 度，几乎垂直于黄道面，右图显示该彗星活动性特征。该成果被列为 2017 年度第二季度“中科院科技创新亮点成果”候选项目。

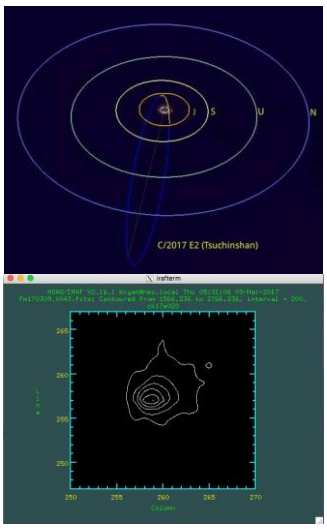

图 1. C/2017 E2 (Tsuchinshan)彗星的轨道和形态

2017年共监测了416个近地小行星的2276个位置数据，截止目前近地天体望远镜总计监测了 1552 个近地小行星，得到了 9938 个位置数据。开展太阳系小天体巡天观测，共计获得244211个(次)太阳系小天体的990452个观测数据，在全球 425 个台站中观测量据第 7 ,在观测量最多的十大地基测站中精度排名第三（位于新加入的 ATLAS 两个测站之后）。2017 年度共发现了 600 个新小行星，其中 51 个小行星获得了正式编号。

开展了大样本小行星光变巡天，2017 年度共计获得了 12277 个小行星的 51720 条光变曲线。开展了快速自转小行星（Fast Rotate Asteroids）的搜索，并发现了一个新的目标 2006 DZ6 为一个快速自转小行星。利用已有的部分小行星样本开展了自转特性的统计分布研究。

近地天体望远镜开展了时域巡天计划，组织开展了“紫台-清华超新星巡天计划”（PTSS），目前超新星搜索方面已经完成北天 SDSS-r，SDSS-i，VR 等 3 个波段北天绝大部份天区的模板库建设和全自动瞬变源数据处理软件，本年度共计发现超新星候选体目标 60 个。

开展了小行星散射法则的研究，以简化的 4 参数 LS 模型来代替复杂的 Hapke 模型，在 Cellinoid 模型小行星形状反演中取得了很好的效果，并且利用 LS 模型参数的主成分分析来进行 C/S 小行星光谱型的分类。另外针对小行星的形状反演，我们研究了利用综合光变曲线来建立小行星的 cellinoid 形状模型的方法，并对 Hebe、Toutatis、Eros 这三个小行星进行了基于实际观测条件的数值模拟，提高了自转周期和自转轴指向参数的反演精度。

利用实际观测数据来加强近地天体望远镜的数据处理软件系统的升级，在近地天体望远镜大视场图像变源检测数据处理过程中引入深度学习方法。建立了光度变源检测系统（Bobey），并且投入线上运行，对可能的目标标注了变源的概率；建立了面向动目标识别的自动检测系统（Tsar），用以辅助人工检视移动目标，提高了人工检视的效率。完成了近地天体望远镜数据库系统的硬件扩容升级，完成了数据库硬件裸容量达到了 200TB ,保证了后续观测数据的存储和发布能力，实现了原始数据和定标数据的实时发布。2017 年度产生的新增原始数据容量为 13.5TB。

大力推进设备的共享观测，开展了 LIGO 引力波天文台光学电磁对应体的巡天搜索，完成了总计 8 次 2017 年度发生的 LIGO 触发事件。接受开放观测项目包括反银心方向窄带巡天观测、Fast rotate asteroid 搜索、引力波事件对应体 Li-Paczynski 巨新星观测研究、中微子事件光学对应体搜索、主带活动彗星观测等。完成了转发式卫星导航试验系统盱眙站分系统运行。

4-07 行星光谱学研究团组（筹）

综合利用轨道与就位巡视探测数据嫦娥三号着陆区系统性研究

嫦娥三号着陆区系统性研究

1、嫦娥三号原位探测数据深入分析、处理与应用研究

嫦娥三号月球车搭载的红外光谱仪实现了首次月面原位光谱测试。过去发表的文献是数据刚获取即发表，存在误解，例如反射率绝对值未考虑大相角影响，矿物解译未认识到1）热效应对光谱的影响，2）测试的对象是土壤而非原始岩石。月岩是由矿物组成的原始产品，而表层月壤是风化产品。嫦娥三号红外光谱探测的信号来源是风化产物（如纳米铁、冲击熔融玻璃）而非矿物。月球无大气导热，温度非常高。地球的热红外波段通常位于 8-10μm，而月球在 2.3μm 就可表现出热效应。嫦娥三号红外光谱曲线在 2.2μm 向着 2.3μm 的抬升并非是过去文献认为的辉石 2.2μm 吸收所致，而是月表热辐射所致。

基于上述对光谱的基础性认识，对嫦娥三号红外光谱开展了深入校正与处理，获得了绝对反射率并提出嫦娥三号着陆点作为新的国际月球定标点（Wu, AJ, 2018）。反演了月壤纳米铁含量（Wang et al., 2017, GRL）。反演了微尺度月壤温度和发射率（Wu et al., EPSL, 2018）等系统性成果。

2、嫦娥三号着陆区地质、构造、成分综合性研究

结合国际上各种先进的绕月轨道探测数据和嫦娥三号就位巡视探测数据，对嫦娥三号着陆区开展了综合性研究，获得了晚期玄武岩矿物（较之于古老的玄武岩富橄榄石，张晓梦等，2017，地学前缘）。发现了嫦娥三号着陆点年轻的构造（<50Ma。过去认为月球 31 亿年就死亡，本发现揭示月球的构造活动持续很近）。揭示着陆区周边高地与典型的斜长岩高地不同，富含铁镁质矿物，命名为一种新的高地——铁镁质高地 MH（Wu et al., Icarus, 2018）。

3、嫦娥三号着陆区晚期玄武岩喷发厚度与体积估算

月海玄武岩的规模,反映了月幔的部分熔融程度和源区的深度,对研究月球玄武岩的成因和热演化具有重要意义。提出了面向玄武岩流特征的厚度估算策略。对于熔岩流锋面清晰可见的地层，采用高精度激光高度计数据测量其厚度；对于熔岩流锋面不可见的地层，依据年轻玄武岩(富含橄榄石）与下伏老地层（富含辉石）光谱特征的不同，利用较小陨石坑（未撞穿顶层地层）和较大陨石坑（撞穿顶层地层）的陨石坑直径与深度比关系，获得晚期玄武岩地层厚度。通过这两种方法，绘制了晚期玄武岩高分辨率厚度分布图并估算了体积（Chen, JGR, 2018）。

三、学术交流与合作

1、国际合作与交流概况

全年办理出访申请 210 人次（含台内审批 27 人次，赴中国台湾地区申请为 20 人次），全年国际合作代理主管赴省外办办事 124 次，平均每周 2-3 次；来访申请 153 人次，台胞来访 11 人次。协助主办/承办国际会议 4 场。

2、主要国际合作项目进展

悟空号获得世界上最精确的 TeV 电子宇宙射线能谱

悟空号采用了紫金山天文台研究人员自主提出的分辨粒子种类的新探测技术方法，实现了对高能（5 GeV-10 TeV）电子、伽马射线的“经济适用型”观测。

悟空号是中国科学院空间科学战略先导专项的首发星，它最早由紫金山天文台的常进研究员于 2005 年提出，在中国科学院基础局、科技部的支持下研制了原理样机。2011 年 12 月 21 日该项目被正式列入中国科学院战略先导专项-空间科学专项，常进研究员担任卫星的首席科学家。该卫星的探测器由紫金山天文台、中国科学技术大学、近代物理研究所、高能物理研究所与国家空间科学中心联合研制。瑞士的日内瓦大学、意大利国家核物理研究院也参与了硅子探测器的研发。卫星平台由中科院微小卫星研究院研发；地面科学应用系统由紫金山天文台牵头，中国科学技术大学、日内瓦大学等合作单位都参与了建设并为物理分析软件的研发做出了重要贡献。

尽管成本相对低（国际上的空间暗物质探测器阿尔法磁谱仪 AMS-02、费米卫星分别耗资 20 亿、7 亿美金），悟空号在“高能电子、伽马射线的能量测量准确度”以及“区分不同种类粒子的本领”这两项关键技术指标方面世界领先，尤其适合寻找暗物质粒子湮灭过程产生的一些非常尖锐的能谱（能谱指的是电子数目随能量的变化情况）信号。

悟空号于 2015 年 12 月 17 日发射成功，是中国的首颗天文卫星。该卫星的数据分析工作获得国家重点研发计划、科技部 973 青年科学家专题项目、国家自然科学基金委员会-中国科学院空间科学卫星联合基金、国家基金委杰出青年基金/优秀青年基金、中国科学院“百人计划”等项目的大力支持。

卫星在轨运行的前 530 天共采集了约 28 亿颗高能宇宙射线，其中包含约 150 万例 25GeV 以上的电子宇宙射线。基于这些数据科研人员成功获取了目前国际上精度最高的 TeV 电子宇宙射线探测结果，如图 1 所示。该成果于北京时间 2017 年 11 月 30 日在 Nature 杂志在线发表。

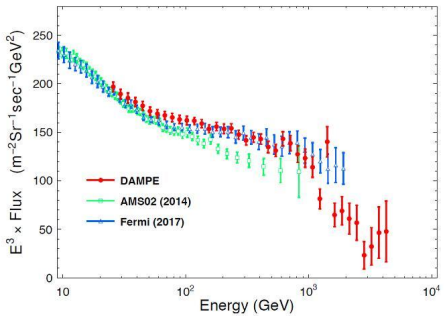

(1)悟空号的电子宇宙射线的能量测量范围比起国外的空间探测设备（AMS-02, Fermi-LAT）有显著提高，拓展了我们观察宇宙的窗口。

(2) 悟空号测量到的 TeV 电子的能量最准、“纯净”程度最高（也就是其中混入的质子数量最少）。

(3) 悟空号首次直接测量到了电子宇宙射线能谱在~1 TeV 处的拐折，该拐折反映了宇宙中高能电子辐射源的典型加速能力，其精确的下降行为对于判定部分（能量低于 1 TeV）电子宇宙射线是否来自于暗物质起着关键性作用。

此外，悟空号的数据初步显示在~1.4 TeV 处存在能谱精细结构。目前悟空号运行状态极佳，正持续收集数据，一旦该精细结构得以确证，将是粒子物理或天体物理领域的重大发现。

2. 南极巡天望远镜成功追踪引力波源重大科学发现

随着 2015 年引力波在观测上被直接证实，寻找产生引力波的宇宙起源就成为全世界天文学家最重要和最紧迫的任务。中国科学院紫金山天文台在南极建设的望远镜就是一台具备追踪探测引力波源的强有力观测设备。2017 年 8 月 17 日，LIGO 和 VIRGO（欧洲“室女座”引力波探测器）共同探测到的引力波事件 GW170817，是人类首次直接探测到由两颗中子星并合产生的引力波事件。北京时间 2017 年 8 月 18 日 21:10 起（即距离引力波事件发生 24 小时后），中国南极巡天望远镜合作团队利用正在中国南极昆仑站运行的第 2 台望远镜 AST3-2 对 GW170817 开展了有效的观测。此次观测持续 10 天，获得了大量的重要数据，探测到此次引力波事件的光学信号。这是我国的望远镜首次直接参与载入人类天文学历史的里程碑事件，并观测到了引力波的辐射源，预示着我国的天文研究逐渐步入国际先进行列。

2016 年 2 月 11 日，美国地基先进激光干涉引力波天文台 LIGO 宣布探测到来自双黑洞并合的引力波辐射，一举证实了广义相对论给出的黑洞和引力波两大预言。2017 年 10 月诺贝尔物理学奖授予 LIGO 的三位奠基者。

2017 年 8 月 17 日，LIGO 和 VIRGO（欧洲“室女座”引力波探测器）共同探测到的引力波事件 GW 170817，是人类首次直接探测到由两颗中子星并合产生的引力波事件。

随后的几秒之内，美国宇航局 Fermi 伽玛射线卫星和欧洲 INTEGRAL 卫星都探测到了一个极弱的短时标伽玛暴 GRB 170817A。全球有几十台天文设备对 GW 170817 开展了后随观测，确定这次的引力波事件发生在距离地球 1.3 亿光年之外的编号为 NGC 4993 的星系中。

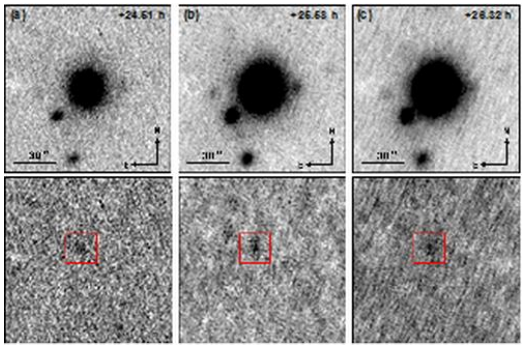

图 1：AST3-2 在 8 月 18 日观测窗口期内引力波光学信号（红色方框内）。

自北京时间 2017 年 8 月 18 日 21:10 起（即距离此次引力波事件发生 24 小时后）,中国南极巡天望远镜 AST3 合作团队利用正在中国南极昆仑站运行的第 2 台望远镜 AST3-2 对 GW 170817 开展了有效的观测，此次观测持续到 8 月 28 日，期间获得了大量的重要数据，并探测到此次引力波事件的光学信号（图 1）。这些数据和全球其他天文台的观测结果一起揭示了此次双中子星并合抛射出 1 %量级太阳质量（超过 3000 个地球质量）的物质，这些物质以 0.3 倍的光速被抛到星际空间，抛射过程中部分物质发生核合成，形成比铁还重的元素。因此，这次引力波光学对应体的发现，证实了双中子星并合事件是宇宙中大部分超重元素（金、银）的起源。

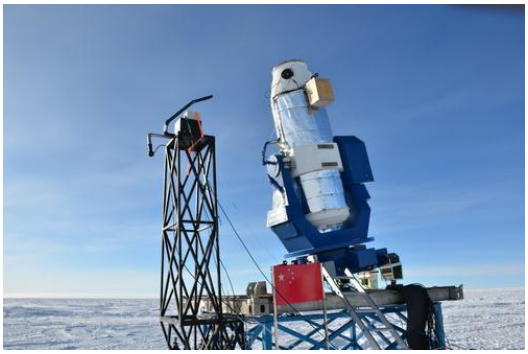

图 2：第二台南极巡天望远镜 AST3-2。

AST3-2 是我国在昆仑站安装的第二台南极巡天望远镜（图 2）。其有效通光口径 50 厘米，是南极现有最大的光学望远镜，并且完全实现了极端环境下的无人值守全自动观测。AST3 望远镜本身就获益于新南威尔士大学所提供的发电系统。在这次对 GW 170817 的观测中，基于中澳天文联合研究中心的双边合作发挥了巨大做用。

ABSTRACT LIST OF PUBLICATIONS IN 2017

I. Dark Matter & Space Astronomy

1-01 Cosmic Gamma Ray Bursts, Neutron Stars, and Relevant Physics

第 1 条 , 共 286 条

A parameterized energy correction method for electromagnetic showers in BGO-ECAL of DAMPE

Yue, C (Yue, Chuan); Zang, JJ (Zang, Jingjing); Dong, TK (Dong, Tiekuang); Li, X (Li, Xiang); Zhang, ZY (Zhang, Zhiyong); Zimmer, S (Zimmer, Stephan); Jiang, W (Jiang, Wei); Zhang, YL (Zhang, Yunlong); Wei, DM (Wei, Daming)
NUCLEAR INSTRUMENTS & METHODS IN PHYSICS RESEARCH SECTION A-ACCELERATORS SPECTROMETERS DETECTORS AND ASSOCIATED EQUIPMENT
卷: 856 页: 11-16
DAMPE is a space-based mission designed as a high energy particle detector measuring cosmic-rays and gamma-rays which was successfully launched on Dec.17, 2015. The BGO electromagnetic calorimeter is one of the key sub detectors of DAMPE for energy measurement of electromagnetic showers produced by e(+/-)/gamma. Due to energy loss in dead material and energy leakage outside the calorimeter, the deposited energy in BGO underestimates the primary energy of incident e(+/-)/gamma In this paper, based on detailed MC simulations, a parameterized energy correction method using the lateral and longitudinal information of electromagnetic showers has been studied and verified with data of electron beam test at CERN. The measurements of energy linearity and resolution are significant improved by applying this correction method for electromagnetic showers.

第 2 条 , 共 286 条

Revealing Physical Activity of GRB Central Engine with Macronova/Kilonova Data

Shen, ZQ (Shen, Zhao-Qiang); Jin, ZP (Jin, Zhi-Ping); Liang, YF (Liang, Yun-Feng); Li, X (Li, Xiang); Fan, YZ (Fan, Yi-Zhong); Wei, DM (Wei, Da-Ming)
ASTROPHYSICAL JOURNAL LETTERS
卷: 835 期: 2 文献号: L22
The modeling of Li-Paczynski macronova/kilonova signals gives a reasonable estimate on the neutron-rich material ejected during the neutron star mergers. Usually the accretion disk is more massive than the macronova ejecta, with which the efficiencies of converting the disk mass into prompt emission of three merger-driven GRBs can hence be directly constrained. Supposing the macronovae/kilonovae associated with GRB 050709, GRB 060614, and GRB 130603B arose from radioactive decay of the r-process material, the upper limit on energy conversion efficiencies are found to be as low as similar to 10(-6) -10(-4). Moreover, for all three events, neutrino annihilation is likely powerful enough to account for the brief gamma-ray flashes. Neutrino annihilation can also explain the "extended" emission lasting similar to 100 s in GRB 050709, but does not work for the one in GRB 060614. These progresses demonstrate that the macronova can serve as a novel probe of the central engine activity.

第 3 条 , 共 286 条

GRB 111005A at z=0.0133 and the Prospect of Establishing Long-Short GRB/GW Association

Wang, YZ (Wang, Yuan-Zhu); Huang, YJ (Huang, Yong-Jia); Liang, YF (Liang, Yun-Feng); Li, X (Li, Xiang); Jin, ZP (Jin, Zhi-Ping); Zhang, FW (Zhang, Fu-Wen); Zou, YC (Zou, Yuan-Chuan); Fan, YZ (Fan, Yi-Zhong); Wei, DM (Wei, Da-Ming)
ASTROPHYSICAL JOURNAL LETTERS
卷: 851 期: 1 文献号: L20
GRB 111005A, a long-duration gamma-ray burst (GRB) that occurred within a metal-rich environment that lacks massive stars with MZAMS >= 15M(circle dot), is not coincident with supernova emission down to a stringent limit and thus should be classified as a "long-short" GRB (lsGRB; also known as an SN-less long GRB or hybrid GRB), like GRB 060505 and GRB 060614. In this work, we show that in the neutron star merger model the non-detection of the optical/infrared emission of GRB 111005A requires sub-relativistic neutron-rich ejecta with a mass of <= 0.01 M-circle dot, which is (significantly) less massive than that of GRB 130603B, GRB 060614, GRB 050709, and GRB 170817A. The lsGRBs are found to have a high rate density and the neutron star merger origin model can be unambiguously tested by the joint observations of the second-generation gravitational-wave (GW) detectors and the full-sky gamma-ray monitors such as Fermi-GBM and the proposed GECAM. If no lsGRB/GW association is observed in the 2020s, alternative scenarios have to be systematically investigated. With the detailed environmental information achievable for the nearby events, a novel kind of merger or explosion origin may be identified.

第 4 条 , 共 286 条

Multi-messenger Observations of a Binary Neutron Star Merger

Abbott, BP (Abbott, B. P.); Abbott, R (Abbott, R.); Abbott, TD (Abbott, T. D.); Acernese, F (Acernese, F.); Ackley, K (Ackley, K.); Adams, C (Adams, C.); Adams, T (Adams, T.); Addesso, P (Addesso, P.); Adhikari, RX (Adhikari, R. X.); Adya, VB (Adya, V. B.); Affeldt, C (Affeldt, C.); Afrough, M (Afrough, M.); Agarwal, B (Agarwal, B.); Agathos, M (Agathos, M.); Agatsuma, K (Agatsuma, K.); Aggarwal, N (Aggarwal, N.); Aguiar, OD (Aguiar, O. D.); Aiello, L (Aiello, L.); Ain, A (Ain, A.); Ajith, P (Ajith, P.); Allen, B (Allen, B.); Allen, G (Allen, G.); Allocca, A (Allocca, A.); Altin, PA (Altin, P. A.); Amato, A (Amato, A.); Ananyeva, A (Ananyeva, A.); Anderson, SB (Anderson, S. B.); Anderson, WG (Anderson, W. G.); Angelova, SV (Angelova, S. V.); Antier, S (Antier, S.); Appert, S (Appert, S.); Arai, K (Arai, K.); Araya, MC (Araya, M. C.); Areeda, JS (Areeda, J. S.); Arnaud, N (Arnaud, N.); Arun, KG (Arun, K. G.); Ascenzi, S (Ascenzi, S.); Ashton, G (Ashton, G.); Ast, M (Ast, M.); Aston, SM (Aston, S. M.); Astone,

P (Astone, P.); Atallah, DV (Atallah, D. V.); Aufmuth, P (Aufmuth, P.); Aulbert, C (Aulbert, C.); AultONeal, K (AultONeal, K.); Austin, C (Austin, C.); Avila-Alvarez, A (Avila-Alvarez, A.); Babak, S (Babak, S.); Bacon, P (Bacon, P.); Bader, MKM (Bader, M. K. M.); Bae, S (Bae, S.); Baker, PT (Baker, P. T.); Baldaccini, F (Baldaccini, F.); Ballardin, G (Ballardin, G.); Ballmer, SW (Ballmer, S. W.); Banagiri, S (Banagiri, S.); Barayoga, JC (Barayoga, J. C.); Barclay, SE (Barclay, S. E.); Barish, BC (Barish, B. C.); Barker, D (Barker, D.); Barkett, K (Barkett, K.); Barone, F (Barone, F.); Barr, B (Barr, B.); Barsotti, L (Barsotti, L.); Barsuglia, M (Barsuglia, M.); Barta, D (Barta, D.); Barthelmy, SD (Barthelmy, S. D.); Bartlett, J (Bartlett, J.); Bartos, I (Bartos, I.); Bassiri, R (Bassiri, R.); Basti, A (Basti, A.); Batch, JC (Batch, J. C.); Bawaj, M (Bawaj, M.); Bayley, JC (Bayley, J. C.); Bazzan, M (Bazzan, M.); Becsy, B (Becsy, B.); Beer, C (Beer, C.); Bejger, M (Bejger, M.); Belahcene, I (Belahcene, I.); Bell, AS (Bell, A. S.); Berger, BK (Berger, B. K.); Bergmann, G (Bergmann, G.); Bero, JJ (Bero, J. J.); Berry, CPL (Berry, C. P. L.); Bersanetti, D (Bersanetti, D.); Bertolini, A (Bertolini, A.); Betzwieser, J (Betzwieser, J.); Bhagwat, S (Bhagwat, S.); Bhandare, R (Bhandare, R.); Bilenko, IA (Bilenko, I. A.); Billingsley, G (Billingsley, G.); Billman, CR (Billman, C. R.); Birch, J (Birch, J.); Birney, R (Birney, R.); Birnholtz, O (Birnholtz, O.); Biscans, S (Biscans, S.); Biscoveanu, S (Biscoveanu, S.); Bisht, A (Bisht, A.); Bitossi, M (Bitossi, M.); Biwer, C (Biwer, C.); Bizouard, MA (Bizouard, M. A.); Blackburn, JK (Blackburn, J. K.); Blackman, J (Blackman, J.); Blair, CD (Blair, C. D.); Blair, DG (Blair, D. G.); Blair, RM (Blair, R. M.); Bloemen, S (Bloemen, S.); Bock, O (Bock, O.); Bode, N (Bode, N.); Boer, M (Boer, M.); Bogaert, G (Bogaert, G.); Bohe, A (Bohe, A.); Bondu, F (Bondu, F.); Bonilla, E (Bonilla, E.); Bonnand, R (Bonnand, R.); Boom, BA (Boom, B. A.); Bork, R (Bork, R.); Boschi, V (Boschi, V.); Bose, S (Bose, S.); Bossie, K (Bossie, K.); Bouffanais, Y (Bouffanais, Y.); Bozzi, A (Bozzi, A.); Bradaschia, C (Bradaschia, C.); Brady, PR (Brady, P. R.); Branchesi, M (Branchesi, M.); Brau, JE (Brau, J. E.); Briant, T (Briant, T.); Brillet, A (Brillet, A.); Brinkmann, M (Brinkmann, M.); Brisson, V (Brisson, V.); Brockill, P (Brockill, P.); Broida, JE (Broida, J. E.); Brooks, AF (Brooks, A. F.); Brown, DA (Brown, D. A.); Brown, DD (Brown, D. D.); Brunett, S (Brunett, S.); Buchanan, CC (Buchanan, C. C.); Buikema, A (Buikema, A.); Bulik, T (Bulik, T.); Bulten, HJ (Bulten, H. J.); Buonanno, A (Buonanno, A.); Buskulic, D (Buskulic, D.); Buy, C (Buy, C.); Byer, RL (Byer, R. L.); Cabero, M (Cabero, M.); Cadonati, L (Cadonati, L.); Cagnoli, G (Cagnoli, G.); Cahillane, C (Cahillane, C.); Bustillo, JC (Bustillo, J. Caldern); Callister, TA (Callister, T. A.); Calloni, E (Calloni, E.); Camp, JB (Camp, J. B.); Canepa, M (Canepa, M.); Canizares, P (Canizares, P.); Cannon, KC (Cannon, K. C.); Cao, H (Cao, H.); Cao, J (Cao, J.); Capano, CD (Capano, C. D.); Capocasa, E (Capocasa, E.); Carbognani, F (Carbognani, F.); Caride, S (Caride, S.); Carney, MF (Carney, M. F.); Diaz, JC (Diaz, J. Casanueva); Casentini, C (Casentini, C.); Caudill, S (Caudill, S.); Cavagli, M (Cavagli, M.); Cavalier, F (Cavalier, F.); Cavalieri, R (Cavalieri, R.); Cella, G (Cella, G.); Cepeda, CB (Cepeda, C. B.); Cerd-Durn, P (Cerd-Durn, P.); Cerretani, G (Cerretani, G.); Cesarini, E (Cesarini, E.); Chamberlin, SJ (Chamberlin, S. J.); Chan, M (Chan, M.); Chao, S (Chao, S.); Charlton, P (Charlton, P.); Chase, E (Chase, E.); Chassande-Mottin, E (Chassande-Mottin, E.); Chatterjee, D (Chatterjee, D.); Chatziioannou, K (Chatziioannou, K.); Cheeseboro, BD (Cheeseboro, B. D.); Chen, HY (Chen, H. Y.); Chen, X (Chen, X.); Chen, Y (Chen, Y.); Cheng, HP (Cheng, H. -P.); Chia, H (Chia, H.); Chincarini, A (Chincarini, A.); Chiummo, A (Chiummo, A.); Chmiel, T (Chmiel, T.); Cho, HS (Cho, H. S.); Cho, M (Cho, M.); Chow, JH (Chow, J. H.); Christensen, N (Christensen, N.); Chu, Q (Chu, Q.); Chua, AJK (Chua, A. J. K.); Chua, S (Chua, S.); Chung, AKW (Chung, A. K. W.); Chung, S (Chung, S.); Ciani, G (Ciani, G.); Ciolfi, R (Ciolfi, R.); Cirelli, CE (Cirelli, C. E.); Cirone, A (Cirone, A.); Clara, F (Clara, F.); Clark, JA (Clark, J. A.); Clearwater, P (Clearwater, P.); Cleva, F (Cleva, F.); Cocchieri, C (Cocchieri, C.); Coccia, E (Coccia, E.); Cohadon, PF (Cohadon, P. -F.); Cohen, D (Cohen, D.); Colla, A (Colla, A.); Collette, CG (Collette, C. G.); Cominsky, LR (Cominsky, L. R.); Constancio, M (Constancio, M.); Conti, L (Conti, L.); Cooper, SJ (Cooper, S. J.); Corban, P (Corban, P.); Corbitt, TR (Corbitt, T. R.); Cordero-Carrion, I (Cordero-Carrion, I.); Corley, KR (Corley, K. R.); Cornish, N (Cornish, N.); Corsi, A (Corsi, A.); Cortese, S (Cortese, S.); Costa, CA (Costa, C. A.); Coughlin, MW (Coughlin, M. W.); Coughlin, SB (Coughlin, S. B.); Coulon, JP (Coulon, J. -P.); Countryman, ST (Countryman, S. T.); Couvares, P (Couvares, P.); Covas, PB (Covas, P. B.); Cowan, EE (Cowan, E. E.); Coward, DM (Coward, D. M.); Cowart, MJ (Cowart, M. J.); Coyne, DC (Coyne, D. C.); Coyne, R (Coyne, R.); Creighton, JDE (Creighton, J. D. E.); Creighton, TD (Creighton, T. D.); Cripe, J (Cripe, J.); Crowder, SG (Crowder, S. G.); Cullen, TJ (Cullen, T. J.); Cumming, A (Cumming, A.); Cunningham, L (Cunningham, L.); Cuoco, E (Cuoco, E.); Dal Canton, T (Dal Canton, T.); Dlya, G (Dlya, G.); Danilishin, SL (Danilishin, S. L.); D'Antonio, S (D'Antonio, S.); Danzmann, K (Danzmann, K.); Dasgupta, A (Dasgupta, A.); Costa, CFDS (Costa, C. F. Da Silva); Dattilo, V (Dattilo, V.); Dave, I (Dave, I.); Davier, M (Davier, M.); Davis, D (Davis, D.); Daw, EJ (Daw, E. J.); Day, B (Day, B.); De, S (De, S.); Debra, D (Debra, D.); Degallaix, J (Degallaix, J.); De Laurentis, M (De laurentis, M.); Deleglise, S (Deleglise, S.); Del Pozzo, W (Del Pozzo, W.); Demos, N (Demos, N.); Denker, T (Denker, T.); Dent, T (Dent, T.); De Pietri, R (De Pietri, R.); Dergachev, V (Dergachev, V.); De Rosa, R (De Rosa, R.); DeRosa, RT (DeRosa, R. T.); De Rossi, C (De Rossi, C.); DeSalvo, R (DeSalvo, R.); De Varona, O (De Varona, O.); Devenson, J (Devenson, J.); Dhurandhar, S (Dhurandhar, S.); Diaz, MC (Diaz, M. C.); Di Fiore, L (Di Fiore, L.); Di Giovanni, M (Di Giovanni, M.); Di Girolamo, T (Di Girolamo, T.); Di Lieto, A (Di Lieto, A.); Di Pace, S (Di Pace, S.); Di Palma, I (Di Palma, I.); Di Renzo, F (Di Renzo, F.); Doctor, Z (Doctor, Z.); Dolique, V (Dolique, V.); Donovan, F (Donovan, F.); Dooley, KL (Dooley, K. L.); Doravari, S (Doravari, S.); Dorrington, I (Dorrington, I.); Douglas, R (Douglas, R.); Alvarez, MD (Alvarez, M. Dovale); Downes, TP (Downes, T. P.); Drago, M (Drago, M.); Dreissigacker, C (Dreissigacker, C.); Driggers, JC (Driggers, J. C.); Du, Z (Du, Z.); Ducrot, M (Ducrot, M.); Dupej, P (Dupej, P.); Dwyer, SE (Dwyer, S. E.); Edo, TB (Edo, T. B.); Edwards, MC (Edwards, M. C.); Effler, A (Effler, A.); Eggenstein, HB (Eggenstein, H. -B.); Ehrens, P (Ehrens, P.); Eichholz, J (Eichholz, J.); Eikenberry, SS (Eikenberry, S. S.); Eisenstein, RA (Eisenstein, R. A.); Essick, RC (Essick, R. C.); Estevez, D (Estevez, D.); Etienne, ZB (Etienne, Z. B.); Etzel, T (Etzel, T.); Evans, M (Evans, M.); Evans, TM (Evans, T. M.); Factourovich, M (Factourovich, M.); Fafone, V (Fafone, V.); Fair, H (Fair, H.); Fairhurst, S (Fairhurst, S.); Fan, X (Fan, X.); Farinon, S (Farinon, S.); Farr, B (Farr, B.); Farr, WM (Farr, W. M.); Fauchon-Jones, EJ (Fauchon-Jones, E. J.); Favata, M (Favata, M.); Fays, M (Fays, M.); Fee, C (Fee, C.); Fehrmann, H (Fehrmann, H.); Feicht, J (Feicht, J.); Fejer, MM (Fejer, M. M.); Fernandez-Galiana, A (Fernandez-Galiana, A.); Ferrante, I (Ferrante, I.); Ferreira, EC (Ferreira, E. C.); Ferrini, F (Ferrini, F.); Fidecaro, F (Fidecaro, F.); Finstad, D (Finstad, D.); Fiori, I (Fiori, I.); Fiorucci, D (Fiorucci, D.); Fishbach, M (Fishbach, M.); Fisher, RP (Fisher, R. P.); Fitz-Axen, M (Fitz-Axen, M.); Flaminio, R (Flaminio, R.); Fletcher, M (Fletcher, M.); Fong, H (Fong, H.); Font, JA (Font, J. A.); Forsyth, PWF (Forsyth, P. W. F.); Forsyth, SS (Forsyth, S. S.); Fournier, JD (Fournier, J. -D.); Frasca, S (Frasca, S.); Frasconi, F (Frasconi, F.); Frei, Z (Frei, Z.); Freise, A (Freise, A.); Frey, R (Frey, R.); Frey, V (Frey, V.); Fries, EM (Fries, E. M.); Fritschel, P (Fritschel, P.); Frolov, VV (Frolov, V. V.); Fulda, P (Fulda, P.); Fyffe, M (Fyffe, M.); Gabbard, H (Gabbard, H.); Gadre, BU (Gadre, B. U.); Gaebel, SM (Gaebel, S. M.); Gair, JR (Gair, J. R.); Gammaitoni, L (Gammaitoni, L.); Ganija, MR (Ganija, M. R.); Gaonkar, SG (Gaonkar, S. G.); Garcia-Quiros, C (Garcia-Quiros, C.); Garufi, F (Garufi, F.); Gateley, B (Gateley, B.); Gaudio, S (Gaudio, S.); Gaur, G (Gaur, G.); Gayathri, V (Gayathri,

V.); Gehrels, N (Gehrels, N.); Gemme, G (Gemme, G.); Genin, E (Genin, E.); Gennai, A (Gennai, A.); George, D (George, D.); George, J (George, J.); Gergely, L (Gergely, L.); Germain, V (Germain, V.); Ghonge, S (Ghonge, S.); Ghosh, A (Ghosh, Abhirup); Ghosh, A (Ghosh, Archisman); Ghosh, S (Ghosh, S.); Giaime, JA (Giaime, J. A.); Giardina, KD (Giardina, K. D.); Giazotto, A (Giazotto, A.); Gill, K (Gill, K.); Glover, L (Glover, L.); Goetz, E (Goetz, E.); Goetz, R (Goetz, R.); Gomes, S (Gomes, S.); Goncharov, B (Goncharov, B.); Gonzlez, G (Gonzlez, G.); Castro, JMG (Castro, J. M. Gonzalez); Gopakumar, A (Gopakumar, A.); Gorodetsky, ML (Gorodetsky, M. L.); Gossan, SE (Gossan, S. E.); Gosselin, M (Gosselin, M.); Gouaty, R (Gouaty, R.); Grado, A (Grado, A.); Graef, C (Graef, C.); Granata, M (Granata, M.); Grant, A (Grant, A.); Gras, S (Gras, S.); Gray, C (Gray, C.); Greco, G (Greco, G.); Green, AC (Green, A. C.); Gretarsson, EM (Gretarsson, E. M.); Griswold, B (Griswold, B.); Groot, P (Groot, P.); Grote, H (Grote, H.); Grunewald, S (Grunewald, S.); Gruning, P (Gruning, P.); Guidi, GM (Guidi, G. M.); Guo, X (Guo, X.); Gupta, A (Gupta, A.); Gupta, MK (Gupta, M. K.); Gushwa, KE (Gushwa, K. E.); Gustafson, EK (Gustafson, E. K.); Gustafson, R (Gustafson, R.); Halim, O (Halim, O.); Hall, BR (Hall, B. R.); Hall, ED (Hall, E. D.); Hamilton, EZ (Hamilton, E. Z.); Hammond, G (Hammond, G.); Haney, M (Haney, M.); Hanke, MM (Hanke, M. M.); Hanks, J (Hanks, J.); Hanna, C (Hanna, C.); Hannam, MD (Hannam, M. D.); Hannuksela, OA (Hannuksela, O. A.); Hanson, J (Hanson, J.); Hardwick, T (Hardwick, T.); Harms, J (Harms, J.); Harry, GM (Harry, G. M.); Harry, IW (Harry, I. W.); Hart, MJ (Hart, M. J.); Haster, CJ (Haster, C. -J.); Haughian, K (Haughian, K.); Healy, J (Healy, J.); Heidmann, A (Heidmann, A.); Heintze, MC (Heintze, M. C.); Heitmann, H (Heitmann, H.); Hello, P (Hello, P.); Hemming, G (Hemming, G.); Hendry, M (Hendry, M.); Heng, IS (Heng, I. S.); Hennig, J (Hennig, J.); Heptonstall, AW (Heptonstall, A. W.); Heurs, M (Heurs, M.); Hild, S (Hild, S.); Hinderer, T (Hinderer, T.); Hoak, D (Hoak, D.); Hofman, D (Hofman, D.); Holt, K (Holt, K.); Holz, DE (Holz, D. E.); Hopkins, P (Hopkins, P.); Horst, C (Horst, C.); Hough, J (Hough, J.); Houston, EA (Houston, E. A.); Howell, EJ (Howell, E. J.); Hreibi, A (Hreibi, A.); Hu, YM (Hu, Y. M.); Huerta, EA (Huerta, E. A.); Huet, D (Huet, D.); Hughey, B (Hughey, B.); Husa, S (Husa, S.); Huttner, SH (Huttner, S. H.); Huynh-Dinh, T (Huynh-Dinh, T.); Indik, N (Indik, N.); Inta, R (Inta, R.); Intini, G (Intini, G.); Isa, HN (Isa, H. N.); Isac, JM (Isac, J. -M.); Isi, M (Isi, M.); Iyer, BR (Iyer, B. R.); Izumi, K (Izumi, K.); Jacqmin, T (Jacqmin, T.); Jani, K (Jani, K.); Jaranowski, P (Jaranowski, P.); Jawahar, S (Jawahar, S.); Jimenez-Forteza, F (Jimenez-Forteza, F.); Johnson, WW (Johnson, W. W.); Jones, DI (Jones, D. I.); Jones, R (Jones, R.); Jonker, RJG (Jonker, R. J. G.); Ju, L (Ju, L.); Junker, J (Junker, J.); Kalaghatgi, CV (Kalaghatgi, C. V.); Kalogera, V (Kalogera, V.); Kamai, B (Kamai, B.); Kandhasamy, S (Kandhasamy, S.); Kang, G (Kang, G.); Kanner, JB (Kanner, J. B.); Kapadia, SJ (Kapadia, S. J.); Karki, S (Karki, S.); Karvinen, KS (Karvinen, K. S.); Kasprzack, M (Kasprzack, M.); Katolik, M (Katolik, M.); Katsavounidis, E (Katsavounidis, E.); Katzman, W (Katzman, W.); Kaufer, S (Kaufer, S.); Kawabe, K (Kawabe, K.); Kefelian, F (Kefelian, F.); Keitel, D (Keitel, D.); Kemball, AJ (Kemball, A. J.); Kennedy, R (Kennedy, R.); Kent, C (Kent, C.); Key, JS (Key, J. S.); Khalili, FY (Khalili, F. Y.); Khan, I (Khan, I.); Khan, S (Khan, S.); Khan, Z (Khan, Z.); Khazanov, EA (Khazanov, E. A.); Kijbunchoo, N (Kijbunchoo, N.); Kim, C (Kim, Chunglee); Kim, JC (Kim, J. C.); Kim, K (Kim, K.); Kim, W (Kim, W.); Kim, WS (Kim, W. S.); Kim, YM (Kim, Y. -M.); Kimbrell, SJ (Kimbrell, S. J.); King, EJ (King, E. J.); King, PJ (King, P. J.); Kinley-Hanlon, M (Kinley-Hanlon, M.); Kirchhoff, R (Kirchhoff, R.); Kissel, JS (Kissel, J. S.); Kleybolte, L (Kleybolte, L.); Klimenko, S (Klimenko, S.); Knowles, TD (Knowles, T. D.); Koch, P (Koch, P.); Koehlenbeck, SM (Koehlenbeck, S. M.); Koley, S (Koley, S.); Kondrashov, V (Kondrashov, V.); Kontos, A (Kontos, A.); Korobko, M (Korobko, M.); Korth, WZ (Korth, W. Z.); Kowalska, I (Kowalska, I.); Kozak, DB (Kozak, D. B.); Krmer, C (Krmer, C.); Kringel, V (Kringel, V.); Krishnan, B (Krishnan, B.); Krlak, A (Krlak, A.); Kuehn, G (Kuehn, G.); Kumar, P (Kumar, P.); Kumar, R (Kumar, R.); Kumar, S (Kumar, S.); Kuo, L (Kuo, L.); Kutynia, A (Kutynia, A.); Kwang, S (Kwang, S.); Lackey, BD (Lackey, B. D.); Lai, KH (Lai, K. H.); Landry, M (Landry, M.); Lang, RN (Lang, R. N.); Lange, J (Lange, J.); Lantz, B (Lantz, B.); Lanza, RK (Lanza, R. K.); Larson, SL (Larson, S. L.); Lartaux-Vollard, A (Lartaux-Vollard, A.); Lasky, PD (Lasky, P. D.); Laxen, M (Laxen, M.); Lazzarini, A (Lazzarini, A.); Lazzaro, C (Lazzaro, C.); Leaci, P (Leaci, P.); Leavey, S (Leavey, S.); Lee, CH (Lee, C. H.); Lee, HK (Lee, H. K.); Lee, HM (Lee, H. M.); Lee, HW (Lee, H. W.); Lee, K (Lee, K.); Lehmann, J (Lehmann, J.); Lenon, A (Lenon, A.); Leonardi, M (Leonardi, M.); Leroy, N (Leroy, N.); Letendre, N (Letendre, N.); Levin, Y (Levin, Y.); Li, TGF (Li, T. G. F.); Linker, SD (Linker, S. D.); Littenberg, TB (Littenberg, T. B.); Liu, J (Liu, J.); Lo, RKL (Lo, R. K. L.); Lockerbie, NA (Lockerbie, N. A.); London, LT (London, L. T.); Lord, JE (Lord, J. E.); Lorenzini, M (Lorenzini, M.); Loriette, V (Loriette, V.); Lormand, M (Lormand, M.); Losurdo, G (Losurdo, G.); Lough, JD (Lough, J. D.); Lousto, CO (Lousto, C. O.); Lovelace, G (Lovelace, G.); Lck, H (Lck, H.); Lumaca, D (Lumaca, D.); Lundgren, AP (Lundgren, A. P.); Lynch, R (Lynch, R.); Ma, Y (Ma, Y.); Macas, R (Macas, R.); Macfoy, S (Macfoy, S.); Machenschalk, B (Machenschalk, B.); MacInnis, M (MacInnis, M.); Macleod, DM (Macleod, D. M.); Hernandez, IM (Hernandez, I. Magaa); Magaa-Sandoval, F (Magaa-Sandoval, F.); Zertuche, LM (Zertuche, L. Magaa); Magee, RM (Magee, R. M.); Majorana, E (Majorana, E.); Maksimovic, I (Maksimovic, I.); Man, N (Man, N.); Mandic, V (Mandic, V.); Mangano, V (Mangano, V.); Mansell, GL (Mansell, G. L.); Manske, M (Manske, M.); Mantovani, M (Mantovani, M.); Marchesoni, F (Marchesoni, F.); Marion, F (Marion, F.); Mrka, S (Mrka, S.); Mrka, Z (Mrka, Z.); Markakis, C (Markakis, C.); Markosyan, AS (Markosyan, A. S.); Markowitz, A (Markowitz, A.); Maros, E (Maros, E.); Marquina, A (Marquina, A.); Marsh, P (Marsh, P.); Martelli, F (Martelli, F.); Martellini, L (Martellini, L.); Martin, IW (Martin, I. W.); Martin, RM (Martin, R. M.); Martynov, DV (Martynov, D. V.); Mason, K (Mason, K.); Massera, E (Massera, E.); Masserot, A (Masserot, A.); Massinger, TJ (Massinger, T. J.); Masso-Reid, M (Masso-Reid, M.); Mastrogiovanni, S (Mastrogiovanni, S.); Matas, A (Matas, A.); Matichard, F (Matichard, F.); Matone, L (Matone, L.); Mavalvala, N (Mavalvala, N.); Mazumder, N (Mazumder, N.); McCarthy, R (McCarthy, R.); McClelland, DE (McClelland, D. E.); McCormick, S (McCormick, S.); McCuller, L (McCuller, L.); McGuire, SC (McGuire, S. C.); McIntyre, G (McIntyre, G.); McIver, J (McIver, J.); McManus, DJ (McManus, D. J.); McNeill, L (McNeill, L.); Mcrae, T (Mcrae, T.); McWilliams, ST (McWilliams, S. T.); Meacher, D (Meacher, D.); Meadors, GD (Meadors, G. D.); Mehmet, M (Mehmet, M.); Meidam, J (Meidam, J.); Mejuto-Villa, E (Mejuto-Villa, E.); Melatos, A (Melatos, A.); Mendell, G (Mendell, G.); Mercer, RA (Mercer, R. A.); Merilh, EL (Merilh, E. L.); Merzougui, M (Merzougui, M.); Meshkov, S (Meshkov, S.); Messenger, C (Messenger, C.); Messick, C (Messick, C.); Metzdorff, R (Metzdorff, R.); Meyers, PM (Meyers, P. M.); Miao, H (Miao, H.); Michel, C (Michel, C.); Middleton, H (Middleton, H.); Mikhailov, EE (Mikhailov, E. E.); Milano, L (Milano, L.); Muller, AL (Mueller, A. L.); Muller, BB (Mueller, B. B.); Miller, J (Miller, J.); Millhouse, M (Millhouse, M.); Milovich-Goff, MC (Milovich-Goff, M. C.); Minazzoli, O (Minazzoli, O.); Minenkov, Y (Minenkov, Y.); Ming, J (Ming, J.); Mishra, C (Mishra, C.); Mitra, S (Mitra, S.); Mitrofanov, VP (Mitrofanov, V. P.); Mitselmakher, G (Mitselmakher, G.); Mittleman, R (Mittleman, R.); Moffa, D (Moffa, D.); Moggi, A (Moggi, A.); Mogushi, K (Mogushi, K.); Mohan, M (Mohan, M.); Mohapatra, SRP (Mohapatra, S. R. P.); Montani, M (Montani, M.); Moore, CJ (Moore, C. J.); Moraru, D (Moraru, D.); Moreno, G (Moreno, G.); Morriss, SR (Morriss, S. R.); Mours, B (Mours, B.); Mow-Lowry, CM (Mow-Lowry, C. M.); Mueller, G (Mueller, G.); Muir, AW (Muir, A. W.); Mukherjee, A (Mukherjee,

Arunava); Mukherjee, D (Mukherjee, D.); Mukherjee, S (Mukherjee, S.); Mukund, N (Mukund, N.); Mullavey, A (Mullavey, A.); Munch, J (Munch, J.); Muiz, EA (Muniz, E. A.); Muratore, M (Muratore, M.); Murray, PG (Murray, P. G.); Napier, K (Napier, K.); Nardecchia, I (Nardecchia, I.); Naticchioni, L (Naticchioni, L.); Nayak, RK (Nayak, R. K.); Neilson, J (Neilson, J.); Nelemans, G (Nelemans, G.); Nelson, TJN (Nelson, T. J. N.); Nery, M (Nery, M.); Neunzert, A (Neunzert, A.); Nevin, L (Nevin, L.); Newport, JM (Newport, J. M.); Newton, G (Newton, G.); Ng, KKY (Ng, K. K. Y.); Nguyen, P (Nguyen, P.); Nguyen, TT (Nguyen, T. T.); Nichols, D (Nichols, D.); Nielsen, AB (Nielsen, A. B.); Nissanke, S (Nissanke, S.); Nitz, A (Nitz, A.); Noack, A (Noack, A.); Nocera, F (Nocera, F.); Nolting, D (Nolting, D.); North, C (North, C.); Nuttall, LK (Nuttall, L. K.); Oberling, J (Oberling, J.); O'Dea, GD (O'Dea, G. D.); Ogin, GH (Ogin, G. H.); Oh, JJ (Oh, J. J.); Oh, SH (Oh, S. H.); Ohme, F (Ohme, F.); Okada, MA (Okada, M. A.); Oliver, M (Oliver, M.); Oppermann, P (Oppermann, P.); Oram, RJ (Oram, Richard J.); O'Reilly, B (O'Reilly, B.); Ormiston, R (Ormiston, R.); Ortega, LF (Ortega, L. F.); O'Shaughnessy, R (O'Shaughnessy, R.); Ossokine, S (Ossokine, S.); Ottaway, DJ (Ottaway, D. J.); Overmier, H (Overmier, H.); Owen, BJ (Owen, B. J.); Pace, AE (Pace, A. E.); Page, J (Page, J.); Page, MA (Page, M. A.); Pai, A (Pai, A.); Pai, SA (Pai, S. A.); Palamos, JR (Palamos, J. R.); Palashov, O (Palashov, O.); Palomba, C (Palomba, C.); Pal-Singh, A (Pal-Singh, A.); Pan, H (Pan, Howard); Pan, HW (Pan, Huang-Wei); Pang, B (Pang, B.); Pang, PTH (Pang, P. T. H.); Pankow, C (Pankow, C.); Pannarale, F (Pannarale, F.); Pant, BC (Pant, B. C.); Paoletti, F (Paoletti, F.); Paoli, A (Paoli, A.); Papa, MA (Papa, M. A.); Parida, A (Parida, A.); Parker, W (Parker, W.); Pascucci, D (Pascucci, D.); Pasqualetti, A (Pasqualetti, A.); Passaquieti, R (Passaquieti, R.); Passuello, D (Passuello, D.); Patil, M (Patil, M.); Patricelli, B (Patricelli, B.); Pearlstone, BL (Pearlstone, B. L.); Pedraza, M (Pedraza, M.); Pedurand, R (Pedurand, R.); Pekowsky, L (Pekowsky, L.); Pele, A (Pele, A.); Penn, S (Penn, S.); Perez, CJ (Perez, C. J.); Perreca, A (Perreca, A.); Perri, LM (Perri, L. M.); Pfeiffer, HP (Pfeiffer, H. P.); Phelps, M (Phelps, M.); Piccinni, OJ (Piccinni, O. J.); Pichot, M (Pichot, M.); Piergiovanni, F (Piergiovanni, F.); Pierro, V (Pierro, V.); Pillant, G (Pillant, G.); Pinard, L (Pinard, L.); Pinto, IM (Pinto, I. M.); Pirello, M (Pirello, M.); Pitkin, M (Pitkin, M.); Poe, M (Poe, M.); Poggiani, R (Poggiani, R.); Popolizio, P (Popolizio, P.); Porter, EK (Porter, E. K.); Post, A (Post, A.); Powell, J (Powell, J.); Prasad, J (Prasad, J.); Pratt, JWW (Pratt, J. W. W.); Pratten, G (Pratten, G.); Predoi, V (Predoi, V.); Prestegard, T (Prestegard, T.); Price, LR (Price, L. R.); Prijatelj, M (Prijatelj, M.); Principe, M (Principe, M.); Privitera, S (Privitera, S.); Prodi, GA (Prodi, G. A.); Prokhorov, LG (Prokhorov, L. G.); Puncken, O (Puncken, O.); Punturo, M (Punturo, M.); Puppo, P (Puppo, P.); Prrer, M (Prrer, M.); Qi, H (Qi, H.); Quetschke, V (Quetschke, V.); Quintero, EA (Quintero, E. A.); Quitzow-James, R (Quitzow-James, R.); Raab, FJ (Raab, F. J.); Rabeling, DS (Rabeling, D. S.); Radkins, H (Radkins, H.); Raffai, P (Raffai, P.); Raja, S (Raja, S.); Rajan, C (Rajan, C.); Rajbhandari, B (Rajbhandari, B.); Rakhmanov, M (Rakhmanov, M.); Ramirez, KE (Ramirez, K. E.); Ramos-Buades, A (Ramos-Buades, A.); Rapagnani, P (Rapagnani, P.); Raymond, V (Raymond, V.); Razzano, M (Razzano, M.); Read, J (Read, J.); Regimbau, T (Regimbau, T.); Rei, L (Rei, L.); Reid, S (Reid, S.); Reitze, DH (Reitze, D. H.); Ren, W (Ren, W.); Reyes, SD (Reyes, S. D.); Ricci, F (Ricci, F.); Ricker, PM (Ricker, P. M.); Rieger, S (Rieger, S.); Riles, K (Riles, K.); Rizzo, M (Rizzo, M.); Robertson, NA (Robertson, N. A.); Robie, R (Robie, R.); Robinet, F (Robinet, F.); Rocchi, A (Rocchi, A.); Rolland, L (Rolland, L.); Rollins, JG (Rollins, J. G.); Roma, VJ (Roma, V. J.); Romano, R (Romano, R.); Romel, CL (Romel, C. L.); Romie, JH (Romie, J. H.); Rosinska, D (Rosinska, D.); Ross, MP (Ross, M. P.); Rowan, S (Rowan, S.); Rdiger, A (Rdiger, A.); Ruggi, P (Ruggi, P.); Rutins, G (Rutins, G.); Ryan, K (Ryan, K.); Sachdev, S (Sachdev, S.); Sadecki, T (Sadecki, T.); Sadeghian, L (Sadeghian, L.); Sakellariadou, M (Sakellariadou, M.); Salconi, L (Salconi, L.); Saleem, M (Saleem, M.); Salemi, F (Salemi, F.); Samajdar, A (Samajdar, A.); Sammut, L (Sammut, L.); Sampson, LM (Sampson, L. M.); Sanchez, EJ (Sanchez, E. J.); Sanchez, LE (Sanchez, L. E.); Sanchis-Gual, N (Sanchis-Gual, N.); Sandberg, V (Sandberg, V.); Sanders, JR (Sanders, J. R.); Sassolas, B (Sassolas, B.); Sathyaprakash, BS (Sathyaprakash, B. S.); Saulson, PR (Saulson, P. R.); Sauter, O (Sauter, O.); Savage, RL (Savage, R. L.); Sawadsky, A (Sawadsky, A.); Schale, P (Schale, P.); Scheel, M (Scheel, M.); Scheuer, J (Scheuer, J.); Schmidt, J (Schmidt, J.); Schmidt, P (Schmidt, P.); Schnabel, R (Schnabel, R.); Schofield, RMS (Schofield, R. M. S.); Schonbeck, A (Schonbeck, A.); Schreiber, E (Schreiber, E.); Schuette, D (Schuette, D.); Schulte, BW (Schulte, B. W.); Schutz, BF (Schutz, B. F.); Schwalbe, SG (Schwalbe, S. G.); Scott, J (Scott, J.); Scott, SM (Scott, S. M.); Seidel, E (Seidel, E.); Sellers, D (Sellers, D.); Sengupta, AS (Sengupta, A. S.); Sentenac, D (Sentenac, D.); Sequino, V (Sequino, V.); Sergeev, A (Sergeev, A.); Shaddock, DA (Shaddock, D. A.); Shaffer, TJ (Shaffer, T. J.); Shah, AA (Shah, A. A.); Shahriar, MS (Shahriar, M. S.); Shaner, MB (Shaner, M. B.); Shao, L (Shao, L.); Shapiro, B (Shapiro, B.); Shawhan, P (Shawhan, P.); Sheperd, A (Sheperd, A.); Shoemaker, DH (Shoemaker, D. H.); Shoemaker, DM (Shoemaker, D. M.); Siellez, K (Siellez, K.); Siemens, X (Siemens, X.); Sieniawska, M (Sieniawska, M.); Sigg, D (Sigg, D.); Silva, AD (Silva, A. D.); Singer, LP (Singer, L. P.); Singh, A (Singh, A.); Singhal, A (Singhal, A.); Sintes, AM (Sintes, A. M.); Slagmolen, BJJ (Slagmolen, B. J. J.); Smith, B (Smith, B.); Smith, JR (Smith, J. R.); Smith, RJE (Smith, R. J. E.); Somala, S (Somala, S.); Son, EJ (Son, E. J.); Sonnenberg, JA (Sonnenberg, J. A.); Sorazu, B (Sorazu, B.); Sorrentino, F (Sorrentino, F.); Souradeep, T (Souradeep, T.); Spencer, AP (Spencer, A. P.); Srivastava, AK (Srivastava, A. K.); Staats, K (Staats, K.); Staley, A (Staley, A.); Steinke, M (Steinke, M.); Steinlechner, J (Steinlechner, J.); Steinlechner, S (Steinlechner, S.); Steinmeyer, D (Steinmeyer, D.); Stevenson, SP (Stevenson, S. P.); Stone, R (Stone, R.); Stops, DJ (Stops, D. J.); Strain, KA (Strain, K. A.); Stratta, G (Stratta, G.); Strigin, SE (Strigin, S. E.); Strunk, A (Strunk, A.); Sturani, R (Sturani, R.); Stuver, AL (Stuver, A. L.); Summerscales, TZ (Summerscales, T. Z.); Sun, L (Sun, L.); Sunil, S (Sunil, S.); Suresh, J (Suresh, J.); Sutton, PJ (Sutton, P. J.); Swinkels, BL (Swinkels, B. L.); Szczepanczyk, MJ (Szczepanczyk, M. J.); Tacca, M (Tacca, M.); Tait, SC (Tait, S. C.); Talbot, C (Talbot, C.); Talukder, D (Talukder, D.); Tanner, DB (Tanner, D. B.); Tpai, M (Tpai, M.); Taracchini, A (Taracchini, A.); Tasson, JD (Tasson, J. D.); Taylor, JA (Taylor, J. A.); Taylor, R (Taylor, R.); Tewari, SV (Tewari, S. V.); Theeg, T (Theeg, T.); Thies, F (Thies, F.); Thomas, EG (Thomas, E. G.); Thomas, M (Thomas, M.); Thomas, P (Thomas, P.); Thorne, KA (Thorne, K. A.); Thorne, KS (Thorne, K. S.); Thrane, E (Thrane, E.); Tiwari, S (Tiwari, S.); Tiwari, V (Tiwari, V.); Tokmakov, KV (Tokmakov, K. V.); Toland, K (Toland, K.); Tonelli, M (Tonelli, M.); Tornasi, Z (Tornasi, Z.); Torres-Forn, A (Torres-Forn, A.); Torrie, CI (Torrie, C. I.); Toyr, D (Toyr, D.); Travasso, F (Travasso, F.); Traylor, G (Traylor, G.); Trinastic, J (Trinastic, J.); Tringali, MC (Tringali, M. C.); Trozzo, L (Trozzo, L.); Tsang, KW (Tsang, K. W.); Tse, M (Tse, M.); Tso, R (Tso, R.); Tsukada, L (Tsukada, L.); Tsuna, D (Tsuna, D.); Tuyenbayev, D (Tuyenbayev, D.); Ueno, K (Ueno, K.); Ugolini, D (Ugolini, D.); Unnikrishnan, CS (Unnikrishnan, C. S.); Urban, AL (Urban, A. L.); Usman, SA (Usman, S. A.); Vahlbruch, H (Vahlbruch, H.); Vajente, G (Vajente, G.); Valdes, G (Valdes, G.); Van Bakel, N (Van Bakel, N.); Van Beuzekom, M (Van Beuzekom, M.); van den Brand, JFJ (van den Brand, J. F. J.); van den Broeck, C (van den Broeck, C.); Vander-Hyde, DC (Vander-Hyde, D. C.); van der Schaaf, L (van der Schaaf, L.); van Heijningen, JV (van Heijningen, J. V.); van Veggel, AA (van Veggel, A. A.); Vardaro, M (Vardaro, M.); Varma, V (Varma, V.); Vass, S (Vass, S.); Vasuth, M (Vasuth, M.); Vecchio, A (Vecchio, A.); Vedovato, G (Vedovato, G.); Veitch, J (Veitch, J.); Veitch, PJ (Veitch, P. J.); Venkateswara, K (Venkateswara, K.); Venugopalan, G (Venugopalan, G.);

Verkindt, D (Verkindt, D.); Vetro, F (Vetro, F.); Vicere, A (Vicere, A.); Viets, AD (Viets, A. D.); Vinciguerra, S (Vinciguerra, S.); Vine, DJ (Vine, D. J.); Vinet, JY (Vinet, J. Y.); Vitale, S (Vitale, S.); Vo, T (Vo, T.); Vocca, H (Vocca, H.); Vorvick, C (Vorvick, C.); Vyatchanin, SP (Vyatchanin, S. P.); Wade, AR (Wade, A. R.); Wade, LE (Wade, L. E.); Wade, M (Wade, M.); Walet, R (Walet, R.); Walker, M (Walker, M.); Wallace, L (Wallace, L.); Walsh, S (Walsh, S.); Wang, G (Wang, G.); Wang, H (Wang, H.); Wang, JZ (Wang, J. Z.); Wang, WH (Wang, W. H.); Wang, YF (Wang, Y. F.); Ward, RL (Ward, R. L.); Warner, J (Warner, J.); Was, M (Was, M.); Watchi, J (Watchi, J.); Weaver, B (Weaver, B.); Wei, LW (Wei, L. -W.); Weinert, M (Weinert, M.); Weinstein, AJ (Weinstein, A. J.); Weiss, R (Weiss, R.); Wen, L (Wen, L.); Wessel, EK (Wessel, E. K.); Wessels, P (Wessels, P.); Westerweck, J (Westerweck, J.); Westphal, T (Westphal, T.); Wette, K (Wette, K.); Whelan, JT (Whelan, J. T.); Whitcomb, SE (Whitcomb, S. E.); Whiting, BF (Whiting, B. F.); Whittle, C (Whittle, C.); Wilken, D (Wilken, D.); Williams, D (Williams, D.); Williams, RD (Williams, R. D.); Williamson, AR (Williamson, A. R.); Willis, JL (Willis, J. L.); Willke, B (Willke, B.); Wimmer, MH (Wimmer, M. H.); Winkler, W (Winkler, W.); Wipf, CC (Wipf, C. C.); Wittel, H (Wittel, H.); Woan, G (Woan, G.); Woehler, J (Woehler, J.); Wofford, J (Wofford, J.); Wong, KWK (Wong, K. W. K.); Worden, J (Worden, J.); Wright, JL (Wright, J. L.); Wu, DS (Wu, D. S.); Wysocki, DM (Wysocki, D. M.); Xiao, S (Xiao, S.); Yamamoto, H (Yamamoto, H.); Yancey, CC (Yancey, C. C.); Yang, L (Yang, L.); Yap, MJ (Yap, M. J.); Yazback, M (Yazback, M.); Yu, H (Yu, Hang); Yu, H (Yu, Haocun); Yvert, M (Yvert, M.); Zadrozny, A (Zadrozny, A.); Zanolin, M (Zanolin, M.); Zelenova, T (Zelenova, T.); Zendri, JP (Zendri, J. -P.); Zevin, M (Zevin, M.); Zhang, L (Zhang, L.); Zhang, M (Zhang, M.); Zhang, T (Zhang, T.); Zhang, YH (Zhang, Y. -H.); Zhao, C (Zhao, C.); Zhou, M (Zhou, M.); Zhou, Z (Zhou, Z.); Zhu, SJ (Zhu, S. J.); Zhu, XJ (Zhu, X. J.); Zimmerman, AB (Zimmerman, A. B.); Zucker, ME (Zucker, M. E.); Zweizig, J (Zweizig, J.); Wilson-Hodge, CA (Wilson-Hodge, C. A.); Bissaldi, E (Bissaldi, E.); Blackburn, L (Blackburn, L.); Briggs, MS (Briggs, M. S.); Burns, E (Burns, E.); Cleveland, WH (Cleveland, W. H.); Connaughton, V (Connaughton, V.); Gibby, MH (Gibby, M. H.); Giles, MM (Giles, M. M.); Goldstein, A (Goldstein, A.); Hamburg, R (Hamburg, R.); Jenke, P (Jenke, P.); Hui, CM (Hui, C. M.); Kippen, RM (Kippen, R. M.); Kocevski, D (Kocevski, D.); McBreen, S (McBreen, S.); Meegan, CA (Meegan, C. A.); Paciesas, WS (Paciesas, W. S.); Poolakkil, S (Poolakkil, S.); Preece, RD (Preece, R. D.); Racusin, J (Racusin, J.); Roberts, OJ (Roberts, O. J.); Stanbro, M (Stanbro, M.); Veres, P (Veres, P.); von Kienlin, A (von Kienlin, A.); Savchenko, V (Savchenko, V.); Ferrigno, C (Ferrigno, C.); Kuulkers, E (Kuulkers, E.); Bazzano, A (Bazzano, A.); Bozzo, E (Bozzo, E.); Brandt, S (Brandt, S.); Chenevez, J (Chenevez, J.); Courvoisier, TJL (Courvoisier, T. J. -L.); Diehl, R (Diehl, R.); Domingo, A (Domingo, A.); Hanlon, L (Hanlon, L.); Jourdain, E (Jourdain, E.); Laurent, P (Laurent, P.); Lebrun, F (Lebrun, F.); Lutovinov, A (Lutovinov, A.); Martin-Carrillo, A (Martin-Carrillo, A.); Mereghetti, S (Mereghetti, S.); Natalucci, L (Natalucci, L.); Rodi, J (Rodi, J.); Roques, JP (Roques, J. -P.); Sunyaev, R (Sunyaev, R.); Ubertini, P (Ubertini, P.); Aartsen, MG (Aartsen, M. G.); Ackermann, M (Ackermann, M.); Adams, J (Adams, J.); Aguilar, JA (Aguilar, J. A.); Ahlers, M (Ahlers, M.); Ahrens, M (Ahrens, M.); Al Samarai, I (Al Samarai, I.); Altmann, D (Altmann, D.); Andeen, K (Andeen, K.); Anderson, T (Anderson, T.); Ansseau, I (Ansseau, I.); Anton, G (Anton, G.); Argelles, C (Argelles, C.); Auffenberg, J (Auffenberg, J.); Axani, S (Axani, S.); Bagherpour, H (Bagherpour, H.); Bai, X (Bai, X.); Barron, JP (Barron, J. P.); Barwick, SW (Barwick, S. W.); Baum, V (Baum, V.); Bay, R (Bay, R.); Beatty, JJ (Beatty, J. J.); Tjus, JB (Tjus, J. Becker); Bernardini, E (Bernardini, E.); Besson, DZ (Besson, D. Z.); Binder, G (Binder, G.); Bindig, D (Bindig, D.); Blaufuss, E (Blaufuss, E.); Blot, S (Blot, S.); Bohm, C (Bohm, C.); Borner, M (Borner, M.); Bos, F (Bos, F.); Bose, D (Bose, D.); Boser, S (Boser, S.); Botner, O (Botner, O.); Bourbeau, E (Bourbeau, E.); Bourbeau, J (Bourbeau, J.); Bradascio, F (Bradascio, F.); Braun, J (Braun, J.); Brayeur, L (Brayeur, L.); Brenzke, M (Brenzke, M.); Bretz, HP (Bretz, H. -P.); Bron, S (Bron, S.); Brostean-Kaiser, J (Brostean-Kaiser, J.); Burgman, A (Burgman, A.); Carver, T (Carver, T.); Casey, J (Casey, J.); Casier, M (Casier, M.); Cheung, E (Cheung, E.); Chirkin, D (Chirkin, D.); Christov, A (Christov, A.); Clark, K (Clark, K.); Classen, L (Classen, L.); Coenders, S (Coenders, S.); Collin, GH (Collin, G. H.); Conrad, JM (Conrad, J. M.); Cowen, DF (Cowen, D. F.); Cross, R (Cross, R.); Day, M (Day, M.); De Andre, JPAM (De Andre, J. P. A. M.); De Clercq, C (De Clercq, C.); DeLaunay, JJ (DeLaunay, J. J.); Dembinski, H (Dembinski, H.); De Ridder, S (De Ridder, S.); Desiati, P (Desiati, P.); De Vries, KD (De Vries, K. D.); De Wasseige, G (De Wasseige, G.); De With, M (De With, M.); DeYoung, T (DeYoung, T.); Diaz-Velez, JC (Diaz-Velez, J. C.); Di Lorenzo, V (Di Lorenzo, V.); Dujmovic, H (Dujmovic, H.); Dumm, JP (Dumm, J. P.); Dunkman, M (Dunkman, M.); Dvorak, E (Dvorak, E.); Eberhardt, B (Eberhardt, B.); Ehrhardt, T (Ehrhardt, T.); Eichmann, B (Eichmann, B.); Eller, P (Eller, P.); Evenson, PA (Evenson, P. A.); Fahey, S (Fahey, S.); Fazely, AR (Fazely, A. R.); Felde, J (Felde, J.); Filimonov, K (Filimonov, K.); Finley, C (Finley, C.); Flis, S (Flis, S.); Franckowiak, A (Franckowiak, A.); Friedman, E (Friedman, E.); Fuchs, T (Fuchs, T.); Gaisser, TK (Gaisser, T. K.); Gallagher, J (Gallagher, J.); Gerhardt, L (Gerhardt, L.); Ghorbani, K (Ghorbani, K.); Giang, W (Giang, W.); Glauch, T (Glauch, T.); Glsenkamp, T (Glsenkamp, T.); Goldschmidt, A (Goldschmidt, A.); Gonzalez, JG (Gonzalez, J. G.); Grant, D (Grant, D.); Griffith, Z (Griffith, Z.); Haack, C (Haack, C.); Hallgren, A (Hallgren, A.); Halzen, F (Halzen, F.); Hanson, K (Hanson, K.); Hebecker, D (Hebecker, D.); Heereman, D (Heereman, D.); Helbing, K (Helbing, K.); Hellauer, R (Hellauer, R.); Hickford, S (Hickford, S.); Hignight, J (Hignight, J.); Hill, GC (Hill, G. C.); Hoffman, KD (Hoffman, K. D.); Hoffmann, R (Hoffmann, R.); Hokanson-Fasig, B (Hokanson-Fasig, B.); Hoshina, K (Hoshina, K.); Huang, F (Huang, F.); Huber, M (Huber, M.); Hultqvist, K (Hultqvist, K.); Hnnefeld, M (Hnnefeld, M.); In, S (In, S.); Ishihara, A (Ishihara, A.); Jacobi, E (Jacobi, E.); Japaridze, GS (Japaridze, G. S.); Jeong, M (Jeong, M.); Jero, K (Jero, K.); Jones, BJP (Jones, B. J. P.); Kalaczynski, P (Kalaczynski, P.); Kang, W (Kang, W.); Kappes, A (Kappes, A.); Karg, T (Karg, T.); Karle, A (Karle, A.); Keivani, A (Keivani, A.); Kelley, JL (Kelley, J. L.); Kheirandish, A (Kheirandish, A.); Kim, J (Kim, J.); Kim, M (Kim, M.); Kintscher, T (Kintscher, T.); Kiryluk, J (Kiryluk, J.); Kittler, T (Kittler, T.); Klein, SR (Klein, S. R.); Kohnen, G (Kohnen, G.); Koirala, R (Koirala, R.); Kolanoski, H (Kolanoski, H.); Kopke, L (Kopke, L.); Kopper, C (Kopper, C.); Kopper, S (Kopper, S.); Koschinsky, JP (Koschinsky, J. P.); Koskinen, DJ (Koskinen, D. J.); Kowalski, M (Kowalski, M.); Krings, K (Krings, K.); Kroll, M (Kroll, M.); Krckl, G (Krckl, G.); Kunnen, J (Kunnen, J.); Kunwar, S (Kunwar, S.); Kurahashi, N (Kurahashi, N.); Kuwabara, T (Kuwabara, T.); Labare, AKM (Kyriacou, A.); Labare, M (Labare, M.); Lanfranchi, JL (Lanfranchi, J. L.); Larson, MJ (Larson, M. J.); Lauber, F (Lauber, F.); Lesiak-Bzdak, M (Lesiak-Bzdak, M.); Leuermann, M (Leuermann, M.); Liu, QR (Liu, Q. R.); Lu, L (Lu, L.); Lnemann, J (Lnemann, J.); Luszczak, W (Luszczak, W.); Madsen, J (Madsen, J.); Maggi, G (Maggi, G.); Mahn, KBM (Mahn, K. B. M.); Mancina, S (Mancina, S.); Maruyama, R (Maruyama, R.); Mase, K (Mase, K.); Maunu, R (Maunu, R.); McNally, F (McNally, F.); Meagher, K (Meagher, K.); Medici, M (Medici, M.); Meier, M (Meier, M.); Menne, T (Menne, T.); Merino, G (Merino, G.); Meures, T (Meures, T.); Miarecki, S (Miarecki, S.); Micallef, J (Micallef, J.); Moment, G (Moment, G.); Montaruli, T (Montaruli, T.); Moore, RW (Moore, R. W.); Moulai, M (Moulai, M.); Nahnhauer, R (Nahnhauer, R.); Nakarmi, P (Nakarmi, P.); Naumann, U (Naumann, U.); Neer, G (Neer, G.); Niederhausen, H (Niederhausen, H.); Nowicki, SC (Nowicki, S. C.); Nygren, DR (Nygren, D. R.); Pollmann, AO (Pollmann, A. Obertacke); Olivas,

A (Olivas, A.); O'Murchadha, A (O'Murchadha, A.); Palczewski, T (Palczewski, T.); Pandya, H (Pandya, H.); Pankova, DV (Pankova, D. V.); Peiffer, P (Peiffer, P.); Pepper, JA (Pepper, J. A.); Heros, CPDL (Heros, C. Perez De Los); Pieloth, D (Pieloth, D.); Pinat, E (Pinat, E.); Price, PB (Price, P. B.); Przybylski, GT (Przybylski, G. T.); Raab, C (Raab, C.); Rdel, L (Rdel, L.); Rameez, M (Rameez, M.); Rawlins, K (Rawlins, K.); Rea, IC (Rea, I. C.); Reimann, R (Reimann, R.); Relethford, B (Relethford, B.); Relich, M (Relich, M.); Resconi, E (Resconi, E.); Rhode, W (Rhode, W.); Richman, M (Richman, M.); Robertson, S (Robertson, S.); Rongen, M (Rongen, M.); Rott, C (Rott, C.); Ruhe, T (Ruhe, T.); Ryckbosch, D (Ryckbosch, D.); Rysewyk, D (Rysewyk, D.); Slzer, T (Slzer, T.); Herrera, SES (Herrera, S. E. Sanchez); Sandrock, A (Sandrock, A.); Sandroos, J (Sandroos, J.); Santander, M (Santander, M.); Sarkar, S (Sarkar, S.); Sarkar, S (Sarkar, S.); Satalecka, K (Satalecka, K.); Schlunder, P (Schlunder, P.); Schmidt, T (Schmidt, T.); Schneider, A (Schneider, A.); Schoenen, S (Schoenen, S.); Schoneberg, S (Schoneberg, S.); Schumacher, L (Schumacher, L.); Seckel, D (Seckel, D.); Seunarine, S (Seunarine, S.); Soedingrekso, J (Soedingrekso, J.); Soldin, D (Soldin, D.); Song, M (Song, M.); Spiczak, GM (Spiczak, G. M.); Spiering, C (Spiering, C.); Stachurska, J (Stachurska, J.); Stamatikos, M (Stamatikos, M.); Stanev, T (Stanev, T.); Stasik, A (Stasik, A.); Stettner, J (Stettner, J.); Steuer, A (Steuer, A.); Stezelberger, T (Stezelberger, T.); Stokstad, RG (Stokstad, R. G.); Stosl, A (Stosl, A.); Strotjohann, NL (Strotjohann, N. L.); Stuttard, T (Stuttard, T.); Sullivan, GW (Sullivan, G. W.); Sutherland, M (Sutherland, M.); Taboada, I (Taboada, I.); Tatar, J (Tatar, J.); Tenholt, F (Tenholt, F.); Ter-Antonyan, S (Ter-Antonyan, S.); Terliuk, A (Terliuk, A.); Tesic, G (Tesic, G.); Tilav, S (Tilav, S.); Toale, PA (Toale, P. A.); Tobin, MN (Tobin, M. N.); Toscano, S (Toscano, S.); Tosi, D (Tosi, D.); Tselengidou, M (Tselengidou, M.); Tung, CF (Tung, C. F.); Turcati, A (Turcati, A.); Turley, CF (Turley, C. F.); Ty, B (Ty, B.); Unger, E (Unger, E.); Usner, M (Usner, M.); Vandenbroucke, J (Vandenbroucke, J.); Van Driessche, W (Van Driessche, W.); Van Eijndhoven, N (Van Eijndhoven, N.); Vanheule, S (Vanheule, S.); Van Santen, J (Van Santen, J.); Vehring, M (Vehring, M.); Vogel, E (Vogel, E.); Vraeghe, M (Vraeghe, M.); Walck, C (Walck, C.); Wallace, A (Wallace, A.); Wallraff, M (Wallraff, M.); Wandler, FD (Wandler, F. D.); Wandkowsky, N (Wandkowsky, N.); Waza, A (Waza, A.); Weaver, C (Weaver, C.); Weiss, MJ (Weiss, M. J.); Wendt, C (Wendt, C.); Werthebach, J (Werthebach, J.); Whelan, BJ (Whelan, B. J.); Wiebe, K (Wiebe, K.); Wiebusch, CH (Wiebusch, C. H.); Wille, L (Wille, L.); Williams, DR (Williams, D. R.); Wills, L (Wills, L.); Wolf, M (Wolf, M.); Wood, TR (Wood, T. R.); Woolsey, E (Woolsey, E.); Woschnagg, K (Woschnagg, K.); Xu, DL (Xu, D. L.); Xu, XW (Xu, X. W.); Xu, Y (Xu, Y.); Yanez, JP (Yanez, J. P.); Yodh, G (Yodh, G.); Yoshida, S (Yoshida, S.); Yuan, T (Yuan, T.); Zoll, M (Zoll, M.); Balasubramanian, A (Balasubramanian, A.); Mate, S (Mate, S.); Bhalerao, V (Bhalerao, V.); Bhattacharya, D (Bhattacharya, D.); Vibhute, A (Vibhute, A.); Dewangan, GC (Dewangan, G. C.); Rao, AR (Rao, A. R.); Vadawale, SV (Vadawale, S. V.); Svinkin, DS (Svinkin, D. S.); Hurley, K (Hurley, K.); Aptekar, RL (Aptekar, R. L.); Frederiks, DD (Frederiks, D. D.); Golenetskii, SV (Golenetskii, S. V.); Kozlova, AV (Kozlova, A. V.); Lysenko, AL (Lysenko, A. L.); Oleynik, PP (Oleynik, Ph. P.); Tsvetkova, AE (Tsvetkova, A. E.); Ulanov, MV (Ulanov, M. V.); Cline, T (Cline, T.); Li, TP (Li, T. P.); Xiong, SL (Xiong, S. L.); Zhang, SN (Zhang, S. N.); Lu, FJ (Lu, F. J.); Song, LM (Song, L. M.); Cao, XL (Cao, X. L.); Chang, Z (Chang, Z.); Chen, G (Chen, G.); Chen, L (Chen, L.); Chen, TX (Chen, T. X.); Chen, Y (Chen, Y.); Chen, YB (Chen, Y. B.); Chen, YP (Chen, Y. P.); Cui, W (Cui, W.); Cui, WW (Cui, W. W.); Deng, JK (Deng, J. K.); Dong, YW (Dong, Y. W.); Du, YY (Du, Y. Y.); Fu, MX (Fu, M. X.); Gao, GH (Gao, G. H.); Gao, H (Gao, H.); Gao, M (Gao, M.); Ge, MY (Ge, M. Y.); Gu, YD (Gu, Y. D.); Guan, J (Guan, J.); Guo, CC (Guo, C. C.); Han, DW (Han, D. W.); Hu, W (Hu, W.); Huang, Y (Huang, Y.); Huo, J (Huo, J.); Jia, SM (Jia, S. M.); Jiang, LH (Jiang, L. H.); Jiang, WC (Jiang, W. C.); Jin, J (Jin, J.); Jin, YJ (Jin, Y. J.); Li, B (Li, B.); Li, CK (Li, C. K.); Li, G (Li, G.); Li, MS (Li, M. S.); Li, W (Li, W.); Li, X (Li, X.); Li, XB (Li, X. B.); Li, XF (Li, X. F.); Li, YG (Li, Y. G.); Li, ZJ (Li, Z. J.); Li, ZW (Li, Z. W.); Liang, XH (Liang, X. H.); Liao, JY (Liao, J. Y.); Liu, CZ (Liu, C. Z.); Liu, GQ (Liu, G. Q.); Liu, HW (Liu, H. W.); Liu, SZ (Liu, S. Z.); Liu, XJ (Liu, X. J.); Liu, Y (Liu, Y.); Liu, YN (Liu, Y. N.); Lu, B (Lu, B.); Lu, XF (Lu, X. F.); Luo, T (Luo, T.); Ma, X (Ma, X.); Meng, B (Meng, B.); Nang, Y (Nang, Y.); Nie, JY (Nie, J. Y.); Ou, G (Ou, G.); Qu, JL (Qu, J. L.); Sai, N (Sai, N.); Sun, L (Sun, L.); Tan, Y (Tan, Y.); Tao, L (Tao, L.); Tao, WH (Tao, W. H.); Tuo, YL (Tuo, Y. L.); Wang, GF (Wang, G. F.); Wang, HY (Wang, H. Y.); Wang, J (Wang, J.); Wang, WS (Wang, W. S.); Wang, YS (Wang, Y. S.); Wen, XY (Wen, X. Y.); Wu, BB (Wu, B. B.); Wu, M (Wu, M.); Xiao, GC (Xiao, G. C.); Xu, H (Xu, H.); Xu, YP (Xu, Y. P.); Yan, LL (Yan, L. L.); Yang, JW (Yang, J. W.); Yang, S (Yang, S.); Yang, YJ (Yang, Y. J.); Zhang, AM (Zhang, A. M.); Zhang, CL (Zhang, C. L.); Zhang, CM (Zhang, C. M.); Zhang, F (Zhang, F.); Zhang, HM (Zhang, H. M.); Zhang, J (Zhang, J.); Zhang, Q (Zhang, Q.); Zhang, S (Zhang, S.); Zhang, T (Zhang, T.); Zhang, W (Zhang, W.); Zhang, WC (Zhang, W. C.); Zhang, WZ (Zhang, W. Z.); Zhang, Y (Zhang, Y.); Zhang, Y (Zhang, Y.); Zhang, YF (Zhang, Y. F.); Zhang, YJ (Zhang, Y. J.); Zhang, Z (Zhang, Z.); Zhang, ZL (Zhang, Z. L.); Zhao, HS (Zhao, H. S.); Zhao, JL (Zhao, J. L.); Zhao, XF (Zhao, X. F.); Zheng, SJ (Zheng, S. J.); Zhu, Y (Zhu, Y.); Zhu, YX (Zhu, Y. X.); Zou, CL (Zou, C. L.); Albert, A (Albert, A.); Andre, M (Andre, M.); Anghinolfi, M (Anghinolfi, M.); Ardid, M (Ardid, M.); Aubert, JJ (Aubert, J. -J.); Aublin, J (Aublin, J.); Avgitas, T (Avgitas, T.); Baret, B (Baret, B.); Barrios-Marti, J (Barrios-Marti, J.); Basa, S (Basa, S.); Belhorma, B (Belhorma, B.); Bertin, V (Bertin, V.); Biagi, S (Biagi, S.); Bormuth, R (Bormuth, R.); Bourret, S (Bourret, S.); Bouwhuis, MC (Bouwhuis, M. C.); Brnzas, H (Brnzas, H.); Bruijn, R (Bruijn, R.); Brunner, J (Brunner, J.); Busto, J (Busto, J.); Capone, A (Capone, A.); Caramete, L (Caramete, L.); Carr, J (Carr, J.); Celli, S (Celli, S.); El Moursli, RC (El Moursli, R. Cherkaoui); Chiarusi, T (Chiarusi, T.); Circella, M (Circella, M.); Coelho, JAB (Coelho, J. A. B.); Coleiro, A (Coleiro, A.); Coniglione, R (Coniglione, R.); Costantini, H (Costantini, H.); Coyle, P (Coyle, P.); Creusot, A (Creusot, A.); Diaz, AF (Diaz, A. F.); Deschamps, A (Deschamps, A.); De Bonis, G (De Bonis, G.); Distefano, C (Distefano, C.); Di Palma, I (Di Palma, I.); Domi, A (Domi, A.); Donzaud, C (Donzaud, C.); Dornic, D (Dornic, D.); Drouhin, D (Drouhin, D.); Eberl, T (Eberl, T.); El Bojaddaini, I (El Bojaddaini, I.); El Khayati, N (El Khayati, N.); Elsasser, D (Elsasser, D.); Enzenhofer, A (Enzenhofer, A.); Ettahiri, A (Ettahiri, A.); Fassi, F (Fassi, F.); Felis, I (Felis, I.); Fusco, LA (Fusco, L. A.); Gay, P (Gay, P.); Giordano, V (Giordano, V.); Glotin, H (Glotin, H.); Gregoire, T (Gregoire, T.); Ruiz, RG (Ruiz, R. Gracia); Graf, K (Graf, K.); Hallmann, S (Hallmann, S.); Van Haren, H (Van Haren, H.); Heijboer, AJ (Heijboer, A. J.); Hello, Y (Hello, Y.); Hernndez-Rey, JJ (Hernndez-Rey, J. J.); Hossl, J (Hossl, J.); Hofestdt, J (Hofestdt, J.); Hugon, C (Hugon, C.); Illuminati, G (Illuminati, G.); James, CW (James, C. W.); De Jong, M (De Jong, M.); Jongen, M (Jongen, M.); Kadler, M (Kadler, M.); Kalekin, O (Kalekin, O.); Katz, U (Katz, U.); Kiessling, D (Kiessling, D.); Kouchner, A (Kouchner, A.); Kreter, M (Kreter, M.); Kreykenbohm, I (Kreykenbohm, I.); Kulikovskiy, V (Kulikovskiy, V.); Lachaud, C (Lachaud, C.); Lahmann, R (Lahmann, R.); LefSvre, D (LefSvre, D.); Leonora, E (Leonora, E.); Lotze, M (Lotze, M.); Loucatos, S (Loucatos, S.); Marcelin, M (Marcelin, M.); Margiotta, A (Margiotta, A.); Marinelli, A (Marinelli, A.); Martinez-Mora, JA (Martinez-Mora, J. A.); Mele, R (Mele, R.); Melis, K (Melis, K.); Michael, T (Michael, T.); Migliozzi, P (Migliozzi, P.); Moussa, A (Moussa, A.); Navas, S (Navas, S.); Nezri, E (Nezri, E.); Organokov, M (Organokov, M.); Pavalas, GE (Pavalas, G. E.); Pellegrino, C (Pellegrino, C.); Perrina, C (Perrina, C.); Piattelli, P (Piattelli, P.); Popa, V (Popa, V.); Pradier, T (Pradier, T.); Quinn, L (Quinn, L.); Racca, C (Racca, C.); Riccobene, G (Riccobene, G.); Snchez-Losa, A (Snchez-Losa, A.);

Saldaa, M (Saldaa, M.); Salvadori, I (Salvadori, I.); Samtleben, DFE (Samtleben, D. F. E.); Sanguineti, M (Sanguineti, M.); Sapienza, P (Sapienza, P.); Sieger, C (Sieger, C.); Spurio, M (Spurio, M.); Stolarczyk, T (Stolarczyk, Th.); Taiuti, M (Taiuti, M.); Tayalati, Y (Tayalati, Y.); Trovato, A (Trovato, A.); Turpin, D (Turpin, D.); Tonnis, C (Tonnis, C.); Vallage, B (Vallage, B.); Van Elewyck, V (Van Elewyck, V.); Versari, F (Versari, F.); Vivolo, D (Vivolo, D.); Vizzoca, A (Vizzoca, A.); Wilms, J (Wilms, J.); Zornoza, JD (Zornoza, J. D.); Zuniga, J (Zuniga, J.); Beardmore, AP (Beardmore, A. P.); Breeveld, AA (Breeveld, A. A.); Burrows, DN (Burrows, D. N.); Cenko, SB (Cenko, S. B.); Cusumano, G (Cusumano, G.); D'Al, A (D'Al, A.); De Pasquale, M (De Pasquale, M.); Emery, SWK (Emery, S. W. K.); Evans, PA (Evans, P. A.); Giommi, P (Giommi, P.); Gronwall, C (Gronwall, C.); Kennea, JA (Kennea, J. A.); Krimm, HA (Krimm, H. A.); Kuin, NPM (Kuin, N. P. M.); Lien, A (Lien, A.); Marshall, FE (Marshall, F. E.); Melandri, A (Melandri, A.); Nousek, JA (Nousek, J. A.); Oates, SR (Oates, S. R.); Osborne, JP (Osborne, J. P.); Pagani, C (Pagani, C.); Page, KL (Page, K. L.); Palmer, DM (Palmer, D. M.); Perri, M (Perri, M.); Siegel, MH (Siegel, M. H.); Sbarufatti, B (Sbarufatti, B.); Tagliaferri, G (Tagliaferri, G.); Tohuvavohu, A (Tohuvavohu, A.); Tavani, M (Tavani, M.); Verrecchia, F (Verrecchia, F.); Bulgarelli, A (Bulgarelli, A.); Evangelista, Y (Evangelista, Y.); Pacciani, L (Pacciani, L.); Feroci, M (Feroci, M.); Pittori, C (Pittori, C.); Giuliani, A (Giuliani, A.); Del Monte, E (Del Monte, E.); Donnarumma, I (Donnarumma, I.); Argan, A (Argan, A.); Trois, A (Trois, A.); Ursi, A (Ursi, A.); Cardillo, M (Cardillo, M.); Piano, G (Piano, G.); Longo, F (Longo, F.); Lucarelli, F (Lucarelli, F.); Munar-Adrover, P (Munar-Adrover, P.); Fuschino, F (Fuschino, F.); Labanti, C (Labanti, C.); Marisaldi, M (Marisaldi, M.); Minervini, G (Minervini, G.); Fioretti, V (Fioretti, V.); Parmiggiani, N (Parmiggiani, N.); Gianotti, F (Gianotti, F.); Trifoglio, M (Trifoglio, M.); Di Persio, G (Di Persio, G.); Antonelli, LA (Antonelli, L. A.); Barbiellini, G (Barbiellini, G.); Caraveo, P (Caraveo, P.); Cattaneo, PW (Cattaneo, P. W.); Costa, E (Costa, E.); Colafrancesco, S (Colafrancesco, S.); D'Amico, F (D'Amico, F.); Ferrari, A (Ferrari, A.); Morselli, A (Morselli, A.); Paoletti, F (Paoletti, F.); Picozza, P (Picozza, P.); Pilia, M (Pilia, M.); Rappoldi, A (Rappoldi, A.); Soffitta, P (Soffitta, P.); Vercellone, S (Vercellone, S.); Foley, RJ (Foley, R. J.); Coulter, DA (Coulter, D. A.); Kilpatrick, CD (Kilpatrick, C. D.); Drout, MR (Drout, M. R.); Piro, AL (Piro, A. L.); Shappee, BJ (Shappee, B. J.); Siebert, MR (Siebert, M. R.); Simon, JD (Simon, J. D.); Ulloa, N (Ulloa, N.); Kasen, D (Kasen, D.); Madore, BF (Madore, B. F.); Murguia-Berthier, A (Murguia-Berthier, A.); Pan, YC (Pan, Y. -C.); Prochaska, JX (Prochaska, J. X.); Ramirez-Ruiz, E (Ramirez-Ruiz, E.); Rest, A (Rest, A.); Rojas-Bravo, C (Rojas-Bravo, C.); Berger, E (Berger, E.); Soares-Santos, M (Soares-Santos, M.); Annis, J (Annis, J.); Alexander, KD (Alexander, K. D.); Allam, S (Allam, S.); Balbinot, E (Balbinot, E.); Blanchard, P (Blanchard, P.); Brout, D (Brout, D.); Butler, RE (Butler, R. E.); Chornock, R (Chornock, R.); Cook, ER (Cook, E. R.); Cowperthwaite, P (Cowperthwaite, P.); Diehl, HT (Diehl, H. T.); Drlica-Wagner, A (Drlica-Wagner, A.); Drout, MR (Drout, M. R.); Durret, F (Durret, F.); Eftekhari, T (Eftekhari, T.); Finley, DA (Finley, D. A.); Fong, W (Fong, W.); Frieman, JA (Frieman, J. A.); Fryer, CL (Fryer, C. L.); Garcia-Bellido, J (Garcia-Bellido, J.); Gruendl, RA (Gruendl, R. A.); Hartley, W (Hartley, W.); Herner, K (Herner, K.); Kessler, R (Kessler, R.); Lin, H (Lin, H.); Lopes, PAA (Lopes, P. A. A.); Lourenco, ACC (Lourenco, A. C. C.); Margutti, R (Margutti, R.); Marshall, JL (Marshall, J. L.); Matheson, T (Matheson, T.); Medina, GE (Medina, G. E.); Metzger, BD (Metzger, B. D.); Muoz, RR (Muoz, R. R.); Muir, J (Muir, J.); Nicholl, M (Nicholl, M.); Nugent, P (Nugent, P.); Palmese, A (Palmese, A.); Paz-Chinchn, F (Paz-Chinchn, F.); Quataert, E (Quataert, E.); Sako, M (Sako, M.); Sauseda, M (Sauseda, M.); Schlegel, DJ (Schlegel, D. J.); Scolnic, D (Scolnic, D.); Secco, LF (Secco, L. F.); Smith, N (Smith, N.); Sobreira, F (Sobreira, F.); Villar, VA (Villar, V. A.); Vivas, AK (Vivas, A. K.); Wester, W (Wester, W.); Williams, PKG (Williams, P. K. G.); Yanny, B (Yanny, B.); Zenteno, A (Zenteno, A.); Zhang, Y (Zhang, Y.); Abbott, TMC (Abbott, T. M. C.); Banerji, M (Banerji, M.); Bechtol, K (Bechtol, K.); Benoit-Levy, A (Benoit-Levy, A.); Bertin, E (Bertin, E.); Brooks, D (Brooks, D.); Buckley-Geer, E (Buckley-Geer, E.); Burke, DL (Burke, D. L.); Capozzi, D (Capozzi, D.); Rosell, AC (Rosell, A. Carnero); Kind, MC (Kind, M. Carrasco); Castander, FJ (Castander, F. J.); Crocce, M (Crocce, M.); Cunha, CE (Cunha, C. E.); D'Andrea, CB (D'Andrea, C. B.); Da Costa, LN (Da Costa, L. N.); Davis, C (Davis, C.); Depoy, DL (Depoy, D. L.); Desai, S (Desai, S.); Dietrich, JP (Dietrich, J. P.); Eifler, TF (Eifler, T. F.); Fernandez, E (Fernandez, E.); Flaugher, B (Flaugher, B.); Fosalba, P (Fosalba, P.); Gaztanaga, E (Gaztanaga, E.); Gerdes, DW (Gerdes, D. W.); Giannantonio, T (Giannantonio, T.); Goldstein, DA (Goldstein, D. A.); Gruen, D (Gruen, D.); Gschwend, J (Gschwend, J.); Gutierrez, G (Gutierrez, G.); Honscheid, K (Honscheid, K.); James, DJ (James, D. J.); Jeltema, T (Jeltema, T.); Johnson, MWG (Johnson, M. W. G.); Johnson, MD (Johnson, M. D.); Kent, S (Kent, S.); Krause, E (Krause, E.); Kron, R (Kron, R.); Kuehn, K (Kuehn, K.); Lahav, O (Lahav, O.); Lima, M (Lima, M.); Maia, MAG (Maia, M. A. G.); March, M (March, M.); Martini, P (Martini, P.); McMahon, RG (McMahon, R. G.); Menanteau, F (Menanteau, F.); Miller, CJ (Miller, C. J.); Miquel, R (Miquel, R.); Mohr, JJ (Mohr, J. J.); Nichol, RC (Nichol, R. C.); Ogando, RLC (Ogando, R. L. C.); Plazas, AA (Plazas, A. A.); Romer, AK (Romer, A. K.); Roodman, A (Roodman, A.); Rykoff, ES (Rykoff, E. S.); Sanchez, E (Sanchez, E.); Scarpine, V (Scarpine, V.); Schindler, R (Schindler, R.); Schubnell, M (Schubnell, M.); Sevilla-Noarbe, I (Sevilla-Noarbe, I.); Sheldon, E (Sheldon, E.); Smith, M (Smith, M.); Smith, RC (Smith, R. C.); Stebbins, A (Stebbins, A.); Suchyta, E (Suchyta, E.); Swanson, MEC (Swanson, M. E. C.); Tarle, G (Tarle, G.); Thomas, RC (Thomas, R. C.); Troxel, MA (Troxel, M. A.); Tucker, DL (Tucker, D. L.); Vikram, V (Vikram, V.); Walker, AR (Walker, A. R.); Wechsler, RH (Wechsler, R. H.); Weller, J (Weller, J.); Carlin, JL (Carlin, J. L.); Gill, MSS (Gill, M. S. S.); Li, TS (Li, T. S.); Marriner, J (Marriner, J.); Neilsen, E (Neilsen, E.); Haislip, JB (Haislip, J. B.); Kouprianov, VV (Kouprianov, V. V.); Reichart, DE (Reichart, D. E.); Sand, DJ (Sand, D. J.); Tartaglia, L (Tartaglia, L.); Valenti, S (Valenti, S.); Yang, S (Yang, S.); Benetti, S (Benetti, S.); Brocato, E (Brocato, E.); Campana, S (Campana, S.); Cappellaro, E (Cappellaro, E.); Covino, S (Covino, S.); D'Avanzo, P (D'Avanzo, P.); D'Elia, V (D'Elia, V.); Getman, F (Getman, F.); Ghirlanda, G (Ghirlanda, G.); Ghisellini, G (Ghisellini, G.); Limatola, L (Limatola, L.); Nicastro, L (Nicastro, L.); Palazzi, E (Palazzi, E.); Pian, E (Pian, E.); Piranomonte, S (Piranomonte, S.); Possenti, A (Possenti, A.); Rossi, A (Rossi, A.); Salafia, OS (Salafia, O. S.); Tomasella, L (Tomasella, L.); Amati, L (Amati, L.); Antonelli, LA (Antonelli, L. A.); Bernardini, MG (Bernardini, M. G.); Bufano, F (Bufano, F.); Capaccioli, M (Capaccioli, M.); Casella, P (Casella, P.); Dadina, M (Dadina, M.); De Cesare, G (De Cesare, G.); Di Paola, A (Di Paola, A.); Giuffrida, G (Giuffrida, G.); Giunta, A (Giunta, A.); Israel, GL (Israel, G. L.); Lisi, M (Lisi, M.); Maiorano, E (Maiorano, E.); Mapelli, M (Mapelli, M.); Masetti, N (Masetti, N.); Pescalli, A (Pescalli, A.); Pulone, L (Pulone, L.); Salvaterra, R (Salvaterra, R.); Schipani, P (Schipani, P.); Spera, M (Spera, M.); Stamerra, A (Stamerra, A.); Stella, L (Stella, L.); Testa, V (Testa, V.); Turatto, M (Turatto, M.); Vergani, D (Vergani, D.); Aresu, G (Aresu, G.); Bachetti, M (Bachetti, M.); Buffa, F (Buffa, F.); Burgay, M (Burgay, M.); Buttu, M (Buttu, M.); Caria, T (Caria, T.); Carretti, E (Carretti, E.); Casasola, V (Casasola, V.); Castangia, P (Castangia, P.); Carboni, G (Carboni, G.); Casu, S (Casu, S.); Concu, R (Concu, R.); Corongiu, A (Corongiu, A.); Deiana, GL (Deiana, G. L.); Egron, E (Egron, E.); Fara, A (Fara, A.); Gaudiomonte, F (Gaudiomonte, F.); Gusai, V (Gusai, V.); Ladu, A (Ladu, A.); Loru, S (Loru, S.); Leurini, S (Leurini, S.); Marongiu, L (Marongiu, L.); Melis, A (Melis, A.); Melis, G (Melis, G.); Migoni, C (Migoni, Carlo); Milia, S (Milia, Sabrina); Navarrini, A (Navarrini,

Alessandro); Orlati, A (Orlati, A.); Ortu, P (Ortu, P.); Palmas, S (Palmas, S.); Pellizzoni, A (Pellizzoni, A.); Perrodin, D (Perrodin, D.); Pisanu, T (Pisanu, T.); Poppi, S (Poppi, S.); Righini, S (Righini, S.); Saba, A (Saba, A.); Serra, G (Serra, G.); Serrau, M (Serrau, M.); Stagni, M (Stagni, M.); Surcis, G (Surcis, G.); Vacca, V (Vacca, V.); Vargiu, GP (Vargiu, G. P.); Hunt, LK (Hunt, L. K.); Jin, ZP (Jin, Z. P.); Klose, S (Klose, S.); Kouveliotou, C (Kouveliotou, C.); Mazzali, PA (Mazzali, P. A.); Moller, P (Moller, P.); Nava, L (Nava, L.); Piran, T (Piran, T.); Selsing, J (Selsing, J.); Vergani, SD (Vergani, S. D.); Wiersema, K (Wiersema, K.); Toma, K (Toma, K.); Higgins, AB (Higgins, A. B.); Mundell, CG (Mundell, C. G.); Alighieri, SDS (Alighieri, S. Di Serego); Gtz, D (Gtz, D.); Gao, W (Gao, W.); Gomboc, A (Gomboc, A.); Kaper, L (Kaper, L.); Kobayashi, S (Kobayashi, S.); Kopac, D (Kopac, D.); Mao, J (Mao, J.); Starling, RLC (Starling, R. L. C.); Steele, I (Steele, I.); Van der Horst, AJ (Van der Horst, A. J.); Acero, F (Acero, F.); Atwood, WB (Atwood, W. B.); Baldini, L (Baldini, L.); Barbiellini, G (Barbiellini, G.); Bastieri, D (Bastieri, D.); Berenji, B (Berenji, B.); Bellazzini, R (Bellazzini, R.); Bissaldi, E (Bissaldi, E.); Blandford, RD (Blandford, R. D.); Bloom, ED (Bloom, E. D.); Bonino, R (Bonino, R.); Bottacini, E (Bottacini, E.); Bregeon, J (Bregeon, J.); Buehler, R (Buehler, R.); Buson, S (Buson, S.); Cameron, RA (Cameron, R. A.); Caputo, R (Caputo, R.); Caraveo, PA (Caraveo, P. A.); Cavazzuti, E (Cavazzuti, E.); Chekhtman, A (Chekhtman, A.); Cheung, CC (Cheung, C. C.); Chiang, J (Chiang, J.); Ciprini, S (Ciprini, S.); Cohen-Tanugi, J (Cohen-Tanugi, J.); Cominsky, LR (Cominsky, L. R.); Costantin, D (Costantin, D.); Cuoco, A (Cuoco, A.); D'Ammando, F (D'Ammando, F.); De Palma, F (De Palma, F.); Digel, SW (Digel, S. W.); Di Lalla, N (Di Lalla, N.); Di Mauro, M (Di Mauro, M.); Di Venere, L (Di Venere, L.); Dubois, R (Dubois, R.); Fegan, SJ (Fegan, S. J.); Focke, WB (Focke, W. B.); Franckowiak, A (Franckowiak, A.); Fukazawa, Y (Fukazawa, Y.); Funk, S (Funk, S.); Fusco, P (Fusco, P.); Gargano, F (Gargano, F.); Gasparrini, D (Gasparrini, D.); Giglietto, N (Giglietto, N.); Giordano, F (Giordano, F.); Giroletti, M (Giroletti, M.); Glanzman, T (Glanzman, T.); Green, D (Green, D.); Grondin, MH (Grondin, M. -H.); Guillemot, L (Guillemot, L.); Guiriec, S (Guiriec, S.); Harding, AK (Harding, A. K.); Horan, D (Horan, D.); Jhannesson, G (Jhannesson, G.); Kamae, T (Kamae, T.); Kensei, S (Kensei, S.); Kuss, M (Kuss, M.); La Mura, G (La Mura, G.); Latronico, L (Latronico, L.); Lemoine-Goumard, M (Lemoine-Goumard, M.); Longo, F (Longo, F.); Loparco, F (Loparco, F.); Lovellette, MN (Lovellette, M. N.); Lubrano, P (Lubrano, P.); Magill, JD (Magill, J. D.); Maldera, S (Maldera, S.); Manfreda, A (Manfreda, A.); Mazziotta, MN (Mazziotta, M. N.); McEnery, JE (McEnery, J. E.); Meyer, M (Meyer, M.); Michelson, PF (Michelson, P. F.); Mirabal, N (Mirabal, N.); Monzani, ME (Monzani, M. E.); Morselli, A (Morselli, A.); Moskalenko, IV (Moskalenko, I. V.); Negro, M (Negro, M.); Nuss, E (Nuss, E.); Ojha, R (Ojha, R.); Omodei, N (Omodei, N.); Orienti, M (Orienti, M.); Orlando, E (Orlando, E.); Palatiello, M (Palatiello, M.); Paliya, VS (Paliya, V. S.); Paneque, D (Paneque, D.); Pesce-Rollins, M (Pesce-Rollins, M.); Piron, F (Piron, F.); Porter, TA (Porter, T. A.); Principe, G (Principe, G.); Rain, S (Rain, S.); Rando, R (Rando, R.); Razzano, M (Razzano, M.); Razzaque, S (Razzaque, S.); Reimer, A (Reimer, A.); Reimer, O (Reimer, O.); Reposeur, T (Reposeur, T.); Rochester, LS (Rochester, L. S.); Parkinson, PMS (Parkinson, P. M. Saz); Sgro, C (Sgro, C.); Siskind, EJ (Siskind, E. J.); Spada, F (Spada, F.); Spandre, G (Spandre, G.); Suson, DJ (Suson, D. J.); Takahashi, M (Takahashi, M.); Tanaka, Y (Tanaka, Y.); Thayer, JG (Thayer, J. G.); Thayer, JB (Thayer, J. B.); Thompson, DJ (Thompson, D. J.); Tibaldo, L (Tibaldo, L.); Torres, DF (Torres, D. F.); Torresi, E (Torresi, E.); Troja, E (Troja, E.); Venters, TM (Venters, T. M.); Vianello, G (Vianello, G.); Zaharijas, G (Zaharijas, G.); Allison, J (Allison, J.); Bannister, KW (Bannister, K. W.); Dobie, D (Dobie, D.); Kaplan, DL (Kaplan, D. L.); Lenc, E (Lenc, E.); Lynch, C (Lynch, C.); Murphy, T (Murphy, T.); Sadler, EM (Sadler, E. M.); Hotan, A (Hotan, A.); James, CW (James, C. W.); Oslowski, S (Oslowski, S.); Raja, W (Raja, W.); Shannon, RM (Shannon, R. M.); Whiting, M (Whiting, M.); Arcavi, I (Arcavi, I.); Howell, DA (Howell, D. A.); McCully, C (McCully, C.); Hosseinzadeh, G (Hosseinzadeh, G.); Hiramatsu, D (Hiramatsu, D.); Poznanski, D (Poznanski, D.); Barnes, J (Barnes, J.); Zaltzman, M (Zaltzman, M.); Vasylyev, S (Vasylyev, S.); Maoz, D (Maoz, D.); Cooke, J (Cooke, J.); Bailes, M (Bailes, M.); Wolf, C (Wolf, C.); Deller, AT (Deller, A. T.); Lidman, C (Lidman, C.); Wang, L (Wang, L.); Gendre, B (Gendre, B.); Andreoni, I (Andreoni, I.); Ackley, K (Ackley, K.); Pritchard, TA (Pritchard, T. A.); Bessell, MS (Bessell, M. S.); Chang, SW (Chang, S. -W.); Moller, A (Moller, A.); Onken, CA (Onken, C. A.); Scalzo, RA (Scalzo, R. A.); Ridden-Harper, R (Ridden-Harper, R.); Sharp, RG (Sharp, R. G.); Tucker, BE (Tucker, B. E.); Farrell, TJ (Farrell, T. J.); Elmer, E (Elmer, E.); Johnston, S (Johnston, S.); Krishnan, VV (Krishnan, V. Venkatraman); Keane, EF (Keane, E. F.); Green, JA (Green, J. A.); Jameson, A (Jameson, A.); Hu, L (Hu, L.); Ma, B (Ma, B.); Sun, T (Sun, T.); Wu, X (Wu, X.); Wang, X (Wang, X.); Shang, Z (Shang, Z.); Hu, Y (Hu, Y.); Ashley, MCB (Ashley, M. C. B.); Yuan, X (Yuan, X.); Li, X (Li, X.); Tao, C (Tao, C.); Zhu, Z (Zhu, Z.); Zhang, H (Zhang, H.); Suntzeff, NB (Suntzeff, N. B.); Zhou, J (Zhou, J.); Yang, J (Yang, J.); Orange, B (Orange, B.); Morris, D (Morris, D.); Cucchiara, A (Cucchiara, A.); Giblin, T (Giblin, T.); Klotz, A (Klotz, A.); Staff, J (Staff, J.); Thierry, P (Thierry, P.); Schmidt, BP (Schmidt, B. P.); Tanvir, NR (Tanvir, N. R.); Levan, AJ (Levan, A. J.); Cano, Z (Cano, Z.); De Ugarte-Postigo, A (De Ugarte-Postigo, A.); Evans, P (Evans, P.); Gonzalez-Fernandez, C (Gonzalez-Fernandez, C.); Greiner, J (Greiner, J.); Hjorth, J (Hjorth, J.); Irwin, M (Irwin, M.); Kruhler, T (Kruhler, T.); Mandel, I (Mandel, I.); Milvang-Jensen, B (Milvang-Jensen, B.); O'Brien, P (O'Brien, P.); Rol, E (Rol, E.); Rosetti, S (Rosetti, S.); Rosswog, S (Rosswog, S.); Rowlinson, A (Rowlinson, A.); Steeghs, DTH (Steeghs, D. T. H.); Thene, CC (Thene, C. C.); Ulaczyk, K (Ulaczyk, K.); Watson, D (Watson, D.); Bruun, SH (Bruun, S. H.); Cutter, R (Cutter, R.); Jaimes, RF (Jaimes, R. Figuera); Fujii, YI (Fujii, Y. I.); Fruchter, AS (Fruchter, A. S.); Gompertz, B (Gompertz, B.); Jakobsson, P (Jakobsson, P.); Hodosan, G (Hodosan, G.); Jergensen, UG (Jergensen, U. G.); Kangas, T (Kangas, T.); Kann, DA (Kann, D. A.); Rabus, M (Rabus, M.); Schroder, SL (Schroder, S. L.); Stanway, ER (Stanway, E. R.); Wijers, RAMJ (Wijers, R. A. M. J.); Lipunov, VM (Lipunov, V. M.); Gorbovskoy, ES (Gorbovskoy, E. S.); Kornilov, VG (Kornilov, V. G.); Tyurina, NV (Tyurina, N. V.); Balanutsa, PV (Balanutsa, P. V.); Kuznetsov, AS (Kuznetsov, A. S.); Vlasenko, DM (Vlasenko, D. M.); Podesta, RC (Podesta, R. C.); Lopez, C (Lopez, C.); Podesta, F (Podesta, F.); Levato, HO (Levato, H. O.); Saffe, C (Saffe, C.); Mallamaci, CC (Mallamaci, C. C.); Budnev, NM (Budnev, N. M.); Gress, OA (Gress, O. A.); Kuvshinov, DA (Kuvshinov, D. A.); Gorbunov, IA (Gorbunov, I. A.); Vladimirov, VV (Vladimirov, V. V.); Zimnukhov, DS (Zimnukhov, D. S.); Gabovich, AV (Gabovich, A. V.); Yurkov, VV (Yurkov, V. V.); Sergienko, YP (Sergienko, Yu. P.); Rebolo, R (Rebolo, R.); Serra-Ricart, M (Serra-Ricart, M.); Tlatov, AG (Tlatov, A. G.); Ishmuhametova, YV (Ishmuhametova, Yu. V.); Abe, F (Abe, F.); Aoki, K (Aoki, K.); Aoki, W (Aoki, W.); Asakura, Y (Asakura, Y.); Baar, S (Baar, S.); Barway, S (Barway, S.); Bond, IA (Bond, I. A.); Doi, M (Doi, M.); Finet, F (Finet, F.); Fujiyoshi, T (Fujiyoshi, T.); Furusawa, H (Furusawa, H.); Honda, S (Honda, S.); Itoh, R (Itoh, R.); Kanda, N (Kanda, N.); Kawabata, KS (Kawabata, K. S.); Kawabata, M (Kawabata, M.); Kim, JH (Kim, J. H.); Koshida, S (Koshida, S.); Kuroda, D (Kuroda, D.); Lee, CH (Lee, C. -H.); Liu, W (Liu, W.); Matsubayashi, K (Matsubayashi, K.); Miyazaki, S (Miyazaki, S.); Morihana, K (Morihana, K.); Morokuma, T (Morokuma, T.); Motohara, K (Motohara, K.); Murata, KL (Murata, K. L.); Nagai, H (Nagai, H.); Nagashima, H (Nagashima, H.); Nagayama, T (Nagayama, T.); Nakaoka, T (Nakaoka, T.); Nakata, F (Nakata, F.); Ohsawa, R (Ohsawa, R.); Ohshima, T (Ohshima, T.); Ohta, K (Ohta, K.); Okita, H (Okita, H.); Saito, T (Saito, T.); Saito, Y (Saito, Y.); Sako, S (Sako, S.);

Sekiguchi, Y (Sekiguchi, Y.); Sumi, T (Sumi, T.); Tajitsu, A (Tajitsu, A.); Takahashi, J (Takahashi, J.); Takayama, M (Takayama, M.); Tamura, Y (Tamura, Y.); Tanaka, I (Tanaka, I.); Tanaka, M (Tanaka, M.); Terai, T (Terai, T.); Tominaga, N (Tominaga, N.); Tristram, PJ (Tristram, P. J.); Uemura, M (Uemura, M.); Utsumi, Y (Utsumi, Y.); Yamaguchi, MS (Yamaguchi, M. S.); Yasuda, N (Yasuda, N.); Yoshida, M (Yoshida, M.); Zenko, T (Zenko, T.); Adams, SM (Adams, S. M.); Allison, JR (Allison, J. R.); Anupama, GC (Anupama, G. C.); Bally, J (Bally, J.); Barway, S (Barway, S.); Bellm, E (Bellm, E.); Blagorodnova, N (Blagorodnova, N.); Cannella, C (Cannella, C.); Chandra, P (Chandra, P.); Chatterjee, D (Chatterjee, D.); Clarke, TE (Clarke, T. E.); Cobb, BE (Cobb, B. E.); Cook, DO (Cook, D. O.); Copperwheat, C (Copperwheat, C.); De, K (De, K.); Emery, SWK (Emery, S. W. K.); Evans, PA (Evans, P. A.); Feindt, U (Feindt, U.); Foster, K (Foster, K.); Frail, ODFDA (Fox, O. D.); Frail, DA (Frail, D. A.); Fremling, C (Fremling, C.); Frohmaier, C (Frohmaier, C.); Garcia, JA (Garcia, J. A.); Ghosh, S (Ghosh, S.); Giacintucci, S (Giacintucci, S.); Goobar, A (Goobar, A.); Gottlieb, O (Gottlieb, O.); Grefenstette, BW (Grefenstette, B. W.); Hallinan, G (Hallinan, G.); Harrison, F (Harrison, F.); Heida, M (Heida, M.); Helou, G (Helou, G.); Ho, AYQ (Ho, A. Y. Q.); Horesh, A (Horesh, A.); Hotokezaka, K (Hotokezaka, K.); Ip, WH (Ip, W. -H.); Itoh, R (Itoh, R.); Jacobs, B (Jacobs, Bob); Jencson, JE (Jencson, J. E.); Kasen, D (Kasen, D.); Kasliwal, MM (Kasliwal, M. M.); Kassim, NE (Kassim, N. E.); Kim, H (Kim, H.); Kiran, BS (Kiran, B. S.); Kuin, NPM (Kuin, N. P. M.); Kulkarni, SR (Kulkarni, S. R.); Kupfer, T (Kupfer, T.); Lau, RM (Lau, R. M.); Madsen, K (Madsen, K.); Mazzali, PA (Mazzali, P. A.); Miller, AA (Miller, A. A.); Miyasaka, H (Miyasaka, H.); Mooley, K (Mooley, K.); Myers, ST (Myers, S. T.); Nakar, E (Nakar, E.); Ngeow, CC (Ngeow, C. -C.); Nugent, P (Nugent, P.); Ofek, EO (Ofek, E. O.); Palliyaguru, N (Palliyaguru, N.); Pavana, M (Pavana, M.); Perley, DA (Perley, D. A.); Peters, WM (Peters, W. M.); Pike, S (Pike, S.); Piran, T (Piran, T.); Qi, H (Qi, H.); Quimby, RM (Quimby, R. M.); Rana, J (Rana, J.); Rosswog, S (Rosswog, S.); Rusu, F (Rusu, F.); Sadler, EM (Sadler, E. M.); Van Sistine, A (Van Sistine, A.); Sollerman, J (Sollerman, J.); Xu, Y (Xu, Y.); Yan, L (Yan, L.); Yatsu, Y (Yatsu, Y.); Yu, PC (Yu, P. -C.); Zhang, C (Zhang, C.); Zhao, W (Zhao, W.); Chambers, KC (Chambers, K. C.); Huber, ME (Huber, M. E.); Schultz, ASB (Schultz, A. S. B.); Bulger, J (Bulger, J.); Flewelling, H (Flewelling, H.); Magnier, EA (Magnier, E. A.); Lowe, TB (Lowe, T. B.); Wainscoat, RJ (Wainscoat, R. J.); Waters, C (Waters, C.); Willman, M (Willman, M.); Ebisawa, K (Ebisawa, K.); Hanyu, C (Hanyu, C.); Harita, S (Harita, S.); Hashimoto, T (Hashimoto, T.); Hidaka, K (Hidaka, K.); Hori, T (Hori, T.); Ishikawa, M (Ishikawa, M.); Isobe, N (Isobe, N.); Iwakiri, W (Iwakiri, W.); Kawai, H (Kawai, H.); Kawai, N (Kawai, N.); Kawamuro, T (Kawamuro, T.); Kawase, T (Kawase, T.); Kitaoka, Y (Kitaoka, Y.); Makishima, K (Makishima, K.); Matsuoka, M (Matsuoka, M.); Mihara, T (Mihara, T.); Morita, T (Morita, T.); Morita, K (Morita, K.); Nakahira, S (Nakahira, S.); Nakajima, M (Nakajima, M.); Nakamura, Y (Nakamura, Y.); Negoro, H (Negoro, H.); Oda, S (Oda, S.); Sakamaki, A (Sakamaki, A.); Sasaki, R (Sasaki, R.); Serino, M (Serino, M.); Shidatsu, M (Shidatsu, M.); Shimomukai, R (Shimomukai, R.); Sugawara, Y (Sugawara, Y.); Sugita, S (Sugita, S.); Sugizaki, M (Sugizaki, M.); Tachibana, Y (Tachibana, Y.); Takao, Y (Takao, Y.); Tanimoto, A (Tanimoto, A.); Tomida, H (Tomida, H.); Tsuboi, Y (Tsuboi, Y.); Tsunemi, H (Tsunemi, H.); Ueda, Y (Ueda, Y.); Ueno, S (Ueno, S.); Yamada, S (Yamada, S.); Yamaoka, K (Yamaoka, K.); Yamauchi, M (Yamauchi, M.); Yatabe, F (Yatabe, F.); Yoneyama, T (Yoneyama, T.); Yoshii, T (Yoshii, T.); Coward, DM (Coward, D. M.); Crisp, H (Crisp, H.); Macpherson, D (Macpherson, D.); Andreoni, I (Andreoni, I.); Laugier, R (Laugier, R.); Noysena, K (Noysena, K.); Klotz, A (Klotz, A.); Gendre, B (Gendre, B.); Thierry, P (Thierry, P.); Turpin, D (Turpin, D.); Im, M (Im, M.); Choi, C (Choi, C.); Kim, J (Kim, J.); Yoon, Y (Yoon, Y.); Lim, G (Lim, G.); Lee, SK (Lee, S. -K.); Lee, CU (Lee, C. -U.); Kim, SL (Kim, S. -L.); Ko, SW (Ko, S. -W.); Joe, J (Joe, J.); Kwon, MK (Kwon, M. -K.); Kim, PJ (Kim, P. -J.); Lim, SK (Lim, S. -K.); Choi, JS (Choi, J. -S.); Fynbo, JPU (Fynbo, J. P. U.); Malesani, D (Malesani, D.); Xu, D (Xu, D.); Smartt, SJ (Smartt, S. J.); Jerkstrand, A (Jerkstrand, A.); Kankare, E (Kankare, E.); Sim, SA (Sim, S. A.); Fraser, M (Fraser, M.); Inserra, C (Inserra, C.); Maguire, K (Maguire, K.); Leloudas, G (Leloudas, G.); Magee, M (Magee, M.); Shingles, LJ (Shingles, L. J.); Smith, KW (Smith, K. W.); Young, DR (Young, D. R.); Kotak, R (Kotak, R.); Gal-Yam, A (Gal-Yam, A.); Lyman, JD (Lyman, J. D.); Homan, DS (Homan, D. S.); Agliozzo, C (Agliozzo, C.); Anderson, JP (Anderson, J. P.); Angus, CR (Angus, C. R.); Ashall, C (Ashall, C.); Barbarino, C (Barbarino, C.); Bauer, FE (Bauer, F. E.); Berton, M (Berton, M.); Botticella, MT (Botticella, M. T.); Bulla, M (Bulla, M.); Cannizzaro, G (Cannizzaro, G.); Cartier, R (Cartier, R.); Cikota, A (Cikota, A.); Clark, P (Clark, P.); De Cia, A (De Cia, A.); Della Valle, M (Della Valle, M.); Dennefeld, M (Dennefeld, M.); Dessart, L (Dessart, L.); Dimitriadis, G (Dimitriadis, G.); Elias-Rosa, N (Elias-Rosa, N.); Firth, RE (Firth, R. E.); Flors, A (Flors, A.); Frohmaier, C (Frohmaier, C.); Galbany, L (Galbany, L.); Gonzlez-Gaitn, S (Gonzlez-Gaitn, S.); Gromadzki, M (Gromadzki, M.); Gutierrez, CP (Gutierrez, C. P.); Hamanowicz, A (Hamanowicz, A.); Harmanen, J (Harmanen, J.); Heintz, KE (Heintz, K. E.); Hernandez, MS (Hernandez, M. -S.); Hodgkin, ST (Hodgkin, S. T.); Hook, IM (Hook, I. M.); Izzo, L (Izzo, L.); James, PA (James, P. A.); Jonker, PG (Jonker, P. G.); Kerzendorf, WE (Kerzendorf, W. E.); Kostrzewa-Rutkowska, Z (Kostrzewa-Rutkowska, Z.); Kromer, M (Kromer, M.); Kuncarayakti, H (Kuncarayakti, H.); Lawrence, A (Lawrence, A.); Manulis, I (Manulis, I.); Mattila, S (Mattila, S.); McBrien, O (McBrien, O.); Mller, A (Mller, A.); Nordin, J (Nordin, J.); O'Neill, D (O'Neill, D.); Onori, F (Onori, F.); Palmerio, JT (Palmerio, J. T.); Pastorello, A (Pastorello, A.); Patat, F (Patat, F.); Pignata, G (Pignata, G.); Podsiadlowski, P (Podsiadlowski, P.); Razza, A (Razza, A.); Reynolds, T (Reynolds, T.); Roy, R (Roy, R.); Ruiter, AJ (Ruiter, A. J.); Rybicki, KA (Rybicki, K. A.); Salmon, L (Salmon, L.); Pumo, ML (Pumo, M. L.); Prentice, SJ (Prentice, S. J.); Seitenzahl, IR (Seitenzahl, I. R.); Smith, M (Smith, M.); Sollerman, J (Sollerman, J.); Sullivan, M (Sullivan, M.); Szegedi, H (Szegedi, H.); Taddia, F (Taddia, F.); Taubenberger, S (Taubenberger, S.); Terreran, G (Terreran, G.); Van Soelen, B (Van Soelen, B.); Vos, J (Vos, J.); Walton, NA (Walton, N. A.); Wright, DE (Wright, D. E.); Wyrzykowski, L (Wyrzykowski, L.); Yaron, O (Yaron, O.); Chen, TW (Chen, T. -W.); Krhler, T (Krhler, T.); Schady, P (Schady, P.); Wiseman, P (Wiseman, P.); Greiner, J (Greiner, J.); Rau, A (Rau, A.); Schweyer, T (Schweyer, T.); Klose, S (Klose, S.); Guelbenzu, AN (Guelbenzu, A. Nicuesa); Palliyaguru, NT (Palliyaguru, N. T.); Shara, MM (Shara, M. M.); Williams, T (Williams, T.); Vaisanen, P (Vaisanen, P.); Potter, SB (Potter, S. B.); Colmenero, ER (Colmenero, E. Romero); Crawford, S (Crawford, S.); Buckley, DAH (Buckley, D. A. H.); Mao, J (Mao, J.); Diaz, MC (Diaz, M. C.); Macri, LM (Macri, L. M.); Lambas, DG (Lambas, D. Garcia); de Oliveira, CM (de Oliveira, C. Mendes); Castellon, JLN (Castellon, J. L. Nilo); Ribeiro, T (Ribeiro, T.); Sanchez, B (Sanchez, B.); Schoenell, W (Schoenell, W.); Abramo, LR (Abramo, L. R.); Akras, S (Akras, S.); Alcaniz, JS (Alcaniz, J. S.); Artola, R (Artola, R.); Beroiz, M (Beroiz, M.); Bonoli, S (Bonoli, S.); Cabral, J (Cabral, J.); Camuccio, R (Camuccio, R.); Chavushyan, V (Chavushyan, V.); Coelho, P (Coelho, P.); Colazo, C (Colazo, C.); Costa-Duarte, MV (Costa-Duarte, M. V.); Larenas, HC (Larenas, H. Cuevas); Romero, MD (Romero, M. Dominguez); Dultzin, D (Dultzin, D.); Fernandez, D (Fernandez, D.); Garcia, J (Garcia, J.); Girardini, C (Girardini, C.); Goncalves, DR (Goncalves, D. R.); Goncalves, TS (Goncalves, T. S.); Gurovich, S (Gurovich, S.); Jimenez-Teja, Y (Jimenez-Teja, Y.); Kanaan, A (Kanaan, A.); Lares, M (Lares, M.); de Oliveira, RL (de Oliveira, R. Lopes); Lopez-Cruz, O (Lopez-Cruz, O.); Melia, R (Melia, R.); Molino, A (Molino, A.); Padilla, N (Padilla, N.); Penuela, T (Penuela, T.); Placco, VM (Placco, V. M.); Quinones, C (Quinones, C.); Rivera, AR (Rivera,

A. Ramirez); Renzi, V (Renzi, V.); Riguccini, L (Riguccini, L.); Rios-Lopez, E (Rios-Lopez, E.); Rodriguez, H (Rodriguez, H.); Sampedro, L (Sampedro, L.); Schneiter, M (Schneiter, M.); Sodre, L (Sodre, L.); Starck, M (Starck, M.); Torres-Flores, S (Torres-Flores, S.); Tornatore, M (Tornatore, M.); Zadrozny, A (Zadrozny, A.); Castro-Tirado, AJ (Castro-Tirado, A. J.); Tello, JC (Tello, J. C.); Hu, YD (Hu, Y. -D.); Zhang, BB (Zhang, B. -B.); Cunniffe, R (Cunniffe, R.); Castelln, A (Castellon, A.); Hiriart, D (Hiriart, D.); Caballero-Garcia, MD (Caballero-Garcia, M. D.); Jelinek, M (Jelinek, M.); Kubnek, P (Kubanek, P.); Del Pulgar, CP (Del Pulgar, C. Perez); Park, IH (Park, I. H.); Jeong, S (Jeong, S.); Ceron, JMC (Ceron, J. M. Castro); Pandey, SB (Pandey, S. B.); Yock, PC (Yock, P. C.); Querel, R (Querel, R.); Fan, Y (Fan, Y.); Wang, C (Wang, C.); Beardsley, A (Beardsley, A.); Brown, IS (Brown, I. S.); Crosse, B (Crosse, B.); Emrich, D (Emrich, D.); Franzen, T (Franzen, T.); Gaensler, BM (Gaensler, B. M.); Horsley, L (Horsley, L.); Johnston-Hollitt, M (Johnston-Hollitt, M.); Kenney, D (Kenney, D.); Morales, MF (Morales, M. F.); Pallot, D (Pallot, D.); Sokolowski, M (Sokolowski, M.); Steele, K (Steele, K.); Tingay, SJ (Tingay, S. J.); Trott, CM (Trott, C. M.); Walker, M (Walker, M.); Wayth, R (Wayth, R.); Williams, A (Williams, A.); Wu, C (Wu, C.); Yoshida, A (Yoshida, A.); Sakamoto, T (Sakamoto, T.); Kawakubo, Y (Kawakubo, Y.); Yamaoka, K (Yamaoka, K.); Takahashi, I (Takahashi, I.); Asaoka, Y (Asaoka, Y.); Ozawa, S (Ozawa, S.); Torii, S (Torii, S.); Shimizu, Y (Shimizu, Y.); Tamura, T (Tamura, T.); Ishizaki, W (Ishizaki, W.); Cherry, ML (Cherry, M. L.); Ricciarini, S (Ricciarini, S.); Penacchioni, AV (Penacchioni, A. V.); Marrocchesi, PS (Marrocchesi, P. S.); Pozanenko, AS (Pozanenko, A. S.); Volnova, AA (Volnova, A. A.); Mazaeva, ED (Mazaeva, E. D.); Minaev, PY (Minaev, P. Yu.); Krugov, MA (Krugov, M. A.); Kusakin, AV (Kusakin, A. V.); Reva, IV (Reva, I. V.); Moskvitin, AS (Moskvitin, A. S.); Rumyantsev, VV (Rumyantsev, V. V.); Inasaridze, R (Inasaridze, R.); Klunko, EV (Klunko, E. V.); Tungalag, N (Tungalag, N.); Schmalz, SE (Schmalz, S. E.); Burhonov, O (Burhonov, O.); Abdalla, H (Abdalla, H.); Abramowski, A (Abramowski, A.); Aharonian, F (Aharonian, F.); Benkhali, FA (Benkhali, F. Ait); Angner, EO (Angner, E. O.); Arakawa, M (Arakawa, M.); Arrieta, M (Arrieta, M.); Aubert, P (Aubert, P.); Backes, M (Backes, M.); Balzer, A (Balzer, A.); Barnard, M (Barnard, M.); Becherini, Y (Becherini, Y.); Tjus, JB (Tjus, J. Becker); Berge, D (Berge, D.); Bernhard, S (Bernhard, S.); Bernlrhr, K (Bernrhr, K.); Blackwell, R (Blackwell, R.); Bottcher, M (Bottcher, M.); Boisson, C (Boisson, C.); Bolmont, J (Bolmont, J.); Bonnefoy, S (Bonnefoy, S.); Bordas, P (Bordas, P.); Bregeon, J (Bregeon, J.); Brun, F (Brun, F.); Brun, P (Brun, P.); Bryan, M (Bryan, M.); Bchele, M (Bchele, M.); Bulik, T (Bulik, T.); Capasso, M (Capasso, M.); Caroff, S (Caroff, S.); Carosi, A (Carosi, A.); Casanova, S (Casanova, S.); Cerruti, M (Cerruti, M.); Chakraborty, N (Chakraborty, N.); Chaves, RCG (Chaves, R. C. G.); Chen, A (Chen, A.); Chevalier, J (Chevalier, J.); Colafrancesco, S (Colafrancesco, S.); Condon, B (Condon, B.); Conrad, J (Conrad, J.); Davids, ID (Davids, I. D.); Decock, J (Decock, J.); Deil, C (Deil, C.); Devin, J (Devin, J.); Dewilt, P (Dewilt, P.); Dirson, L (Dirson, L.); Djannati-Atao, A (Djannati-Atao, A.); Donath, A (Donath, A.); Drury, LO (Drury, L. O'C.); Dutson, K (Dutson, K.); Dyks, J (Dyks, J.); Edwards, T (Edwards, T.); Egberts, K (Egberts, K.); Emery, G (Emery, G.); Ernenwein, JP (Ernenwein, J. -P.); Eschbach, S (Eschbach, S.); Farnier, C (Farnier, C.); Fegan, S (Fegan, S.); Fernandes, MV (Fernandes, M. V.); Fiasson, A (Fiasson, A.); Fontaine, G (Fontaine, G.); Funk, S (Funk, S.); Fssling, M (Fssling, M.); Gabici, S (Gabici, S.); Gallant, YA (Gallant, Y. A.); Garrigoux, T (Garrigoux, T.); Gate, F (Gate, F.); Giavitto, G (Giavitto, G.); Giebels, B (Giebels, B.); Glawion, D (Glawion, D.); Glicenstein, JF (Glicenstein, J. F.); Gottschall, D (Gottschall, D.); Grondin, MH (Grondin, M. -H.); Hahn, J (Hahn, J.); Haupt, M (Haupt, M.); Hawkes, J (Hawkes, J.); Heinzelmann, G (Heinzelmann, G.); Henri, G (Henri, G.); Hermann, G (Hermann, G.); Hinton, JA (Hinton, J. A.); Hofmann, W (Hofmann, W.); Hoischen, C (Hoischen, C.); Holch, TL (Holch, T. L.); Holler, M (Holler, M.); Horns, D (Horns, D.); Ivascenko, A (Ivascenko, A.); Iwasaki, H (Iwasaki, H.); Jacholkowska, A (Jacholkowska, A.); Jamrozy, M (Jamrozy, M.); Jankowsky, D (Jankowsky, D.); Jankowsky, F (Jankowsky, F.); Jingo, M (Jingo, M.); Jouvin, L (Jouvin, L.); Jung-Richardt, I (Jung-Richardt, I.); Kastendieck, MA (Kastendieck, M. A.); Katarzynski, K (Katarzynski, K.); Katsuragawa, M (Katsuragawa, M.); Khangulyan, D (Khangulyan, D.); Khelifi, B (Khelifi, B.); King, J (King, J.); Klepser, S (Klepser, S.); Klochkov, D (Klochkov, D.); Kluzniak, W (Kluzniak, W.); Komin, N (Komin, Nu.); Kosack, K (Kosack, K.); Krakau, S (Krakau, S.); Kraus, M (Kraus, M.); Krger, PP (Krger, P. P.); Laffon, H (Laffon, H.); Lamanna, G (Lamanna, G.); Lau, J (Lau, J.); Lees, JP (Lees, J. -P.); Lefaucheur, J (Lefaucheur, J.); Lemiere, A (Lemiere, A.); Lemoine-Goumard, M (Lemoine-Goumard, M.); Lenain, JP (Lenain, J. -P.); Leser, E (Leser, E.); Lohse, T (Lohse, T.); Lorentz, M (Lorentz, M.); Liu, R (Liu, R.); Lypova, I (Lypova, I.); Malyshev, D (Malyshev, D.); Marandon, V (Marandon, V.); Marcowith, A (Marcowith, A.); Mariaud, C (Mariaud, C.); Marx, R (Marx, R.); Maurin, G (Maurin, G.); Maxted, N (Maxted, N.); Mayer, M (Mayer, M.); Meintjes, PJ (Meintjes, P. J.); Meyer, M (Meyer, M.); Mitchell, AMW (Mitchell, A. M. W.); Moderski, R (Moderski, R.); Mohamed, M (Mohamed, M.); Mohrmann, L (Mohrmann, L.); Mor, K (Mor, K.); Moulin, E (Moulin, E.); Murach, T (Murach, T.); Nakashima, S (Nakashima, S.); De Naurois, M (De Naurois, M.); Ndiyavala, H (Ndiyavala, H.); Niederwanger, F (Niederwanger, F.); Niemiec, J (Niemiec, J.); Oakes, L (Oakes, L.); O'Brien, P (O'Brien, P.); Odaka, H (Odaka, H.); Ohm, S (Ohm, S.); Ostrowski, M (Ostrowski, M.); Oya, I (Oya, I.); Padovani, M (Padovani, M.); Panter, M (Panter, M.); Parsons, RD (Parsons, R. D.); Pekeur, NW (Pekeur, N. W.); Pelletier, G (Pelletier, G.); Perennes, C (Perennes, C.); Petrucci, PO (Petrucci, P. -O.); Peyaud, B (Peyaud, B.); Piel, Q (Piel, Q.); Pita, S (Pita, S.); Poireau, V (Poireau, V.); Poon, H (Poon, H.); Prokhorov, D (Prokhorov, D.); Prokoph, H (Prokoph, H.); Phlhofer, G (Phlhofer, G.); Punch, M (Punch, M.); Quirrenbach, A (Quirrenbach, A.); Raab, S (Raab, S.); Rauth, R (Rauth, R.); Reimer, A (Reimer, A.); Reimer, O (Reimer, O.); Renaud, M (Renaud, M.); Reyes, RDL (Reyes, R. De Los); Rieger, F (Rieger, F.); Rinchiuso, L (Rinchiuso, L.); Romoli, C (Romoli, C.); Rowell, G (Rowell, G.); Rudak, B (Rudak, B.); Rulten, CB (Rulten, C. B.); Sahakian, V (Sahakian, V.); Saito, S (Saito, S.); Sanchez, DA (Sanchez, D. A.); Santangelo, A (Santangelo, A.); Sasaki, M (Sasaki, M.); Schlickeiser, R (Schlickeiser, R.); Schssler, F (Schssler, F.); Schulz, A (Schulz, A.); Schwanke, U (Schwanke, U.); Schwemmer, S (Schwemmer, S.); Seglar-Arroyo, M (Seglar-Arroyo, M.); Settimo, M (Settimo, M.); Seyffert, AS (Seyffert, A. S.); Shafi, N (Shafi, N.); Shilon, I (Shilon, I.); Shiningayamwe, K (Shiningayamwe, K.); Simoni, R (Simoni, R.); Sol, H (Sol, H.); Spanier, F (Spanier, F.); Spir-Jacob, M (Spir-Jacob, M.); Stawarz, L (Stawarz, L.); Steenkamp, R (Steenkamp, R.); Stegmann, C (Stegmann, C.); Steppa, C (Steppa, C.); Sushch, I (Sushch, I.); Takahashi, T (Takahashi, T.); Tavernet, JP (Tavernet, J. -P.); Tavernier, T (Tavernier, T.); Taylor, AM (Taylor, A. M.); Terrier, R (Terrier, R.); Tibaldo, L (Tibaldo, L.); Tiziani, D (Tiziani, D.); Tluczykont, M (Tluczykont, M.); Trichard, C (Trichard, C.); Tsirou, M (Tsirou, M.); Tsuji, N (Tsuji, N.); Tuffs, R (Tuffs, R.); Uchiyama, Y (Uchiyama, Y.); Van der Walt, DJ (Van der Walt, D. J.); Van Eldik, C (Van Eldik, C.); Van Rensburg, C (Van Rensburg, C.); Van Soelen, B (Van Soelen, B.); Vasileiadis, G (Vasileiadis, G.); Veh, J (Veh, J.); Venter, C (Venter, C.); Viana, A (Viana, A.); Vincent, P (Vincent, P.); Vink, J (Vink, J.); Voisin, F (Voisin, F.); Volk, HJ (Volk, H. J.); Vuillaume, T (Vuillaume, T.); Wadiasingh, Z (Wadiasingh, Z.); Wagner, SJ (Wagner, S. J.); Wagner, P (Wagner, P.); Wagner, RM (Wagner, R. M.); White, R (White, R.); Wierzcholska, A (Wierzcholska, A.); Willmann, P (Willmann, P.); WRnlein, A (WRnlein, A.); Wouters, D (Wouters, D.); Yang, R (Yang, R.); Zaborov, D (Zaborov, D.); Zacharias, M (Zacharias, M.); Zanin, R (Zanin, R.); Zdziarski, AA (Zdziarski, A. A.); Zech, A

(Zech, A.); Zefi, F (Zefi, F.); Ziegler, A (Ziegler, A.); Zorn, J (Zorn, J.); Zywucka, N (Zywucka, N.); Fender, RP (Fender, R. P.); Broderick, JW (Broderick, J. W.); Rowlinson, A (Rowlinson, A.); Wijers, RAMJ (Wijers, R. A. M. J.); Stewart, AJ (Stewart, A. J.); Ter Veen, S (Ter Veen, S.); Shulevski, A (Shulevski, A.); Kavic, M (Kavic, M.); Simonetti, JH (Simonetti, J. H.); League, C (League, C.); Tsai, J (Tsai, J.); Obenberger, KS (Obenberger, K. S.); Nathaniel, K (Nathaniel, K.); Taylor, GB (Taylor, G. B.); Dowell, JD (Dowell, J. D.); Liebling, SL (Liebling, S. L.); Estes, JA (Estes, J. A.); Lippert, M (Lippert, M.); Sharma, I (Sharma, I.); Vincent, P (Vincent, P.); Farella, B (Farella, B.); Abeysekara, AU (Abeysekara, A. U.); Albert, A (Albert, A.); Alfaro, R (Alfaro, R.); Alvarez, C (Alvarez, C.); Arceo, R (Arceo, R.); Arteaga-Velzquez, JC (Arteaga-Velzquez, J. C.); Rojas, DA (Rojas, D. Avila); Solares, HAA (Solares, H. A. Ayala); Barber, AS (Barber, A. S.); Gonzalez, JB (Gonzalez, J. Becerra); Becerril, A (Becerril, A.); Belmont-Moreno, E (Belmont-Moreno, E.); BenZvi, SY (BenZvi, S. Y.); Berley, D (Berley, D.); Bernal, A (Bernal, A.); Braun, J (Braun, J.); Brisbois, C (Brisbois, C.); Caballero-Mora, KS (Caballero-Mora, K. S.); Capistrn, T (Capistrn, T.); Carramiana, A (Carramiana, A.); Casanova, S (Casanova, S.); Castillo, M (Castillo, M.); Cotti, U (Cotti, U.); Cotzomi, J (Cotzomi, J.); De Leon, SC (De Leon, S. Coutio); De Leon, C (De Leon, C.); De la Fuente, E (De la Fuente, E.); Hernandez, RD (Hernandez, R. Diaz); Dichiara, S (Dichiara, S.); Dingus, BL (Dingus, B. L.); DuVernois, MA (DuVernois, M. A.); Diaz-Velez, JC (Diaz-Velez, J. C.); Ellsworth, RW (Ellsworth, R. W.); Engel, K (Engel, K.); Enriquez-Rivera, O (Enriquez-Rivera, O.); Fiorino, DW (Fiorino, D. W.); Fleischhack, H (Fleischhack, H.); Fraija, N (Fraija, N.); Garcia-Gonzlez, JA (Garcia-Gonzlez, J. A.); Garfias, F (Garfias, F.); Gerhardt, M (Gerhardt, M.); Muoz, AG (Muoz, A. Gonzolez); Gonzlez, MM (Gonzlez, M. M.); Goodman, JA (Goodman, J. A.); Hampel-Arias, Z (Hampel-Arias, Z.); Harding, JP (Harding, J. P.); Hernandez, S (Hernandez, S.); Hernandez-Almada, A (Hernandez-Almada, A.); Hona, B (Hona, B.); Hntemeyer, P (Hntemeyer, P.); Iriarte, A (Iriarte, A.); Jardin-Blicq, A (Jardin-Blicq, A.); Joshi, V (Joshi, V.); Kaufmann, S (Kaufmann, S.); Kieda, D (Kieda, D.); Lara, A (Lara, A.); Lauer, RJ (Lauer, R. J.); Lennarz, D (Lennarz, D.); Vargas, HL (Vargas, H. Leon); Linnemann, JT (Linnemann, J. T.); Longinotti, AL (Longinotti, A. L.); Raya, GL (Raya, G. Luis); Luna-Garcia, R (Luna-Garcia, R.); Lopez-Coto, R (Lopez-Coto, R.); Malone, K (Malone, K.); Marinelli, SS (Marinelli, S. S.); Martinez, O (Martinez, O.); Martinez-Castellanos, I (Martinez-Castellanos, I.); Martinez-Castro, J (Martinez-Castro, J.); Martinez-Huerta, H (Martinez-Huerta, H.); Matthews, JA (Matthews, J. A.); Miranda-Romagnoli, P (Miranda-Romagnoli, P.); Moreno, E (Moreno, E.); Mostaf, M (Mostaf, M.); Nellen, L (Nellen, L.); Newbold, M (Newbold, M.); Nisa, MU (Nisa, M. U.); Noriega-Papaqui, R (Noriega-Papaqui, R.); Pelayo, R (Pelayo, R.); Pretz, J (Pretz, J.); Perez-Perez, EG (Perez-Perez, E. G.); Ren, Z (Ren, Z.); Rho, CD (Rho, C. D.); Riviere, C (Riviere, C.); Rosa-Gonzlez, D (Rosa-Gonzlez, D.); Rosenberg, M (Rosenberg, M.); Ruiz-Velasco, E (Ruiz-Velasco, E.); Salazar, H (Salazar, H.); Greus, FS (Greus, F. Salesa); Sandoval, A (Sandoval, A.); Schneider, M (Schneider, M.); Schoorlemmer, H (Schoorlemmer, H.); Sinnis, G (Sinnis, G.); Smith, AJ (Smith, A. J.); Springer, RW (Springer, R. W.); Surajbali, P (Surajbali, P.); Tibolla, O (Tibolla, O.); Tollefson, K (Tollefson, K.); Torres, I (Torres, I.); Ukwatta, TN (Ukwatta, T. N.); Weisgarber, T (Weisgarber, T.); Westerhoff, S (Westerhoff, S.); Wisher, IG (Wisher, I. G.); Wood, J (Wood, J.); Yapici, T (Yapici, T.); Yodh, GB (Yodh, G. B.); Younk, PW (Younk, P. W.); Zhou, H (Zhou, H.); Alvarez, JD (Alvarez, J. D.); Aab, A (Aab, A.); Abreu, P (Abreu, P.); Aglietta, M (Aglietta, M.); Albuquerque, IFM (Albuquerque, I. F. M.); Albury, JM (Albury, J. M.); Allekotte, I (Allekotte, I.); Almela, A (Almela, A.); Castillo, JA (Castillo, J. Alvarez); Alvarez-Muiz, J (Alvarez-Muiz, J.); Anastasi, GA (Anastasi, G. A.); Anchordoqui, L (Anchordoqui, L.); Andrada, B (Andrada, B.); Andringa, S (Andringa, S.); Aramo, C (Aramo, C.); Arsene, N (Arsene, N.); Asorey, H (Asorey, H.); Assis, P (Assis, P.); Avila, G (Avila, G.); Badescu, AM (Badescu, A. M.); Balaceanu, A (Balaceanu, A.); Barbato, F (Barbato, F.); Luz, RJB (Luz, R. J. Barreira); Becker, KH (Becker, K. H.); Bellido, JA (Bellido, J. A.); Berat, C (Berat, C.); Bertaina, ME (Bertaina, M. E.); Bertou, X (Bertou, X.); Biermann, PL (Biermann, P. L.); Biteau, J (Biteau, J.); Blaess, SG (Blaess, S. G.); Blanco, A (Blanco, A.); Blazek, J (Blazek, J.); Bleve, C (Bleve, C.); Bohacova, M (Bohacova, M.); Bonifazi, C (Bonifazi, C.); Borodai, N (Borodai, N.); Botti, AM (Botti, A. M.); Brack, J (Brack, J.); Brancus, I (Brancus, I.); Bretz, T (Bretz, T.); Bridgeman, A (Bridgeman, A.); Briechle, FL (Briechle, F. L.); Buchholz, P (Buchholz, P.); Bueno, A (Bueno, A.); Buitink, S (Buitink, S.); Buscemi, M (Buscemi, M.); Caballero-Mora, KS (Caballero-Mora, K. S.); Caccianiga, L (Caccianiga, L.); Cancio, A (Cancio, A.); Canfora, F (Canfora, F.); Caruso, R (Caruso, R.); Castellina, A (Castellina, A.); Catalani, F (Catalani, F.); Cataldi, G (Cataldi, G.); Cazon, L (Cazon, L.); Chavez, AG (Chavez, A. G.); Chinellato, JA (Chinellato, J. A.); Chudoba, J (Chudoba, J.); Clay, RW (Clay, R. W.); Cerutti, ACC (Cerutti, A. C. Cobos); Colalillo, R (Colalillo, R.); Coleman, A (Coleman, A.); Collica, L (Collica, L.); Coluccia, MR (Coluccia, M. R.); Conceicao, R (Conceicao, R.); Consolati, G (Consolati, G.); Contreras, F (Contreras, F.); Cooper, MJ (Cooper, M. J.); Coutu, S (Coutu, S.); Covault, CE (Covault, C. E.); Cronin, J (Cronin, J.); D'Amico, S (D'Amico, S.); Daniel, B (Daniel, B.); Dasso, S (Dasso, S.); Daumiller, K (Daumiller, K.); Dawson, BR (Dawson, B. R.); Day, JA (Day, J. A.); De Almeida, RM (De Almeida, R. M.); De Jong, SJ (De Jong, S. J.); De Mauro, G (De Mauro, G.); Neto, JRTDM (Neto, J. R. T. De Mello); De Mitri, I (De Mitri, I.); De Oliveira, J (De Oliveira, J.); De Souza, V (De Souza, V.); Debatin, J (Debatin, J.); Deligny, O (Deligny, O.); Castro, MLD (Castro, M. L. Diaz); Diogo, F (Diogo, F.); Dobrigkeit, C (Dobrigkeit, C.); D'Olivo, JC (D'Olivo, J. C.); Dorosti, Q (Dorosti, Q.); Dos Anjos, RC (Dos Anjos, R. C.); Dova, MT (Dova, M. T.); Dundovic, A (Dundovic, A.); Ebr, J (Ebr, J.); Engel, R (Engel, R.); Erdmann, M (Erdmann, M.); Erfani, M (Erfani, M.); Escobar, CO (Escobar, C. O.); Espadanal, J (Espadanal, J.); Etchegoyen, A (Etchegoyen, A.); Falcke, H (Falcke, H.); Farmer, J (Farmer, J.); Farrar, G (Farrar, G.); Fauth, AC (Fauth, A. C.); Fazzini, N (Fazzini, N.); Feldbusch, F (Feldbusch, F.); Fenu, F (Fenu, F.); Fick, B (Fick, B.); Figueira, JM (Figueira, J. M.); Filipcic, A (Filipcic, A.); Freire, MM (Freire, M. M.); Fujii, T (Fujii, T.); Fuster, A (Fuster, A.); Gaior, R (Gaior, R.); Garcia, B (Garcia, B.); Gate, F (Gate, F.); Gemmeke, H (Gemmeke, H.); Gherghel-Lascu, A (Gherghel-Lascu, A.); Ghia, PL (Ghia, P. L.); Giaccari, U (Giaccari, U.); Giammarchi, M (Giammarchi, M.); Giller, M (Giller, M.); Glas, D (Glas, D.); Glaser, C (Glaser, C.); Golup, G (Golup, G.); Berisso, MG (Berisso, M. Gomez); Vitale, PFG (Vitale, P. F. Gomez); Gonzlez, N (Gonzlez, N.); Gorgi, A (Gorgi, A.); Gottowik, M (Gottowik, M.); Grillo, AF (Grillo, A. F.); Grubb, TD (Grubb, T. D.); Guarino, F (Guarino, F.); Guedes, GP (Guedes, G. P.); Halliday, R (Halliday, R.); Hampel, MR (Hampel, M. R.); Hansen, P (Hansen, P.); Harari, D (Harari, D.); Harrison, TA (Harrison, T. A.); Harvey, VM (Harvey, V. M.); Haungs, A (Haungs, A.); Hebbeker, T (Hebbeker, T.); Heck, D (Heck, D.); Heimann, P (Heimann, P.); Herve, AE (Herve, A. E.); Hill, GC (Hill, G. C.); Hojvat, C (Hojvat, C.); Holt, EW (Holt, E. W.); Homola, P (Homola, P.); Horandel, JR (Horandel, J. R.); Horvath, P (Horvath, P.); Hrabovsky, M (Hrabovsky, M.); Huege, T (Huege, T.); Hulsman, J (Hulsman, J.); Insolia, A (Insolia, A.); Isar, PG (Isar, P. G.); Jandt, I (Jandt, I.); Johnsen, JA (Johnsen, J. A.); Josebachuili, M (Josebachuili, M.); Jurysek, J (Jurysek, J.); Kaapa, A (Kaapa, A.); Kampert, KH (Kampert, K. H.); Keilhauer, B (Keilhauer, B.); Kemmerich, N (Kemmerich, N.); Kemp, J (Kemp, J.); Kieckhafer, RM (Kieckhafer, R. M.); Klages, HO (Klages, H. O.); Kleifges, M (Kleifges, M.); Kleinfeller, J (Kleinfeller, J.); Krause, R (Krause, R.); Krohm, N (Krohm, N.); Kuempel, D (Kuempel, D.); Mezek, GK (Mezek, G. Kukec); Kunka, N (Kunka, N.); Awad, AK

(Awad, A. Kuotb); Lago, BL (Lago, B. L.); LaHurd, D (LaHurd, D.); Lang, RG (Lang, R. G.); Lauscher, M (Lauscher, M.); Legumina, R (Legumina, R.); De Oliveira, MAL (De Oliveira, M. A. Leigui); Letessier-Selvon, A (Letessier-Selvon, A.); Lhenry-Yvon, I (Lhenry-Yvon, I.); Link, K (Link, K.); Lo Presti, D (Lo Presti, D.); Lopes, L (Lopes, L.); Lopez, R (Lopez, R.); Casado, AL (Casado, A. Lopez); Lorek, R (Lorek, R.); Luce, Q (Luce, Q.); Lucero, A (Lucero, A.); Malacari, M (Malacari, M.); Mallamaci, M (Mallamaci, M.); Mandat, D (Mandat, D.); Mantsch, P (Mantsch, P.); Mariazzi, AG (Mariazzi, A. G.); Maris, IC (Maris, I. C.); Marsella, G (Marsella, G.); Martello, D (Martello, D.); Martinez, H (Martinez, H.); Bravo, OM (Bravo, O. Martinez); Meza, JJM (Meza, J. J. Masias); Mathes, HJ (Mathes, H. J.); Mathys, S (Mathys, S.); Matthews, J (Matthews, J.); Matthiae, G (Matthiae, G.); Mayotte, E (Mayotte, E.); Mazur, PO (Mazur, P. O.); Medina, C (Medina, C.); Medina-Tanco, G (Medina-Tanco, G.); Melo, D (Melo, D.); Menshikov, A (Menshikov, A.); Merenda, KD (Merenda, K. -D.); Michal, S (Michal, S.); Micheletti, MI (Micheletti, M. I.); Middendorf, L (Middendorf, L.); Miramonti, L (Miramonti, L.); Mitrica, B (Mitrica, B.); Mockler, D (Mockler, D.); Mollerach, S (Mollerach, S.); Montanet, F (Montanet, F.); Morello, C (Morello, C.); Morlino, G (Morlino, G.); Muller, AL (Mueller, A. L.); Muller, G (Mueller, G.); Muller, MA (Mueller, M. A.); Muller, S (Mueller, S.); Mussa, R (Mussa, R.); Naranjo, I (Naranjo, I.); Nguyen, PH (Nguyen, P. H.); Niculescu-Oglinzanu, M (Niculescu-Oglinzanu, M.); Niechciol, M (Niechciol, M.); Niemietz, L (Niemietz, L.); Niggemann, T (Niggemann, T.); Nitz, D (Nitz, D.); Nosek, D (Nosek, D.); Novotny, V (Novotny, V.); Nozka, L (Nozka, L.); Nunez, LA (Nunez, L. A.); Oikonomou, F (Oikonomou, F.); Olinto, A (Olinto, A.); Palatka, M (Palatka, M.); Pallotta, J (Pallotta, J.); Papenbreer, P (Papenbreer, P.); Parente, G (Parente, G.); Parra, A (Parra, A.); Paul, T (Paul, T.); Pech, M (Pech, M.); Pedreira, F (Pedreira, F.); Kala, JP (Kala, J. P.); Pea-Rodriguez, J (Pea-Rodriguez, J.); Pereira, LAS (Pereira, L. A. S.); Perlin, M (Perlin, M.); Perrone, L (Perrone, L.); Peters, C (Peters, C.); Petrera, S (Petrera, S.); Phuntsok, J (Phuntsok, J.); Pierog, T (Pierog, T.); Pimenta, M (Pimenta, M.); Pirronello, V (Pirronello, V.); Platino, M (Platino, M.); Plum, M (Plum, M.); Poh, J (Poh, J.); Porowski, C (Porowski, C.); Prado, RR (Prado, R. R.); Privitera, P (Privitera, P.); Prouza, M (Prouza, M.); Quel, EJ (Quel, E. J.); Querchfeld, S (Querchfeld, S.); Quinn, S (Quinn, S.); Ramos-Pollan, R (Ramos-Pollan, R.); Rautenberg, J (Rautenberg, J.); Ravignani, D (Ravignani, D.); Ridky, J (Ridky, J.); Riehn, F (Riehn, F.); Risse, M (Risse, M.); Ristori, P (Ristori, P.); Rizi, V (Rizi, V.); De Carvalho, WR (De Carvalho, W. Rodrigues); Fernandez, GR (Fernandez, G. Rodriguez); Rojo, JR (Rojo, J. Rodriguez); Roncoroni, MJ (Roncoroni, M. J.); Roth, M (Roth, M.); Roulet, E (Roulet, E.); Rovero, AC (Rovero, A. C.); Ruehl, P (Ruehl, P.); Saffi, SJ (Saffi, S. J.); Saftoiu, A (Saftoiu, A.); Salamida, F (Salamida, F.); Salazar, H (Salazar, H.); Saleh, A (Saleh, A.); Salina, G (Salina, G.); Sanchez, F (Sanchez, F.); Sanchez-Lucas, P (Sanchez-Lucas, P.); Santos, EM (Santos, E. M.); Santos, E (Santos, E.); Sarazin, F (Sarazin, F.); Sarmento, R (Sarmento, R.); Sarmiento-Cano, C (Sarmiento-Cano, C.); Sato, R (Sato, R.); Schauer, M (Schauer, M.); Scherini, V (Scherini, V.); Schieler, H (Schieler, H.); Schimp, M (Schimp, M.); Schmidt, D (Schmidt, D.); Scholten, O (Scholten, O.); Schovnek, P (Schovnek, P.); Schroder, FG (Schroder, F. G.); Schroder, S (Schroder, S.); Schulz, A (Schulz, A.); Schumacher, J (Schumacher, J.); Sciutto, SJ (Sciutto, S. J.); Segreto, A (Segreto, A.); Shadkam, A (Shadkam, A.); Shellard, RC (Shellard, R. C.); Sigl, G (Sigl, G.); Silli, G (Silli, G.); Smida, R (Smida, R.); Snow, GR (Snow, G. R.); Sommers, P (Sommers, P.); Sonntag, S (Sonntag, S.); Soriano, JF (Soriano, J. F.); Squartini, R (Squartini, R.); Stanca, D (Stanca, D.); Stanic, S (Stanic, S.); Stasielak, J (Stasielak, J.); Stassi, P (Stassi, P.); Stolpovskiy, M (Stolpovskiy, M.); Strafella, F (Strafella, F.); Streich, A (Streich, A.); Suarez, F (Suarez, F.); Suarez-Duran, M (Suarez-Duran, M.); Sudholz, T (Sudholz, T.); Suomijarvi, T (Suomijarvi, T.); Supanitsky, AD (Supanitsky, A. D.); Supik, J (Supik, J.); Swain, J (Swain, J.); Szadkowski, Z (Szadkowski, Z.); Taboada, A (Taboada, A.); Taborda, OA (Taborda, O. A.); Timmermans, C (Timmermans, C.); Tomankova, CJT (Peixoto, C. J. Todero); Tomankova, L (Tomankova, L.); Tom, B (Tome, B.); Elipe, GT (Elipe, G. Torralba); Travnicek, P (Travnicek, P.); Trini, M (Trini, M.); Tueros, M (Tueros, M.); Ulrich, R (Ulrich, R.); Unger, M (Unger, M.); Urban, M (Urban, M.); Galicia, JFV (Galicia, J. F. Valdes); Valio, I (Valio, I.); Valore, L (Valore, L.); Van Aar, G (Van Aar, G.); Van Bodegom, P (Van Bodegom, P.); Van den Berg, AM (Van den Berg, A. M.); Van Vliet, A (Van Vliet, A.); Varela, E (Varela, E.); Cardenas, BV (Cardenas, B. Vargas); Vazquez, RA (Vazquez, R. A.); Veberic, D (Veberic, D.); Ventura, C (Ventura, C.); Quispe, IDV (Quispe, I. D. Vergara); Verzi, V (Verzi, V.); Vicha, J (Vicha, J.); Villaseor, L (Villaseor, L.); Vorobiov, S (Vorobiov, S.); Wahlberg, H (Wahlberg, H.); Wainberg, O (Wainberg, O.); Walz, D (Walz, D.); Watson, AA (Watson, A. A.); Weber, M (Weber, M.); Weindl, A (Weindl, A.); Wiedenski, M (Wiedenski, M.); Wiencke, L (Wiencke, L.); Wilczynski, H (Wilczynski, H.); Wirtz, M (Wirtz, M.); Wittkowski, D (Wittkowski, D.); Wundheiler, B (Wundheiler, B.); Yang, L (Yang, L.); Yushkov, A (Yushkov, A.); Zas, E (Zas, E.); Zavrtanik, D (Zavrtanik, D.); Zavrtanik, M (Zavrtanik, M.); Zepeda, A (Zepeda, A.); Zimmermann, B (Zimmermann, B.); Ziolkowski, M (Ziolkowski, M.); Zong, Z (Zong, Z.); Zuccarello, F (Zuccarello, F.); Kim, S (Kim, S.); Schulze, S (Schulze, S.); Bauer, FE (Bauer, F. E.); Corral-Santana, JM (Corral-Santana, J. M.); De Gregorio-Monsalvo, I (De Gregorio-Monsalvo, I.); Gonzlez-Lopez, J (Gonzlez-Lopez, J.); Hartmann, DH (Hartmann, D. H.); Ishwara-Chandra, CH (Ishwara-Chandra, C. H.); Martin, S (Martin, S.); Mehner, A (Mehner, A.); Misra, K (Misra, K.); Michalowski, MJ (Michalowski, M. J.); Resmi, L (Resmi, L.); Paragi, Z (Paragi, Z.); Agudo, I (Agudo, I.); An, T (An, T.); Beswick, R (Beswick, R.); Casadio, C (Casadio, C.); Frey, S (Frey, S.); Jonker, P (Jonker, P.); Kettenis, M (Kettenis, M.); Marcote, B (Marcote, B.); Moldon, J (Moldon, J.); Szomoru, A (Szomoru, A.); Langevelde, HJ (Langevelde, H. J.); Yang, J (Yang, J.); Cwiek, A (Cwiek, A.); Cwiok, M (Cwiok, M.); Czyrkowski, H (Czyrkowski, H.); Dabrowski, R (Dabrowski, R.); Kasprowicz, G (Kasprowicz, G.); Mankiewicz, L (Mankiewicz, L.); Nawrocki, K (Nawrocki, K.); Opiela, R (Opiela, R.); Piotrowski, LW (Piotrowski, L. W.); Wrochna, G (Wrochna, G.); Zaremba, M (Zaremba, M.); Zarnecki, AF (Zarnecki, A. F.); Haggard, D (Haggard, D.); Nynka, M (Nynka, M.); Ruan, JJ (Ruan, J. J.); Bland, PA (Bland, P. A.); Booler, T (Booler, T.); Devillepoix, HAR (Devillepoix, H. A. R.); De Gois, JS (De Gois, J. S.); Hancock, PJ (Hancock, P. J.); Howie, RM (Howie, R. M.); Paxman, J (Paxman, J.); Sansom, EK (Sansom, E. K.); Towner, MC (Towner, M. C.); Tonry, J (Tonry, J.); Coughlin, M (Coughlin, M.); Stubbs, CW (Stubbs, C. W.); Denneau, L (Denneau, L.); Heinze, A (Heinze, A.); Stalder, B (Stalder, B.); Weiland, H (Weiland, H.); Eatough, RP (Eatough, R. P.); Kramer, M (Kramer, M.); Kraus, A (Kraus, A.); Troja, E (Troja, E.); Piro, L (Piro, L.); Gonzlez, JB (Gonzlez, J. Becerra); Butler, NR (Butler, N. R.); Fox, OD (Fox, O. D.); Khandrika, HG (Khandrika, H. G.); Kutyrev, A (Kutyrev, A.); Lee, WH (Lee, W. H.); Ricci, R (Ricci, R.); Ryan, RE (Ryan, R. E., Jr.); Sanchez-Ramirez, R (Sanchez-Ramirez, R.); Veilleux, S (Veilleux, S.); Watson, AM (Watson, A. M.); Wieringa, MH (Wieringa, M. H.); Burgess, JM (Burgess, J. M.); Van Eerten, H (Van Eerten, H.); Fontes, CJ (Fontes, C. J.); Fryer, CL (Fryer, C. L.); Korobkin, O (Korobkin, O.); Wollaeger, RT (Wollaeger, R. T.); Camilo, F (Camilo, F.); Foley, AR (Foley, A. R.); Goedhart, S (Goedhart, S.); Makhathini, S (Makhathini, S.); Oozeer, N (Oozeer, N.); Smirnov, OM (Smirnov, O. M.); Fender, RP (Fender, R. P.); Woudt, PA (Woudt, P. A.)

团体作者: LIGO Sci Collaboration & Virgo; Fermi GBM; INTERGRAL; IceCube Collaboration; AstroSat Cadmium Zinc Telluride; IPN Collaboration; Insight-Hxmt Collaboration; ANTARES Collaboration; Swift Collaboration; AGILE Team; The 1M2H Team; Dark Energy Camera GW-EM; DLT40 Collaboration;

GRAWITA GRAvitational Wave; Fermi Large Area Telescope; ATCA Australia Telescope; ASKAP Australian SKA Pathfinder; Las Cumbres Observatory Grp; OzGrav DWF Deeper Wider Faster; VINROUGE Collaboration; MASTER Collaboration; J-GEM; GROWTH JAGWAR CALTECH; Pan-STARRS; MAXI Team; TZAC Consortium; KU Collaboration; Nordic Optical Telescope; ePESSTO; GROUND; Texas Tech Univ; Salt Grp; Toros Transient Robotic Observat; BOOTES Collaboration; MWA Murchison Widefield Array; CALET Collaboration; IKI-GW Follow-up Collaboration; H E S S Collaboration; LOFAR Collaboration; LWA Long Wavelength Array; HAWC Collaboration; Pierre Auger Collaboration; ALMA Collaboration; Euro VLBI Team; Pi Sky Collaboration; Chandra Team McGill Univ; DFN Desert Fireball Network; ATLAS; High Time Resolution Universe; RIMAS RATIR; SKA South Africa MeerKAT
ASTROPHYSICAL JOURNAL LETTERS
卷: 848 期: 2 文献号: L12
On 2017 August 17 a binary neutron star coalescence candidate (later designated GW170817) with merger time 12:41:04 UTC was observed through gravitational waves by the Advanced LIGO and Advanced Virgo detectors. The Fermi Gamma-ray Burst Monitor independently detected a gamma-ray burst (GRB 170817A) with a time delay of similar to 1.7 s with respect to the merger time. From the gravitational-wave signal, the source was initially localized to a sky region of 31 deg(2) at a luminosity distance of 40(-8)(+8) Mpc and with component masses consistent with neutron stars. The component masses were later measured to be in the range 0.86 to 2.26 M-circle dot. An extensive observing campaign was launched across the electromagnetic spectrum leading to the discovery of a bright optical transient (SSS17a, now with the IAU identification of AT 2017gfo) in NGC 4993 (at similar to 40 Mpc) less than 11 hours after the merger by the One-Meter, Two Hemisphere (1M2H) team using the 1 m Swope Telescope. The optical transient was independently detected by multiple teams within an hour. Subsequent observations targeted the object and its environment. Early ultraviolet observations revealed a blue transient that faded within 48 hours. Optical and infrared observations showed a redward evolution over similar to 10 days. Following early non-detections, X-ray and radio emission were discovered at the transient's position similar to 9 and similar to 16 days, respectively, after the merger. Both the X-ray and radio emission likely arise from a physical process that is distinct from the one that generates the UV/optical/near-infrared emission. No ultra-high-energy gamma-rays and no neutrino candidates consistent with the source were found in follow-up searches. These observations support the hypothesis that GW170817 was produced by the merger of two neutron stars in NGC4993 followed by a short gamma-ray burst (GRB 170817A) and a kilonova/macronova powered by the radioactive decay of r-process nuclei synthesized in the ejecta.

第 5 条 , 共 286 条

The GW170817/GRB 170817A/AT 2017gfo Association: Some Implications for Physics and Astrophysics

Wang, H (Wang, Hao); Zhang, FW (Zhang, Fu-Wen); Wang, YZ (Wang, Yuan-Zhu); Shen, ZQ (Shen, Zhao-Qiang); Liang, YF (Liang, Yun-Feng); Li, X (Li, Xiang); Liao, NH (Liao, Neng-Hui); Jin, ZP (Jin, Zhi-Ping); Yuan, Q (Yuan, Qiang); Zou, YC (Zou, Yuan-Chuan); Fan, YZ (Fan, Yi-Zhong); Wei, DM (Wei, Da-Ming)
ASTROPHYSICAL JOURNAL LETTERS
卷: 851 期: 1 文献号: L18
On 2017 August 17, a gravitational-wave event (GW170817) and an associated short gamma-ray burst (GRB 170817A) from a binary neutron star merger had been detected. The follow-up optical/infrared observations also identified the macronova/kilonova emission (AT 2017gfo). In this work, we discuss some implications of the remarkable GW170817/GRB 170817A/AT 2017gfo association. We show that the similar to 1.7 s time delay between the gravitational-wave (GW) and GRB signals imposes very tight constraints on the superluminal movement of gravitational waves (i.e., the relative departure of GW velocity from the speed of light is. <= 4.3 x 10(-16)) or the possible violation of the weak equivalence principle (i.e., the difference of the gamma-ray and GW trajectories in the gravitational field of the galaxy and the local universe should be within a factor of similar to 3.4 x 10(-9)). The so-called Dark Matter Emulators and a class of contender models for cosmic acceleration ("Covariant Galileon") are ruled out as well. The successful identification of lanthanide elements in the macronova/kilonova spectrum also excludes the possibility that the progenitors of GRB 170817A are a binary strange star system. The high neutron star merger rate (inferred from both the local sGRB data and the gravitational-wave data) together with the significant ejected mass strongly suggest that such mergers are the prime sites of heavy r-process nucleosynthesis.

1-02 High-energy Solar physics

第 6 条 , 共 286 条

Shapes of Ne-20 de-excitation line in solar flare

Chen, W (Chen, Wei); Gan, WQ (Gan, Wei Qun)
ASTROPHYSICS AND SPACE SCIENCE
卷: 362 期: 9 文献号: 150
Since almost all de-excitation lines from nuclear states excited by flare-accelerated protons and a-particles are emitted promptly after nuclear collisions, the emission photon's energy depends on the velocity of the recoiling nucleus. The energies and widths of gamma-ray lines provide a wealth of information on the directionality and spectra of ions in solar flares. In this paper, we use TALYS code to improve the cross sections of gamma-ray lines production, and calculate the shapes of the 1.634 MeV line from de-excitation of Ne-20 as a function of ion's energy spectra and the heliocentric angle. Taking this line shape as an example, we try to develop a new method of line shape analysis to study the properties of accelerated ions in solar flares.

第 7 条 , 共 286 条

The Confined X-class Flares of Solar Active Region 2192 (vol 801, L23, 2015)

Thalmann, JK (Thalmann, J. K.); *Su, Y* (Su, Y.); Temmer, M (Temmer, M.); Veronig, AM (Veronig, A. M.)
ASTROPHYSICAL JOURNAL LETTERS
卷: 844 期: 2 文献号: L27
react-text: 252 We report high-cadence H-alpha observations of a distinct Moreton wave observed at Kanzelhoehe Solar Observatory associated with the 3B/X3.8 flare and CME event of 2005 January 17. The Moreton wave can be identified in about 40 H-alpha frames over a period of 7 min. The EIT wave is observed in only one frame but the derived propagation distance is close to that of the simultaneously measured.

第 8 条 , 共 286 条

On the time evolution of brightness, volume and height of a coronal source in an M-class flare

Firoz, KA (Firoz, Kazi A.); *Gan, WQ* (Gan, W. Q.); Li, YP (Li, Y. P.); Rodriguez-Pacheco, J (Rodriguez-Pacheco, J.); Su, Y (Su, Y.)
ASTROPHYSICS AND SPACE SCIENCE
卷: 362 期: 6 文献号: 113
We study brightness, volume and heights of the X-ray thermal emission components for an M-class solar flare on 17 May 2012. Based on the RHESSI data availability, we present the results for 01:42-01:58 UT over the lateflare phase. It is observed that the spatial evolution of the thermal emission components 6-12 and 12-18 keV are well associated with the hottest plasma in the corona. Results show that the ascending height (similar to 1.35x10(4) km) and speed (similar to 14.0 kms(-1)) of coronal source component 6-12 keV is slightly smaller than the ascending height (similar to 1.45x10(4) km) and speed (similar to 15.1 kms(-1)) of the coronal source component 12-18 keV. Mean flux intensity (I-mean) of the 6-12 keV maintained a good fit (chi(2) = 0.41) with the corresponding volume (V) following strongly the power law [I-mean = (15.8 +/- 0.21) V-1.28 +/- 0.03]. In contrast, the 12-18 keV maintained a weak fit (chi(2) = 2.37) following still the power law [I-mean = (0.19 +/- 0.01) V-1.88 +/- 0.16]. The power law indices (-1.28 +/- 0.03;-1.88 +/- 0.16) obtained by the observation

第 9 条，共 286 条

Generation Mechanisms of Quasi-parallel and Quasi-circular Flare Ribbons in a Confined Flare

Hernandez-Perez, A (Hernandez-Perez, Aaron); Thalmann, JK (Thalmann, Julia K.); Veronig, AM (Veronig, Astrid M.); *Su, Y* (Su, Yang); Gomory, P (Gomory, Peter); Dickson, EC (Dickson, Ewan C.)
ASTROPHYSICAL JOURNAL
卷: 847 期: 2 文献号: 124
We analyze a confined multiple-ribbon M2.1 flare (SOL2015-01-29T11:42) that originated from a fan-spine coronal magnetic field configuration, within active region NOAA 12268. The observed ribbons form in two steps. First, two primary ribbons form at the main flare site, followed by the formation of secondary ribbons at remote locations. We observe a number of plasma flows at extreme-ultraviolet temperatures during the early phase of the flare (as early as 15 minutes before the onset) propagating toward the formation site of the secondary ribbons. The secondary ribbon formation is co-temporal with the arrival of the pre-flare generated plasma flows. The primary ribbons are co-spatial with Ramaty High Energy Spectroscopic Imager (RHESSI) hard X-ray sources, whereas no enhanced X-ray emission is detected at the secondary ribbon sites. The (E)UV emission, associated with the secondary ribbons, peaks similar to 1 minute after the last RHESSI hard X-ray enhancement. A nonlinear force-free model of the coronal magnetic field reveals that the secondary flare ribbons are not directly connected to the primary ribbons, but to regions nearby. Detailed analysis suggests that the secondary brightenings are produced due to dissipation of kinetic energy of the plasma flows (heating due to compression), and not due to non-thermal particles accelerated by magnetic reconnection, as is the case for the primary ribbons.

第 10 条，共 286 条

Formation and Initiation of Erupting Flux Rope and Embedded Filament Driven by Photospheric Converging Motion

Zhao, XZ (Zhao, Xiaozhou); Xia, C (Xia, Chun); Keppens, R (Keppens, Rony); Gan, WQ (Gan, Weiqun)
ASTROPHYSICAL JOURNAL
卷: 841 期: 2 文献号: 106
In this paper, we study how a flux rope (FR) is formed and evolves into the corresponding structure of a coronal mass ejection (CME) numerically driven by photospheric converging motion. A two-and-a-half-dimensional magnetohydrodynamics simulation is conducted in a chromosphere-transition-corona setup. The initial arcade-like linear force-free magnetic field is driven by an imposed slow motion converging toward the magnetic inversion line at the bottom boundary. The convergence brings opposite-polarity magnetic flux to the polarity inversion, giving rise to the formation of an FR by magnetic reconnection and eventually to the eruption of a CME. During the FR formation, an embedded prominence gets formed by the levitation of chromospheric material. We confirm that the converging flow is a potential mechanism for the formation of FRs and a possible triggering mechanism for CMEs. We investigate the thermal, dynamical, and magnetic properties of the FR and its embedded prominence by tracking their thermal evolution, analyzing their force balance, and measuring their kinematic quantities. The phase transition from the initiation phase to the acceleration phase of the kinematic evolution of the FR was observed in our simulation. The FR undergoes a series of quasi-static equilibrium states in the initiation phase; while in the acceleration phase the FR is driven by Lorentz force and the impulsive acceleration occurs. The underlying physical reason for the phase transition is the change of the reconnection mechanism from the Sweet-Parker to the unsteady bursty regime of reconnection in the evolving current sheet underneath the FR.

第 11 条，共 286 条

Search for the gamma-ray emission from M33 with the Fermi Large Area Telescope

Fu, L (Fu, L.); Xia, ZQ (Xia, Z. Q.); Shen, ZQ (Shen, Z. Q.)
MONTHLY NOTICES OF THE ROYAL ASTRONOMICAL SOCIETY
卷: 471 期: 2 页: 1737-1742
We searched for the gamma-ray signal from M33, one of the largest galaxies in the Local Group, using the Pass8 data from the Fermi Large Area Telescope (LAT). No statistically significant gamma-ray emission has been detected in the direction of M33, and we report a new upper limit of the high-energy (>100 MeV) photon flux of 2.3 x 10(-9) ph cm(-2) s(-1), which is stricter than previous constraints and implies a cosmic ray density for M33 that is lower than that suggested previously. The current limit is still, however, in agreement with the correlation of star formation rate and gamma-ray luminosity inferred from the Local group galaxies and a few nearby starburst galaxies.

第 12 条，共 286 条

Molecular Gas toward the Gemini OB1 Molecular Cloud Complex. I. Observation Data

Wang, C (Wang, Chen); Yang, J (Yang, Ji); Xu, Y (Xu, Ye); Li, FC (Li, Facheng); Su, Y (Su, Yang); Zhang, SB (Zhang, Shaobo)
ASTROPHYSICAL JOURNAL SUPPLEMENT SERIES
卷: 230 期: 1 文献号: 5
We present a large-scale mapping toward the GEM OB1 association in the galactic anti-center direction. The 9 degrees x 6 degrees.5 area was mapped in (CO)-C-12, (CO)-C-13, and (CO)-O-18 with similar to 50" angular resolution at 30" sampling. The region was divided into four main components based on spatial distribution and velocity: the Gemini OB1 Giant Molecular Cloud (GGMC) Complex, the Lynds Dark Clouds and the West Front Clouds, the Swallow and Horn, and

the Remote Clouds. The GGMC Complex is located in the Perseus arm, while the Lynds Dark Clouds and the West Front Clouds are located in the Local arm. Swallow and Horn are revealed for the first time in this paper. The two clouds have a similar velocity interval ([11, 21] km s(-1)) and have similar sizes (0.6 and 0.8 deg(2)). We analyzed the structure of these clouds in detail and calculated their parameters (mass, temperature, etc.). Two elongated structures were discovered in a longitude-velocity map in the velocity interval [11, 30] km s(-1). We also found an interesting filament that shows a 0.8 km s(-1) pc(-1) gradient perpendicular to the direction of the long axis.

第 13 条，共 286 条

The Molecular Structures of the Local Arm and Perseus Arm in the Galactic Region of l = [139 degrees.75, 149 degrees.75], b = [-5 degrees.25, 5 degrees.25]

Du, XY (Du, Xinyu); Xu, Y (Xu, Ye); Yang, J (Yang, Ji); Sun, Y (Sun, Yan)
ASTROPHYSICAL JOURNAL SUPPLEMENT SERIES
卷: 229 期: 2 文献号: 24
Using the Purple Mountain Observatory Delingha (PMODLH) 13.7m telescope, we report a 96 deg(2) (CO)-C-12/(CO)-C-13/(CO)-O-18 mapping observation toward the Galactic region of l = [139 degrees. 75,149 degrees. 75], b = [-5 degrees. 25, 5 degrees. 25]. The molecular structures of the Local Arm and Perseus Arm are presented. Combining H I data and part of the Outer Arm results, we obtain that the warp structure of both atomic and molecular gas is obvious, while the flare structure only exists in atomic gas in this observing region. In addition, five filamentary giant molecular clouds on the Perseus Arm are identified. Among them, four are newly identified. Their relations with the Milky Way large-scale structure are discussed.

第 14 条，共 286 条

Characteristics of events with metric-to-decahectometric type II radio bursts associated with CMEs and flares in relation to SEP events

Prakash, O (Prakash, O.); *Feng, L* (Feng, Li); Michalek, G (Michalek, G.); Gan, WQ (Gan, Weiqun); Lu, L (Lu, Lei); Shanmugaraju, A (Shanmugaraju, A.); Umapathy, S (Umapathy, S.)
ASTROPHYSICS AND SPACE SCIENCE
卷: 362 期: 3 文献号: 56
A gradual solar energetic particle (SEP) event is thought to happen when particles are accelerated at a shock due to a fast coronal mass ejection (CME). To quantify what kind of solar eruptions can result in such SEP events, we have conducted detailed investigations on the characteristics of CMEs, solar flares and metric-to-decahectometric wavelength type II radio bursts (herein after m-to-DH type II bursts) for SEP-associated and non-SEP-associated events, observed during the period of 1997-2012. Interestingly, 65% of m-to-DH type II bursts associated with CMEs and flares produced SEP events. The SEP-associated CMEs have higher sky-plane mean speed, projection corrected speed, and sky-plane peak speed than those of non-SEP-associated CMEs respectively by 30%, 39%, and 25%, even though the two sets of CMEs achieved their sky-plane peak speeds at nearly similar heights within LASCO field of view. We found Pearson's correlation coefficients between the speeds of CMEs (sky-plane speed and corrected speed) and logarithmic peak intensity of SEP events are cc = 0.62 and cc = 0.58, respectively. We also found that the SEPassociated CMEs are on average of three times more decelerated (-21.52 ms(-2)) than the non-SEP-associated CMEs (-5.63 ms(-2)). The SEP-associated flares have a mean peak flux (1.85 x 10(-4) Wm(-2)) three times larger than that of non-SEP-associated flares, even though the flare duration (rise time) of both sets of events is similar. The SEPassociated m type II bursts have higher frequency drift rate and associated shock speed than those of the non-SEPassociated events by 70% and 25% respectively. The average formation heights of m and DH type II radio bursts for SEP-associated events (1.31 R-o and 3.54 R-o, respectively) are lower than for non-SEP-associated events (1.61 R-o and 3.91 R-o, respectively). 93% of SEP-associated events originate from the western hemisphere and 65% of SEPassociated events are associated with interacting CMEs. The obtained results indicate that, at least for the set of CMEs associated with m-to-DH type II bursts, SEP-associated CMEs are more energetic than those not associated with SEPs, thus suggesting that they are effective particle accelerators.

第 15 条，共 286 条

Observational Evidence of Magnetic Reconnection for Brightenings and Transition Region Arcades in IRIS Observations

Zhao, J (Zhao, Jie); Schmieder, B (Schmieder, Brigitte); Li, H (Li, Hui); Pariat, E (Pariat, Etienne); Zhu, XS (Zhu, Xiaoshuai); Feng, L (Feng, Li); Grubecka, M (Grubecka, Michalina)
ASTROPHYSICAL JOURNAL
卷: 836 期: 1 文献号: 52
By using a new method of forced-field extrapolation, we study the emerging flux region AR11850 observed by the Interface Region Imaging Spectrograph and Solar Dynamical Observatory. Our results suggest that the bright points(BPs) in this emerging region exhibit responses in lines formed from the upper photosphere to the transition region, which have relatively similar morphologies. They have an oscillation of several minutes according to the Atmospheric Imaging Assembly data at 1600 and 1700 angstrom. The ratio between the BP intensities measured in 1600 and 1700 angstrom filtergrams reveals that these BPs are heated differently. Our analysis of the Helioseismic and Magnetic Imager vector magnetic field and the corresponding topology in AR11850 indicates that the BPs are located at the polarity inversion line and most of them are related to magnetic reconnection or cancelation. The heating of the BPs might be different due to different magnetic topology. We find that the heating due to the magnetic cancelation would be stronger than the case of bald patch reconnection. The plasma density rather than the magnetic field strength could play a dominant role in this process. Based on physical conditions in the lower atmosphere, our forced-field extrapolation shows consistent results between the bright arcades visible in slit-jaw image 1400 angstrom and the extrapolated field lines that pass through the bald patches. It provides. reliable observational evidence for testing the mechanism of magnetic reconnection for the BPs and arcades in the. emerging flux region, as proposed in simulation studies.

第 16 条，共 286 条

Spectroscopic Observations of Magnetic Reconnection and Chromospheric Evaporation in an X-shaped Solar Flare

Li, Y (Li, Y.); Kelly, M (Kelly, M.); Ding, MD (Ding, M. D.); Qiu, J (Qiu, J.); Zhu, XS (Zhu, X. S.); Gan, WQ (Gan, W. Q.)
ASTROPHYSICAL JOURNAL
卷: 848 期: 2 文献号: 118
We present observations of distinct UV spectral properties at different locations during an atypical X-shaped flare (SOL2014-11-09T15:32) observed by the Interface Region Imaging Spectrograph (IRIS). In this flare, four chromospheric ribbons appear and converge at an X-point where a separator is anchored. Above the X-point, two sets of non-coplanar

coronal loops approach laterally and reconnect at the separator. The IRIS. slit was located close to the X-point, cutting across some of the flare ribbons and loops. Near the location of the separator, the Si IV 1402.77 angstrom line exhibits significantly broadened line wings extending to 200 km s(-1) with an unshifted line core. These spectral features suggest the presence of bidirectional flows possibly related to the separator reconnection. While at the flare ribbons, the hot Fe XXI 1354.08 angstrom line shows blueshifts and the cool Si IV 1402.77 angstrom, C II 1335.71 angstrom, and Mg II 2803.52 angstrom lines show evident redshifts up to a velocity of 80 km s(-1), which are consistent with the scenario of chromospheric evaporation/condensation.

第 17 条，共 286 条

Spectroscopic Observations of Magnetic Reconnection and Chromospheric Evaporation in an X-shaped Solar Flare

Li, Y (Li, Y.); Kelly, M (Kelly, M.) ; Ding, MD (Ding, M. D.) ; Qiu, J (Qiu, J.) ; Zhu, XS (Zhu, X. S.)[; Gan, WQ (Gan, W. Q.)
ASTROPHYSICAL JOURNAL
卷: 848　期: 2 文献号: 118
We present observations of distinct UV spectral properties at different locations during an atypical X-shaped flare (SOL2014-11-09T15:32) observed by the Interface Region Imaging Spectrograph (IRIS). In this flare, four chromospheric ribbons appear and converge at an X-point where a separator is anchored. Above the X-point, two sets of non-coplanar coronal loops approach laterally and reconnect at the separator. The IRIS. slit was located close to the X-point, cutting across some of the flare ribbons and loops. Near the location of the separator, the Si IV 1402.77 angstrom line exhibits significantly broadened line wings extending to 200 km s(-1) with an unshifted line core. These spectral features suggest the presence of bidirectional flows possibly related to the separator reconnection. While at the flare ribbons, the hot Fe XXI 1354.08 angstrom line shows blueshifts and the cool Si IV 1402.77 angstrom, C II 1335.71 angstrom, and Mg II 2803.52 angstrom lines show evident redshifts up to a velocity of 80 km s(-1), which are consistent with the scenario of chromospheric evaporation/condensation.

第 18 条，共 286 条

A Study of Fermi-LAT GeV gamma-Ray Emission toward the Magnetar-harboring Supernova Remnant Kesteven 73 and Its Molecular Environment

Liu, B (Liu, Bing); Chen, Y (Chen, Yang); Zhang, X (Zhang, Xiao); Liu, QC (Liu, Qian-Cheng); He, TL (He, Ting-Lan); Zhou, X (Zhou, Xin); Zhou, P (Zhou, Ping); Su, Y (Su, Yang)
ASTROPHYSICAL JOURNAL
卷: 851 期: 1 文献号: 37
We report our independent Gey gamma-ray study the young shell-type supernova remnant (SNR) Kes 73, which harbors a central magnetar, and CO-line millimeter observations toward the SNR. Using 7.6 years of Fermi-LAT observation data, we detected an extended gamma-ray source ("source A") with centroid on the west of the SNR, with a significance of 21 sigma in 0.1-300 GeV and an error circle of 5'.4n angular radius. The gamma-ray spectrum cannot be reproduced by a pure leptonic emission or a pure emission from the magnetar, and thus a hadronic emission component is needed. The CO-line observations reveal a molecular cloud (MC) at V-LSR similar to 90 km s(-1), which demonstrates morphological correspondence with the western boundary of the SNR brightened in multiwavelength. The (CO)-C-12 (J-1)/(CO)-C-12 (J-1-0)retioin the left (blue) wing 85-88 km s(-1) is prominently elevated to similar to 1.1 along the northwestern boundary, providing kinematic evidence of the SNR-MC interaction. This SNR-MC association yields a kinematic distance 9 kpc to Kes 73. The MC is shown to be capable of accounting for the hadronic gamma ray emission component. The gamma-ray spectrum can be interpreted with a pure hadronic emission or a magnetar+ hadronic hybrid emission. In the case of pure hadronic emission, the spectral index of the protons is 2.4, very similar to that of the radio-emitting electrons, essentially consistent with the diffusive shock acceleration theory. In the case of magnetar+ hadronic hybrid emission, a magnetic field decay rate. 1036 erg s(-1) is needed to power the magnetar's curvature radiation.

第 19 条，共 286 条

Generation Mechanisms of Quasi-parallel and Quasi-circular Flare Ribbon in a Confined Flare

Hernandez-Perez, A (Hernandez-Perez, Aaron) ; Thalmann, JK (Thalmann, Julia K.) ; Veronig, AM (Veronig, Astrid M.); *Su, Y* (Su, Yang); Gomory, P (Gomory, Peter) ; Dickson, EC (Dickson, Ewan C.)
ASTROPHYSICAL JOURNAL
卷: 847　期: 2 文献号: 124
We analyze a confined multiple-ribbon M2.1 flare (SOL2015-01-29T11:42) that originated from a fan-spine coronal magnetic field configuration, within active region NOAA 12268. The observed ribbons form in two steps. First, two primary ribbons form at the main flare site, followed by the formation of secondary ribbons at remote locations. We observe a number of plasma flows at extreme-ultraviolet temperatures during the early phase of the flare (as early as 15 minutes before the onset) propagating toward the formation site of the secondary ribbons. The secondary ribbon formation is co-temporal with the arrival of the pre-flare generated plasma flows. The primary ribbons are co-spatial with Ramaty High Energy Spectroscopic Imager (RHESSI) hard X-ray sources, whereas no enhanced X-ray emission is detected at the secondary ribbon sites. The (E)UV emission, associated with the secondary ribbons, peaks similar to 1 minute after the last RHESSI hard X-ray enhancement. A nonlinear force-free model of the coronal magnetic field reveals that the secondary flare ribbons are not directly connected to the primary ribbons, but to regions nearby. Detailed analysis suggests that the secondary brightenings are produced due to dissipation of kinetic energy of the plasma flows (heating due to compression), and not due to non-thermal particles accelerated by magnetic reconnection, as is the case for the primary ribbons.

第 20 条，共 286 条

Statistical study of co-rotating interaction region properties with STEREO and ACE observations

Huang, Y (Huang, Yu); Song, QW (Song, Qi-Wu); Li, D (Li, Dong)
RESEARCH IN ASTRONOMY AND ASTROPHYSICS
卷: 17 期: 11 文献号: 111
We analyzed the data on co-rotating interaction regions (CIRs) measured by the Advanced Composition Explorer (ACE) and Solar TErrestrial RElations Observatory (STEREO) from 2007 to 2010. The CIRs were observed by STEREO B (STB), ACE and STEREO A (STA) one after another, and a total of 28 CIRs were identified in this work. Since the same characteristics of CIRs were detected by these three spacecraft at three different locations and times, these data can help us to study the evolutions of CIRs. For a single event, the properties of CIRs observed by the three spacecraft were quite different and could be explained by spatial or temporal variations. For all these 28 CIRs, STA and STB observed similar mean parameters,

such as peak magnetic field strength (offset 11%), peak and change in solar wind speed (offset 3% and 10% respectively), peak proton temperature (offset 14%) and peak perpendicular pressure (offset 15%). Surprisingly, STA detected much higher (41%) peak density of protons than STB.

1-03 Multi-Band Observation Solar Activity

第 21 条，共 286 条

Simultaneous Transverse and Longitudinal Oscillations in a Quiescent Prominence Triggered by a Coronal Jet

Zhang, QM (Zhang, Q. M.); Li, D (Li, D.); Ning, ZJ (Ning, Z. J.)
ASTROPHYSICAL JOURNAL
卷: 851 期: 1 文献号: 47
In this paper, we report our multiwavelength observations of the simultaneous transverse and longitudinal oscillations in a quiescent prominence. The prominence was observed by the Global Oscillation Network Group and by the Atmospheric Imaging Assembly on board the Solar Dynamics Observatory on 2015 June 29. A GOES C2.4 flare took place in NOAA active region 12373, which was associated with a pair of short ribbons and a remote ribbon. During the impulsive phase of the flare, a coronal jet spurted out of the primary flare site and propagated in the northwest direction at an apparent speed of similar to 224 km s(-1). Part of the jet stopped near the remote ribbon. The remaining part continued moving forward before stopping to the east of the prominence. Once the jet encountered the prominence, it pushed the prominence to oscillate periodically. The transverse oscillation of the eastern part (EP) of prominence can be divided into two phases. In phase I, the initial amplitude, velocity, period, and damping timescale are similar to 4.5 Mm, similar to 20 km s(-1), similar to 25 minutes, and similar to 7.5 hr, respectively. The oscillation lasted for two cycles. In phase II, the initial amplitude increases to similar to 11.3 Mm, while the initial velocity halves to similar to 10 km s(-1). The period increases by a factor of similar to 3.5. With a damping timescale of similar to 4.4 hr, the oscillation lasted for about three cycles. The western part of prominence also experienced transverse oscillation. The initial amplitude is only similar to 2 Mm and the velocity is less than 10 km s(-1). The period (similar to 27 minutes) is slightly longer than that of the EP in phase I. The oscillation lasted for about four cycles with the shortest damping timescale (similar to 1.7 hr). To the east of prominence, a handful of horizontal threads experienced longitudinal oscillation. The initial amplitude, velocity, period, and damping timescale are similar to 52 Mm, similar to 50 km s(-1), similar to 99 minutes, and 2.5 hr, respectively. To our knowledge, this is the first report of simultaneous transverse and longitudinal prominence oscillations triggered by a coronal jet.

第 22 条，共 286 条

INITIATION PROCESSES FOR THE 2013 MAY 13 X1.7 LIMB FLARE

Shen, JH (Shen, Jinhua); Wang, Y (Wang, Ya); Zhou, TH (Zhou, Tuanhui); Ji, HS (Ji, Haisheng)
ASTROPHYSICAL JOURNAL
卷: 835 期: 1 文献号: 43
For the X1.7 class flare on 2013 May 13 (SOL2013-05-13T01: 53), its initiation process was well observed by the Atmospheric Imaging Assembly (AIA) on board the Solar Dynamic Observatory. and the Extreme UltraViolet Imager (EUVI) on board STEREO-B. The initiation process incorporates the following phenomena: an X-ray precursor that started similar to 9 minutes before flare onset, two hot magnetic loops (as seen with AIA hot channels) forming a sigmoidal core magnetic structure (as seen with the EUVI), a rapidly formed magnetic flux rope (MFR) that expands outward, and a flare loop that contracts inward. The two hot magnetic loops were activated after the occurrence of the X-ray precursor. After activation, magnetic reconnection occurred between the two hot magnetic loops (inside the sigmoid structure), which produced the expanding MFR and the contracting flare loop (CFL). The MFR and CFL can only be seen with AIA hot and cool channels, respectively. For this flare, the real initiation time can be regarded as being from the starting time of the precursor, and its impulsive phase started when the MFR began its fast expansion. In addition, the CFL and the growing postflare magnetic loops are different loop systems, and the CFL was the product of magnetic reconnection between sheared magnetic fields that also produced the MFR.

第 23 条，共 286 条

THE INTERPRETATION OF THE MULTI-WAVELENGTH AFTERGLOW EMISSION OF SHORT GRB 140903A

Zhang, S (Zhang, Shuai); *Jin, ZP* (Jin, Zhi-Ping); Wang, YZ (Wang, Yuan-Zhu); Wei, DM (Wei, Da-Ming)
ASTROPHYSICAL JOURNAL
卷: 835 期: 1 文献号: 73
GRB 140903A, a short duration gamma-ray burst (SGRB) detected by Swift, is characterized by its long-lasting radio emission among SGRBs. In addition to the similar to 10(6) s radio afterglow emission, the afterglow of GRB 140903A displays a plateau from 10(3) s to 7 x 10(3) s in the X-rays. In this work, we attribute the X-ray plateau to the energy injection into the decelerating blast wave and then model the later radio/optical/X-ray afterglow emission within the standard fireball afterglow model. The afterglow emission has been well reproduced with reasonable physical parameters, including a jet half-opening angle of similar to 0.05.

第 24 条，共 286 条

NIHAO - VIII. Circum-galactic medium and outflows - The puzzles of H I and O VI gas distributions Gutcke,

TA (Gutcke, Thales A.); Stinson, GS (Stinson, Greg S.); Maccio, AV (Maccio, Andrea V.); *Wang, L* (Wang, Liang); Dutton, AA (Dutton, Aaron A.)
MONTHLY NOTICES OF THE ROYAL ASTRONOMICAL SOCIETY
卷: 464 期: 3 页: 2796-2815
We study the hot and cold circum-galactic medium (CGM) of 86 galaxies of the cosmological, hydrodynamical simulation suite, Numerical Investigation of a Hundred Astrophysical Objects (NIHAO). NIHAO allows a study of how the z = 0 CGM varies across five orders of magnitude of stellar mass using O VI and HI as proxies for hot and cold gas. The cool HI covering fraction and column density profiles match observations well, particularly in the inner CGM. O VI shows increasing column densities with mass, a trend seemingly echoed in the observations. As in multiple previous simulations, the O VI column densities in simulations are lower than observed and optically thick HI does not extend as far out as in observations. We take a look at the collisional ionization fraction of O VI as a function of halo mass. We make observable predictions of the bipolarity of outflows and their effect on the general shape of the CGM. Bipolar outflows can be seen out to around 40 kpc in intermediate-and low-mass haloes (M-Halo < 10(11) M-circle

dot), but outside that radius, the CGM is too well mixed to detect an elongated shape. Larger haloes have extended gas discs beyond the stellar disc that dominate the shape of the inner CGM. The simulated CGM is remarkably spherical even in low-mass simulations. The chemical enrichment of both halo and disc gas follow expected increasing trends as a function of halo mass that are well fit with power laws. These relations can be used in non-hydrodynamic models, such as semi-analytic models.

第 25 条，共 286 条

Quasi-periodic pulsations with periods that change depending on whether the pulsations have thermal or nonthermal components

Li, D (Li, D.); Zhang, QM (Zhang, Q. M.); Huang, Y (Huang, Y.); Ning, ZJ (Ning, Z. J.); Su, YN (Su, Y. N.)
ASTRONOMY & ASTROPHYSICS
卷: 597 文献号: L4
Context. Quasi-periodic pulsations (QPPs) typically display periodic and regular peaks in the light curves during the flare emissions. Sometimes, QPPs show multiple periods at the same wavelength. However, changing periods in various channels are rare.
Aims. We report QPPs in a solar flare on 2014 October 27. They showed a period change that depended on whether thermal or nonthermal components were included. The flare was simultaneously observed by many instruments.
Methods. Using the fast Fourier transform (FFT), we decomposed the light curves at multiple wavelengths into slowly varying and rapidly varying signals. Then we identified the QPPs as the regular and periodic peaks from the rapidly varying signals. The periods are derived with the wavelet method and confirmed based on the FFT spectra of the rapidly varying signals.
Results. We find a period of similar to 50 s from the thermal emissions during the impulsive phase of the flare, that is, in the soft X-ray bands. At the same time, a period of about 100 s is detected from the nonthermal emissions, such as hard X-ray and microwave channels. The period ratio is exactly 2.0, which might be due to the modulations of the magnetic reconnection rate by the fundamental and harmonic modes of magnetohydrodynamic waves. Our results further show that the similar to 100 s period is present over a broad wavelength, such as hard X-rays, extreme-UV/UV, and microwave emissions, indicating the periodic magnetic reconnection in this flare.
Conclusions. To our knowledge, this is the first report about period changes from thermal to nonthermal components in a single flare that occur at almost the same time. This new observational finding could be a challenge to the theory of flare QPPs.

第 26 条，共 286 条

One-Minute Quasi-Periodic Pulsations Seen in a Solar Flare

Ning, Z (Ning, Z.)
SOLAR PHYSICS
卷: 292 期: 1 文献号: 11
We study quasi-periodic pulsations (QPPs) in the SOL2014-09-10 event that was detected by the Geostationary Operational Environmental Satellites (GOES), the Atmospheric Imaging Assembly (AIA) and the Extreme Ultraviolet Variability Experiment (EVE) onboard the Solar Dynamics Observatory (SDO), and the Gamma Ray Burst Monitor (GBM) onboard the Fermi satellite. Previous studies have found that this flare displays four-minute QPPs in a broad range of wavelengths. In this article, we find that this event also shows QPPs with a period of around one minute. Using the Fast Fourier Transform (FFT) method, the light curves are decomposed into fast- and slowly varying components with a separation at approximate to 100 seconds. The four-minute QPPs are in the slowly varying component, and the one-minute QPPs are identified with the fast-varying components in the impulsive and maximum phases. Similarly as the four-minute QPPs, the one-minute QPPs are simultaneously found in soft X-rays (SXR), extreme ultraviolet (EUV), and hard X-ray (HXR) emission. High correlations are found between the fast-varying components at the different wavelengths, especially between SXR and HXR. The spatial location of the sources of one-minute QPPs differ from those of the four-minute QPPs. The four-minute QPPs appear in the whole flare region, while the one-minute QPPs tend to originate from the flare loop footpoints. This finding provides an observational constraint for the physical origin of the QPPs.

第 27 条，共 286 条

The Eruption of a Small-scale Emerging Flux Rope as the Driver of an M-class Flare and of a Coronal Mass Ejection

Yan, XL (Yan, X. L.); Jiang, CW (Jiang, C. W.); Xue, ZK (Xue, Z. K.); Wang, JC (Wang, J. C.); Priest, ER (Priest, E. R.); Yang, LH (Yang, L. H.); Kong, DF (Kong, D. F.); Cao, WD (Cao, W. D.); Ji, HS (Ji, H. S.)
ASTROPHYSICAL JOURNAL
卷: 845 期: 1 文献号: 18
Solar flares and coronal mass ejections are the most powerful explosions in the Sun. They are major sources of potentially destructive space weather conditions. However, the possible causes of their initiation remain controversial. Using high-resolution data observed by the New Solar Telescope of Big Bear Solar Observaotry, supplemented by Solar Dynamics Observatory observations, we present unusual observations of a small-scale emerging flux rope near a large sunspot, whose eruption produced an M-class flare and a coronal mass ejection. The presence of the small-scale flux rope was indicated by static nonlinear force-free field extrapolation as well as data-driven magnetohydrodynamics modeling of the dynamic evolution of the coronal three-dimensional magnetic field. During the emergence of the flux rope, rotation of satellite sunspots at the footpoints of the flux rope was observed. Meanwhile, the Lorentz force, magnetic energy, vertical current, and transverse fields were increasing during this phase. The free energy from the magnetic flux emergence and twisting magnetic fields is sufficient to power the M-class flare. These observations present, for the first time, the complete process, from the emergence of the small-scale flux rope, to the production of solar eruptions.

第 28 条，共 286 条

High-resolution Observations of Sympathetic Filament Eruptions by NVST

Li, SW (Li, Shangwei); Su, YN (Su, Yingna); Zhou, TH (Zhou, Tuanhui); van Ballegooijen, A (van Ballegooijen, Adriaan); Sun, XD (Sun, Xudong); Ji, HS (Ji, Haisheng)
ASTROPHYSICAL JOURNAL
卷: 844 期: 1 文献号: 70
We investigate two sympathetic filament eruptions observed by the New Vacuum Solar Telescope on 2015 October 15. The full picture of the eruptions is obtained from the corresponding Solar Dynamics Observatory (SDO)/Atmospheric Imaging Assembly (AIA) observations. The two filaments start from active region NOAA 12434 in the north and end in one large quiescent filament channel in the south. The left filament erupts first, followed by the right filament eruption about 10 minutes later. Clear twist structure and rotating motion are observed in both filaments during the eruption. Both eruptions failed, since the filaments first rise up, then flow toward the

south and merge into the southern large quiescent filament. We also observe repeated activations of mini filaments below the right filament after its eruption. Using magnetic field models constructed based on SDO/ HMI magnetograms via the flux rope insertion method, we find that the left filament eruption is likely to be triggered by kink instability, while the weakening of overlying magnetic fields due to magnetic reconnection at an X-point between the two filament systems might play an important role in the onset of the right filament eruption.

第 29 条，共 286 条

Large-amplitude Longitudinal Oscillations in a Solar Filament

Zhang, QM (Zhang, Q. M.); Li, T (Li, T.); Zheng, RS (Zheng, R. S.); Su, YN (Su, Y. N.); Ji, HS (Ji, H. S.)
ASTROPHYSICAL JOURNAL
卷: 842 期: 1 文献号: 27
In this paper, we report our multiwavelength observations of the large-amplitude longitudinal oscillations of a filament observed. on 2015 May 3. Located next to active region 12335, the sigmoidal filament was observed by the ground-based H alpha telescopes from the Global Oscillation Network Group and by the Atmospheric Imaging Assembly instrument on. board the Solar Dynamics Observatory. The filament oscillations were most probably triggered by the magnetic reconnection in the filament channel, which is characterized by the bidirectional flows, brightenings in EUV and soft X-ray, and magnetic cancellation in the photosphere. The directions of oscillations have angles of 4 degrees-36 degrees with respect to the filament axis. The whole filament did not oscillate in phase as a rigid body. Meanwhile, the oscillation. periods (3100-4400 s). have a spatial dependence, implying that the curvature radii (R) of the magnetic dips are different at different positions. The values of R are estimated to be 69.4-133.9 Mm, and the minimum transverse magnetic field of the dips is estimated to be 15 G. The amplitudes of S5-S8 grew with time, while the amplitudes of S9-S14 damped with time. The oscillation. amplitudes. range from a few to ten Mm, and the maximum. velocity can reach 30 km s(-1). Interestingly, the filament experienced mass drainage southward. at a speed of similar to 27 km s(-1). The oscillations continued after the mass drainage and lasted for more than 11 hr. After the mass drainage, the oscillation. phases. did not change much. The periods of S5-S8 decreased, while the periods of S9-S14 increased. The amplitudes of S5-S8 damped with time, while the amplitudes of S9-S14 grew. Most of the damping (growing) ratios are between -9 and 14. We offer. a schematic cartoon to explain the complex behaviors of oscillations by introducing thread-thread interaction.

第 30 条，共 286 条

Solar Tornadoes Triggered by Interaction between Filaments and EUV Jets

Chen, HD (Chen, Huadong); Zhang, J (Zhang, Jun); Ma, SL (Ma, Suli); Yan, XL (Yan, Xiaoli); Xue, JC (Xue, Jianchao)
ASTROPHYSICAL JOURNAL LETTERS
卷: 841 期: 1 文献号: L13
We investigate the formations and evolutions of two successive solar tornadoes in/near AR 12297 during 2015 March 19-20. Recurrent EUV jets close to two filaments were detected along a large-scale coronal loop prior to the appearances of the tornadoes. Under the disturbances from the activities, the filaments continually ascended and finally interacted with the loops tracked by the jets. Subsequently, the structures of the filaments and the loop were merged together, probably via magnetic reconnections, and formed tornado-like structures with a long spiral arm. Our observations suggest that solar tornadoes can be triggered by the interaction between filaments and nearby coronal jets, which has rarely been reported before. At the earlier development phase of the first tornado, about 30 small-scale sub-jets appeared in the tornado's arm, accompanied by local EUV brightenings. They have an ejection direction approximately vertical to the axis of the arm and a typical maximum speed of similar to 280 km s(-1). During the ruinations of the two tornadoes, fast plasma outflows from the strong EUV brightenings inside tornadoes are observed, in company with the untangling or unwinding of the highly twisted tornado structures. These observational features indicate that self reconnections probably occurred between the tangled magnetic fields of the tornadoes and resulted in the rapid disintegrations and disappearances of the tornadoes. According to the reconnection theory, we also derive the field strength of the tornado core to be similar to 8G.

第 31 条，共 286 条

Explosive Chromospheric Evaporation Driven by Nonthermal Electrons around One Footpoint of a Solar Flare Loop

Li, D (Li, D.); Ning, ZJ (Ning, Z. J.); Huang, Y (Huang, Y.); Zhang, QM (Zhang, Q. M.)
ASTROPHYSICAL JOURNAL LETTERS
卷: 841 期: 1 文献号: L9
We explore the temporal relationship between microwave/hard X-ray (HXR) emission and Doppler velocity during the impulsive phase of a solar flare on 2014 October 27 (SOL2014-10-27) that displays a pulse on the light curves in the microwave (34 GHz) and HXR (25-50 keV) bands before the flare maximum. Imaging observation shows that this pulse mainly comes from one footpoint of a solar flare loop. The slit of the Interface Region Imaging Spectrograph (IRIS) stays at this footpoint during this solar flare. The Doppler velocities of Fe XXI. 1354.09 angstrom and Si IV. 1402.77. angstrom are extracted from the Gaussian fitting method. We find that the hot line of Fe XXI. 1354.09 angstrom (log T similar to 7.05) in the corona exhibits blueshift, while the cool line of Si IV. 1402.77 angstrom (log T similar to 4.8) in the transition region exhibits redshift, indicating explosive chromospheric evaporation. Evaporative upflows along the flare loop are also observed in the AIA 131 angstrom image. To our knowledge, this is the first report of chromospheric evaporation evidence from both spectral and imaging observations in the same flare. Both microwave and HXR pulses are well correlated with the Doppler velocities, suggesting that the chromospheric evaporation is driven by nonthermal electrons around this footpoint of a solar flare loop.

第 32 条，共 286 条

Blob Formation and Ejection in Coronal Jets due to the Plasmoid and Kelvin-Helmholtz Instabilities

Ni, L (Ni, Lei); *Zhang, QM* (Zhang, Qing-Min); Murphy, NA (Murphy, Nicholas A.); Lin, J (Lin, Jun)
ASTROPHYSICAL JOURNAL
卷: 841 期: 1 文献号: 27
We perform 2D resistive magnetohydrodynamic simulations of coronal jets driven by flux emergence along the lower boundary. The reconnection layers are susceptible to the formation of blobs that are ejected in the jet. Our simulation with low plasma beta (Case I) shows that magnetic islands form easily and propagate upward in the jet. These islands are multithermal and thus are predicted to show up in hot channels (335 angstrom and 211 angstrom) and the cool channel (304 angstrom) in observations by the Atmospheric Imaging Assembly (AIA) on the Solar Dynamics Observatory.

The islands have maximum temperatures of 8 MK, lifetimes of 120 s, diameters of 6 Mm, and velocities of 200 km s(-1). These parameters are similar to the properties of blobs observed in extreme-ultraviolet (EUV) jets by AIA. The Kelvin-Helmholtz instability develops in our simulation with moderately high plasma beta (Case II) and leads to the formation of bright vortex-like blobs above the multiple high magnetosonic Mach number regions that appear along the jet. These vortex-like blobs can also be identified in the AIA channels. However, they eventually move downward and disappear after the high magnetosonic Mach number regions disappear. In the lower plasma beta case, the lifetime for the jet is shorter, the jet and magnetic islands are formed with higher velocities and temperatures, the current-sheet fragments are more chaotic, and more magnetic islands are generated. Our results show that the plasmoid instability and Kelvin-Helmholtz instability along the jet are both possible causes of the formation of blobs observed at EUV wavelengths.

第 33 条，共 286 条

Steep Decay Phase Shaped by the Curvature Effect. II. Spectral Evolution

Lin, DB (Lin, Da-Bin); Mu, HJ (Mu, Hui-Jun); Liang, YF (Liang, Yun-Feng); Liu, T (Liu, Tong); Gu, WM (Gu, Wei-Min); Lu, RJ (Lu, Rui-Jing); Wang, XG (Wang, Xiang-Gao); Liang, EW (Liang, En-Wei)
ASTROPHYSICAL JOURNAL
卷: 840 期: 2 文献号: 118
We derive a simple analytical formula to describe the evolution of spectral index beta in the steep decay phase shaped by the curvature effect with the. assumption that the spectral parameters and Lorentz factor of the. jet shell are. the same for different latitudes. Here, the value of beta is estimated in the 0.3-10 keV energy band. For a spherical thin shell with a cutoff power-law (CPL) intrinsic radiation spectrum, the spectral evolution can be read as a linear function of observer time. For the situation with the. Band function intrinsic radiation spectrum, the spectral evolution may be complex. If the observed break energy of the. radiation spectrum is larger than 10 keV, the spectral evolution is the same as that shaped by jet shells with a CPL spectrum. If the observed break energy is less than 0.3 keV, the value of beta would be a constant. For others, the spectral evolution can be approximated as a logarithmal function of the observer time in general.

第 34 条，共 286 条

Steep Decay Phase Shaped by the Curvature Effect. I. Flux Evolution

Lin, DB (Lin, Da-Bin); Mu, HJ (Mu, Hui-Jun); Lu, RJ (Lu, Rui-Jing); Liu, T (Liu, Tong); Gu, WM (Gu, Wei-Min); Liang, YF (Liang, Yun-Feng); Wang, XG (Wang, Xiang-Gao); Liang, EW (Liang, En-Wei)
ASTROPHYSICAL JOURNAL
卷: 840 期: 2 文献号: 95
The curvature effect may be responsible for the steep decay phase observed in gamma-ray bursts. To test the curvature effect with observations, the zero time point t(0) adopted to plot the observer time and flux on a logarithmic scale should be appropriately selected. In practice, however, the true t0 cannot be directly constrained from the data. Thus, we move t0 to a certain time in the steep decay phase, which can be easily identified. In this situation, we derive an analytical formula to describe the flux evolution of the steep decay phase. The analytical formula reads as F-v proportional to (1 +(t) over bar obs /(t) over bar obs) (-alpha,) with alpha((t) over bar (obs) =2 + integral(0) log(1+(t) over bar obs /(t) over barc) ss(T)d[log (1 +(t) over barc)]/1+(t) over bar obs /(t) over barc) F-v is the flux observed at frequency v, (t) over bar obs is the observer time by setting t(0) at a certain time in the steep decay phase, beta is the spectral index estimated around v, (t) over bar c and is the decay timescale of the phase with (t) over bar obs We test the analytical formula with the data from numerical calculations. It is found that the analytical formula presents a good estimate of the evolution of the flux shaped by the curvature effect. Our analytical formula can be used to confront the curvature effect with observations and estimate the decay timescale of the steep decay phase.

第 35 条，共 286 条

Statistical properties of bipolar magnetic regions

Li, D (Li, Dong)
RESEARCH IN ASTRONOMY AND ASTROPHYSICS
卷: 17 期: 5 文献号: 40
Using observations from the Michelson Doppler Imager (MDI) onboard Solar and Heliospheric Observatory (SOHO), we develop a computational algorithm to automatically identify bipolar magnetic regions (BMRs) in active regions (ARs), and then study their statistical properties. The individual magnetic (positive or negative) pole of a BMR is determined from the region with an absolute strength above 55G and with an area larger than 250 pixel(2) (similar to 495 Mm(2)), while a BMR is identified as a pair of positive and negative poles with the shortest area-weight distance between them. Based on this method, 2234 BMRs are identified fromMDI synoptic magnetograms between Carrington Rotations 1909 (1996 May 06) and 2104 (2010 December 10). 1005 of them are located in the northern hemisphere, while the other 1229 are in the southern hemisphere. We find that the BMR parameters (e.g., latitude, separation, fragment number and strength) are similar to those of ARs. Moreover, based on the maximum likelihood estimation (MLE) method, the frequency distributions representing the occurrence of these BMRs as functions of area and magnetic flux exhibit a power-law behavior, i.e., dN/d x alpha x (-alpha x), with indices of alpha(A) = 1.98 +/- 0.06 and alpha(F) = 1.93 +/- 0.05 respectively. We also find that their orientation angles (theta) follow "Hale's Polarity Law" and deviate slightly toward the direction of the solar equator. Consistent with previous findings, we obtain the dependence of orientation angles on latitudes for normal BMRs during the 23rd solar cycle. The north-south asymmetry of these BMRs is also detected here.

第 36 条，共 286 条

Terrestrial planet formation under migration: systems near the 4:2:1 mean motion resonance

Sun, Z (Sun, Zhao); Ji, JH (Ji, Jianghui); Wang, S (Wang, Su); Jin, S (Jin, Sheng)
MONTHLY NOTICES OF THE ROYAL ASTRONOMICAL SOCIETY
卷: 467 期: 1 页: 619-632
In this work, we investigate extensively the formation of near 4:2:1 mean motion resonance (MMR) configurations by performing two sets of N-body simulations. We model the eccentricity damping, gas drag, type I and type II planetary migration of planetesimals, planetary embryos and giant planets in the first set. For simulations of giant planets with type II migration, massive terrestrial planets with a mass up to several Earth masses are likely produced in these systems. We further show that by shepherding and/ or scattering mechanisms through a Jovian planet's type II migration, the terrestrial and giant planets in the systems can be evolved into near 4:2:1 MMRs. Moreover, the models are applicable to the formation of the Kepler-238 and 302 systems. In the second set of simulations, we study 4:2:1 MMR formation in terrestrial planetary systems, where the planets undergo type I migration

and eccentricity damping. By considering type I migration, similar to 17.1 per cent of the simulations indicate that terrestrial planets are evolved into 4:2:1 MMRs. However, this probability should depend on the initial conditions of the planets. Hence, we conclude that both type I and type II migration can play a crucial role in close-in terrestrial planet formation.

第 37 条，共 286 条

Interaction of Two Filaments in a Long Filament Channel Associated with Twin Coronal Mass Ejections

Zheng, RS (Zheng, Ruisheng); *Zhang, QM* (Zhang, Qingmin); Chen, Y (Chen, Yao); Wang, B (Wang, Bing); Du, GH (Du, Guohui); Li, CY (Li, Chuanyang); Yang, K (Yang, Kai)
ASTROPHYSICAL JOURNAL
卷: 836 期: 2 文献号: 160
Using the high-quality observations of the Solar Dynamics Observatory, we present the interaction of two filaments (F1 and F2) in a long filament channel associated with twin coronal mass ejections (CMEs) on 2016 January 26. Before the eruption, a sequence of rapid cancellation and emergence of the magnetic flux has been observed, which likely triggered the ascending of the west filament (F1). The east footpoints of rising F1 moved toward the east far end of the filament channel, accompanied by post-eruption loops and flare ribbons. This likely indicated a large-scale eruption involving the long filament channel, which resulted from the interaction between F1 and the east filament (F2). Some bright plasma flew over F2, and F2 stayed at rest during the eruption, likely due to the confinement of its overlying lower magnetic field. Interestingly, the impulsive F1 pushed its overlying magnetic arcades to form the first CME, and F1 finally evolved into the second CME after the collision with the nearby coronal hole. We suggest that the interaction of F1 and the overlying magnetic field of F2 led to the merging reconnection that forms a longer eruptive filament loop. Our results also provide a possible picture of the origin of twin CMEs and show that the large-scale magnetic topology of the coronal hole is important for the eventual propagation direction of CMEs.

第 38 条，共 286 条

Location of energy source for coronal heating on the photosphere

Hong, ZX (Hong, Zhen-Xiang); Yang, X (Yang, Xu); Wang, Y (Wang, Ya); Ji, KF (Ji, Kai-Fan); *Ji, HS* (Ji, Hai-Sheng); Cao, WD (Cao, Wen-Da)
RESEARCH IN ASTRONOMY AND ASTROPHYSICS
卷: 17 期: 3 文献号: 25
It is reported that ultra-fine dynamic ejections along magnetic loops of an active region originate from intergranular lanes and they are associated with subsequent heating in the corona. As continuing work, we analyze the same set of data but focus on a quiet region and the overlying EUV/UV emission as observed by the Atmospheric Imaging Assembly (AIA) on board Solar Dynamics Observatory (SDO). We find that there appear to be dark patches scattered across the quiet region and the dark patches always stay along intergranular lanes. Over the dark patches, the average UV/EUV emission at 131, 171, 304 and 1600 angstrom (middle temperature) is more intense than that of other regions and EUV brightness is negatively correlated with 10830 angstrom intensity, though, such a trend does not exist for high temperature lines at 94, 193, 211 and 335 angstrom. For the same quiet region, where both TiO 7057 angstrom broad band images and 10830 angstrom filtergrams are available, contours for the darkest lane areas on TiO images and dark patches on 10830 angstrom filtergrams frequently differ in space. The results suggest that the dark patches do not simply reflect the areas with the darkest lanes but are associated with a kind of enhanced absorption (EA) at 10830 angstrom. A strict definition for EA with narrow band 10830 angstrom filtergrams is found to be difficult. In this paper, we define enhanced absorption patches (EAPs) of a quiet region as the areas where emission is less than similar to 90% of the mean intensity of the region. The value is equivalent to the average intensity along thin dark loops connecting two moss regions of the active region. A more strict definition for EAPs, say 88%, gives even more intense UV/EUV emission over those in the middle temperature range. The results provide further observational evidence that energy for heating the upper solar atmosphere comes from the intergranular lane area where the magnetic field is constantly brought in by convection motion in granules.

第 39 条，共 286 条

Pre-flare coronal dimmings

Zhang, QM (Zhang, Q. M.); Su, YN (Su, Y. N.); Ji, HS (Ji, H. S.)
ASTRONOMY & ASTROPHYSICS
卷: 598 文献号: A3
Context. Coronal dimmings are regions of decreased extreme-ultravoilet (EUV) and/or X-ray (originally Skylab, then Yohkoh/SXT) intensities, which are often associated with flares and coronal mass ejections (CMEs). The large-scale impulsive dimmings have been thoroughly observed and investigated. The pre-flare dimmings before the flare impulsive phase, however, have rarely been studied in detail.
Aims. We focus on the pre-flare coronal dimmings. We report our multiwavelength observations of the GOES X1.6 solar flare and the accompanying halo CME that was produced by the eruption of a sigmoidal magnetic flux rope (MFR) in NOAA active region (AR) 12158 on 2014 September 10.
Methods. The eruption was observed by the Atmospheric Imaging Assembly (AIA) on board the Solar Dynamic Observatory (SDO). The photospheric line-of-sight magnetograms were observed by the Helioseismic and Magnetic Imager (HMI) on board SDO. The soft X-ray (SXR) fluxes were recorded by the GOES spacecraft. The halo CME was observed by the white-light coronagraphs of the Large Angle Spectroscopic Coronagraph (LASCO) on board SOHO.
Results. About 96 min before the onset of the flare /CME, narrow pre-flare coronal dimmings appeared at the two ends of the twisted MFR. They extended very slowly, with their intensities decreasing with time, while their apparent widths (8 9 Mm) continued to be nearly constant. During the impulsive and decay phases of flare, typical fan-like twin dimmings appeared and expanded, with a much larger extent and lower intensities than the pre-flare dimmings. The percentage of the 171 angstrom intensity decrease reac40%. The pre-flare dimmings are most striking in 171, 193, and 211 angstrom with formation temperatures 0.6-2.5 MK. The northern part of the pre-flare dimmings could also be recognized in 131 and 335 angstrom.
Conclusions. To our knowledge, this is the first detailed study of pre-flare coronal dimmings; they can be explained by density depletion as a result of the gradual expansion of the coronal loop system surrounding the MFR during the slow rise of the MFR.

第 40 条，共 286 条

LITTLE THINGS (vol 144, 134, 2012)

Hunter, DA (Hunter, Deidre A.); Ficut-Vicas, D (Ficut-Vicas, Dana); Ashley, T (Ashley, Trisha); Brinks, E (Brinks, Elias); Cigan, P (Cigan, Phil); Elmegreen, BG (Elmegreen, Bruce G.); Heesen, V (Heesen, Volker); Herrmann, KA (Herrmann, Kimberly A.); Johnson, M (Johnson, Megan); Oh, SH (Oh, Se-Heon); Rupen,

MP (Rupen, Michael P.); Schruba, A (Schruba, Andreas); Simpson, CE (Simpson, Caroline E.); Walter, F (Walter, Fabian); Westpfahl, DJ (Westpfahl, David J.); Young, LM (Young, Lisa M.); *Zhang, HX* (Zhang, Hong-Xin)
ASTRONOMICAL JOURNAL
卷: 153 期: 1 文献号: 47
DOI: 10.3847/1538-3881/153/1/47
出版年: JAN 2017

第 41 条，共 286 条

Design Study on the Digital Correlator Using for Radio Holography

Xu, LF (Xu, Linfen); Zuo, YX (Zuo, Yingxi)
Xhafa, F (Xhafa, F); Patnaik, S (Patnaik, S); Yu, Z (Yu, Z)
RECENT DEVELOPMENTS IN INTELLIGENT SYSTEMS AND INTERACTIVE APPLICATIONS (IISA2016)
丛书标题: Advances in Intelligent Systems and Computing
卷: 541 页: 377-382
In this paper the author presents a digital correlation design for the radio holography receiver of DATE5 (the 5-m Dome A Terahertz Explorer). Signal digitization is made at the IF outputs of the receiver and correlation is implemented in time domain. A 4-component algorithm for complex correlation is proposed. With this algorithm, the systematic error is much lower and the SNR is expected to have a 3 dB improvement comparing with the previous 3-component algorithm.
会议名称: International Conference on Intelligent and Interactive Systems and Applications (IISA)
会议日期: JUN 25-26, 2016
会议地点: Shanghai, PEOPLES R CHINA

第 42 条，共 286 条

Metal enrichment signatures of the first stars on high-z DLAs

Ma, Q (Ma, Q.); Maio, U (Maio, U.); Ciardi, B (Ciardi, B.); Salvaterra, R (Salvaterra, R.)
MONTHLY NOTICES OF THE ROYAL ASTRONOMICAL SOCIETY
卷: 472 期: 3 页: 3532-3542
We use numerical N-body hydrodynamical simulations with varying PopIII stellar models to investigate the possibility of detecting first star signatures with observations of high-redshift damped Lya absorbers (DLAs). The simulations include atomic and molecular cooling, star formation, energy feedback and metal spreading due to the evolution of stars with a range of masses and metallicities. Different initial mass functions (IMFs) and corresponding metaldependent yields and lifetimes are adopted to model primordial stellar populations. The DLAs in the simulations are selected according to either the local gas temperature (temperature selected) or the host mass (mass selected). We find that 3 per cent (40 per cent) of mass (temperature)-selected high-z (z = 5.5) DLAs retain signatures of pollution from PopIII stars, independent of the first star model. Such DLAs have low halo mass (< 109.6 M-circle dot), metallicity (< 10(-3) Z(circle dot)) and star formation rate (< 10(-1.5) M-circle dot yr(-1)). Metal abundance ratios of DLAs imprinted in the spectra of quasi-stellar object can be useful as tools to infer the properties of the polluting stellar generation and to constrain the first star mass ranges. Comparing the abundance ratios derived from our simulations to those observed in DLAs at z = 5, we find that most of these DLAs are consistent within errors with PopII star dominated enrichment and strongly disfavour the pollution pattern of very massive first stars (i.e. 100-500 M-circle dot). However, some of them could still result from the pollution of first stars in the mass range [0.1, 100] M-circle dot. In particular, we find that the abundance ratios from SDSS J1202+ 3235 are consistent with those expected from PopIII enrichment dominated by massive (but not extreme) first stars.

第 43 条，共 286 条

Doppler Shift Oscillations from a Hot Line Observed by IRIS

Li, D (Li, D.); Ning, ZJ (Ning, Z. J.); Huang, Y (Huang, Y.); Chen, NH (Chen, N. -H.); Zhang, QM (Zhang, Q. M.); Su, YN (Su, Y. N.); Su, W (Su, W.)
ASTROPHYSICAL JOURNAL
卷: 849 期: 2 文献号: 113
We present a detailed investigation of the Doppler shift oscillations in a hot loop during an M7.1 flare on 2014 October 27 observed by the Interface Region Imaging Spectrograph. The periodic oscillations are observed in the Doppler shift of Fe XXI. 1354.09 angstrom (log T similar to 7.05), and the dominant period is about 3.1. minutes. However, such 3.1 minute oscillations are not found in the line-integrated intensity of Fe XXI. 1354.09 angstrom, AIA EUV fluxes, or microwave emissions. Solar Dynamics Observatory/AIA and Hinode/XRT imaging observations indicate that the Doppler shift oscillations locate at the hot loop-top region (>= 11 MK). Moreover, the differential emission measure results show that the temperature is increasing rapidly when the Doppler shift oscillates, but the number density does not exhibit the corresponding increases nor oscillations, implying that the flare loop is likely to oscillate in an incompressible mode. All of these facts suggest that the Doppler shift oscillations at the shorter period are most likely the standing kink oscillations in a flare loop. Meanwhile, a longer period of about 10. minutes is identified in the time series of Doppler shift and line-integrated intensity, GOES SXR fluxes, and AIA EUV light curves, indicating the periodic energy release in this flare, which may be caused by a slow mode wave.

第 44 条，共 286 条

Quasi-periodic pulsations with multiple periods in hard X-ray emission

Li, D (Li, D.); Zhang, QM (Zhang, Q. M.)
MONTHLY NOTICES OF THE ROYAL ASTRONOMICAL SOCIETY
卷: 471 期: 1 页: L6-L10
We explore quasi-periodic pulsations with multiple periods in hard X-ray (HXR) emission from the Fermi Gamma-ray Burst Monitor during the impulsive phase of a solar flare (SOL2014-09-10). The completely new observational result is that the shorter periods appear at lower energies of the X-ray photons at the beginning and the longer periods appear at higher energies at the end, with some intersection of the periods at medium energies. We also find shorter and then longer periods during the same phase of this flare. Using the wavelet power spectrum and fast Fourier transform spectrum, we analyse the normalized rapidly varying signal divided by its slowly varying signal, which is the smoothed original HXR flux. The periods of 27 and 37 s are derived at lower-energy channels between 17: 25 and 17: 29 UT (i.e. 12.0-27.3 and 27.3-50.9 keV). Then, the periods of 27, 46 and 60 s are observed at the medium-energy channel from 17: 26 to 17: 33 UT, such as 50.9-102.3 keV. Also, the period of 80 s is detected at the higher-energy channel from 17: 28 to 17: 33 UT, such as 102.3-296.4 keV.

第 45 条，共 286 条

Large-amplitude Longitudinal Oscillations Triggered by the Merging of Two Solar Filaments: Observations and Magnetic Field Analysis

Luna, M (Luna, M.); *Su, Y* (Su, Y.); Schmieder, B (Schmieder, B.); Chandra, R (Chandra, R.); Kucera, TA (Kucera, T. A.)
ASTROPHYSICAL JOURNAL
卷: 850 期: 2 文献号: 143
We follow the eruption of two related intermediate filaments observed in Ha (from GONG) and EUV (from Solar Dynamics Observatory SDO/Atmospheric Imaging assembly AIA) and the resulting large-amplitude longitudinal oscillations of the plasma in the filament channels. The events occurred in and around the decayed active region AR12486 on 2016 January 26. Our detailed study of the oscillation reveals that the periods of the oscillations are about one hour. In H alpha, the period decreases with time and exhibits strong damping. The analysis of 171 angstrom images shows that the oscillation has two phases: an initial long-period phase and a subsequent oscillation with a shorter period. In this wavelength, the damping appears weaker than in Ha. The velocity is the largest ever detected in a prominence oscillation, approximately 100 km s(-1). Using SDO/HMI magnetograms, we reconstruct the magnetic field of the filaments, modeled as flux ropes by using a flux-rope insertion method. Applying seismological techniques, we determine that the radii of curvature of the field lines in which cool plasma is condensed are in the range 75-120. Mm, in agreement with the reconstructed field. In addition, we infer a field strength of >= 7 to 30 Gauss, depending on the electron density assumed, that is also in agreement with the values from the reconstruction (8-20 Gauss). The poloidal flux is zero and the axis flux is on the order of 10(20) to 10(21) Mx, confirming the high shear existing even in a non-active filament.

1-04 Acceleration and Radiation of High-Energy Cosmic Particles

第 46 条，共 286 条

EVOLUTION OF HIGH-ENERGY PARTICLE DISTRIBUTION IN MATURE SHELL-TYPE SUPERNOVA REMNANTS

Zeng, HD (Zeng, Houdun); Xin, YL (Xin, Yuliang); Liu, SM (Liu, Siming); Jokipii, JR (Jokipii, J. R.); Zhang, L (Zhang, Li); Zhang, SN (Zhang, Shuinai)
ASTROPHYSICAL JOURNAL
卷: 834 期: 2 文献号: 153
Multi-wavelength observations of mature supernova remnants (SNRs), especially with recent advances in gamma-ray astronomy, make it possible to constrain energy distribution of energetic particles within these remnants. In consideration of the SNR origin of Galactic cosmic rays and physics related to particle acceleration and radiative processes, we use a simple one-zone model to fit the nonthermal emission spectra of three shell-type SNRs located within 2 degrees on the sky: RX J1713.7-3946, CTB 37B, and CTB 37A. Although radio images of these three sources all show a shell (or half-shell) structure, their radio, X-ray, and gamma-ray spectra are quite different, offering an ideal case to explore evolution of energetic particle distribution in SNRs. Our spectral fitting shows that (1) the particle distribution becomes harder with aging of these SNRs, implying a continuous acceleration process, and the particle distributions of CTB 37A and CTB 37B in the GeV range are harder than the hardest distribution that can be produced at a shock via the linear diffusive shock particle acceleration process, so spatial transport may play a role; (2) the energy loss timescale of electrons at the high-energy cutoff due to synchrotron radiation appears to be always a bit (within a factor of a few) shorter than the age of the corresponding remnant, which also requires continuous particle acceleration; (3) double power-law distributions are needed to fit the spectra of CTB 37B and CTB 37A, which may be attributed to shock interaction with molecular clouds.

第 47 条，共 286 条

Anomalous Distributions of Primary Cosmic Rays as Evidence for Time-dependent Particle Acceleration in Supernova Remnants

Zhang, YR (Zhang, Yiran); *Liu, SM* (Liu, Siming); Yuan, Q (Yuan, Qiang)
ASTROPHYSICAL JOURNAL LETTERS
卷: 844 期: 1 文献号: L3
Recent precise measurements of cosmic-ray (CR) spectra show that the energy distribution of protons is softer than those of heavier nuclei, and there are spectral hardenings for all nuclear compositions above similar to 200 GV. Models proposed for these anomalies generally assume steady-state solutions of the particle acceleration process. We show that if the diffusion coefficient has a weak dependence on the particle rigidity near shock fronts of supernova remnants (SNRs), time-dependent solutions of the linear diffusive shock acceleration at two stages of SNR evolution can naturally account for these anomalies. The high-energy component of CRs is dominated by acceleration in the free expansion and adiabatic phases with enriched heavy elements and a high shock speed. The low-energy component may be attributed to acceleration by slow shocks propagating in dense molecular clouds with low metallicity in the radiative phase. Instead of a single power-law distribution, the spectra of time-dependent solutions soften gradually with the increase of energy, which may be responsible for the "knee" of CRs.

第 48 条，共 286 条

Evaluation of dimension of fractal time series with the least square method

Qiao, BQ (Qiao, BingQiang); Liu, SM (Liu, SiMing); Zeng, HD (Zeng, HouDun); Li, X (Li, Xiang); Dai, BZ (Dai, BenZhong)
SCIENCE CHINA-PHYSICS MECHANICS & ASTRONOMY
卷: 60 期: 4 文献号: 040521
Properties of fractional Brownian motions (fBms) have been investigated by researchers in different fields, e.g. statistics, hydrology, biology, finance, and public transportation, which has helped us better understand many complex time series observed in nature [1-4]. The Hurst exponent H ($0 < H < 1$) is the most important parameter characterizing any given time series F(t), where t represents the time steps, and the fractal dimension D is determined via the relation $D = 2 - H$. The Hurst exponent H is defined with the following expression [5]: $\log(h|F(t+\tau) - F(t)|i) \propto H\log(\tau)$, (1) where "hi" represents averaging over t. Using the Lowen method for $0 < H < 0.5$ and the circulant embedding method for $0.5 < H < 1$, Qiao and Liu [5] carried out extensive simulations of fBms with different H to obtain the standard deviation of the re-scaled range $h|\Delta F\tau|i = h|F(t+\tau) - F(t)|i$ for different sampling methods. This letter extends this study to apply the commonly used least square (LS) method to the $\log(h|F(t+\tau) - F(t)|i)$ v.s. $\log(\tau)$ plot for evaluation of H.

第 49 条，共 286 条

Measure the Propagation of a Halo CME and Its Driven Shock with the Observations from a Single Perspective at Earth

Lu, L (Lu, Lei); Inhester, B (Inhester, Bernd); Feng, L (Feng, Li); Liu, SM (Liu, Siming); Zhao, XH (Zhao, Xinhua)
ASTROPHYSICAL JOURNAL
卷: 835 期: 2 文献号: 188
We present a detailed study of an Earth-directed coronal mass ejection (full-halo CME) event that happened on 2011 February 15, making use of white-light observations by three coronagraphs and radio observations by Wind/WAVES. We applied three different methods to reconstruct the propagation direction and traveling distance of the CME and its driven shock. We measured the kinematics of the CME leading edge from white-light images observed by Solar Terrestrial Relations Observatory (STEREO) Aand B, tracked the CME-driven shock using the frequency drift observed by Wind/WAVES together with an interplanetary density model, and obtained the equivalent scattering centers of the CME by the polarization ratio (PR) method. For the first time, we applied the PR method to different features distinguished from LASCO/C2 polarimetric observations and calculated their projections onto white-light images observed by STEREO-A and STEREO-B. By combining the graduated cylindrical shell (GCS) forward modeling with the PR method, we proposed a new GCS-PR method to derive 3D parameters of a CME observed from a single perspective at Earth. Comparisons between different methods show a good degree of consistence in the derived 3D results.

第 50 条，共 286 条

Calibration of the Mengcheng Solar Radio Spectrometer

Wang Lu; Zhang Ping; Liu Siming; Liu Rui; Pan Zonghao; Song Qiwu; Ning Zongjun; Ma Kaixue
Acta Astronomica Sinica
卷: 58 期: 1 页: 4-1-4-13 文献号: 0001-5245(2017)58:1<4:MCTYSD>2.0.TX;2-V
Observations of solar radio bursts are one of the most important tools to study solar activities. Based on the analysis of the Mengcheng Solar Radio Spectrometer observations of an M2.9 class flare occurred on 2015 August 27,we find that the classical calibration method does not give satisfactory results, due to the influence of the electronic apparatuses of the instrument. By using the X-ray and radio data of Geostationary Operational Environmental Satellites (GOES), and Nobeyama Radio Polarimeter (NoRP)/Nobeyama Radioheliograph (NoRH), and combined with the relevant radiative mechanisms, the calibration method is improved. Compared to the classical method, the improved calibration method provides better results, which are consistent with the NoRP/NoRH observations and reveal the typical evolution of the radio spectrum for a flare.

1-05 Physics of Dark Matter Indirect Detection

第 51 条，共 286 条

A gamma-ray Quasi-periodic Modulation in the Blazar PKS 0301-243?

Zhang, PF (Zhang, Peng-Fei); Yan, DH (Yan, Da-Hai); Zhou, JN (Zhou, Jia-Neng); Fan, YZ (Fan, Yi-Zhong); Wang, JC (Wang, Jian-Cheng); Zhang, L (Zhang, Li)
ASTROPHYSICAL JOURNAL
卷: 845 期: 1 文献号: 82
We report a nominally high-confidence gamma-ray quasi-periodic modulation in the blazar PKS 0301-243. For this target, we analyze its Fermi-LAT Pass 8 data from 2008 August to 2017 May. Two techniques, i.e., maximum likelihood optimization and exposure-weighted aperture photometry, are used to build the gamma-ray light curves. Then, both the Lomb-Scargle periodogram and the weighted wavelet Z-transform are applied to the light curves to search for period signals. A quasi-periodicity with a period of 2.1 +/- 0.3 yr appears at the significance level of similar to 5 sigma, although it should be noted that this putative quasi-period variability is seen in a data set that is barely four times longer. We speculate that this gamma-ray quasi-periodic modulation may be evidence of a binary supermassive black hole.

第 52 条，共 286 条

Neutron Star-Black Hole Coalescence Rate Inferred from Macronova Observations

Li, X (Li, Xiang); Hu, YM (Hu, Yi-Ming); Jin, ZP (Jin, Zhi-Ping); Fan, YZ (Fan, Yi-Zhong); Wei, DM (Wei, Da-Ming)
ASTROPHYSICAL JOURNAL LETTERS
卷: 844 期: 2 文献号: L22
Neutron star-black hole (NS-BH) coalescences are widely believed to be promising gravitational-wave sources in the era of advanced detectors of LIGO/Virgo, but the rate of this population is highly uncertain due to the lack of direct detection of such binaries. There is growing evidence for the connection between the observed three luminous macronova (also known as kilonova) events and NS-BH mergers. In this work, we propose, for the first time based on such a link, a fiducial lower limit of NS-BH coalescence rate density R-nsbh approximate to 18.8(-8.6)(+12.5) Gpc(-3) yr(-0.1) (theta(j)/0.1 rad)(-2) ,where theta(j) is the typical half-opening angle of the GRB ejecta. After marginalizing over distributions of black hole masses and spins, we find a rate density R-nsbh >= 10(2) Gpc(-3) yr(-1), depending upon the equation of state (EoS) of NS material and the properties of the NS-BH system. With the O1 non-observation by advanced LIGO, we show a preference for NS-BH systems with a stiffer NS EoS and a larger contribution from low-mass/high-spin BHs. Our estimate predicts the first detection of an NS-BH system can be as early as the late O2 run or the early O3 run. We expect that future multi-messenger observations can much better constrain NS-BH systems' properties.

第 53 条，共 286 条

Possible Correlations between the Emission Properties of SGRBs and Their Offsets from the Host Galaxies

Zhang, S (Zhang, Shuai); *Jin, ZP* (Jin, Zhi-Ping); Zhang, FW (Zhang, Fu-Wen); Li, X (Li, Xiang); Fan, YZ (Fan, Yi-Zhong); Wei, DM (Wei, Da-Ming)
ASTROPHYSICAL JOURNAL
卷: 844 期: 1 文献号: 55
Short gamma-ray bursts (SGRBs) are widely believed to be from mergers of binary compact objects involving at least one neutron star and hence have a broad range of spatial offsets from their host galaxies. In this work, we search for possible correlations between the emission properties of 18 SGRBs and their offsets from the host galaxies. The SGRBs with and without extended emission do not show significant differences between their offset distributions, in agreement with some previous works. There are, however, possible correlations between the optical and X-ray afterglow emission and the offsets. The underlying physical origins are examined.

第 54 条，共 286 条

Revisiting SNR Puppis A with Seven Years of Fermi Large Area Telescope Observations

Xin, YL (Xin, Yu-Liang); Guo, XL (Guo, Xiao-Lei); Liao, NH (Liao, Neng-Hui); Yuan, Q (Yuan, Qiang); Liu, SM (Liu, Si-Ming); Wei, DM (Wei, Da-Ming)
ASTROPHYSICAL JOURNAL
卷: 843 期: 2 文献号: 90
Puppis A is a very famous and extensively studied supernova remnant that shows strong evidence of shock-cloud interaction. We reanalyze its GeV gamma-ray emission using seven years of Pass 8 data recorded by the Fermi Large Area Telescope. The morphology of the gamma-ray emission is more compatible with that of the thermal X-ray and IR emissions than the radio image, which suggests a possible correlation between the gamma-ray-emitting region and dense clouds. The gamma-ray spectrum in the energy range of 1-500 GeV shows a break at 7.92 +/- 1.91 GeV, with photon indices of 1.81 +/- 0.08 below the break and 2.53 +/- 0.12 above the break, which can naturally explain the lack of TeV gamma-ray emission from Puppis A. The multi-wavelength observations favor a hadronic origin for the gamma-ray emission.

第 55 条，共 286 条

Millimeter observations of the disk around GW Orionis

Fang, M (Fang, M.); Sicilia-Aguilar, A (Sicilia-Aguilar, A.); Wilner, D (Wilner, D.); Wang, Y (Wang, Y.); Roccatagliata, V (Roccatagliata, V.); Fedele, D (Fedele, D.); Wang, JZ (Wang, J. Z.)
ASTRONOMY & ASTROPHYSICS
卷: 603 文献号: A132
The GW Ori system is a pre-main sequence triple system (GW Ori A/B/C) with companions (GW Ori B/C) at similar to 1AU and similar to 8AU, respectively, from the primary (GW Ori A). The primary of the system has a mass of 3.9 M-circle dot, but shows a spectral type of G8. Thus, GW Ori A could be a precursor of a B star, but it is still at an earlier evolutionary stage than Herbig Be stars. GW Ori provides an ideal target for experiments and observations (being a "blown-up" solar system with a very massive sun and at least two upscaled planets). We present the first spatially resolved millimeter interferometric observations of the disk around the triple pre-main sequence system GW Ori, obtained with the Submillimeter Array, both in continuum and in the (CO)-C-12 J = 2-1, (CO)-C-13 J = 2 1, and (CO)-O-18 J = 2-1 lines. These new data reveal a huge, massive, and bright disk in the GW Ori system. The dust continuum emission suggests a disk radius of around 400AU, but the 12CO J = 2 1 emission shows a much more extended disk with a size around 1300AU. Owing to the spatial resolution (similar to 1"), we cannot detect the gap in the disk that is inferred from spectral energy distribution (SED) modeling. We characterize the dust and gas properties in the disk by comparing the observations with the predictions from the disk models with various parameters calculated with a Monte Carlo radiative transfer code RADMC-3D. The disk mass is around 0.12 M-circle dot, and the disk inclination with respect to the line of sight is around similar to 35 degrees. The kinematics in the disk traced by the CO line emission strongly suggest that the circumstellar material in the disk is in Keplerian rotation around GW Ori. Tentatively substantial (CO)-O-18 depletion in gas phase is required to explain the characteristics of the line emission from the disk.

第 56 条，共 286 条

Possible Quasi-periodic Modulation in the z=1.1 Gamma-Ray Blazar PKS 0426-380

Zhang, PF (Zhang, Peng-fei); Yan, DH (Yan, Da-hai); Liao, NH (Liao, Neng-hui); Zeng, W (Zeng, Wei); Wang, JC (Wang, Jian-cheng); Cao, LJ (Cao, Li-jia)
ASTROPHYSICAL JOURNAL
卷: 842 期: 1 文献号: 10
We search for gamma-ray and optical periodic modulations in distant flat-spectrum radio quasar (FSRQ) PKS 0426-380 (the redshift z = 1.1). Using two techniques (i. e., the maximum likelihood optimization and the exposure-weighted aperture photometry), we obtain gamma-ray light curves from Fermi-LAT Pass 8 data covering from 2008 August to 2016 December. We then analyze the light curves with the Lomb-Scargle periodogram and the weighted wavelet Z-transform. A gamma-ray quasi-periodicity with a period of 3.35 +/- 0.68 yr is found at the significance level of. 3.6 s. The optical-UV flux covering from 2005 August to 2013 April provided by the ASI Science Data Center is also analyzed, but no significant quasi-periodicity is found. It should be pointed out that the result of the optical-UV data could be tentative because of the incompleteness of the data. Further long-term multiwavelength monitoring of this FSRQ is needed to confirm its quasi-periodicity.

第 57 条，共 286 条

Possible Dark Matter Annihilation Signal in the AMS-02 Antiproton Data

Cui, MY (Cui, Ming-Yang); Yuan, Q (Yuan, Qiang); Tsai, YLS (Tsai, Yue-Lin Sming); Fan, YZ (Fan, Yi-Zhong)
PHYSICAL REVIEW LETTERS
卷: 118 期: 19 文献号: 191101
Using the latest AMS-02 cosmic-ray antiproton flux data, we search for a potential dark matter annihilation signal. The background parameters about the propagation, source injection, and solar modulation are not assumed a priori but based on the results inferred from the recent B/C ratio and proton data measurements instead. The possible dark matter signal is incorporated into the model self-consistently under a Bayesian framework. Compared with the astrophysical background-only hypothesis, we find that a dark matter signal is favored. The rest mass of the dark matter particles is similar to 20-80 GeV, and the velocity-averaged hadronic annihilation cross section is about (0.2-5) x 10(-26) cm(3) s(-1), in agreement with that needed to account for the Galactic center GeV excess and/or the weak GeV emission from dwarf spheroidal galaxies Reticulum 2 and Tucana III. Tight constraints on the dark matter annihilation models are also set in a wide mass region.

第 58 条，共 286 条

Light bending in infinite derivative theories of gravity

Feng, L (Feng, Lei)
PHYSICAL REVIEW D
卷: 95 期: 8 文献号: 084015
Light bending is one of the significant predictions of general relativity (GR) and it has been confirmed with great accuracy during the past one hundred years. In this paper, we semiclassically calculate the deflection angle for the photons that just graze the Sun in the infinite derivative theories of gravity (IDG) which is a ghost and singularity free theory of gravity. From our calculations, we find that the deflection angle. only depends on Lambda/E. theta -> theta(E) when Lambda/E -> infinity and decrease to zero when Lambda/E -> 0. The transition interval occurs at 10(4) < E/Lambda < 10(7). It should be pointed out that this model can be tested by the Chandra X-ray Observatory if 0.01 eV < Lambda < 0.1 eV.

第 59 条，共 286 条

Constraining the PopIII IMF with high-z GRBs

Ma, Q (Ma, Q.); Maio, U (Maio, U.); Ciardi, B (Ciardi, B.); Salvaterra, R (Salvaterra, R.)
MONTHLY NOTICES OF THE ROYAL ASTRONOMICAL SOCIETY
卷: 466 期: 1 页: 1140-1148
We study the signatures of enrichment from PopIII stars in observations of PopII GRBs (GRBIIs) at high redshift by using numerical N-body/hydrodynamical simulations including atomic and molecular cooling, star formation and metal spreading from stellar populations with different initial mass functions (IMFs), yields and lifetimes. PopIII and PopII star formation regimes are followed simultaneously and both a top-heavy and a Salpeter-like IMF for pristine PopIII star formation are adopted. We find that the fraction of GRBIIs hosted in a medium previously enriched by PopIII stars (PopIII-dominated) is model-independent. Typical abundance ratios, such as [Si/O] versus[C/O] and [Fe/C] versus[Si/C], can help to disentangle enrichment from massive and intermediate PopIII stars, while low-mass first stars are degenerate with regular PopII generations. The properties of galaxies hosting PopIII-dominated GRBIIs are not very sensitive to the particular assumption on the mass of the first stars.

第 60 条，共 286 条

Limits on dark matter annihilation cross sections to gamma-ray lines with subhalo distributions in N-body simulations and Fermi LAT data

Liang, YF (Liang, Yun-Feng); Xia, ZQ (Xia, Zi-Qing); Duan, KK (Duan, Kai-Kai); Shen, ZQ (Shen, Zhao-Qiang); Li, X (Li, Xiang); Fan, YZ (Fan, Yi-Zhong)
PHYSICAL REVIEW D
卷: 95 期: 6 文献号: 063531
In this work, we simulate a set of realizations of the local volume dark matter subhalo population based on the distributions and relations derived from Via Lactea II N-body simulation. We calculate the J-factors of these subhalos, and find that the low mass subhalos contribute a lot to the total J-factors. Combining with 91 months of the Fermi LAT observation, we constrain on the cross section of dark matter annihilating directly to two gamma rays. This is the first work combining numerical simulation results and Fermi LAT observations to constrain the dark matter cross section to the gamma-ray line with the subhalo population. Though the constraints derived from the subhalo population are weaker than those from the Fermi LAT observation of the Galactic center, they are supportive of and complementary to these other results.

第 61 条，共 286 条

gamma-Ray emission signals in the massive graviton mediated dark matter model

Zhang, C (Zhang, Cun); Cui, MY (Cui, Ming-Yang); Feng, L (Feng, Lei); Fan, YZ (Fan, Yi-Zhong); Ren, ZZ (Ren, Zhong-Zhou)
NUCLEAR PHYSICS B
卷: 916 页: 208-218
Dark matter may interact with Standard Model (SM) particle through the exchange of a massive spin-2 graviton producing signals that can be detected. In this work we examine the gamma-ray emission signals, including the line emission and the continuous spectrum component in such a massive graviton-mediated dark matter model. The constraints of LHC data, dark matter relic density as well as the dark matter indirect detection data have been applied to narrow down the parameter space. We focus on the vector dark matter model which could produce detectable gamma-ray line signal. It is found that the gamma-ray line data is effective on constraining the model parameters and the ongoing and upcoming space or ground-based gamma-ray experiments can constrain the model further. As for the continuous gamma-ray emission, the total effective annihilation cross section is similar to 10(-26) cm(3) s(-1) except at the region where dark matter mass is around the graviton mass or half of it, which is consistent with current observational data and will be reliably probed by the upcoming CTA. (C) 2017 The Authors. Published by Elsevier B.V.

第 62 条，共 286 条

Evaluating the Bulk Lorentz Factors of Outflow Material: Lessons Learned from the Extremely Energetic Outburst GRB 160625B

Wang, YZ (Wang, Yuan-Zhu); Wang, H (Wang, Hao); Zhang, S (Zhang, Shuai); Liang, YF (Liang, Yun-Feng); Jin, ZP (Jin, Zhi-Ping); He, HN (He, Hao-Ning); Liao, NH (Liao, Neng-Hui); Fan, YZ (Fan, Yi-Zhong); Wei, DM (Wei, Da-Ming)
ASTROPHYSICAL JOURNAL
卷: 836 期: 1 文献号: 81
GRB 160625B is an extremely bright outburst with well-monitored afterglow emission. The geometry-corrected energy is high, up to similar to 5.2 x 10(52) erg or even similar to 8 x 10(52) erg, rendering it the most energetic GRB prompt emission recorded so far. We analyzed the time-resolved spectra of the prompt emission and found that in some intervals there were likely thermal-radiation components and the high energy emission was characterized by significant cutoff. The bulk Lorentz factors of the outflow material are estimated accordingly. We found out that the Lorentz factors derived in the thermal- radiation model are consistent with the luminosity-Lorentz factor correlation found in other bursts, as well as in GRB 090902B for the time-esolved thermal-radiation components, while the spectral cutoff model yields much lower Lorentz factors that are in tension with the constraints set by the electron pair Compton scattering process. We then suggest that these spectral cutoffs are more likely related to the particle acceleration process and that one should be careful in estimating the Lorentz factors if the spectrum cuts at a rather low energy (e.g., similar to tens of MeV). The nature of the central engine has also been discussed, and a stellarmass black hole is favored.

第 63 条，共 286 条

Revisiting Quasi-periodic Modulation in gamma- Ray Blazar PKS 2155-304 with Fermi Pass 8 Data

Zhang, PF (Zhang, Peng-fei); Yan, DH (Yan, Da-hai); Liao, NH (Liao, Neng-hui); Wang, JC (Wang, Jian-cheng)
ASTROPHYSICAL JOURNAL
卷: 835 期: 2 文献号: 260
We examine the gamma-ray quasi-periodic variability of PKS 2155-304 with the latest publicly available Fermi-LAT Pass 8 data, which covers the years from 2008 August to 2016 October. We produce the light curves in two ways: the exposure-weighted aperture photometry and the maximum likelihood optimization. The light curves are then analyzed by using Lomb-Scargle Periodogram (LSP) and Weighted Wavelet Z-transform, and the results reveal a significant quasi-periodicity with a period of 1.74. +/- 0.13 years and a significance of similar to 4.9 sigma. The constraint of multifrequencies quasi-periodic variabilities on blazar emission model is discussed.

第 64 条，共 286 条

Spectroscopic identification of r-process nucleosynthesis in a double neutron-star merger

Pian, E (Pian, E.); D'Avanzo, P (D'Avanzo, P.); Enetti, SB (Enetti, S. B.); Branchesi, M (Branchesi, M.); Rocato, EB (Rocato, E. B.); Campana, S (Campana, S.); Cappellaro, E (Cappellaro, E.); Covino, S (Covino, S.); D'Elia, V (D'Elia, V.); Fynbo, JPU (Fynbo, J. P. U.); Getman, F (Getman, F.); Ghirlanda, G (Ghirlanda, G.); Ghisellini, G (Ghisellini, G.); Grado, A (Grado, A.); Greco, G (Greco, G.); Hjorth, J (Hjorth, J.); Kouveliotou, C (Kouveliotou, C.); Levan, A (Levan, A.); Limatola, L (Limatola, L.); Alesani, DM (Alesani, D. M.); Azzali, PAM (Azzali, P. A. M.); Elandri, AM (Elandri, A. M.); Oller, PM (Oller, P. M.); Icastro, LN (Icastro, L. N.); Palazzi, E (Palazzi, E.); Piranomonte, S (Piranomonte, S.); Rossi, A (Rossi, A.); Salafia, OS (Salafia, O. S.); Selsing, J (Selsing, J.); Stratta, G (Stratta, G.); Tanaka, M (Tanaka, M.); Tanvir, NR (Tanvir, N. R.); Tomasella, L (Tomasella, L.); Watson, D (Watson, D.); Yang, S (Yang, S.); Amati, L (Amati, L.); Antonelli, LA (Antonelli, L. A.); Ascenzi, S (Ascenzi, S.); Ernardini, MGB (Ernardini, M. G. B.); Boer, M (Boer, M.); Ufano, FB (Ufano, F. B.); Ulgarelli, AB (Ulgarelli, A. B.); Capaccioli, M (Capaccioli, M.); Casella, P (Casella, P.); Castro-Tirado, AJ (Castro-Tirado, A. J.); Chassande-Mottin, E (Chassande-Mottin, E.); Ciolfi, R (Ciolfi, R.); Copperwheat, CM (Copperwheat, C. M.); Dadina, M (Dadina, M.); De Cesare, G (De Cesare, G.); Di Paola, A (Di Paola, A.); *Fan, YZ* (Fan, Y. Z.); Gendre, B (Gendre, B.); Giuffrida, G (Giuffrida, G.); Giunta, A (Giunta, A.); Hunt, LK (Hunt, L. K.); Israel, GL (Israel, G. L.); Jin, ZP (Jin, Z. -P.); Kasliwal, MM (Kasliwal, M. M.); Klose, S (Klose, S.); Lisi, M (Lisi, M.); Longo, F (Longo, F.); Aiorano, EM (Aiorano, E. M.); Apelli, MM (Apelli, M. M.); Asetti, NM (Asetti, N. M.); Ava, LN (Ava, L. N.); Patricelli, B (Patricelli, B.); Perley, D (Perley, D.); Pescalli, A (Pescalli, A.); Piran, T (Piran, T.); Possenti, A (Possenti, A.); Pulone, L (Pulone, L.); Azzano, MR (Azzano, M. R.); Salvaterra, R (Salvaterra, R.); Schipani, P (Schipani, P.); Spera, M (Spera, M.); Stamerra, A (Stamerra, A.); Stella, L (Stella, L.); Tagliaferri, G (Tagliaferri, G.); Testa, V (Testa, V.); Troja, E (Troja, E.); Turatto, M (Turatto, M.); Ergani, SDV (Ergani, S. D. V.); Ergani, DV (Ergani, D. V.)
NATURE
卷: 551 期: 7678 页: 67-+
The merger of two neutron stars is predicted to give rise to three major detectable phenomena: a short burst of gamma-rays, a gravitational-wave signal, and a transient optical-near-infrared source powered by the synthesis of large amounts of very heavy elements via rapid neutron capture (the r-process)(1-3). Such transients, named 'macronovae' or 'kilonovae'(4-7), are believed to be centres of production of rare elements such as gold and platinum(8). The most compelling evidence so far for a kilonova was a very faint near-infrared rebrightening in the afterglow of a short gamma-ray burst(9,10) at redshift z = 0.356, although findings indicating bluer events have been reported(11). Here we report the spectral identification and describe the physical properties of a bright kilonova associated with the gravitational-wave source(12) GW170817 and gamma-ray burst(13,14) GRB 170817A associated with a galaxy at a distance of 40 megaparsecs from Earth. Using a series of spectra from ground-based observatories covering the wavelength range from the ultraviolet to the near-infrared, we find that the kilonova is characterized by rapidly expanding ejecta with spectral features similar to those predicted by current models(15,16). The ejecta is optically thick early on, with a velocity of about 0.2 times light speed, and reaches a radius of about 50 astronomical units in only 1.5 days. As the ejecta expands, broad absorption-like lines appear on the spectral continuum, indicating atomic species produced by nucleosynthesis that occurs in the post-merger fast-moving dynamical ejecta and in two slower (0.05 times light speed) wind regions. Comparison with spectral models suggests that the merger ejected 0.03 to 0.05 solar masses of material, including high-opacity lanthanides.

第 65 条，共 286 条

An X-Ray Periodicity of similar to 1.8 hr in Narrow-line Seyfert 1 Galaxy Mrk 766

Zhang, P (Zhang, Peng); Zhang, PF (Zhang, Peng-fei); Yan, JZ (Yan, Jing-zhi); Fan, YZ (Fan, Yi-zhong); Liu, QZ (Liu, Qing-zhong)
ASTROPHYSICAL JOURNAL
卷: 849 期: 1 文献号: 9
In the narrow-line Seyfert 1 galaxy Mrk 766, a quasi-periodic oscillation (QPO) signal with a period of similar to 6450 s is detected in the XMM-Newton data collected on 2005 May 31. This QPO signal is highly statistically significant at the similar to 5 sigma confidence level, with a quality factor of Q = f / Delta f > 13.6. The X-ray intensity changed by a factor of 3, with a root mean square fractional variability of 14.3%. Furthermore, this QPO signal is present in the data of all three EPIC detectors and two RGS cameras and its frequency follows the f(QPO)-M-BH relation spanning from stellar-mass to supermassive black holes. Interestingly, a possible QPO signal with a period of similar to 4200 s had been reported in the literature. The frequency ratio of these two QPO signals is similar to 3:2. Our result is also in support of the hypothesis that the QPO signals can just be transient. The spectral analysis reveals that the contribution of the soft excess component below similar to 1 keV is different between epochs with and without QPO. This property, as well as the former frequency ratio, are well-detected in X-ray BH binaries, which may shed some light on the physical origins of our event.

第 66 条，共 286 条

Direct detection of a break in the teraelectronvolt cosmic-ray spectrum of electrons and positrons

Ambrosi, G (Ambrosi, G.); An, Q (An, Q.); Asfandiyarov, R (Asfandiyarov, R.); Azzarello, P (Azzarello, P.); Bernardini, P (Bernardini, P.); Bertucci, B (Bertucci, B.); Cai, MS (Cai, M. S.); Chang, J (Chang, J.); Chen, DY (Chen, D. Y.); Chen, HF (Chen, H. F.); Chen, JL (Chen, J. L.); *Chen, W* (Chen, W.); Cui, MY (Cui, M. Y.); Cui, TS (Cui, T. S.); D'Amone, A (D'Amone, A.); De Benedittis, A (De Benedittis, A.); De Mitri, I (De Mitri, I.); Di Santo, M (Di Santo, M.); Dong, JN (Dong, J. N.); Dong, TK (Dong, T. K.); Dong, YF (Dong, Y. F.); Dong, ZX (Dong, Z. X.); Donvito, G (Donvito, G.); Droz, D (Droz, D.); Duan, KK (Duan, K. K.); Duan, JL (Duan, J. L.); Duranti, M (Duranti, M.); D'Urso, D (D'Urso, D.); Fan, RR (Fan, R. R.); Fan, YZ (Fan, Y. Z.); Fang, F (Fang, F.); Feng, CQ (Feng, C. Q.); Feng, L (Feng, L.); Fusco, P (Fusco, P.); Gallo, V (Gallo, V.); Gan, FJ (Gan, F. J.); Gao, M (Gao, M.); Gao, SS (Gao, S. S.); Gargano, F (Gargano, F.); Garrappa, S (Garrappa, S.); Gong, K (Gong, K.); Gong, YZ (Gong, Y. Z.); Guo, DY (Guo, D. Y.); Guo, JH (Guo, J. H.); Hu, YM (Hu, Y. M.); Huang, GS (Huang, G. S.); Huang, YY (Huang, Y. Y.); Ionica, M (Ionica, M.); Jiang, D (Jiang, D.); Jiang, W (Jiang, W.); Jin, X (Jin, X.); Kong, J (Kong, J.); Lei, SJ (Lei, S. J.); Li, S (Li, S.); Li, X (Li, X.); Li, WL (Li, W. L.); Li, Y (Li, Y.); Liang, YF (Liang, Y. F.); Liang, YM (Liang, Y. M.); Liao, NH (Liao, N. H.); Liu, H (Liu, H.); Liu, J (Liu, J.); Liu, SB (Liu, S. B.); Liu, WQ (Liu, W. Q.); Liu, Y (Liu, Y.); Loparco, F (Loparco, F.); Ma, M (Ma, M.); Ma, PX (Ma, P. X.); Ma, SY (Ma, S. Y.); Ma, T (Ma, T.); Ma, XQ (Ma, X. Q.); Ma, XY (Ma, X. Y.); Marsella, G (Marsella, G.); Mazziotta, MN (Mazziotta, M. N.); Mo, D (Mo, D.); Niu, XY (Niu, X. Y.); Peng, XY (Peng, X. Y.); Peng, WX (Peng, W. X.); Qiao, R (Qiao, R.); Rao, JN (Rao, J. N.); Salinas, MM (Salinas, M. M.); Shang, GZ (Shang, G. Z.); Shen, WH (Shen, W. H.); Shen, ZQ (Shen, Z. Q.); Shen, ZT (Shen, Z. T.); Song, JX (Song, J. X.); Su, H (Su, H.); Su, M (Su, M.); Sun, ZY (Sun, Z. Y.); Surdo, A (Surdo, A.); Teng, XJ (Teng, X. J.); Tian, XB (Tian, X. B.); Tykhonov, A (Tykhonov, A.); Vagelli, V

(Vagelli, V.); Vitillo, S (Vitillo, S.); Wang, C (Wang, C.); Wang, H (Wang, H.); Wang, HY (Wang, H. Y.); Wang, JZ (Wang, J. Z.); Wang, LG (Wang, L. G.); Wang, Q (Wang, Q.); Wang, S (Wang, S.); Wang, XH (Wang, X. H.); Wang, XL (Wang, X. L.); Wang, YF (Wang, Y. F.); Wang, YP (Wang, Y. P.); Wang, YZ (Wang, Y. Z.); Wen, SC (Wen, S. C.); Wang, ZM (Wang, Z. M.); Wei, DM (Wei, D. M.); Wei, JJ (Wei, J. J.); Wei, YF (Wei, Y. F.); Wu, D (Wu, D.); Wu, J (Wu, J.); Wu, LB (Wu, L. B.); Wu, SS (Wu, S. S.); Wu, X (Wu, X.); Xi, K (Xi, K.); Xia, ZQ (Xia, Z. Q.); Xin, YL (Xin, Y. L.); Xu, HT (Xu, H. T.); Xu, ZL (Xu, Z. L.); Xu, ZZ (Xu, Z. Z.); Xue, GF (Xue, G. F.); Yang, HB (Yang, H. B.); Yang, P (Yang, P.); Yang, YQ (Yang, Y. Q.); Yang, ZL (Yang, Z. L.); Yao, HJ (Yao, H. J.); Yu, YH (Yu, Y. H.); Yuan, Q (Yuan, Q.); Yue, C (Yue, C.); Zang, JJ (Zang, J. J.); Zhang, C (Zhang, C.); Zhang, DL (Zhang, D. L.); Zhang, F (Zhang, F.); Zhang, JB (Zhang, J. B.); Zhang, JY (Zhang, J. Y.); Zhang, JZ (Zhang, J. Z.); Zhang, L (Zhang, L.); Zhang, PF (Zhang, P. F.); Zhang, SX (Zhang, S. X.); Zhang, WZ (Zhang, W. Z.); Zhang, Y (Zhang, Y.); Zhang, YJ (Zhang, Y. J.); Zhang, YQ (Zhang, Y. Q.); Zhang, YL (Zhang, Y. L.); Zhang, YP (Zhang, Y. P.); Zhang, Z (Zhang, Z.); Zhang, ZY (Zhang, Z. Y.); Zhao, H (Zhao, H.); Zhao, HY (Zhao, H. Y.); Zhao, XF (Zhao, X. F.); Zhou, CY (Zhou, C. Y.); Zhou, Y (Zhou, Y.); Zhu, X (Zhu, X.); Zhu, Y (Zhu, Y.); Zimmer, S (Zimmer, S.)

NATURE

卷: 552 期: 7683 页: 63-+

High-energy cosmic-ray electrons and positrons (CREs), which lose energy quickly during their propagation, provide a probe of Galactic high-energy processes(1-7) and may enable the observation of phenomena such as dark-matter particle annihilation or decay(8-10). The CRE spectrum has been measured directly up to approximately 2 teraelectronvolts in previous balloon-or space-borne experiments(11-16), and indirectly up to approximately 5 teraelectronvolts using ground-based Cherenkov gamma-ray telescope arrays(17,18). Evidence for a spectral break in the teraelectronvolt energy range has been provided by indirect measurements(17,18), although the results were qualified by sizeable systematic uncertainties. Here we report a direct measurement of CREs in the energy range 25 gigaelectronvolts to 4.6 teraelectronvolts by the Dark Matter Particle Explorer (DAMPE)(19) with unprecedentedly high energy resolution and low background. The largest part of the spectrum can be well fitted by a 'smoothly broken power-law' model rather than a single power-law model. The direct detection of a spectral break at about 0.9 teraelectronvolts confirms the evidence found by previous indirect measurements(17,18), clarifies the behaviour of the CRE spectrum at energies above 1 teraelectronvolt and sheds light on the physical origin of the sub-teraelectronvolt CREs.

第 67 条，共 286 条

The unpolarized macronova associated with the gravitational wave event GW 170817

Covino, S (Covino, S.); Wiersema, K (Wiersema, K.); *Fan, YZ* (Fan, Y. Z.); Toma, K (Toma, K.); Higgins, AB (Higgins, A. B.); Melandri, A (Melandri, A.); D'Avanzo, P (D'Avanzo, P.); Mundell, CG (Mundell, C. G.); Palazzi, E (Palazzi, E.); Tanvir, NR (Tanvir, N. R.); Bernardini, MG (Bernardini, M. G.); Branchesi, M (Branchesi, M.); Brocato, E (Brocato, E.); Campana, S (Campana, S.); Alighieri, SD (Alighieri, S. di Serego); Gotz, D (Gotz, D.); Fynbo, JPU (Fynbo, J. P. U.); Gao, W (Gao, W.); Gomboc, A (Gomboc, A.); Gompertz, B (Gompertz, B.); Greiner, J (Greiner, J.); Hjorth, J (Hjorth, J.); Jin, ZP (Jin, Z. P.); Kaper, L (Kaper, L.); Klose, S (Klose, S.); Kobayashi, S (Kobayashi, S.); Kopac, D (Kopac, D.); Kouveliotou, C (Kouveliotou, C.); Levan, AJ (Levan, A. J.); Mao, J (Mao, J.); Malesani, D (Malesani, D.); Pian, E (Pian, E.); Rossi, A (Rossi, A.); Salvaterra, R (Salvaterra, R.); Starling, RLC (Starling, R. L. C.); Steele, I (Steele, I.); Tagliaferri, G (Tagliaferri, G.); Troja, E (Troja, E.); van der Horst, AJ (van der Horst, A. J.); Wijers, RAMJ (Wijers, R. A. M. J.)

NATURE ASTRONOMY

卷: 1 期: 11 页: 791-794

The merger of two dense stellar remnants including at least one neutron star is predicted to produce gravitational waves (GWs) and short-duration gamma ray burststs. In the process, neutron-rich material is ejected from the system and heavy elements are synthesized by r-process nucleosynthesis(1,3). The radioactive decay of these heavy elements produces additional transient radiation termed kilonova or macronova(4-10). We report the detection of linear optical polarization, P= (0.50 +/- 0.07)%, 1.46 days after detection of the GWs from GW170817-a double neutron star merger associated with an optical macronova counterpart and a short gamma ray burst(11-14). The optical emission from a macronova is expected to be characterized by a blue, rapidly decaying component and a red, more slowly evolving component due to material rich in heavy elements-the lanthanidess(15). The polarization measurement was made when the macronova was still in its blue phase, during which there was an important contribution from a lanthanide-free outflow. The low degree of polarization is consistent with intrinsically unpolarized emission scattered by galactic dust, suggesting a symmetric geometry of the emitting region and low inclination of the merger system. Stringent upper limits to the polarization degree from 2.45-9.48 days post-burst are consistent with the lanthanides-rich macronova interpretation.

第 68 条，共 286 条

GRB 111005A at z = 0.0133 and the Prospect of Establishing Long-Short GRB/GW Association

Wang, Yuan-Zhu; Huang, Yong-Jia; Liang, Yun-Feng; Li, Xiang; Jin, Zhi-Ping; Zhang, Fu-Wen; Zou, Yuan-Chuan; Fan, Yi-Zhong; Wei, Da-Ming

ASTROPHYSICAL JOURNAL LETTERS

卷号: 851, 期号:1, 页码:L20

GRB 111005A, a long-duration gamma-ray burst (GRB) that occurred within a metal-rich environment that lacks massive stars with MZAMS >= 15M(circle dot), is not coincident with supernova emission down to a stringent limit and thus should be classified as a "long-short" GRB (lsGRB; also known as an SN-less long GRB or hybrid GRB), like GRB 060505 and GRB 060614. In this work, we show that in the neutron star merger model the non-detection of the optical/infrared emission of GRB 111005A requires sub-relativistic neutron-rich ejecta with a mass of <= 0.01 M-circle dot, which is (significantly) less massive than that of GRB 130603B, GRB 060614, GRB 050709, and GRB 170817A. The lsGRBs are found to have a high rate density and the neutron star merger origin model can be unambiguously tested by the joint observations of the second-generation gravitational-wave (GW) detectors and the full-sky gamma-ray monitors such as Fermi-GBM and the proposed GECAM. If no lsGRB/GW association is observed in the 2020s, alternative scenarios have to be systematically investigated. With the detailed environmental information achievable for the nearby events, a novel kind of merger or explosion origin may be identified.

1-06 Laboratory for Dark Matter and Space Astronomy

第 69 条，共 286 条

LIKEDM: Likelihood calculator of dark matter detection

Huang, XY (Huang, Xiaoyuan); Tsai, YLS (Tsai, Yue-Lin Sming); Yuan, Q (Yuan, Qiang)
COMPUTER PHYSICS COMMUNICATIONS
卷: 213 页: 252-263
With the large progress in searches for dark matter (DM) particles with indirect and direct methods, we develop a numerical tool that enables fast calculations of the likelihoods of specified DM particle models given a number of observational data, such as charged cosmic rays from space-borne experiments (e.g., PAMELA, AMS-02), gamma-rays from the Fermi space telescope, and underground direct detection experiments. The purpose of this tool - LIKEDM, likelihood calculator for dark matter detection - is to bridge the gap between a particle model of DM and the observational data. The intermediate steps between these two, including the astrophysical backgrounds, the propagation of charged particles, the analysis of Fermi gamma-ray data, as well as the DM velocity distribution and the nuclear form factor, have been dealt with in the code. We release the first version (v1.0) focusing on the constraints from indirect detection of DM with charged cosmic and gamma rays. Direct detection will be implemented in the next version. This manual describes the framework, usage, and related physics of the code.
Program summary
Program Title: LIKEDM
Program Files doi: http://dx.doi.org/10.17632/p93d3ksfvd.1
Licensing provisions: GPLv3
Programming language: FORTRAN 90 and Python
Nature of problem: Dealing with the intermediate steps between a dark matter model and data.
Solution method: Fast computation of the likelihood of a given dark matter model (defined by a mass, cross section or decay rate, and annihilation or decay yield spectrum), without digging into the details of cosmic-ray propagation, Fermi-LAT data analysis, or related astrophysical backgrounds. (C) 2017 Elsevier B.V. All rights reserved.

第 70 条，共 286 条

HESS J1427-608: AN UNUSUAL HARD, UNBROKEN gamma-RAY SPECTRUM IN A VERY WIDE ENERGY RANGE

Guo, XL (Guo, Xiao-Lei); Xin, YL (Xin, Yu-Liang); Liao, NH (Liao, Neng-Hui); Yuan, Q (Yuan, Qiang); Gao, WH (Gao, Wei-Hong); He, HN (He, Hao-Ning); Fan, YZ (Fan, Yi-Zhong); Liu, SM (Liu, Si-Ming)
ASTROPHYSICAL JOURNAL
卷: 835 期: 1 文献号: 42
We report the detection of a GeV gamma-ray source that. spatially overlaps. and is. thus very likely associated with the unidentified very. high. energy (VHE) gamma-ray source HESS J1427-608 with the Pass 8 data recorded by the Fermi Large Area Telescope. The photon spectrum of this source is best described by a power law with an index of 1.85 +/- 0.17 in the energy range of 3-500 GeV, and the measured flux connects smoothly with that of HESS J1427 -608 at a few hundred gigaelectronvolts. This source shows no significant extension and time variation. The broadband GeV to TeV emission over four decades of energies can be well fitted by a single power-law function with an index of 2.0, without obvious indication of spectral cutoff toward high energies. Such a result implies that HESS J1427-608 may be a PeV particle accelerator. We discuss the possible nature of HESS J1427-608 according to the multiwavelength spectral fittings. Given the relatively large errors, either a leptonic or a hadronic model can explain the multiwavelength data from radio to VHE gamma-rays. The inferred magnetic field strength is a few micro-Gauss, which is smaller than the. typical values of supernova remnants (SNRs). and is consistent with some pulsar wind nebulae (PWNe). On the other hand, the flat gamma-ray spectrum is slightly different from typical PWNe but is. similar to that of some known SNRs.

第 71 条，共 286 条

On-orbit Status and Light Attenuation Behavior of the DAMPE-PSD

Li Yao; Zhang Yapeng; Zhang Yongjie; Sun Zhiyu; Yu Yuhong; Dong Tiekuang; Ma Pengxiong; Wang Yuanpeng; Yuan Qiang
Acta Astronomica Sinica
卷：58 期：6 页：54-1-54-9 文献号：0001-5245(2017)58:6<54:AWZLZT>2.0.TX;2-9
The DArk Matter Particle Explorer(DAMPE) is a high-resolution multi-purpose space-borne device for detecting the high-energy cosmic-rays like e, gamma-rays, protons, and heavy-ions, which was launched on 2015 December 17th. The Plastic Scintillator Detector(PSD) is the top-most sub-detector of DAMPE. The PSD is designed to measure the charge of incident high-energy particles, and to serve as a veto detector for discriminating gamma-rays from the charged particles. In this paper, the on-orbit status of the PSD after launching in terms of high voltage(HV) and temperature stabilities is presented. The temperature and the HV variations of the PSD are less than 1°C and 0.5%, respectively. By using the on-orbit data, the attenuation lengths of PSD bars are obtained according to an empirical formula. A preliminary charge spectrum reconstructed from the X-layer of the PSD is obtained.

第 72 条，共 286 条

A radiation transfer model for the Milky Way: I. Radiation fields and application to high-energy astrophysics

Popescu, CC (Popescu, C. C.); *Yang, R* (Yang, R.); Tuffs, RJ (Tuffs, R. J.); Natale, G (Natale, G.); Rushton, M (Rushton, M.); Aharonian, F (Aharonian, F.)
MONTHLY NOTICES OF THE ROYAL ASTRONOMICAL SOCIETY
卷: 470 期: 3 页: 2539-2558
We present a solution for the ultraviolet - submillimetre (submm) interstellar radiation fields (ISRFs) of the Milky Way (MW), derived from modelling COBE, IRAS and Planck maps of the all-sky emission in the near-, mid-, far-infrared and submm. The analysis uses the axisymmetric radiative transfer model that we have previously implemented to model the panchromatic spectral energy distributions (SEDs) of star-forming galaxies in the nearby universe, but with a new methodology allowing for optimization of the radial and vertical geometry of stellar emissivity and dust opacity, as deduced from the highly resolved emission seen from the vantage point of the Sun. As such, this is the first self-consistent model of the broad-band continuum emission from the MW. In this paper, we present model predictions for the spatially integrated SED of the MW as seen from the Sun, showing good agreement with the data, and give a detailed description of the solutions for the distribution of ISRFs, as well as their physical origin, throughout the volume of the galaxy. We explore how the spatial and spectral distributions of our

new predictions for the ISRF in the MW affects the amplitude and spectral distributions of the gamma rays produced via inverse Compton scattering for cosmic ray (CR) electrons situated at different positions in the galaxy, as well as the attenuation of the gamma rays due to interactions of the gamma-ray photons with photons of the ISRF. We also compare and contrast our solutions for the ISRF with those incorporated in the GALPROP package used for modelling the high-energy emission from CR in the MW.

第 73 条，共 286 条

Compact Resolved Ejecta in the Nearest Tidal Disruption Event

Perlman, ES (Perlman, Eric S.); Meyer, ET (Meyer, Eileen T.); Wang, QD (Wang, Q. Daniel); *Yuan, Q* (Yuan, Qiang); Henriksen, R (Henriksen, Richard); Irwin, J (Irwin, Judith); Krause, M (Krause, Marita); Wiegert, T (Wiegert, Theresa); Murphy, EJ (Murphy, Eric J.); Heald, G (Heald, George); Dettmar, RJ (Dettmar, Ralf-Juergen)
ASTROPHYSICAL JOURNAL
卷: 842 期: 2 文献号: 126
Tidal disruption events (TDEs) occur when a star or substellar object passes close enough to a galaxy's supermassive black hole to be disrupted by tidal forces. NGC 4845 (d - 17 Mpc) was host to a TDE, IGR J12580 vertical bar 0134, detected in 2010 November. Its proximity offers us a unique close-up of the TDE and its aftermath. We discuss new Very Long Baseline Array (VLBA) and Karl G. Jansky Very Large Array observations, which show that the radio flux from the active nucleus created by the TDE has decayed in a manner consistent with predictions from a jet-circumnuclear medium interaction model. This model explains the source's broadband spectral evolution, which shows a spectral peak that has moved from the submillimeter (at the end of 2010) to GHz radio frequencies (in 2011-2013) to < 1 GHz in 2015. The milliarcsecond-scale core is circularly polarized at 1.5 GHz but not at 5 GHz, consistent with the model. The VLBA images show a complex structure at 1.5 GHz that includes an east-west extension that is similar to 40 mas (3 pc) long, as well as a resolved component that is 52 mas (4.1 pc) northwest of the flat-spectrum core, which is all that can be seen at 5 GHz. If ejected in 2010, the northwest component must have had v = 0.96c over five years. However, this is unlikely, as our model suggests strong deceleration to speeds < 0.5c within months and a much smaller, sub-parsec size. In this interpretation, the northwest component could have either a non-nuclear origin or be from an earlier event.

第 74 条，共 286 条

3FGL J1924.8-1034: A spatially extended stable unidentified GeV source?

Xia, ZQ (Xia, Zi-Qing); Duan, KK (Duan, Kai-Kai); Li, S (Li, Shang); Liang, YF (Liang, Yun-Feng); Shen, ZQ (Shen, Zhao-Qiang); Yue, C (Yue, Chuan); Wang, YP (Wang, Yuan-Peng); Yuan, Q (Yuan, Qiang); Fan, YZ (Fan, Yi-Zhong); Wu, J (Wu, Jian); Chang, J (Chang, Jin)
PHYSICAL REVIEW D
卷: 95 期: 10 文献号: 102001
Milky Way-like galaxies are predicted to host a very large number of dark matter subhalos. Some massive and nearby subhalos could generate detectable gamma rays, appearing as unidentified, spatially extended and stable gamma-ray sources. We search for such sources in the third Fermi Large Area Telescope source list (3FGL) and report the identification of a new candidate, 3FGL J1924.8-1034. With the Fermi-LAT Pass 8 data, we find that 3FGL J1924.8-1034 is spatially extended at a high confidence level of 5.4 sigma, with a best-fit extension radius of similar to 0.15 degrees. No significant variability has been found and its gammaray spectrum is well fitted by the dark matter annihilation into b (b) over bar with a mass of similar to 43 GeV. All these facts make 3FGL J1924.8-1034 a possible dark matter subhalo candidate. However, due to the limited angular resolution, the possibility of that the spatial extension of 3FGL J1924.8-1034 is caused by the contamination from the other unresolved point source cannot be ruled out.

第 75 条，共 286 条

Quality control of mass production of PMT modules for DAMPE

Dong, JN (Dong, J. N.); Zhang, YL (Zhang, Y. L.); Zhang, ZY (Zhang, Z. Y.); Wei, YF (Wei, Y. F.); Wu, LB (Wu, L. B.); Wang, C (Wang, C.); Shen, ZT (Shen, Z. T.); Feng, CQ (Feng, C. Q.); Gao, SS (Gao, S. S.); Gan, FJ (Gan, F. J.); Wen, SC (Wen, S. C.); Hu, YM (Hu, Y. M.); Chen, DY (Chen, D. Y.); Gong, YZ (Gong, Y. Z.); Huang, HS (Huang, H. S.); Wang, XL (Wang, X. L.); Xu, ZZ (Xu, Z. Z.); Liu, SB (Liu, S. B.); An, Q (An, Q.)
JOURNAL OF INSTRUMENTATION
卷: 12 文献号: T05004
Photomultiplier tube (PMT) modules were selected to read out the signals in the BGO electromagnetic calorimeter for the Dark Matter Particle Explorer satellite. The test procedure and the related quality control of mass production PMT modules are described, with a summary of PMT module quality and the results from tests. With strict quality control throughout the production and test process, over 88% of the PMT modules meet the criteria required by DAMPE.

第 76 条，共 286 条

Propagation of cosmic rays in the AMS-02 era

Yuan, Q (Yuan, Qiang); Lin, SJ (Lin, Su-Jie); Fang, K (Fang, Kun); Bi, XJ (Bi, Xiao-Jun)
PHYSICAL REVIEW D
卷: 95 期: 8 文献号: 083007
In this work we use the newly reported boron-to-carbon ratio (B/C) from AMS-02 and the time-dependent proton fluxes from PAMELA and AMS-02 to constrain the source and propagation parameters of cosmic rays in the Milky Way. A linear correlation of the solar modulation parameter with solar activities is assumed to account for the time-varying cosmic ray fluxes. A comprehensive set of propagation models, with or without reacceleration or convection, has been discussed and compared. We find that only the models with reacceleration can self-consistently fit both the proton and B/C data. The rigidity dependence slope of the diffusion coefficient, delta, is found to be about 0.38-0.50 for the diffusion-reacceleration models. The plain diffusion and diffusion-convection models fit the data poorly. We compare different model predictions of the positron and antiprotonfluxes with the data. We find that the diffusion-reacceleration models overproduce low energy positrons, while nonreacceleration models give better fit to the data. As for antiprotons, reacceleration models tend to underpredict low energy antiproton fluxes, unless a phenomenological modification of the velocity dependence of the diffusion coefficient is applied. Our results suggest that there could be important differences of the propagation for nuclei and leptons, in either the Milky Way or the solar heliosphere.

第 77 条，共 286 条

Calibrating a physical model based on Geant4 to calculate cosmogenic nuclide production rates on lunar surface

Chen, J (Chen, Jian); Dong, TK (Dong, Tiekuang); Ren, ZZ (Ren, Zhongzhou)

METEORITICS & PLANETARY SCIENCE
卷: 52 期: 4 页: 646-655
A physical model based on the open-source toolkit Geant4 for production rates of cosmogenic nuclei on the lunar surface is proposed and calibrated. The fluxes of proton and neutron beneath the lunar surface are obtained by simulating the physical processes between the cosmic-ray particles and the lunar surface material. By combining the experimental proton cross sections and the a posteriori neutron cross sections, we calculate the production rate depth profiles of long-lived nuclei (Be-10, C-14, Al-26, Cl-36, and Mn-53). Through comparing experimental and theoretical data for these nuclei, we find that for all the selected nuclei, experimental and theoretical production rate depth profiles agree well with each other by introducing a single normalization factor. It means that the physical model based on Geant4 can also reproduce the depth profiles of cosmogenic nuclei, and that this model can be used by everyone worldwide. In addition, we predict the production rates of three stable nuclei (Ne-21, Ne-22, and Ar-38).

第 78 条，共 286 条

AMS-02 positron excess and indirect detection of three-body decaying dark matter

Cheng, HC (Cheng, Hsin-Chia); Huang, WC (Huang, Wei-Chih); Huang, XY (Huang, Xiaoyuan); Low, I (Low, Ian); Tsai, YLS (Tsai, Yue-Lin Sming); Yuan, Q (Yuan, Qiang)
JOURNAL OF COSMOLOGY AND ASTROPARTICLE PHYSICS
期: 3 文献号: 041
We consider indirect detection of meta-stable dark matter particles decaying into a stable neutral particle and a pair of standard model fermions. Due to the softer energy spectra from the three-body decay, such models could potentially explain the AMS-02 positron excess without being constrained by the Fermi-LAT gamma-ray data and the cosmic ray anti-proton measurements. We scrutinize over different final state fermions, paying special attention to handling of the cosmic ray background and including various contributions from cosmic ray propagation with the help of the Like DM package. It is found that primary decays into an electron-positron pair and a stable neutral particle could give rise to the AMS-02 positron excess and, at the same time, stay unscathed against the gamma-ray and antiproton constraints. Decays to a muon pair or a mixed flavor electron-muon pair may also be viable depending on the propagation models. Decays to all other standard model fermions are severely disfavored.

第 79 条，共 286 条

Thermal Design and Validation of DAMPE BGO Calorimeter

Hu Yiming; Chang Jin; Chen Dengyi; Liu Shubin; Feng Changqing; Zhang Yunlong
Chinese Journal of Space Science
卷：37 期：1 页：114-121 文献号：0254-6124(2017)37:1<114:YWZLZT>2.0.TX;2-#
Dark Matter Particle Explorer (DAMPE) is one of the first scientific exploration satellites of China, aiming to search dark matter by measuring the spectrum of electron/positron and gamma ray. DAMPE mainly consists of four sub-detectors including Plastic Scintillator Detector (PSD), Silicon Tungsten Tracker (STK), BGO Calorimeter (BGO) and Neutron Detector (NUD). As the most important sub-detector of DAMPE, BGO calorimeter plays a key role in precisely measuring energy of the incident cosmic ray and identifying particles. In this paper, thermal design of the calorimeter is introduced. Based on this design, the Finite Element Analysis (FEA) on temperature field of the BGO calorimeter is performed with the given on-orbit conditions. In the end, Thermal Vacuum (TV) test has been carried out in March, 2015 to prove the FEA is correct and the methodology in this paper is effective.

第 80 条，共 286 条

Synthesis of ZnO nanoporous structure materials by two-step thermal oxidation of Zn film

Xu, Q (Xu, Qiang); Hong, RD (Hong, Rongdun); Chen, XP (Chen, Xiaping); Wei, JJ (Wei, Jiaju); Wu, ZY (Wu, Zhengyun)
CERAMICS INTERNATIONAL
卷: 43 期: 18 页: 16391-16394
We describe the synthesis of ZnO nanostructures materials on quartz substrates by a simple two-step thermal oxidation process. Firstly, a thin layer of metallic Zn films are oxidized in nitrogen atmosphere at 350 degrees C, and then the samples annealed at high temperature (from 600 to 800 degrees C) to improve the crystal quality. The properties of the materials are characterized with X-ray diffraction (XRD), scanning electron microscopy (SEM), Raman spectroscopy and UV-Visible spectroscopy at room temperature. The results show that nano porous structure materials have been formed after the samples annealed at high temperature. Since the small grain size and grain boundary induced effect of conduction band bending, the optical band gap shifts to low energy.

第 81 条，共 286 条

CALIFA reveals prolate rotation in massive early-type galaxies: A polar galaxy merger origin?

Tsatsi, A (Tsatsi, A.); Lyubenova, M (Lyubenova, M.); de Ven, GV (de Ven, G. van); *Chang, J* (Chang, J.); Aguerri, JAL (Aguerri, J. A. L.); Falcon-Barroso, J (Falcon-Barroso, J.); Maccio, AV (Maccio, A. V.)
ASTRONOMY & ASTROPHYSICS
卷: 606 文献号: A62
We present new evidence for eight early-type galaxies (ETGs) from the CALIFA Survey that show clear rotation around their major photometric axis ("prolate rotation"). These are LSBCF560-04, NGC 0647, NGC 0810, NGC 2484, NGC 4874, NGC 5216, NGC 6173, and NGC 6338. Including NGC 5485, a known case of an ETG with stellar prolate rotation, as well as UGC 10695, a further candidate for prolate rotation, we report ten CALIFA galaxies in total that show evidence for such a feature in their stellar kinematics. Prolate rotators correspond to similar to 9% of the volume-corrected sample of CALIFA ETGs, a fraction much higher than previously reported. We find that prolate rotation is more common (similar to 27%) among the most massive ETGs (M* greater than or similar to 2x 10(11) M circle dot). We investigated the implications of these findings by studying N-body merger simulations, and we show that a prolate ETG with rotation around its major axis could be the result of a major polar merger, with the amplitude of prolate rotation depending on the initial bulgeto-total stellar mass ratio of its progenitor galaxies. Additionally, we find that prolate ETGs resulting from this formation scenario show a correlation between their stellar line-of-sight velocity and higher order moment h(3), opposite to typical oblate ETGs, as well as a double peak of their stellar velocity dispersion along their minor axis. Finally, we investigated the origin of prolate rotation in polar galaxy merger remnants. Our findings suggest that prolate rotation in massive ETGs might be more common than previously expected, and can help toward a better understanding of their dynamical structure and formation origin.

第 82 条，共 286 条

The DArk Matter Particle Explorer mission

Chang, J (Chang, J.); Ambrosi, G (Ambrosi, G.); An, Q (An, Q.);

Asfandiyarov, R (Asfandiyarov, R.); Azzarello, P (Azzarello, P.); Bernardini, P (Bernardini, P.); Bertucci, B (Bertucci, B.); Cai, MS (Cai, M. S.); Caragiulo, M (Caragiulo, M.); Chen, DY (Chen, D. Y.); Chen, HF (Chen, H. F.); Chen, JL (Chen, J. L.); Chen, W (Chen, W.); Cui, MY (Cui, M. Y.); Cui, TS (Cui, T. S.); D'Amone, A (D'Amone, A.); De Benedittis, A (De Benedittis, A.); De Mitri, I (De Mitri, I.); Di Santo, M (Di Santo, M.); Dong, JN (Dong, J. N.); Dong, TK (Dong, T. K.); Dong, YF (Dong, Y. F.); Dong, ZX (Dong, Z. X.); Donvito, G (Donvito, G.); Droz, D (Droz, D.); Duan, KK (Duan, K. K.); Duan, JL (Duan, J. L.); Duranti, M (Duranti, M.); D'Urso, D (D'Urso, D.); Fan, RR (Fan, R. R.); Fan, YZ (Fan, Y. Z.); Fang, F (Fang, F.); Feng, CQ (Feng, C. Q.); Feng, L (Feng, L.); Fusco, P (Fusco, P.); Gallo, V (Gallo, V.); Gan, FJ (Gan, F. J.); Gan, WQ (Gan, W. Q.); Gao, M (Gao, M.); Gao, SS (Gao, S. S.); Gargano, F (Gargano, F.); Gong, K (Gong, K.); Gong, YZ (Gong, Y. Z.); Guo, JH (Guo, J. H.); Hu, YM (Hu, Y. M.); Huang, GS (Huang, G. S.); Huang, YY (Huang, Y. Y.); Ionica, M (Ionica, M.); Jiang, D (Jiang, D.); Jiang, W (Jiang, W.); Jin, X (Jin, X.); Kong, J (Kong, J.); Lei, SJ (Lei, S. J.); Li, S (Li, S.); Li, X (Li, X.); Li, WL (Li, W. L.); Li, Y (Li, Y.); Liang, YF (Liang, Y. F.); Liang, YM (Liang, Y. M.); Liao, NH (Liao, N. H.); Liu, QZ (Liu, Q. Z.); Liu, H (Liu, H.); Liu, J (Liu, J.); Liu, SB (Liu, S. B.); Liu, QZ (Liu, Q. Z.); Liu, WQ (Liu, W. Q.); Liu, Y (Liu, Y.); Loparco, F (Loparco, F.); Lu, J (Lu, J.); Ma, M (Ma, M.); Ma, PX (Ma, P. X.); Ma, SY (Ma, S. Y.); Ma, T (Ma, T.); Ma, XQ (Ma, X. Q.); Ma, XY (Ma, X. Y.); Marsella, G (Marsella, G.); Mazziotta, MN (Mazziotta, M. N.); Mo, D (Mo, D.); Miao, TT (Miao, T. T.); Niu, XY (Niu, X. Y.); Pohl, M (Pohl, M.); Peng, XY (Peng, X. Y.); Peng, WX (Peng, W. X.); Qiao, R (Qiao, R.); Rao, JN (Rao, J. N.); Salinas, MM (Salinas, M. M.); Shang, GZ (Shang, G. Z.); Shen, WH (Shen, W. H.); Shen, ZQ (Shen, Z. Q.); Shen, ZT (Shen, Z. T.); Song, JX (Song, J. X.); Su, H (Su, H.); Su, M (Su, M.); Sun, ZY (Sun, Z. Y.); Surdo, A (Surdo, A.); Teng, XJ (Teng, X. J.); Tian, XB (Tian, X. B.); Tykhonov, A (Tykhonov, A.); Vagelli, V (Vagelli, V.); Vitillo, S (Vitillo, S.); Wang, C (Wang, C.); Wang, C (Wang, Chi); Wang, H (Wang, H.); Wang, HY (Wang, H. Y.); Wang, JZ (Wang, J. Z.); Wang, LG (Wang, L. G.); Wang, Q (Wang, Q.); Wang, S (Wang, S.); Wang, XH (Wang, X. H.); Wang, XL (Wang, X. L.); Wang, YF (Wang, Y. F.); Wang, YP (Wang, Y. P.); Wang, YZ (Wang, Y. Z.); Wen, SC (Wen, S. C.); Wang, ZM (Wang, Z. M.); Wei, DM (Wei, D. M.); Wei, JJ (Wei, J. J.); Wei, YF (Wei, Y. F.); Wu, D (Wu, D.); Wu, J (Wu, J.); Wu, SS (Wu, S. S.); Wu, X (Wu, X.); Xi, K (Xi, K.); Xia, ZQ (Xia, Z. Q.); Xin, YL (Xin, Y. L.); Xu, HT (Xu, H. T.); Xu, ZL (Xu, Z. L.); Xu, ZZ (Xu, Z. Z.); Xue, GF (Xue, G. F.); Yang, HB (Yang, H. B.); Yang, J (Yang, J.); Yang, P (Yang, P.); Yang, YQ (Yang, Y. Q.); Yang, ZL (Yang, Z. L.); Yao, HJ (Yao, H. J.); Yu, YH (Yu, Y. H.); Yuan, Q (Yuan, Q.); Yue, C (Yue, C.); Zang, JJ (Zang, J. J.); Zhang, C (Zhang, C.); Zhang, DL (Zhang, D. L.); Zhang, F (Zhang, F.); Zhang, JB (Zhang, J. B.); Zhang, JY (Zhang, J. Y.); Zhang, JZ (Zhang, J. Z.); Zhang, L (Zhang, L.); Zhang, PF (Zhang, P. F.); Zhang, SX (Zhang, S. X.); Zhang, WZ (Zhang, W. Z.); Zhang, Y (Zhang, Y.); Zhang, YJ (Zhang, Y. J.); Zhang, YQ (Zhang, Y. Q.); Zhang, YL (Zhang, Y. L.); Zhang, YP (Zhang, Y. P.); Zhang, Z (Zhang, Z.); Zhang, ZY (Zhang, Z. Y.); Zhao, H (Zhao, H.); Zhao, HY (Zhao, H. Y.); Zhao, XF (Zhao, X. F.); Zhou, CY (Zhou, C. Y.); Zhou, Y (Zhou, Y.); Zhu, X (Zhu, X.); Zhu, Y (Zhu, Y.); Zimmer, S (Zimmer, S.)

ASTROPARTICLE PHYSICS
卷: 95 页: 6-24

The DArk Matter Particle Explorer (DAMPE), one of the four scientific space science missions within the framework of the Strategic Pioneer Program on Space Science of the Chinese Academy of Sciences, is a general purpose high energy cosmic-ray and gamma-ray observatory, which was successfully launched on December 17th, 2015 from the Jiuquan Satellite Launch Center. The DAMPE scientific objectives include the study of galactic cosmic rays up to similar to 10 TeV and hundreds of TeV for electrons/gammas and nuclei respectively, and the search for dark matter signatures in their spectra. In this paper we illustrate the layout of the DAMPE instrument, and discuss the results of beam tests and calibrations performed on ground. Finally we present the expected performance in space and give an overview of the mission key scientific goals. (C) 2017 Elsevier B.V. All rights reserved.

第 83 条，共 286 条

Offline software for the DAMPE experiment

Wang, C (Wang, Chi); Liu, D (Liu, Dong); Wei, YF (Wei, Yifeng); Zhang, ZY (Zhang, Zhiyong); Zhang, YL (Zhang, Yunlong); Wang, XL (Wang, Xiaolian); Xu, ZZ (Xu, Zizong); Huang, GS (Huang, Guangshun); Tykhonov, A (Tykhonov, Andrii); Wu, X (Wu, Xin); Zang, JJ (Zang, Jingjing); Liu, Y (Liu, Yang); Jiang, W (Jiang, Wei); Wen, SC (Wen, Sicheng); Wu, J (Wu, Jian); Chang, J (Chang, Jin)

CHINESE PHYSICS C
卷: 41 期: 10 文献号: 106201

A software system has been developed for the DArk Matter Particle Explorer (DAMPE) mission, a satellite-based experiment. The DAMPE software is mainly written in C++ and steered using a Python script. This article presents an overview of the DAMPE offline software, including the major architecture design and specific implementation for simulation, calibration and reconstruction. The whole system has been successfully applied to DAMPE data analysis. Some results obtained using the system, from simulation and beam test experiments, are presented.

第 84 条，共 286 条

Temperature effects on MIPs in the BGO calorimeters of DAMPE

Wang, YP (Wang, Yuan-Peng); Wen, SC (Wen, Si-Cheng); Jiang, W (Jiang, Wei); Yue, C (Yue, Chuan); Zhang, ZY (Zhang, Zhi-Yong); Wei, YF (Wei, Yi-Feng); Zhang, YL (Zhang, YunLong); Zang, JJ (Zang, Jing-Jing); Wu, J (Wu, Jian)

CHINESE PHYSICS C
卷: 41 期: 10 文献号: 106001

In this paper, we present a study of temperature effects on BGO calorimeters using proton MIPs collected in the first year of operation of DAMPE. By directly comparing MIP calibration constants used by the DAMPE data production pipe line, we find an experimental relation between the temperature and signal amplitudes of each BGO bar: a general deviation of -1.162%/degrees C, and -0.47%/degrees C to -1.60%/degrees C statistically for each detector element. During 2016, DAMPE's temperature changed by similar to 8 degrees C due to solar elevation angle, and the corresponding energy scale bias is about 9%. By frequent MIP calibration operation, this kind of bias is eliminated to an acceptable value.

第 85 条，共 286 条

Validation of the Ability of Full Configuration Interaction Quantum Monte Carlo for Studying the 2D Hubbard Model

Yun, SJ (Yun, Su-Jun); Dong, TK (Dong, Tie-Kuang); Zhu, SN (Zhu, Shi-Ning)

CHINESE PHYSICS LETTERS
卷: 34 期: 8 文献号: 080201

To validate the ability of full configuration interaction quantum Monte Carlo (FCIQMC) for studying the 2D Hubbard model near half-filling regime, the ground state energies of a 4 x 4 square lattice system with various interaction strengths are calculated. It is found that the calculated results are in good agreement with those obtained by exact diagonalization (i.e., the exact values for a given basis set) when the population of psi particles (psips) is higher than the critical population required to correctly sample the ground state wave function.

In addition, the variations of the average computational time per 20 Monte Carlo cycles with the coupling strength and the number of processors are also analyzed. The calculated results show that the computational efficiency of an FCIQMC calculation is mainly affected by the total population of psips and the communication between processors. These results can provide useful references for understanding the FCIQMC algorithm, studying the ground state properties of the 2D Hubbard model for the larger system size by the FCIQMC method and using a computational budget as effectively as possible.

第 86 条，共 286 条

Statistical study of co-rotating interaction region properties with STEREO and ACE observations

Yu Huang Qi-Wu Song Dong Li
Research in Astronomy and Astrophysics
卷: 31 期: 8
We analyzed the data on co-rotating interaction regions(CIRs) measured by the Advanced Composition Explorer(ACE) and Solar TErrestrial RElations Observatory(STEREO) from 2007 to2010. The CIRs were observed by STEREO B(STB), ACE and STEREO A(STA) one after another, and a total of 28 CIRs were identified in this work. Since the same characteristics of CIRs were detected by these three spacecraft at three different locations and times, these data can help us to study the evolutions of CIRs. For a single event, the properties of CIRs observed by the three spacecraft were quite different and could be explained by spatial or temporal variations. For all these 28 CIRs,STA and STB observed similar mean parameters, such as peak magnetic field strength(offset 11%), peak and change in solar wind speed(offset 3% and 10% respectively), peak proton temperature(offset 14%) and peak perpendicular pressure(offset 15%). Surprisingly, STA detected much higher(41%) peak density of protons than STB.

1-07 UV/X-ray Astronomy Research Group

第 87 条，共 286 条

A timing view of the heartbeat state of GRS 1915+105

Yan, SP (Yan, Shu-Ping); *Ji, L* (Ji, Li); Mendez, M (Mendez, Mariano); Liu, SM (Liu, Si-Ming); Wang, N (Wang, Na); Li, XD (Li, Xiang-Dong); Ge, MY (Ge, Ming-Yu); Liao, JY (Liao, Jin-Yuan); Niu, S (Niu, Shu); Qu, JL (Qu, Jin-Lu); Ding, GQ (Ding, Guo-Qiang); Liu, QZ (Liu, Qing-Zhong); Sun, W (Sun, Wei)
MONTHLY NOTICES OF THE ROYAL ASTRONOMICAL SOCIETY
卷: 465 期: 2 页: 1926-1933
We present a timing analysis of two Rossi X-ray Timing Explorer observations of the micro-quasar GRS 1915+ 105 during the heartbeat state. The phase-frequency-power maps show that the intermediate-frequency aperiodic X-ray variability weakens as the source softens in the slow rise phase, and when the quasi-periodic oscillation disappears in the rise phase of the pulse of the double-peaked class, its sub-harmonic is still present with a hard phase lag. In the slow rise phase, the energy-frequency-power maps show that most of the aperiodic variability is produced in the corona, and may also induce the aperiodic variability observed at low energies from an accretion disc, which is further supported by the soft phase lag especially in the intermediate-frequency range (with a time delay up to 20 ms). In the rise phase of the pulse, the low-frequency aperiodic variability is enhanced significantly and there is a prominent hard lag (with a time delay up to 50 ms), indicating that the variability is induced by extension of the disc towards small radii as implied by the increase in flux and propagates into the corona. However, during the hard pulse of the double-peaked class, the variability shows no significant lag, which may be attributed to an optically thick corona. These timing results are generally consistent with the spectral results presented by Neilsen, Remillard & Lee which indicated that the slow rise phase corresponds to a local Eddington limit and the rise phase of the pulse corresponds to a radiation pressure instability in the disc.

第 88 条，共 286 条

Joint fit of Warm Absorbers in COS and HETG spectra of NGC 3783

Fu, XD (Fu, Xiao-Dan); Zhang, SN (Zhang, Shui-Nai); Sun, W (Sun, Wei); Niu, S (Niu, Shu); Ji, L (Ji, Li)
RESEARCH IN ASTRONOMY AND ASTROPHYSICS
卷: 17 期: 9
Warm Absorbers (WAs), as an important form of AGN outflows, show absorption in both the UV and X-ray bands. Using XSTAR generated photoionization models, for the first time we present a joint fit to the simultaneous observations of HST/COS and Chandra/HETG on NGC 3783. A total of five WAs explain well all absorption features from the AGN outflows, which are spread over a wide range of parameters: ionization parameter log xi from 0.6 to 3.8, column density log N-H from 19.5 to 22.3 cm(-2), velocity v from 380 to 1060 km s(-1), and covering factor from 0.33 to 0.75. Not all the five WAs are consistent in pressure. Two of them are likely different parts of the same absorbing gas, and two of the other WAs may be smaller discrete clouds that are blown out from the inner region of the torus at different periods. The five WAs suggest a total mass outflowing rate within the range of 0.22-4.1 solar mass per year.

第 89 条，共 286 条

Current Investigations on Young Star Cluster NGC 3603 in X-ray

Wang Qian; Sun Wei; Ji Li
Progress in Astronomy
卷 : 35 期 : 1 页 : 1-15 文 献 号 : 1000-8349(2017)35:1<1:YHXNQX>2.0.TX;2-C
NGC 3603 is a dense young cluster located in the Carina spiral arm of the Milky Way. The mechanical energy released by the winds from massive stars alters the property of the ambient medium, and has very important influences on the star formation and the galaxy evolution process. The X-ray emission in massive star formation region is produced by the pre-main sequence star, OB star, and diffuse hot gas etc. In this paper, we reviewed the X-ray radiation mechanisms of those three kinds of sources and presented the X-ray radiation of point sources and diffuse hot gas in NGC 3603, respectively. For the point sources, Moffat et al.(2002)detected the X-rays from 43 early-type sources, and found that they follow the canonical relationship between the X-ray luminosity and the bolometric luminosity: L_X/L_(bol) ~ 10~(-7). They also found that MTT 68 and MTT 71, two O stars far away from the core region, have enhanced X-ray emission: L_X/L_(bol) ~ 10-5. For the diffuse emission, Townsley et al.(2011)found that the diffuse plasma in NGC 3603 is in nonequilibrium state. Ji et al.(2006)fitted the diffuse X-rays in the central annulus region with the 1-D self-consistent non-equilibrium ionization cluster wind model, and determined related stellar wind parameters. Besides that, they both found that the X-rays from un-resolved

pre-main sequence stars contribute ~ 10% in total X-ray luminosity. The prospect of X-ray research on NGC 3603 based on the archival 0.5 Ms Chandra observation is also discussed in the end.

II. Antarctic Astronomy Radio Astronomy

2-01 Stellar Structure, Evolution and Pulsation

第 90 条，共 286 条

On the effect of turbulent anisotropy on pulsation stability of stars

Zhang, CG (Zhang, Chun-Guang); Deng, LC (Deng, Li-Cai); Xiong, DR (Xiong, Da-Run)
RESEARCH IN ASTRONOMY AND ASTROPHYSICS
卷: 17 期: 3
Within the framework of a non- local time- dependent stellar convection theory, we study in detail the effect of turbulent anisotropy on stellar pulsation stability. The results show that anisotropy has no substantial influence on pulsation stability of g modes and low- order (radial order n(r) < 5) p modes. The effect of turbulent anisotropy increases as the radial order increases. When turbulent anisotropy is neglected, most high- order (n(r) > 5) p modes of all low-temperature stars become unstable. Fortunately, within a wide range of the anisotropic parameter c(3), stellar pulsation stability is not sensitive to the specific value of c(3.) Therefore it is safe to say that calibration errors of the convective parameter c (3) do not cause any uncertainty in the calculation of stellar pulsation stability.

第 91 条，共 286 条

Turbulent Convection and Pulsation Stability of Stars

Xiong Darun
Acta Astronomica Sinica
卷：58 期：2 页：10-1-10-17 文献号：0001-5245(2017)58:2<10:TDDLYB>2.0.TX;2-4
The controversies about the excitation mechanism for cool variables are reviewed: (1) Most people believe that gamma Doradus stars are excited by so called convective blocking. Our researches show that the excitation of gamma Doradus has no difference from that of delta Scuti. They are two subgroups of a broader type of delta Stuti-gamma Doradus stars: delta Scuti is the p-mode subgroup, while gamma Doradus is the g-mode subgroup. (2) Most people believe that the Solar- and Solar-like oscillations of stars are damped by convection, and they are excited by so called stochastic effects of turbulence. Our researches show that convection is not solely a damping mechanism for stellar oscillations, otherwise it is not able to explain the excitation of Mira and Mira-like stars. It can be repeated not only the delta Scuti and gamma Doradus strip, but also the characteristics of Solar-like and Mira-like oscillations, respectively, for the low- and high- luminosity red stars by using our non-local and time-dependent theory of convection.

2-02 Center for Antarctic Astronomy

第 92 条，共 286 条

INTERSTELLAR-MEDIUM MAPPING IN M82 THROUGH LIGHT ECHOES AROUND SUPERNOVA 2014

J Yang, Y (Yang, Yi); *Wang, LF* (Wang, Lifan); Baade, D (Baade, Dietrich); Brown, PJ (Brown, Peter. J.); Cracraft, M (Cracraft, Misty); Hoflich, PA (Hoflich, Peter A.); Maund, J (Maund, Justyn); Patat, F (Patat, Ferdinando); Sparks, WB (Sparks, William B.); Spyromilio, J (Spyromilio, Jason); Stevance, HF (Stevance, Heloise F.); Wang, XF (Wang, Xiaofeng); Wheeler, JC (Wheeler, J. Craig)
ASTROPHYSICAL JOURNAL
卷: 834 期: 1 文献号: 60
We present multiple-epoch measurements of the size and surface brightness of the light echoes from supernova (SN) 2014J in the nearby starburst galaxy M82. Hubble Space Telescope (HST) ACS/WFC images were taken similar to 277 and similar to 416 days after B-band maximum in the filters F475W, F606W, and F775W. Observations with HST WFC3/UVIS images at epochs similar to 216 and similar to 365 days are included for a more complete analysis. The images reveal the temporal evolution of at least two major light-echo components. The first one exhibits a filled ring structure with position-angle-dependent intensity. This radially extended, diffuse echo indicates the presence of an inhomogeneous interstellar dust cloud ranging from similar to 100 to similar to 500 pc in the foreground of the SN. The second echo component appears as an unresolved luminous quarter-circle arc centered on the SN. The wavelength dependence of scattering measured in different dust components suggests that the dust producing the luminous arc favors smaller grain sizes, while that causing the diffuse light echo may have sizes similar to those of the Milky Way dust. Smaller grains can produce an optical depth consistent with that along the supernova-Earth line of sight measured by previous studies around maximum light. Therefore, it is possible that the dust slab from which the luminous arc arises is also responsible for most of the extinction toward SN. 2014J. The optical depths determined from the Milky Way-like dust in the scattering matters are lower than the optical depth produced by the dust slab.

第 93 条，共 286 条

Optical Sky Brightness and Transparency during the Winter Season at Dome A Antarctica from the Gattini-All-Sky Camera

Yang, Y (Yang, Yi); Moore, AM (Moore, Anna M.); Krisciunas,

K (Krisciunas, Kevin); Wang, LF (Wang, Lifan); Ashley, MCB (Ashley, Michael C. B.); Fu, JN (Fu, Jianning); Brown, PJ (Brown, Peter J.); Cui, XQ (Cui, Xiangqun); Feng, LL (Feng, Long-Long); Gong, XF (Gong, Xuefei); Hu, ZW (Hu, Zhongwen); Lawrence, JS (Lawrence, Jon S.); Luong-Van, D (Luong-Van, Daniel); Riddle, RL (Riddle, Reed L.); Shang, ZH (Shang, Zhaohui); Sims, G (Sims, Geoff); Storey, JWV (Storey, John W. V.); Suntzeff, NB (Suntzeff, Nicholas B.); Tothill, N (Tothill, Nick); Travouillon, T (Travouillon, Tony); Yang, HG (Yang, Huigen); Yang, J (Yang, Ji); Zhou, X (Zhou, Xu); Zhu, ZX (Zhu, Zhenxi)
ASTRONOMICAL JOURNAL
卷: 154 期: 1 文献号: 6
The summit of the Antarctic plateau, Dome A, is proving to be an excellent site for optical, near-infrared, and terahertz astronomical observations. Gattini is a wide-field camera installed on the PLATO instrument module as part of the Chinese-led traverse to Dome A in 2009 January. We present here the measurements of sky brightness with the Gattini ultra-large field of view (90 degrees X 90 degrees) in the photometric B-, V-, and R-bands; cloud cover statistics measured during the 2009 winter season; and an estimate of the sky transparency. A cumulative probability distribution indicates that the darkest 10% of the nights at Dome A have sky brightness of S-B = 22.98, S-V = 21.86, and S-R = 21.68 mag arcsec(-2). These values were obtained during the year 2009 with minimum aurora, and they are comparable to the faintest sky brightness at Maunakea and the best sites of northern Chile. Since every filter includes strong auroral lines that effectively contaminate the sky brightness measurements, for instruments working around the auroral lines, either with custom filters or with high spectral resolution instruments, these values could be easily obtained on a more routine basis. In addition, we present example light curves for bright targets to emphasize the unprecedented observational window function available from this ground-based site. These light curves will be published in a future paper.

第 94 条，共 286 条

IC 630: Piercing the Veil of the Nuclear Gas

Durre, M (Durre, Mark); Mould, J (Mould, Jeremy); Schartmann, M (Schartmann, Marc); Uddin, SA (Uddin, Syed Ashraf); Cotter, G (Cotter, Garrett)
ASTROPHYSICAL JOURNAL
卷: 838 期: 2 文献号: 102
IC 630 is a nearby early-type galaxy with a mass of 6 x 10(10) M-circle dot with an intense burst of recent (6Myr) star formation (SF). It shows strong nebular emission lines, with radio and X-ray emission, which classifies it as an active galactic nucleus (AGN). With VLT-SINFONI and Gemini North-NIFS adaptive optics observations (plus supplementary ANU 2.3m WiFeS optical IFU observations), the excitation diagnostics of the nebular emission species show no sign of standard AGN engine excitation; the stellar velocity dispersion also indicates that a supermassive black hole (if one is present) is small (M. = 2.25 x 10(5)M(circle dot)). The luminosity at all wavelengths is consistent with SF at a rate of about 1-2M(circle dot) yr(-1). We measure gas outflows driven by SF at a rate of 0.18M(circle dot) yr(-1) in a face-on truncated cone geometry. We also observe a nuclear cluster or disk and other clusters. Photoionization from young, hot stars is the main excitation mechanism for [Fe II] and hydrogen, whereas shocks are responsible for the H-2 excitation. Our observations are broadly comparable with simulations where a Toomre-unstable, self-gravitating gas disk triggers a burst of SF, peaking after about 30 Myr and possibly cycling with a period of about 200 Myr.

第 95 条，共 286 条

Evolution of Mass and Velocity Field in the Cosmic Web: Comparison Between Baryonic and Dark Matter

Zhu, WS (Zhu, Weishan); Feng, LL (Feng, Long-Long)
ASTROPHYSICAL JOURNAL
卷: 838 期: 1 文献号: 21
We investigate the evolution of the cosmic web since z. =. 5 in grid-based cosmological hydrodynamical simulations, focusing on the mass and velocity fields of both baryonic and cold dark matter. The tidal tensor of density is used as the main method for web identification, with lambda(th). =. 0.2-1.2. The evolution trends in baryonic and dark matter are similar, although moderate differences are observed. Sheets appear early, and their large-scale pattern may have been set up by z. =. 3. In terms of mass, filaments supersede sheets as the primary collapsing structures from z. similar to 2-3. Tenuous filaments assembled with each other to form prominent ones at z. <.. 2. In accordance with the construction of the frame of the sheets, the cosmic divergence velocity, vdiv, was already welldeveloped above 2-3 Mpc by z. =. 3. Afterwards, the curl velocity, vcurl, grew dramatically along with the rising of filaments, becoming comparable to vdiv, for < 2-3 Mpc at z. =. 0. The scaling of vcurl can be described by the hierarchical turbulence model. The alignment between the vorticity and the eigenvectors of the shear tensor in the baryonic matter field resembles that in the dark matter field, and is even moderately stronger between w and e1, and. and e3. Compared with dark matter, there is slightly less baryonic matter found residing in filaments and clusters, and its vorticity developed more significantly below 2-3 Mpc. These differences may be underestimated because of the limited resolution and lack of star formation in our simulation. The impact of the change of dominant structures in overdense regions at z. similar to 2-3 on galaxy formation and evolution is shortly discussed.

第 96 条，共 286 条

Superluminous Supernovae at High Redshift

Abbott, T (Abbott, Tim); Cooke, J (Cooke, Jeff); Curtin, C (Curtin, Chris); Joudaki, S (Joudaki, Shahab); Katsianis, A (Katsianis, Antonios); Koekemoer, A (Koekemoer, Anton); Mould, J (Mould, Jeremy); Tescari, E (Tescari, Edoardo); Uddin, S (Uddin, Syed); *Wang, LF* (Wang, Lifan)
PUBLICATIONS OF THE ASTRONOMICAL SOCIETY OF AUSTRALIA
卷: 34 文献号: e012
Superluminous supernovae are beginning to be discovered at redshifts as early as the epoch of reionisation. A number of candidate mechanisms is reviewed, together with the discovery programmes.

第 97 条，共 286 条

Variable Stars Observed in the Galactic Disk by AST3-1 from Dome A, Antarctica

Wang, LZ (Wang, Lingzhi); Ma, B (Ma, Bin); Li, G (Li, Gang); Hu, Y (Hu, Yi); Fu, JN (Fu, Jianning); *Wang, LF* (Wang, Lifan); Ashley, MCB (Ashley, Michael C. B.); Cui, XQ (Cui, Xiangqun); Du, FJ (Du, Fujia); Gong, XF (Gong, Xuefei); Li, XY (Li, Xiaoyan);

Li, ZY (Li, Zhengyang); Liu, Q (Liu, Qiang); Pennypacker, CR (Pennypacker, Carl R.); Shang, ZH (Shang, Zhaohui); Yuan, XY (Yuan, Xiangyan); York, DG (York, Donald G.); Zhou, JL (Zhou, Jilin)
ASTRONOMICAL JOURNAL
卷: 153 期: 3 文献号: 104
AST3-1 is the second-generation wide-field optical photometric telescope dedicated to time-domain astronomy at Dome A, Antarctica. Here, we present the results of an i-band images survey from AST3-1 toward one Galactic disk field. Based on time-series photometry of 92,583 stars, 560 variable stars were detected with i magnitude <= 16.5 mag during eight days of observations; 339 of these are previously unknown variables. We tentatively classify the 560 variables as 285 eclipsing binaries (EW, EB, and EA), 27 pulsating variable stars (delta Scuti, gamma Doradus, delta Cephei variable, and RR Lyrae stars), and 248 other types of variables (unclassified periodic, multiperiodic, and aperiodic variable stars). Of the eclipsing binaries, 34 show O'Connell effects. One of the aperiodic variables shows a plateau light curve and another variable shows a secondary maximum after peak brightness. We also detected a complex binary system with an RS CVn-like light-curve morphology; this object is being followed-up spectroscopically using the Gemini South telescope.

第 98 条，共 286 条

Cosmological Inference from Host-Selected Type Ia Supernova Samples

Uddin, SA (Uddin, Syed A.); *Mould, J* (Mould, Jeremy); Lidman, C (Lidman, Chris); Ruhlmann-Kleider, V (Ruhlmann-Kleider, Vanina); Hardin, D (Hardin, Delphine)
PUBLICATIONS OF THE ASTRONOMICAL SOCIETY OF AUSTRALIA
卷: 34 文献号: e009
We compare two Type Ia supernova samples that are drawn from a spectroscopically confirmed Type Ia supernova sample: a host-selected sample in which SNe Ia are restricted to those that have a spectroscopic redshift from the host; and a broader, more traditional sample in which the redshift could come from either the SN or the host. The host-selected sample is representative of SN samples that will use the redshift of the host to infer the SN redshift, long after the SN has faded from view. We find that SNe Ia that are selected on the availability of a redshift from the host differ from SNe Ia that are from the broader sample. The former tend to be redder, have narrower light curves, live in more massive hosts, and tend to be at lower redshifts. We find that constraints on the equation of state of dark energy, omega, and the matter density, Omega(M), remain consistent between these two types of samples. Our results are important for ongoing and future supernova surveys, which unlike previous supernova surveys, will have limited real-time follow-up to spectroscopically classify the SNe they discover. Most of the redshifts in these surveys will come from the hosts.

第 99 条，共 286 条

Detection of a possible superluminous supernova in the Epoch of Reionization

Mould, J (Mould, Jeremy); Abbott, T (Abbott, Tim); Cooke, J (Cooke, Jeff); Curtin, C (Curtin, Chris); Katsianis, A (Katsianis, Antonios); Koekemoer, A (Koekemoer, Anton); Tescari, E (Tescari, Edoardo); Uddin, S (Uddin, Syed); Wang, LF (Wang, Lifan); Wyithe, S (Wyithe, Stuart)
SCIENCE BULLETIN
卷: 62 期: 10 页: 675-678
An interesting transient has been detected in one of our three Dark Energy Camera deep fields. Observations of these deep fields take advantage of the high red sensitivity of DECam on the Cerro Tololo Interamerican Observatory Blanco telescope. The survey includes the Y band with rest wavelength 1430{\AA} at z = 6. Survey fields (the Prime field 0555-6130, the 16hr field 1600-75 and the SUDSS New Southern Field) are deeper in Y than other infrared surveys. They are circumpolar, allowing all night to be used efficiently, exploiting the moon tolerance of 1 micron observations to minimize conflict with the Dark Energy Survey. As an i-band dropout (meaning that the flux decrement shortward of Lyman alpha is in the i bandpass), the transient we report here is a supernova candidate with z ~ 6, with a luminosity comparable to the brightest known current epoch superluminous supernova (i.e., ~ 2 x 10^11 solar luminosities).

第 100 条，共 286 条

OzDES multifibre spectroscopy for the Dark Energy Survey: 3-yr results and first data release

Childress, MJ (Childress, M. J.); Lidman, C (Lidman, C.); Davis, TM (Davis, T. M.); Tucker, BE (Tucker, B. E.); Asorey, J (Asorey, J.); Yuan, F (Yuan, F.); Abbott, TMC (Abbott, T. M. C.); Abdalla, FB (Abdalla, F. B.); Allam, S (Allam, S.); Annis, J (Annis, J.); Banerji, M (Banerji, M.); Benoit-Levy, A (Benoit-Levy, A.); Bernard, SR (Bernard, S. R.); Bertin, E (Bertin, E.); Brooks, D (Brooks, D.); Buckley-Geer, E (Buckley-Geer, E.); Burke, DL (Burke, D. L.); Rosell, AC (Rosell, A. Carnero); Carollo, D (Carollo, D.); Kind, MC (Kind, M. Carrasco); Carretero, J (Carretero, J.); Castander, FJ (Castander, F. J.); Cunha, CE (Cunha, C. E.); da Costa, LN (da Costa, L. N.); D'Andrea, CB (D'Andrea, C. B.); Doel, P (Doel, P.); Eifler, TF (Eifler, T. F.); Evrard, AE (Evrard, A. E.); Flaugher, B (Flaugher, B.); Foley, RJ (Foley, R. J.); Fosalba, P (Fosalba, P.); Frieman, J (Frieman, J.); Garcia-Bellido, J (Garcia-Bellido, J.); Glazebrook, K (Glazebrook, K.); Goldstein, DA (Goldstein, D. A.); Gruen, D (Gruen, D.); Gruendl, RA (Gruendl, R. A.); Gschwend, J (Gschwend, J.); Gupta, RR (Gupta, R. R.); Gutierrez, G (Gutierrez, G.); Hinton, SR (Hinton, S. R.); Hoormann, JK (Hoormann, J. K.); James, DJ (James, D. J.); Kessler, R (Kessler, R.); Kim, AG (Kim, A. G.); King, AL (King, A. L.); Kovacs, E (Kovacs, E.); Kuehn, K (Kuehn, K.); Kuhlmann, S (Kuhlmann, S.); Kuropatkin, N (Kuropatkin, N.); Lagattuta, DJ (Lagattuta, D. J.); Lewis, GF (Lewis, G. F.); Li, TS (Li, T. S.); Lima, M (Lima, M.); Lin, H (Lin, H.); Macaulay, E (Macaulay, E.); Maia, MAG (Maia, M. A. G.); Marriner, J (Marriner, J.); March, M (March, M.); Marshall, JL (Marshall, J. L.); Martini, P (Martini, P.); McMahon, RG (McMahon, R. G.); Menanteau, F (Menanteau, F.); Miquel, R (Miquel, R.); Moller, A (Moller, A.); Morganson, E (Morganson, E.); *Mould, J* (Mould, J.); Mudd, D (Mudd, D.); Muthukrishna, D (Muthukrishna, D.); Nichol, RC (Nichol, R. C.); Nord, B (Nord, B.); Ogando, RLC (Ogando, R. L. C.); Ostrovski, F (Ostrovski, F.); Parkinson, D (Parkinson, D.); Plazas, AA (Plazas, A. A.); Reed, SL (Reed, S. L.); Reil, K (Reil, K.); Romer, AK (Romer, A. K.); Rykoff, ES (Rykoff, E. S.); Sako, M (Sako, M.); Sanchez, E (Sanchez, E.); Scarpine, V (Scarpine, V.); Schindler, R (Schindler, R.); Schubnell, M (Schubnell, M.); Scolnic, D (Scolnic, D.); Sevilla-Noarbe, I (Sevilla-Noarbe, I.); Seymour, N (Seymour, N.); Sharp, R (Sharp, R.); Smith, M (Smith, M.); Soares-Santos,

M (Soares-Santos, M.); Sobreira, F (Sobreira, F.); Sommer, NE (Sommer, N. E.); Spinka, H (Spinka, H.); Suchyta, E (Suchyta, E.); Sullivan, M (Sullivan, M.); Swanson, MEC (Swanson, M. E. C.); Tarle, G (Tarle, G.); Uddin, SA (Uddin, S. A.); Walker, AR (Walker, A. R.); Wester, W (Wester, W.); Zhang, BR (Zhang, B. R.)
MONTHLY NOTICES OF THE ROYAL ASTRONOMICAL SOCIETY
卷: 472 期: 1 页: 273-288
We present results for the first three years of OzDES, a six year programme to obtain redshifts for objects in the Dark Energy Survey (DES) supernova fields using the 2dF fibre positioner and AAOmega spectrograph on the Anglo-Australian Telescope. OzDES is a multi-object spectroscopic survey targeting multiple types of targets at multiple epochs over a multiyear baseline and is one of the first multi-object spectroscopic surveys to dynamically include transients into the target list soon after their discovery. At the end of three years, OzDES has spectroscopically confirmed almost 100 supernovae, and has measured redshifts for 17 000 objects, including the redshifts of 2566 supernova hosts. We examine how our ability to measure redshifts for targets of various types depends on signal-to-noise ratio (S/N), magnitude and exposure time, finding that our redshift success rate increases significantly at a S/N of 2-3 per 1-angstrom bin. We also find that the change in S/N with exposure time closely matches the Poisson limit for stacked exposures as long as 10 h. We use these results to predict the redshift yield of the full OzDES survey, as well as the potential yields of future surveys on other facilities such as (i.e. the 4-m Multi-Object Spectroscopic Telescope, the Subaru Prime Focus Spectrograph and the Maunakea Spectroscopic Explorer). This work marks the first OzDES data release, comprising 14 693 redshifts. OzDES is on target to obtain over 30 000 redshifts over the 6-yr duration of the survey, including a yield of approximately 5700 supernova host-galaxy redshifts.

第 101 条，共 286 条

The Influence of Host Galaxies in Type Ia Supernova Cosmology

Uddin, SA (Uddin, Syed A.); *Mould, J* (Mould, Jeremy); Lidman, C (Lidman, Chris); Ruhlmann-Kleider, V (Ruhlmann-Kleider, Vanina); Zhang, BR (Zhang, Bonnie R.)
ASTROPHYSICAL JOURNAL
卷: 848 期: 1 文献号: 56
We use a sample of 1338 spectroscopically confirmed and photometrically classified Type Ia supernovae (SNe Ia) sourced from Carnegie Supernova Project, Center for Astrophysics Supernova Survey, Sloan Digital Sky Survey-II, and SuperNova Legacy Survey SN samples to examine the relationships between SNe Ia and the galaxies that host them. Our results provide confirmation with improved statistical significance that SNe Ia, after standardization, are on average more luminous in massive hosts (significance. > 5 sigma), and decline more rapidly in massive hosts (significance. > 9 sigma) and in hosts with low specific star formation rates (significance. > 8 sigma). We study the variation of these relationships with redshift and detect no evolution. We split SNe Ia into pairs of subsets that are based on the properties of the hosts and fit cosmological models to each subset. Including both systematic and statistical uncertainties, we do not find any significant shift in the best-fit cosmological parameters between the subsets. Among different SN Ia subsets, we find that SNe Ia in hosts with high specific star formation rates have the least intrinsic scatter (sigma(int) = 0.08 +/- 0.01) in luminosity after standardization.

第 102 条，共 286 条

A hybrid type Ia supernova with an early flash triggered by helium-shell detonation

Jiang, JA (Jiang, Ji-an); Doi, M (Doi, Mamoru); Maeda, K (Maeda, Keiichi); Shigeyama, T (Shigeyama, Toshikazu); Nomoto, K (Nomoto, Ken'ichi); Yasuda, N (Yasuda, Naoki); Jha, SW (Jha, Saurabh W.); Tanaka, M (Tanaka, Masaomi); Morokuma, T (Morokuma, Tomoki); Tominaga, N (Tominaga, Nozomu); Ivezic, Z (Ivezic, Zeljko); Ruiz-Lapuente, P (Ruiz-Lapuente, Pilar); Stritzinger, MD (Stritzinger, Maximilian D.); Mazzali, PA (Mazzali, Paolo A.); Ashall, C (Ashall, Christopher); *Mould, J* (Mould, Jeremy); Baade, D (Baade, Dietrich); Suzuki, N (Suzuki, Nao); Connolly, AJ (Connolly, Andrew J.); Patat, F (Patat, Ferdinando); Wang, LF (Wang, Lifan); Yoachim, P (Yoachim, Peter); Jones, D (Jones, David); Furusawa, H (Furusawa, Hisanori); Miyazaki, S (Miyazaki, Satoshi)
NATURE
卷: 550 期: 7674 页: 80-+
Type Ia supernovae arise from the thermonuclear explosion of white-dwarf stars that have cores of carbon and oxygen(1,2). The uniformity of their light curves makes these supernovae powerful cosmological distance indicators(3,4), but there have long been debates about exactly how their explosion is triggered and what kind of companion stars are involved(2,5,6). For example, the recent detection of the early ultraviolet pulse of a peculiar, subluminous type Ia supernova has been claimed as evidence for an interaction between a red-giant or a main-sequence companion and ejecta from a whited-warf explosion(7,8). Here we report observations of a prominent but red optical flash that appears about half a day after the explosion of a type Ia supernova. This supernova shows hybrid features of different supernova subclasses, namely a light curve that is typical of normal-brightness supernovae, but with strong titanium absorption, which is commonly seen in the spectra of subluminous ones. We argue that this early flash does not occur through previously suggested mechanisms such as the companion-ejecta interaction(8-10). Instead, our simulations show that it could occur through detonation of a thin helium shell either on a near-Chandrasekhar- mass white dwarf, or on a sub-Chandrasekhar-mass white dwarf merging with a less-massive white dwarf. Our finding provides evidence that one branch of previously proposed explosion models-the helium-ignition branch- does exist in nature, and that such a model may account for the explosions of white dwarfs in a mass range wider than previously supposed(11-14).

第 103 条，共 286 条

Preheating of the Intergalactic Medium by Gravitational Collapse and Ultraviolet Background

Zhu, WS (Zhu, Weishan); *Feng, LL* (Feng, Long-Long)
ASTROPHYSICAL JOURNAL
卷: 847 期: 1 文献号: 17
The preheating of the intergalactic medium by structure collapse and ultraviolet background (UVB) is investigated in cosmological hydrodynamical simulations. When gravitational collapse is the sole heating mechanism, we find that (1) 60% and 45% of the IGM are heated up to S > 8 and 17 keV cm(2), respectively, at z = 0, but the fractions drop

rapidly to a few percent at z = 2; (2) the entropy of the circumhalo gas S-cir is higher than the virial entropy for more than 75% of the halos with masses M < 10(11.5) M-circle dot since z = 2, but the fraction higher than the entropy, S-pr, required in the preventive model of galaxy formation is only 15%-20% for halos with M < 10(10.5) M-circle dot at z = 0, and decreases as redshift increases; (3) assuming a metallicity of Z <= 0.03 Z(circle dot), the fraction of halos whose circumhalo gas has a cooling time longer than the Hubble time t(cool,cir) > t(H) is merely 5%-10% at z less than or similar to 0.5, and even less at z >= 1 for halos with M < 10(10.5) M-circle dot; and (4) gas in the filaments undergoes the strongest preheating. Furthermore, we show that the UVB cannot enhance the fraction of the IGM with S > 17 keV cm(2), but can increase the fraction of low-mass halos (<10(10.5) M-circle dot) having S-cir > S-pr to similar to 70% at z = 0 and that having t(cool,cir) > t(H) to 15%-30% at z less than or similar to 0.5. Our results indicate that preheating due to gravitational collapse and UVB is inadequate to fulfill the needs of the preventative model, especially for halos with 10(10.5) M-circle dot < M< 10(11.5) M-circle dot. Nevertheless, these two mechanisms might cause large-scale galactic conformity.

第 104 条，共 286 条

Follow Up of GW170817 and Its Electromagnetic Counterpart by Australian-Led Observing Programmes

Andreoni, I (Andreoni, I.); Ackley, K (Ackley, K.); Cooke, J (Cooke, J.); Acharyya, A (Acharyya, A.); Allison, JR (Allison, J. R.); Anderson, GE (Anderson, G. E.); Ashley, MCB (Ashley, M. C. B.); Baade, D (Baade, D.); Bailes, M (Bailes, M.); Bannister, K (Bannister, K.); Beardsley, A (Beardsley, A.); Bessell, MS (Bessell, M. S.); Bian, F (Bian, F.); Bland, PA (Bland, P. A.); Boer, M (Boer, M.); Booler, T (Booler, T.); Brandeker, A (Brandeker, A.); Brown, IS (Brown, I. S.); Buckley, DAH (Buckley, D. A. H.); Chang, SW (Chang, S. -W.); Coward, DM (Coward, D. M.); Crawford, S (Crawford, S.); Crisp, H (Crisp, H.); Crosse, B (Crosse, B.); Cucchiara, A (Cucchiara, A.); Cupak, M (Cupak, M.); de Gois, JS (de Gois, J. S.); Deller, A (Deller, A.); Devillepoix, HAR (Devillepoix, H. A. R.); Dobie, D (Dobie, D.); Elmer, E (Elmer, E.); Emrich, D (Emrich, D.); Farah, W (Farah, W.); Farrell, TJ (Farrell, T. J.); Franzen, T (Franzen, T.); Gaensler, BM (Gaensler, B. M.); Galloway, DK (Galloway, D. K.); Gendre, B (Gendre, B.); Giblin, T (Giblin, T.); Goobar, A (Goobar, A.); Green, J (Green, J.); Hancock, PJ (Hancock, P. J.); Hartig, BAD (Hartig, B. A. D.); Howell, EJ (Howell, E. J.); Horsley, L (Horsley, L.); Hotan, A (Hotan, A.); Howie, RM (Howie, R. M.); Hu, L (Hu, L.); Hu, Y (Hu, Y.); James, CW (James, C. W.); Johnston, S (Johnston, S.); Johnston-Hollitt, M (Johnston-Hollitt, M.); Kaplan, DL (Kaplan, D. L.); Kasliwal, M (Kasliwal, M.); Keane, EF (Keane, E. F.); Kenney, D (Kenney, D.); Klotz, A (Klotz, A.); Lau, R (Lau, R.); Laugier, R (Laugier, R.); Lenc, E (Lenc, E.); Li, X (Li, X.); Liang, E (Liang, E.); Lidman, C (Lidman, C.); Luvaul, LC (Luvaul, L. C.); Lynch, C (Lynch, C.); Ma, B (Ma, B.); Macpherson, D (Macpherson, D.); Mao, J (Mao, J.); McClelland, DE (McClelland, D. E.); McCully, C (McCully, C.); Moller, A (Moller, A.); Morales, MF (Morales, M. F.); Morris, D (Morris, D.); Murphy, T (Murphy, T.); Noysena, K (Noysena, K.); Onken, CA (Onken, C. A.); Orange, NB (Orange, N. B.); Oslowski, S (Oslowski, S.); Pallot, D (Pallot, D.); Paxman, J (Paxman, J.); Potter, SB (Potter, S. B.); Pritchard, T (Pritchard, T.); Raja, W (Raja, W.); Ridden-Harper, R (Ridden-Harper, R.); Romero-Colmenero, E (Romero-Colmenero, E.); Sadler, EM (Sadler, E. M.); Sansom, EK (Sansom, E. K.); Scalzo, RA (Scalzo, R. A.); Schmidt, BP (Schmidt, B. P.); Scott, SM (Scott, S. M.); Seghouani, N (Seghouani, N.); Shang, Z (Shang, Z.); Shannon, RM (Shannon, R. M.); Shao, L (Shao, L.); Shara, MM (Shara, M. M.); Sharp, R (Sharp, R.); Sokolowski, M (Sokolowski, M.); Sollerman, J (Sollerman, J.); Staff, J (Staff, J.); Steele, K (Steele, K.); Sun, T (Sun, T.); Suntzeff, NB (Suntzeff, N. B.); Tao, C (Tao, C.); Tingay, S (Tingay, S.); Towner, MC (Towner, M. C.); Thierry, P (Thierry, P.); Trott, C (Trott, C.); Tucker, BE (Tucker, B. E.); Vaisanen, P (Vaisanen, P.); Krishnan, VV (Krishnan, V. Venkatraman); Walker, M (Walker, M.); Wang, L (Wang, L.); Wang, X (Wang, X.); Wayth, R (Wayth, R.); Whiting, M (Whiting, M.); Williams, A (Williams, A.); Williams, T (Williams, T.); Wolf, C (Wolf, C.); Wu, C (Wu, C.); Wu, X (Wu, X.); *Yang, J* (Yang, J.); Yuan, X (Yuan, X.); Zhang, H (Zhang, H.); Zhou, J (Zhou, J.); Zovaro, H (Zovaro, H.)

PUBLICATIONS OF THE ASTRONOMICAL SOCIETY OF AUSTRALIA

卷: 34 文献号: e069

The discovery of the first electromagnetic counterpart to a gravitational wave signal has generated follow-up observations by over 50 facilities world-wide, ushering in the new era of multi-messenger astronomy. In this paper, we present follow-up observations of the gravitational wave event GW170817 and its electromagnetic counterpart SSS17a/DLT17ck (IAU label AT2017gfo) by 14 Australian telescopes and partner observatories as part of Australian-based and Australian-led research programs. We report early- to late-time multi-wavelength observations, including optical imaging and spectroscopy, mid-infrared imaging, radio imaging, and searches for fast radio bursts. Our optical spectra reveal that the transient source emission cooled from approximately 6 400 K to 2 100 K over a 7-d period and produced no significant optical emission lines. The spectral profiles, cooling rate, and photometric light curves are consistent with the expected outburst and subsequent processes of a binary neutron star merger. Star formation in the host galaxy probably ceased at least a Gyr ago, although there is evidence for a galaxy merger. Binary pulsars with short (100 Myr) decay times are therefore unlikely progenitors, but pulsars like PSR B1534+12 with its 2.7 Gyr coalescence time could produce such a merger. The displacement (similar to 2.2 kpc) of the binary star system from the centre of the main galaxy is not unusual for stars in the host galaxy or stars originating in the merging galaxy, and therefore any constraints on the kick velocity imparted to the progenitor are poor.

第 105 条，共 286 条

Optical observations of LIGO source GW 170817 by the Antarctic Survey Telescopes at Dome A, Antarctica

Hu, L (Hu, Lei); Wu, XF (Wu, Xuefeng); Andreoni, I (Andreoni, Igor); Ashley, MCB (Ashley, Michael C. B.); Cooke, J (Cooke, Jeff); Cui, XQ (Cui, Xiangqun); Du, FJ (Du, Fujia); Dai, ZG (Dai, Zigao); Gu, BZ (Gu, Bozhong); Hu, Y (Hu, Yi); Lu, HP (Lu, Haiping); Li, XY (Li, Xiaoyan); Li, ZY (Li, Zhengyang); Liang, ES (Liang, Ensi); Liu, LD (Liu, Liangduan); Ma, B (Ma, Bin); Shang, ZH (Shang, Zhaohui); Sun, TR (Sun, Tianrui); Suntzeff, NB (Suntzeff, N. B.); Tao, C (Tao, Charling); Uddin, SA (Uddin, Syed A.); Wang, LF (Wang, Lifan); Wang, XF (Wang, Xiaofeng); Wen, HK (Wen, Haikun); Xiao, D (Xiao, Di); Xu, J (Xu, Jin); Yang, J (Yang, Ji); Yang, SH (Yang, Shihai); Yuan, XY (Yuan, Xiangyan); Zhou, HY (Zhou, Hongyan); Zhang, H (Zhang, Hui); Zhou, JL (Zhou, Jilin); Zhu, ZH (Zhu, Zonghong)

SCIENCE BULLETIN

卷: 62 期: 21 页: 1433-1438

The LIGO detection of gravitational waves (GW) from merging black holes in 2015 marked the beginning of a new era in observational astronomy. The detection of an electromagnetic signal from a GW source is the critical next step to explore in detail the physics involved. The Antarctic Survey Telescopes (AST3), located at Dome A, Antarctica, is uniquely situated for rapid response time-domain astronomy with its continuous night-time coverage during the austral winter. We report optical observations of the GW source (GW 170817) in the nearby galaxy NGC 4993 using AST3. The data show a rapidly fading transient at around 1 day after the GW trigger, with the i-band magnitude declining from 17.23 +/- 0.13 magnitude to 17.72 +/- 0.09 magnitude in similar to 1.8 h. The brightness and time evolution of the optical transient associated with GW 170817 are broadly consistent with the predictions of models involving merging binary neutron stars. We infer from our data that the merging process ejected about similar to 10(-2) solar mass of radioactive material at a speed of up to 30% the speed of light. (C) 2017 Science China Press. Published by Elsevier B.V. and Science China Press. All rights reserved.

第 106 条，共 286 条

Average Spectral Properties of Type Ia Supernova Host Galaxies

Uddin, SA (Uddin, Syed A.); Mould, J (Mould, Jeremy); *Wang, LF* (Wang, Lifan)
ASTROPHYSICAL JOURNAL
卷: 850 期: 2 文献号: 135
We construct the average spectra of host galaxies of slower, faster, bluer, and redder Type Ia supernovae (SNe Ia) from the SDSS-II supernova survey. The average spectrum of slower declining (broader light curve width or higher stretch) SN Ia hosts shows stronger emission lines compared to the average spectrum of faster declining (narrower light curve width or lower stretch) SN Ia hosts. Using pPXF, we find that hosts of slower declining SNe Ia have metallicities that are, on average, 0.24 dex lower than average metallicities of faster declining SN Ia hosts. Similarly, redder SN Ia hosts have slightly higher metallicities than bluer SN Ia hosts. Lick index analysis of metallic lines and Balmer lines shows that faster declining SN Ia hosts have relatively higher metal content and have relatively older stellar populations compared with slower declining SN Ia hosts. We calculate average Ha star formation rate (SFR), stellar mass, and the specific SFR (sSFR) of host galaxies in these subgroups of SNe Ia. We find that slower declining SN Ia hosts have significantly higher (> 5 sigma) sSFR than faster declining SN Ia hosts. A Kolmogorov-Smirnov test shows that these two types of hosts originate from different parent distributions. Our results, when compared with the models of Childress et al., indicate that slower declining SNe Ia, being hosted in actively star-forming galaxies, are young (prompt) SNe Ia, originating from similar progenitor age groups.

第 107 条，共 286 条

Average Spectral Properties of Type Ia Supernova Host Galaxies

Uddin, SA (Uddin, Syed A.); Mould, J (Mould, Jeremy); *Wang, LF* (Wang, Lifan)
ASTROPHYSICAL JOURNAL
卷: 850 期: 2 文献号: 135
We construct the average spectra of host galaxies of slower, faster, bluer, and redder Type Ia supernovae (SNe Ia) from the SDSS-II supernova survey. The average spectrum of slower declining (broader light curve width or higher stretch) SN Ia hosts shows stronger emission lines compared to the average spectrum of faster declining (narrower light curve width or lower stretch) SN Ia hosts. Using pPXF, we find that hosts of slower declining SNe Ia have metallicities that are, on average, 0.24 dex lower than average metallicities of faster declining SN Ia hosts. Similarly, redder SN Ia hosts have slightly higher metallicities than bluer SN Ia hosts. Lick index analysis of metallic lines and Balmer lines shows that faster declining SN Ia hosts have relatively higher metal content and have relatively older stellar populations compared with slower declining SN Ia hosts. We calculate average Ha star formation rate (SFR), stellar mass, and the specific SFR (sSFR) of host galaxies in these subgroups of SNe Ia. We find that slower declining SN Ia hosts have significantly higher (> 5 sigma) sSFR than faster declining SN Ia hosts. A Kolmogorov-Smirnov test shows that these two types of hosts originate from different parent distributions. Our results, when compared with the models of Childress et al., indicate that slower declining SNe Ia, being hosted in actively star-forming galaxies, are young (prompt) SNe Ia, originating from similar progenitor age groups.

2-03 Galaxy Cosmology and Dark Energy

第 108 条，共 286 条

Backflows by active galactic nuclei jets: global properties and influence on supermassive black hole accretion

Cielo, S (Cielo, S.); Antonuccio-Delogu, V (Antonuccio-Delogu, V.); Silk, J (Silk, J.); *Romeo, AD* (Romeo, A. D.)
MONTHLY NOTICES OF THE ROYAL ASTRONOMICAL SOCIETY
卷: 467 期: 4 页: 4526-4539
Jets from active galactic nuclei (AGN) inflate large cavities in the hot gas environment around galaxies and galaxy clusters. The large-scale gas circulation promoted within such cavities by the jet itself gives rise to backflows that propagate back to the centre of the jet-cocoon system, spanning all the physical scales relevant for the AGN. Using an adaptive mesh refinement code, we study these backflows through a series of numerical experiments, aiming at understanding how their global properties depend on jet parameters. We are able to characterize their mass flux down to a scale of a few kiloparsecs to about 0.5 M(circle dot)yr(-1) for as long as 15 or 20 Myr, depending on jet power. We find that backflows are both spatially coherent and temporally intermittent, independently of jet power in the range 10(43)-10(45) erg s(-1). Using the mass flux thus measured, we model analytically the effect of backflows on the central accretion region, where a magnetically arrested disc lies at the centre of a thin circumnuclear disc. Backflow accretion on to the disc modifies its density profile, producing a flat core and tail. We use this analytic model to predict how accretion beyond the black hole magnetopause is modified, and thus how the jet power is temporally modulated. Under the assumption that the magnetic flux stays frozen in the accreting matter, and that the jets are always launched via the Blandford-Znajek mechanism, we find that backflows are

capable of boosting the jet power up to tenfold during relatively short time episodes (a few Myr).

第 109 条，共 286 条

NIHAO XII: galactic uniformity in a Lambda CDM universe

Dutton, AA (Dutton, Aaron A.); Obreja, A (Obreja, Aura); Wang, L (Wang, Liang); Gutcke, TA (Gutcke, Thales A.); Buck, T (Buck, Tobias); Udrescu, SM (Udrescu, Silviu M.); Frings, J (Frings, Jonas); Stinson, GS (Stinson, Gregory S.); *Kang, X* (Kang, Xi); Maccio, AV (Maccio, Andrea V.)
MONTHLY NOTICES OF THE ROYAL ASTRONOMICAL SOCIETY
卷: 467 期: 4 页: 4937-4950
We use a sample of 83 high-resolution cosmological zoom-in simulations and a semi-analytic model (SAM) to study the stochasticity of galaxy formation in haloes ranging from dwarf to Milky Way masses. Our simulated galaxies reproduce the observed inefficiency of galaxy formation as expressed through the stellar, gas and baryonic Tully-Fisher relations. For HI velocities in the range (70 less than or similar to V less than or similar to 220 km s(-1)), the scatter is just 0.08 to 0.14 dex, consistent with the observed intrinsic scatter at these scales. At low velocities (20 less than or similar to V less than or similar to 70 km s(-1)), the simulated scatter is 0.2-0.25 dex, which could be tested with future observations. The scatter in the stellar mass versus dark halo velocity relation is constant for 30 less than or similar to V less than or similar to 180 km s(-1), and smaller (similar or equal to 0.17 dex) when using the maximum circular velocity of the dark-matter-only simulation, V-max(DMO), compared to the virial velocity (V-200 or V-200(DMO)). The scatter in stellar mass is correlated with halo concentration, and is minimized when using a circular velocity at a fixed fraction of the virial radius similar or equal to 0.4R(200) or with V-alpha = V-200(DMO)(V-max(DMO) / V-200(DMO))(alpha) with alpha similar or equal to 0.7, consistent with constraints from halo clustering. Using the SAM we show the correlation between halo formation time and concentration is essential in order to reproduce this result. This uniformity in galaxy formation efficiency we see in our hydrodynamical simulations and an SAM proves the simplicity and self-regulating nature of galaxy formation in a Lambda cold dark matter (Lambda CDM) universe.

第 110 条，共 286 条

NIHAO VII: predictions for the galactic baryon budget in dwarf to Milky Way mass haloes

Wang, LA (Wang, Liang); Dutton, AA (Dutton, Aaron A.); Stinson, GS (Stinson, Gregory S.); Maccio, AV (Maccio, Andrea V.); Gutcke, T (Gutcke, Thales); Kang, X (Kang, Xi)
MONTHLY NOTICES OF THE ROYAL ASTRONOMICAL SOCIETY
卷: 466 期: 4 页: 4858-4867
We use the Numerical Investigation of a Hundred Astrophysical Objects (NIHAO) galaxy formation simulations to make predictions for the baryonic budget in present day galaxies ranging from dwarf (M-200 similar to 10(10)M circle dot) toMilkyWay (M-200 similar to 10(12)M circle dot) masses. The sample is made of 88 independent high-resolution cosmological zoom-in simulations. NIHAO galaxies reproduce key properties of observed galaxies, such as the stellar mass versus halo mass and cold gas versus stellar mass relations. Thus they make plausible predictions for the baryon budget. We present the mass fractions of stars, cold gas (T< 10(4) K), cool gas (10(4) < T< 10(5) K), warm-hot gas (10(5) < T < 5 x 10(6) K) and hot gas (T > 5 x 10(6) K), inside the virial radius, R200. Compared to the predicted baryon mass, using the dark halo mass and the universal baryon fraction, f(b) = Omega(b)/Omega(m) = 0.15, we find that all of our haloes are missing baryons. The missing mass has been relocated past 2 virial radii, and cool gas dominates the corona at low mass (M-200 Alpha less than or similar to 3 x 10(11)M circle dot) while the warm-hot gas dominates at high mass (M-200 less than or similar to 3 x 10(11)M circle dot). Haloes of mass M-200 greater than or similar to 10(10)M circle dot are missing similar to 90 per cent of their baryons. More massive haloes (M-200 similar to 10(12)M circle dot) retain a higher fraction of their baryons, with similar to 30 per cent missing, consistent with recent observational estimates. Moreover, these more massive haloes reproduce the observed fraction of cold, warm-hot and hot gases. The fraction of cool gas we predict (0.11 +/- 0.06) is significantly lower than the observation from COS-Halos (0.3-0.47), but agrees with the alternative analysis of Stern et al. (2016).

第 111 条，共 286 条

Constraints on the Evolution of the Galaxy Stellar Mass Function. I. Role of Star Formation, Mergers, and Stellar Stripping

Contini, E (Contini, E.); *Kang, X* (Kang, Xi); Romeo, AD (Romeo, A. D.); Xia, Q (Xia, Q.)
ASTROPHYSICAL JOURNAL
卷: 837 期: 1 文献号: 27
We study the connection between the observed star formation rate-stellar mass (SFR-M-*) relation and the evolution of the stellar mass function (SMF) by means of a subhalo abundance matching technique coupled to merger trees extracted from an N-body simulation. Our approach, which considers both galaxy mergers and stellar stripping, is to force the model to match the observed SMF at redshift z > 2, and let it evolve down to the present time according to the observed SFR-M-* relation. In this study, we use two different sets of SMFs and two SFR-M-* relations: a simple power law and a relation with a mass-dependent slope. Our analysis shows that the evolution of the SMF is more consistent with an SFR-M-* relation with a mass-dependent slope, in agreement with predictions from other models of galaxy evolution and recent observations. In order to fully and realistically describe the evolution of the SMF, both mergers and stellar stripping must be considered, and we find that both have almost equal effects on the evolution of SMF at the massive end. Taking into account the systematic uncertainties in the observed data, the high-mass end of the SMF obtained by considering stellar stripping results in good agreement with recent observational data from the Sloan Digital Sky Survey. At log M-* < 11.2, our prediction at z = 0.1 is close to Li & White data, but the high-mass end (log M-* > 11.2) is in better agreement with D'Souza et al. data which account for more massive galaxies.

第 112 条，共 286 条

What is the right way to quench star formation in semi-analytic models of galaxy formation?

Luo, Y (Luo, Yu); Kang, X (Kang, Xi)
RESEARCH IN ASTRONOMY AND ASTROPHYSICS
卷: 17 期: 2 文献号: 12
Semi-analytic models of galaxy formation are powerful tools to study the evolution of a galaxy population in a cosmological context. However, most models overpredict

the number of lowmass galaxies at high redshifts and the colors of model galaxies are not right in the sense that low-mass satellite galaxies are too red and centrals are too blue. The recent version of the L-Galaxies model by Henriques et al. (H15) is a step forward to solve these problems by reproducing the evolution of stellar mass function and the overall fraction of red galaxies. In this paper we compare the two model predictions of L-Galaxies (the other is Guo et al., G13) to SDSS data in detail. We find that in the H15 model the red fraction of central galaxies now agrees with the data due to their implementation of strong AGN feedback, but the stellar mass of centrals in massive halos is now slightly lower than what is indicated by the data. For satellite galaxies, the red fraction of low-mass galaxies (log M+/M-circle dot < 10) also agrees with the data, but the color of massive satellites (10 < log M-*/M-circle dot < 11) is slightly bluer. The correct color of centrals and the bluer color of massive satellites indicate that quenching in massive satellites is not strong enough. We also find that there are too many red spirals and less bulge-dominated galaxies in both H15 and G13 models. Our results suggest that additional mechanisms, such as more minor mergers or disk instability, are needed to slightly increase the stellar mass of the central galaxy in massive galaxies, mainly in the bulge component, and bulge dominated galaxies will be quenched not only by minor mergers, but also by some other mechanisms.

第 113 条，共 286 条

The spatial alignment of galaxies on different scales:A review on the theoretical and observational progress

Kang Xi; Wang Peng; Luo Yu; Xia Qianli; Pan Hengxing
Scientia Sinica Physica, Mechanica & Astronomica
卷：47 期：4 页：049803-1-049803-21 文献号：1674-7275(2017)47:4<049803:XXKJQX>2.0.TX;2-O
The spatial distribution of galaxies in our universe is not random, and they demonstrate different alignment patterns on different scales. On the scale of galaxy and galaxy clusters, satellite galaxies tend to be distributed along the major axis of the central galaxy. On large scales, major axis of a central galaxy tends to point towards large scale matter distribution, for example, along the large scale filamentary structure. Even on larger scales, the major axes of different galaxies still have non-negligible correlations. Besides, the angular momentums of galaxies are also correlated with the mass distribution on large scales, with different correlations. This article will review the relative theories and observational developments in galaxies alignment and spatial distribution, it will show that the anisotropic distributions of galaxies on small scales are determined by the non-spherical nature of dark matter halo, and the correlations with large-scale mass distribution are also the natural predictions of cold dark matter theory, and this article also indicates that studies of galaxy alignment help us to understand the physics of galaxy formation and could be used to constrain the nature of dark matter and dark energy.

第 114 条，共 286 条

The Frontier Fields lens modelling comparison project

Meneghetti, M (Meneghetti, M.); Natarajan, P (Natarajan, P.); Coe, D (Coe, D.); *Contini, E* (Contini, E.); De Lucia, G (De Lucia, G.); Giocoli, C (Giocoli, C.); Acebron, A (Acebron, A.); Borgani, S (Borgani, S.); Bradac, M (Bradac, M.); Diego, JM (Diego, J. M.); Hoag, A (Hoag, A.); Ishigaki, M (Ishigaki, M.); Johnson, TL (Johnson, T. L.); Jullo, E (Jullo, E.); Kawamata, R (Kawamata, R.); Lam, D (Lam, D.); Limousin, M (Limousin, M.); Liesenborgs, J (Liesenborgs, J.); Oguri, M (Oguri, M.); Sebesta, K (Sebesta, K.); Sharon, K (Sharon, K.); Williams, LLR (Williams, L. L. R.); Zitrin, A (Zitrin, A.)
MONTHLY NOTICES OF THE ROYAL ASTRONOMICAL SOCIETY
卷: 472 期: 3 页: 3177-3216
Gravitational lensing by clusters of galaxies offers a powerful probe of their structure and mass distribution. Several research groups have developed techniques independently to achieve this goal. While these methods have all provided remarkably high-precision mass maps, particularly with exquisite imaging data from the Hubble Space Telescope (HST), the reconstructions themselves have never been directly compared. In this paper, we present for the first time a detailed comparison of methodologies for fidelity, accuracy and precision. For this collaborative exercise, the lens modelling community was provided simulated cluster images that mimic the depth and resolution of the ongoing HST Frontier Fields. The results of the submitted reconstructions with the un-blinded true mass profile of these two clusters are presented here. Parametric, free-form and hybrid techniques have been deployed by the participating groups and we detail the strengths and trade-offs in accuracy and systematics that arise for each methodology. We note in conclusion that several properties of the lensing clusters are recovered equally well by most of the lensing techniques compared in this study. For example, the reconstruction of azimuthally averaged density and mass profiles by both parametric and free-form methods matches the input models at the level of similar to 10 per cent. Parametric techniques are generally better at recovering the 2D maps of the convergence and of the magnification. For the best-performing algorithms, the accuracy in the magnification estimate is similar to 10 per cent at mu(true) = 3 and it degrades to similar to 30 per cent at mu(true) similar to 10.

第 115 条，共 286 条

Halo Intrinsic Alignment: Dependence on Mass, Formation Time, and Environment

Xia, QL (Xia, Qianli); Kang, X (Kang, Xi); Wang, P (Wang, Peng); Luo, Y (Luo, Yu); Yang, XH (Yang, Xiaohu); Jing, YP (Jing, Yipeng); Wang, HY (Wang, Huiyuan); Mo, HJ (Mo, Houjun)
ASTROPHYSICAL JOURNAL
卷: 848 期: 1 文献号: 22
In this paper we use high-resolution cosmological simulations to study halo intrinsic alignment and its dependence on mass, formation time, and large-scale environment. In agreement with previous studies using N-body simulations, it is found that massive halos have stronger alignment. For the first time, we find that for a given halo mass older halos have stronger alignment and halos in cluster regions also have stronger alignment than those in filaments. To model these dependencies, we extend the linear alignment model with inclusion of halo bias and find that the halo alignment with its mass and formation time dependence can be explained by halo bias. However, the model cannot account for the environment dependence, as it is found that halo bias is lower in clusters and higher in filaments. Our results suggest that halo bias and environment are independent factors in determining halo alignment. We also study the halo alignment correlation function and find that halos are strongly clustered along

their major axes and less clustered along the minor axes. The correlated halo alignment can extend to scales as large as 100 h(-1) Mpc, where its feature is mainly driven by the baryon acoustic oscillation effect.

第 116 条，共 286 条

A general explanation on the correlation of dark matter halo spin with the large-scale environment

Wang, P (Wang, Peng); Kang, X (Kang, Xi)
MONTHLY NOTICES OF THE ROYAL ASTRONOMICAL SOCIETY
卷: 468 期: 1 页: L123-L127
Both simulations and observations have found that the spin of halo/galaxy is correlated with the large-scale environment, and particularly the spin of halo flips in filament. A consistent picture of halo spin evolution in different environments is still lacked. Using N-body simulation, we find that halo spin with its environment evolves continuously from sheet to cluster, and the flip of halo spin happens both in filament and nodes. The flip in filament can be explained by halo formation time and migrating time when its environment changes from sheet to filament. For low-mass haloes, they form first in sheets and migrate into filaments later, so their mass and spin growth inside filament are lower, and the original spin is still parallel to filament. For high-mass haloes, they migrate into filaments first, and most of their mass and spin growth are obtained in filaments, so the resulted spin is perpendicular to filament. Our results well explain the overall evolution of cosmic web in the cold dark matter model and can be tested using high-redshift data. The scenario can also be tested against alternative models of dark matter, such as warm/hot dark matter, where the structure formation will proceed in a different way.

第 117 条，共 286 条

How to co-add images? I. A new iterative method for image reconstruction of dithered observations

Wang, L (Wang, Lei); Li, GL (Li, Guo-Liang)
RESEARCH IN ASTRONOMY AND ASTROPHYSICS
卷: 17 期: 10 文献号: 100
By employing the previous Voronoi approach and replacing its nearest neighbor approximation with Drizzle in iterative signal extraction, we develop a fast iterative Drizzle algorithm, named fiDrizzle, to reconstruct the underlying band-limited image from undersampled dithered frames. Compared with the existing iDrizzle, the new algorithm improves rate of convergence and accelerates the computational speed. Moreover, under the same conditions (e.g. the same number of dithers and iterations), fiDrizzle can make a better quality reconstruction than iDrizzle, due to the newly discovered High Sampling caused Decelerating Convergence (HSDC) effect in the iterative signal extraction process. fiDrizzle demonstrates its powerful ability to perform image deconvolution from undersampled dithers.

第 118 条，共 286 条

Constraints on the Evolution of the Galaxy Stellar Mass Function. II. The Quenching Timescale of Galaxies and Its Implication for Their Star Formation Rates

Contini, E (Contini, E.); Kang, X (Kang, X.); Romeo, AD (Romeo, A. D.); Xia, Q (Xia, Q.); Yi, SK (Yi, S. K.)
ASTROPHYSICAL JOURNAL
卷: 849 期: 2 文献号: 156
We study the connection between the observed star formation rate-stellar mass (SFR-M-*) relation and the evolution of the stellar mass function (SMF) by means of a subhalo abundance matching technique coupled to merger trees extracted from an N-body simulation. Our approach consists of forcing the model to match the observed SMF at redshift z similar to 2.3, and letting it evolve down to z similar to 0.3 according to a tau model, an exponentially declining functional form that describes the star formation rate decay of both satellite and central galaxies. In this study, we use three different sets of SMFs: ZFOURGE data from Tomczak et al., UltraVISTA data from Ilbert et al., and COSMOS data from Davidzon et al. We also build a mock survey combining UltraVISTA with ZFOURGE. Our modeling of quenching timescales is consistent with the evolution of the SMF down to z similar to 0.3, with different accuracy depending on the particular survey used for calibration. We tested our model against the observed SMFs at low redshift, and it predicts residuals (observation versus model) within 1 sigma observed scatter along most of the stellar mass range investigated, and with mean residuals below 0.1 dex in the range similar to[10(8.7)-10(11.7)]M-circle dot. We then compare the SFR-M-* relation predicted by the model with the observed one at different redshifts. The predicted SFR-M-* relation underpredicts the median SFR at fixed stellar mass relative to observations at all redshifts. Nevertheless, the shapes are consistent with the observed relations up to intermediate-mass galaxies, followed by a rapid decline for massive galaxies.

第 119 条，共 286 条

The Sloan Lens ACS Survey. XIII. Discovery of 40 New Galaxy-scale Strong Lenses

Shu, YP (Shu, Yiping); Brownstein, JR (Brownstein, Joel R.); Bolton, AS (Bolton, Adam S.); Koopmans, LVE (Koopmans, Leon V. E.); Treu, T (Treu, Tommaso); Montero-Dorta, AD (Montero-Dorta, Antonio D.); Auger, MW (Auger, Matthew W.); Czoske, O (Czoske, Oliver); Gavazzi, R (Gavazzi, Raphael); Marshall, PJ (Marshall, Philip J.); Moustakas, LA (Moustakas, Leonidas A.)
ASTROPHYSICAL JOURNAL
卷: 851 期: 1 文献号: 48
We present the full sample of 118 galaxy-scale strong-lens candidates in the Sloan Lens ACS (SLACS) Survey for the Masses (S4TM) Survey, which are spectroscopically selected from the final data release of the Sloan Digital Sky Survey. Follow-up Hubble Space Telescope (HST) imaging observations confirm that 40 candidates are definite strong lenses with multiple lensed images. The foreground-lens galaxies are found to be early-type galaxies (ETGs) at redshifts 0.06-0.44, and background sources are emission-line galaxies at redshifts 0.22-1.29. As an extension of the SLACS Survey, the S4TM Survey is the first attempt to preferentially search for strong-lens systems with relatively lower lens masses than those in the pre-existing strong-lens samples. By fitting HST data with a singular isothermal ellipsoid model, we find that the total projected mass within the Einstein radius of the S4TM strong-lens sample ranges from 3 x 10(10) M-circle dot to 2 x 10(11) M-circle dot. In Shu et al., we have derived the total stellar mass of the S4TM lenses to be 5 x 10(10) M-circle dot to 1 x 10(12) M-circle dot. Both the total enclosed mass and stellar mass of the S4TM lenses are on average almost a factor of 2 smaller than those of the SLACS lenses, which also represent

the typical mass scales of the current strong-lens samples. The extended mass coverage provided by the S4TM sample can enable a direct test, with the aid of strong lensing, for transitions in scaling relations, kinematic properties, mass structure, and dark-matter content trends of ETGs at intermediate-mass scales as noted in previous studies.

第 120 条，共 286 条

The Sloan Lens ACS Survey. XIII. Discovery of 40 New Galaxy-scale Strong Lenses

Shu, YP (Shu, Yiping); Brownstein, JR (Brownstein, Joel R.); Bolton, AS (Bolton, Adam S.); Koopmans, LVE (Koopmans, Leon V. E.); Treu, T (Treu, Tommaso); Montero-Dorta, AD (Montero-Dorta, Antonio D.); Auger, MW (Auger, Matthew W.); Czoske, O (Czoske, Oliver); Gavazzi, R (Gavazzi, Raphael); Marshall, PJ (Marshall, Philip J.); Moustakas, LA (Moustakas, Leonidas A.)

ASTROPHYSICAL JOURNAL
卷: 851 期: 1 文献号: 48

We present the full sample of 118 galaxy-scale strong-lens candidates in the Sloan Lens ACS (SLACS) Survey for the Masses (S4TM) Survey, which are spectroscopically selected from the final data release of the Sloan Digital Sky Survey. Follow-up Hubble Space Telescope (HST) imaging observations confirm that 40 candidates are definite strong lenses with multiple lensed images. The foreground-lens galaxies are found to be early-type galaxies (ETGs) at redshifts 0.06-0.44, and background sources are emission-line galaxies at redshifts 0.22-1.29. As an extension of the SLACS Survey, the S4TM Survey is the first attempt to preferentially search for strong-lens systems with relatively lower lens masses than those in the pre-existing strong-lens samples. By fitting HST data with a singular isothermal ellipsoid model, we find that the total projected mass within the Einstein radius of the S4TM strong-lens sample ranges from 3 x 10(10) M-circle dot to 2 x 10(11) M-circle dot. In Shu et al., we have derived the total stellar mass of the S4TM lenses to be 5 x 10(10) M-circle dot to 1 x 10(12) M-circle dot. Both the total enclosed mass and stellar mass of the S4TM lenses are on average almost a factor of 2 smaller than those of the SLACS lenses, which also represent the typical mass scales of the current strong-lens samples. The extended mass coverage provided by the S4TM sample can enable a direct test, with the aid of strong lensing, for transitions in scaling relations, kinematic properties, mass structure, and dark-matter content trends of ETGs at intermediate-mass scales as noted in previous studies.

第 121 条，共 286 条

Testing PSF Interpolation in Weak Lensing with Real Data

Lu, TH (Lu, Tianhuan); Zhang, J (Zhang, Jun); Dong, FY (Dong, Fuyu); Li, YK (Li, Yingke); Liu, DZ (Liu, Dezi); Fu, LP (Fu, Liping); Li, GL (Li, Guoliang); Fan, ZH (Fan, Zuhui)

ASTRONOMICAL JOURNAL
卷: 153 期: 4 文献号: 197

Reconstruction of the point-spread function (PSF) is a critical process in weak lensing measurement. We develop a real-data based and galaxy-oriented pipeline to compare the performances of various PSF reconstruction schemes. Making use of a large amount of the CFHTLenS data, the performances of three classes of interpolating schemes-polynomial, Kriging, and Shepard-are evaluated. We find that polynomial interpolations with optimal orders and domains perform the best. We quantify the effect of the residual PSF reconstruction error on shear recovery in terms of the multiplicative and additive biases, and their spatial correlations using the shear measurement method of Zhang et al. We find that the impact of PSF reconstruction uncertainty on the shear-shear correlation can be significantly reduced by cross correlating the shear estimators from different exposures. It takes only 0.2 stars (S/N greater than or similar to > 100) per square arcmin on each exposure to reach the best performance of PSF interpolation, a requirement that is satisfied in most of the CFHTlenS data.

2-04 Star Formation in Galaxies

第 122 条，共 286 条

Dense gas in low-metallicity galaxies

Braine, J (Braine, J.); Shimajiri, Y (Shimajiri, Y.); Andre, P (Andre, P.); Bontemps, S (Bontemps, S.); *Gao, Y* (Gao, Yu); Chen, H (Chen, Hao); Kramer, C (Kramer, C.)

ASTRONOMY & ASTROPHYSICS
卷: 597 文献号: A44

Stars form out of the densest parts of molecular clouds. Far-IR emission can be used to estimate the star formation rate (SFR) and high dipole moment molecules, typically HCN, trace the dense gas. A strong correlation exists between HCN and far-IR emission, with the ratio being nearly constant, over a large range of physical scales. A few recent observations have found HCN to be weak with respect to the far-IR and CO in subsolar metallicity (low-Z) objects. We present observations of the Local Group galaxies M 33, IC 10, and NGC 6822 with the IRAM 30 m and NRO 45 m telescopes, greatly improving the sample of low-Z galaxies observed. HCN, HCO+, CS, C2H, and HNC have been detected. Compared to solar metallicity galaxies, the nitrogen-bearing species are weak (HCN, HNC) or not detected (CN, HNCO, N2H+) relative to far-IR or CO emission. HCO+ and C2H emission is normal with respect to CO and far-IR. While (CO)-C-13 is the usual factor 10 weaker than (CO)-C-12, (CO)-O-18 emission was not detected down to very low levels. Including earlier data, we find that the HCN/HCO+ ratio varies with metallicity (O/H) and attribute this to the sharply decreasing nitrogen abundance. The dense gas fraction, traced by the HCN/CO and HCO+/CO ratios, follows the SFR but in the low-Z objects the HCO+ is much easier to measure. Combined with larger and smaller scale measurements, the HCO+ line appears to be an excellent tracer of dense gas and varies linearly with the SFR for both low and high metallicities.

第 123 条，共 286 条

HIFI Spectroscopy of H2O Submillimeter Lines in Nuclei of Actively Star-forming Galaxies

Liu, L (Liu, L.); Weiss, A (Weiss, A.); Perez-Beaupuits, JP (Perez-Beaupuits, J. P.); Gusten, R (Guesten, R.); Liu, D (Liu, D.); Gao, Y (Gao, Y.); Menten, KM (Menten, K. M.); van der Werf, P (van der Werf, P.); Israel, FP (Israel, F. P.); Harris, A (Harris, A.); Martin-Pintado, J (Martin-Pintado, J.); Requena-Torres, MA (Requena-Torres, M. A.); Stutzki, J (Stutzki, J.)

ASTROPHYSICAL JOURNAL
卷: 846 期: 1 文献号: 5

We present a systematic survey of multiple velocity-resolved H2O spectra using Herschel/Heterodyne Instrument for the Far Infrared (HIFI) toward nine nearby actively star-forming galaxies. The ground-state and low-excitation lines (E-up <= 130 K) show profiles with emission and absorption blended together, while absorption-free medium-excitation lines (130 K <= E-up <= 350 K) typically display line shapes similar to CO. We analyze the HIFI observation together with archival SPIRE/PACS H2O data using a state-of-the-art 3D radiative transfer code that includes the interaction between continuum and line emission. The water excitation models are combined with information on the dust and CO spectral line energy distribution to determine the physical structure of the interstellar medium (ISM). We identify two ISM components that are common to all galaxies: a warm (T-dust similar to 40-70 K), dense (n(H) similar to 10(5)-10(6) cm(-3)) phase that dominates the emission of medium-excitation H2O lines. This gas phase also dominates the far-IR emission and the CO intensities for J(up) > 8. In addition, a cold (T-dust similar to 20-30 K), dense (n(H) similar to 10(4)-10(5)cm(-3)), more extended phase is present. It outputs the emission in the low-excitation H2O lines and typically also produces the prominent line absorption features. For the two ULIRGs in our sample (Arp 220 and Mrk 231) an even hotter and more compact (R-s <= 100 pc) region is present, which is possibly linked to AGN activity. We find that collisions dominate the water excitation in the cold gas and for lines with E-up <= 300 K and E-up <= 800 K in the warm and hot component, respectively. Higher-energy levels are mainly excited by IR pumping.

第 124 条，共 286 条

ALMA Maps of Dust and Warm Dense Gas Emission in the Starburst Galaxy IC 5179

Zhao, YH (Zhao, Yinghe); Lu, NY (Lu, Nanyao); Diaz-Santos, T (Diaz-Santos, Tanio); Xu, CK (Xu, C. Kevin); Gao, Y (Gao, Yu); Charmandaris, V (Charmandaris, Vassilis); van der Werf, P (van der Werf, Paul); Zhang, ZY (Zhang, Zhi-Yu); Cao, C (Cao, Chen)

ASTROPHYSICAL JOURNAL
卷: 845 期: 1 文献号: 58

We present our high-resolution (0."15 x 0."13, similar to 34pc) observations of the CO (6-5) line emission, which probes the warm and dense molecular gas, and the 434 mu m dust continuum emission in the nuclear region of the starburst galaxy IC 5179, conducted with the Atacama Large Millimeter Array (ALMA). The CO. (6-5) emission is spatially distributed in filamentary structures with many dense cores and shows a velocity field that is characteristic of a circumnuclear rotating gas disk, with 90% of the rotation speed arising within a radius of less than or similar to 150 pc. At the scale of our spatial resolution, the CO. (6-5) and dust emission peaks do not always coincide, with their surface brightness ratio varying by a factor of similar to 10. This result suggests that their excitation mechanisms are likely different, as further evidenced by the southwest to northeast spatial gradient of both CO-to-dust continuum ratio and Pa-alpha equivalent width. Within the nuclear region (radius similar to 300 pc) and with a resolution of similar to 34 pc, the CO line flux (dust flux density) detected in our ALMA observations is 180 +/- 18 Jy km s(-1) (71 +/- 7 mJy), which accounts for 22% (2.4%) of the total value measured by Herschel.

第 125 条，共 286 条

Testing the universality of the star-formation efficiency in dense molecular gas

Shimajiri, Y (Shimajiri, Y.); Andre, P (Andre, Ph.); Braine, J (Braine, J.); Konyves, V (Koenyves, V.); Schneider, N (Schneider, N.); Bontemps, S (Bontemps, S.); Ladjelate, B (Ladjelate, B.); Roy, A (Roy, A.); *Gao, Y* (Gao, Y.); Chen, H (Chen, H.)

ASTRONOMY & ASTROPHYSICS
卷: 604 文献号: A74

Context. Recent studies with, for example, Spitzer and Herschel have suggested that star formation in dense molecular gas may be governed by essentially the same "law" in Galactic clouds and external galaxies. This conclusion remains controversial, however, in large part because different tracers have been used to probe the mass of dense molecular gas in Galactic and extragalactic studies.

Aims. We aimed to calibrate the HCN and HCO + lines commonly used as dense gas tracers in extragalactic studies and to test the possible universality of the star-formation efficiency in dense gas (greater than or similar to 10(4) cm(-3)), SFEdense.

Methods. We conducted wide-field mapping of the Aquila, Ophiuchus, and Orion B clouds at similar to 0.04 pc resolution in the J = 1-0 transition of HCN, HCO+, and their isotopomers. For each cloud, we derived a reference estimate of the dense gas mass M-Herschel(AV > 8), as well as the strength of the local far-ultraviolet (FUV) radiation field, using Herschel Gould Belt survey data products, and estimated the star-formation rate from direct counting of the number of Spitzer young stellar objects.

Results. The (HCO+)-C-13 (1-0) and (HCN)-C-13(1-0) lines were observed to be good tracers of the dense star-forming filaments detected with Herschel. Comparing the luminosities L-HCN and LHCO+ measured in the HCN and HCO+ lines with the reference masses M-Herschel(AV > 8), the empirical conversion factors alpha(Herschel-HCN) (=M-Herschel(AV > 8)/ L-HCN) and alpha(Herschel-HCO+) (=M-Herschel(AV > 8)/LHCO+) were found to be significantly anti-correlated with the local FUV strength. In agreement with a recent independent study of Orion B by Pety et al., the HCN and HCO+ lines were found to trace gas down to A(V) greater than or similar to 2. As a result, published extragalactic HCN studies must be tracing all of the moderate density gas down to n(H2) less than or similar to 10(3) cm(-3). Estimating the contribution of this moderate density gas from the typical column density probability distribution functions in nearby clouds, we obtained the following G(0)-dependent HCN conversion factor for external galaxies: alpha(fit)(Herschel)' (HCN) = 64 x G(0)(0.340). Re-estimating the dense gas masses in external galaxies with alpha(fit)(Herschel)' (HCN) (G(0)), we found that SFEdense is remarkably constant, with a scatter of less than 1.5 orders of magnitude around 4.5 x 10(-8) yr(-1), over eight orders of magnitude in dense gas mass.

Conclusions. Our results confirm that SFEdense of galaxies is quasi-universal on a wide range of scales from similar to 1-10 pc to >10 kpc. Based on the tight link between star formation and filamentary structure found in Herschel studies of nearby clouds, we argue that SFEdense is primarily set by the "microphysics" of core and star formation along filaments.

第 126 条，共 286 条

ALMA [N II] 205 mu m Imaging Spectroscopy of the Interacting Galaxy System BRI 1202-0725 at Redshift 4.7

Lu, NY (Lu, Nanyao); Zhao, YH (Zhao, Yinghe); Diaz-Santos, T (Diaz-Santos, Tanio); Xu, CK (Kevin Xu, C.); Charmandaris, V (Charmandaris, Vassilis); Gao, Y (Gao, Yu); van der Werf, PP (van der Werf, Paul P.); Privon, GC (Privon, George C.); Inami, H (Inami, Hanae); Rigopoulou, D (Rigopoulou, Dimitra); Sanders, DB (Sanders, David B.); Zhu, L (Zhu, Lei)
ASTROPHYSICAL JOURNAL LETTERS
卷: 842 期: 2 文献号: L16
We present the results from Atacama Large Millimeter/submillimeter Array imaging in the [N II] 205 mu m fine-structure line (hereafter [N II]) and the underlying continuum of BRI 1202-0725, an interacting galaxy system at z = 4.7, consisting of a quasi-stellar object (QSO), a submillimeter galaxy (SMG), and two Ly alpha emitters, all within similar to 25 kpc of the QSO. We detect the QSO and SMG in both [N II] and continuum. At the similar to 1 '' (or 6.6 kpc) resolution, both the QSO and SMG are resolved in [N II], with the de-convolved major axes of similar to 9 and similar to 14 kpc, respectively. In contrast, their continuum emissions are much more compact and unresolved even at an enhanced resolution of similar to 0 ''.7. The ratio of the [N II] flux to the existing CO(7-6) flux is used to constrain the dust temperature (T-dust) for a more accurate determination of the FIR luminosity L-FIR. Our best estimated T-dust equals 43 (+/- 2) K for both galaxies (assuming an emissivity index beta = 1.8). The resulting LCO(7-6)/LFIR ratios are statistically consistent with that of local luminous infrared galaxies, confirming that LCO(7-6) traces the star formation (SF) rate (SFR) in these galaxies. We estimate that the ongoing SF of the QSO (SMG) has an SFR of 5.1 (6.9) x 10(3) M-circle dot yr(-1) (+/- 30%) assuming Chabrier initial mass function, takes place within a diameter (at half maximum) of 1.3 (1.5) kpc, and will consume the existing 5 (5) x 10(11) M-circle dot of molecular gas in 10 (7) x 10(7) years.

第 127 条，共 286 条

Neutral Carbon Emission in Luminous Infrared Galaxies: The [CI] Lines as Total Molecular Gas Tracers

Jiao, Q (Jiao, Qian); Zhao, YH (Zhao, Yinghe); Zhu, M (Zhu, Ming); Lu, NY (Lu, Nanyao); Gao, Y (Gao, Yu); Zhang, ZY (Zhang, Zhi-Yu)
ASTROPHYSICAL JOURNAL LETTERS
卷: 840 期: 2 文献号: L18
We present a statistical study of the [C I] (P-3(1) (R) P-3(0)), [C I] (P-3(2) (R) P-3(1)) lines (hereafter [C I] (1-0) and [C I] (2-1), respectively) and the CO(1-0) line for a sample of (ultra-) luminous infrared galaxies ((U) LIRGs). We explore the correlations between the luminosities of CO(1-0) and [C I] lines, and find that L'(CO(1-0)) correlates almost linearly with both L'[C I] (1-0) and L'[C I] (2-1), suggesting that [C I] lines can trace total molecular gas mass, at least for (U) LIRGs. We also investigate the dependence of L'([C I] (1-0))/L'(CO (1-0)), L'([C I] (2-1))/L'(CO (1-0)), and L'([C I] (2-1))/L'([C I] (1-0)) on the far-infrared color of 60-to-100 mu m, and find non-correlation, a weak correlation, and a modest correlation, respectively. Under the assumption that these two carbon transitions are optically thin, we further calculate the [C I] line excitation temperatures, atomic carbon masses, and mean [C I] line flux-to-H-2 mass conversion factors for our sample. The resulting H-2 masses using these [C I]-based conversion factors roughly agree with those derived from L'(CO (1-0)) and CO-to-H-2 conversion factor.

第 128 条，共 286 条

A Herschel Space Observatory Spectral Line Survey of Local Luminous Infrared Galaxies from 194 to 671 Microns

Lu, NY (Lu, Nanyao); Zhao, YG (Zhao, Yinghe); Diaz-Santos, T (Diaz-Santos, Tanio); Xu, CK (Kevin Xu, C.); Gao, Y (Gao, Yu); Armus, L (Armus, Lee); Isaak, KG (Isaak, Kate G.); Mazzarella, JM (Mazzarella, Joseph M.); van der Werf, PP (van der Werf, Paul P.); Appleton, PN (Appleton, Philip N.); Charmandaris, V (Charmandaris, Vassilis); Evans, AS (Evans, Aaron S.); Howell, J (Howell, Justin); Iwasawa, K (Iwasawa, Kazushi); Leech, J (Leech, Jamie); Lord, S (Lord, Steven); Petric, AO (Petric, Andreea O.); Privon, GC (Privon, George C.); Sanders, DB (Sanders, David B.); Schulz, B (Schulz, Bernhard); Surace, JA (Surace, Jason A.)
ASTROPHYSICAL JOURNAL SUPPLEMENT SERIES
卷: 230 期: 1 文献号: 1
We describe a Herschel Space Observatory 194-671 mu m spectroscopic survey of a sample of 121 local luminous infrared galaxies and report the fluxes of the CO J to J-1 rotational transitions for 4 <= J <= 13, the [N II] 205 mu m line, the [C I] lines at 609 and 370 mu m, as well as additional and usually fainter lines. The CO spectral line energy distributions (SLEDs) presented here are consistent with our earlier work, which was based on a smaller sample, that calls for two distinct molecular gas components in general: (i) a cold component, which emits CO lines primarily at J less than or similar to 4 and likely represents the same gas phase traced by CO (1-0), and (ii) a warm component, which dominates over the mid-J regime (4 < J less than or similar to 10) and is intimately related to current star formation. We present evidence that the CO line emission associated with an active galactic nucleus is significant only at J > 10. The flux ratios of the two [C I] lines imply modest excitation temperatures of 15-30 K; the [C I] 370 mu m line scales more linearly in flux with CO (4-3) than with CO (7-6). These findings suggest that the [C I] emission is predominantly associated with the gas component defined in (i) above. Our analysis of the stacked spectra in different far-infrared (FIR) color bins reveals an evolution of the SLED of the rotational transitions of H2O vapor as a function of the FIR color in a direction consistent with infrared photon pumping.

第 129 条，共 286 条

HC3N observations of nearby galaxies

Jiang, XJ (Jiang, Xue-Jian); Wang, JZ (Wang, Jun-Zhi); Gao, Y (Gao, Yu); Gu, QS (Gu, Qiu-Sheng)
ASTRONOMY & ASTROPHYSICS
卷: 600 文献号: A15
Aims. We aim to systematically study the properties of the different transitions of the dense molecular gas tracer HC3N in galaxies.
Methods. We have conducted single-dish observations of HC3N emission lines towards a sample of nearby gas-rich galaxies. HC3N(J = 2-1) was observed in 20 galaxies with the Effelsberg 100-m telescope. HC3N(J = 24-23) was observed in nine galaxies with the 10-m Submillimeter Telescope (SMT).
Results. HC3N 2-1 is detected in three galaxies: IC 342, M 66, and NGC 660 (>3 sigma). HC3N 24-23 is detected in three galaxies: IC 342, NGC 1068, and IC 694. These are the first measurements of HC3N 2-1 in a relatively large sample of

external galaxies, although the detection rate is low. For the HC3N 2-1 non-detections, upper limits (2 sigma) are derived for each galaxy, and stacking the non-detections is attempted to recover the weak signal of HC3N. The stacked spectrum, however, does not show any significant signs of HC3N 2-1 emission. The results are also compared with other transitions of HC3N observed in galaxies.
Conclusions. The low detection rate of both transitions suggests low abundance of HC3N in galaxies, which is consistent with other observational studies. The comparison between HC3N and HCN or HCO+ shows a large diversity in the ratios between HC3N and HCN or HCO+. More observations are needed to interpret the behavior of HC3N in different types of galaxies.

第 130 条，共 286 条

Dense Gas in the Outer Spiral Arm of M51

Chen, H (Chen, Hao); Braine, J (Braine, Jonathan); Gao, Y (Gao, Yu); Koda, J (Koda, Jin); Gu, QS (Gu, Qiusheng)
ASTROPHYSICAL JOURNAL
卷: 836 期: 1 文献号: 101
There is a linear relation between the mass of dense gas traced by the HCN(1- 0) luminosity and the star formation rate (SFR) traced by the far-infrared luminosity. Recent observations of galactic disks have shown some systematic variations. In order to explore the SFR-dense gas link at high resolution (similar to 4 '', similar to 150 pc) in the outer disk of an external galaxy, we have mapped a region about 5 kpc from the center along the northern spiral arm of M51 in the HCN(1- 0), HCO+(1- 0), and HNC(1- 0) emission lines using the Northern Extended Millimeter Array interferometer. The HCN and HCO+ lines were detected in six giant molecular associations (GMAs), while HNC emission was only detected in the two brightest GMAs. One of the GMAs hosts a powerful H II region, and HCN is stronger than HCO+ there. Comparing observations of GMAs in the disks of M31 and M33 at similar angular resolution (similar to 100 pc), we find that GMAs in the outer disk of M51 are brighter in both the HCN and the HCO+ lines by a factor of 3, on average. However, the I-HCN /I-CO and I-HCO(+) /I-CO ratios are similar to the ratios in nearby galactic disks and the Galactic plane. Using the Herschel 70 mu m data to trace the total IR luminosity at the resolution of the GMAs, we find that both the LIR/LHCN and LIR/LHCO+ relations in the outer disk GMAs are consistent with the proportionality between the LIR and the dense gas mass established globally in galaxies within the scatter. The IR/HCN and IR/HCO+ ratios of the GMAs vary by a factor of 3, probably depending on whether massive stars are forming.

第 131 条，共 286 条

Extinction Correction Significantly Influences the Estimate of the Ly alpha Escape Fraction

An, FX (An, Fang Xia); Zheng, XZ (Zheng, Xian Zhong); Hao, CN (Hao, Cai-Na); Huang, JS (Huang, Jia-Sheng); Xia, XY (Xia, Xiao-Yang)
ASTROPHYSICAL JOURNAL
卷: 835 期: 2 文献号: 116
The Ly alpha escape fraction is a key measure to constrain the neutral state of the intergalactic medium and then to understand how the universe was fully reionized. We combine deep narrowband imaging data from the custom-made filter NB393 and the H2S1 filter centered at 2.14 mu m to examine the Ly alpha emitters and H alpha emitters at the same redshift z - 2.24. The combination of these two populations allows us to determine the Ly alpha escape fraction at z = 2.24. Over an area of 383 arcmin(2) in the Extended Chandra Deep Field South (ECDFS), 124 Ly alpha emitters are detected down to NB393 = 26.4 mag at the 5 sigma level, and 56 H alpha emitters come from An et al. Of these, four have both Ly alpha and H alpha emissions (LAHAEs). We also collect the Ly alpha emitters and H alpha emitters at z = 2.24 in the COSMOS field from the literature, and increase the number of LAHAEs to 15 in total. About one-third of them are AGNs. We measure the individual/volumetric Ly alpha escape fraction by comparing the observed Ly alpha luminosity/luminosity density to the extinction-corrected Ha luminosity/luminosity density. We revisit the extinction correction for H alpha emitters using the Galactic extinction law with color excess for nebular emission. We also adopt the Calzetti extinction law together with an identical color excess for stellar and nebular regions to explore how the uncertainties in extinction correction affect the estimate of individual and global Ly alpha escape fractions. In both cases, an anti-correlation between the Ly alpha escape fraction and dust attenuation is found among the LAHAEs, suggesting that dust absorption is responsible for the suppression of the escaping Ly alpha photons. However, the estimated Ly alpha escape fraction of individual LAHAEs varies by up to similar to 3 percentage points between the two methods of extinction correction. We find the global Ly alpha escape fraction at z = 2.24 to be (3.7 +/- 1.4)% in the ECDFS. The variation in the color excess of the extinction causes a discrepancy of similar to 1 percentage point in the global Ly alpha escape fraction.

第 132 条，共 286 条

High Dense Gas Fraction in Intensely Star-forming Dusty Galaxies

Oteo, I (Oteo, I.); *Zhang, ZY* (Zhang, Z-Y.); Yang, C (Yang, C.); Ivison, RJ (Ivison, R. J.); Omont, A (Omont, A.); Bremer, M (Bremer, M.); Bussmann, S (Bussmann, S.); Cooray, A (Cooray, A.); Cox, P (Cox, P.); Dannerbauer, H (Dannerbauer, H.); Dunne, L (Dunne, L.); Eales, S (Eales, S.); Furlanetto, C (Furlanetto, C.); Gavazzi, R (Gavazzi, R.); Gao, Y (Gao, Y.); Greve, TR (Greve, T. R.); Nayyeri, H (Nayyeri, H.); Negrello, M (Negrello, M.); Neri, R (Neri, R.); Riechers, D (Riechers, D.); Tunnard, R (Tunnard, R.); Wagg, J (Wagg, J.); Van der Werf, P (Van der Werf, P.)
ASTROPHYSICAL JOURNAL
卷: 850 期: 2 文献号: 170
We present ALMA J = 3-2 and VLA J = 1-0 observations of the dense molecular gas tracers HCN, HCO+, and HNC in two lensed, high-redshift starbursts selected from the Herschel-ATLAS survey: H-ATLAS J090740.0 -004200 (SDP.9, z(spec) = 1.575) and H-ATLAS J091043.1-000321 (SDP.11, z(spec) = 1.786). In SDP.9 we have detected all J = 3-2 transitions and also HCN(1-0) and HCO+(1-0). In SDP.11 we have detected HCN(3-2) and HCO+(3-2). The amplification factors for both galaxies have been determined from subarcsecond-resolution CO and dust emission observations carried out with NOEMA and the SMA. The HNC(1-0)/HCN(1-0) line ratio in SDP.9 suggests the presence of photon-dominated regions, as happens in most local (U)LIRGs. The CO, HCN, and HCO+ spectral line energy distribution (SLEDs) of SDP. 9 are compatible to those found for many local, IR-bright galaxies, indicating that the molecular gas in local and high-redshift dusty starbursts can

have similar excitation conditions. We obtain that the correlation between total IR (L-IR) and dense line (L-dense) luminosity in SDP.9 and SDP.11 and local star-forming galaxies can be represented by a single relation. We argue that the scatter of the L-IR-L-dense correlation, together with the lack of sensitive dense molecular gas tracer observations for a homogeneous sample of high-redshift galaxies, prevents us from distinguishing differential trends with redshift. Our results suggest that the intense star formation found in some high-redshift, dusty, luminous starbursts is associated with more massive dense molecular gas reservoirs and higher dense molecular gas fractions.

第 133 条，共 286 条

VALES: IV. Exploring the transition of star formation efficiencies between normal and starburst galaxies using APEX/SEPIA Band-5 and ALMA at low redshift

C Cheng ， E Ibar ， TM Hughes ， V Villanueva ， R Leiton
In this work we present new APEX/SEPIA Band-5 observations targeting the CO ($J=2\text{-}1$) emission line of 24 Herschel-detected galaxies at $z=0.1-0.2$. Combining this sample {with} our recent new Valpara\'iso ALMA Line Emission Surve...

第 134 条，共 286 条

Molecular gas in the Herschel-selected strongly lensed submillimeter galaxies at z 2-4 as probed by multi-J CO lines

C Yang ， A Omont ， A Beelen ， Y Gao ， PVD Werf
Astronomy & Astrophysics, 2017 , 608
We present the IRAM-30 m observations of multiple-J CO (Jup mostly from 3 up to 8) and [C I](3P2 → 3P1) ([C I](2–1) hereafter) line emissi...

第 135 条，共 286 条

Molecular gas in the Herschel-selected strongly lensed submillimeter galaxies at z similar to 2-4 as probed by multi-J CO lines

Yang, C (Yang, C.); Omont, A (Omont, A.); Beelen, A (Beelen, A.); Gao, Y (Gao, Y.); van der Werf, P (van der Werf, P.); Gavazzi, R (Gavazzi, R.); Zhang, ZY (Zhang, Z. -Y.); Ivison, R (Ivison, R.); Lehnert, M (Lehnert, M.); Liu, D (Liu, D.); Oteo, I (Oteo, I.); Gonzalez-Alfonso, E (Gonzalez-Alfonso, E.); Dannerbauer, H (Dannerbauer, H.); Cox, P (Cox, P.); Krips, M (Krips, M.); Neri, R (Neri, R.); Riechers, D (Riechers, D.); Baker, AJ (Baker, A. J.); Michalowski, MJ (Michalowski, M. J.); Cooray, A (Cooray, A.); Smail, I (Smail, I.)
ASTRONOMY & ASTROPHYSICS
卷: 608 文献号: A144
We present the IRAM-30m observations of multiple-J CO (J(up) mostly from 3 up to 8) and [CI](P-3(2) -> P-3(1)) ([CI](2-1) hereafter) line emission in a sample of redshift similar to 2-4 submillimeter galaxies (SMGs). These SMGs are selected among the brightest-lensed galaxies discovered in the Herschel-Astrophysical Terahertz Large Area Survey (H-ATLAS). Forty-seven CO lines and 7 [CI](2-1) lines have been detected in 15 lensed SMGs. A non-negligible effect of differential lensing is found for the CO emission lines, which could have caused significant underestimations of the linewidths, and hence of the dynamical masses. The CO spectral line energy distributions (SLEDs), peaking around J(up) similar to 5-7, are found to be similar to those of the local starburst-dominated ultra-luminous infrared galaxies and of the previously studied SMGs. After correcting for lensing amplification, we derived the global properties of the bulk of molecular gas in the SMGs using non-LTE radiative transfer modelling, such as the molecular gas density n(H2) similar to 10(2.5)-10(4.1) cm(-3) and the kinetic temperature T-k similar to 20-750 K. The gas thermal pressure P-th ranging from similar to 10(5) Kcm(-3) to 10(6) Kcm(-3) is found to be correlated with star formation efficiency. Further decomposing the CO SLEDs into two excitation components, we find a low-excitation component with n(H2) similar to 10(2.8)-10(4.6) cm(-3) and T-k similar to 20-30 K, which is less correlated with star formation, and a high-excitation one (n(H2) similar to 10(2.7)-10(4.2) cm(-3), T-k similar to 60-400 K) which is tightly related to the on-going star-forming activity. Additionally, tight linear correlations between the far-infrared and CO line luminosities have been confirmed for the J(up) >= 5 CO lines of these SMGs, implying that these CO lines are good tracers of star formation. The [C I](2-1) lines follow the tight linear correlation between the luminosities of the [C I](2-1) and the CO(1-0) line found in local starbursts, indicating that [C I] lines could serve as good total molecular gas mass tracers for high-redshift SMGs as well. The total mass of the molecular gas reservoir, (1-30) x 10(10) M circle dot, derived based on the CO(3-2) fluxes and alpha(CO(1-0)) = 0.8 M circle dot (K km s(-1) pc(2))(-1), suggests a typical molecular gas depletion time t(dep) similar to 20-100 Myr and a gas to dust mass ratio delta(GDR) similar to 30-100 with similar to 20%-60% uncertainty for the SMGs. The ratio between CO line luminosity and the dust mass L'(CO)/M-dust appears to be slowly increasing with redshift for high-redshift SMGs, which need to be further confirmed by a more complete SMG sample at various redshifts. Finally, through comparing the linewidth of CO and H2O lines, we find that they agree well in almost all our SMGs, confirming that the emitting regions of the CO and H2O lines are co-spatially located.

第 136 条，共 286 条

Molecular gas in the Herschel-selected strongly lensed submillimeter galaxies at z similar to 2-4 as probed by multi-J CO lines

Yang, C (Yang, C.); Omont, A (Omont, A.); Beelen, A (Beelen, A.); Gao, Y (Gao, Y.); van der Werf, P (van der Werf, P.); Gavazzi, R (Gavazzi, R.); Zhang, ZY (Zhang, Z. -Y.); Ivison, R (Ivison, R.); Lehnert, M (Lehnert, M.); Liu, D (Liu, D.); Oteo, I (Oteo, I.); Gonzalez-Alfonso, E (Gonzalez-Alfonso, E.); Dannerbauer, H (Dannerbauer, H.); Cox, P (Cox, P.); Krips, M (Krips, M.); Neri, R (Neri, R.); Riechers, D (Riechers, D.); Baker, AJ (Baker, A. J.); Michalowski, MJ (Michalowski, M. J.); Cooray, A (Cooray, A.); Smail, I (Smail, I.)
ASTRONOMY & ASTROPHYSICS
卷: 608 文献号: A144
We present the IRAM-30m observations of multiple-J CO (J(up) mostly from 3 up to 8) and [CI](P-3(2) -> P-3(1)) ([CI](2-1) hereafter) line emission in a sample of redshift similar to 2-4 submillimeter galaxies (SMGs). These SMGs are selected among the brightest-lensed galaxies discovered in the Herschel-Astrophysical Terahertz Large Area Survey (H-ATLAS). Forty-seven CO lines and 7 [CI](2-1) lines have been detected in 15 lensed SMGs. A non-negligible effect of differential lensing is found for the CO emission lines, which could have caused significant underestimations of the

linewidths, and hence of the dynamical masses. The CO spectral line energy distributions (SLEDs), peaking around J(up) similar to 5-7, are found to be similar to those of the local starburst-dominated ultra-luminous infrared galaxies and of the previously studied SMGs. After correcting for lensing amplification, we derived the global properties of the bulk of molecular gas in the SMGs using non-LTE radiative transfer modelling, such as the molecular gas density n(H2) similar to 10(2.5)-10(4.1) cm(-3) and the kinetic temperature T-k similar to 20-750 K. The gas thermal pressure P-th ranging from similar to 10(5) Kcm(-3) to 10(6) Kcm(-3) is found to be correlated with star formation efficiency. Further decomposing the CO SLEDs into two excitation components, we find a low-excitation component with n(H2) similar to 10(2.8)-10(4.6) cm(-3) and T-k similar to 20-30 K, which is less correlated with star formation, and a high-excitation one (n(H2) similar to 10(2.7)-10(4.2) cm(-3), T-k similar to 60-400 K) which is tightly related to the on-going star-forming activity. Additionally, tight linear correlations between the far-infrared and CO line luminosities have been confirmed for the J(up) >= 5 CO lines of these SMGs, implying that these CO lines are good tracers of star formation. The [C I](2-1) lines follow the tight linear correlation between the luminosities of the [C I](2-1) and the CO(1-0) line found in local starbursts, indicating that [C I] lines could serve as good total molecular gas mass tracers for high-redshift SMGs as well. The total mass of the molecular gas reservoir, (1-30) x 10(10) M circle dot, derived based on the CO(3-2) fluxes and alpha(CO(1-0)) = 0.8 M circle dot (K km s(-1) pc(2))(-1), suggests a typical molecular gas depletion time t(dep) similar to 20-100 Myr and a gas to dust mass ratio delta(GDR) similar to 30-100 with similar to 20%-60% uncertainty for the SMGs. The ratio between CO line luminosity and the dust mass L'(CO)/M-dust appears to be slowly increasing with redshift for high-redshift SMGs, which need to be further confirmed by a more complete SMG sample at various redshifts. Finally, through comparing the linewidth of CO and H2O lines, we find that they agree well in almost all our SMGs, confirming that the emitting regions of the CO and H2O lines are co-spatially located.

第 137 条，共 286 条

Homologous Circular-ribbon Flares Driven by Twisted Flux Emergence

Xu, Z (Xu, Z.); Yang, K (Yang, K.); Guo, Y (Guo, Y.); Zhao, J (Zhao, J.); Zhao, ZJ (Zhao, Z. J.); Kashapova, L (Kashapova, L.)
ASTROPHYSICAL JOURNAL
卷: 851 期: 1 文献号: 30
In this paper, we report two homologous circular-ribbon flares associated with two filament eruptions. They were well observed by the New Vacuum Solar Telescope and the Solar Dynamics Observatory on 2014 March 5. Prior to the flare, two small-scale filaments enclosed by a circular pre-flare brightening lie along the circular polarity inversion line around the parasitic polarity, which has shown a continuous rotation since its first appearance. Two filaments eventually erupt in sequence associated with two homologous circular-ribbon flares and display an apparent writhing signature. Supplemented by the nonlinear force-free field extrapolation and the magnetic field squashing factor investigation, the following are revealed. (1) This event involves the emergence of magnetic flux ropes into a pre-existing polarity area, which yields the formation of a 3D null-point topology in the corona. (2) Continuous input of the free energy in the form of a flux rope from beneath the photosphere may drive a breakout-type reconnection occurring high in the corona, supported by the pre-flare brightening. (3) This initiation reconnection could release the constraint on the flux rope and trigger the MHD instability to first make filament F1 lose equilibrium. The subsequent more violent magnetic reconnection with the overlying flux is driven during the filament rising. In return, the eruption of filament F2 is further facilitated by the reduction of the magnetic tension force above. These two processes form a positive feedback to each other to cause the energetic mass eruption and flare.

2-05 Molecular Clouds and Star Formation

第 138 条，共 286 条

A simple criterion for selecting disks with evidence for dust growth and settling

Liu, Y (Liu, Yao); Wang, HC (Wang, Hongchi); Henning, T (Henning, Thomas)
ASTROPHYSICS AND SPACE SCIENCE
卷: 362 期: 11 文献号: 208
Dust growth and settling, as an initial step of planet formation in protoplanetary disks, have an important impact on the appearance of the spectral energy distribution (SED). Selecting a promising sample of disks with signs of these processes helps to guide future observations towards a better understanding of the initial conditions for planet formation and disk evolution. Using a standard flared disk model, we conducted a large parameter study to investigate the effects of various disk parameters on the overall shape of the SED. We found that the flaring index and scale height can be used to mimic the effects of dust evolution on the SED. The influences of these two parameters on the infrared excess are very similar to that caused by dust evolution which have been shown in previous simulations where grain growth and settling are treated directly. Based on a statistic analysis of all the models in our grid, we proposed a criterion of Psi >= 0.6 to diagnose signs of dust evolution, where Psi is a ratio defined by dividing a linearly interpolated (between 24 mu m and 1.3 mm) flux at 70 mu m by the observed 70 mu m photometry. We tested the applicability of our criterion with the class II disks in the Taurus star formation region.

第 139 条，共 286 条

Kinetic temperature of massive star-forming molecular clumps measured with formaldehyde III. The Orion molecular cloud 1

Tang, XD (Tang, X. D.); Henkel, C (Henkel, C.); Menten, KM (Menten, K. M.); Wyrowski, F (Wyrowski, F.); Brinkmann, N (Brinkmann, N.); Zheng, XW (Zheng, X. W.); Gong, Y (Gong, Y.); Lin, YX (Lin, Y. X.); Esimbek, J (Esimbek, J.); Zhou, JJ (Zhou, J. J.); Yuan, Y (Yuan, Y.); Li, DL (Li, D. L.); He, YX (He, Y. X.)
ASTRONOMY & ASTROPHYSICS
卷: 609 文献号: A16
We mapped the kinetic temperature structure of the Orion molecular cloud 1 (OMC-1) with para-H2CO(J(KaKc) = 3(03)-2(02), 3(22)- 2(21), and 3(21)-2(20)) using the APEX 12m telescope. This is compared with the temperatures derived

from the ratio of the NH3 (2, 2)/(1, 1) inversion lines and the dust emission. Using the RADEX non-LTE model, we derive the gas kinetic temperature modeling the measured averaged line ratios of para-H(2)CO3(22)-2(21)/3(03)-2(02) and 3(21)-2(20)/3(03)-2(02). The gas kinetic temperatures derived from the para-H(2)COline ratios are warm, ranging from 30 to > 200K with an average of 62 +/- 2K at a spatial density of 105 cm(-3). These temperatures are higher than those obtained from NH3 (2, 2) /(1, 1) and CH3CCH(6-5) in the OMC-1 region. The gas kinetic temperatures derived from para-H2CO agree with those obtained from warm dust components measured in the mid infrared (MIR), which indicates that the para-H2CO(3-2) ratios trace dense and warm gas. The cold dust components measured in the far infrared (FIR) are consistent with those measured with NH3 (2, 2) /(1, 1) and the CH3CCH(6-5) line series. With dust at MIR wavelengths and para-H2CO(3-2) on one side, and dust at FIR wavelengths, NH3 (2, 2) /(1, 1), and CH3CCH(6-5) on the other, dust and gas temperatures appear to be equivalent in the dense gas (n(H-2) greater than or similar to 104 cm 3) of the OMC-1 region, but provide a bimodal distribution, one more directly related to star formation than the other. The non-thermal velocity dispersions of para-H2CO are positively correlated with the gas kinetic temperatures in regions of strong non-thermal motion (Mach number > greater than or similar to 2 : 5) of the OMC-1, implying that the higher temperature traced by para-H2CO is related to turbulence on a similar to 0.06 pc scale. Combining the temperature measurements with para-H2CO and NH3 (2, 2) /(1, 1) line ratios, we find direct evidence for the dense gas along the northern part of the OMC-1 10 km s(-1) filament heated by radiation from the central Orion nebula.

第 140 条，共 286 条

L1188: A Promising Candidate for Cloud-Cloud Collisions Triggering the Formation of Low-and Intermediate-mass Stars

Gong, Y (Gong, Yan); Fang, M (Fang, Min); Mao, RQ (Mao, Ruiqing); Zhang, SB (Zhang, Shaobo); Wang, Y (Wang, Yuan); Su, Y (Su, Yang); Chen, XP (Chen, Xuepeng); Yang, J (Yang, Ji); Wang, HC (Wang, Hongchi); Lu, DR (Lu, Dengrong)
ASTROPHYSICAL JOURNAL LETTERS
卷: 835 期: 1 文献号: L14
We present a new large-scale (2 degrees x 2 degrees) simultaneous (CO)-C-12, (CO)-C-13, and (CO)-O-18 (J = 1-0) mapping of L1188 with the Purple Mountain Observatory 13.7 m telescope. Our observations have revealed that L1188 consists of two nearly orthogonal filamentary molecular clouds at two clearly separated velocities. Toward the intersection showing large velocity spreads, we find several bridging features connecting the two clouds in velocity, and an open arc structure that exhibits high excitation temperatures, enhanced (CO)-C-12 and (CO)-C-13 emission, and broad (CO)-C-12 line wings. This agrees with the scenario that the two clouds are colliding with each other. The distribution of young stellar object (YSO) candidates implies an enhancement of star formation in the intersection of the two clouds. We suggest that a cloud-cloud collision happened in L1188 about 1 Myr ago, possibly triggering the formation of low-and intermediate-mass YSOs in the intersection.

第 141 条，共 286 条

On the local stellar populations

Fuhrmann, K (Fuhrmann, Klaus); Chini, R (Chini, Rolf); Kaderhandt, L (Kaderhandt, Lena); *Chen, ZW* (Chen, Zhiwei)
MONTHLY NOTICES OF THE ROYAL ASTRONOMICAL SOCIETY
卷: 464 期: 3 页: 2610-2621
We present a study of the local stellar populations from a volume-complete all-sky survey of the about 500 bright stars with distances less than 25 pc and down to main-sequence effective temperatures T-eff >= 5300 K. The sample is dominated by a 93 per cent fraction of Population I stars, only 22 sources (5 per cent) are Population II stars, and 9 sources (2 per cent) are intermediate-disc stars. No source belongs to the halo. By following the mass of the stars instead of their light, the resulting subset of 136 long-lived stars distributes as 22 (16.2 per cent): 6 (4.4 per cent): 108 (79.4 per cent) for the Population II: intermediate disc: Population I, respectively. Along with the much larger scaleheight reached by Population II, this unbiased census of long-lived stars provides plain evidence for a starburst epoch in the early Milky Way, with the formation of a massive, rotationally supported, and dark Population II. The same conclusion arises from the substantial early chemical enrichment levels, exemplified here by the elements magnesium and iron, as it arises also from the local Population II white dwarfs. The kinematics, metallicity distribution functions, star formation rates, age-metallicity relations, the inventory of young stars, and the occurrence of blue straggler stars are discussed. A potentially new aspect of the survey is the possibility for substructure among the local Population II stars that may further subdivide into metal-poor and metal-rich sources.

第 142 条，共 286 条

The barium-to-iron enrichment versus age relation of ancient disc stars

Fuhrmann, K (Fuhrmann, K.); Chini, R (Chini, R.); Kaderhandt, L (Kaderhandt, L.); *Chen, Z* (Chen, Z.); Lachaume, R (Lachaume, R.)
MONTHLY NOTICES OF THE ROYAL ASTRONOMICAL SOCIETY
卷: 471 期: 3 页: 3768-3774
We report an intrinsically precise relation of the barium-to-iron enrichment as a function of age for a local, volume-complete (N = 30) sample of ancient Population II (tau >= 12 Gyr) and intermediate-disc stars (tau similar or equal to 10 Gyr), which suggests a common, r-process-dominated nucleosynthesis site for both elements in the early stages of the Milky Way. Deviants from this empirical relation are to a large extent identified as formerly known or new blue straggler stars. We report in particular the striking case of the Population II star HD159062, whose barium overabundance is difficult to explain without wind accretion of s-process material from a former asymptotic giant branch (AGB) primary that very likely survived as a white dwarf companion. The weak but significant barium enhancement that we measure for HR3578 and 104 Tau also suggests that both may be accompanied by faint degenerate companions. If confirmed through precision astrometry or direct imaging observations, this would mean a very efficient method to uncover ancient stellar remnant companions around solar-type stars.

第 143 条，共 286 条

SiS in the Circumstellar Envelope of IRC+10216: Maser and Quasi-thermal Emission

Gong, Y (Gong, Y.); Henkel, C (Henkel, C.); Ott, J (Ott, J.); Menten, KM (Menten, K. M.); Morris, MR (Morris, M. R.); Keller, D (Keller, D.); Claussen, MJ (Claussen, M. J.); Grasshoff, M (Grasshoff, M.); Mao, RQ (Mao, R. Q.)
ASTROPHYSICAL JOURNAL
卷: 843 期: 1 文献号: 54
We present new Effelsberg 100-m, Australia Telescope Compact Array (ATCA), and Very Large Array observations of rotational SiS transitions in the circumstellar envelope (CSE) of IRC +10216. Thanks to the high angular resolution achieved by the ATCA observations, we unambiguously confirm that the molecule's J= 1 (R) 0 transition exhibits maser action in this CSE, as first suggested more than 30 years ago. The maser emission's radial velocity, peaking at a local standard of rest velocity of -39.862 +/- 0.065 km s-1, indicates that it arises from an almost fully accelerated shell. Monitoring observations show time variability of the SiS (1 (R) 0) maser. The two lowest-J SiS quasi-thermal emission lines trace a much more extended emitting region than previous high-J SiS observations. Their distributions show that the SiS quasi-thermal emission consists of two components: one is very compact (radius < 1."5, corresponding to <3 x 10(15) cm), and the other extends out to a radius >11''. An incomplete shell-like structure is found in the northeast, which is indicative of existing SiS shells. Clumpy structures are also revealed in this CSE. The gain of the SiS (1 (R) 0) maser (optical depths of about -5 at the blueshifted side and, assuming inversion throughout the entire line's velocity range, about -2 at the redshifted side) suggests that it is unsaturated. The SiS (1 (R) 0) maser can be explained in terms of ro-vibrational excitation caused by infrared pumping, and we propose that infrared continuum emission is the main pumping source.

第 144 条，共 286 条

First Results from BISTRO: A SCUBA-2 Polarimeter Survey of the Gould Belt

Ward-Thompson, D (Ward-Thompson, Derek); Pattle, K (Pattle, Kate); Bastien, P (Bastien, Pierre); Furuya, RS (Furuya, Ray S.); Kwon, W (Kwon, Woojin); Lai, SP (Lai, Shih-Ping); Qiu, KP (Qiu, Keping); Berry, D (Berry, David); Choi, M (Choi, Minho); Coude, S (Coude, Simon); Di Francesco, J (Di Francesco, James); Hoang, T (Hoang, Thiem); Franzmann, E (Franzmann, Erica); Friberg, P (Friberg, Per); Graves, SF (Graves, Sarah F.); Greaves, JS (Greaves, Jane S.); Houde, M (Houde, Martin); Johnstone, D (Johnstone, Doug); Kirk, JM (Kirk, Jason M.); Koch, PM (Koch, Patrick M.); Kwon, J (Kwon, Jungmi); Lee, CW (Lee, Chang Won); *Li, D* (Li, Di); Matthews, BC (Matthews, Brenda C.); Mottram, JC (Mottram, Joseph C.); Parsons, H (Parsons, Harriet); Pon, A (Pon, Andy); Rao, R (Rao, Ramprasad); Rawlings, M (Rawlings, Mark); Shinnaga, H (Shinnaga, Hiroko); Sadavoy, S (Sadavoy, Sarah); van Loo, S (van Loo, Sven); Aso, Y (Aso, Yusuke); Byun, DY (Byun, Do-Young); Eswaraiah, C (Eswaraiah, Chakali); Chen, HR (Chen, Huei-Ru); Chen, MCY (Chen, Mike C. -Y.); Chen, WP (Chen, Wen Ping); Ching, TC (Ching, Tao-Chung); Cho, J (Cho, Jungyeon); Chrysostomou, A (Chrysostomou, Antonio); Chung, EJ (Chung, Eun Jung); Doi, YS (Doi, Yasuo); Drabek-Maunder, E (Drabek-Maunder, Emily); Eyres, SPS (Eyres, Stewart P. S.); Fiege, J (Fiege, Jason); Friesen, RK (Friesen, Rachel K.); Fuller, G (Fuller, Gary); Gledhill, T (Gledhill, Tim); Griffin, MJ (Griffin, Matt J.); Gu, QL (Gu, Qilao); Hasegawa, T (Hasegawa, Tetsuo); Hatchell, J (Hatchell, Jennifer); Hayashi, SS (Hayashi, Saeko S.); Holland, W (Holland, Wayne); Inoue, T (Inoue, Tsuyoshi); Inutsuka, S (Inutsuka, Shu-ichiro); Iwasaki, K (Iwasaki, Kazunari); Jeong, IG (Jeong, Il-Gyo); Kang, JH (Kang, Ji-hyun); Kang, M (Kang, Miju); Kang, SJ (Kang, Sung-ju); Kawabata, KS (Kawabata, Koji S.); Kemper, F (Kemper, Francisca); Kim, G (Kim, Gwanjeong); Kim, J (Kim, Jongsoo); Kim, KT (Kim, Kee-Tae); Kim, KH (Kim, Kyoung Hee); Kim, MR (Kim, Mi-Ryang); Kim, S (Kim, Shinyoung); Lacaille, KM (Lacaille, Kevin M.); Lee, JE (Lee, Jeong-Eun); Lee, SS (Lee, Sang-Sung); Li, DL (Li, Dalei); Li, HB (Li, Hua-bai); Liu, HL (Liu, Hong-Li); Liu, JH (Liu, Junhao); Liu, SY (Liu, Sheng-Yuan); Liu, T (Liu, Tie); Lyo, AR (Lyo, A-Ran); Mairs, S (Mairs, Steve); Matsumura, M (Matsumura, Masafumi); Moriarty-Schieven, GH (Moriarty-Schieven, Gerald H.); Nakamura, F (Nakamura, Fumitaka); Nakanishi, H (Nakanishi, Hiroyuki); Ohashi, N (Ohashi, Nagayoshi); Onaka, T (Onaka, Takashi); Peretto, N (Peretto, Nicolas); Pyo, TS (Pyo, Tae-Soo); Qian, L (Qian, Lei); Retter, B (Retter, Brendan); Richer, J (Richer, John); Rigby, A (Rigby, Andrew); Robitaille, JF (Robitaille, Jean-Francois); Savini, G (Savini, Giorgio); Scaife, AMM (Scaife, Anna M. M.); Soam, A (Soam, Archana); Tamura, M (Tamura, Motohide); Tang, YW (Tang, Ya-Wen); Tomisaka, K (Tomisaka, Kohji); Wang, HC (Wang, Hongchi); Wang, JW (Wang, Jia-Wei); Whitworth, AP (Whitworth, Anthony P.); Yen, HW (Yen, Hsi-Wei); Yoo, H (Yoo, Hyunju); Yuan, JH (Yuan, Jinghua); Zhang, CP (Zhang, Chuan-Peng); Zhang, GY (Zhang, Guoyin); Zhou, JJ (Zhou, Jianjun); Zhu, L (Zhu, Lei); Andre, P (Andre, Philippe); Dowell, CD (Dowell, C. Darren); Falle, S (Falle, Sam); Tsukamoto, Y (Tsukamoto, Yusuke)
ASTROPHYSICAL JOURNAL
卷: 842 期: 1 文献号: 66
We present the first results from the B-fields In STar-forming Region Observations (BISTRO) survey, using the Sub-millimetre Common-User Bolometer Array. 2 camera, with its associated polarimeter (POL-2), on the James Clerk Maxwell Telescope in Hawaii. We discuss the survey's aims and objectives. We describe the rationale behind the survey, and the questions that. the survey will aim to answer. The most important of these is the role of magnetic fields in the star formation process on the scale of individual filaments and cores in dense regions. We describe the data acquisition and reduction processes for POL-2, demonstrating both repeatability and consistency with previous data. We present a first-look analysis of the first results from the BISTRO survey in the OMC 1 region. We see that the magnetic field lies approximately perpendicular to the famous "integral filament" in the densest regions of that filament. Furthermore, we see an "hourglass" magnetic field morphology extending beyond the densest region of the integral filament into the less-dense surrounding material, and discuss possible causes for this. We also discuss the more complex morphology seen along the Orion Bar region. We examine the morphology of the field along the lower-density northeastern filament. We find consistency with previous theoretical models that predict magnetic fields lying parallel to low-density, non-self-gravitating filaments, and perpendicular to higher-density, self-gravitating filaments.

第 145 条，共 286 条

First Millimeter Detection of the Disk around a Young, Isolated, Planetary-mass Object

Bayo, A (Bayo, Amelia); Joergens, V (Joergens, Viki); *Liu, Y* (Liu, Yao); Brauer, R (Brauer, Robert); Olofsson, J (Olofsson,

Johan); Arancibia, J (Arancibia, Javier); Pinilla, P (Pinilla, Paola); Wolf, S (Wolf, Sebastian); Ruge, JP (Ruge, Jan Philipp); Henning, T (Henning, Thomas); Natta, A (Natta, Antonella); Johnston, KG (Johnston, Katharine G.); Bonnefoy, M (Bonnefoy, Mickael); Beuther, H (Beuther, Henrik); Chauvin, G (Chauvin, Gael)
ASTROPHYSICAL JOURNAL LETTERS
卷: 841 期: 1 文献号: L11
OTS44 is one of only four free-floating planets known to have a disk. We have previously shown that it is the coolest and least massive known free-floating planet (similar to 12 M-Jup) with a substantial disk that is actively accreting. We have obtained Band 6 (233 GHz) ALMA continuum data of this very young disk-bearing object. The data show a clear unresolved detection of the source. We obtained disk-mass estimates via empirical correlations derived for young, higher-mass, central (substellar) objects. The range of values obtained are between 0.07 and 0.63 M-circle plus (dust masses). We compare the properties of this unique disk with those recently reported around higher-mass (brown dwarfs) young objects in order to infer constraints on its mechanism of formation. While extreme assumptions on dust temperature yield disk-mass values that could slightly diverge from the general trends found for more massive brown dwarfs, a range of sensible values provide disk masses compatible with a unique scaling relation between M-dust and M* through the substellar domain down to planetary masses.

第 146 条，共 286 条

NGC 1980 Is Not a Foreground Population of Orion: Spectroscopic Survey of Young Stars with Low Extinction in Orion

Fang, M (Fang, Min); Kim, JS (Kim, Jinyoung Serena); Pascucci, I (Pascucci, Ilaria); Apai, D (Apai, Daniel); Zhang, L (Zhang, Lan); Sicilia-Aguilar, A (Sicilia-Aguilar, Aurora); Alonso-Martinez, M (Alonso-Martinez, Miguel); Eiroa, C (Eiroa, Carlos); Wang, HC (Wang, Hongchi)
ASTRONOMICAL JOURNAL
卷: 153 期: 4 文献号: 188
We perform a spectroscopic survey of the foreground population in Orion. A with MMT/Hectospec. We use these data, along with archival spectroscopic data and photometric data, to derive spectral types, extinction values, and masses for 691 stars. Using the Spitzer Space Telescope data, we characterize the disk properties of these sources. We identify 37 new transition disk (TD) objects, 1 globally depleted disk candidate, and 7 probable young debris disks. We discover an object with a mass of. less than 0.018-0.030 M-circle dot, which harbors a flaring disk. Using the Ha emission line, we characterize the accretion activity of the sources with disks, and confirm that the. fraction of accreting TDs is lower than that of optically thick disks (46% +/- 7% versus 73% +/- 9%, respectively). Using kinematic data from the Sloan Digital Sky Survey and APOGEE INfrared Spectroscopy of the Young Nebulous Clusters program (IN-SYNC), we confirm that the foreground population shows similar kinematics to their local molecular clouds and other young stars in the same regions. Using the isochronal ages, we find that the foreground population has a median age of. around 1-2 Myr, which is similar to that of other young stars in Orion. A. Therefore, our results argue against the presence of a large and old foreground cluster in front of Orion. A.

第 147 条，共 286 条

A Curved Magnetic Field in the Ring-like Shell of Bubble N4

Chen, ZW (Chen, Zhiwei); Jiang, ZB (Jiang, Zhibo); Tamura, M (Tamura, Motohide); Kwon, J (Kwon, Jungmi); Roman-Lopes, A (Roman-Lopes, A.)
ASTROPHYSICAL JOURNAL
卷: 838 期: 2 文献号: 80
We report the detection of a curved magnetic field in the ring-like shell of the bubble N4, derived from near-infrared polarization of reddened diskless stars located behind this bubble. The magnetic field in the shell is curved and parallel to the ring-like shell, and its strength is estimated to be similar to 120 mu G in the plane of the sky. The magnetic field strength in the shell is significantly enhanced compared to the local field strength. We calculate the mass-to-flux ratio for the submillimeter clumps in the shell and find that they are all magnetically subcritical. Our results demonstrate that the magnetic field strengthens as the interstellar medium is compressed into a shell, and suggest that the magnetic field has the potential to hinder star formation triggered by H II region expansion.

第 148 条，共 286 条

Multiplicity among Solar-type Stars

Fuhrmann, K (Fuhrmann, K.); Chini, R (Chini, R.); Kaderhandt, L (Kaderhandt, L.); *Chen, Z* (Chen, Z.) ASTROPHYSICAL JOURNAL
卷: 836 期: 1 文献号: 139
We present a multiplicity census for a volume-complete all-sky survey of 422 stars with distances less than 25 pc and primary main-sequence effective temperatures T-eff >= 5300. K. Very similar to previous results that have been presented for various subsets of this survey, we confirm the positive correlation of the stellar multiplicities with primary mass. We find for the F-and G-type Population. I stars that 58% are non-single and 21% are in triple or higher level systems. For the old intermediate-disk and Population. II stars-virtually all of G type and less massive -even two out of three sources prove to be non-single. These numbers being lower limits because of the continuous flow of new discoveries, the unbiased survey clearly demonstrates that the standard case for solar-type field stars is a hydrogen-burning source with at least one ordinary or degenerate stellar companion, and a surprisingly large number of stars are organized in multiple systems. A principal consequence is that orbital evolution, including the formation of blue straggler stars, is a potentially important issue on all spatial scales and timescales for a significant percentage of the stellar systems, in particular among Population. II stars. We discuss a number of recent observations of known or suspected companions in the local survey, including a new detection of a double- lined Ba- Bb subsystem to the visual binary HR 8635.

第 149 条，共 286 条

How Do Stars Gain Their Mass? A JCMT/SCUBA-2 Transient Survey of Protostars in Nearby Star-forming Regions

Herczeg, GJ (Herczeg, Gregory J.); Johnstone, D (Johnstone, Doug); Mairs, S (Mairs, Steve); Hatchell, J (Hatchell, Jennifer); Lee, JE (Lee, Jeong-Eun); Bower, GC (Bower, Geoffrey C.); Chen, HRV (Chen, Huei-Ru Vivien); Aikawa, Y (Aikawa, Yuri); Yoo, H (Yoo, Hyunju); Kang, SJ (Kang, Sung-Ju); Kang, M

(Kang, Miju); *Chen, WP* (Chen, Wen-Ping); Williams, JP (Williams, Jonathan P.); Bae, J (Bae, Jaehan); Dunham, MM (Dunham, Michael M.); Vorobyov, EI (Vorobyov, Eduard I.); Zhu, ZH (Zhu, Zhaohuan); Rao, R (Rao, Ramprasad); Kirk, H (Kirk, Helen); Takahashi, S (Takahashi, Satoko); Morata, O (Morata, Oscar); Lacaille, K (Lacaille, Kevin); Lane, J (Lane, James); Pon, A (Pon, Andy); Scholz, A (Scholz, Aleks); Samal, MR (Samal, Manash R.); Bell, GS (Bell, Graham S.); Graves, S (Graves, Sarah); Lee, EM (Lee, E'lisa M.); Parsons, H (Parsons, Harriet); He, YX (He, Yuxin); Zhou, JJ (Zhou, Jianjun); Kim, MR (Kim, Mi-Ryang); Chapman, S (Chapman, Scott); Drabek-Maunder, E (Drabek-Maunder, Emily); Chung, EJ (Chung, Eun Jung); Eyres, SPS (Eyres, Stewart P. S.); Forbrich, J (Forbrich, Jan); Hillenbrand, LA (Hillenbrand, Lynne A.); Inutsuka, S (Inutsuka, Shu-ichiro); Kim, G (Kim, Gwanjeong); Kim, KH (Kim, Kyoung Hee); Kuan, YJ (Kuan, Yi-Jehng); Kwon, W (Kwon, Woojin); Lai, SP (Lai, Shih-Ping); Lalchand, B (Lalchand, Bhavana); Lee, CW (Lee, Chang Won); Lee, CF (Lee, Chin-Fei); Long, F (Long, Feng); Lyo, AR (Lyo, A-Ran); Qian, L (Qian, Lei); Scicluna, P (Scicluna, Peter); Soam, A (Soam, Archana); Stamatellos, D (Stamatellos, Dimitris); Takakuwa, S (Takakuwa, Shigehisa); Tang, YW (Tang, Ya-Wen); Wang, HC (Wang, Hongchi); Wang, YR (Wang, Yiren)
ASTROPHYSICAL JOURNAL
卷: 849 期: 1 文献号: 43
Most protostars have luminosities that are fainter than expected from steady accretion over the protostellar lifetime. The solution to this problem may lie in episodic mass accretion -- prolonged periods of very low accretion punctuated by short bursts of rapid accretion. However, the timescale and amplitude for variability at the protostellar phase is almost entirely unconstrained. In "A JCMT/SCUBA-2 Transient Survey of Protostars in Nearby Star Forming Regions", we are monitoring monthly with SCUBA-2 the sub-mm emission in eight fields within nearby (<500 pc) star forming regions to measure the accretion variability of protostars. The total survey area of similar to 1.6 sq.deg. includes similar to 105 peaks with peaks brighter than 0.5 Jy/beam (43 associated with embedded protostars or disks) and 237 peaks of 0.125-0.5 Jy/beam (50 with embedded protostars or disks). Each field has enough bright peaks for flux calibration relative to other peaks in the same field, which improves upon the nominal flux calibration uncertainties of sub-mm observations to reach a precision of similar to 2-3% rms, and also provides quantified confidence in any measured variability. The timescales and amplitudes of any sub-mm variation will then be converted into variations in accretion rate and subsequently used to infer the physical causes of the variability. This survey is the first dedicated survey for sub-mm variability and complements other transient surveys at optical and near-IR wavelengths, which are not sensitive to accretion variability of deeply embedded protostars.

第 150 条，共 286 条

A simple criterion for selecting disks with evidence for dust growth and settling

Liu, Y (Liu, Yao); Wang, HC (Wang, Hongchi); Henning, T (Henning, Thomas)
ASTROPHYSICS AND SPACE SCIENCE
卷: 362 期: 11 文献号: 208
Dust growth and settling, as an initial step of planet formation in protoplanetary disks, have an important impact on the appearance of the spectral energy distribution (SED). Selecting a promising sample of disks with signs of these processes helps to guide future observations towards a better understanding of the initial conditions for planet formation and disk evolution. Using a standard flared disk model, we conducted a large parameter study to investigate the effects of various disk parameters on the overall shape of the SED. We found that the flaring index and scale height can be used to mimic the effects of dust evolution on the SED. The influences of these two parameters on the infrared excess are very similar to that caused by dust evolution which have been shown in previous simulations where grain growth and settling are treated directly. Based on a statistic analysis of all the models in our grid, we proposed a criterion of Psi >= 0.6 to diagnose signs of dust evolution, where Psi is a ratio defined by dividing a linearly interpolated (between 24 mu m and 1.3 mm) flux at 70 mu m by the observed 70 mu m photometry. We tested the applicability of our criterion with the class II disks in the Taurus star formation region.

第 151 条，共 286 条

The properties of the inner disk around HL Tau: Multi-wavelength modeling of the dust emission

Liu, Y (Liu, Yao); Henning, T (Henning, Thomas); Carrasco-Gonzalez, C (Carrasco-Gonzalez, Carlos); Chandler, CJ (Chandler, Claire J.); Linz, H (Linz, Hendrik); Birnstiel, T (Birnstiel, Til); van Boekel, R (van Boekel, Roy); Perez, LM (Perez, Laura M.); Flock, M (Flock, Mario); Testi, L (Testi, Leonardo); Rodriguez, LF (Rodriguez, Luis F.); Galvan-Madrid, R (Galvan-Madrid, Roberto)
ASTRONOMY & ASTROPHYSICS
卷: 607 文献号: A74
We conducted a detailed radiative transfer modeling of the dust emission from the circumstellar disk around HL Tau. The goal of our study is to derive the surface density profile of the inner disk and its structure. In addition to the Atacama Large Millimeter/submillimeter Array images at Band 3 (2.9 mm), Band 6 (1.3 mm), and Band 7 (0.87 mm), the most recent Karl G. Jansky Very Large Array (VLA) observations at 7mm were included in the analysis. A simulated annealing algorithm was invoked to search for the optimum model. The radiative transfer analysis demonstrates that most radial components (i.e., > 6AU) of the disk become optically thin at a wavelength of 7 mm, which allows us to constrain, for the first time, the dust density distribution in the inner region of the disk. We found that a homogeneous grain size distribution is not sufficient to explain the observed images at different wavelengths simultaneously, while models with a shallower grain size distribution in the inner disk work well. We found clear evidence that larger grains are trapped in the first bright ring. Our results imply that dust evolution has already taken place in the disk at a relatively young (i.e., similar to 1 Myr) age. We compared the midplane temperature distribution, optical depth, and properties of various dust rings with those reported previously. Using the Toomre parameter, we briefly discussed the gravitational instability as a potential mechanism for the origin of the dust clump detected in the first bright ring via the VLA observations.

第 152 条，共 286 条

Stellar variability from Dome A, Antarctica

Wang, LZ (Wang, Lingzhi); Macri, LM (Macri, L. M.); Ma, B (Ma, B.); Wang, LF (Wang, L. F.); Ashley, MCB (Ashley, M. C. B.); Cui, X (Cui, X.); Du, FJ (Du, F. J.); Fu, JN (Fu, J. N.); Feng,

LL (Feng, L. L.); Gong, X (Gong, X.); Hu, Y (Hu, Y.); Li, G (Li, G.); Li, XY (Li, X. Y.); Li, ZY (Li, Z. Y.); Lawrence, JS (Lawrence, J. S.); Luong-Van, D (Luong-Van, D.); Pennypacker, CR (Pennypacker, C. R.); Shang, Z (Shang, Z.); Storey, JWV (Storey, J. W. V.); Yang, H (Yang, H.); Yuan, X (Yuan, X.); York, DG (York, D. G.); Zhou, X (Zhou, X.); Zhu, ZH (Zhu, Z. H.); Zhu, ZX (Zhu, Z. X.); Zhou, JL (Zhou, J. L.)
WIDE-FIELD VARIABILITY SURVEYS: A 21ST CENTURY PERSPECTIVE
EPJ Web of Conferences
卷: 152 文献号: UNSP 02010
The Antarctic plateau is one of the best observing sites on the surface of the Earth thanks to its extremely cold, dry, stable and transparent atmosphere conditions. Various astronomical activities are underway there and the Chinese Center for Antarctic Astronomy (CCAA) is dedicated to developing Antarctic astronomy at the highest point, Dome A or the Chinese Kunlun station. So far a large number of images have been collected from a 14.5-cm quad-telescope called the Chinese Small Telescope AR-ray (CSTAR) and the first two of a trio of 50-cm Antarctic Survey Telescopes (AST3-1 and AST3-2).
会议名称: 22nd Los Alamos Stellar Pulsation Conference
会议日期: NOV 28-DEC 02, 2016
会议地点: San Pedro de Atacama, CHILE

2-06 Galaxy formation and wide Field Sky Survey

第 153 条，共 286 条

THE QUENCHED MASS PORTION OF STAR-FORMING GALAXIES AND THE ORIGIN OF THE STAR FORMATION SEQUENCE SLOPE

Pan, ZZ (Pan, Zhizheng); Zheng, XZ (Zheng, Xianzhong); Kong, X (Kong, Xu)
ASTROPHYSICAL JOURNAL
卷: 834 期: 1 文献号: 39
Observationally, a massive disk galaxy can harbor a bulge component that is comparably inactive as a quiescent galaxy. It has been speculated that the quenched component contained in star-forming galaxies (SFGs) is the reason why the star formation main sequence (MS) has a shallow slope at high masses. In this paper, we present a toy model to quantify the quenched mass portion of SFGs (f(Q)) at fixed stellar mass (M-*) and to reconcile the MS slopes in both the low-and the high-mass regimes. In this model, each SFG is composed of a star-forming plus a quenched component. The mass of the star-forming component (M-SF) correlates with the star formation rate (SFR) following a relation SFR alpha M-SF(alpha SF), where alpha(SF) similar to 1.0. The quenched component contributes to the stellar mass but not to the SFR. It is thus possible to quantify f(Q) based on the departure of the observed MS slope a from aSF. Adopting the redshift-dependent MS slope reported by Whitaker et al., we explore the evolution of the f(Q) -M-* relations over z = [0.5, 2.5]. We find that Milky Way-like SFGs (with M-* approximate to 10(10.7) M-circle dot) typically have an f(Q) = 30%-40% at z similar to 2.25, whereas this value rapidly rises up to 70%-80% at z similar to 0.75. The origin of an alpha similar to 1.0 MS slope seen in the low-mass regime is also discussed. We argue for a scenario in which the majority of low-mass SFGs stay in a "steady-stage" star formation phase. In this phase, the SFR is mainly regulated by stellar feedback and not significantly influenced by the quenching mechanisms, thus remaining roughly constant over cosmic time. This scenario successfully produces an alpha similar to 1.0 MS slope, as well as the observed MS evolution from z = 2.5 to z - 0 at low masses.

第 154 条，共 286 条

First Spectroscopic Confirmations of z similar to 7.0 Ly alpha Emitting Galaxies in the LAGER Survey

Hu, WD (Hu, Weida); Wang, JX (Wang, Junxian); Zheng, ZY (Zheng, Zhen-Ya); Malhotra, S (Malhotra, Sangeeta); Infante, L (Infante, Leopoldo); Rhoads, J (Rhoads, James); Gonzalez, A (Gonzalez, Alicia); Walker, AR (Walker, Alistair R.); Jiang, LH (Jiang, Linhua); Jiang, CY (Jiang, Chunyan); Hibon, P (Hibon, Pascale); Barrientos, LF (Felipe Barrientos, L.); Finkelstein, S (Finkelstein, Steven); Galaz, G (Galaz, Gaspar); Kang, WY (Kang, Wenyong); Kong, X (Kong, Xu); Tilvi, V (Tilvi, Vithal); Yang, H (Yang, Huan); Zheng, XZ (Zheng, XianZhong)
ASTROPHYSICAL JOURNAL LETTERS
卷: 845 期: 2 文献号: L16
Narrowband imaging is a highly successful approach for finding large numbers of high-redshift Ly alpha emitting galaxies (LAEs) up to z similar to 6.6. However, at z greater than or similar to 7 there are as of yet only three narrowband selected LAEs with spectroscopic confirmations (two at z similar to 6.9-7.0, one at z similar to 7.3), which hinders extensive studies on cosmic reionization and galaxy evolution at this key epoch. We have selected 23 candidate z similar to 6.9 LAEs in COSMOS field with the large area narrowband survey Lyman-Alpha Galaxies at the End of Reionization (LAGER). In this work, we present spectroscopic follow-up observations of 12 candidates using the Inamori Magellan Areal Camera and Spectrograph on Magellan. For nine of these, the observations are sufficiently deep to detect the expected lines. Ly alpha emission lines are identified in six sources (yielding a success rate of 2/3), including three luminous LAEs with Ly alpha luminosities of L-Ly alpha similar to 10(43.5) erg s(-1), the highest among known spectroscopically confirmed galaxies at greater than or similar to 7.0. This triples the sample size of spectroscopically confirmed narrowband selected LAEs at z greater than or similar to 7, and confirms the bright-end bump in the Ly alpha luminosity function we previously derived based on the photometric sample, supporting a patchy reionization scenario. Two luminous LAEs appear physically linked with a projected distance of 1.1 pMpc and velocity difference of similar to 170 km s(-1). They likely sit in a common ionized bubble produced by themselves or with close neighbors, which reduces the intergalactic medium attenuation of Ly alpha. A tentative narrow N V lambda 1240 line is seen in one source, hinting at activity of a central massive black hole with metal-rich line-emitting gas.

第 155 条，共 286 条

The Origins of UV-optical Color Gradients in Star-forming Galaxies at z similar to 2: Predominant Dust Gradients but Negligible sSFR Gradients

Liu, FS (Liu, F. S.); Jiang, DF (Jiang, Dongfei); Faber, SM (Faber,

S. M.); Koo, DC (Koo, David C.); Yesuf, HM (Yesuf, Hassen M.); Tacchella, S (Tacchella, Sandro); Mao, SD (Mao, Shude); Wang, WC (Wang, Weichen); Guo, YC (Guo, Yicheng); Fang, JJ (Fang, Jerome J.); Barro, G (Barro, Guillermo); Zheng, XZ (Zheng, Xianzhong); Jia, M (Jia, Meng); Tong, W (Tong, Wei); Liu, L (Liu, Lu); Meng, XM (Meng, Xianmin)
ASTROPHYSICAL JOURNAL LETTERS
卷: 844 期: 1 文献号: L2
The rest-frame UV-optical (i.e., NUV - B) color is sensitive to both low-level recent star formation (specific star formation rate-sSFR) and dust. In this Letter, we extend our previous work on the origins of NUV - B color gradients in star-forming galaxies (SFGs) at z similar to 1 to those at z similar to 2. We use a sample of 1335 large (semimajor axis radius R-SMA > 0.'' 18) SFGs with extended UV emission out to 2R(SMA) in the mass range M-* = 10(9)-10(11) M-circle dot at 1.5 < z < 2.8 in the CANDELS/GOODS-S and UDS fields. We show that these SFGs generally have negative NUV - B color gradients (redder centers), and their color gradients strongly increase with galaxy mass. We also show that the global rest-frame FUV - NUV color is approximately linear with A(V), which is derived by modeling the observed integrated FUV to NIR spectral energy distributions of the galaxies. Applying this integrated calibration to our spatially resolved data, we find a negative dust gradient (more dust extinguished in the centers), which steadily becomes steeper with galaxy mass. We further find that the NUV - B color gradients become nearly zero after correcting for dust gradients regardless of galaxy mass. This indicates that the sSFR gradients are negligible and dust reddening is likely the principal cause of negative UV-optical color gradients in these SFGs. Our findings support that the buildup of the stellar mass in SFGs at Cosmic Noon is self-similar inside 2R(SMA).

第 156 条，共 286 条

An Imperfectly Passive Nature: Bright Submillimeter Emission from Dust-obscured Star Formation in the z=3.717 "Passive" System, ZF 20115

Simpson, JM (Simpson, J. M.); Smail, I (Smail, Ian); *Wang, WH* (Wang, Wei-Hao); Riechers, D (Riechers, D.); Dunlop, JS (Dunlop, J. S.); Ao, Y (Ao, Y.); Bourne, N (Bourne, N.); Bunker, A (Bunker, A.); Chapman, SC (Chapman, S. C.); Chen, CC (Chen, Chian-Chou); Dannerbauer, H (Dannerbauer, H.); Geach, JE (Geach, J. E.); Goto, T (Goto, T.); Harrison, CM (Harrison, C. M.); Hwang, HS (Hwang, H. S.); Ivison, RJ (Ivison, R. J.); Kodama, T (Kodama, Tadayuki); Lee, CH (Lee, C. -H.); Lee, HM (Lee, H. -M.); Lee, M (Lee, M.); Lim, CF (Lim, C. -F.); Michalowski, MJ (Michalowski, M. J.); Rosario, DJ (Rosario, D. J.); Shim, H (Shim, H.); Shu, XW (Shu, X. W.); Swinbank, AM (Swinbank, A. M.); Tee, WL (Tee, W. -L.); Toba, Y (Toba, Y.); Valiante, E (Valiante, E.); Wang, JX (Wang, Junxian); Zheng, XZ (Zheng, X. Z.)
ASTROPHYSICAL JOURNAL LETTERS
卷: 844 期: 1 文献号: L10
The identification of high-redshift, massive galaxies with old stellar populations may pose challenges to some models of galaxy formation. However, to securely classify a galaxy as quiescent, it is necessary to exclude significant ongoing star formation, something that can be challenging to achieve at high redshifts. In this Letter, we analyze deep ALMA/870 mu m and SCUBA-2/450 mu m imaging of the claimed "post-starburst" galaxy ZF 20115 at z = 3.717 that exhibits a strong Balmer break and absorption lines. The rest-frame far-infrared imaging identifies a luminous starburst 0.'' 4 +/- 0.'' 1 (similar to 3 kpc in projection) from the position of the ultraviolet/optical emission and is consistent with lying at the redshift of ZF 20115. The star-forming component, with an obscured star formation rate of 100(-70)(+15) M-circle dot yr(-1), is undetected in the rest-frame ultraviolet but contributes significantly to the lower angular resolution photometry at rest-frame wavelengths greater than or similar to 3500 angstrom. This contribution from the obscured starburst, especially in the Spitzer/IRAC wavebands, significantly complicates the determination of a reliable stellar mass for the ZF 20015 system, and we conclude that this source does not pose a challenge to current models of galaxy formation. The multi-wavelength observations of ZF 20115 unveil a complex system with an intricate and spatially varying star formation history. ZF 20115 demonstrates that understanding high-redshift obscured starbursts will only be possible with multi-wavelength studies that include high-resolution observations, available with the James Webb Space Telescope, at mid-infrared wavelengths.

第 157 条，共 286 条

First Results from the Lyman Alpha Galaxies in the Epoch of Reionization (LAGER) Survey: Cosmological Reionization at z similar to 7

Zheng, ZY (Zheng, Zhen-Ya); Wang, JX (Wang, Junxian); Rhoads, J (Rhoads, James); Infante, L (Infante, Leopoldo); Malhotra, S (Malhotra, Sangeeta); Hu, WD (Hu, Weida); Walker, AR (Walker, Alistair R.); Jiang, LH (Jiang, Linhua); Jiang, CY (Jiang, Chunyan); Hibon, P (Hibon, Pascale); Gonzalez, A (Gonzalez, Alicia); Kong, X (Kong, Xu); Zheng, XZ (Zheng, XianZhong); Galaz, G (Galaz, Gaspar); Barrientos, LF (Felipe Barrientos, L.)
ASTROPHYSICAL JOURNAL LETTERS
卷: 842 期: 2 文献号: L22
We present the first results from the ongoing Lyman Alpha Galaxies in the Epoch of Reionization (LAGER) project, which is the largest narrowband survey for z similar to 7 galaxies to date. Using a specially built narrowband filter NB964 for the superb large-area Dark Energy Camera (DECam) on the NOAO/CTIO 4 m Blanco telescope, LAGER has collected 34 hr NB964 narrowband imaging data in the 3 deg(2) COSMOS field. We have identified 23 Ly alpha Emitter candidates at z = 6.9 in the central 2-deg(2) region, where DECam and public COSMOS multi-band images exist. The resulting luminosity function (LF) can be described as a Schechter function modified by a significant excess at the bright end (four galaxies with L-Ly alpha similar to 10(43.4 +/- 0.2) erg s(-1)). The number density at L-Ly alpha similar to 10(43.4 +/- 0.2) erg s(-1) is little changed from z = 6.6, while at fainter L-Ly alpha it is substantially reduced. Overall, we see a fourfold reduction in Ly alpha luminosity density from z = 5.7 to z = 6.9. Combined with a more modest evolution of the continuum UV luminosity density, this suggests a factor of similar to 3 suppression of Ly alpha by radiative transfer through the z similar to 7 intergalactic medium (IGM). It indicates an IGM neutral fraction of x(HI) similar to 0.4-0.6 (assuming Ly alpha velocity offsets of 100-200 km s(-1)). The changing shape of the Ly alpha LF between z less than or similar to 6.6 and z = 6.9 supports the hypothesis of ionized bubbles in a patchy reionization at z similar to 7.

第 158 条，共 286 条

AGN-host connection at 0.5 < z < 2.5: A rapid evolution of AGN fraction in red galaxies during the last 10 Gyr

Wang, T (Wang, Tao); Elbaz, D (Elbaz, D.); Alexander, DM (Alexander, D. M.); Xue, YQ (Xue, Y. Q.); Gabor, JM (Gabor, J. M.); Juneau, S (Juneau, S.); Schreiber, C (Schreiber, C.); Zheng, XZ (Zheng, X. -Z.); Wuyts, S (Wuyts, S.); Shi, Y (Shi, Y.); Daddi, E (Daddi, E.); Shu, XW (Shu, X. -W.); Fang, GW (Fang, G. -W.); Huang, JS (Huang, J. -S.); Luo, B (Luo, B.); Gu, QS (Gu, Q. -S.)

ASTRONOMY & ASTROPHYSICS

卷: 601 文献号: A63

We explore the dependence of the incidence of moderate-luminosity (L0.5-8 keV = 10(41.9-43.7) erg s(-1)) active galactic nuclei (AGNs) and the distribution of their accretion rates on host color at 0.5 < z < 2.5. Based on the deepest X-ray and UV-to-far-infrared data in the two The Great Observatories Origins Deep Survey (GOODS) fields, we identify 221 AGNs within a mass-complete parent galaxy sample down to M-* > 10(10) M-circle dot. We use extinction-corrected rest-frame U-V colors to divide both AGN hosts and non-AGN galaxies into red sequence (red), green valley (green), and blue cloud (blue) populations. We find that the fraction of galaxies hosting an AGN at fixed X-ray luminosity increases with stellar mass and redshift for all the three galaxy populations, independent of their colors. However, both the AGN fraction at fixed stellar mass and its evolution with redshift are clearly dependent on host colors. Most notably, red galaxies have the lowest AGN fraction (similar to 5%) at z similar to 1 yet with most rapid evolution with redshift, increasing by a factor of similar to 5 (24%) at z similar to 2. Green galaxies exhibit the highest AGN fraction across all redshifts, which is most pronounced at z similar to 2 with more than half of them hosting an AGN at M-* > 10(10.6) M-circle dot. Together with the high AGN fraction in red galaxies at z similar to 2, this indicates that (X-ray) AGNs could be important in both transforming (quenching) star-forming galaxies into quiescent ones and subsequently maintaining their quiescence at high redshift. Furthermore, consistent with previous studies at lower redshifts, we show that the probability of hosting an AGN for the total galaxy population can be characterized by a universal Eddington ratio (as approximated by L-X/M-*) distribution (p(lambda(Edd)) similar to lambda(-0.4)(Edd) Edd), which is independent on host mass. Yet consistent with their different AGN fractions, galaxies with different colors appear to also have different p(lambda(Edd)) with red galaxies exhibiting more rapid redshift evolution compared with that for green and blue galaxies. Evidence for a steeper power-law distribution of p(lambda(Edd)) in red galaxies (p(lambda(Edd)) similar to lambda(-0.6)(Edd) Edd) is also presented, though larger samples are needed to confirm. These results suggest that the AGN accretion or the growth of supermassive black holes is related to their host properties, and may also influence their hosts in a different mode dependent on the host color.

第 159 条，共 286 条

DEEP CFHT Y-BAND IMAGING OF VVDS-F22 FIELD. I. DATA PRODUCTS AND PHOTOMETRIC REDSHIFTS

Liu, DZ (Liu, Dezi); Yang, JY (Yang, Jinyi); Yuan, S (Yuan, Shuo); Wu, XB (Wu, Xue-Bing); Fan, ZH (Fan, Zuhui); Shan, HY (Shan, Huanyuan); Yan, HJ (Yan, Haojing); Zheng, XZ (Zheng, Xianzhong)

ASTRONOMICAL JOURNAL

卷: 153 期: 2 文献号: 53

We present our deep Y-band imaging data of a two square degree field within the F22 region of the VIMOS VLT Deep Survey. The observations were conducted using the WIRCam instrument mounted at the Canada-France-Hawaii Telescope (CFHT). The total on-sky time was 9 hours, distributed uniformly over 18 tiles. The scientific goals of the project are to select faint quasar candidates at redshift z > 2.2, and constrain the photometric redshifts for quasars and galaxies. In this paper, we present the observation and the image reduction, as well as the photometric redshifts that we derived by combining our Y-band data with the CFHTLenS u*g'r'i'z' optical data and UKIDSS DXS JHK near-infrared data. With J-band image as reference total similar to 80,000 galaxies are detected in the final mosaic down to Y-band 5 sigma point source limiting depth of 22.86 mag. Compared with the similar to 3500 spectroscopic redshifts, our photometric redshifts for galaxies with z < 1.5 and i'less than or similar to 24.0 mag have a small systematic offset of vertical bar Delta z vertical bar less than or similar to 0.2, 1 sigma scatter 0.03< (sigma)Delta(z) < 0.06, and less than 4.0% of catastrophic failures. We also compare to the CFHTLenS photometric redshifts, and find that ours are more reliable at z greater than or similar to 0.6 because of the inclusion of the near-infrared bands. In particular, including the Y-band data can improve the accuracy at z similar to 1.0-2.0 because the location of the 4000 angstrom-break is better constrained. The Y-band images, the multi-band photometry catalog and the photometric redshifts are released at http://astro.pku.edu.cn/astro/data/DYI.html.

2-07 High – energy time-domain astronomy

第 160 条，共 286 条

A Further Test of Lorentz Violation from the Rest-frame Spectral Lags of Gamma-Ray Bursts

Wei, JJ (Wei, Jun-Jie); Wu, XF (Wu, Xue-Feng)

ASTROPHYSICAL JOURNAL

卷: 851 期: 2 文献号: 127

Lorentz invariance violation (LIV) can manifest itself by an energy-dependent vacuum dispersion of light, which leads to arrival time differences of photons with different energies originating from the same astronomical source. The spectral lags of gamma-ray bursts (GRBs) have been widely used to investigate the possible LIV effect. However, all current investigations used lags extracted in the observer frame only. In this work, we present, for the first time, an analysis of the LIV effect and its redshift dependence in the cosmological rest frame. Using a sample of 56 GRBs with known redshifts, we obtain a robust limit on LIV by fitting their rest-frame spectral lag data using both a maximization of the likelihood function and a minimum chi(2) statistic. Our analysis indicates that there is no evidence of LIV. Additionally, we test the LIV in different redshift ranges by dividing the full sample into four redshift bins. We also find no evidence for the redshift variation of the LIV effect.

第 161 条，共 286 条

A New Measurement of the Spectral Lag of Gamma-Ray Bursts and its Implications for Spectral Evolution Behaviors

Shao, L (Shao, Lang); Zhang, BB (Zhang, Bin-Bin); Wang, FR (Wang, Fu-Ri); Wu, XF (Wu, Xue-Feng); Cheng, YH (Cheng, Ye-Hao); Zhang, X (Zhang, Xi); Yu, BY (Yu, Bang-Yao); Xi, BJ (Xi, Bao-Jia); Wang, X (Wang, Xue); Feng, HX (Feng, Huan-Xue); *Zhang, M* (Zhang, Meng); Xu, D (Xu, Dong)
ASTROPHYSICAL JOURNAL
卷: 844 期: 2 文献号: 126
We carry out a systematical study of the spectral lag properties of 50 single-pulsed gamma-ray bursts (GRBs) detected by the Fermi Gamma-Ray Burst Monitor. By dividing the light curves into multiple consecutive energy channels, we provide a new measurement of the spectral lag that is independent of energy channel selections. We perform a detailed statistical study of our new measurements. We find two similar power-law energy dependencies of both the pulse arrival time and pulse width. Our new results on the power-law indices would favor the relativistic geometric effects for the origin of spectral lag. However, a complete theoretical framework that can fully account for the diverse energy dependencies of both arrival time and pulse width revealed in this work is still lacking. We also study the spectral evolution behaviors of the GRB pulses. We find that a GRB pulse with negligible spectral lag would usually have a shorter pulse duration and would appear to have a "hardness-intensity tracking" behavior, and a GRB pulse with a significant spectral lag would usually have a longer pulse duration and would appear to have a "hard-to-soft" behavior.

第 162 条，共 286 条

Constraining Anisotropic Lorentz Violation via the Spectral-lag Transition of GRB 160625B

Wei, JJ (Wei, Jun-Jie); Wu, XF (Wu, Xue-Feng); Zhang, BB (Zhang, Bin-Bin); Shao, L (Shao, Lang); Meszaros, P (Meszaros, Peter); Kostelecky, VA (Kostelecky, V. Alan)
ASTROPHYSICAL JOURNAL
卷: 842 期: 2 文献号: 115
Violations of Lorentz invariance can lead to an energy-dependent vacuum dispersion of light, which results in arrival-time differences of photons with different energies arising from a given transient source. In this work, direction-dependent dispersion constraints are obtained on nonbirefringent Lorentz-violating effects using the observed spectral lags of the gamma-ray burst GRB 160625B. This burst has unusually large high-energy photon statistics, so we can obtain constraints from the true spectral time lags of bunches of high-energy photons rather than from the rough time lag of a single highest-energy photon. Also, GRB 160625B is the only burst to date having a well-defined transition from positive lags to negative lags, providing a unique opportunity to distinguish Lorentz-violating effects from any source-intrinsic time lag in the emission of photons of different energy bands. Our results place comparatively robust two-sided constraints on a variety of isotropic and anisotropic coefficients for Lorentz violation, including the first bounds on Lorentz-violating effects from operators of mass dimension 10 in the photon sector.

第 163 条，共 286 条

New test of weak equivalence principle using polarized light from astrophysical events

Wu, XF (Wu, Xue-Feng); Wei, JJ (Wei, Jun-Jie); Lan, MX (Lan, Mi-Xiang); Gao, H (Gao, He); Dai, ZG (Dai, Zi-Gao); Meszaros, P (Meszaros, Peter)
PHYSICAL REVIEW D
卷: 95 期: 10 文献号: 103004
Einstein's weak equivalence principle (WEP) states that any freely falling, uncharged test particle follows the same identical trajectory independent of its internal structure and composition. Since the polarization of a photon is considered to be part of its internal structure, we propose that polarized photons from astrophysical transients, such as gamma-ray bursts (GRBs) and fast radio bursts (FRBs), can be used to constrain the accuracy of the WEP through the Shapiro time delay effect. Assuming that the arrival time delays of photons with different polarizations are mainly attributed to the gravitational potential of the Laniakea supercluster of galaxies, we show that a strict upper limit on the differences of the parametrized post-Newtonian parameter. value for the polarized optical emission of GRB 120308A is Delta(gamma) < 1.2 x 10(-10), for the polarized gamma-ray emission of GRB 100826A is Delta(gamma) < 1.2 x 10(-10), and for the polarized radio emission of FRB 150807 is Delta(gamma) < 2.2 x 10(-6). These are the first direct verifications of the WEP for multiband photons with different polarizations. In particular, the result from FRB 150807 provides the most stringent limit to date on a deviation from the WEP, improving by one order of magnitude the previous best result based on Crab pulsar photons with different energies.

第 164 条，共 286 条

An Improved Method to Measure the Cosmic Curvature

Wei, JJ (Wei, Jun-Jie); Wu, XF (Wu, Xue-Feng)
ASTROPHYSICAL JOURNAL
卷: 838 期: 2 文献号: 160
In this paper, we propose an improved model-independent method to constrain the cosmic curvature by combining the most recent Hubble parameter H(z) and supernovae Ia (SNe Ia) data. Based on the H(z) data, we first use the model-independent smoothing technique, Gaussian processes, to construct a distance modulus mu(H)(z) which is susceptible to the cosmic curvature parameter Omega(k). In contrary to previous studies, the light-curve-fitting parameters, which account for the distance estimation of SN (mu(SN)(z)), are set free to investigate whether Omega(k) has a dependence on them. By comparing mu(H)(z) to mu(SN)(z), we put limits on Omega(k). Our results confirm that Omega(k) is independent of the SN light-curve parameters. Moreover, we show that the measured Omega(k) is in good agreement with zero cosmic curvature, implying that there is no significant deviation from a flat universe at the current observational data level. We also test the influence of different H(z) samples and different Hubble constant H-0 values, finding that different H(z) samples do not have a significant impact on the constraints. However, different H-0 priors can affect the constraints of Ok to some degree. The prior of H-0 = 73.24 +/- 1.74 km s(-1) Mpc(-1) gives a value of Omega(k), a little bit above the 1 sigma confidence level away from 0, but H-0 = 69.6 +/-. 0.7 km s(-1) Mpc(-1) gives it below 1 sigma.

第 165 条，共 286 条

Impact of a Locally Measured H-0 on the Interpretation of Cosmic-chronometer Data

Wei, JJ (Wei, Jun-Jie); Melia, F (Melia, Fulvio); Wu, XF (Wu, Xue-Feng)
ASTROPHYSICAL JOURNAL
卷: 835 期: 2 文献号: 270
Many measurements in cosmology depend on the use of integrated distances or time, but. galaxies evolving passively on a timescale much longer than their age difference allow us to determine the expansion rate H(z) solely as a function of the redshift-time derivative dz/dt. These model-independent "cosmic chronometers" can therefore be powerful discriminators for testing different cosmologies. In previous applications, the available sources strongly disfavored models (such as Lambda CDM) predicting a variable acceleration, preferring instead a steady expansion rate over the redshift range 0 less than or similar to z less than or similar to 2. A more recent catalog of 30 objects appears to suggest non-steady expansion. In this paper, we show that such a result is entirely due to the inclusion of a high, locally inferred value of the Hubble constant H-0 as an additional datum in a set of otherwise pure cosmic-chronometer measurements. This H-0, however, is not the same as the background Hubble constant if the local expansion rate is influenced by a Hubble Bubble. Used on their own, the cosmic chronometers completely reverse this conclusion, favoring instead a constant expansion rate out to z similar to 2.

第 166 条，共 286 条

New limits on the photon mass with radio pulsars in the Magellanic clouds

Wei, JJ (Wei, Jun-Jie); Zhang, EK (Zhang, Er-Kang); Zhang, SB (Zhang, Song-Bo); Wu, XF (Wu, Xue-Feng)
RESEARCH IN ASTRONOMY AND ASTROPHYSICS
卷: 17 期: 2 文献号: 13
A conservative constraint on the rest mass of the photon can be estimated under the assumption that the frequency dependence of dispersion from astronomical sources is mainly contributed by the nonzero photon mass effect. Photon mass limits have been set earlier through the optical emissions of the Crab Nebula pulsar, but we demonstrate that these limits can be significantly improved with the dispersion measure (DM) measurements of radio pulsars in the Large and Small Magellanic Clouds. The combination of DM measurements of pulsars and distances of the Magellanic Clouds provides a strict upper limit on the photon mass as low as m(gamma) <= 2.0 x 10(-45) g, which is at least four orders of magnitude smaller than the constraint from the Crab Nebula pulsar. Although our limit is not as tight as the current best result (similar to 10(-47) g) from a fast radio burst (FRB 150418) at a cosmological distance, the cosmological origin of FRB 150418 remains under debate; and our limit can reach the same high precision of FRB 150418 when it has an extragalactic origin (similar to 10(-45) g).

第 167 条，共 286 条

Gamma-ray burst cosmology: Hubble diagram and star formation history

Wei, JJ (Wei, Jun-Jie); Wu, XF (Wu, Xue-Feng)
INTERNATIONAL JOURNAL OF MODERN PHYSICS D
卷: 26 期: 2 文献号: 1730002
We briefly introduce the disadvantages for Type Ia supernovae (SNe Ia) as standard candles to measure the universe, and suggest Gamma-ray bursts (GRBs) can serve as a powerful tool for probing the properties of high redshift universe. We use GRBs as distance indicators in constructing the Hubble diagram at redshifts beyond the current reach of SNe Ia observations. Since the progenitors of long GRBs (LGRBs) are confirmed to be massive stars, they are deemed as an effective approach to study the cosmic star formation rate (SFR). A detailed representation of how to measure high-z SFR using GRBs is presented. Moreover, first stars can form only in structures that are suitably dense, which can be parametrized by defining the minimum dark matter halo mass M-min. Mmin must play a crucial role in star formation. The association of LGRBs with the collapses of massive stars also indicates that the GRB data can be applied to constrain the minimum halo mass Mmin and to investigate star formation in dark matter halos.

第 168 条，共 286 条

A New Test of Lorentz Invariance Violation: The Spectral Lag Transition of GRB 160625B

Wei, JJ (Wei, Jun-Jie); Zhang, BB (Zhang, Bin-Bin); Shao, L (Shao, Lang); Wu, XF (Wu, Xue-Feng); Meszaros, P (Meszaros, Peter)
ASTROPHYSICAL JOURNAL LETTERS
卷: 834 期: 2 文献号: L13
Possible violations of Lorentz invariance (LIV) have been investigated for a long time using the observed spectral lags of gamma-ray bursts (GRBs). However, these generally have relied on using a single photon in the highest energy range. Furthermore, the search for LIV lags has been hindered by our ignorance concerning the intrinsic time lag in different energy bands. GRB 160625B, the only burst so far with a well-defined transition from positive lags to negative lags provides a unique opportunity to put new constraints on LIV. Using multi-photon energy bands we consider the contributions to the observed spectral lag from both the intrinsic time lag and the lag by LIV effects, and assuming the intrinsic time lag to have a positive dependence on the photon energy, we obtain robust limits on LIV by directly fitting the spectral lag data of GRB 160625B. Here we show that these robust limits on the quantum gravity energy scales are E-QG,E-1 >= 0.5 x 10(16) GeV for the linear, and E-QG,E-2 >= 1.4 x 10(7) GeV for the quadratic LIV effects, respectively. In addition, we give, for the first time, a reasonable formulation of the intrinsic energy-dependent time lag.

第 169 条，共 286 条

The Observer's Guide to the Gamma-Ray Burst Supernova Connection

Cano, Z (Cano, Zach); Wang, SQ (Wang, Shan-Qin); Dai, ZG (Dai, Zi-Gao); Wu, XF (Wu, Xue-Feng)
ADVANCES IN ASTRONOMY
文献号: 8929054
We present a detailed report of the connection between long-duration gamma-ray bursts (GRBs) and their accompanying supernovae (SNe). The discussion presented here places emphasis on how observations, and the modelling of observations, have constrained what we know about GRB-SNe. We discuss their photometric and spectroscopic properties, their role as cosmological probes, including their measured luminosity-decline relationships, and how they can be used to measure the Hubble constant.

We present a statistical summary of their bolometric properties and use this to determine the properties of the "average" GRB-SN. We discuss their geometry and consider the various physical processes that are thought to power the luminosity of GRB-SNe and whether differences exist between GRB-SNe and the SNe associated with ultra-long-duration GRBs. We discuss how observations of their environments further constrain the physical properties of their progenitor stars and give a brief overview of the current theoretical paradigms of their central engines. We then present an overview of the radioactively powered transients that have been photometrically associated with short-duration GRBs, and we conclude by discussing what additional research is needed to further our understanding of GRB-SNe, in particular the role of binary-formation channels and the connection of GRB-SNe with superluminous SNe.

第 170 条，共 286 条

Strongly lensed gravitational waves and electromagnetic signals as powerful cosmic rulers

Wei, JJ (Wei, Jun-Jie); Wu, XF (Wu, Xue-Feng)
MONTHLY NOTICES OF THE ROYAL ASTRONOMICAL SOCIETY
卷: 472 期: 3 页: 2906-2912
In this paper, we discuss the possibility of using strongly lensed gravitational waves (GWs) and their electromagnetic (EM) counterparts as powerful cosmic rulers. In the EM domain, it has been suggested that joint observations of the time delay (Delta tau) between lensed quasar images and the velocity dispersion (sigma) of the lensing galaxy (i.e. the combination Delta tau/sigma(2)) are able to constrain the cosmological parameters more strongly than Delta tau or sigma(2) separately. Here, for the first time, we propose that this Delta tau/sigma(2) method can be applied to the strongly lensed systems observed in both GW and EM windows. Combining the redshifts, images and sigma observed in the EM domain with the very precise Delta tau derived from lensed GW signals, we expect that accurate multimessenger cosmology can be achieved in the era of third-generation GW detectors. Comparing with the constraints from the Delta tau method, we prove that using Delta tau/sigma(2) can improve the discrimination between cosmological models. Furthermore, we demonstrate that with similar to 50 strongly lensed GW-EM systems, we can reach a constraint on the dark energy equation of state w comparable to the 580 Union2.1 Type Ia supernovae data. Much more stringent constraints on w can be obtained when combining the Delta tau and Delta tau/sigma(2) methods.

第 171 条，共 286 条

Hyperaccreting Black Hole as Gamma-Ray Burst Central Engine. II. Temporal Evolution of the Central Engine Parameters during the Prompt and Afterglow Phases

Lei, WH (Lei, Wei-Hua); Zhang, B (Zhang, Bing); Wu, XF (Wu, Xue-Feng); Liang, EW (Liang, En-Wei)
ASTROPHYSICAL JOURNAL
卷: 849 期: 1 文献号: 47
A hyperaccreting stellar-mass black hole (BH) has been proposed as the candidate central engine of gamma-ray bursts (GRBs). The rich observations of GRBs by Fermi and Swift make it possible to constrain the central engine model by comparing the model predictions against data. This paper is dedicated to studying the temporal evolution of the central engine parameters for both the prompt emission and afterglow phases. We consider two jet-launching mechanisms, i.e., nu(nu) over bar annihilations and the Blandford-Znajek (BZ) process, and obtain analytical solutions to these two models. We then investigate the BH central engine parameters, such as the jet power, the dimensionless entropy eta, and the central engine parameter mu(0) = eta (1 + sigma(0)) (where sigma(0) is the initial magnetization of the engine) at the base of the jet. The BH may be spun up by accretion or spun down by the BZ process, leaving imprints in the GRB light curves. Usually, a BZ jet is more powerful and is likely responsible for the late-time central engine activities. However, an initially non-spinning BH central engine may first launch a thermal "fireball" via neutrino annihilations, and then launch a Poynting-flux-dominated jet via the BZ process. Multiple flares, giant bumps, and plateaus in GRB afterglows can be produced as the result of late-time accretion onto the BH.

第 172 条，共 286 条

Model-independent Constraints on Cosmic Curvature and Opacity

Wang, GJ (Wang, Guo-Jian); Wei, JJ (Wei, Jun-Jie); Li, ZX (Li, Zheng-Xiang); Xia, JQ (Xia, Jun-Qing); Zhu, ZH (Zhu, Zong-Hong)
ASTROPHYSICAL JOURNAL
卷: 847 期: 1 文献号: 45
In this paper, we propose to estimate the spatial curvature of the universe and the cosmic opacity in a model-independent way with expansion rate measurements, H(z), and type Ia supernova (SNe Ia). On the one hand, using a nonparametric smoothing method Gaussian process, we reconstruct a function H(z) from opacity-free expansion rate measurements. Then, we integrate the H(z) to obtain distance modulus mu(H), which is dependent on the cosmic curvature. On the other hand, distances of SNe Ia can be determined by their photometric observations and thus are opacity-dependent. In our analysis, by confronting distance moduli mu(H) with those obtained from SNe Ia, we achieve estimations for both the spatial curvature and the cosmic opacity without any assumptions for the cosmological model. Here, it should be noted that light curve fitting parameters, accounting for the distance estimation of SNe Ia, are determined in a global fit together with the cosmic opacity and spatial curvature to get rid of the dependence of these parameters on cosmology. In addition, we also investigate whether the inclusion of different priors for the present expansion rate (H-0: global estimation, 67.74 +/- 0.46 km s(-1) Mpc(-1), and local measurement, 73.24 +/- 1.74 km s(-1) Mpc(-1)) exert influence on the reconstructed H(z) and the following estimations of the spatial curvature and cosmic opacity. Results show that, in general, a spatially flat and transparent universe is preferred by the observations. Moreover, it is suggested that priors for H-0 matter a lot. Finally, we find that there is a strong degeneracy between the curvature and the opacity.

第 173 条，共 286 条

Lorentz factor - Beaming corrected energy/luminosity correlations and GRB central engine models

Yi, SX (Yi, Shuang-Xi); *Lei, WH* (Lei, Wei-Hua); Zhang, B (Zhang, Bing); Dai, ZG (Dai, Zi-Gao); Wu, XF (Wu, Xue-Feng); Liang, EW (Liang, En-Wei)
JOURNAL OF HIGH ENERGY ASTROPHYSICS

卷: 13-14 页: 1-9
We work on a GRB sample whose initial Lorentz factors (Gamma(0)) are constrained by the afterglow onset method and the jet opening angles (theta j) are determined by the jet break time. We confirm the Gamma(0)-E-gamma,E-iso correlation by Liang etal.(2010), and the Gamma(0)-L-gamma,L-iso correlation by Lu etal.(2012). Furthermore, we find correlations between Gamma(0) and the beaming corrected gamma-ray energy (E-gamma) and mean gamma-ray luminosity (L-gamma). By also including the kinetic energy of the afterglow, we find rough correlations (with larger scatter) between Gamma(0) and the total (gamma- ray plus kinetic) energy and the total mean luminosity, both for isotropic values and beaming corrected values: these correlations allow us to test the data with GRB central engine models. Limiting our sample to the GRBs that likely have a black hole central engine, we compare the data with theoretical predictions of two types of jet launching mechanisms from BHs, i. e. the nonmagnetized v (v) over bar -annihilation mechanism, and the strongly magnetized Blandford- Znajek (BZ) mechanism. We find that the data are more consistent with the latter mechanism, and discuss the implications of our findings for GRB jet composition. (C) 2017 Elsevier B.V. All rights reserved.

第 174 条，共 286 条

Afterglows and Kilonovae Associated with Nearby Low-luminosity Short-duration Gamma-Ray Bursts: Application to GW170817/GRB 170817A

Xiao, D (Xiao, Di); Liu, LD (Liu, Liang-Duan); Dai, ZG (Dai, Zi-Gao); Wu, XF (Wu, Xue-Feng)
ASTROPHYSICAL JOURNAL LETTERS
卷: 850 期: 2 文献号: L41
Very recently, the gravitational-wave (GW) event GW170817 was discovered to be associated with the short gamma-ray burst (GRB) 170817A. Multi-wavelength follow-up observations were carried out, and X-ray, optical, and radio counterparts to GW170817 were detected. The observations undoubtedly indicate that GRB 170817A originates from a binary neutron star merger. However, the GRB falls into the low-luminosity class that could have a higher statistical occurrence rate and detection probability than the normal (high-luminosity) class. This implies the possibility that GRB 170817A is intrinsically powerful, but we are off-axis and only observe its side emission. In this Letter, we provide a timely modeling of the multi-wavelength afterglow emission from this GRB and the associated kilonova signal from the merger ejecta, under the assumption of a structured jet, a two-component jet, and an intrinsically less-energetic quasi-isotropic fireball, respectively. Comparing the afterglow properties with the multi-wavelength follow-up observations, we can distinguish between these three models. Furthermore, a few model parameters (e.g., the ejecta mass and velocity) can be constrained.

第 175 条，共 286 条

Multimessenger tests of the weak equivalence principle from GW170817 and its electromagnetic counterparts

Wei, JJ (Wei, Jun-Jie); Zhang, BB (Zhang, Bin-Bin); Wu, XF (Wu, Xue-Feng); Gao, H (Gao, He); Meszaros, P (Meszaros, Peter); Zhang, B (Zhang, Bing); Dai, ZG (Dai, Zi-Gao); Zhang, SN (Zhang, Shuang-Nan); Zhu, ZH (Zhu, Zong-Hong)
JOURNAL OF COSMOLOGY AND ASTROPARTICLE PHYSICS
期: 11 文献号: 035
The coincident detection of a gravitational-wave (GW) event GW170817 with electromagnetic (EM) signals (e.g., a short gamma-ray burst SGRB 170817A or a macronova) from a binary neutron star merger within the nearby galaxy NGC 4933 provides a new, multi-messenger test of the weak equivalence principle (WEP), extending the WEP test with GWs and photons. Assuming that the arrival time delay between the GW signals from GWT70817 and the photons from SGRB 170817A or the macronova is mainly attributed to the gravitational potential of the Milky Way, we demonstrate that the strict upper limits on the deviation from the WEP are delta gamma < 1.4 x 10(-3) for GW170817/macronova and delta gamma < 5.9 x 10(-8) for GW170817/SGRB 170817A. A much more severe constraint on the WEP accuracy can be achieved (similar to 0.9 x 10(-10)) for GW170817/SGRB 170817A when we consider the gravitational potential of the Virgo Cluster, rather than the Milky Way's gravity. This provides the tightest limit to date on the WEP through the relative differential variations of the gamma parameter for two different species of particles. Compared with other multimessenger (photons and neutrinos) results, our limit is 7 orders of magnitude tighter than that placed by the neutrinos and photons from supernova 1987A, and is almost as good as or is an improvement of 6 orders of magnitude over the limits obtained by the low-significance neutrinos correlated with GRBs and a blazar flare.

第 176 条，共 286 条

A Further Test of Lorentz Violation from the Rest-frame Spectral Lags of Gamma-Ray Bursts

Wei, JJ (Wei, Jun-Jie); Wu, XF (Wu, Xue-Feng)
ASTROPHYSICAL JOURNAL
卷: 851 期: 2 文献号: 127
Lorentz invariance violation (LIV) can manifest itself by an energy-dependent vacuum dispersion of light, which leads to arrival time differences of photons with different energies originating from the same astronomical source. The spectral lags of gamma-ray bursts (GRBs) have been widely used to investigate the possible LIV effect. However, all current investigations used lags extracted in the observer frame only. In this work, we present, for the first time, an analysis of the LIV effect and its redshift dependence in the cosmological rest frame. Using a sample of 56 GRBs with known redshifts, we obtain a robust limit on LIV by fitting their rest-frame spectral lag data using both a maximization of the likelihood function and a minimum chi(2) statistic. Our analysis indicates that there is no evidence of LIV. Additionally, we test the LIV in different redshift ranges by dividing the full sample into four redshift bins. We also find no evidence for the redshift variation of the LIV effect.

2-08 Gas distribution and Properties of the Milky Way

第 177 条，共 286 条

Is HESS J1912+101 Associated with an Old Supernova Remnant?

Su, Y (Su, Yang); Zhou, X (Zhou, Xin); Yang, J (Yang, Ji); Chen, Y (Chen, Yang); Chen, XP (Chen, Xuepeng); Gong, Y (Gong, Yan); Zhang, SB (Zhang, Shaobo)
ASTROPHYSICAL JOURNAL
卷: 845 期: 1 文献号: 48
HESS J1912+101 is a shell-like TeV source that has no clear counterpart in multiwavelength. Using CO and H I data, we reveal that V-LSR similar to + 60 km s(-1) molecular clouds (MCs), together with shocked molecular gas and high-velocity neutral atomic shells, are concentrated toward HESS J1912+101. The prominent wing profiles up to V-LSR similar to + 80 km s(-1) seen in (CO)-C-12 (J = 1-0 and J = 3-2) data, as well as the high-velocity expanding H I shells up to V-LSR similar to + 100 km s(-1), exhibit striking redshifted-broadening relative to the quiescent gas. These features provide compelling evidences for large-scale perturbation in the region. We argue that the shocked MCs and the high-velocity H I shells may originate from an old supernova remnant (SNR). The distance to the SNR is estimated to be similar to 4.1. kpc based on the H I self-absorption method, which leads to a physical radius of 29.0 pc for the similar to(0.7-2.0) x 10(5). years old remnant with an expansion velocity of >= 40 km s(-1). The +60 km s(-1) MCs and the disturbed gas are indeed found to coincide with the bright TeV emission, supporting the physical association between them. Naturally, the shell-like TeV emission comes from the decay of neutral pions produced by interactions between the accelerated hadrons from the SNR and the surrounding high-density molecular gas.

第 178 条，共 286 条

Multifrequency VLBA polarimetry of the high-redshift GPS quasar OQ172

Liu, Y (Liu, Yi); Jiang, DR (Jiang, D. R.); Gu, MF (Gu, Minfeng); Gurvits, LI (Gurvits, L. I.)
MONTHLY NOTICES OF THE ROYAL ASTRONOMICAL SOCIETY
卷: 468 期: 3 页: 2699-2712
Multifrequency Very Long Baseline Array (VLBA) polarimetry observation of the GHz-peaked spectrum (GPS) quasar OQ172 (J1445+ 0958) has been performed at 1.6, 2.2, 4.8, 8.3 and 15.3 GHz in 2005. Core-jet structures are detected in all bands with the jet strongly bent at about 3 mas from the core. The radio emission of the source is polarized at all five bands. We study the Faraday rotation in the core and jet components at all five bands, and find good linear fits of Faraday rotation in the core and jet components at 4.8 and 8.3 GHz. At these two frequencies, the rotation measure (RM) is similar to 2000 rad m(-2) in the core and similar to 700 rad m(-2) in the inner jet components and continues to decrease at the outer jet parts. We find that the depolarization at 4.8 and 8.3 GHz might be caused by the internal medium in the source. We investigate consistency of the turnover spectra of VLBI components with the synchrotron self-absorption and free-free absorption models. Although these two models cannot be easily distinguished due to the lack of low-frequency data, the physical parameters can be constrained for each model. We find that the large width of the [O III](5007) line is likely caused by a jet interaction with a narrow line region (NLR) medium. The jet bending, significant RM variations, Faraday depolarization, spectral turnover and broad line width of [O III](5007) could be closely related, likely caused by the same nucleus medium, presumably NLR.

第 179 条，共 286 条

Molecular Clouds in the Extreme Outer Galaxy between l.=34 degrees.75 to 45 degrees.25

Sun, Y (Sun, Yan); Su, Y (Su, Yang); Zhang, SB (Zhang, Shao-Bo); Xu, Y (Xu, Ye); Chen, XP (Chen, Xue-Peng); Yang, J (Yang, Ji); Jiang, ZB (Jiang, Zhi-Bo); Fang, M (Fang, Min)
ASTROPHYSICAL JOURNAL SUPPLEMENT SERIES
卷: 230 期: 2 文献号: 17
We present the results of an unbiased CO survey in the Galactic range of 34 degrees 75..l..45 degrees 25 and -5 degrees.25 <= b <= 5 degrees 25, and the velocity range beyond the Outer armA total of 168 molecular clouds (MCs) are identified within the Extreme Outer Galaxy(EOG) region, and 31 of these MCs are associated with 13CO. emissionHowever, none of them show significant (CO)-O-18 emission under the current detection limitThe typical size and mass of these MCs are 5pc and 3x10(3)M(circle dot), implying a lack of large and massive MCs in the EOG regionSimilar to MCs in the outer Galaxy, the velocity dispersions of EOG clouds are also correlated with their sizes; however, they are well displaced below the scaling relationship defined by the inner Galaxy MCsThese MCs with a median Galactocentric radius of 12.6 kpc show very different distributions from those of the MCs in the Outer arm published in our previous paper, while roughly following the Outer Scutum-Centaurus arm defined by Dame & ThaddeusThis result may provide robust evidence for the existence of the Outer Scutum-Centaurus armThe lower limit of the total mass of this segment is about 2.7x105Me, which is about one magnitude lower than that of the Outer armThe mean thickness of the gaseous disk is about 1 degrees 45 or 450pc, and the scale height is about 1 degrees 27, or 400pc above the b=0 degrees planeThe warp traced by CO emission is very obvious in the EOG region and its amplitude is consistent with the predictions by other warp models using different tracers, such as dust, H I, and stellar components of our Galaxy.

第 180 条，共 286 条

Kinematics of a Young Low-mass Star-forming Core: Understanding the Evolutionary State of the First-core Candidate L1451-mm

Maureira, MJ (Maureira, Maira Jose); Arce, HG (Arce, Hector G.); Dunham, MM (Dunham, Michael M.); Pineda, JE (Pineda, Jaime E.); Fernandez-Lopez, M (Fernandez-Lopez, Manuel); *Chen, XP* (Chen, Xuepeng); Mardones, D (Mardones, Diego)
ASTROPHYSICAL JOURNAL
卷: 838 期: 1 文献号: 60
We use 3 mm multiline and continuum CARMA observations toward the first hydrostatic core (FHSC) candidate L1451-mm to characterize the envelope kinematics at 1000 au scales and investigate its evolutionary state. We detect evidence of infall and rotation in the NH2D(11,110,1), N2H+(10), and HCN(10) molecular lines. We compare the

positionvelocity diagram of the NH2D(11,110,1) line with a simple kinematic model and find that it is consistent with an envelope that is both infalling and rotating while conserving angular momentum around a central mass of about 0.06 M-circle dot. The N2H+(10) LTE mass of the envelope along with the inferred infall velocity leads to a mass infall rate of approximately 6 x 10(-6) M-circle dot yr(-1), implying a young age of 10(4) years for this FHSC candidate. Assuming that the accretion onto the central object is the same as the infall rate, we obtain a minimum source size of 1.55 au, consistent with the size expected for a first core. We do not see any evidence of outflow motions or signs of outflowenvelope interaction at scales greater than or similar to 2000 au. This is consistent with previous observations that revealed a very compact outflow (less than or similar to 500 au). We conclude that L1451-mm is indeed at a very early stage of evolution, either a first core or an extremely young Class 0 protostar. Our results provide strong evidence that L1451-mm is the best candidate for being a bona fide first core.

第 181 条，共 286 条

Molecular Environments of Three. Large Supernova Remnants in the Third Galactic Quadrant: G205.5+0.5, G206.9+2.3, and G213.0-0.6

Su, Y (Su, Yang); Zhou, X (Zhou, Xin); Yang, J (Yang, Ji); Chen, XP (Chen, Xuepeng); Chen, Y (Chen, Yang); Liu, Y (Liu, Yi); Wang, H (Wang, Hongchi); Li, C (Li, Chong); Zhang, SB (Zhang, Shaobo)
ASTROPHYSICAL JOURNAL
卷: 836 期: 2 文献号: 211
We present CO observations toward three large supernova remnants (SNRs) in the third Galactic quadrant using the Purple Mountain Observatory Delingha 13.7 m millimeter-wavelength telescope. The observations are part of the high-resolution CO survey of the Galactic plane between Galactic longitudes l = -10 degrees to 250 degrees and latitudes b = -5 degrees to 5 degrees CO emission was detected toward the three SNRs: G205.5+0.5 (Monoceros Nebula), G206.9+2.3 (PKS 0646+06), and G213.0-0.6. Both SNRs G205.5+0.5 and G213.0-0.6 exhibit the morphological agreement (or spatial correspondences) between the remnant and the surrounding molecular clouds (MCs), as well as kinematic signatures of shock perturbation in the molecular gas. We confirm that the two SNRs are physically associated with their ambient MCs and the shock of SNRs is interacting with the dense, clumpy molecular gas. SNR G206.9+2.3, which is close to the northeastern edge of the Monoceros Nebula, displays the spatial coincidence with molecular partial shell structures at V-LSR similar to 15 km s(-1). While no significant line broadening has been detected within or near the remnant, the strong morphological correspondence between the SNR and the molecular cavity implies that SNR G206.9+2.3 is probably associated with the CO gas and is evolving in the low-density environment. The physical features of individual SNRs, together with the relationship between SNRs and their nearby objects, are also discussed.

第 182 条，共 286 条

A Turbulent Origin for the Complex Envelope Kinematics in the Young Low-mass Core Per-bolo 58 Maureira,

MJ (Maureira, Maria Jose); Arce, HG (Arce, Hector G.); Offner, SSR (Offner, Stella S. R.); Dunham, MM (Dunham, Michael M.); Pineda, JE (Pineda, Jaime E.); Fernandez-Lopez, M (Fernandez-Lopez, Manuel); *Chen, XP* (Chen, Xuepeng); Mardones, D (Mardones, Diego)
ASTROPHYSICAL JOURNAL
卷: 849 期: 2 文献号: 89
We use CARMA 3 mm continuum and molecular lines (NH2D, N2H+, HCO+, HCN, and CS) at similar to 1000 au resolution to characterize the structure and kinematics of the envelope surrounding the deeply embedded first core candidate Per-bolo 58. The line profile of the observed species shows two distinct peaks separated by 0.4-0.6 km. s(-1), which most likely arise from two different optically thin velocity components rather than the product of self-absorption in an optically thick line. The two velocity components, each with a mass of similar to 0.5-0.6 M circle dot, overlap spatially at the position of the continuum emission and produce a general gradient along the outflow direction. We investigate whether these observations are consistent with infall in a turbulent and magnetized envelope. We compare the morphology and spectra of the N2H+ (1-0) with synthetic observations of an MHD simulation that considers the collapse of an isolated core that is initially perturbed with a turbulent field. The proposed model matches the data in the production of two velocity components, traced by the isolated hyperfine line of the N2H+ (1-0) spectra, and shows a general agreement in morphology and velocity field. We also use large maps of the region to compare the kinematics of the core with that of the surrounding large-scale filamentary structure and find that accretion from the large-scale filament could also explain the complex kinematics exhibited by this young dense core.

第 183 条，共 286 条

A Turbulent Origin for the Complex Envelope Kinematics in the Young Low-mass Core Per-bolo 58

Maureira, MJ (Maureira, Maria Jose); Arce, HG (Arce, Hector G.); Offner, SSR (Offner, Stella S. R.); Dunham, MM (Dunham, Michael M.); Pineda, JE (Pineda, Jaime E.); Fernandez-Lopez, M (Fernandez-Lopez, Manuel); *Chen, XP* (Chen, Xuepeng); Mardones, D (Mardones, Diego)
ASTROPHYSICAL JOURNAL
卷: 849 期: 2 文献号: 89
We use CARMA 3 mm continuum and molecular lines (NH2D, N2H+, HCO+, HCN, and CS) at similar to 1000 au resolution to characterize the structure and kinematics of the envelope surrounding the deeply embedded first core candidate Per-bolo 58. The line profile of the observed species shows two distinct peaks separated by 0.4-0.6 km. s(-1), which most likely arise from two different optically thin velocity components rather than the product of self-absorption in an optically thick line. The two velocity components, each with a mass of similar to 0.5-0.6 M circle dot, overlap spatially at the position of the continuum emission and produce a general gradient along the outflow direction. We investigate whether these observations are consistent with infall in a turbulent and magnetized envelope. We compare the morphology and spectra of the N2H+ (1-0) with synthetic observations of an MHD simulation that considers the collapse of an isolated core that is initially perturbed with a turbulent field. The proposed model matches the data in the production of two velocity components, traced by the isolated hyperfine line of the N2H+ (1-0) spectra, and shows a general agreement in morphology and velocity field. We also use large maps of the region to compare the kinematics

of the core with that of the surrounding large-scale filamentary structure and find that accretion from the large-scale filament could also explain the complex kinematics exhibited by this young dense core.

2-09 Millimeter & Sub-Millimeter Wave Laboratory

第 184 条，共 286 条

Characterization of a Free-Standing Membrane Supported Superconducting Ti Transition Edge Sensor

Zhang, W (Zhang, Wen); Miao, W (Miao, Wei); Wang, Z (Wang, Zheng); Liu, D (Liu, Dong); Zhong, JQ (Zhong, Jia-Qiang); Guo, XH (Guo, Xiao-Hui); Wu, F (Wu, F.); Yao, QJ (Yao, QiJun); Shi, SC (Shi, Sheng-Cai)
IEEE TRANSACTIONS ON APPLIED SUPERCONDUCTIVITY
卷: 27 期: 4 文献号: 2100606
Superconducting transition edge sensors (TES) based on a Ti microbridge on Si substrate have demonstrated a very low noise equivalent power. Their effective response time, however, is in the order of microseconds due to relatively high transition temperature (i.e., 300-400 mK) of the Ti microbridge, making it difficult to read out the signal of a large Ti TES array with a SQUID-based multiplexer. We propose a twin-slot antenna coupled superconducting Ti microbridge separated from the antenna feed and supported by a free-standing membrane. Its resistive transition (R-T) and current-voltage (I-V) curves are measured before and after KOH wet etching of the Si substrate underneath the Ti microbridge. The free-standing membrane supported Ti TES with a thickness of 40 nm shows slightly lower transition temperature and higher normal resistance. Its thermal conductance is reduced to similar to 800 pW/ K from similar to 3000 pW/ K. In addition, its effective response time measured with a current pulse signal is about 5 mu s. The uniformity of the 8 x 8 TES array is studied by measuring the distribution of normal resistance and critical temperature. In order to improve the uniformity, we increase the Ti film thickness to 64 nm, and characterize its thermal and electrical features.

第 185 条，共 286 条

Optoelectronic Control of an External Cavity Quantum Cascade Laser Using a Graphene Loaded Metamaterial Array

Kindness, SJ (Kindness, S. J.); Jessop, DS (Jessop, D. S.); *Wei, B* (Wei, B.); Wallis, R (Wallis, R.); Kamboj, VS (Kamboj, V. S.); Xiao, L (Xiao, L.); Ren, Y (Ren, Y.); Braeuninger-Weimer, P (Braeuninger-Weimer, P.); Hofmann, S (Hofmann, S.); Beere, HE (Beere, H. E.); Ritchie, DA (Ritchie, D. A.); Degl'Innocenti, R (Degl'Innocenti, R.)
书籍团体作者: IEEE
2017 CONFERENCE ON LASERS AND ELECTRO-OPTICS (CLEO)
We present the optoelectronic frequency and amplitude modulation of a terahertz quantum cascade laser, achieved by implementing a graphene loaded split ring resonator array into an external cavity feedback set-up. Amplitude modulation depths as high as 100% are achieved and the output frequency is lithographically and optoelectronically tuned.
会议名称: Conference on Lasers and Electro-Optics (CLEO)
会议日期: MAY 14-19, 2017
会议地点: San Jose, CA
会议赞助商: IEEE

第 186 条，共 286 条

Observations of the Hydroxyl Radical in C/2013 US10 (Catalina) at 18cm Wavelength

Wang, Z (Wang, Zhen); Chen, X (Chen, Xi); Gao, F (Gao, Feng); Zhang, SB (Zhang, Shaobo); Zheng, XW (Zheng, Xing-Wu); Ip, WH (Ip, Wing-Huen); Wang, N (Wang, Na); Liu, X (Liu, Xiang); Zuo, XT (Zuo, Xiu-Ting); Gou, W (Gou, Wei); Chang, SQ (Chang, Sheng-Qi)
ASTRONOMICAL JOURNAL
卷: 154 期: 6 文献号: 249
The hydroxyl (OH) radical produced by photodissociation of water molecule is one of the most important indicators for cometary outgassing activity. The absorption lines of the OH radical at 1665 and 1667 MHz in the coma of comet C/2013 US10 Catalina were detected between 2015 December 3 and 5 by the Tian Ma Radio Telescope of Shanghai Astronomical Observatory. The source flux intensity was derived to be about - 209 mJy km s(-1) and -86 mJy km s(-1) at 1665 MHz and 1667 MHz, respectively. The corresponding gas production rate was estimated to be (8.78 +/- 1.47) x 10(28) H2O s(-1) and (5.94 +/- 1.27) x 10(28) H2O s(-1), accordingly.

第 187 条，共 286 条

Guest Editorial Mini-Special Issue on the 27th International Symposium on Space Terahertz Technology

Shi, SC (Shi, Sheng-Cai); Mehdi, I (Mehdi, Imran)
IEEE TRANSACTIONS ON TERAHERTZ SCIENCE AND TECHNOLOGY
卷: 7 期: 1 页: 1-1
DOI: 10.1109/TTHZ.2016.2636058
出版年: JAN 2017
在 BIOSIS Citation Index 中的被引频次: 0
SciELO Citation Index 中的 "被引频次": 0
Russian Science Citation Index 中的 "被引频次": 0
在中国科学引文数据库中的被引频次: 0

第 188 条，共 286 条

THz Vector Field Measurement Comparison Between On-the-Fly and Step Scan Method

Hu, J (Hu, Jie); Lou, Z (Lou, Zheng); Yao, QJ (Yao, Qi-Jun); Miao, W (Miao, Wei); Yang, JP (Yang, Jin-Ping); Lin, ZH (Lin, Zhen-Hui); Shi, SC (Shi, Sheng-Cai)
IEEE TRANSACTIONS ON TERAHERTZ SCIENCE AND TECHNOLOGY
卷: 7 期: 1 页: 27-35
A fast terahertz vector field measurement system based on the on-the-fly (OTF) scan method is investigated. Compared with the step scan method, which samples at certain step, the OTF scan obtains the data with the scanner moving continuously, thus improving the measurement efficiency to some extent. The phase stability of the system is fully

studied. Demonstration at approximately 500 GHz is compared with the result by the step scan method, showing that the OTF method can improve the measurement speed by a factor of 7 while the data accuracy is almost the same. Measurements at different scanning speeds and with different probes are also compared to understand their effects.
会议名称: 27th International Symposium on Space Terahertz Technology (ISSTT)
会议日期: APR 12-15, 2016
会议地点: Purple Mt Observ, Nanjing, PEOPLES R CHINA
会议赞助商: Key Lab Radio Astron
会议主办方: Purple Mt Observ

第 189 条，共 286 条

External amplitude and frequency modulation of a terahertz quantum cascade laser using metamaterial/graphene devices

Kindness, SJ (Kindness, S. J.); Jessop, DS (Jessop, D. S.); Wei, B (Wei, B.); Wallis, R (Wallis, R.); Kamboj, VS (Kamboj, V. S.); Xiao, L (Xiao, L.); *Ren, Y* (Ren, Y.); Braeuninger-Weimer, P (Braeuninger-Weimer, P.); Aria, AI (Aria, A. I.); Hofmann, S (Hofmann, S.); Beere, HE (Beere, H. E.); Ritchie, DA (Ritchie, D. A.); Degl'Innocenti, R (Degl'Innocenti, R.)
SCIENTIFIC REPORTS
卷: 7 文献号: 7657
Active control of the amplitude and frequency of terahertz sources is an essential prerequisite for exploiting a myriad of terahertz applications in imaging, spectroscopy, and communications. Here we present a optoelectronic, external modulation technique applied to a terahertz quantum cascade laser which holds the promise of addressing a number of important challenges in this research area. A hybrid metamaterial/graphene device is implemented into an external cavity set-up allowing for optoelectronic tuning of feedback into a quantum cascade laser. We demonstrate powerful, all-electronic, control over the amplitude and frequency of the laser output. Full laser switching is performed by electrostatic gating of the metamaterial/graphene device, demonstrating a modulation depth of 100%. External control of the emission spectrum is also achieved, highlighting the flexibility of this feedback method. By taking advantage of the frequency dispersive reflectivity of the metamaterial array, different modes of the QCL output are selectively suppressed using lithographic tuning and single mode operation of the multi-mode laser is enforced. Side mode suppression is electrically modulated from similar to 6 dB to similar to 21 dB, demonstrating active, optoelectronic modulation of the laser frequency content between multi-mode and single mode operation.

第 190 条，共 286 条

Analysis of 220-GHz Low-Loss Quasi-Elliptic Waveguide Bandpass Filter

Ding, JQ (Ding, Jiang-Qiao); Shi, SC (Shi, Sheng-Cai); Zhou, K (Zhou, Kang); Liu, D (Liu, Dong); Wu, W (Wu, Wen)
IEEE MICROWAVE AND WIRELESS COMPONENTS LETTERS
卷: 27 期: 7 页: 648-650
A 220-GHz low-loss and wideband waveguide bandpass filter with fourth-order quasi-elliptic response is presented and analyzed in this letter. An electric cross-coupling realized by easily manufactured capacitive iris is introduced in the classical folded quadruplet topology. The prototype fabricated by conventional computer numerical control (CNC)-metal-milling technology exhibits meaningful results of an insertion loss of around 0.6 dB and a 3-dB fractional bandwidth of 9.8% centered at 214.3 GHz, which are in excellent agreement with the simulated ones. The effects of tolerance and surface roughness on the filter performance are discussed in detail. All the results indicate that the present CNC process can meet the accuracy and roughness requirement of such waveguide filter in WR-4 band.

第 191 条，共 286 条

WR-3 Band Quasi-Elliptical Waveguide Filters Using Higher Order Mode Resonances

Ding, JQ (Ding, Jiang-Qiao); Shi, SC (Shi, Sheng-Cai); Zhou, K (Zhou, Kang); Zhao, Y (Zhao, Yun); Liu, D (Liu, Dong); Wu, W (Wu, Wen)
IEEE TRANSACTIONS ON TERAHERTZ SCIENCE AND TECHNOLOGY
卷: 7 期: 3 页: 302-309
Two types of WR-3 band quasi-elliptical waveguide bandpass filters (BPFs) using higher order mode resonators are presented based on physical cross coupling and modal bypass coupling, respectively. Under the situation of physical folded structure, a TE102-mode in an oversized waveguide resonator is utilized to reverse the magnetic field direction of main path to implement a negative cross coupling (Filter-I). Limited to the structure of Filter-I itself, the simulated 3 dB fractional bandwidth (FBW) of 8.5% is slightly narrower than desired 10% FBW. For the other case, two TE101/TE201 overmode resonant cavities with suitable input and output coupling locations are employed to generate two transmission zeros in the vicinity of the passband through modal bypass couplings (Filter-II). The benefit from the realization of the wide-band source and load couplings in the fringe first and fourth oversized cavities is that the FBW of 10% is achieved in the Filter-II. The two BPFs fabricated by computer numerical control milling technology exhibit an insertion loss (IL) of about 0.7 dB and a 3 dB FBW of 8.77% centered at 257.7 GHz (Filter-I), IL of around 0.5 dB, and FBW of 9.83% with center frequency of 256.3 GHz (Filter-II), which are all in good agreement with the simulations. The performance of the two BPFs based on one or two oversized waveguide resonators is highlighted comparing with the reported similar terahertz waveguide filters.

第 192 条，共 286 条

A 240-GHz Wideband Ridged Waveguide Filter Based on MEMS Process

Ding, JQ (Ding, Jiangqiao); Hu, J (Hu, Jie); Liu, D (Liu, Dong); Wang, DW (Wang, Daowei); Shi, SC (Shi, Shengcai); Wu, W (Wu, Wen)
JOURNAL OF INFRARED MILLIMETER AND TERAHERTZ WAVES
卷: 38 期: 3 页: 283-291
Terahertz (THz) bandpass filter (BPF) is one of important components in some detectors for astronomical observations. In this paper, a BPF with a relative bandwidth of 50% centered at 240 GHz is presented. This wideband BPF is made up of six ridged waveguide resonators and developed by silicon-based micro-electro-mechanical systems (MEMS) process. The transmission response of the filter is measured by a quasi-optical setup incorporating a sensitive superconducting mixer, and the result is in good agreement with the simulated one. Details of the design, simulation, and measurement are discussed in this paper.

第 193 条，共 286 条

Development of ultra high sensitivity superconducting THz detectors

Li Jing; Zhang Wen; Miao Wei; Shi Shengcai
Chinese Optics
卷：10 期：1 页：122-130 文献号：2095-1531(2017)10:1<122:CGLMDT>2.0.TX;2-B
Nearly half of the photon energy is occupied in Terahertz waveband after the cosmic microwave background(CMB) radiation in space,which plays an irreplaceable role in the study of astronomy. So the terahertz astronomy research has extremely important scientific significance. In this paper,we introduce the development of the terahertz coherent detectors bosed on ultra high sensitivity superconducting terahertz detection technology,including superconducting tunnel junction the mixer(SIS) and superconducting hot electron mixer (HEB),and non coherent detectors such as superconducting dynamic inductance detector(MKIDs) and superconducting transition edge detector(TES). The future development trend is also prospected. The review for superconducting THz detectors has the reference significance for the development of astronomical terahertz detection technique in our country.

第 194 条，共 286 条

Terahertz and far-infrared windows opened at Dome A in Antarctica

Shi, SC (Shi, Sheng-Cai); Paine, S (Paine, Scott); Yao, QJ (Yao, Qi-Jun); Lin, ZH (Lin, Zhen-Hui); Li, XX (Li, Xin-Xing); Duan, WY (Duan, Wen-Ying); Matsuo, H (Matsuo, Hiroshi); Zhang, QZ (Zhang, Qizhou); Yang, J (Yang, Ji); Ashley, MCB (Ashley, M. C. B.); Shang, ZH (Shang, Zhaohui); Hu, ZW (Hu, Zhong-Wen)
NATURE ASTRONOMY
卷: 1 期: 1 文献号: 0001
The terahertz and far-infrared band, ranging from approximately 0.3 THz to 15 THz (1 mm to 20 mu m), is important for astrophysics as it hosts the peak of the thermal radiation of the cold component of the Universe as well as many spectral lines that trace the cycle of interstellar matter1-8. However, water vapour makes the terrestrial atmosphere opaque to this frequency band over nearly all of the Earth's surface9. Early radiometric measurements10 below 1 THz at Dome A (80 degrees 22'S, 77 degrees 21' E), the highest point of the cold and dry Antarctic ice sheet, suggest that this site may offer the best possible access for ground-based astronomical observations in the terahertz and far-infrared band. To fully assess the site conditions and to address the uncertainties in radiative transfer modelling of the atmosphere, we carried out measurements of atmospheric radiation from Dome A with a Fourier transform spectrometer, spanning the entire water vapour pure rotation band from 20 mu m to 350 mu m. Our measurements reveal substantial transmission in atmospheric windows throughout the whole band. By combining our broad-band spectra with data on the atmospheric state over Dome A, we set new constraints on the spectral absorption of water vapour at upper tropospheric temperatures, which is important for accurate modelling of the terrestrial climate. We find that current spectral models significantly underestimate the H2O continuum absorption.

第 195 条，共 286 条

High Efficiency and Wideband 300 GHz Frequency Doubler Based on Six Schottky Diodes

Ding, JQ (Ding, Jiangqiao); Maestrini, A (Maestrini, Alain); Gatilova, L (Gatilova, Lina); Cavanna, A (Cavanna, Antonella); Shi, SC (Shi, Shengcai); Wu, W (Wu, Wen)
JOURNAL OF INFRARED MILLIMETER AND TERAHERTZ WAVES
卷: 38 期: 11 页: 1331-1341
A high efficiency and wideband 300 GHz frequency doubler based on six Schottky diodes is presented in this paper. This balanced doubler features a compact and robust circuit on a 5-mu m-thick, 0.36-mm-wide, and 1-mm-long GaAs membrane, fabricated by LERMA-C2N Schottky process. The conversion efficiency is mainly better than 16% across the wide bandwidth of 266-336 GHz (3 dB fractional bandwidth of 24%) when pumping with 20-60 mW input power (P (in)) at the room temperature. A peak output power of 14.75 mW at 332 GHz with a 61.18 mW P (in), an excellent peak efficiency of 30.5% at 314 GHz with 43.86 mW P (in) and several frequency points with outstanding efficiency of higher than 25% are delivered. This doubler served as the second stage of the 600 GHz frequency multiplier chain is designed, fabricated, and measured. The performance of this 300 GHz doubler is highlighted comparing to the state-of-art terahertz frequency doublers.

第 196 条，共 286 条

超高灵敏度太赫兹超导探测技术发展

李婧 ， 张文 ， 缪巍 ， 史生才
中国光学,
2017 , 10 (1) :122-130
太赫兹波段占有宇宙微波背景(CMB)辐射以后宇宙空间近一半的光子能量,该波段在天文学研究中具有不可替代的作用,因此太赫兹天文学的研究,具有极其重要的科学意义。本文系统介绍了基于超高灵敏度太赫兹超导探测技术的太赫兹相干探测器发展状况,包括超导隧道结混频器(SIS)和超导热电子混频器(HEB),以及以超导动态电感探测器(MKIDs)和超导相变边缘探测器(TES)为代表的非相干探测器的研究。在此基础上,展望了该领域未来发展趋势,对我国太赫兹天文探测技术的发展具有一定的参考意义。

2-10 Telescope Technology Laboratory

第 197 条，共 286 条

Failure analysis of a frangible composite cover: A transient-dynamics study

Cai, DA (Cai, Deng'an); Zhou, GM (Zhou, Guangming); Qian, Y (Qian, Yuan); Silberschmidt, VV (Silberschmidt, Vadim V.)
JOURNAL OF COMPOSITE MATERIALS
卷: 51 期: 18 页: 2607-2617
A transient-dynamics model based on the approximate Riemann algorithm is proposed for the failure analysis of a frangible composite canister cover. The frangible cover,

manufactured with a traditional manual lay-up method, is designed to conduct a simulated missile launch test using a specially developed test device. Deformation of the cover's centre is determined using a transient-dynamics finite element model; failure pressure for the frangible cover is obtained based on a failure criterion and compared with simulated experimental results. Weak-zone position of the frangible cover has a significant effect on failure pressure compared to that of deformation of the cover's centre. With the same structure of the weak-zone, an increase in its height can first raise and then reduce the level of failure pressure of the frangible cover. Close agreements between the experimental and numerical results are observed.

第 198 条，共 286 条

Two Methods to Broaden the Bandwidth of a Nonlinear Piezoelectric Bimorph Power Harvester

Hu, HP (Hu, Hongping); Dai, LX (Dai, Longxiang); Chen, H (Chen, Hao); Jiang, S (Jiang, Shan); Wang, HR (Wang, Hairen); Laude, V (Laude, Vincent)
JOURNAL OF VIBRATION AND ACOUSTICS-TRANSACTIONS OF THE ASME
卷: 139 期: 3 文献号: 031008
We propose two methods to broaden the operation bandwidth of a nonlinear pinned-pinned piezoelectric bimorph power harvester. The energy-scavenging structure consists of a properly poled and electroded flexible bimorph with a metallic layer in the middle, and is subjected to flexural vibration. Nonlinear effects at large deformations near resonance are considered by taking the in-plane extension of the bimorph into account. The resulting output powers are multivalued and exhibit jump phenomena. Two methods to broaden the operation bandwidth are proposed: The first method is to extend the operation frequency to the left single-valued region through optimal design. The second method is to excite optimal initial conditions with a voltage source. Larger output powers in the multivalued region of the nonlinear harvester are obtained. Hence, the operation bandwidth is broadened from the left single-valued region to the whole multivalued region.

第 199 条，共 286 条

Research on a bimorph piezoelectric deformable mirror for adaptive optics in optical telescope

Wang, HR (Wang, Hairen)
OPTICS EXPRESS
卷: 25 期: 7 页: 8115-8122
We have proposed a discrete-layout bimorph piezoelectric deformable mirror (DBPDM) and developed its realistic electromechanical model. Compared with the conventional piezoelectric deformable mirror (CPDM) and the bimorph piezoelectric deformable mirror (BPDM), the DBPDM has both a larger stroke and a higher resonance frequency by integrating the strengths of the CPDM and the BPDM. To verify the advancement, a 21-elements DBPDM is studied in this paper. The results have suggested that the stroke of the DBPDM is larger than 10 microns and its resonance frequency is 53.3 kHz. Furthermore, numerical simulation is conducted on the deformation of the mirror using the realistic electromechanical model, and the dependence of the influence function upon the size of the radius of push pad is analyzed. (C) 2017 Optical Society of America

第 200 条，共 286 条

Linear and nonlinear analysis of the thermal effects of beam piezoelectric bending actuator on adaptive optics

Wang, HR (Wang, Hairen); Hu, L (Hu, Lin)
JOURNAL OF INTELLIGENT MATERIAL SYSTEMS AND STRUCTURES
卷: 28 期: 20 页: 3016-3024
The beam piezoelectric bending actuator, of a simple structure and at a low cost, can be a good match for the large adaptive optics telescopes, for it has a large stroke and a high resonance frequency. In this article, the thermal effects of a beam piezoelectric bending actuator are analyzed in the aspects of the statics, dynamics, and nonlinear dynamics. The results of the linear statics and dynamics have shown that the thermal effects will produce the zero offsets to the static strokes of the beam piezoelectric bending actuator and have little influence on the resonant frequency. Besides, finite element analysis methods are applied to validate the analytic methods. The conclusions have shown that the analytic results and the finite element analysis results are reasonably consistent with each other. Furthermore, the nonlinear behaviors of the beam piezoelectric bending actuator in dynamics are studied, and through the changeable curves of the frequency, it can be observed that the results of the strokes imposed on the actuator have exhibited multiple values and jumps near the resonance.

第 201 条，共 286 条

A combined analysis of PandaX, LUX, and XENON1T experiments within the framework of dark matter effective theory

Liu, ZW (Liu, Zuowei); Su, YS (Su, Yushan); Tsai, YLS (Tsai, Yue-Lin Sming); Yu, BR (Yu, Bingrong);
JOURNAL OF HIGH ENERGY PHYSICS
期: 11 文献号: 024
Weakly interacting massive particles are a widely well-probed dark matter candidate by the dark matter direct detection experiments. Theoretically, there are a large number of ultraviolet completed models that consist of a weakly interacting massive particle dark matter. The variety of models makes the comparison with the direct detection data complicated and often non-trivial. To overcome this, in the non-relativistic limit, the effective theory was developed in the literature which works very well to significantly reduce the complexity of dark matter-nucleon interactions and to better study the nuclear response functions. In the effective theory framework for a spin-1/2 dark matter, we combine three independent likelihood functions from the latest PandaX, LUX, and XENON1T data, and give a joint limit on each effective coupling. The astrophysical uncertainties of the dark matter distribution are also included in the likelihood. We further discuss the isospin violating cases of the interactions. Finally, for both dimension-five and dimension-six effective theories above the electroweak scale, we give updated limits of the new physics mass scales.

2-11 Delingha millimeter wave Observation Station

第 202 条，共 286 条

Two-dimensional Molecular Gas and Ongoing Star Formation around H II Region Sh2-104

Xu, JL (Xu, Jin-Long); Xu, Y (Xu, Ye); Yu, NP (Yu, Naiping); Zhang, CP (Zhang, Chuan-peng); Liu, XL (Liu, Xiao-Lan); Wang, JJ (Wang, Jun-Jie); Ning, CC (Ning, Chang-chun); Ju, BG (Ju, Bing-Gang); Zhang, GY (Zhang, Guo-Yin)
ASTROPHYSICAL JOURNAL
卷: 849 期: 2 文献号: 140
We performed a multi-wavelength study toward H II region Sh2-104. New maps of (CO)-C-12 J = 1 - 0 and (CO)-C-13 J = 1 - 0 were obtained from the Purple Mountain Observatory 13.7 m radio telescope. Sh2-104 displays a double-ring structure. The outer ring with a radius of 4.4 pc is dominated by 12, 500 mu m, (CO)-C-12 J = 1 - 0, and (CO)-C-13 J = 1 - 0 emission, while the inner ring with a radius of 2.9 pc is dominated by 22 mu m and 21 cm emission. We did not detect CO emission inside the outer ring. The north-east portion of the outer ring is blueshifted, while the south-west portion is redshifted. The present observations have provided evidence that the collected outer ring around Sh2-104 is a two-dimensional structure. From the column density map constructed by the Hi-GAL survey data, we extract 21 clumps. About 90% of all the clumps will form low-mass stars. A power-law fit to the clumps yields M = 281 M-circle dot(r/pc)(1.31 +/- 0.8). The selected YSOs are associated with the collected material on the edge of Sh2-104. The derived dynamical age of Sh2-104 is 1.6 x 10(6) yr. Comparing the Sh2-104 dynamical age with the YSO timescale and the fragmentation time of the molecular ring, we further confirm that the collect-and-collapse process operates in this region, indicating positive feedback from a massive star for surrounding gas.

第 203 条，共 286 条

Towards a three-dimensional distribution of the molecular clouds in the Galactic Centre

Yan, QZ (Yan, Qing-Zeng); Walsh, AJ (Walsh, A. J.); Dawson, JR (Dawson, J. R.); Macquart, JP (Macquart, J. P.); Blackwell, R (Blackwell, R.); Burton, MG (Burton, M. G.); Rowell, GP (Rowell, G. P.); Zhang, B (Zhang, Bo); Xu, Y (Xu, Ye); Tang, ZH (Tang, Zheng-Hong); Hancock, PJ (Hancock, P. J.)
MONTHLY NOTICES OF THE ROYAL ASTRONOMICAL SOCIETY
卷: 471 期: 3 页: 2523-2536
We present a study of the three-dimensional structure of the molecular clouds in the Galactic Centre (GC) using CO emission and OH absorption lines. Two CO isotopologue lines, (CO)-C-12(J = 1 -> 0) and (CO)-C-13(J = 1 -> 0), and four OH ground-state transitions, surveyed by the Southern Parkes Large-Area Survey in Hydroxyl, contribute to this study. We develop a novel method to calculate the OH column density, excitation temperature and optical depth precisely using all four OH lines, and we employ it to derive a three-dimensional model for the distribution of molecular clouds in the GC for six slices in Galactic latitude. The angular resolution of the data is 15.5 arcmin, which at the distance of the GC (8.34 kpc) is equivalent to 38 pc. We find that the total mass of OH in the GC is in the range of 2400-5100 M-circle dot. The face-on view at a Galactic latitude of b = 0 degrees. displays a bar-like structure with an inclination angle of 67.5 +/- 2.1 degrees with respect to the line of sight. No ring-like structure in the GC is evident in our data, likely due to the low-spatial resolution of the CO and OH maps.

第 204 条，共 286 条

Large-field CO(1-0) observations toward the Galactic historical supernova remnants: a large cavity around Tycho's supernova remnant

Chen, X (Chen, X.); Xiong, F (Xiong, F.); Yang, J (Yang, J.)
ASTRONOMY & ASTROPHYSICS
卷: 604 文献号: A13
Context. The investigation of the interaction between the supernova remnants (SNRs) and interstellar gas is not only necessary to improve our knowledge of SNRs, but also to understand the nature of the progenitor systems.
Aims. As a part of the Milky Way Imaging Scroll Painting CO line survey, the aim is to study the interstellar gas surrounding the Galactic historical SNRs. In this work, we present the CO results of Tycho's SNR.
Methods. Using the 3 x 3 Superconducting Spectroscopic Array Receiver (SSAR) at the PMO 13.7-m telescope, we performed large-field (3 degrees x 2 degrees) and high-sensitivity CO(1-0) molecular line observations toward Tycho's SNR.
Results. The CO observations reveal large molecular clouds, stream-like structures, and an inner rim around the remnant. We derived the basic properties (column density, mass, and kinematics) of these objects based on the CO observations. The large molecular clouds individually show an arc toward the remnant center, outlining a large cavity with radii of similar to 0.3 degrees x 0.6 degrees (or 13 pc x 27 pc at a distance of 2.5 kpc) around the remnant. The CO line broadenings and asymmetries detected in the surrounding clouds, the observed expansion of the cavity, in concert with enhanced (CO)-C-12(2-1)/(1-0) intensity ratio detected in previous studies, suggest the interaction of the large cavity with a wind in the region. After excluding the scenario of a large bubble produced by bright massive stars, we suggest that the large cavity could be explained by accretion wind from the progenitor system of Tycho's supernova. Nevertheless, the possibility of the random distribution of a large cavity around Tycho's SNR cannot be ruled out thus far. Further observations are needed to confirm the physical association of the large cavity with Tycho's SNR.

第 205 条，共 286 条

A 95 GHz methanol emission survey toward eight small supernova remnants

Li, YJ (Li, Ying-Jie); Xu, Y (Xu, Ye); Chen, X (Chen, Xi); Lu, DR (Lu, Deng-Rong); Sun, Y (Sun, Yan); Du, XY (Du, Xin-Yu); Shen, ZQ (Shen, Zhi-Qiang)
RESEARCH IN ASTRONOMY AND ASTROPHYSICS
卷: 17 期: 12 文献号: 125
We report on a 95GHz (8(0)-7(1) A(+)) methanol (CH3OH) emission survey with the Purple Mountain Observatory Delingha 13.7 m telescope. Eight supernova remnants (SNRs) with angular size less than or similar to 10' were observed, but emission was only detected in three SNRs near the Galactic center (Sgr A East, G 0.1-0.1 and G 359.92-0.09). CH3OH emission mainly surrounds the SNRs and can be decomposed into nine spatial peaks with the velocity range of eight peaks being (-30, 70) km s(-1), and the other is (70, 120) km s(-1). They are probably excited by interaction with these SNRs and adjacent molecular gas in the central molecular zone (CMZ), although star formation may play an

important role in exciting CH3OH emission in some regions of CMZ. We infer that tidal action is unlikely to be an excitation source for CH3OH emission.

第 206 条，共 286 条

A New 95GHz Methanol Maser Catalog. I. Data

Yang, WJ (Yang, Wenjin); Xu, Y (Xu, Ye); Chen, X (Chen, Xi); Ellingsen, SP (Ellingsen, Simon P.); Lu, DR (Lu, Dengrong); Ju, BG (Ju, Binggang); Li, YJ (Li, Yingjie)
ASTROPHYSICAL JOURNAL SUPPLEMENT SERIES
卷: 231 期: 2 文献号: 20
The Purple Mountain Observatory 13.7 m radio telescope has been used to search for 95 GHz (8(0)-7(1)A(+)) class I methanol masers toward 1020 Bolocam Galactic Plane Survey (BGPS) sources, leading to 213 detections. We have compared the line width of the methanol and HCO+ thermal emission in all of the methanol detections, and on that basis, we find that 205 of the 213 detections are very likely to be masers. This corresponds to an overall detection rate of 95 GHz methanol masers toward our BGPS sample of 20%. Of the 205 detected masers, 144 (70%) are new discoveries. Combining our results with those of previous 95 GHz methanol maser searches, a total of 481 95 GHz methanol masers are now known. We have compiled a catalog listing the locations and properties of all known 95 GHz methanol masers.

第 207 条，共 286 条

Techniques for Accurate Parallax Measurements for 6.7 GHz Methanol Masers

Reid, MJ (Reid, M. J.); Brunthaler, A (Brunthaler, A.); Menten, KM (Menten, K. M.); Sanna, A (Sanna, A.); *Xu, Y* (Xu, Y.); Li, JJ (Li, J. J.); Wu, Y (Wu, Y.); Hu, B (Hu, B.); Zheng, XW (Zheng, X. W.); Zhang, B (Zhang, B.); Immer, K (Immer, K.); Rygl, K (Rygl, K.); Moscadelli, L (Moscadelli, L.); Sakai, N (Sakai, N.); Bartkiewicz, A (Bartkiewicz, A.); Choi, YK (Choi, Y. K.)
ASTRONOMICAL JOURNAL
卷: 154 期: 2 文献号: 63
The BeSSeL Survey is mapping the spiral structure of the Milky Way by measuring trigonometric parallaxes of hundreds of maser sources associated with high-mass star formation. While parallax techniques for water masers at high frequency (22 GHz) have been well documented, recent observations of methanol masers at lower frequency (6.7 GHz) have revealed astrometric issues associated with signal propagation through the ionosphere that could significantly limit parallax accuracy. These problems displayed as a "parallax gradient" on the sky when measured against different background quasars. We present an analysis method in which we generate position data relative to an "artificial quasar" at the target maser position at each epoch. Fitting parallax to these data can significantly mitigate the problems and improve parallax accuracy.

第 208 条，共 286 条

CO(J=1-0) Observations of a Filamentary Molecular Cloud in the Galactic Region Centered at l=150 degrees, b=3 degrees.5

Xiong, F (Xiong, Fang); Chen, XP (Chen, Xuepeng); Yang, J (Yang, Ji); Fang, M (Fang, Min); Zhang, SB (Zhang, Shaobo); Zhang, MM (Zhang, Miaomiao); Du, XY (Du, Xinyu); Long, WS (Long, Wenshan)
ASTROPHYSICAL JOURNAL
卷: 838 期: 1 文献号: 49
We present large-field (4.25 x 3.75 deg(2)) mapping observations toward the Galactic region centered at l = 150 degrees, b = 3 degrees.5 in the J = 1-0 emission line of CO isotopologues ((CO)-C-12, (CO)-C-13, and (CO)-O-18), using the 13.7 m millimeter-wavelength telescope of the Purple Mountain Observatory. Based on the (CO)-C-13 observations, we reveal a filamentary cloud in the Local Arm at a velocity range of -0.5 to 6.5 km s(-1). This molecular cloud contains 1 main filament and 11 sub-filaments, showing the so-called "ridge-nest" structure. The main filament and three sub-filaments are also detected in the (CO)-O-18 line. The velocity structures of most identified filaments display continuous distribution with slight velocity gradients. The measured median excitation temperature, line width, length, width, and linear mass of the filaments are similar to 9.28 K, 0.85 km s(-1), 7.30 pc, 0.79 pc, and 17.92 M-circle dot pc(-1), respectively, assuming a distance of 400 pc. We find that the four filaments detected in the (CO)-O-18 line are thermally supercritical, and two of them are in the virialized state, and. thus tend to be gravitationally bound. We identify in total 146 (CO)-C-13 clumps in the cloud, about 77% of the clumps are distributed along the filaments. About 56% of the virialized clumps are found to be associated with the supercritical filaments. Three young stellar object candidates are also identified in the supercritical filaments, based on the complementary infrared data. These results indicate that the supercritical filaments, especially the virialized filaments, may contain star-forming activities.

第 209 条，共 286 条

Molecular Lines of CO Isotopes of the High Galactic Latitude Cloud HSVMT 27

He Zhihong; Xu Ye; Yang Ji; Du Xinyu; Li Facheng; Lu Dengrong; Yan Qingzeng
Acta Astronomica Sinica
卷：58 期：1 页：6-1-6-13 文献号：0001-5245(2017)58:1<6:GYWQYH>2.0.TX;2-9
A study on ~(12)CO,~(13)CO, and C~(18)O] of the high galactic latitude cloud HSVMT 27, located in Ursa Major, was conducted. A relatively low ~(12)CO excitation temperature was found. While some C~(18)O emissions were detected, they were too weak to be mapped. With the linear resolution of 0.08 pc and the velocity resolution of 0.17 km·s~(-1), 26 ~(13)CO cores were identified in the dense regions. All the local thermodynamic equilibrium masses of these cores are less than their Virial masses, ranging in 0.5-10 M_⊙,and have no infrared point sources associated with them. Overall, the data indicate that there is no recent or ongoing star formation in this cloud.

III. Applied Celestial Mechanics and Space Object & Debris Research

3-01 Center for Space Object and Debris Research

第 210 条，共 286 条

The secular analytical solution of the orbital plane using Lindstedt-Poincare method

Yu, SX (Yu, Shengxian); Zhao, CY (Zhao, Changyin); Zhang, W (Zhang, Wei)
ADVANCES IN SPACE RESEARCH
卷: 60 期: 10 页: 2166-2180
Nowadays, the increasing amount of space objects makes the space so crowded that the satellites in orbit endure severe environment. Hence how to efficiently search and catalog these space objects becomes an urgent problem to be solved. In the paper, in order to contribute to this problem, the secular analytical solution of the orbital plane for medium and high orbit objects is studied. For medium and high orbit objects, the Earth's oblateness and the lunisolar gravitational perturbations are considered. The double averaging method is used to first average the system. For small to medium orbit inclinations and small eccentricities, and then the differential equations can be rewritten in an expansion form. Combining the Lindstedt-Poincare procedure and the solution for differential equations with special coefficients, the third-order analytical solutions can be derived step by step. Finally, two kinds of comparisons are carried out. One is the comparison between the analytical solution and the results derived by integrating the simplified model. It aims to verify the validity of these methods. The other one is the comparison with the integration results of the normal model to show the accuracy of the analytical solution. Both of the two comparisons results work well. The accuracy of the analytical solution can be maintained at the order of O(10(-3)) for the duration of 200 yrs.

第 211 条，共 286 条

Approximate expressions of mean eddy current torque acted on space debris

Lin, HY (Lin, Hou-yuan); Zhao, CY (Zhao, Chang-yin)
ASTROPHYSICS AND SPACE SCIENCE
卷: 362 期: 2 文献号: 34
Rotational state of space debris will be influenced by eddy current torque which is produced by the conducting body rotating within the geomagnetic field. Former expressions of instantaneous torque established in body-fixed coordinate system will change in space during rotation due to the variation of the coordinate system. In order to further investigate the evolution of the rotation of space debris subjected to the eddy current torque, approximate expressions of mean eddy current torque in inertial coordinate system are obtained from the average of the Euler dynamics equations under the assumption that two of the principal moments of inertia of the space debris are similar. Then the expressions are verified through numerical simulation, in which the orientation of the averaged variation of angular momentum is in agreement with the torque from the expressions, which is on an identical plane with magnetic field and the angular momentum. The torque and the averaged variation of the angular momentum have the same evolution trend during rotation in spite of minor deviations of their values.

第 212 条，共 286 条

Long-term dynamical evolution of Tundra-type orbits

Zhang, MJ (Zhang, Ming-Jiang); Zhao, CY (Zhao, Chang-Yin); Hou, YG (Hou, Yong-Gang); Zhu, TL (Zhu, Ting-Lei); Wang, HB (Wang, Hong-Bo); Sun, RY (Sun, Rong-Yu); Zhang, W (Zhang, Wei)
ADVANCES IN SPACE RESEARCH
卷: 59 期: 2 页: 682-697
Tundra-type orbits are elliptical geosynchronous orbits located at the critical inclination. The long-term dynamical evolution of this type of special orbit is investigated in this paper. First, the effect of Earth's gravitational potential is examined. A simplified Hamiltonian of Tundra-type orbits subjected to Earth's gravitational potential is presented through a strict magnitude comparison of the involved terms. Based on this simplified Hamiltonian with two degrees of freedom, the equilibrium points of the orbits subjected to Earth's gravitational potential and their stabilities are discussed. This simplified Hamiltonian is then reduced to a one-degree-of-freedom system dominating the intermediate-period motion of the orbits approximately. In particular, the main characteristic parameters of the intermediate-period motion for nominal Tundra-type orbits and the corresponding specific results for three Sirius satellites in such orbits are presented. Second, the effect of lunisolar perturbations is examined. A magnitude comparison elementarily illustrates that the effect of tesseral harmonics of the Earth's gravitational potential on the long timespan evolution of Tundra-type orbits is negligible compared to that of lunisolar perturbations. A simplified dynamical model including lunisolar perturbations is then presented. Based on this simplified dynamical model, the influences of lunar precession, the initial longitude of the ascending node, the initial argument of perigee, and the initial epoch on the long-term dynamical evolution of the orbits are comparatively analyzed. Finally, numerical calculations with exact perturbation models are conducted to verify the theoretical analysis and to provide more information about the dynamical evolution of Tundra-type orbits.

第 213 条，共 286 条

The fast co-adding algorithm of QCT

Ping, YD (Ping, Yiding); Zhang, C (Zhang, Chen)
ADVANCES IN SPACE RESEARCH
卷: 60 期: 5 页: 907-914
This paper presents a fast co-adding algorithm designed to stack the images coming from different channels of QCT in real-time. The algorithm calculates the transformation

coefficients for every single exposure to eliminate the effects of the possible shifts of the lenses. The way of reprojection and co-adding applied here is a linear method similar to Drizzle, and a reasonable simplification is applied to accelerate the computation. All the calculation can be finished in about 100 ms on a 3.4 GHz CPU with 4 cores, which matches the needs for the observation of space debris perfectly, while the limiting magnitude is improved by about 0.8. The co-adding results of our algorithm are very close to SWarp's, even slightly better in terms of SNRs. (C) 2017 COSPAR. Published by Elsevier Ltd. All rights reserved.

第 214 条，共 286 条

Blind deconvolution with principal components analysis for wide-field and small-aperture telescopes

Jia, P (Jia, Peng); Sun, RY (Sun, Rongyu); Wang, WN (Wang, Weinan); Cai, DM (Cai, Dongmei); Liu, HG (Liu, Huigen)
MONTHLY NOTICES OF THE ROYAL ASTRONOMICAL SOCIETY
卷: 470 期: 2 页: 1950-1959
Telescopes with a wide field of view (greater than 1 degrees) and small apertures (less than 2 m) are workhorses for observations such as sky surveys and fast-moving object detection, and play an important role in time-domain astronomy. However, images captured by these telescopes are contaminated by optical system aberrations, atmospheric turbulence, tracking errors and wind shear. To increase the quality of images and maximize their scientific output, we propose a new blind deconvolution algorithm based on statistical properties of the point spread functions (PSFs) of these telescopes. In this new algorithm, we first construct the PSF feature space through principal component analysis, and then classify PSFs from a different position and time using a self-organizing map. According to the classification results, we divide images of the same PSF types and select these PSFs to construct a prior PSF. The prior PSF is then used to restore these images. To investigate the improvement that this algorithm provides for data reduction, we process images of space debris captured by our small-aperture wide-field telescopes. Comparing the reduced results of the original images and the images processed with the standard Richardson-Lucy method, our method shows a promising improvement in astrometry accuracy.

第 215 条，共 286 条

Satellite-based entanglement distribution over 1200 kilometers

Yin, J (Yin, Juan); Cao, Y (Cao, Yuan); Li, YH (Li, Yu-Huai); Liao, SK (Liao, Sheng-Kai); Zhang, L (Zhang, Liang); Ren, JG (Ren, Ji-Gang); Cai, WQ (Cai, Wen-Qi); Liu, WY (Liu, Wei-Yue); Li, B (Li, Bo); Dai, H (Dai, Hui); Li, GB (Li, Guang-Bing); Lu, QM (Lu, Qi-Ming); Gong, YH (Gong, Yun-Hong); Xu, Y (Xu, Yu); Li, SL (Li, Shuang-Lin); Li, FZ (Li, Feng-Zhi); Yin, YY (Yin, Ya-Yun); Jiang, ZQ (Jiang, Zi-Qing); Li, M (Li, Ming); Jia, JJ (Jia, Jian-Jun); Ren, G (Ren, Ge); He, D (He, Dong); Zhou, YL (Zhou, Yi-Lin); Zhang, XX (Zhang, Xiao-Xiang); Wang, N (Wang, Na); Chang, X (Chang, Xiang); Zhu, ZC (Zhu, Zhen-Cai); Liu, NL (Liu, Nai-Le); Chen, YA (Chen, Yu-Ao); Lu, CY (Lu, Chao-Yang); Shu, R (Shu, Rong); Peng, CZ (Peng, Cheng-Zhi); Wang, JY (Wang, Jian-Yu); Pan, JW (Pan, Jian-Wei)
SCIENCE
卷: 356 期: 6343 页: 1180-1184
Long-distance entanglement distribution is essential for both foundational tests of quantum physics and scalable quantum networks. Owing to channel loss, however, the previously achieved distance was limited to similar to 100 kilometers. Here we demonstrate satellite-based distribution of entangled photon pairs to two locations separated by 1203 kilometers on Earth, through two satellite-to-ground downlinks with a summed length varying from 1600 to 2400 kilometers. We observed a survival of two-photon entanglement and a violation of Bell inequality by 2.37 +/- 0.09 under strict Einstein locality conditions. The obtained effective link efficiency is orders of magnitude higher than that of the direct bidirectional transmission of the two photons through telecommunication fibers.

第 216 条，共 286 条

Investigations of associated multi-band observations for GEO space debris

Lu, Y (Lu, Yao); Zhang, C (Zhang, Chen); Sun, RY (Sun, Rong-yu); Zhao, CY (Zhao, Chang-yin); Xiong, JN (Xiong, Jian-ning)
ADVANCES IN SPACE RESEARCH
卷: 59 期: 10 页: 2501-2511
According to the proposal of active space debris removal, the knowledge of the shape, rotational state and surface characteristics of space debris is demanding. An associated multi-band observation of the Geosynchronous Earth Orbit space debris is performed to investigate the improvement and promotion while infrared and g'Vr'i' information are provided. The Quad-Channel Telescope and the famous United Kingdom Infrared Telescope are adopted in our observation, along with other two dedicated space debris telescopes. Due to the limitation of geometry, the infrared data of 13 objects are acquired, and the photometry results are obtained. The tumbling motion is analyzed with the brightness variations, and the color indices are investigated according to the bus type of objects. At last the frequency analysis of the multi-band light curves is performed, the consistency and non-consistency of the results under different circumstances are presented. It is demonstrated that the adoption of multi-band observations is useful for increasing the knowledge of space debris, and the applications are deserved to be further promoted. (C) 2017 COSPAR. Published by Elsevier Ltd. All rights reserved.

第 217 条，共 286 条

Analytic model for the long-term evolution of circular Earth satellite orbits including lunar node regression

Zhu, TL (Zhu, Ting-Lei); Zhao, CY (Zhao, Chang-Yin); Zhang, MJ (Zhang, Ming-Jiang)
ASTROPHYSICS AND SPACE SCIENCE
卷: 362 期: 4 文献号: 69
This paper aims to obtain an analytic approximation to the evolution of circular orbits governed by the Earth's J(2) and the luni-solar gravitational perturbations. Assuming that the lunar orbital plane coincides with the ecliptic plane, Allan and Cook (Proc. R. Soc. A, Math. Phys. Eng. Sci. 280(1380):97, 1964) derived an analytic solution to the orbital plane evolution of circular orbits. Using their result as an intermediate solution, we establish an approximate analytic model with lunar orbital inclination and its node regression be taken into account. Finally, an approximate analytic expression is derived, which is accurate compared to the numerical results except for the resonant cases when the

period of the reference orbit approximately equals the integer multiples (especially 1 or 2 times) of lunar node regression period.

第 218 条，共 286 条

Image Restoration Based on Statistic PSF Modeling for Improving the Astrometry of Space Debris

Sun, RY (Sun, Rongyu); Jia, P (Jia, Peng)
PUBLICATIONS OF THE ASTRONOMICAL SOCIETY OF THE PACIFIC
卷: 129 期: 974 文献号: UNSP 044502
Space debris is a special kind of fast-moving, near-Earth objects, and it is also considered to be an interesting topic in time-domain astronomy. Optical survey is the main technique for observing space debris, which contributes much to the studies of space environment. However, due to the motion of registered objects, image degradation is critical in optical space debris observations, as it affects the efficiency of data reduction and lowers the precision of astrometry. Therefore, the image restoration in the form of deconvolution can be applied to improve the data quality and reduction accuracy. To promote the image processing and optimize the reduction, the image degradation across the field of view is modeled statistically with principal component analysis and the efficient mean point-spread function (PSF) is derived from raw images, which is further used in the image restoration. To test the efficiency and reliability, trial observations were made for both low-Earth orbital and high-Earth orbital objects. The positions of all targets were measured using our novel approach and compared with the reference positions. The performance of image restoration employing our estimated PSF was compared with several competitive approaches. The proposed image restoration outperformed the others so that the influence of image degradation was distinctly reduced, which resulted in a higher signal-to-noise ratio and more precise astrometric measurements.

第 219 条，共 286 条

The Representation of OTA Images' Astrometric Results with WCS-SIP Coefficients

Ping Yiding; Zhang Chen; Lu Chunlin
Acta Astronomica Sinica
卷: 58 期: 3 页: 25-1-25-10
Cross-matching the sources extracted from observed images with reference catalogs or earlier records is a necessary procedure for seeking the variation of sources in terms of position or brightness for the Optical Telescopes Array (OTA) survey. Knowing the celestial positions of these objects on images is prerequisite therefore. A method based on matrix manipulation is applied to transform the existing calculated plate constants of OTA images into World Coordinate System (WCS) coefficients and Simple Imaging Polynomial (SIP) coefficients, which map image positions into celestial positions so as to facilitate the mining of the FITS (Flexible Image Transport System) images of OTA. An improvement of OTA's astrometry coming with this method, as well as the discussion about some problems of OTA's astrometry are also presented.

第 220 条，共 286 条

Probabilistic Data Association Method for Space Object Tracking

Xu Zhanwei; Wang Xin
Acta Astronomica Sinica
卷: 58 期: 3 页: 26-1-26-8 文献号: 0001-5245(2017)58:3<26:KJMBGZ>2.0.TX;2-O
In the optical tracking of space objects, multiple measurements are often detected in the observing gate, which brings about the uncertainty in the tracking accuracy and causes the unstability along the tracking path. This kind of condition will eventually interrupt the track and lead to the lost of the target. A new approach, combining the Kalman filter and probabilistic data association, is proposed for the adaptive tracking of space objects. This method employs Kalman filter to predict the gate of association, and uses probabilistic data association to obtain the equivalent measurement as an effective feed instead. The experiments show that this technique can effectively improve the tracking accuracy as well as the robustness for the automatic tracking of space objects.

第 221 条，共 286 条

Analysis of Nighttime Infrared Cloud Cover at Yaoan Astronomical Station

Fan Liang; Lei Chengming; Shi Dongdong; Huang Xuehai
Acta Astronomica Sinica
卷: 58 期: 2 页: 13-1-13-8 文献号: 0001-5245(2017)58:2<13:TATWGC>2.0.TX;2-D
Clouds have important effects on astronomical observations. Cloud cover is an important indicator of the quality of an astronomical site. The infrared cloud imager which locates in Yaoan astronomical station, is used for the real-time acquisition of all-sky infrared cloud image with high spatial resolution. Combining the actual observations of space debris, according to astronomical nights strictly, we make statistics and analysis of cloud cover at night accumulated in one year (from 2015-08-01 to 2016- 07-31). Annual average cloud cover at night at Yaoan astronomical station is 4.42 ten percent, and there are 236 available astronomy nights, including 98 photometric nights, 44 half-photometric nights, and 94 spectroscopic nights. The cloud cover has obvious characteristics of two seasons: the rainy season with a significant increase in cloud cover is from May to October, and the observation conditions are worst in July; The dry season is from November to April with low cloud cover, there are more than 23 available astronomy nights monthly, the most numerous photometric nights are in January, and the most available astronomy nights are in March. Combined with the threat level of cloud for astronomical observation, we make statistics of the total time of different cloud covers and the monthly distribution of cloud covers, to assess the meteorological conditions of the station, and to provide a reference for reasonable arrangements of the astronomical observations.

第 222 条，共 286 条

Research Progress on Ground-based Infrared Observations of Space Objects

Fan Liang; Lei Chengming; Sun Rongyu; Lu Yao; Zhang Chen
Progress in Astronomy
卷: 35 期: 1 页: 93-106 文献号: 1000-8349(2017)35:1<93:KJMBDD>2.0.TX;2-Z
As a new research field, ground-based infrared observations of space objects may extend the horizons of traditional radar

and optical observations, improving the mechanism of space surveillance. With broad wavelength range and thermal radiation bands, infrared band has a greater potential in daytime observations and spectral analysis for development. In recent years, the United States began the exploration of infrared characteristics on space objects, by gaining access to large infrared telescope or transforming optical telescope. In this paper, we give a review of the telescopes participated in the ground-based infrared observations of space objects. And we conclude the research progress of the infrared survey, daytime observations, infrared photometry and spectral analysis in infrared space surveillance for nearly a decade. Finally, a summary and prospects on ground-based infrared observations of space objects will be given.

第 223 条，共 286 条

Deep Learning for Mid-Term Forecast of Daily Index of Solar 10.7 cm Radio Flux

Wang Xin
Journal of Spacecraft TT & C Technology
卷：36 期：2 页：118-122 文献号：1674-5620(2017)36:2<118:JYSDXX>2.0.TX;2-C
For mid-term forecast of the daily index of solar 10.7 cm radio flux with deep learning method,a neural network based on classical multi-layer perception model is proposed.The network contains only one hidden layer with 90 neutrons,and an autoregressive model of time series is implemented non-parametrically.In the forecast, historical daily indices as well as historical forecast error are considered.The model gives forecast of next 27 days with values of past 27 days.The network is trained and validated with historical data over 50 years,and the result clearly shows that the mean relative error is significantly reduced compared to the traditional methods.Unlike most of previous studies,in which the parameters of the model need to be rolling-updated,the parameters are fixed after the training with this model.The proposed model greatly simplifies daily operation of forecast and is extremely advantageous to the promotion in other applications.

第 224 条，共 286 条

姚安天文观测站的夜间红外云量特征分析

樊亮 雷成明 师冬冬 黄学海
云对天文观测具有重要影响,云量是衡量天文台址质量的重要指标.位于姚安天文观测站的红外云量仪,用于获取实时的全天高空间分辨率云图.结合空间碎片的实际观测,严格按照天文夜对累积 1yr(2015-08-01—2016-07-31)的夜间云量数据进行统计和分析.姚安站的年平均夜间云量为 4.42 成,年天文可用夜为 236 个,其中测光夜 98 个,半测光夜 44 个,光谱夜 94 个.云量具有明显的两季特征:5 月至 10 月间为雨季,云量显著增多,其中 7 月份观测条件最差;11 月至次年 4 月为旱季,云量较少,每月的天文可用夜均在 23 个以上,其中 1 月份的测光夜最多,3 月份的天文可用夜最多.结合云层对天文观测的威胁程度,统计不同云量的总时间和每月的云量分布情况,评估观测站的气象条件,为合理安排观测计划提供参考.
基金：中国科学院国防科技创新基金项目(CXJJ-14-S106)资助；
关键词：天体测量; 仪器:红外云量仪; 望远镜; 技术:图像处理; 方法:观测; 数据分析;
DOI：10.15940/j.cnki.0001-5245.2017.02.004
分类号：P112

第 225 条，共 286 条

空间目标的地基红外观测研究进展

樊亮 雷成明 孙荣煜 鹿瑶 张晨
Progress in Astronomy
作为一个新兴的研究方向,空间目标的地基红外观测能够与传统雷达和光学观测形成互补,完善空间监测机制。红外具有宽阔的波段范围和特有的热辐射波段,在光谱分析和白天观测方面蕴藏着更大的发展潜力。近年来美国开始征用大型的红外望远镜,或者通过改造光学望远镜,研究空间目标在红外波段的特性。综述了参与空间目标地基红外观测的望远镜工作状况,以及近 10 年来空间目标监测在红外巡天、白天观测、测光和光谱分析方面的研究进展,最后对空间目标的地基红外观测研究进行总结与展望。
基金：中国科学院国防科技创新基金(CXJJ-14-S106)； 国家自然科学基金(11403108)；
关键词：空间目标; 红外观测; 物理特征; 光谱;
分类号：V556;V528

第 226 条，共 286 条

The secular analytical solution of the orbital plane using Lindstedt-Poincaré method

Shengxian Yu; Changyin Zhao; Wei Zhang;
Advances in Space Research
DOI:10.1016/j.asr.2017.08.032
Nowadays, the increasing amount of space objects makes the space so crowded that the satellites in orbit endure severe environment. Hence how to efficiently search and catalog these space objects becomes an urgent problem to be solved. In the paper, in order to contribute to this problem, the secular analytical solution of the orbital plane for medium and high orbit objects is studied. For medium and high orbit objects, the Earth's oblateness and the lunisolar gravitational perturbations are considered. The double averaging method is used to first average the system. For small to medium orbit inclinations and small eccentricities, and then the differential equations can be rewritten in an expansion form. Combining the Lindstedt-Poincaré procedure and the solution for differential equations with special coefficients, the third-order analytical solutions can be derived step by step. Finally, two kinds of comparisons are carried out. One is the comparison between the analytical solution and the results derived by integrating the simplified model. It aims to verify the validity of these methods. The other one is the comparison with the integration results of the normal model to show the accuracy of the analytical solution. Both of the two comparisons results work well. The accuracy of the analytical solution can be maintained at the order of O (10 - 3) for the duration

3-02 Satellite Precise Orbit Determination and Application

第 227 条，共 286 条

农村资本流动涡旋模型及应用——以山东商河大蒜产业为例

侯永刚

济南大学学报(社会科学版)

通过分析山东商河县大蒜产业发展的过程、现状和未来,借鉴流体力学中已经发展比较成熟的流体运动理论,建立了农村资本流动的涡旋模型。此模型能够简洁明了地显示大蒜产业从单纯的农作物生产发展到农作物生产、加工、销售一条龙的资本运动状况,能够说明农村企业和个体经营者资本积累的速度和来源,能够对农村产业多元化的资本流向加以说明并且对其盈利能力做出评估。此外,文章还拓展了此模型的应用范围,对于不同尺度的资本流动现象,均可以通过此模型进行相关研究。

关键词：农村经济; 资本流动; 涡旋模型; 大蒜产业;
分类号：F326.13

IV. Planetary Sciences and Deep Space Exploration

4-01 Near Earth Object Survey and Solar System Bodies

第 228 条，共 286 条

Obliquity evolution of the minor satellites of Pluto and Charon

Quillen, AC (Quillen, Alice C.); Nichols-Fleming, F (Nichols-Fleming, Fiona); *Chen, YY* (Chen, Yuan-Yuan); Noyelles, B (Noyelles, Benoit)

ICARUS

卷: 293 页: 94-113

New Horizons mission observations show that the small satellites Styx, Nix, Kerberos and Hydra, of the Pluto-Charon system, have not tidally spun-down to near synchronous spin states and have high obliquities with respect to their orbit about the Pluto-Charon binary (Weaver, 2016). We use a damped mass spring model within an N-body simulation to study spin and obliquity evolution for single spinning non round bodies in circumbinary orbit. Simulations with tidal dissipation alone do not show strong obliquity variations from tidally induced spin-orbit resonance crossing and this we attribute to the high satellite spin rates and low orbital eccentricities. However, a tidally evolving Styx exhibits intermittent obliquity variations and episodes of tumbling. During a previous epoch where Charon migrated away from Pluto, the minor satellites could have been trapped in orbital mean motion inclination resonances. An outward migrating Charon induces large variations in Nix and Styx's obliquities. The cause is a commensurability between the mean motion resonance frequency and the spin precession rate of the spinning body. As the minor satellites are near mean motion resonances, this mechanism could have lifted the obliquities of all four minor satellites. The high obliquities need not be primordial if the minor satellites were at one time captured into mean motion resonances. (C) 2017 Elsevier Inc. All rights reserved.

第 229 条，共 286 条

Transiting Exoplanet Monitoring Project (TEMP). II. Refined System Parameters and Transit Timing Analysis of HAT-P-33b

Wang, YH (Wang, Yong-Hao); Wang, S (Wang, Songhu); Liu, HG (Liu, Hui-Gen); Hinse, TC (Hinse, Tobias C.); Laughlin, G (Laughlin, Gregory); Wu, DH (Wu, Dong-Hong); Zhang, XJ (Zhang, Xiaojia); Zhou, X (Zhou, Xu); Wu, ZY (Wu, Zhenyu); Zhou, JL (Zhou, Ji-Lin); Wittenmyer, RA (Wittenmyer, R. A.); Eastman, J (Eastman, Jason); Zhang, H (Zhang, Hui); Hori, Y (Hori, Yasunori); Narita, N (Narita, Norio); Chen, YY (Chen, Yuanyuan); Ma, J (Ma, Jun); Peng, XY (Peng, Xiyan); Zhang, TM (Zhang, Tian-Meng); Zou, H (Zou, Hu); Nie, JD (Nie, Jun-Dan); Zhou, ZM (Zhou, Zhi-Min)

ASTRONOMICAL JOURNAL

卷: 154 期: 2 文献号: 49

We present 10. R-band photometric observations of eight different transits of the hot Jupiter HAT-P-33b, which has

been targeted by our Transiting Exoplanet Monitoring Project. The data were obtained by two telescopes at the Xinglong Station of National Astronomical Observatories of China (NAOC) from 2013 December through 2016 January, and exhibit photometric scatter of 1.6-3.0 mmag. After jointly analyzing the previously published photometric data, radial-velocity (RV) measurements, and our new light curves, we revisit the system parameters and orbital ephemeris for the HAT-P-33b system. Our results are consistent with the published values except for the planet to. star radius ratio (RP/R-*), the ingress/egress duration (tau) and the total duration (T-14), which together indicate a slightly shallower and shorter transit shape. Our results are based on more complete light curves, whereas the previously published work had only one complete transit light curve. No significant anomalies in Transit Timing Variations (TTVs) are found, and we place upper mass limits on potential perturbers, largely supplanting the loose constraints provided by the extant RV data. The TTV limits are stronger near mean-motion resonances, especially for the low-order commensurabilities. We can exclude the existence of a perturber with mass larger than 0.6, 0.3, 0.5, 0.5, and 0.3 M-circle plus near the 1: 3, 1: 2, 2: 3, 3: 2, and 2: 1 resonances, respectively.

第 230 条，共 286 条

Feature-rich transmission spectrum for WASP-127b Cloud-free skies for the puffiest known super-Neptune?

Palle, E (Palle, E.); *Chen, G* (Chen, G.); Prieto-Arranz, J (Prieto-Arranz, J.); Nowak, G (Nowak, G.); Murgas, F (Murgas, F.); Nortmann, L (Nortmann, L.); Pollacco, D (Pollacco, D.); Lam, K (Lam, K.); Montanes-Rodriguez, P (Montanes-Rodriguez, P.); Parviainen, H (Parviainen, H.); Casasayas-Barris, N (Casasayas-Barris, N.)
ASTRONOMY & ASTROPHYSICS
卷: 602 文献号: L15
Context. WASP-127b is a planet with one of the lowest densities discovered to date. With a sub-Saturn mass (M-p = 0.18 +/- 0.02 M-J) and super-Jupiter radius (R-p = 1.37 +/- 0.04 R-J), it orbits a bright G5 star that is about to leave the main-sequence.
Aims. We aim to explore the atmosphere of WASP-127b in order to retrieve its main atmospheric components, and to find hints for its intriguing inflation and evolutionary history.
Methods. We used the ALFOSC spectrograph at the NOT telescope to observe a low-resolution (R similar to 330, seeing limited) long-slit spectroscopic time series during a planetary transit, and present here the first transmission spectrum for WASP-127b.
Results. We find a strong Rayleigh slope at blue wavelengths and a hint of Na absorption, although the quality of the data does not allow us to claim a detection. At redder wavelengths the absorption features of TiO and VO are the best explanation to fit the data.
Conclusions. Although observations with a higher signal-to-noise ratio are needed to conclusively confirm the absorption features, WASP-127b seems to posses a cloud-free atmosphere and is one of the best targets on which to perform further characterization studies in the near future.

第 231 条，共 286 条

The GTC exoplanet transit spectroscopy survey VI. Detection of sodium in WASP-52b's cloudy

Chen, G (Chen, G.); Palle, E (Palle, E.); Nortmann, L (Nortmann, L.); Murgas, F (Murgas, F.); Parviainen, H (Parviainen, H.); Nowak, G (Nowak, G.)
ASTRONOMY & ASTROPHYSICS
卷: 600 文献号: L11
We report the first detection of sodium absorption in the atmosphere of the hot Jupiter WASP-52b. We observed one transit of WASP-52b with the low-resolution Optical System for Imaging and low-Intermediate-Resolution Integrated Spectroscopy (OSIRIS) at the 10.4 m Gran Telescopio Canarias (GTC). The resulting transmission spectrum, covering the wavelength range from 522 nm to 903 nm, is flat and featureless, except for the significant narrow absorption signature at the sodium doublet, which can be explained by an atmosphere in solar composition with clouds at 1 mbar. A cloud-free atmosphere is stringently ruled out. By assessing the absorption depths of sodium in various bin widths, we find that temperature increases towards lower atmospheric pressure levels, with a positive temperature gradient of 0.88 +/- 0.65 K km(-1), possibly indicative of upper atmospheric heating and a temperature inversion.

第 232 条，共 286 条

The GTC exoplanet transit spectroscopy survey V. A spectrally-resolved Rayleigh scattering slope in GJ 3470b

Chen, G (Chen, G.); Guenther, EW (Guenther, E. W.); Palle, E (Palle, E.); Nortmann, L (Nortmann, L.); Nowak, G (Nowak, G.); Kunz, S (Kunz, S.); Parviainen, H (Parviainen, H.); Murgas, F (Murgas, F.)
ASTRONOMY & ASTROPHYSICS
卷: 600 文献号: A138
Aims. As a sub-Uranus-mass low-density planet, GJ 3470b has been found to show a flat featureless transmission spectrum in the infrared and a tentative Rayleigh scattering slope in the optical. We conducted an optical transmission spectroscopy project to assess the impacts of stellar activity and to determine whether or not GJ 3470b hosts a hydrogen-rich gas envelop.
Methods. We observed three transits with the low-resolution Optical System for Imaging and low-Intermediate-Resolution Integrated Spectroscopy (OSIRIS) at the 10.4 m Gran Telescopio Canarias, and one transit with the high-resolution Ultraviolet and Visual Echelle Spectrograph (UVES) at the 8.2 m Very Large Telescope.
Results. From the high-resolution data, we find that the difference of the Ca II H+K lines in-and out-of-transit is only 0 : 67 +/- 0 : 22%, and determine a magnetic filling factor of about 10-15%. From the low-resolution data, we present the first optical transmission spectrum in the 435-755 nm band, which shows a slope consistent with Rayleigh scattering.
Conclusions. After exploring the potential impacts of stellar activity in our observations, we confirm that Rayleigh scattering in an extended hydrogen-helium atmosphere is currently the best explanation. Further high-precision observations that simultaneously cover optical and infrared bands are required to answer whether or not clouds and hazes exist at high-altitude.

第 233 条，共 286 条

The GTC exoplanet transit spectroscopy survey VII. An optical transmission spectrum of WASP-48b

Murgas, F (Murgas, F.); Palle, E (Palle, E.); Parviainen, H (Parviainen, H.); *Chen, G* (Chen, G.); Nortmann, L (Nortmann, L.); Nowak, G (Nowak, G.); Cabrera-Lavers, A (Cabrera-Lavers, A.); Iro, N (Iro, N.)
ASTRONOMY & ASTROPHYSICS
卷: 605 文献号: A114
Context. Transiting planets off er an excellent opportunity for characterizing the atmospheres of extrasolar planets under very different conditions from those found in our solar system.
Aims. We are currently carrying out a ground-based survey to obtain the transmission spectra of several extrasolar planets using the 10 m Gran Telescopio Canarias. In this paper we investigate the extrasolar planet WASP-48b, a hot Jupiter orbiting around an F-type star with a period of 2.14 days.
Methods. We obtained long-slit optical spectroscopy of one transit of WASP-48b with the Optical System for Imaging and low-Intermediate-Resolution Integrated Spectroscopy (OSIRIS) spectrograph. We integrated the spectrum of WASP-48 and one reference star in several channels with different wavelength ranges, creating numerous color light curves of the transit. We fit analytic transit curves to the data taking into account the systematic effects present in the time series in an effort to measure the change of the planet-to-star radius ratio (R-p/R-s) across wavelength. The change in transit depth can be compared with atmosphere models to infer the presence of particular atomic or molecular compounds in the atmosphere of WASP-48b.
Results. After removing the transit model and systematic trends to the curves we reached precisions between 261 ppm and 455755 ppm for the white and spectroscopic light curves, respectively. We obtained R-p/R-s uncertainty values between 0.8 x 10(3) and 1.5 x 10(3) for all the curves analyzed in this work. The measured transit depth for the curves made by integrating the wavelength range between 530 nm and 905 nm is in agreement with previous studies. We report a relatively flat transmission spectrum for WASP-48b with no statistical significant detection of atmospheric species, although the theoretical models that fit the data more closely include TiO and VO.

第 234 条，共 286 条

Obliquity evolution of the minor satellites of Pluto and Charon

AC Quillen F Nichols-Fleming *YY Chen* B Noyelles
Icarus,
2017 , 293 :94-113
New Horizons mission observations show that the small satellites Styx, Nix, Kerberos and Hydra, of the Pluto-Charon system, have not tidally spun-down to near synchronous spin states and have high obliquities with respect to their orbit about the Pluto-Charon binary (Weaver, 2016). We use a damped mass-spring model within an N-body simulation to study spin and obliquity evolution for single spinning non-round bodies in circumbinary orbit. Simulations with tidal dissipation alone do not show strong obliquity variations from tidally induced spin-orbit resonance crossing and this we attribute to the high satellite spin rates and low orbital eccentricities. However, a tidally evolving Styx exhibits intermittent obliquity variations and episodes of tumbling. During a previous epoch where Charon migrated away from Pluto, the minor satellites could have been trapped in orbital mean motion inclination resonances. An outward migrating Charon induces large variations in Nix and Styx 欽樓 obliquities. The cause is a commensurability between the mean motion resonance frequency and the spin precession rate of the spinning body. As the minor satellites are near mean motion resonances, this mechanism could have lifted the obliquities of all four minor satellites. The high obliquities need not be primordial if the minor satellites were at one time captured into mean motion resonances.

4-02 Ephemerial Astronomy and Astronomical Reference System

第 235 条，共 286 条

Solar System and stellar tests of noncommutative spectral geometry

Deng, XM (Deng, Xue-Mei)
EUROPEAN PHYSICAL JOURNAL PLUS
卷: 132 期: 2 文献号: 85
By using purely geometric forces on a noncommutative spacetime, noncommutative spectral geometry (NCSG) was proposed as a possible way to unify gravitation with the other known fundamental forces. The correction of the NCSG solution to Einstein's general relativity (GR) in the four-dimensional spacetime can be characterized by a parameter beta similar to 1/root f(0), where f(0) denotes the coupling constants at the unification. The parameter beta contributes a Yukawa-type correction exp(-beta r)/r to the Newtonian gravitational potential at the leading order, which can be interpreted as either the massive component of the gravitational field or the typical range of interactions carried by that component of the field. As an extension of previous works, we mainly focus on the Solar System and stellar tests of the theory, and the constraints on similar to obtained by the present work is independent of the previous ones. In the Solar System, we investigate the effects of the NCSG on the perihelion shift of a planet, deflection of light, time delay at superior conjunction (SC) and inferior conjunction (IC), and the Cassini experiment by modeling new observational results and adopting new datasets. In the binary pulsars system, based on the observational data sets of four systems of binary pulsars, PSR B1913+ 16, PSR B1534+ 12, PSR J0737-3039, and PSR B2127+ 11C, the secular periastron precessions are used to constrain this theory. These effects in the scale of the Solar System and binary pulsars were not considered in previous works. We find that the lower bounds given by these experiments are beta similar or equal to 10(-9) similar to 10(-10) m(-1),

considerably smaller than those obtained in laboratory experiments. This confirms that experiments and observations at smaller scales are more favorable for testing the NCSG theory.

第 236 条，共 286 条

Deep Imaging of the HCG 95 Field. I. Ultra-diffuse Galaxies

Shi, DD (Shi, Dong Dong); Zheng, XZ (Zheng, Xian Zhong); *Bin Zhao, H* (Bin Zhao, Hai); Pan, ZZ (Pan, Zhi Zheng); Li, B (Li, Bin); Zou, H (Zou, Hu); Zhou, X (Zhou, Xu); Guo, KX (Guo, KeXin); An, FX (An, Fang Xia); Bin Li, Y (Bin Li, Yu)
ASTROPHYSICAL JOURNAL
卷: 846 期: 1 文献号: 26
We present a detection of 89 candidates of ultra-diffuse galaxies (UDGs) in a 4.9 degree(2) field centered on the Hickson Compact Group 95 (HCG 95) using deep g- and r-band images taken with the Chinese Near Object Survey Telescope. This field contains one rich galaxy cluster (Abell 2588 at z. = .0.199) and two poor clusters (Pegasus I at z = .0.013 and Pegasus II at z = .0.040). The 89 candidates are likely associated with the two poor clusters, giving about 50-60 true UDGs with a half-light radius r(e) > 1.5 kpc and a central surface brightness mu(g, 0) > 24.0 mag arcsec(-2). Deep z'-band images are available for 84 of the 89 galaxies from the Dark Energy Camera Legacy Survey (DECaLS), confirming that these galaxies have an extremely low central surface brightness. Moreover, our UDG candidates are spread over a wide range in g - r color, and similar to 26% are as blue as normal star-forming galaxies, which is suggestive of young UDGs that are still in formation. Interestingly, we find that one UDG linked with HCG 95 is a gas-rich galaxy with H I mass 1.1 x 10(9) M-circle dot detected by the Very Large Array, and has a stellar mass of M-star similar to 1.8 x 10(8) M-circle dot. This indicates that UDGs at least partially overlap with the population of nearly dark galaxies found in deep H I surveys. Our results show that the high abundance of blue UDGs in the HCG 95 field is favored by the environment of poor galaxy clusters residing in H I-rich large-scale structures.

第 237 条，共 286 条

The orbital configuration of the two interacting Jupiters in HD 155358 system

Ma, DZ (Ma, Da-Zhu); Fu, YN (Fu, Yan-Ning); Wang, XL (Wang, Xiao-Li)
MONTHLY NOTICES OF THE ROYAL ASTRONOMICAL SOCIETY
卷: 470 期: 1 页: 706-712
Recent observation reveals two interacting Jupiters possibly trapped in a 2: 1 mean motion resonance (MMR) around the star HD 155358. For the 2:1 MMR, Beauge et al. found that as long as the orbital decay was sufficiently slow, the trapped planets should also be in apsidal co-rotation. So it is very interesting to explore whether HD 155358 did undergo such an evolution and presents an apsidal co-rotation. Based on the existing results of spectroscopic orbital determination, the global dynamics of the system shows that the two planets are in an apsidal co-rotation if the eccentricity of the outer planet (ec) takes values very close to the lower limit of its 1 sigma confidence interval. This makes us conjecture that the globally minimizing solution could be missed in the previous orbital determination. Using an efficient global optimization method, we do find a better solution, reducing chi(2) from 1.4 to 1.2. This new solution is significantly different from the previous one, and in particular, with smaller ec. However, the increased possibility for the system to be trapped in a 2: 1 MMR with apsidal co-rotation is still not high. A set of simulations of the adiabatic convergent migration process are then performed. The results consistently indicate that the 2: 1 MMR forms before apsidal co-rotation. Finally, the long-term stability of the formed system and of its resonant structure is extensively explored, and the resulting statistics are given. A conclusion is that the 2: 1 MMR with apsidal co-rotation is a very stable structure.

第 238 条，共 286 条

Classical tests of photons coupled to Weyl tensor in the Solar System

Li, G (Li, Gang); Deng, XM (Deng, Xue-Mei)
ANNALS OF PHYSICS
卷: 382 页: 136-142
With the purpose of deeply understanding the fundamental interaction between the electromagnetic and gravitational fields, photons coupled to the Weyl tensor was proposed, which could be derived from the Maxwell equation with a Weyl correction. This correction with respect to general relativity in a 4-dimensional spacetime can be characterized by a coupling strength parameter a. By taking such a coupling into account, we investigate its effects on the classical tests in the Solar System, including the deflection of light, the gravitational time delay and the Cassini tracking experiment, and constrain the parameter a with new datasets. None of these works were done before and these data of the experiments are used for testing the photons coupled to the Weyl tensor for the first time. We find that the experimental upper bounds are vertical bar alpha vertical bar less than or similar to 4 x 10(11) - 5 x 10(13) m(2), in which the strongest bound comes from the Cassini tracking. Therefore, it is expected that when more sophisticated frequency standards can be implemented in the al analysis slightly differ from the power law index (-1.67) obtained by a theoretical model. The observations are consistent with adiabatic expansion of the coronal source component.

第 239 条，共 286 条

A prediction method for ground-based stellar occultations by ellipsoidal solar system bodies and its application

Yuan, Y (Yuan, Ye); Fu, YN (Fu, Yan-Ning); Cheng, Z (Cheng, Zhuo)
RESEARCH IN ASTRONOMY AND ASTROPHYSICS
卷: 17 期: 5 文献号: 45
A new programmable prediction method is developed to refine the occultation band by taking into consideration the triaxiality of an occulting body, as well as two more factors, namely, the barycenter offset of an occulting planet from the relevant planetary satellite system and the gravitational deflection of light rays due to an occulting planet. Although these factors can be neglected in most cases, it is shown that there are cases when these factors can cause a variation ranging from several tens to thousands of kilometers in the boundaries of occultation bands. Knowledge of analytic geometry simplifies the process of derivation and computation. This method is applied to long-term predictions of Jovian and Saturnian events.

第 240 条，共 286 条

Improved Solar System bounds on the cosmologically viable f (G) gravity

Deng, XM (Deng, Xue-Mei); Xie, Y (Xie, Yi)
ASTROPHYSICS AND SPACE SCIENCE
卷: 362 期: 3 文献号: 59
By making use of the supplementary advances of the perihelia provided by INPOP10a and INPOP15a (France) and EPM2011 (Russia) ephemerides, we obtain improved Solar System bounds on the cosmologically viable f (G) gravity, where f is an arbitrary function of the Gauss-Bonnet invariant G. When we estimate new bounds on its model parameters, we consider the Lense-Thirring effect caused by the Sun's angular momentum and the uncertainty of the Sun's quadrupole moment, neither of which were included in related works before. The bounds we obtain in the present work are tighter than the previous ones by at least 5 orders of magnitude.

第 241 条，共 286 条

Gravitational time advancement under gravity's rainbow

Deng, XM (Deng, Xue-Mei); Xie, Y (Xie, Yi)
PHYSICS LETTERS B
卷: 772 页: 152-158
Under gravity's rainbow, we investigate its effects on the gravitational time advancement, which is a natural consequence of measuring proper time span for a photon's round trip. This time advancement can be complementary to the time delay for testing the gravity's rainbow, because they are sensitive to different modified dispersion relations (MDRs). Its observability on ranging a spacecraft far from the Earth by two radio and a laser links is estimated at superior conjunction (SC) and inferior conjunction (IC). We find that (1) the IC is more favorable than the SC for measurement on the advancement caused by the rainbow; (2) aspecific type of MDR has a significantly larger effect on the advancement than others in both SC and IC cases; and (3) acombination of available optical clocks and the realization of planetary laser ranging in the future will benefit distinguishing the gravity's rainbow from GR by measuring the gravitational time advancement. (C) 2017 The Author(s). Published by Elsevier B.V.

第 242 条，共 286 条

Application of Close Encounters in Determining the Masses of Asteroids

Tang Huaijin; Li Fan; Fu Yanning
Acta Astronomica Sinica
卷：58 期：6 页：59-1-59-8 文献号：0001-5245(2017)58:6<59:MJJHZQ>2.0.TX;2-V
Asteroids are important part of the solar system. So far, the number of known asteroids is more than seven hundred thousand, and the total number is probably more than one million. Among many events of encounters among asteroids, those very close ones can be used to improve the precision of the masses of asteroids. To achieve this, it's necessary to search for the latter events in advance by making an accurate assessment of the effectiveness of an encounter in the mass determination. In this context, the previous dynamical models and assessing indicators are not precise enough. By using a more realistic dynamical model and introducing a properly defined Signal-to-Noise ratio, we are able to estimate the precision of the mass determination based on observations made from the Earth. Moreover, the best observation time span can be quantitatively given, which is useful in collecting observational data and planning further observations. We search systematically for the useful asteroid encounters involving one of the 773 massive asteroids with equivalent diameter larger than 50 km, for which the searched time span is from the year 2000 to 2030.

第 243 条，共 286 条

Solar system and binary pulsars tests of the minimal momentum uncertainty principle

Deng, XM (Deng, Xue-Mei)
卷: 120 期: 6 文献号: 60004
In order to explore a minimal momentum uncertainty principle in Heisenberg's uncertainty principle, the minimal momentum uncertainty principle (MMUP) was proposed. The correction on the canonical commutation relation of MMUP can be parametrized by a and alpha'. In the macroscopic scale, MMUP could change bodies' orbital motion, which is different from the results of general relativity (GR). In the present work, we mainly focus on the influence of MMUP on the tests of the Solar System and the binary pulsars. In the Solar System, the perihelion shift of a planet has been remodeled under MMUP by the data of INPOP10a, EPM2011 and INPOP15a. In five systems of binary pulsars, the upper bounds of a and alpha' are obtained by using the data of the secular periastron precessions. These five systems are PSR B1913+16, PSR B1534+12, PSR J1756-2251, PSR B2127+11C and PSR J0737-3039. Few studies about the tests have been done before and the effects of MMUP on these systems are investigated for the first time. They show that the upper bounds of a and a alpha' constrained by planets of the Solar System and the binary pulsars are alpha + alpha'= 10- 28 similar to 10(-36) m(-2), tighter than the previous result by at least 2 orders of magnitude. It is expected that the bounds on MMUP will be further improved by tremendous advances in techniques for deep space exploration and by new tracking data sets. Copyright (C) EPLA, 2018.

第 244 条，共 286 条

Stability Analysis of the Two Possible 2:1 MMR Systems

Ma Dazhu; Fu Yanning; Wang Xiaoli
Acta Astronomica Sinica
卷：58 期：6 页：60-1-60-8 文献号：0001-5245(2017)58:6<60:LGKNJY>2.0.TX;2-K
Based on the existing orbital parameters determined with the radial velocity(RV) data, the planets in HD 155358 and 24 Sextanis systems are found possibly trapped in the 2:1 mean motion resonance(MMR), respectively. For each system, the dynamical behavior of the best-fitting solution is discussed, and the 1sigma confidence around the best-fitting initial phase point is explored using the chaos indicator Δe_(max) . The results reveal that HD 155358 could be stable without the 2:1 MMR protection, but the case is different for 24 Sextanis system.

4-03 The Sun and Solar System Plasmas

第 245 条，共 286 条

Low-frequency electromagnetic cyclotron waves in and around magnetic clouds: STEREO observations during 2007-2013

Zhao, GQ (Zhao, G. Q.); Chu, YH (Chu, Y. H.); Lin, PH (Lin, P. H.); Yang, YH (Yang, Y. H.); Feng, HQ (Feng, H. Q.); *Wu, DJ* (Wu, D. J.); Liu, Q (Liu, Q.)
JOURNAL OF GEOPHYSICAL RESEARCH-SPACE PHYSICS
卷: 122 期: 5 页: 4879-4894
Wave activities in the solar wind are an important topic and magnetic clouds (MCs) are a common phenomenon in interplanetary space, though waves activities associated with MCs have not been well documented. Based on a survey of 120 MCs observed by STEREO spacecraft during the years 2007-2013, this work studies electromagnetic cyclotron waves (ECWs) near the proton cyclotron frequency in and around MCs. For total 7807 ECW events, 24% of them occurred in the regions within MCs while 76% occurred in the regions around MCs. Statistics indicate that ECWs around MCs have higher frequencies, wider bandwidths, and stronger powers relative to the waves in MCs. More ECWs, on the other hand, tend to be related to a plasma with higher temperature, lower density, and larger velocity. In particular, it is found that there exist positive power law correlations between plasma betas and the wave frequencies, bandwidths, and powers. The results imply that the plasma beta should play an important role in determining the properties of ECWs, which is consistent with previous theory studies and the recent simulation results.

第 246 条，共 286 条

Effects of ion thermal pressure on wave properties of electromagnetic ion cyclotron waves in a H+-He+-O+ plasma

Tang, Y (Tang, Ying); Zhao, JS (Zhao, Jinsong); Sun, HY (Sun, Heyu); Lu, JY (Lu, Jianyong); Wang, M (Wang, Ming)
PHYSICS OF PLASMAS
卷: 24 期: 5 文献号: 052120
Electromagnetic ion cyclotron (EMIC) waves in the H+, He+, and O+ bands are frequently observed in the magnetosphere. This study examines the effects of the thermal pressure of heavy He+ and O+ ions on EMIC wave properties. It illustrates that hot and isotropic heavy ions may completely suppress the growth of He+ band EMIC waves, whereas H+ band waves are growing irrespective of whether the heavy ions are cool or hot. At large O+ ion concentration, O+ band waves grow considerably as hot protons, and heavy ions are anisotropic. Results from the hot fluid model show that anisotropic thermal pressures of heavy ions result in the resonance frequency of EMIC waves larger than that from the cold fluid model, and therefore, narrowing the corresponding stop bands. Furthermore, the anisotropic ion thermal pressures lead to the minimum resonant energy of electrons interacting with EMIC waves at higher frequencies than that predicted by the cold fluid model. Published by AIP Publishing.

第 247 条，共 286 条

Magnetospheric Multiscale Observations of Electron Vortex Magnetic Hole in the Turbulent Magnetosheath Plasma

Huang, SY (Huang, S. Y.); Sahraoui, F (Sahraoui, F.); Yuan, ZG (Yuan, Z. G.); He, JS (He, J. S.); Zhao, JS (Zhao, J. S.); Le Contel, O (Le Contel, O.); Deng, XH (Deng, X. H.); Zhou, M (Zhou, M.); Fu, HS (Fu, H. S.); Shi, QQ (Shi, Q. Q.); Lavraud, B (Lavraud, B.); Pang, Y (Pang, Y.); Yang, J (Yang, J.); Wang, DD (Wang, D. D.); Li, HM (Li, H. M.); Yu, XD (Yu, X. D.); Pollock, CJ (Pollock, C. J.); Giles, BL (Giles, B. L.); Torbert, RB (Torbert, R. B.); Russell, CT (Russell, C. T.); Goodrich, KA (Goodrich, K. A.); Gershman, DJ (Gershman, D. J.); Moore, TE (Moore, T. E.); Ergun, RE (Ergun, R. E.); Khotyaintsev, YV (Khotyaintsev, Y. V.); Lindqvist, PA (Lindqvist, P. -A.); Strangeway, RJ (Strangeway, R. J.); Magnes, W (Magnes, W.); Bromund, K (Bromund, K.); Leinweber, H (Leinweber, H.); Plaschke, F (Plaschke, F.); Anderson, BJ (Anderson, B. J.); Burch, JL (Burch, J. L.)
ASTROPHYSICAL JOURNAL LETTERS
卷: 836 期: 2 文献号: L27
We report on the observations of an electron vortex magnetic hole corresponding to a new type of coherent structure in the turbulent magnetosheath plasma using the Magnetospheric Multiscale mission data. The magnetic hole is characterized by a magnetic depression, a density peak, a total electron temperature increase (with a parallel temperature decrease but a perpendicular temperature increase), and strong currents carried by the electrons. The current has a dip in the core region and a peak in the outer region of the magnetic hole. The estimated size of the magnetic hole is about 0.23 rho(i) (similar to 30 rho(e)) in the quasi-circular cross-section perpendicular to its axis, where rho(i) and rho(e) are respectively the proton and electron gyroradius. There are no clear enhancements seen in high-energy electron fluxes. However, there is an enhancement in the perpendicular electron fluxes at 90 degrees pitch angle inside the magnetic hole, implying that the electrons are trapped within it. The variations of the electron velocity components V-em and V-en suggest that an electron vortex is formed by trapping electrons inside the magnetic hole in the cross-section in the M-N plane. These observations demonstrate the existence of a new type of coherent structures behaving as an electron vortex magnetic hole in turbulent space plasmas as predicted by recent kinetic simulations.

第 248 条，共 286 条

Radial Variations of Outward and Inward Alfvenic Fluctuations Based on Ulysses Observations

Yang, L (Yang, L.); Lee, LC (Lee, L. C.); Li, JP (Li, J. P.); Luo, QY (Luo, Q. Y.); Kuo, CL (Kuo, C. L.); Shi, JK (Shi, J. K.); Wu, DJ (Wu, D. J.)
ASTROPHYSICAL JOURNAL
卷: 850 期: 2 文献号: 177
Ulysses magnetic and plasma data are used to study hourly scale Alfvenic fluctuations in the solar polar wind. The calculated energy ratio R-vA(2) (cal) of inward to outward Alfven waves is obtained from the observed Walen slope through an analytical expression, and the observed R-vA(2) (obs) is based on a direct decomposition of original Alfvenic fluctuations into outward-and inward-propagating Alfven waves. The radial variation of R-vA(2) (cal) shows a monotonically increasing trend with heliocentric distance r, implying the increasing local generation or contribution of inward Alfven waves. The contribution is also shown by the

radial increase in the occurrence of dominant inward fluctuations. We further pointed out a higher occurrence (similar to 83% of a day in average) of dominant outward Alfvenic fluctuations in the solar wind than previously estimated. Since R-vA(2) (cal) is more accurate than R-vA(2) (obs) in the measurement of the energy ratio for dominant outward fluctuations, the values of R-vA(2) (cal) in our results are likely more realistic in the solar wind than those previously estimated as well as R-vA(2) (obs) in our results. The duration ratio R-T of dominant inward to all Alfvenic fluctuations increases monotonically with r, and is about two or more times that from Voyager 2 observations at r >= 4 au. These results reveal new qualitative and quantitative features of Alfvenic fluctuations therein compared with previous studies and put constraints on modeling the variation of solar wind fluctuations.

第 249 条，共 286 条

Research Progress of Electron Cyclotron Maser Emission on Solar Physics

Tang Jianfei; Wu Dejin; Zhao Guoqing; Chen Ling
Progress in Astronomy
卷：35 期：2 页：149-174 文献号：1000-8349(2017)35:2<149:DZHXMZ>2.0.TX;2-F
Electron-cyclotron maser (ECM) emission is a well-known radiation emission mechanism in astrophysics. It has been extensively applied to various nonthermal coherent radio emission, especially to the short-timescale coherent radio bursts. Excitation of electron cyclotron maser radiation requires two basic conditions. One is the inversion distribution of the energetic electrons in the direction perpendicular to the ambient magnetic field. The other is the escape difficulty that requires the local electron cyclotron frequency over the plasma frequency. These two conditions are hardly satisfied in the corona under the conventional solar atmosphere models, which limit the application of ECM emission mechanism to solar radio astronomy. In general, flare associated energetic electrons are accelerated initially mainly along the magnetic field, it means that these energetic electrons do not have enough free energy to drive ECM emission. After the energetic electrons leave the acceleration site and propagate in the solar atmosphere, the energy of the energetic electrons in the parallel orientation can be transfer to the perpendicular orientation, and form an anisotropic distribution due to the interaction of energetic electrons with magnetic field and plasma waves. For the escape difficulty, a density depletion duct in the corona is necessary and may be rational as optical observations show fibrous density structures exist commonly in the corona. This paper presents a systematic review on the recent development of ECM emission mechanism, especially on the new models which may overcome the above difficulties and can be applied in several kinds of solar radio bursts, such as type I bursts, type II bursts, and type V bursts. Some perspectives on the study of ECM mechanism and solar radio emission processes are also presented.

第 250 条，共 286 条

A self-consistent mechanism for electron cyclotron maser emission and its application to type III solar radio bursts

Chen, L (Chen, L.); Wu, DJ (Wu, D. J.); Zhao, GQ (Zhao, G. Q.); Tang, JF (Tang, J. F.)
JOURNAL OF GEOPHYSICAL RESEARCH-SPACE PHYSICS
卷: 122 期: 1 页: 35-49
Type III solar radio bursts (SRBs) produced by fast electron beams (FEBs) traveling along solar magnetic fields are the best known and the most important kind of SRBs because of their clearest association with FEBs as well as most frequent observations during solar activities. However, the physics of their emitting mechanism has been a controversial issue. Based on the electron cyclotron maser (ECM) instability driven directly by a magnetized FEB, whose physics is fairly well known from the Earth's auroral kilometric radiation, this paper proposes a self-consistent mechanism for type III SRBs, in which the Alfven wave (AW) produced by the current instability of the beam-return current system associated with the FEB, called the self-generated AW, plays an important and crucial role. Taking into account the return-current effect of the FEB, the growth rate and the saturation intensity of the self-generated AW are estimated. Then the effects of the self-generated AW on the ECM emission via the ECM instability driven by the magnetized FEB are further investigated. The results show that the self-generated AW can significantly influence and change the physical properties of the ECM emission. In particular, this novel ECM emission mechanism can effectively overcome the main difficulties of the conventional ECM emission mechanism in application to type III SRBs and may potentially provide a self-consistent physics scenario for type III SRBs.

第 251 条，共 286 条

Chaos-induced resistivity of collisionless magnetic reconnection in the presence of a guide field Shang,

M (Shang, Meng); *Wu, DJ* (Wu, De-Jin); Chen, L (Chen, Ling); Chen, PF (Chen, Peng-Fei)
RESEARCH IN ASTRONOMY AND ASTROPHYSICS
卷: 17 期: 1 文献号: 3
One of the most puzzling problems in astrophysics is to understand the anomalous resistivity in collisionless magnetic reconnection that is believed extensively to be responsible for the energy release in various eruptive phenomena. The magnetic null point in the reconnecting current sheet, acting as a scattering center, can lead to chaotic motions of particles in the current sheet, which is one of the possible mechanisms for anomalous resistivity and is called chaos-induced resistivity. In many interesting cases, however, instead of the magnetic null point, there is a nonzero magnetic field perpendicular to the merging field lines, usually called the guide field, whose effect on chaos-induced resistivity has been an open problem. By use of the test particle simulation method and statistical analysis, we investigate chaos-induced resistivity in the presence of a constant guide field. The characteristics of particle motion in the reconnecting region, in particular, the chaotic behavior of particle orbits and evolving statistical features, are analyzed. The results show that as the guide field increases, the radius of the chaos region increases and the Lyapunov index decreases. However, the effective collision frequency, and hence the chaos-induced resistivity, reach their peak values when the guide field approaches half of the characteristic strength of the reconnection magnetic field. The presence of a guide field can significantly influence the chaos of the particle orbits and hence the chaos-induced resistivity in the reconnection sheet, which decides the collisionless reconnection rate. The present result is helpful

for us to understand the micro physics of anomalous resistivity in collisionless reconnection with a guide field.

第 252 条，共 286 条

Time-dependent Occurrence Rate of Electromagnetic Cyclotron Waves in the Solar Wind: Evidence for the Effect of Alpha Particles?

Zhao, GQ (Zhao, G. Q.); Feng, HQ (Feng, H. Q.); *Wu, DJ* (Wu, D. J.); Chu, YH (Chu, Y. H.); Huang, J (Huang, J.)
ASTROPHYSICAL JOURNAL LETTERS
卷: 847 期: 1 文献号: L8
Previous studies revealed that electromagnetic cyclotron waves (ECWs) near the proton cyclotron frequency exist widely in the solar wind, and the majority of ECWs are left-handed (LH) polarized waves. Using the magnetic field data from the STEREO mission, this Letter carries out a survey of ECWs over a long period of 7 years and calculates the occurrence rates of ECWs with different polarization senses. Results show that the occurrence rate is nearly a constant for the ECWs with right-handed polarization, but it varies significantly for the ECWs with LH polarization. Further investigation of plasma conditions reveals that the LH ECWs take place preferentially in a plasma characterized by higher temperature, lower density, and larger velocity. Some considerable correlations between the occurrence rate of LH ECWs and the properties of ambient plasmas are discussed. The present research may provide evidence for the effect of alpha particles on the generation of ECWs.

第 253 条，共 286 条

A statistical study of kinetic-size magnetic holes in turbulent magnetosheath: MMS observations

Huang, SY (Huang, S. Y.); Du, JW (Du, J. W.); Sahraoui, F (Sahraoui, F.); Yuan, ZG (Yuan, Z. G.); He, JS (He, J. S.); Zhao, JS (Zhao, J. S.); Le Contel, O (Le Contel, O.); Breuillard, H (Breuillard, H.); Wang, DD (Wang, D. D.); Yu, XD (Yu, X. D.); Deng, XH (Deng, X. H.); Fu, HS (Fu, H. S.); Zhou, M (Zhou, M.); Pollock, CJ (Pollock, C. J.); Torbert, RB (Torbert, R. B.); Russell, CT (Russell, C. T.); Burch, JL (Burch, J. L.)
JOURNAL OF GEOPHYSICAL RESEARCH-SPACE PHYSICS
卷: 122 期: 8 页: 8577-8588
Kinetic-size magnetic holes (KSMHs) in the turbulent magnetosheath are statistically investigated using high time resolution data from the Magnetospheric Multiscale mission. The KSMHs with short duration (i.e., < 0.5 s) have their cross section smaller than the ion gyroradius. Superposed epoch analysis of all events reveals that an increase in the electron density and total temperature significantly increases (resp. decrease) the electron perpendicular (resp. parallel) temperature and an electron vortex inside KSMHs. Electron fluxes at similar to 90 degrees pitch angles with selective energies increase in the KSMHs are trapped inside KSMHs and form the electron vortex due to their collective motion. All these features are consistent with the electron vortex magnetic holes obtained in 2-D and 3-D particle-in-cell simulations, indicating that the observed KSMHs seem to be best explained as electron vortex magnetic holes. It is furthermore shown that KSMHs are likely to heat and accelerate the electrons.
Plain Language Summary A nonlinear energy cascade in magnetized turbulent plasmas leads to the formation of different coherent structures which are thought to play an important role in dissipating energy and transporting particles. This study statistically investigate one new type of coherent structure, named electron vortex magnetic hole, used by Magnetospheric Multiscale data. It reveals the common features of this structure, including an increase in the electron density and total temperature, significantly increase (resp. decrease) the electron perpendicular (resp. parallel) temperature and an electron vortex inside these holes. The increase of electron temperature inside the holes indicates that these holes are likely to heat and accelerate the electrons. This gives new clue for energy dissipation in turbulent plasmas.

第 254 条，共 286 条

电子回旋脉泽辐射机制在太阳物理中的进展

唐建飞 吴德金 赵国清 陈玲
Progress in Astronomy
电子回旋脉泽辐射是一种重要的射电辐射机制,将其应用在太阳物理中,需要解决两个困难:一是自由能来源问题;二是辐射的逃逸问题。高能电子束离开加速区后,在磁等离子体中与磁场、波等相互作用可以形成不同的速度空间分布,可以为脉泽辐射提供自由能。对于辐射逃逸问题,日冕低密度导管的假设可以解决这一困难。介绍了近几年回旋脉泽辐射研究的进展及其在太阳射电爆发中的应用,以及阐述了该领域未来研究方向。
基金：新疆维吾尔自治区自然科学基金青年项目(2013211B40)；
关键词：辐射机制；电子回旋脉泽不稳定性；射电暴；幂律谱；
分类号：P182

第 255 条，共 286 条

Radial Variations of Outward and Inward Alfv é nic Fluctuations Based on Ulysses Observations,

L Yang LC Lee JP Li QY Luo CL Kuo ，
《Astrophysical Journal》
2017 , 850 (2) :177
Ulysses magnetic and plasma data are used to study hourly scale Alfvénic fluctuations in the solar polar wind. The calculated energy ratio {R}(cal) of inward to outward Alfvén waves is obtained from the observed Walén slope through an analytical expression, and the observed {R}(obs) is based on a direct decomposition of original Alfvénic fluctuations into outward- and inward-propagating Alfvén waves. The radial variation of {R}(cal) shows a monotonically increasing trend with heliocentric distance r, implying the increasing local generation or contribution of inward Alfvén waves. The contribution is also shown by the radial increase in the occurrence of dominant inward fluctuations. We further pointed out a higher occurrence (65 83 % of a day in average) of dominant outward Alfvénic fluctuations in the solar wind than previously estimated. Since {R}(cal) is more accurate than {R}(obs) in the measurement of the energy ratio for dominant outward fluctuations, the values of {R}(cal) in our results are likely more realistic in the solar wind than those previously estimated as well as {R}(obs) in our results. The duration ratio R of dominant inward to all Alfvénic fluctuations increases monotonically with r, and is about two or more times that from Voyager 2 observations at r≥ slant 4 {au}. These results reveal new qualitative and quantitative features of Alfv é nic fluctuations therein

compared with previous studies and put constraints on modeling the variation of solar wind fluctuations.

第 256 条，共 286 条

Properties of Whistler Waves in Warm Electron Plasmas

Zhao, JS (Zhao, Jinsong)
ASTROPHYSICAL JOURNAL
卷: 850 期: 1 文献号: 13
Dispersion relation and electromagnetic properties of obliquely propagating whistler waves are investigated on the basis of a warm electron fluid model. The magnetic field of whistler waves is nearly circularly polarized with respect to the wave vector in a plasma where the electron plasma frequency Omega(pe) is much larger than the electron cyclotron frequency Omega(ce), and the magnetic field polarization can become elliptical, or even linear, polarization as Omega(pe) less than or similar to Omega(ce). In the plasmas with Omega(pe) < Omega(ce), the resonant frequency is about Omega(ce) cos theta, which is different from Omega(pe) cos theta predicted by the cold electron fluid model. Near the resonant frequency, the whistler wave approximates a quasi-magnetostatic mode, not a quasi-electrostatic mode in the cold electron plasmas. Moreover, the detailed mode properties are given in Earth's magnetosphere, the solar active region, and Jupiter's polar cap. Furthermore, the study proposes that the ratio of the electrostatic to electromagnetic component of the electric field can be used to distinguish the whistler mode from the Z-mode in the frequency range of Omega(pe) < omega < Omega(ce) in the solar active region and Jupiter's polar cap.

第 257 条，共 286 条

Applying the cold plasma dispersion relation to whistler mode chorus waves: EMFISIS wave measurements from the Van Allen Probes

Zhao, JS (Zhao, Jinsong)
Wiley Online Library
卷:230 期: 1 文献号: 11
Most theoretical wave models require the power in the wave magnetic field in order to determine the effect of chorus waves on radiation belt electrons. However, researchers typically use the cold plasma dispersion relation to approximate the magnetic wave power when only electric field data are available. In this study, the validity of using the cold plasma dispersion relation in this context is tested using Electric and Magnetic Field Instrument Suite and Integrated Science (EMFISIS) observations of both the electric and magnetic spectral intensities in the chorus wave band (0.1–0.9 fce). Results from this study indicate that the calculated wave intensity is least accurate during periods of enhanced wave activity. For observed wave intensities >10−3 nT2, using the cold plasma dispersion relation results in an underestimate of the wave intensity by a factor of 2 or greater 56% of the time over the full chorus wave band, 60% of the time for lower band chorus, and 59% of the time for upper band chorus. Hence, during active periods, empirical chorus wave models that are reliant on the cold plasma dispersion relation will underestimate chorus wave intensities to a significant degree, thus causing questionable calculation of wave‐particle resonance effects on MeV electrons.

4-04 Near Earth Object Telescope

第 258 条，共 286 条

Detection of Faint Asteroids Based on Image Shifting and Stacking Method

Wang Bin; Zhao Haibin; Li Bin
Acta Astronomica Sinica
卷: 58 期: 5 页: 49-1-49-13 文献号: 0001-5245(2017)58:5<49:JYTXWY>2.0.TX;2-R
In order to improve the ability to find faint small solar system bodies, a method of shifting and stacking images which improves the detection efficiency of faint moving objects is applied to process the sequential optical images. This method determines the existence of moving objects by using False Position Method to estimate the apparent velocities of moving objects, then determines iteratively accurate position of moving objects based on SNR (Signal-to-Noise Ratio) and elongation. Using the sequential images of the China Near Earth Object Survey Telescope (CNEOST), we carry out a trial experiment and succeed in detecting asteroids fainter than 21 magnitude which are invisible on a single image. At last the feasibility of this method is proved.

第 259 条，共 286 条

Analysis for Cellinoid shape model in inverse process from lightcurves

Lu, XP (Lu, Xiao-Ping); Ip, WH (Ip, Wing-Huen); Huang, XJ (Huang, Xiang-Jie); Zhao, HB (Zhao, Hai-Bin)
PLANETARY AND SPACE SCIENCE
卷: 135 页: 74-85
Based on the special shape first introduced by Alberto Cellino, which consists of eight ellipsoidal octants with the constraint that adjacent octants must have two identical semi-axes, an efficient algorithm to derive the physical parameters, such as the rotational period, pole orientation, and overall shape from either lightcurves or sparse photometric data of asteroids, is developed by Lu et al. and named as 'Cellinoid' shape model. For thoroughly investigating the relationship between the morphology of the synthetic lightcurves generated by the Cellinoid shape and its six semi-axes as well as rotational period and pole, the numerical tests are implemented to compare the synthetic lightcurves generated by three Cellinoid models with different parameters in this article. Furthermore, from the synthetic lightcurves generated by two convex shape models of (6) Hebe and (4179) Toutatis, the inverse process based on Cellinoid shape model is applied to search the best-fit parameters. Especially, for better simulating the real observations, the synthetic lightcurves are generated under the orbit limit of the two asteroids. By comparing the results derived from synthetic lightcurves observed in one apparition and multiple apparitions, the performance of Cellinoid shape model is confirmed and the suggestions for observations are presented. Finally, the whole process is also applied to real observed lightcurves of (433) Eros and the derived results are consistent with the known results.

第 260 条，共 286 条

Scattering Law Analysis Based on Hapke and Lommel-Seeliger Models for Asteroidal Taxonomy

Huang, XJ (Huang, Xiang-Jie); Lu, XP (Lu, Xiao-Ping); Li, JY (Li, Jian-Yang); Mei, B (Mei, Bao); Hsia, CH (Hsia, Chih-Hao); Zhao, HB (Zhao, Hai-Bin)
RESEARCH IN ASTRONOMY AND ASTROPHYSICS
卷: 17 期: 10 文献号: 106
In deriving the physical properties of asteroids from their photometric data, the scattering law plays an important role, although the shape variations of asteroids result in the main variations in lightcurves. By following the physical behaviors of light reflections, Hapke et al. deduced complex functions to represent the scattering process, however, it is very hard to accurately simulate the surface scattering law in reality. For simplicity, other numerical scattering models are presented for efficiently calculating the physical properties of asteroids, such as the Lommel-Seeliger (LS) model. In this article, these two models are compared numerically. It is found that in some numerical applications the LS model in simple form with four parameters can be exploited to replace the Hapke model in complex form with five parameters. Furthermore, the generated synthetic lightcurves by the Cellinoid shape model also show that the LS model can perform as well as the Hapke model in the inversion process. Finally, by applying the Principal Component Analysis (PCA) technique to the parameters of the LS model, we present an efficient method to classify C and S type asteroids, instead of the conventional method using the parameters of the Hapke model.

4-05 Laboratory for Planetary Science and Deep Space Exploration

第 261 条，共 286 条

Drilling, sampling, and sample-handling system for China's asteroid exploration mission

Zhang, T (Zhang, Tao); Zhang, WM (Zhang, Wenming); Wang, K (Wang, Kang); Gao, S (Gao, Sheng); Hou, L (Hou, Liang); Ji, JH (Ji, Jianghui); Ding, XL (Ding, Xilun)
ACTA ASTRONAUTICA
卷: 137 页: 192-204
Asteroid exploration has a significant importance in promoting our understanding of the solar system and the origin of life on Earth. A unique opportunity to study near-Earth asteroid 99942 Apophis will occur in 2029 because it will be at its perigee. In the current work, a drilling, sampling, and sample-handling system (DSSHS) is proposed to penetrate the asteroid regolith, collect regolith samples at different depths, and distribute the samples to different scientific instruments for in situ analysis. In this system, a rotary-drilling method is employed for the penetration, and an inner sampling tube is utilized to collect and discharge the regolith samples. The sampling tube can deliver samples up to a maximum volume of 84 mm(3) at a maximum penetration depth of 300 mm to 17 different ovens. To activate the release of volatile substances, the samples will be heated up to a temperature of 600 degrees C by the ovens, and these substances will be analyzed by scientific instruments such as a mass spectrometer, an isotopic analyzer, and micro -cameras, among other instruments. The DSSHS is capable of penetrating rocks with a hardness value of six, and it can be used for China's asteroid exploration mission in the foreseeable future.

第 262 条，共 286 条

Surface thermophysical properties on the potentially hazardous asteroid (99942) Apophis

Yu, LL (Yu, Liang-Liang); Ji, JH (Ji, Jianghui); Ip, WH (Ip, Wing-Huen)
RESEARCH IN ASTRONOMY AND ASTROPHYSICS
卷: 17 期: 7 文献号: 70
We investigate the surface thermophysical properties (thermal emissivity, thermal inertia, roughness fraction and geometric albedo) of asteroid (99942) Apophis, using the currently available mid-infrared observations from CanariCain on Gran Telescopio CANARIAS and far-infrared data from PACS on Herschel, based on the Advanced Thennophysical Model. We show that the thermal emissivity of Apophis should be wavelength dependent from 8.70 mu m to 160 mu m, and the maximum emissivity may appear around 20 mu m, similar to that of Vesta. Moreover, we further derive the thermal inertia, roughness fraction, geometric albedo and effective diameter of Apophis within a possible 1 sigma scale of Gamma = 100(-52)(+100) Jm(-2) S-0.5 K-1, integral(r) = 0.78 similar to 1.0, p(v) = 0.286(-0.026)(+0.030) and D-eff = 378(-25)(+19)m, and 3 sigma scale of Gamma = 100(-100)(+240) Jm(-2) s(-0.5) K-1, f(r) = 0.2 similar to 1.0, p(v) = 0.286(-0.029)(+0.039) and D-eff = 378(-29)(+27) m. The derived low thermal inertia but high roughness fraction may imply that Apophis could have regolith on its surface, where stronger space weathering but weaker regolith migration has happened in comparison with asteroid Itokawa. Our results show that small-size asteroids could also have fine regolith on the surface, and further infer that Apophis may have been delivered from the Main Belt by the Yarkovsky effect.

第 263 条，共 286 条

Long-lived Dust Asymmetries at Dead Zone Edges in Protoplanetary Disks

Miranda, R (Miranda, Ryan); *Li, H* (Li, Hui); Li, ST (Li, Shengtai); Jin, S (Jin, Sheng)
ASTROPHYSICAL JOURNAL
卷: 835 期: 2 文献号: 118
A number of transition disks exhibit significant azimuthal asymmetries in thermal dust emission. One possible origin for these asymmetries is dust trapping in vortices formed at the edges of dead zones. We carry out high-resolution, two-dimensional hydrodynamic simulations of this scenario, including the effects of dust feedback. We find that, although feedback weakens the vortices and slows down the process of dust accumulation, the dust distribution in the disk can nonetheless remain asymmetric for many thousands of orbits. We show that even after 104 orbits, or 2.5 Myr when scaled to the parameters of Oph IRS 48 (a significant fraction of its age), the dust is not dispersed into an axisymmetric ring, in contrast to the case of a vortex formed by a planet. This is because accumulation of mass at the dead zone edge constantly replenishes the vortex, preventing it from being fully destroyed. We produce synthetic dust emission images using our simulation results. We find that multiple small clumps of dust may be distributed azimuthally. These clumps, if not resolved from one another, appear as a single large feature. A defining

characteristic of a disk with a dead zone edge is that an asymmetric feature is accompanied by a ring of dust located about twice as far from the central star.

第 264 条，共 286 条

Thermophysical characteristics of the large main-belt asteroid (349) Dembowska

Yu, LL (Yu, Liang Liang); Yang, B (Yang, Bin); Ji, JH (Ji, Jianghui); Ip, WH (Ip, Wing-Huen)
MONTHLY NOTICES OF THE ROYAL ASTRONOMICAL SOCIETY
卷: 472 期: 2 页: 2388-2397
(349) Dembowska is a large, bright main-belt asteroid that has a fast rotation and an oblique spin axis. It might have experienced partial melting and differentiation. We constrain Dembowska's thermophysical properties, such as thermal inertia, roughness fraction, geometric albedo and effective diameter within 3s uncertainty of Gamma = 20(-7)(+12) Jm(-2) s(-0.5) K-1, fr = 0.25(-0.25)(+0.60), p(v) = 0.309(-0.038)(+0.026) and D-eff = 155.8(-6.2)(+7.5) km, by utilizing the advanced thermophysical model to analyse four sets of thermal infrared data obtained by the Infrared Astronomy Satellite (IRAS), AKARI, the Wide-field Infrared Survey Explorer (WISE) and the Subaru/Cooled Mid-Infrared Camera and Spectrometer (COMICS) at different epochs. In addition, by modelling the thermal light curve observed by WISE, we obtain the rotational phases of each data set. These rotationally resolved data do not reveal significant variations of thermal inertia and roughness across the surface, indicating that the surface of Dembowska should be covered by a dusty regolith layer with few rocks or boulders. Besides, the low thermal inertia of Dembowska shows no significant difference with other asteroids larger than 100 km, which indicates that the dynamical lives of these large asteroids are long enough to make their surfaces have sufficiently low thermal inertia. Furthermore, based on the derived surface thermophysical properties, as well as the known orbital and rotational parameters, we can simulate Dembowska's surface and subsurface temperatures throughout its orbital period. The surface temperature varies from similar to 40 to similar to 220 K, showing significant seasonal variation, whereas the subsurface temperature achieves equilibrium temperature about 120-160 K below a depth of 30-50 cm.

第 265 条，共 286 条

The Scattering Outcomes of Kepler Circumbinary Planets: Planet Mass Ratio

Gong, YX (Gong, Yan-Xiang); Ji, JH (Ji, Jianghui)
ASTRONOMICAL JOURNAL
卷: 154 期: 5 文献号: 179
DOI: 10.3847/1538-3881/aa8c7c
Recent studies reveal that the free eccentricities of Kepler-34b and Kepler-413b are much larger than their forced eccentricities, implying that scattering events may take place in their formation. The observed orbital configuration of Kepler-34b cannot be well reproduced in disk-driven migration models, whereas a two-planet scattering scenario can play a significant role of shaping the planetary configuration. These studies indicate that circumbinary planets discovered by Kepler may have experienced scattering process. In this work, we extensively investigate the scattering outcomes of circumbinary planets focusing on the effects of planet mass ratio. We find that the planetary mass ratio and the the initial relative locations of planets act as two important parameters that affect the eccentricity distribution of the surviving planets. As an application of our model, we discuss the observed orbital configurations of Kepler-34b and Kepler-413b. We first adopt the results from the disk-driven models as the initial conditions, then simulate the scattering process that occurs in the late evolution stage of circumbinary planets. We show that the present orbital configurations of Kepler-34b and Kepler-413b can be well reproduced when considering a two unequal-mass planet ejection model. Our work further suggests that some of the currently discovered circumbinary single-planet systems may be survivors of original multiple-planet systems. The disk-driven migration and scattering events occurring in the late stage both play an irreplaceable role in sculpting the final systems.

第 266 条，共 286 条

Tidal Evolution of the Kepler Planets with Radii Less than 4 R_

Dong Yao; Ji Jianghui; Wang Su
Acta Astronomica Sinica
卷：58 期：4 页：31-1-31-11 文献号：0001-5245(2017)58:4<31:DZLKXX>2.0.TX;2-J
The planets with a radius<4 R_ observed by the Kepler mission exhibit a unique feature,and propose a challenge for current planetary formation models. The tidal effects between the planet and the host star play an essential role in reconfiguring the final orbits of the short-period planets. In this work, based on various initial Rayleigh distributions of the orbital elements, the final semi-major axis distributions of the planets with a radius<4 R_ after suffering tidal evolution are investigated. Our simulations qualitatively reveal various statistical properties:the peaks of semi- major axes increase with the mean semi-major axis, and the peak amplitude of the final semi-major axis distribution increases with the mean eccentricity for all kinds of semi-major axis distributions. For the case that the mean semi-major axis is about 0.1 au and the mean eccentricity is larger than 0.25, the amplitude peaks of the final semi-major axis are approximately consistent with observations. In addition, the roles of other parameters such as the tidal dissipation factor, stellar, and planetary mass etc, are explored in this study by performing numerical simulations, and it is found that they have little effect on the amplitudes of the peaks. Our simulation results provide some clues of planetary formation for such low-mass planets. We speculate that these low-mass planets are possible to form in a farther place of the proto-planetary disk with a moderate eccentricity via type I migration, and it is possible to form in situ too.

第 267 条，共 286 条

基于图像位移叠加方法探测暗弱小行星

王斌 赵海斌 李彬
为了提高对太阳系内暗弱小天体的探测能力,将位移叠加方法应用于时序光学图像的处理,提高了暗弱小行星的识别效率.通过试位法预估动目标的视运动速度,确定动目标的存在性,进一步根据目标星象特征判据(信噪比和星象伸长率)迭代确定动目标的精确位置.将位移叠加方法运用在近地天体望远镜同一天区连续曝光的多幅图像的处理中,成功探测到暗于 21 mag 的单帧不可见动目标,验证了图像位移叠加方法探测暗弱动目标的可行性.
基金：国家自然科学基金项目(11633009、11503090、

11273067、11661161013)； 澳门科学技术发展基金项目(095/2013/A3)； 紫金山天文台小行星基金会和澳门科技大学月球与行星科学实验室-中国科学院月球与深空探测重点实验室伙伴实验室资助；
关键词：天体测量学; 仪器; 望远镜; 技术:图像处理; 方法:观测; 方法:数据分析;
DOI：10.15940/j.cnki.0001-5245.2017.05.008
分类号：P185.7

第 268 条，共 286 条

晚期月海玄武岩的矿物变化

张迅与 欧阳自远 *吴昀昭* 许敖敖 陈媛 蔡伟 卢瑜
月球火山活动的最后一个主要阶段大部分都发生在月球的风暴洋和雨海地区,并产出了一套光谱独特的高铁、钛玄武岩(Hiesinger et al.,2003;Staid et al.,2011)。早期地基望远镜观测的研究发现,这些低反射率的中-高钛玄武岩具有较强的 1μm 吸收特征和较弱的 2μm 吸收特征(Johnson et al.,1977;Pieters et al.,1980)。这说明晚期月海玄武
基金：澳门科学技术发展基金项目(039/2013/A2 和 091/2013/A3)；
会议名称：中国矿物岩石地球化学学会第九次全国会员代表大会暨第 16 届学术年会
会议时间：2017-04-18
会议地点：中国陕西西安
分类号：P184

第 269 条，共 286 条

Using Chebyshev polynomial interpolation to improve the computational efficiency of gravity models near an irregularly-shaped asteroid

Hu, SC (Hu, Shou-Cun); Ji, JH (Ji, Jiang-Hui)
RESEARCH IN ASTRONOMY AND ASTROPHYSICS
卷: 17 期: 12 文献号: 120
In asteroid rendezvous missions, the dynamical environment near an asteroid's surface should be made clear prior to launch of the mission. However, most asteroids have irregular shapes, which lower the efficiency of calculating their gravitational field by adopting the traditional polyhedral method. In this work, we propose a method to partition the space near an asteroid adaptively along three spherical coordinates and use Chebyshev polynomial interpolation to represent the gravitational acceleration in each cell. Moreover, we compare four different interpolation schemes to obtain the best precision with identical initial parameters. An error-adaptive octree division is combined to improve the interpolation precision near the surface. As an example, we take the typical irregularly-shaped near-Earth asteroid 4179 Toutatis to demonstrate the advantage of this method; as a result, we show that the efficiency can be increased by hundreds to thousands of times with our method. Our results indicate that this method can be applicable to other irregularly-shaped asteroids and can greatly improve the evaluation efficiency.

第 270 条，共 286 条

Near Mean-motion Resonances in the System Observed by Kepler: Affected by Mass Accretion and Type I Migration

Wang, S (Wang, Su); Ji, JH (Ji, Jianghui)
ASTRONOMICAL JOURNAL
卷: 154 期: 6 文献号: 236
The Kepler mission has released over 4496 planetary candidates, among which 3483 planets have been confirmed as of 2017 April. The statistical results of the planets show that there are two peaks around 1.5 and 2.0 in the distribution of orbital period ratios. The observations indicate that plenty of planet pairs could have first been captured into mean-motion resonances (MMRs) in planetary formation. Subsequently, these planets depart from exact resonant locations to be near-MMR configurations. Through type I migration, two low-mass planets have a tendency to be trapped in first-order MMRs (2:1 or 3:2 MMRs); however, two scenarios of mass accretion of planets and potential outward migration play important roles in reshaping their final orbital configurations. Under the scenario of mass accretion, the planet pairs can cross 2:1 MMRs and then enter into 3:2 MMRs, especially for the inner pairs. With such a formation scenario, the possibility that two planets are locked into 3:2 MMRs can increase if they are formed in a flat disk. Moreover, the outward migration can make planets have a high likelihood to be trapped into 3:2 MMRs. We perform additional runs to investigate the mass relationship for those planets in three-planet systems, and we show that two peaks near 1.5 and 2.0 for the period ratios of two planets can be easily reproduced through our formation scenario. We further show that the systems in chain resonances (e.g., 4:2:1, 3:2:1, 6:3:2, and 9:6:4 MMRs), have been observed in our simulations. This mechanism can be applicable to understand the formation of systems of Kepler-48, Kepler-53, Kepler-100, Kepler-192, Kepler-297, Kepler-399, and Kepler-450.

第 271 条，共 286 条

Near Mean-motion Resonances in the System Affected by Mass Accretion and Type I MigrationObserved by Kepler:

S Wang ， J Ji
Astronomical Journal
The Kepler mission has released over 4496 planetary candidates, among which 3483 planets have been confirmed as of April 2017. The statistical results

4-06 Laboratory for Astrochemistry and Planetary Sciences

第 272 条，共 286 条

Optical spectroscopic characterizations of laser irradiated olivine grains

Yang, YZ (Yang, Yazhou); Zhang, H (Zhang, Hao); Wang, ZW (Wang, Ziwei); Yuan, Y (Yuan, Ye); Li, SL (Li, Shaolin); Hsu, WB (Hsu, Weibiao); Liu, CJ (Liu, Chujian)
ASTRONOMY & ASTROPHYSICS
卷: 597 文献号: A50
Context. Visible and near-infrared spectra of asteroids are known to be susceptible to nanophase irons produced by space weathering processes, thus making mineral identifications difficult. Mid-infrared spectroscopy may

retain more mineral features owing to its lattice vibrational nature.
Aims. We investigate the structure and reflectance spectral feature changes of olivine grains before and after simulated space weathering.
Methods. We irradiate olivine grains by using pulsed laser to simulate varying degrees of micrometeorite bombardments. Reflectance measurements from 0.5 to 25 mu m and radiative transfer calculations were carried out in order to compare them with each other.
Results. Both the experimental simulations and modeling results indicate that the mid-infrared spectral features of olivine grains can survive the intense irradiations. Although the Christansen Feature is slightly shifted to longer wavelength, major vibrational bands remain essentially unchanged, because the lattice structure is quite immune to even the strongest irradiations, as revealed by both the X-ray diffraction and Raman scattering measurements.
Conclusions. Mid-infrared spectroscopy is much more immune to productions of nanophase irons and amorphous materials and thus may be used more reliably in remote detections of minerals on asteroid surfaces.

第 273 条，共 286 条

Late Oligocene crustal anatexis and melt/fluid migration in the Ailao Shan tectonic belt: Evidences from zircon U-Pb ages and trace element compositions

Wang, DB (Wang DongBing); Tang, Y (Tang Yuan); Luo, L (Luo Liang); Liao, SY (Liao ShiYong); Yin, FG (Yin FuGuang); Wang, BD (Wang BaoDi)
ACTA PETROLOGICA SINICA
卷: 33 期: 7 页: 2037-2053
The Ailao Shan tectonic belt is an important tectonic boundary in southeast of the Qinghai-Tibetan Plateau and consists mainly of high-grade metamorphic rocks previously thought to be Paleoproterozoic basement rocks. In-situ LA-ICP-MS U-Pb age and trace element of zircons were determined for the Ailao Shan high-grade metamorphic rocks. Zircon U-Pb geochronological data indicate that the high-grade metamorphic rocks have various parent rocks with different intrusive/depositional ages of 728 +/- 8Ma, 727 +/- 3Ma and 231 +/- 4Ma and similar metamorphic ages of 27. 8 similar to 23. 7Ma. Our new results demonstrate that the high-grade metamorphic rocks from the Ailao Shan belt zone are a mixture of metamorphic both igneous and sedimentary rocks of different times, instead of solely Paleoproterozoic basement rocks. Migmatization and metamorphic crystallization of these rocks took place at 27. 8 similar to 23. 7Ma, indicating a significant period of crustal anatexis in the Ailao Shan tectonic belt. The syntectonic felsic dykes hosted by gneiss were derived from a mixture of locally-derived and allochthonous melts. The migmatized rocks from the Ailao Shan deformation zone were most probably the results of decompression melting following peak metamorphism. The crustal anatexis and left-lateral shearing were two synchronous metamorphic patterns resulted from a shared geological event. They interact and influence each other during exhumation of the Ailao Shan metamorphic zone in Late Oligocene.

第 274 条，共 286 条

New understanding on Ximeng Group in Three River area, western Yunnan: Evidence from structural characterization and zircon U-Pb dating

Tang, Y (Tang Yuan); Wang, DB (Wang DongBing); Liao, SY (Liao ShiYong); Yin, FG (Yin FuGuang)
ACTA PETROLOGICA SINICA
卷: 33 期: 7 页: 2054-2072
Located in the eastern margin of Baoshan-Shan Thai block, the Ximeng Group was long regarded as the only Precambrian metamorphic basement rocks exposed in China of this block. Without scientific and reliable data of geochronology and paleontology, the age of the metamorphic rocks is still controversial. Based on detailed macro- and micro-structural observations, the metamorphic rocks of Ximeng Group which shows domelike uplift can be divided into granitic mylonites and low grade metamorphic rocks. The former are distributed in core of the uplift and have experienced intensively ductile deformation. The latter are distributed in the rim and have the similar features of Pake Formation and Wangya-Yungou Formation. According to EBSD fabric analysis of quartz in the deformed rocks of Ximeng Group, it can reveal that the rocks closed to the core have experienced an early stage of deformation at intermediate temperatures (550 similar to 650 degrees C, corresponding to amphibolite facies) and a late deformation at low temperature (400 similar to 550 degrees C, greenschist facies), while the rocks near the rim of uplift have been deformed at low temperature (400 550 degrees C). In this paper, three samples of granitic mylonites were chosen for LA-ICP-MS zircon U-Pb dating, giving ages of 455 +/- 3Ma, 456 +/- 3Ma and 454 +/- 3Ma respectively. Combined with previous research results of geochronology and paleontology, it indicates that the protolith of the Ximeng metamorphic rocks may be composed of two parts. The first part is the Ordovician granite (similar to 460Ma) and the other mainly comprises Cambrian carbonate, elastic rocks and minor basic volcanic rock. The former is highly deformed into mylonites during the ductile shearing, and the latter is transformed into phylite, schist and marble due to low grade metamorphism at low temperature (400 550 degrees C, greenschist facies). It also can be concluded that Ximeng Group should not be regarded as the Precambrian metamorphic basement rocks of Baoshan block.

第 275 条，共 286 条

The petrology and chronology of NWA 8009 impact melt breccia: Implication for early thermal and impact histories of Vesta

Liao, SY (Liao, Shiyong); Hsu, WB (Hsu, Weibiao)
GEOCHIMICA ET COSMOCHIMICA ACTA
卷: 204 页: 159-178
Studies of petrology, mineralogy and geochronology of eucrites are keys to reconstruct the thermal and impact history of 4 Vesta, the proposed parent body for HED meteorites. Here we report the petrography, mineralogy and geochemistry of NWA 8009, a newly found eucritic impact-melt breccia, and present SIMS U-Pb ages of zircon and phosphates. NWA 8009 consists of coarse-and fine-grained lithic and mineral clasts set in fine-grained recrystallized matrix. It was derived from a protolith of monomict non-cumulate eucrite. Evidence for intense shock metamorphism observed in NWA 8009 includes mosaicism, deformed exsolution lamellae and partial melting of pyroxene, melting and incipient flow of plagioclase, planar fractures and granular textures of zircon. These shock

effects indicate NWA 8009 was subjected to an impact metamorphism with peak pressure of similar to 50-60 GPa and post-shock temperature of similar to 1160-1200 degrees C. NWA 8009 is among the most intensely shocked HEDs reported yet. After the impact, the sample was buried near the surface in target rocks and experienced rapid cooling (similar to 23 degrees C/h) and annealing, resulting in recrystallization of the matrix and devitrification of plagioclase and silica glasses. U-Pb isotopic system of apatite within plagioclase groundmass of lithic clasts is completely reset and constrains the timing of impact at 4143 +/- 61 Ma, providing a new robust impact age on Vesta. Combined with the presence of synchronous impact resetting events, especially those recorded by Lu-Hf, Sm-Nd, and Pb-Pb isotopic systems, we identified a period of high impacts flux at ca. 4.1-4.2 Ga on Vesta. This impact flux occurred coincident with the uptick at ca. 4.1-4.2 Ga in impact age spectra of the moon, probably reflects widespread intense bombardment throughout the inner solar system at ca. 4.1-4.2 Ga. Based on evidence from zircon chemical zoning, petrographic occurrences, as well as the distinctive Zr/Hf ratios, we suggested that zircons in NWA 8009 have had a metamorphic, instead of magmatic origin. They mainly crystallized from melts produced by partial melting of mesostasis area due to reheating event during early global thermal metamorphism, rather than by Zr release from Zr-rich minerals. The U-Pb isotopic system in zircons was not disturbed by subsequent impacts, the weighted-mean Pb-207/Pb-206 age of 4560 +/- 8 Ma represents the timing of zircon growth during thermal metamorphism. Zircons from NWA 8009 and other eucrites may share a common origin during metamorphic growth events, and constraining the global thermal metamorphism on Vesta at ca. 4.55 Ga. The main heat sources responsible for global metamorphism in basaltic crust of Vesta might be heating from the hot interior, especially heat flow related to magmatism, rather than impact. (C) 2017 Elsevier Ltd. All rights reserved.

第 276 条，共 286 条

Petrogenesis of late Eocene high Ba-Sr potassic rocks from western Yangtze Block, SE Tibet: A magmatic response to the Indo-Asian collision

Liu, Z (Liu, Zheng); Liao, SY (Liao, Shi-Yong); Wang, JR (Wang, Jin-Rong); Ma, Z (Ma, Zhen); Liu, YX (Liu, Yi-Xin); Wang, DB (Wang, Dong-Bing); Tang, Y (Tang, Yuan); Yang, J (Yang, Jing)
JOURNAL OF ASIAN EARTH SCIENCES
卷: 135 页: 95-109
The Indo-Asian collision resulted in extrusion of the Indochina Block along the Ailao Shan-Red River (ASRR) shear zone in the Cenozoic, with the emplacement of widespread potassic magmatic rocks. In this contribution, we investigated five potassic felsic intrusions exposed in the western Yangtze Block adjacent to the ASRR shear zone, including the Xiaoqiaotou, Jianchuan, Yuzhaokuai, Laojunshan and South Taohuacun intrusions. New LA-ICP-MS zircon U-Pb results in combination with previous data indicate that these felsic rocks have identical crystallization ages of similar to 36-35 Ma. They are characterized by high Ba (mostly >1500 ppm) and Sr (mostly >1000 ppm) abundances, with high K2O contents and K2O/Na2O ratios. They exhibit similar Sr-Nd isotopic components as the coeval shoshonitic mafic rocks exposed in the studied area. Elemental and isotopic data suggest that the five intrusions were likely derived from fractional crystallization of shoshonitic mafic magmas originating from an enriched lithospheric mantle. On the basis of previously published data and results in this paper, we considered that the lithospheric mantle underneath the western Yangtze might have undergone enrichment events twice at least, including the Neoproterozoic oceanic subduction and the Neo-Tethyan oceanic subduction. (C) 2016 Elsevier Ltd. All rights reserved.

第 277 条，共 286 条

Chronology,Petrogenesis and Links with Extrusion Tectonics of Cangyuan Cenozoic Intermediate to Acid Intrusive Rocks in Baoshan Block,Eastern Tibetan Plateau

Wang Dongbing; Tang Yuan; Ye Chunlin; Yin Fuguang; Luo Liang; Liao Shiyong
Bulletin of Mineralogy Petrology and Geochemistry
卷 : 36 期 : 2 页 : 245-258 文 献 号 : 1007-2802(2017)36:2<245:QZGYDY>2.0.TX;2-P
In order to investigate the geochronology,petrogenesis and geodynamicsettingof the Cenozoic igneous rocks in Baoshan block,we have concentrated on the petrology,zircon U-Pb chronology and whole-rock geochemical composition of the Early Cenozoic igneous rock in Cangyuan,southeastern Baoshan block. The results of dating indicate that the intermediate to flesic intrusions and dykes in Cangyuan emplaced at 40-41 Ma,synchronous with those in Lancang region. The Early Cenozoic igneous rock in Cangyuan and Lancang exhibits high Sr /Y,La /Yb,Gd /Yb ratios and significant REE fractionation,with no significant Sr,Eu negative anomaly,similar to C-type adakite. They have enriched initial ~(86)Sr / ~(87)Sr ratios of 0.7065-0.7103,epsilon_(Nd) (t) values of -3.6 to -5.6. We infer that the Cangyuan Cenozoic magmatism resulted from partial melting of garnet amphibolite in lower crust at a depth of 30 ~ 40 km. In addition,we report for the first time that there has ~ 41 Ma A-type granite in Cangyuan region in this study. The early Cenozoic igneous rock in both Cangyuan and Lancang have close spatial,temporal and possibly has genetic linkage with the eastward extrusion of Tibet.

第 278 条，共 286 条

PETROLOGY, MINERALOGY AND IN SITU U-PB DATING OF NORTHWEST AFRICA 11042.

Wu, Y (Wu, Y.); Hsu, W (Hsu, W.)
METEORITICS & PLANETARY SCIENCE
卷: 52 特刊: SI 页: A391-A391
会议摘要: 6190
增刊: 1
出版年: AUG 2017
会议名称: 80th Annual Meeting of the Meteoritical-Society
会议日期: JUL 23-28, 2017
会议地点: Santa Fe, NM
会议赞助商: Meteorit Soc

第 279 条，共 286 条

滇西三江地区西盟群的再认识——来自构造变形特征及锆石 U-Pb 年代学的证据

唐 渊 王冬兵 廖世勇 尹福光

位于保山-掸泰地块东缘的西盟群,长期以来被认为是该地块在我国境内唯一出露的"前寒武纪"基底变质岩系,但其缺乏可靠的年代学数据和化石支持。本文基于详细地野外考察和显微构造分析认为,西盟群变质岩系可解体为花岗质糜棱岩和浅变质岩。前者主要出露于西盟穹形隆起的核部,遭受了强烈的韧性剪切变形;后者分布于隆起的边缘及东西两侧,归属为帕克组、王雅-允沟组。通过变形岩石的石英 EBSD 组构分析,揭示出位于西盟隆起核部的岩石经历了中等温度条件(550~650℃,角闪岩相)下的变形作用,并叠加了较低温度条件(400~550℃,绿片岩相)下的变形作用;而靠近西盟隆起边部的岩石仅经历了较低温度条件(400~550℃,绿片岩相)下的变形作用。本文还对西盟群变质岩中的 3 个花岗质糜棱岩样品进行了 LA-ICP-MS 锆石 U-Pb 测年,得到的锆石 U-Pb 年龄分别为 455±3Ma、456±3Ma 和 454±3Ma。结合前人获得的年代学数据和化石资料,认为西盟群变质岩系的原岩主要由两个不同时期的物质组成,即中-晚奥陶世(~460Ma)侵入的花岗岩及寒武纪的碳酸盐岩和碎屑岩夹少量基性火山岩等;前者遭受强烈变质变形作用的改造,形成花... 更多

基金：国家重点研究发展计划项目(2015CB452601)； 深地专项(2016YFC0600305)； 国家自然科学基金项目(41302170 、 41302157)； 中国地质调查局项目(DD20160021、DD20160016)联合资助；
关键词：西盟群; 花岗质糜棱岩; 韧性剪切作用; EBSD 组构分析; U-Pb 定年;
分类号：P542;P597.3

第 280 条，共 286 条

哀牢山构造带晚渐新世地壳深熔与熔/流体迁移:锆石 U-Pb 年龄与微量元素证据

王冬兵 唐渊 罗亮 廖世勇 尹福光 王保弟

哀牢山构造带是青藏高原东南缘重要的边界构造带,其内出露的深变质岩系一直被认为是古老的变质基底岩石。利用 LA-ICP-MS 原位微区分析技术对哀牢山深变质岩系锆石进行 U-Pb 年龄、微量元素分析。结果表明深变质岩系的原岩有 728±8Ma、727±3Ma、231±4Ma 的花岗质岩石和其它年龄的碎屑岩,变质时代为 27.8~23.7Ma。综合野外地质特征和分析结果,我们认为哀牢山深构造带在晚渐新世 27.8~23.7Ma 发生了大规模的地壳深熔作用,现今所见深变质岩系是由不同时代、不同岩性的原岩在晚渐新世(27.8~23.7Ma)变质形成,不全是古老的变质基底岩石。深熔过程中熔/流体发生了明显的迁移。哀牢山变质带具有混合岩化特征的岩石很可能是峰期变质作用后减压熔融的产物。晚渐新世地壳深熔作用与左行走滑剪切是哀牢山深变质带折返过程中近似同时发生的两种不同变质表现形式,两者相互影响、相互制约。

基金：国家重点研究发展计划项目(2015CB452601)； 深地专项(2016YFC0600305)； 国家自然科学基金项目(41302157 、 41302170)； 中国地质调查局项目(DD20160016、DD20160021)联合资助；
关键词：地壳深熔作用; 熔/流体迁移; 深变质岩系; 锆石 U-Pb 定年; 哀牢山构造带;
分类号：P588.3;P597.3

第 281 条，共 286 条

青藏高原东缘保山地块沧源新生代中酸性侵入岩年代学、岩石成因与地块挤出

王冬兵 唐渊 叶春林 尹福光 罗 亮 廖世勇

为探讨保山地块新生代岩浆侵位时代,揭示其成因和形成动力学机制,重建保山地块新生代演化历史,对保山地块东南缘沧源新生代岩浆岩中部分中酸性岩体和岩墙开展了岩石学、锆石 U-Pb 年代学和地球化学研究。结果表明,沧源地区新生代中酸性岩体和岩墙均侵位于 40~41Ma,与澜沧新生代花岗质侵入岩年龄相当,为保山地块新生代早期岩浆活动的重要组成。沧源和澜沧新生代岩浆岩总体具有较强的轻-重稀土、特别是中-重稀土分馏,无明显 Sr、Eu 负异常,具高的 Sr/Y、La/Yb、Gd/Yb 值,与 C 型埃达克岩类似。样品的 86Sri/87Sri 为 0.7065~0.7103, ε Nd(t)为-3.6~-5.6。沧源新生代岩浆岩很可能来自石榴斜长角闪岩源区在 30~40km 深度的部分熔融。通过岩相学和地球化学分析,首次在沧源新生代岩浆岩中识别出~41Ma 的 A 型花岗岩。结合区域构造-岩浆研究成果,认为沧源-澜沧新生代岩浆带与青藏高原碰撞导致的东部岩石圈块体南东向挤出作用存在密切联系。

基金：江苏省自然科学基金(BK20151609,BK20161098)； 国家自然科学基金项目(41202048,41302157,41302170)； 中国地质调查局项目(1212011085119,1212011220412)；
关键词：保山地块; 新生代; C 型埃达克; A 型花岗岩; 锆石 U-Pb 年龄; 岩石成因; 地块挤出;
分类号：P597.3;P588.12

第 282 条，共 286 条

NWA 4898 月球高铝玄武岩岩石成因研究

李少林,徐伟彪,管云彬,王英

月球高铝玄武岩以其较高的 Al2O3 含量（11%16%）为特征,是目前已知的最古老的月球玄武岩样品之一,其成因对于研究月球早期岩浆作用具有重要的意义。Apollo 14,Luna 16 探月任务返回了绝大部分的高铝玄武岩样品。Apollo 12 样品中仅发现一块高铝玄武岩（12038）,在 Apollo 16 月壤样品（60053,2-9）中也发现了一块疑似高铝玄武质的岩屑(Zeigler 等,2

基金：国家自然科学基金项目(41273079,41573059)； 中国科学院小行星基金会；
会议名称：中国矿物岩石地球化学学会第九次全国会员代表大会暨第 16 届学术年会
会议时间：2017-04-18
会议地点：中国陕西西安
分类号：P184

第 283 条，共 286 条

月海玄武岩 NWA 10597 的岩相特征及成因探讨

吴蘧华,徐伟彪

目前地球上发现的月球陨石样品多数为角砾岩,非角砾的月海玄武岩则很稀有,通常认为月海玄武岩形成于月幔深部堆晶岩不同程度重熔、上升、喷发(Shearer and Papike,1999)。对月海玄武岩的研究是了解月球深部化学成分、岩浆演化过程的重要手段之一。NWA 10597 是 1 块新命名的低钛月海玄武岩,在 2015 年发现于摩洛哥,保留有完整新鲜的熔壳。

基金：中国科学院小行星基金会(41573059)；
会议名称：中国矿物岩石地球化学学会第九次全国会员代表大会暨第 16 届学术年会
会议时间：2017-04-18
会议地点：中国陕西西安

分类号：P184

第 284 条，共 286 条

Optical spectroscopic characterizations of laser irradiated olivine grains

Y Yang， H Zhang， Z Wang， Y Yuan， S Li
Astronomy & Astrophysics
Context. Visible and near-infrared spectra of asteroids are known to be susceptible to nanophase irons produced by space weathering processes, thus making mineral identifications difficult. Mid-infrared spectroscopy may retain more mineral features owing to its lattice vibrational nature. Aims. We investigate the structure and reflectance spectral feature changes of olivine grains before and after simulated space weathering. Methods. We irradiate olivine grains by using pulsed laser to simulate varying degrees of micrometeorite bombardments. Reflectance measurements from 0.5 to 25 μm and radiative transfer calculations were carried out in order to compare them with each other. Results. Both the experimental simulations and modeling results indicate that the mid-infrared spectral features of olivine grains can survive the intense irradiations. Although the Christansen Feature is slightly shifted to longer wavelength, major vibrational bands remain essentially unchanged, because the lattice structure is quite immune to even the strongest irradiations, as revealed by both the X-ray diffraction and Raman scattering measurements. Conclusions. Mid-infrared spectroscopy is much more immune to productions of nanophase irons and amorphous materials and thus may be used more reliably in remote detections of minerals on asteroid surfaces.

4-07 Planetary Spectroscopy Group

第 285 条，共 286 条

Submicroscopic metallic iron in lunar soils estimated from the in situ spectra of the Chang'E-3 mission

Wang, ZC (Wang, Zhenchao); Wu, YZ (Wu, Yunzhao); Blewett, DT (Blewett, David T.); Cloutis, EA (Cloutis, Edward A.); Zheng, YC (Zheng, Yongchun); Chen, J (Chen, Jun)
GEOPHYSICAL RESEARCH LETTERS
卷: 44 期: 8 页: 3485-3492
Submicroscopic metallic iron (SMFe) created by space weathering has strong effects on the optical properties of the lunar surface. Spectra measured in situ by the visible-near-infrared spectrometer (VNIS) on board the Chang'E-3 Yutu rover were used to investigate optical maturity differences at the CE-3 landing site caused by lander exhaust. SMFe abundances were estimated using Hapke's radiative transfer model. Analysis of the spectrum for a minimally disturbed soil indicates that it contains 0.368 wt% SMFe, corresponding to an I-s/FeO maturity index of similar to 53 and indicating that the landing site is submature. The soil at a location that was more disturbed contains 0.217 wt% SMFe, suggesting that the material removed by the rocket blast is more weathered than the regolith that remained behind. We conclude that maturity differences related to removal of the finest, highly mature particles play a major role in the observed reflectance changes associated with rocket blast.

第 286 条，共 286 条

Effect of Topography Degradation on Crater Size-Frequency Distributions: Implications for Populations of Small Craters and Age Dating

Xie, MG (Xie, Minggang); Zhu, MH (Zhu, Meng-Hua); Xiao, ZY (Xiao, Zhiyong); Wu, YZ (Wu, Yunzhao); Xu, AA (Xu, Aoao)
GEOPHYSICAL RESEARCH LETTERS
卷: 44 期: 20 页: 10171-10179
Whether or not background secondary craters dominate populations of small impact craters on terrestrial bodies is a half-century controversy. It has been suggested that small craters on some planetary bodies are dominated by background secondary craters based partly on the steepened slope of crater size-frequency distribution (CSFD) toward small diameters, such as the less than similar to 1 km diameter crater population on the lunar mare. Here we show that topography degradation enlarges craters and increases CSFD slopes with time. When topography degradation is taken into account, for various-aged crater populations, the observed steep CSFD at small diameters is uniformly consistent with an originally shallower CSFD, whose slope is undifferentiated from the CSFD slope estimated from near-Earth objects and terrestrial bolides. The results show that the effect of topography degradation on CSFD is important in dating planetary surfaces, and the steepening of CSFD slopes is not necessarily caused by secondary cratering, but rather a natural consequence of topography degradation.

紫台历年发表论文情况

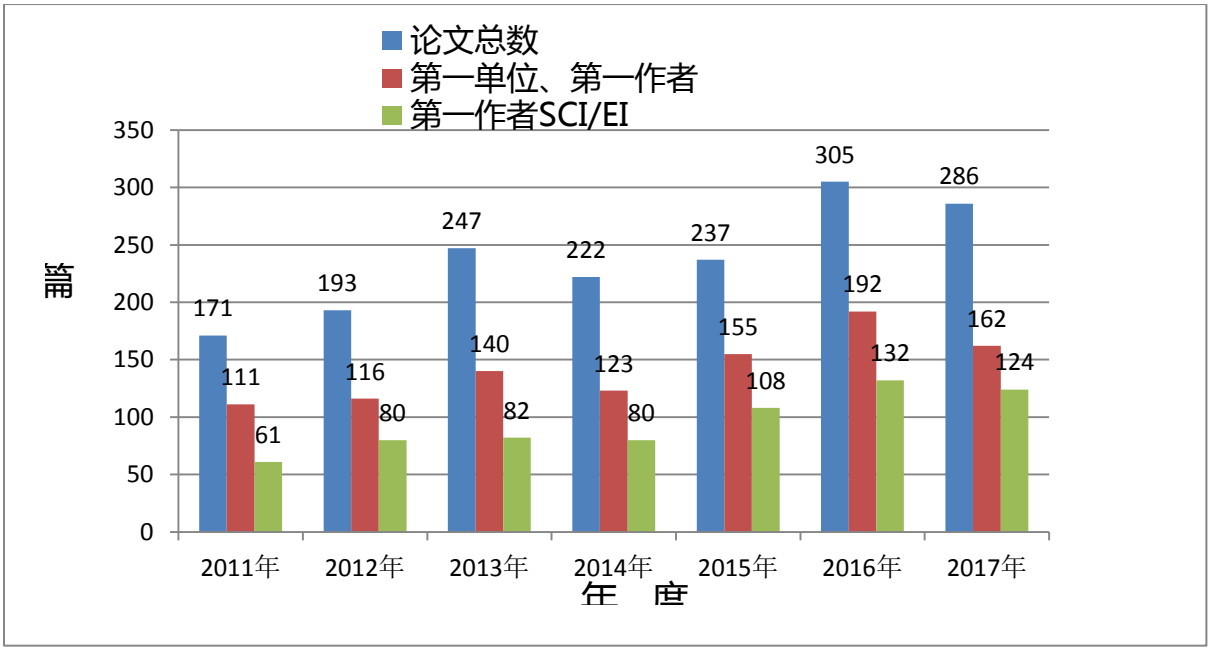

学术报告

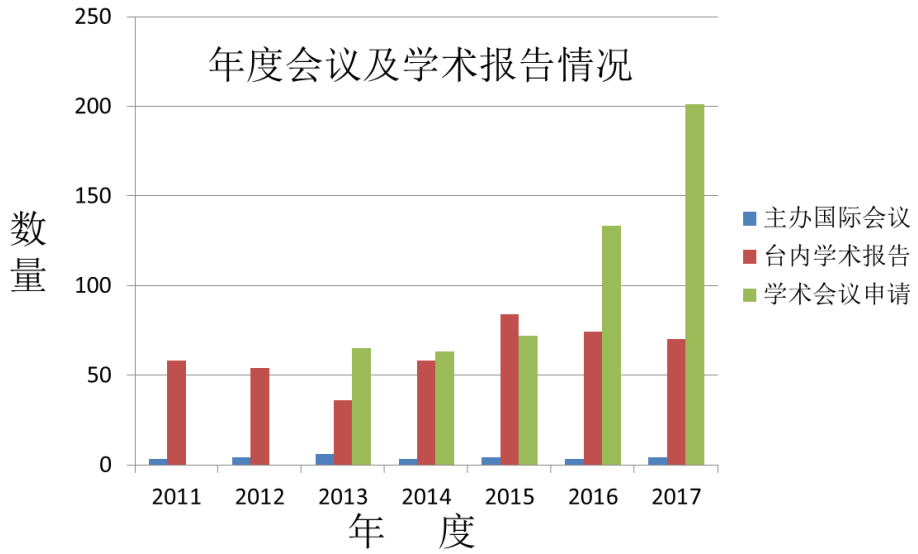

专利

序号	申请号/专利号	发明名称	专利类型	发明人	状态
1	201711282708 0	一种南极天文保障平台发电机组带时间限制的控制方法	发明专利	王慧慧、柳磊、朱镇熹、蒙克来	申请
2	201711282709 5	一种南极天文保障平台发电机组分布控制方法	发明专利	王慧慧、管旭、朱镇熹、柳磊、蒙克来	申请
3	201711152874 9	一种新型的太赫兹碳纤维复合材料面板结构	发明专利	钱元、郝旭峰、娄铮、左营喜、杨戟	申请
4	201711152875 3	一种新型的保温结构	发明专利	钱元、张守玉、陈同海、赵忠博、娄铮、左营喜、杨戟	申请
5	201711082011 9	一种数字 FFT 频谱仪系统及运行方法	发明专利	林镇辉、段文英、姚骑均	申请
6	201710846796 6	热电子混频器和太赫兹量子级联激光器的集成装置及方法	发明专利	高鲁、缪巍、史生才	申请
7	201710560132 3	一种真空阀远程控制系统及方法	发明专利	姚骑均、周超	申请
8	201710405813 2	利用蒸镀法在光阻掩膜衬底上制备超导钛薄膜的方法	发明专利	王争、张文、缪巍、史生才	申请
9		一种基于超导探测器的太赫兹波段大气发射谱线测量装置	发明专利	李升	申请
10	201810261153 .X	一种无人值守柴油发电机组远程定量更换润滑油系统	发明专利	柳磊、王慧慧、朱镇熹、蒙克来	申请
11	201711380705	一种基于数字摄影测量技术的高精度转动测量方法	发明专利	娄铮	申请
12	201710307681 X	FiDrizzle 多次采样图像重建技术	发明专利	王蕾，李国亮	申请
13	201711321275 5	铺装简单曲面多次曝光图像重建技术	发明专利	王蕾，李国亮	申请
14	201711331038 7	基于分立小波变换的快速迭代(多次曝光)图像重建技术	发明专利	王蕾，李国亮	申请
1	201621289176 4	滤光片磁定位更换装置	实用新型	姚大志、杨戟、郑宪忠、刘伟、娄铮、华园园	授权
2	201621284235	一种中子探测装置	实用	黄永益	授

	9		新型		权
3	201621285447 9	一种高压供电装置	实用 新型	黄永益	授 权
4	201610319948 2	一种 KID 探测器阵列的多功能读出电路系统	发明 专利	林镇辉、杨瑾屏、史生才、李升	授 权
5	201610132088 1	太赫兹探测器及读出电路系统频响测量方法	发明 专利	林镇辉、史生才、李绍亮	授 权
6	201610132090 9	太赫兹外差阵列接收机偏置复用装置	发明 专利	张文、张坤、史生才、缪巍、姚骑均	授 权
7	201510599033 7	低温面形摄影测量方法	发明 专利	钱元、娄铮、刘昌儒、范生宏、王海仁、左营喜、杨戟	授 权
8	201510294511 3	一种星载空间晶体阵列探测器的保护结构	发明 专利	常进、胡一鸣、陈灯意、郭建华、蔡明生、宫一忠	授 权
9	201410780651 7	一种空间探测仪器加热装置	发明 专利	胡一鸣、张家宇、崔兴柱、常进	授 权
10	201410114485 7	单接收机太赫兹矢量场形测量装置及其测量方法	发明 专利	娄铮、胡洁、周康敏、林镇辉、姚骑均、史生才	授 权

2017 年度发表科研论文、专著、专利一览表

团组与学科片	论文总数	第一单位论文	SCI论文	第一单位SCI论文	第一单位EI论文	国际合作	著作	专利申请	专利授权	软件登记
宇宙伽马暴、中子星及相关物理研究团组	4	3	4	3	0	2	0	0	0	0
太阳高能及相关物理过程研究团组	13	8	13	8	0	9	0	0	0	0
太阳活动的多波段观测研究团组	25	15	24	14	1	6	0	0	0	0
宇宙高能粒子的加速和辐射研究团组	5	5	4	4	0	2	1	0	0	0
暗物质间接探测的相关物理研究团组	20	15	16	12	0	3	0	0	0	0
暗物质和空间天文实验室	18	6	17	5	0	7	0	0	4	0
紫外及 X 射线天文研究	2	2	2	2	0	1	0	0	0	0
暗物质和空间天文研究部　合计	**87**	**54**	**80**	**48**	**1**	**30**	**1**	**0**	**4**	**0**
恒星结构、演化和脉动研究团组	3	2	1	0	0	0	0	0	0	0
南极天文中心	15	4	15	4	0	12	0	2	0	0
星系宇宙学和暗能量研究团组	15	11	12	8	0	7	0	3	0	0
星系中的恒星形成研究团组	13	3	13	3	0	10	0	0	0	0
分子云与恒星形成研究团组	12	6	12	6	0	10	0	0	0	0
星系形成与大视场巡天研究团组	8	1	8	1	0	6	0	0	0	0
高能时域天文研究团组	17	10	16	10	0	11	0	0	0	0
银河系气体分布与性质研究团组	6	4	6	4	0	3	0	0	0	0
毫米波和亚毫米波技术实验室	11	7	8	4	1	4	0	3	3	4
天文望远镜技术实验室	6	3	5	2	0	2	0	6	2	2
德令哈毫米波观测基地	7	5	5	3	0	3	0	0	0	3
南极天文和射电天文研究部　合计	**##**	**56**	**101**	**45**	**1**	**68**	**0**	**14**	**5**	**9**

空间目标与碎片观测研究中心	20	18	10	8	2	1	1	0	1	3
卫星精密定轨及应用研究团组	1	1	0	0	0	0	0	0	0	0
应用天体力学和空间目标与碎片研究部合计	**21**	**19**	**10**	**8**	**2**	**1**	**0**	**0**	**1**	**3**
近地天体探测和太阳系天体研究团组	8	0	8	0	0	7	0	0	0	0
历算和天文参考系研究团组	10	10	8	8	0	0	0	0	0	0
太阳和太阳系等离子体研究团组	11	5	9	5	0	2	0	0	0	0
近地天体望远镜团组	1	0	1	0	0	0	0	0	0	0
行星科学与深空探测实验室	10	5	7	3	0	2	0	0	0	0
天体化学和行星科学实验室	17	8	10	5	0	0	0	0	0	0
盱眙天文观测站	0	0	0	0	0	0	0	0	0	0
行星光谱学研究团组	2	0	0	0	0	0	0	0	0	0
行星科学和深空探测研究部　合计	**59**	**29**	**45**	**22**	**0**	**13**	**0**	**0**	**0**	**0**
其他	6	6	0	0	0	0	0	0	0	0
其他　合计	0	6	0	0	0	0	0	0	0	0
合计	286	163	234	122	4	110	2	14	10	12

紫台历年主要科研项目统计

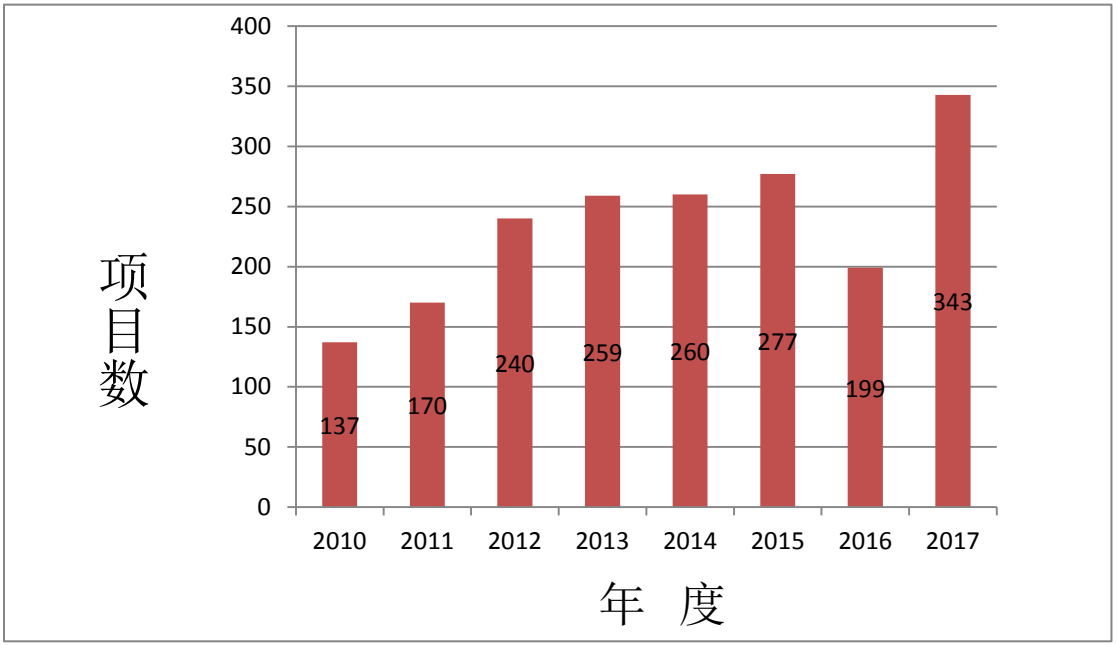

2017 年度在研科研项目

项目类型	在研项目数	占比	当年项目到账经费/万
国家任务	171	52%	10344
中科院任务	98	30%	3289
地方任务	26	8%	184
横向委托	29	9%	617
研究生自选	0	0%	0
其他	2	1%	5
总和	326	100%	14439

学术报告

序号	日期	报告人	单位	职称	题目
001	2017.1.3	黄狮勇	武汉大学	研究员	地球磁鞘湍流的卫星观测研究：从 MHD 尺度到电子尺度
002	2017.1.13	Seog-Tae Han	韩国天文与空间学院	研究员	A Millimeter-Wave Quasi-optical Circuitfor Compact Triple Bands Receiving System.
003	2017.1.12	王铁砚	北京航天航空大学	博士	Turbulent dissipation and structure in the space plasma flows
004	2017.2.15	王为豪	台湾中研院	副研究员	Mapping the Dust Obscured Cosmic Star Formation
005	2017.3.14	侯贤	云南天文台	副研究员	Observations of M31 and M33 with the Fermi Large Area Telescope: a galactic center excess in Andromeda?
006	2017.3.14	袁尊理	云南天文台	助理研究员	A Mixture Evolution Scenario of the AGN Radio Luminosity Function
007	2017.4.6	Paul van der Werf	莱顿大学	教授	Water emission and molecular gas outflows in (ultra)luminous infrared galaxies at low and high redshift
008	2017.4.11	Matin Bureau	University of Oxford	教授	3D Observations of Molecular Gas in Galaxies: From Global Dynamics to Supermassive Black Holes
009	2017.4.12	仲佳勇	北京师范大学	教授	实验室天体物理介绍
010	2017.4.19	李广兴	Universitäts-Sternwarte München	博士	Impact of molecular clouds on galactic disk clumpiness
011	2017.4.20	杨睿智	德国马普核物理研究	博士后	Pinning down the origin of Galactic cosmic rays by using gamma-ray observations
012	2017.4.24	Victor Melnikov	Pulkovo Observatory, Saint Petersburg		Spatial Distribution of Intensity and Polarization of Hard X-Ray and Gamma-Ray Emission in a Flare Loop
013	2017.4.27	王华沛	中国地质大学	教授	利用古磁学来研究太阳系早期演化和行星体内部动力学过程
014	2017.5.2	许丹丹	Heidelberg Institute for Theoretical Studies	博士后	inner structure of early-type galaxies since z=1.0: a simulation perspective
015	2017.5.5	陈枫	美国高山天文台	博士后	Formation of Active Regions and Sunspots through Emergence of Magnetic Flux Generated in a Solar Convective Dynamo
016	2017.5.8	Sergey Kuzin	俄罗斯科学院列别捷夫物理研究所	博士	Results of Solar Space Experiments of LPI
017	2017.5.11	Nithaya Chetty	南非 NRF 天文负责人	教授	Enhancing Chinese-South African cooperation in Astronomy
018	2017.5.22	郭静楠	德国基尔大学	博士	Space Weather and Space Radiation and their effects on space explorations
019	2017.5.19	刘洋	美国西南研究所	博士	Remote Sensing and Spectroscopic Studies of Mars and the Moon: from Thermal Infrared to Far-Ultraviolet
020	2017.5.25	Chang FENG	University of California, Irvine	博士	Recent measurements from POLARBEAR, CIBER, Planck and Fermi-LAT experiments
021	2017.5.31	Jonathan Braine	University de Bordeaux	教授	Dense gas in low metallicity environments
022	2017.6.12	Zhiyu Zhang	University of Edinburgh/ESO	博士	Losing sight of CO and dust in galaxies: the CMB effect, cosmic rays, and their implications for the stellar IMF
023	2017.6.1	蔡振翼	中科大	博士	AGN variability - a powerful tool to probe and test AGN structures in the era of time domain astronomy
024	2017.6.6	冯劼	中山大学	博士	Precision measurement of antiproton to proton ratio by AMS-02

025	2017.6.12	沈嗣钧	俄亥俄州立大学	教授	Constraint Studies on the Interior Structure of Planetary Bodies Using Satellite Geodesy
026	2017.6.17	Yu Gao	Wayne State Univ., USA)		Indirect Search Aspects of Right Handed Neutrinos
027	2017.6.14	Shuo Zhang	MIT	博士后	Revealing the Origin of Cosmic-rays in the Galactic Center
028	2017.6.14	Rainer Schoedel	IAA-CSIC, Spain	教授	Near-infrared studies of the nearest galactic nucleus
029	2017.6.14	柳若愚	Max Planck Institute for Nuclear Physics		A fading particle accelerator for multi-TeV emissions in the Galactic Center
030	2017.6.19	林郁	Physics Department, Auburn University	教授	Understanding Transport Processes in the Magnetosphere Using Hybrid Simulation
031	2017.6.27	Jian-Yang Li	Planetary Science Institute	博士	Disk-Resolved Photometric Analysis and Applications on Dawn Vesta Data
032	2017.7.4	吕行	日本国立天文台	博士	Gas Accretion and High-Mass Star Formation in Filamentary Molecular Clouds
033	2017.7.5	Jie Zhang	George Mason University	教授	Compound Solar Eruptions: the phenomena, processes and possible causes
034	2017.7.20	季索清	University of California	博士	Make it, Mix it and Shake it — a recipe for cold gas in circumgalactic medium
035	2017.7.14	François PAJOT	Recherche au CNRS	教授	X-IFU, the high resolution X-ray imaging spectrometer of the Athena mission
036	2017.7.25	Xianming L. Han	美国巴特勒大学	教授	Asteroids, Eclipsing Binaries and Active Galactic Nuclei
037	2017.7.24	许伟伟	麻省理工	博士后	Properties of Elementary Particle Fluxes in Primary Cosmic Rays Measured with the Alpha Magnetic Spectrometer on the ISS
038	2017.8.16	高扬	清华大学	助理研究员	Cloud core dynamics and protostellar mass accretion history in star formation
039	2017.8.14	赵璐璐	Florida Institute of Technology	博士	Solar Energetic Particle Acceleration and Transport in the Inner Heliosphere
040	2017.8.28	Zhoujian Zhang	PhD, University of Hawaii	博士	A Pan-STARRS1 View of the Taurus Star Formation History in the Substellar Regime
041	2017.9.4	Mousumi Das	Indian Institute of Astrophysics	Associate ProfessorI	Star Formation in the Extended Disks of Spiral Galaxies and what it tells us about the Disk Mass Distribution
042	2017.8.31	Guoqing Zhao	洛阳师范	博士	Low frequency electromagnetic cyclotron waves in and around magnetic clouds: STEREO observations during 2007-2013
043	2017.9.7	Ting Li	Fermi National Accelerator Laboratory	Lederman Fellow	Constraining the Nature of Dark Matter with the Milky Way Satellite Galaxies Discovered in the Dark Energy Survey
044	2017.9.2	N.-H. Chen	Korea Astronomy and Space Science		Temperature of source regions of 3He-rich impulsive solar energetic particle events
045	2017.9.4	范锡龙	湖北第二师范学院	副教授	高频引力波天文学
046	2017.9.4	郑普	工程物理院	副研究员	中子探测基础
047	2017.9.4	郑普	工程物理院	副研究员	基于反冲质子法的快中子能谱测量技术研究
048	2017.9.22	ZIMOVETS IVAN	Space Research Institute (IKI) of Russian Academy of Sciences	博士	Spatially-resolved observations of the sources of hard X-ray pulsations and their links with the magnetic structure in solar flare regions
049	2017.9.22	许浩杰	美国犹他大学	博士生	Conditional Color-Magnitude Distribution of Galaxies from Color/Luminosity Dependent Galaxy Clustering

非学术型报告	2017.9.25	Marios Karouzos	美国	副主编	What is Nature Astronomy and how do I get published in it?
050	2017.9.28	Tongjiang Wang	Catholic University of America and NASA GSFC		Coronal seismology by flare-excited standing slow-mode waves
051	2017.10.24	Eli Waxman	Weizmann Institute of Science	教授	High energy neutrino astronomy: What have we learned?
052	2017.10.27	陈宇翱	中科大	教授	构建中国－全球的量子通讯网络
053	2017.11.8	David Elbaz	CEA-Saclay, France	博士	Universality and peculiarity in galaxy formation
非学术型报告	2017.11.16	Ravi Guntupalli	Vice President, Sales & Marketing		Latest Technology and Application in Astronomy
054	2017.11.29	何建森	北京大学	研究员	太阳风湍流多点测量的研究回顾与展望
055	2017.12.13	Peter Mészáros	Pennsylvania State University	教授	Gamma-Ray Bursts, Neutron Star Mergers and Muti-Messenger Astrophysics
056	2017.12.15	刘彤	厦门大学	教授	伽玛射线暴不同中心引擎释放引力波的对比研究
057	2017.12.15	顾为民	厦门大学	教授	A Black Hole – White Dwarf Compact Binary Model for Long Gamma-ray Bursts without Supernova Association

国际合作与台内学术报告统计

团组与学科片	出访人次	占比	来访人次	占比	台内学术报告	占比	PMO Colloquium	占比
宇宙伽玛暴、中子星及相关物理研究				0%	2	4%	1	8%
太阳高能及相关物理过程研究	5	3%	15	10%	9	16%	1	8%
太阳活动的多波段观测研究	11	7%	17	11%	1	2%		
暗物质和空间天文实验室	31	20%	15	10%	2	4%		
宇宙高能粒子的加速和辐射研究			3	2%	6	11%	1	8%
暗物质间接探测的相关物理研究	2	1%	5	3%	3	5%		
暗物质和空间天文								
恒星结构、演化和脉动研究团组								
南极天文中心	**9**	**6%**	**1**	**1%**				
星系宇宙学和暗能量研究团组	**5**	**3%**	**4**	**3%**	**4**	**7%**		**0%**
星系中的恒星形成研究团组	**16**	**10%**	**20**	**13%**	**7**	**12%**	**3**	**23%**
分子云与恒星形成研究团组	**6**	**4%**	**50**	**33%**	**1**	**2%**		
毫米波和亚毫米波技术实验室	23	15%	4	3%	2	**4%**	1	**8%**
德令哈毫米波观测基地	**9**	**6%**			**1**	**2%**		
星系形成与大视场巡天研究团组	**2**	**1%**			**1**	**2%**		**0%**
高能时域天文研究团组	**3**	**2%**	**3**	**2%**	**1**	**2%**	**2**	**15%**
银河系气体分布与性质研究团组	**2**	**1%**			**1**	**2%**		
天文望远镜技术实验室								
紫外及 X 射线天文研究	**4**	**3%**	**7**	**5%**	**2**	**4%**	**1**	**8%**
南极天文和射电天文								
空间目标与碎片观测研究	**8**	**5%**	**4**	**3%**	**5**	**9%**		
卫星精密定轨及应用研究								
应用天体力学和空间目标与碎片								
近地天体探测和太阳系天体研究	1	1%			1			
历算和天文参考系研究	1	1%						
太阳和太阳系等离子体研究	3	2%	1	1%	4	7%		
行星科学与深空探测实验室	8	5%	2	1%	4	7%	2	15%
天体化学和行星科学实验室	4	3%						
行星光谱学	5	3%	1	1%			1	3%
近地天体望远镜								
行星科学和深空探测								
总计	158	**100%**	152	**100%**	57		13	**100%**

中国 2017 年度“十大天文科技进展”

（紫金山天文台相关部分）

1、暗物质粒子探测卫星发布首批科学成果；

暗物质粒子探测卫星（悟空号）是中国科学卫星系列的首发星，也是我国成功发射的首颗天文卫星。悟空号于 2011 年 12 月 1 日正式立项，2015 年 12 月 17 日发射，随后进行了为期 3 个月的在轨标定实验，并于 2016 年 3 月 17 日正式交付使用。

悟空号在轨工作状态优异，每天约收集 500 万例宇宙线事例。基于其在轨前 530 天所收集到的数据，悟空号合作组从中证认出约 150 万例能量高于 25GeV 的电子宇宙射线，进而获得了 25GeV-4.6TeV 的高精度电子宇宙射线能谱，该成果于 2017 年 12 月 7 日在《Nature》杂志正式发表(http://www.nature.com/articles/nature24475)。

如图 1 所示：悟空号的电子宇宙射线的能量测量范围比起国外的空间探测设备（AMS-02, Fermi-LAT）有显著提高，拓展了人类在太空中观察宇宙的窗口； 悟空号测量到的 TeV 电子的“纯净”程度最高(也就是其中混入的质子数量最少)，能谱的准确性高；悟空号首次直接测量到了电子宇宙射线能谱在~1 TeV 处的拐折，该拐折反映了宇宙中高能电子辐射源的典型加速能力，其精确的下降行为对于判定部分电子宇宙射线是否来自于暗物质起着关键性作用。此外，悟空号的数据初步显示在~1.4 TeV 处存在能谱精细结构，但尚需更多的数据予以确认或排除。

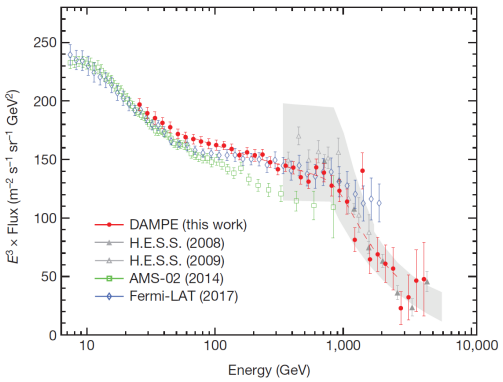

图 1：悟空号工作 530 天得到的高精度宇宙射线电子能谱（红色数据点），以及和美国费米卫星测量结果（蓝点）、丁肇中先生领导的阿尔法磁谱仪的测量结果(绿点)、欧洲的地面间接探测实验 H.E.S.S 结果(灰点)的比较。

2、中国南极巡天望远镜团队追踪探测引力波事件首例光学信号；

2017 年 8 月 17 日，美国地基先进激光干涉引力波天文台 LIGO 和欧洲“室女座”引力波探测器 VIRGO 共同探测到的引力波事件 GW 170817。随后几秒内，美国宇航局 Fermi 伽玛射线卫星和欧洲 INTEGRAL 卫星都探测到了一个极弱的短时标伽玛暴 GRB 170817A。全球有几十台天文设备对 GW 170817 开展了后随观测，确定这次的引力波事件发生在距离地球 1.3 亿光年之外的 NGC 4993 的星系中。这是人类首次直接探测到双中子星合并引力波事件及其光学对应体，对天文学的发展具有重大意义。

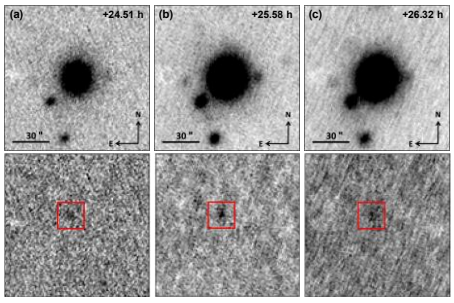

图 1：AST3-2 在 8 月 18 日观测窗口期内引力波光学信号（红色方框内）

自北京时间 2017 年 8 月 18 日 21:10 起（即距离此次引力波事件发生 24 小时后），中国南极巡天望远镜 AST3 合作团队利用正在中国南极昆仑站运行的第 2 台望

远镜 AST3-2 对 GW 170817 开展了有效的观测，此次观测持续到 8 月 28 日，期间获得了大量的重要数据，并探测到此次引力波事件的光学信号（图 1）。AST3-2 得到的数据和全球其他天文台的观测结果一起揭示了此次双中子星并合抛射出 1 %量级太阳质量（超过 3000 个地球质量）的物质，这些物质以 0.3 倍光速被抛到星际空间，抛射过程中部分物质发生核合成，形成比铁还重的元素。因此，这次引力波光学对应体的发现，证实了双中子星并合事件是宇宙中大部分超重元素（金、银）的起源。

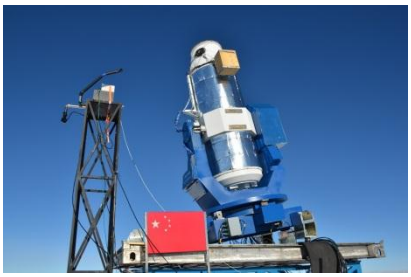

图 2：第二台南极巡天望远镜 AST3-2

AST3-2 是我国在昆仑站安装的第二台南极巡天望远镜（图 2）。有效通光口径 50 厘米，是南极现有最大的光学巡天望远镜，并完全实现了极端环境下无人值守全自动观测。AST3 的研制和运行是跨学科成功合作的典范。在国家海洋局南极科考大力支持下，项目主要参与单位包括中科院紫金山天文台、中科院国家天文台、中科院南京天文光学技术研究所、海洋局中国极地研究中心、天津师范大学、南京大学、清华大学、北京师范大学、天津大学、澳大利亚新南威尔士大学、英澳天文台和斯威本科技大学。在南极天文近 10 年的发展中，项目也先后获得多方经费支持，包括国家自然科学基金委、中科院方向性重点、紫金山天文台、国家天文台、南京天文光学技术研究所、清华大学、南京大学、北京师范大学以及科技部 973 项目。

著名的中国旗舰期刊《科学通报》英文版 Science Bulletin 于北京时间 2017 年 10 月 16 日 22:00 同步上线由紫金山天文台联合中外各个单位的研究论文。

相关论文：

1、 Hu, Lei; Wu, Xuefeng etal, Optical Observations of LIGO Source GW 170817 by the Antarctic Survey Telescopes at Dome A, Antarctica, Science Bulletin， Volume 62, Issue 21, （2017）.

2、 LIGO Scientific Collaboration and Virgo Collaboration et al, Multi-messenger Observations of a Binary Neutron Star Merger, The Astrophysical Journal Letters, Volume 848, Issue 2, article id. L12, 59 pp. (2017).

3、 Andreoni, I. et al, Follow up of GW170817 and its electromagnetic counterpart by Australian-led observing programs, eprint arXiv:1710.05846.

3,太赫兹超导成像阵列研制成功

太赫兹波段在当代天文学前沿研究（如宇宙生命环境和极高红移早期宇宙）中具有特别重要的作用。为此，我国将在地面最优良的太赫兹、远红外天文台址--南极冰穹 A 建设一台 5 米太赫兹望远镜（DATE5）。DATE5 望远镜除了将配备针对宇宙生命环境研究的太赫兹谱线观测接收机，还拟布局多像元宽场太赫兹相机，为行星、恒星、星系和宇宙学研究提供这一独特波段的巡天“传世”数据库。针对这一重要科学需求，我们提出了“太赫兹超导阵列成像系统”项目，并被遴选为国家基金委 2011 年首批启动的 9 项国家重大科研仪器研制项目（部门推荐）之一。

项目组历时 5 年时间，攻克了太赫兹超导阵列成像系统的核“芯”—国际前沿的超导动态电感探测器（Kinetic Inductance Detectors，简称 KID）和超导相变边缘探测器（Transition Edge Sensor，简称 TES）技术，实现了我国大规模二维阵列超导探测器芯片技术“零”的突破，其中 KID 超导探测器在阵列规模、灵敏度及工作频段等指标方面均处于国际同类探测器的前沿水平。此外，项目组还攻克了系统研制中的三项主要关键技术：大规模 KID 探测器阵列频分复用读出技术、太赫兹波段大视场成像光学设计仿真技术、以及低漏热亚 K 低温制冷平台技术。基于上述研究成果，成功研制了一台 850 微米波段 8×8 像元和一台 350 微米波段 32x32 像元超导阵列成像系统（参见下图），灵敏度均优于地面观测设备背景极限。研制的两套超导阵列成像系统分别实现了天文试验观测及实验室演示实验。该系统的成功研制使我国跻身大规模阵列超导探测器技术领域国际前沿，为我国天文观测研究提供了一种全新的成像探测手段。除了南极太赫兹天文观测应用以外，KID 与 TES 探测器技术还有望应用于宇宙微波背景

探测、3D 成像频谱探测、X 射线及光学红外天文、量子信息及国家安全等领域。该项目已顺利通过了国家基金委组织的项目验收（参见 http://www.cas.cn/syky/201707/t20170703_4607328.shtml）。

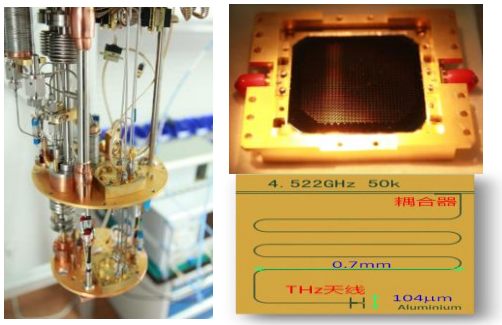

图，工作在亚 K 温区的 350 微米波段 32x32 像元超导阵列成像系统内部照片（左）、32x32 像元 KID 探测器（右上）和包含太赫兹天线与微波超导谐振器的单一 KID 探测器照片（右下）

If you are interested in the work of PMO please contact division of Science & Technology Management at

+86-(0)25-83332288, 83332103

pmokjc@pmo.ac.cn